Claudia Heindl
aus Tirschenreuth, geb. am 03.07.1986

Studium: Chemie, Biologie für das Lehramt an Gymnasien
Abschluss: 1. Staatsexamen
Promotion: Prof. Dr. Manfred Scheer,
Institut für Anorganische Chemie

Die vorliegende Dissertation beschäftigt sich mit Polyphospholylliganden als Bausteine zum Aufbau von polymeren und sphärischen Aggregaten. Insbesondere wird das Koordinationsverhalten von 1,2,4-Triphosphaferrocenen, 1,2,4-Triphospholylsalzen und Pentaphosphaferrocenen gegenüber Cu(I)-Halogeniden untersucht. Die ersten beiden Substanzklassen zeigen dabei eine hohe Tendenz zur Bildung von neuartigen ein-, zwei- und dreidimensionalen Polymeren mit seltenen oder gar bisher unbekannten Strukturmotiven. Pentaphosphaferrocene eignen sich hingegen hervorragend zum templatgesteuerten Aufbau von diskreten Supramolekülen im Nanometerbereich. Systematisch wurden im Rahmen der Arbeit die Bedingungen dieser Wirt-Gast-Chemie untersucht und so eine Reihe an neuen Einschlussverbindungen erhalten. Auch ermöglichte dies die Bildung neuer Gerüste, die sich in Ladung, Größe und Aufbau unterscheiden. Neben den koordinationschemischen Untersuchungen konnten zudem auch bisher nicht zugängliche Moleküle und Salze synthetisiert und charakterisiert werden, welche sich als Ausgangsverbindungen für den Aufbau von Makromolekülen eignen.

Alumniverein Chemie der Universität Regensburg e.V.
alumniverein@chemie.uni-regensburg.de
http://www.alumnichemie-uniregensburg.de

ISBN 978-3-86845-129-0

Fakultät für
Chemie und Pharmazie
Universität Regensburg
Universitätsstraße 31
93053 Regensburg
www.uni-regensburg.de

Claudia Heindl | 2015

Polyphospholyl Ligands as Building Blocks

5

Institut für Anorganische Chemie
Fakultät für Chemie und Pharmazie

Polyphospholyl Ligands as Building Blocks for the Formation of Polymeric and Spherical Assemblies

Claudia Heindl
2015

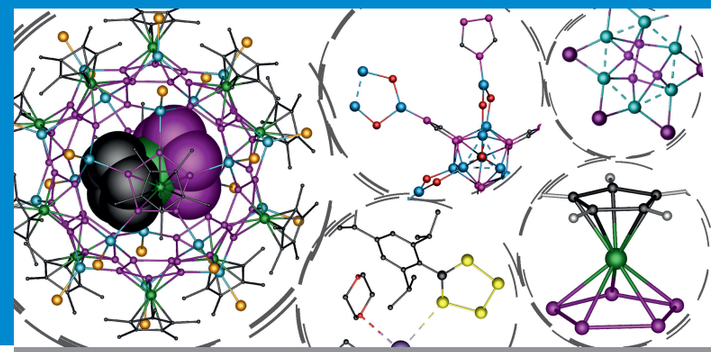

Universität Regensburg

Claudia Heindl

Polyphospholyl Ligands as Building Blocks for the Formation of Polymeric and Spherical Assemblies

Polyphospholyl Ligands as Building Blocks for the Formation of Polymeric and Spherical Assemblies

Dissertation zur Erlangung des Doktorgrades der Naturwissenschaften (Dr. rer. nat.)
der Fakultät für Chemie und Pharmazie der Universität Regensburg
vorgelegt von

Claudia Heindl

Tirschenreuth
2015

Die Arbeit wurde von Prof. Dr. Manfred Scheer angeleitet.
Das Promotionsgesuch wurde am 10.08.2015 eingereicht.
Das Kolloquium fand am 10.09.2015 statt.

Prüfungsausschuss:	Vorsitzender:	Prof. Dr. Arnd Vogler
	1. Gutachter:	Prof. Dr. Manfred Scheer
	2. Gutachter:	Prof. Dr. Henri Brunner
	weiterer Prüfer:	Prof. Dr. Oliver Tepner

Dissertationsreihe der Fakultät für Chemie und Pharmazie der Universität Regensburg, Band 5

Herausgegeben vom Alumniverein Chemie der Universität Regensburg e.V.
in Zusammenarbeit mit Prof. Dr. Burkhard König, Prof. Dr. Joachim Wegener,
Prof. Dr. Arno Pfitzner und Prof. Dr. Werner Kunz.

Polyphospholyl Ligands as Building Blocks for the Formation of Polymeric and Spherical Assemblies

Claudia Heindl

Universitätsverlag Regensburg

Bibliografische Informationen der Deutschen Bibliothek.
Die Deutsche Bibliothek verzeichnet diese Publikation
in der Deutschen Nationalbibliografie. Detailierte bibliografische Daten
sind im Internet über http://dnb.ddb.de abrufbar.

1. Auflage 2015

Leibnizstraße 13, 93055 Regensburg

Umschlagentwurf: Alumniverein Chemie der Universität Regensburg e.V.
Layout: Claudia Heindl
Druck: Docupoint, Magdeburg
ISBN: 978-3-86845-129-0

Weitere Informationen zum Verlagsprogramm erhalten Sie unter:
www.univerlag-regensburg.de

This thesis was elaborated within the period from September 2011 till August 2015 in the Institute of Inorganic Chemistry at the University of Regensburg, under the supervision of Prof. Dr. Manfred Scheer.

Parts of this thesis have already been published or submitted, including results from collaborations, which are not mentioned within this work:
(* = Co-First Authorship: These authors contributed equally to this work.)

- C. Heindl, S. Reisinger, C. Schwarzmaier, L. Rummel, E. V. Peresypkina, A. V. Virovets, M. Scheer, *Eur. J. Inorg. Chem.* 2015, accepted. (Chapter 7)
- C. Heindl, E. V. Peresypkina, A. V. Virovets, W. Kremer, M. Scheer, *J. Am. Chem. Soc.* 2015, *137*, 10938-10941. (Chapter 14)
- C. Heindl, A. Schindler, M. Bodensteiner, E. V. Peresypkina, A. V. Virovets, M. Scheer, *Phosphorus, Sulfur Silicon Rel. Elem.* 2015, *190*, 397-403.
- C. Heindl, E. V. Peresypkina, A. V. Virovets, V. Komarov, M. Scheer, *Dalton Trans.* 2015, *44*, 10245-10252. (Chapter 5)
- C. Heindl, A. Kuntz, E. V. Peresypkina, A. V. Virovets, M. Zabel, D. Luedeker, G. Brunklaus, M. Scheer, *Dalton Trans.* 2015, *44*, 6502-6509. (Chapter 4)
- F. Dielmann,* M. Fleischmann,* C. Heindl,* E. V. Peresypkina, A. V. Virovets, R. M. Gschwind, M. Scheer, *Chem. Eur. J.* 2015, *21*, 6208-6214.
- C. Heindl, S. Heinl, D. Luedeker, G. Brunklaus, W. Kremer, M. Scheer, *Inorg. Chim. Acta* 2014, *422*, 218-223. (Chapter 8)
- F. Dielmann,* C. Heindl,* F. Hastreiter, E. V. Peresypkina, A. V. Virovets, R. M. Gschwind, M. Scheer, *Angew. Chem., Int. Ed.* 2014, *53*, 13605-13608; *Angew. Chem.* 2014, *126*, 13823-13827.
- E. V. Peresypkina, C. Heindl, A. Schindler, M. Bodensteiner, A. V. Virovets and M. Scheer, *Z. Kristallogr.* 2014, *229*, 735-740.
- C. Schwarzmaier, A. Schindler, C. Heindl, S. Scheuermayer, E. V. Peresypkina, A. V. Virovets, M. Neumeier, R. Gschwind, M. Scheer, *Angew. Chem. Int. Ed.* 2013, *52*, 10663; *Angew. Chem.* 2013, *125*, 11097-11100.
- M. Fleischmann, C. Heindl, M. Seidl, G. Balázs, A. V. Virovets, E. V. Peresypkina, M. Tsunoda, F. P. Gabbaï, M. Scheer, *Angew. Chem. Int. Ed.* 2012, *51*, 9918-9921; *Angew. Chem.* 2012, *124*, 10056-10059.
- Schindler, C. Heindl, G. Balázs, C. Groeger, A. V. Virovets, E. V. Peresypkina, M. Scheer, *Chem.-Eur. J.* 2012, *18*, 829-835.

To Sebastian

Preface

During the period of this thesis (September 2011 – August 2015) some results have already been published (*vide supra*). These are also summarized in the present work, reprinted with permission of the respective scientific publisher. The corresponding license numbers are given in the beginning of the particular chapters.

At the beginning of each chapter a list of authors, who contributed to the respective part, is given. In addition, each capter contains the section 'author contributions', which accurately describes the extent of involvement. If results from collaborations are in part also discussed in other theses, it is stated there.

To ensure a uniform design of this work, all chapters are subdivided into 'Introduction', 'Results and Discussion', 'Experimental Part', 'Crystallographic Details', 'Author Contributions' and 'References'. Furthermore, all chapters have the same text settings and the compound numeration begins anew. In addition, a general introduction is given at the beginning and a comprehensive conclusion of all chapters is presented at the end of this thesis.

Table of Contents

1. Introduction

1.1 Supramolecular Chemistry

'When a substrate binds to an enzyme, a drug sticks to its target, or signals propagate between cells, […]'[1]

…then we are talking about supramolecular chemistry. With these words Jean-Marie Lehn started an article about this interdisciplinary and fascinating field of chemistry, a few years after the award of the Nobel Prize together with Donald J. Cram[2] and Charles Pedersen.[3] The mentioned biological actions all refer to highly complex systems that are based on small subunits and held together by weak interactions, such as hydrogen bonds, π-π-interactions and/or van-der-Waals-forces. To differentiate these key factors from the conventional synthetic approach based on generally strong covalent bonds he coined the new term 'chemistry beyond the molecule'.[4] During the last decades supramolecular chemistry was successfully implemented in non-biological systems for the synthesis of polymeric and spherical assemblies built by small building blocks.

Supramolecular chemistry can be divided into two broad categories, yet partly overlapping: Self-assembly and host-guest chemistry.[5] Here, the self-assembly principle characterizes '*the spontaneous and reversible association of two or more components to form a larger, non-covalently bound aggregate'*, whereas host-guest chemistry is defined as '*the study of large 'host' molecules that are capable of enclosing smaller 'guest' molecules via non-covalent interactions*'.[5] Hence, the construction of a larger aggregate by small 'lego® bricks' *via* weak interactions they both have in common, whereas they differ in their mutual size ratio. Therefore, one speaks of host-guest chemistry, when one kind of bricks is significantly larger (host) and wraps around a second, smaller type of brick (guest). If this is not the case, the aggregates are rather referred to the self-assembly approach.[5]

Since especially coordinative bonds are relatively strong, but often still labile enough to show dynamic behavior in solution, also the Lewis acid/base interaction between a metal and a ligand is included into this field as subcategory named metallosupramolecular chemistry.[6] In addition, metal ions mostly prefer a certain coordination number and geometry, so in combination with characteristic binding sites of the ligand a rational design of architectures is achievable.[6a] Pioneering work on this field has already been done by the group of Lehn in 1987, when they obtained di- and trinuclear double stranded helicates from bipyridine ligands and Cu(I) ions.[7]

1.2 Coordination Polymers

According to an early definition of J. C. Bailar the term 'coordination polymer' describes infinite systems built up by metal ions and organic ligands.[8] This concept has recently been slightly broadened by IUPAC defining it as *‚coordination compound with repeating coordination entities extending in 1, 2, or 3 dimensions'*.[9] Therefore, it is not restricted to an organic nature of the ligand any more and organometallic building blocks are also included (see chapter 1.3). Rather, the ligand is characterized by multiple donation sites to bridge the metal centers *via* a Lewis acid/base relationship, hence any type of atom with a lone pair displays such a donation site. Especially oxygen (e.g. in polycarboxylates) and nitrogen (e.g. in polypyridines and polynitriles) are preferably used,[10] whereas linker molecules based on sulfur (e.g. in dithiocarboxylates)[11] and phosphorus (e.g. in phosphanes)[12] only play a subordinate role. A selection of multidentate ligands, neutral and anionic, is displayed in *Figure 1.1*.

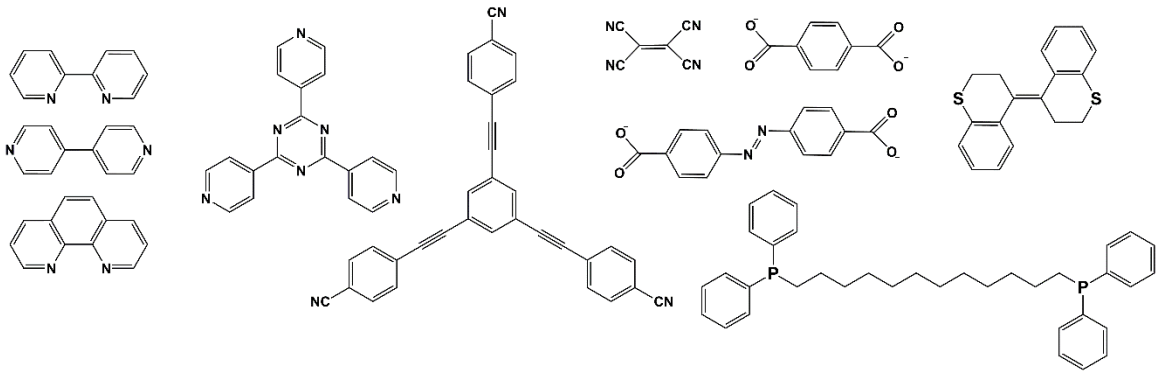

Figure 1.1 Selected multidentate ligands used for the construction of coordination polymers.

A classification of coordination polymers is often done according to dimensionality: 1D, 2D, or 3D. Discrete supramolecules are often referred as (*pseudo*-) 0D coordination polymers, but as they are not polymeric in terms of infinite, they are not considered here and will be discussed in chapter 1.3. In their capacity as nodes, the metal fragments/ions or, more precise, their available coordination sites often predetermine the dimensionality of the polymer.[10c] A linear or zig-zag chain can be obtained using metal ions with two connecting points, whereas three or four may lead to two-dimensional architectures, such as a grid or honeycomb net. Finally, tetrahedral or octahedral nodes can build up a three-dimensional network, e.g. an octahedral or diamandoid net. However, these guidelines are not mandatory, exemplarily three free coordination sites may also lead to a one-dimensional ladder. A summary of the just mentioned motifs, which certainly display only a small excerpt of possible arrangements, is shown in *Figure 1.2*.

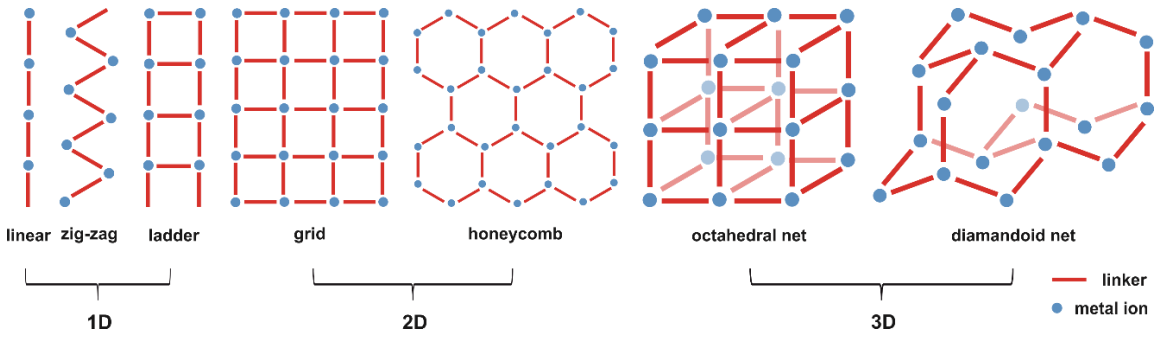

Figure 1.2 Schematic representation of selected structural motifs in coordination polymers.

Metal-organic frameworks (MOFs) are classified as a subcategory of coordination polymers and are, according to IUPAC, defined as *'coordination networks with organic ligands containing potential voids'*.[9] Contrary to the commonly held view, this term is not restricted to 3D architectures, also mesh-like 2D networks may be regarded as porous.[9,13] However, the majority of MOFs are characterized by their three-dimensionality in combination with ultrahigh porosity and enormous internal surface areas.[14] These properties are advantageous for promising applications, such as gas storage (hydrogen, methane, carbon dioxide),[15] adsorption for separation processes,[16] chemical sensor technology,[17] luminescence[18] and heterogeneous catalysis.[19] An unprecedented application attracted special attention recently: A porous 3D network of cages can be applied as a crystalline sponge allowing X-ray analysis of liquids on a nanogram scale by reversible guest uptake of the molecules in the pores or cavities (*Figure 1.3*).[20]

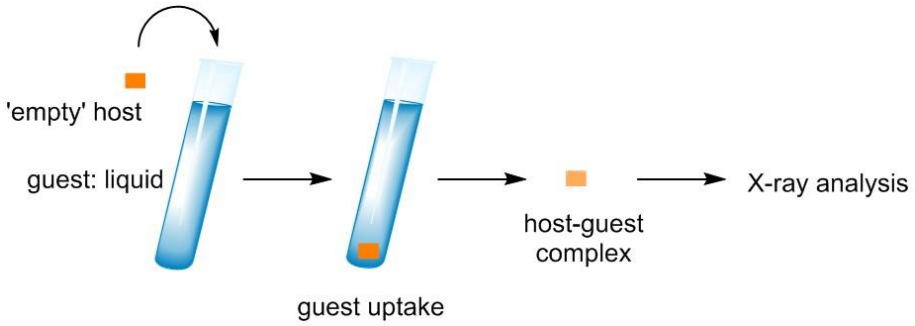

Figure 1.3 Basic functioning of a crystalline 'sponge'.

A prime example of a metal-organic framework is MOF-5 (*Figure 1.4*),[21] synthesized by the group of O. M. Yaghi, who created the term metal-organic framework and unambiguously is the pioneer in this field.[22] MOF-5 is synthesized under solvothermal conditions from zinc nitrate hexahydrate and terephthalic acid and consists of 1,4-benzenedicarboxylate anions as linking units and $[Zn_4O]^{6+}$ cluster as nodes.[23] Although MOFs are often mentioned in connection with zeolites and COFs (covalent organic frameworks) due to their porous 3D structures, the latter two classes of compounds have to be differentiated from coordination polymers. Since they show a lack of

coordinative bonds, a reversible bond formation and cleavage process is not possible in these systems.

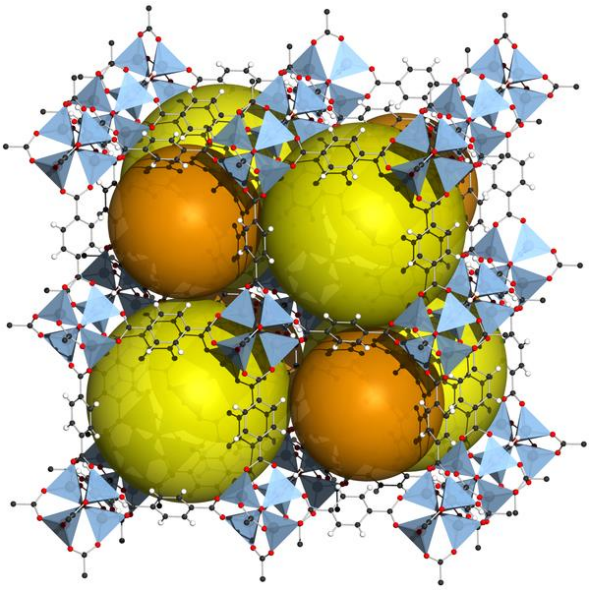

Figure 1.4 Section of the polymeric structure of MOF-5 illustrating the pores by yellow balls. The figure is reused with permission of the copyright holder Tony Boehle (Creative Commons license, view online).

1.3 Discrete Nano-Sized Supramolecules

Discrete nano-sized supramolecules, especially spheres with defined inner cavities, show auspicious potential for widespread applications, e.g. as storage containers for small molecules or as reaction vessels, in catalysis and for molecular recognition. Regarding the latter point, crown ethers (cyclic polyethers), cryptands (polycyclic ligands with ether groups and amine 'caps') and calixarenes (macrocycles obtained by the condensation reaction between phenol and formaldehyde) have to be mentioned (*Figure 1.5*), albeit not yet on a nanometer scale. They all are capable of the selective binding of cations in the interior of the ring or cavity, respectively. Furthermore, Rebek *et al.* make use of calixarene derivatives, resorcinarenes, which form capsules of cylindrical or even bent shape *via* hydrogen bonds.[24]

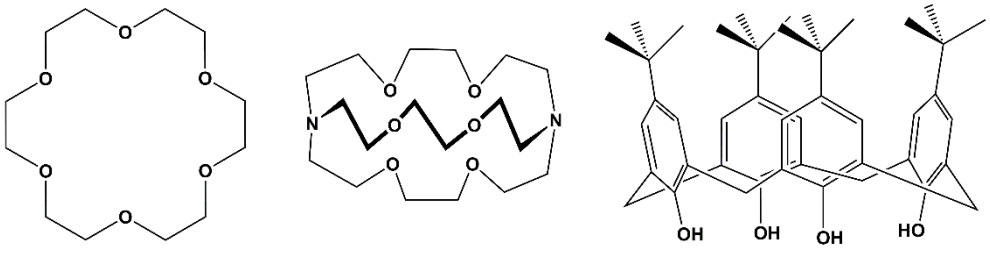

Figure 1.5 The typical representatives for a crown ether, a cryptand and a calixarene, respectively.

With respect to host-guest chemistry a large variety of metallosupramolecular assemblies is known. Within this field, the directed metal-ligand bond can be used for the rational design of supramolecules with a certain shape or size and defined inner voids. Sometimes, reactive intermediates can be stabilized in such cavities[25] and selected catalytic transformations are accelerated inside such metallosupramolecular arrangements.[26] Due to the great number of contributions to this field,[27] only selected examples are given hereafter. For example, the group of Fujita obtained structural motifs ranging from tetrahedral and octahedra to ball-like spheres by using M(II) (M = Pd, Zn, Co) moieties linked by multidentate pyridyl ligands (*Figure 1.6*).[28] These spheres are able to incorporate suitable guest molecules and can be applied as molecular flasks allowing different reactions than in bulk solvents.[28a,f] Another fascinating research area is pursued by Stang *et al.*: They mainly focus on the formation of catenated systems, such as molecular necklaces (*Figure 1.7*).[29]

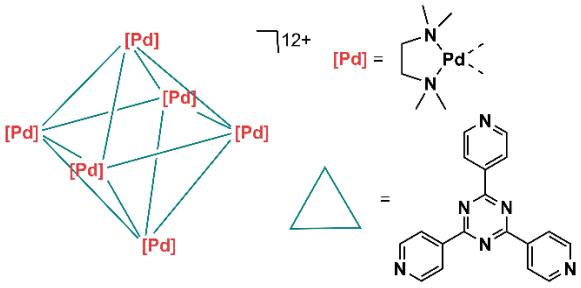

Figure 1.6 Octahedral supramolecule built up by a tridentate linker.

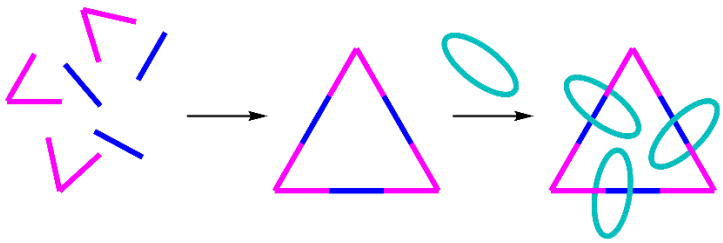

Figure 1.7 Molecular necklace consisting of a preorganized Pt(II) acceptor as node (pink), 1,2-bis(pyridinium)ethane as linker (blue) and a crown ether (cyan) for catenation.

Beside these spherical architectures, also metallamacrocycles can be obtained by self-assembly processes with similar building blocks. Severin *et al.* published many examples in this field, concentrating on half sandwich complexes of precious metals and Pd salts,[30] as well as the group of Hahn, who succeeded in the formation of metallo-organic-cycles by the use of ditopic carbenes as connecting moiety.[31]

Based on the principles of self-assembly and supramolecular chemistry, the mentioned supramolecules are connected *via* weak and reversible interactions, therefore dynamic behavior and/or fragmentation is observed in solution.

In the field of discrete, nano-sized spheres also covalently linked assemblies have an important contribution due to their high rigidity and are therefore discussed below, yet they have to be differentiated from supramolecular assemblies.

Polyoxometallates (POMs), known for almost 200 years, are a prominent example.[32] They are defined by MO_6 octahedra (M = Mo, W, V, Mn…) joint *via* their vertices, edges or faces to build up large supramolecules with the basic structural motif of the Keggin ion, $[(XO_4)(M_{12}O_{36})]^{n-}$ (X = P^{5+}, Si^{4+}, B^{3+}, … ; M = Mo^{6+}, W^{6+}, V^{5+}, …).[33] Despite their early discovery the exploration of its variety and applications is still investigated, especially by contributions of A. Müller *et al.* and L. Cronin *et al.*[34]

Among them is the largest structurally characterized inorganic cluster: $[H_xMo_{368}O_{1032}(H_2O)_{240}(SO_4)_{48}]^{48-}$ (x ~ 16), named 'hedgehog', which reaches an outer diameter of *ca.* 6 nm (*Figure 1.8*a).[35] The results of Fenske and coworkers also display record holders: Although smaller in size, they synthesized $[Ag_{490}S_{188}(StC_5H_{11})_{114}]$ representing the structurally characterized discrete cluster with the highest number of metal atoms so far (*Figure 1.8*b).[36] This and similar chalcogenide clusters of copper and silver can be regarded as initial nanoparticles on the way to form binary phases like, e.g. α-Ag_2S.[37] Concerning the heavier homologue Au, a highlight is the X-ray structural analysis of a $[Au_{102}(p\text{-}MBA)_{44}]$ (p-MBA = p-mercaptobenzoic acid) nanoparticle, in which the thiol ligands form a monolayer around the gold decahedron.[38] Very recently, Dass et al. reported on the structural characterization of the even larger 'nanomolecule' $[Au_{133}(SPh\text{-}^tBu)_{52}]$ bearing bulky and rigid ligands that comprise the outer shell and shield the inner gold core.[39]

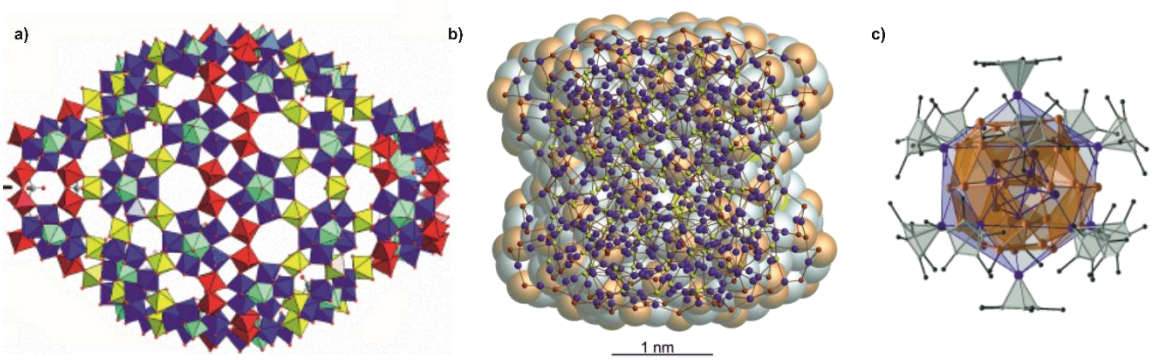

Figure 1.8 a) ‚Hedgehog' cluster $[H_xMo_{368}O_{1032}(H_2O)_{240}(SO_4)_{48}]^{48-}$; b) $[Ag_{490}S_{188}(StC_5H_{11})_{114}]$ cluster; c) intermetalloid $[Al_{50}Cp^*_{12}]$ cluster; figures are reproduced with permission of John Wiley & Sons from a) ref. [35b], license number 3625980187005; b) ref. [36], license number 3626471108896; c) ref. [40b], license number 3626470457488.

Furthermore, the group of Schnöckel defined the class of 'metalloid clusters' for compounds, which contain more metal-metal than metal-ligand bonds.[40] They succeeded in the formation of the *pseudo*-fullerene $[Al_{50}Cp^*_{12}]$ (Cp* = η^5-C_5Me_5) with the Cp* ligands covering and protecting the Al_{50} core[40b] (*Figure 1.8*c). Also $[Ga_{64}\{GaN(SiMe_3)_2\}_{20}]^{4-}$, the largest Ga cluster synthesized so far, has been reported by them.[40e] Another approach to metalloid clusters is the extraction of discrete Zintl anions (e.g. $[Ge_9]^{4-}$) from the solid state, as it is applied by the group of Fässler. In combination with transition metal complexes they obtain linked compounds and intermetalloid clusters containing interstitial metal atoms or even encapsulated cages.[41a] In addition, Dahl *et al.* were able to

synthesize large Pd clusters like $[Pd_{145}(CO)_x(PEt_3)_{30}]$ (x ~ 60) containing an extended three-shell Pd core of icosahedral symmetry surrounded by phosphine and carbonyl ligands.[42]

As a matter of course, in the field of covalently connected spherical molecules the third allotropic modification of carbon, the fullerenes, needs to be included. Their discovery[43] was honoured by the Noble Prize to H. Kroto,[44] R. Curl[45] and R. Smalley[46] in 1996, although previously hints of their existence have been collected.[47] Fullerenes gain a remarkable cage stability if only consisting of 12 five- and any even number of six-membered rings (Euler's theorem) and additionally with the pentagons not abutting to each other (isolated pentagon rule; IPR).[48] The smallest possible fullerene to obey these rules is the Buckminster fullerene I_h-C_{60} (12 five-membered and 20 six-membered rings), which is also the most prominent representative by far (*Figure 1.9*). Remarkably, mass-spectrometric evidences have been obtained for much larger spheres up to C_{418}.[49] However, structurally characterized derivatives are only known for up to 104 carbon atoms: the chlorinated compounds $C_{104}Cl_{16}$ and $C_{104}Cl_{24}$[50] as well as the endohedral fullerene $Sm_2@C_{104}$ with two enclosed samarium atoms.[51] These elongated C_{104} cages already resemble a tiny carbon tube with I_h-C_{80} caps. The distinct advantage of the synthesis of such endohedral metallofullerenes is the formation of novel fullerenes of different size and symmetry. For instance, the icosahedral I_h-C_{80} cage is formed in higher quantities (milligram scale) in the presence of nitrogen and scandium and therefore X-ray structural analysis of $Sc_3N@I_h$-C_{80} was possible.[52] Beside these examples also non-metal doped fullerenes, e.g. with a noble gas atom ($He@C_{60}$, $Ne@C_{60}$,...)[53] or small molecules ($H_2@C_{60}$,[54] $H_2O@C_{60}$[55]) exist.

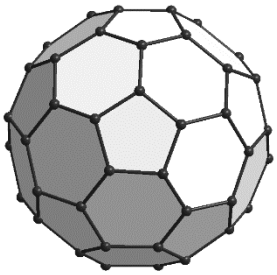

Figure 1.9 Buckminster fullerene C_{60}.

1.4 Organometallic Building Blocks

The previously described metallosupramolecular examples (coordination polymers as well as discrete supramolecules) are all composed of relatively simple metal ions and organic ligands. A completely different approach therefore is the replacement of one type of building block by an organometallic compound.[56] On the contrary to the omnipresent metal-organic assemblies, its use as a node leads to the formation of an organometallic-organic architecture, whereas its application as a ligand gives a metal-organometallic hybrid compound. The first approach has successfully been applied by the combination of half sandwich complexes of ruthenium, rhodium and iridium with multitopic organic ligands such as diisocyanides, bipyridine and dihydroxypyridines, respectively.[30b,57] Due to three available coordination sites of (arene)Ru(II) and $Cp^RM(II)$ (M = Rh,

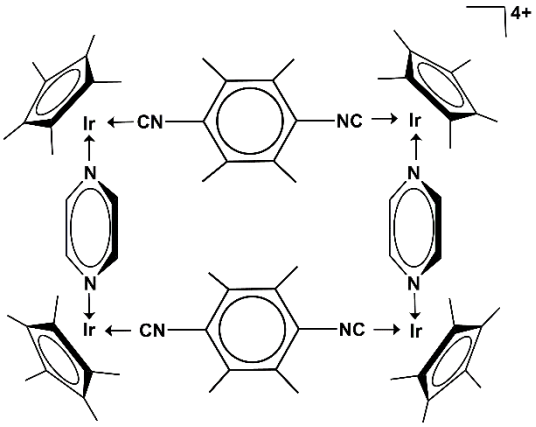

Figure 1.11 An organometallic-organic metallamacrocycle.

Ir), coordination cages and metallamacrocycles are constructed. One selected example is shown in *Figure 1.11*. A further example of an organometallic node in a molecular rectangle is reported by Hahn and coworkers.[31a,58] In this complex, dicarbene and bipyridine ligands bridge [NiCp] fragments, yet its synthesis is not based on self-assembly in a narrow sense due to ligand abstraction and substitution. Also rather simple systems, e.g. the 1:1 adduct of $CdMe_2$ and dioxane to give a 1D chain, are included in this category.[59]

For the second approach (organometallic compound as bridging ligand) Braga *et al.* are cited at this point exemplarily. They use 1,1'-bis(4-pyridyl)ferrocene (*Figure 1.10*) as a preorganized bidentate ligand to build up macrocyclic complexes with M(II) salts (M = Ag, Cu, Zn, Cd).[60]

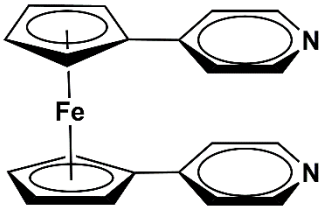

Figure 1.10 1,1'-bis(4-pyridyl)ferrocene

Furthermore, Fukino *et al.* recently presented a highlight in ferrocene-based supramolecular chemistry when they reported on the assembly and disassembly of nanotubes based on a tetratopic pyridyl ferrocene ligand (*Figure 1.12*A).[61] This sandwich complex in combination with Ag^+ builds up metal-organometallic nanotubes, held together by π-stacking and metallophilic interactions (*Figure 1.12*B). Upon oxidation of the ferrocene unit they disassemble into giant cationic rings with a diameter of several nanometers (*Figure 1.12*C), which in turn can be attached onto an anionic surface (*Figure 1.12*D). On the other hand, reduction again leads to the formation of the nanotubes. This example vividly shows the benefits of the involvement of further metal atoms so that one can take advantage of their manifold properties, like the reversible oxidation of ferrocene in this case.

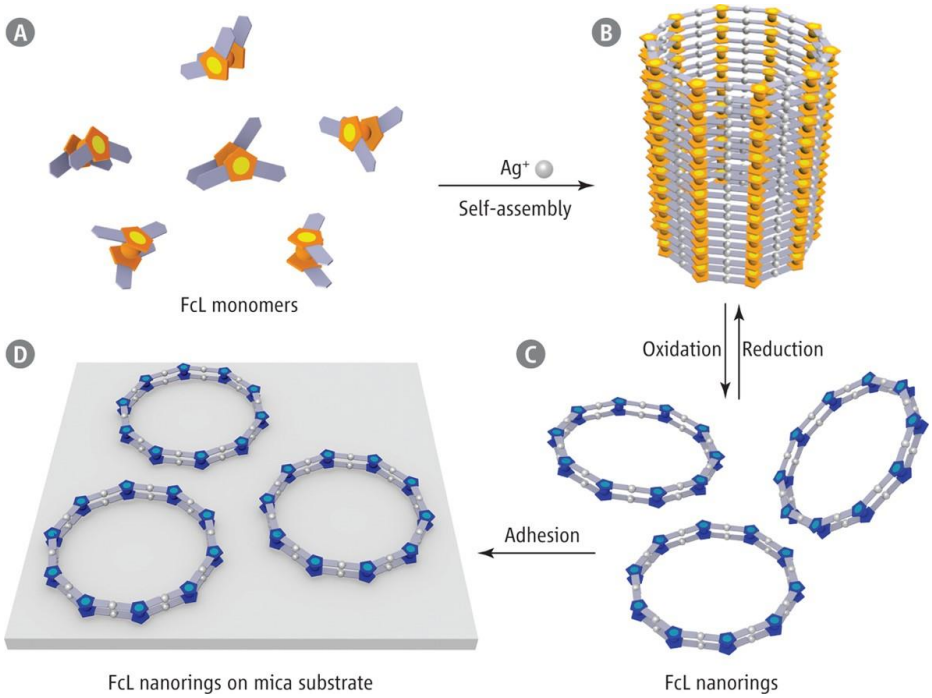

Figure 1.12 Assembly, disassembly and adhesion of ferrocene-based nanotubes and –rings reported by Fukino *et al.* (Figure from ref. [61b]: Z. M. Hudson, I. Manners, *Science* **2014**, *344*, 482-483. Reprinted with permission from AAAS)

Ferrocene derivatives are also incorporated in coronands and cryptands performing multiple functions.[62] They might contain functional groups capable of hydrogen bonding and therefore facilitate the binding of neutral molecules. Furthermore, due to the easy oxidizability of ferrocene, it can bear positive charges and thus serve as a host even for an anionic guest.[63]

1.5 Phosphorus as a Donating Element

As discussed in the previous chapters, the dimensionality and symmetry of a metallosupramolecular assembly is predetermined by the nature, geometry and the number of binding sites of both the metal and the linking unit. However, the majority of reported findings is based on bi-, tri- or tetradentate ligands with oxygen and nitrogen as donating element (*Figure 1.1*). Far more exceptionally sulfur- and phosphorus-based linkers appear, the latter in terms of phosphanes, if at all. On the contrary, our group focuses on phosphorus linkers belonging to the (not clearly distinctive) substance classes of P_n ligand complexes and phosphaferrocenes.

Representatives of the former category are characterized by substituent-free phosphorus atoms, which are solely bound to metal and/or other phosphorus atoms and therefore do not bear any organic group (*Figure 1.13*). In contrast, the latter term describes ferrocene derivatives, in which one or more methine moieties are replaced isolobally by phosphorus (*Figure 1.15*). Of course, numerous other examples of both types of phosphorus containing complexes are known.[64]

Their reactivity towards unsaturated transition metal complexes is partly well explored,[65] yet their description exceeds the scope of this introduction. Hence, only selected examples important for the construction of polymeric or spherical assemblies will be discussed below.

P_n Ligand Complexes in Supramolecular Chemistry

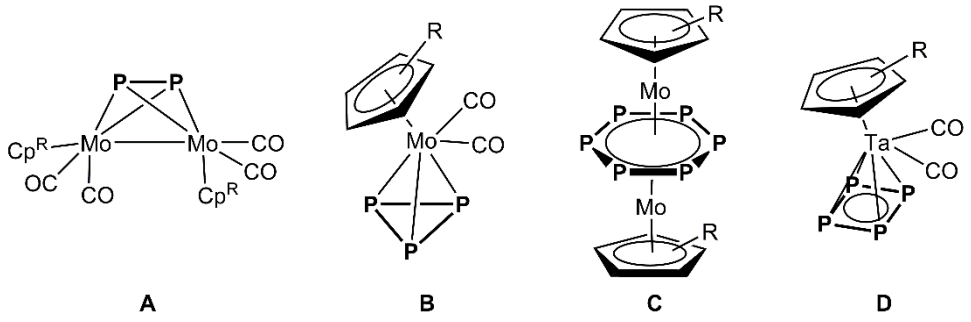

Figure 1.13 Selected P_n ligand complexes (n = 2 – 6) as building blocks for supramolecular chemistry.

The tetrahedrane complexes $[\{Cp^RMo(CO)_2\}_2(\eta^2\text{-}P_2)]$ (**A**) and $[Cp^RMo(CO)_2(\eta^3\text{-}P_3)]$ (**B**) as well as the triple decker complex $[(Cp^RMo)_2(\mu,\eta^{6:6}\text{-}P_6)]$ (**C**), which are all obtained by the thermolysis of $[Cp^RMo(CO)_3]_2$ (Cp^R = Cp, Cp*) with white phosphorus (P_4),[66] should display well-suited building blocks for the formation of polymers. In fact, the self-assembly processes of $[\{CpMo(CO)_2\}_2(\eta^2\text{-}P_2)]$ (type **A**) with $AgNO_3$, CuX (X = Cl, Br, I) and CuX_2 (X = Cl, Br), respectively, all give 1D chains.[67] Despite different oxidation states in the starting materials, all copper-containing polymers are isostructural and set up by $\{Cu_2X_2\}$ four-membered and $\{Cu_2P_4\}$ six-membered rings (*Figure 1.14*). In contrast, metal ions with non- or weakly coordinating anions, such as BF_4^-, PF_6^-, ClO_4^- and $CF_3SO_3^-$, all lead to dimeric complexes.[68] Only upon addition of an organic linker as third component to the combination $[\{CpMo(CO)_2\}_2(\eta^2\text{-}P_2)]/[Cu(CH_3CN)_4][BF_4]$ also a 2D network can be obtained.[69] Despite three available coordination sites, which would possibly allow the self-assembly to form two-dimensional polymers, complexes of type **B** exclusively form positively charged 1D chains in combination with Cu(I) and Ag(I) salts, respectively, *via* coordination of only two phosphorus atoms.[70] Depending on the Cp^R ligand (Cp^R = Cp, Cp*) and the counter anion the structural motifs slightly differ; one example is depicted in *Figure 1.14*.

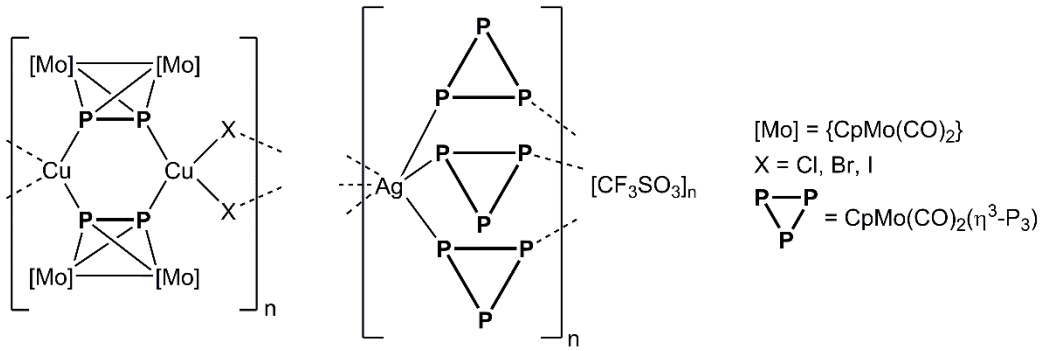

Figure 1.14 Repeating units of selected 1D polymers built up by complexes of type **A** (left) and **B** (right), respectively.

Due to the all-phosphorus analogue of benzene, the triple decker complexes of type **C** are of special interest in supramolecular chemistry, since one might think of inorganic graphene-like sheet structures upon coordination. However, reactions of the Cp* derivative with $[Cu(CH_3CN)_4][BF_4]$[71] and $[Ag(CH_2Cl_2)][Al\{OC(CF_3)_3\}_4]$,[72] respectively, only allow the isolation of a dimeric complex with two linked moieties of the P_n ligand complex as well as the oxidized species $[(Cp^*Mo)_2(\mu,\eta^{6:6}\text{-}P_6)]^+$. With CuX (X = Br, I) as a metal salt at least 1D polymers are obtained in which a $\eta^2{:}\eta^1{:}\eta^1$ coordination mode of the hexaphosphabenzene ligand to copper is observed.[71] Finally, the self-assembly with CuCl leads to the formation of a 2D polymer of an undulated sheet-like structure containing an extended CuCl framework with many different ring sizes in addition to the P_6 rings.[72]

Phosphaferrocenes in Supramolecular Chemistry

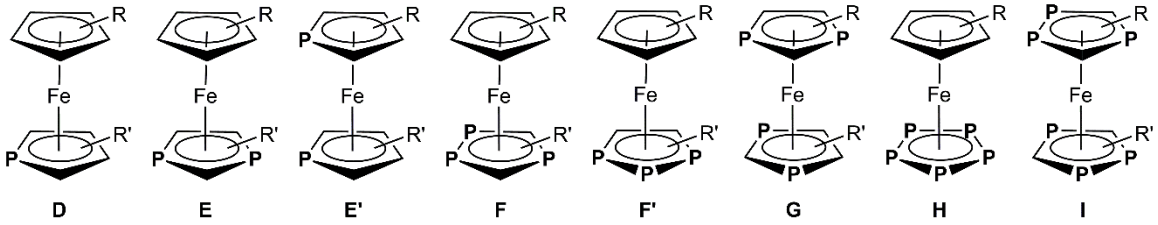

Figure 1.15 Selected types of phosphaferrocenes regardless of the real conformation (staggered/eclipsed).

Phosphaferrocenes, more precisely of type **F**, **H** and **I** (*Figure 1.15*), provide an even greater diversity of supramolecular assemblies, especially in combination with Cu(I) halides.

The accessibility and stability of the respective building blocks underlie the isolobal principle of CH moieties and P atoms. Depending on the number of phosphorus atoms in the Cp^R ligand, different synthetic strategies are applied. Exemplarily for the ^{t}Bu substituted derivative, starting from phosphaalkene and $K[P(SiMe_3)_2]$, the 1,2,4-triphospholyl potassium salt is obtained (*Equation 1.1*).[73]

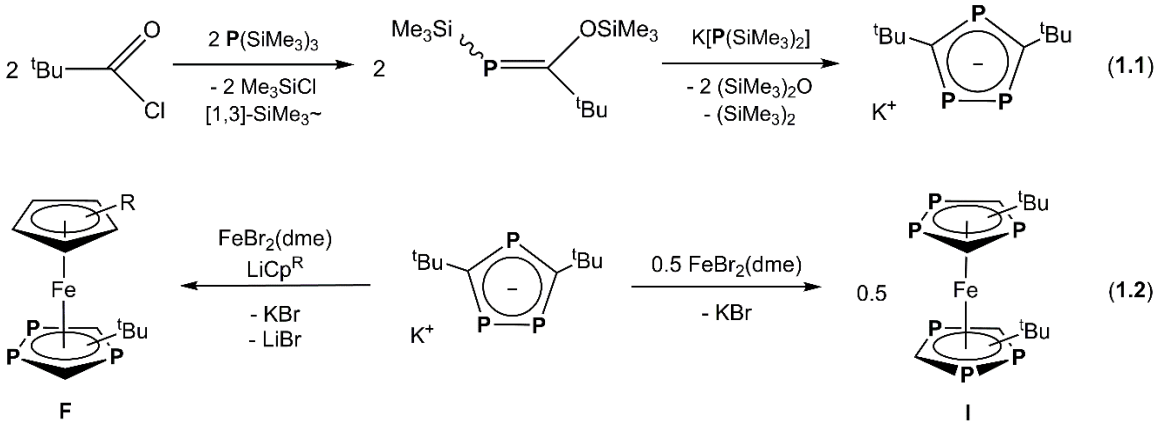

The subsequent salt metathesis reaction with $FeBr_2$(dme) leads to the formation of the corresponding hexaphosphaferrocene **I**[74] or, in presence of $LiCp^R$, the 1,2,4-triphosphaferrocene **F** (*Equation 1.2*).[75] Recently, Ionkin *et al.* reported on a one-pot synthesis for tri- and tetraphospholyl anions from $P(SiMe_3)_3$, the Mes* substituted acyl chloride (Mes* = $C_6H_2{}^tBu_3$) and CsF (*Equation 1.3*).[76]

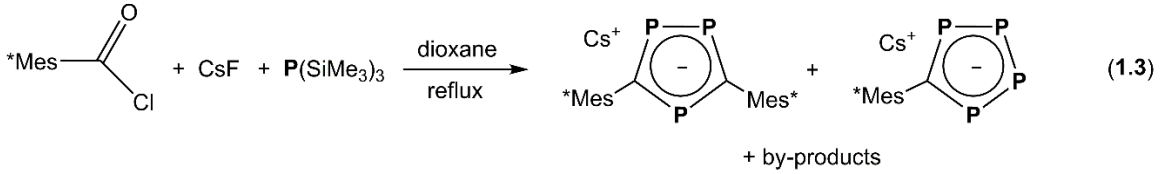

A completely different approach is used for type **H** complexes: In this case the thermolysis reaction of $[Cp^RFe(CO)_2]_2$ with white phosphorus is expedient (*Equation 1.4*).[77] The obtained sandwich complexes $[Cp^RFe(\eta^5\text{-}P_5)]$ are also assigned to the class of P_n ligand complexes due to the lack of P-C bonds.

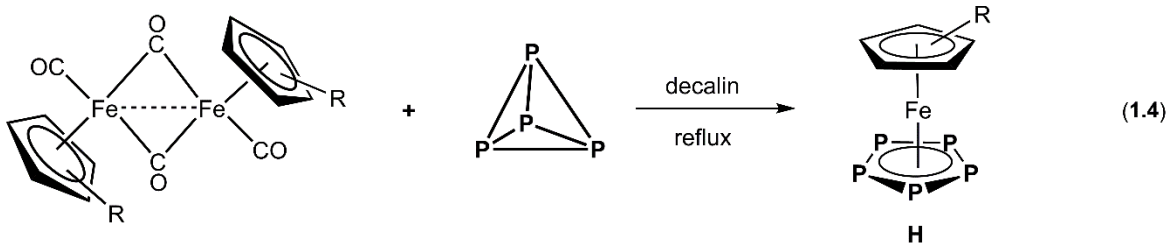

The coordination chemistry of type **F** complexes (R' = ^{t}Bu) towards CuX (X = Cl, Br, I) strongly depends on the nature of the Cp^R ligand (Cp, Cp*, Cp''' = $\eta^5\text{-}C_5H_2{}^tBu_3$). Whereas the Cp and Cp''' derivatives tend to the formation of simple dimers (*Figure 1.16*a), the Cp* derivative is also capable of oligomeric assemblies.[78] However, three supramolecular products are worth being mentioned explicitly: The combination of $[Cp^*Fe(\eta^5\text{-}P_3C_2{}^tBu_2)]$ and 4 eq. of CuI leads to the coordination of all

three phosphorus atoms for the first time and the expansion of the network in two dimensions (*Figure 1.16*b).[78b] Even more remarkable, the reaction of [Cp'''Fe(η^5-$P_3C_2{}^tBu_2$)] with an excess of CuCl involves a fragmentation of the $P_3C_2{}^tBu$ ring into a tetraphosphabutadiene chain, which is stabilized by two {Cp'''Fe} fragments and in combination with $\{Cu_2Cl_2\}$ rings part of a 1D strain (*Figure 1.16*c).[78c] The same triphosphaferrocene undergoes a further, yet different fragmentation when reacted with CuBr. In this case, a formal elimination of a P atom can be obtained, resulting in a 1,2-disphospha*cyclo*butadiene sandwich complex (*Figure 1.16*d).[78a]

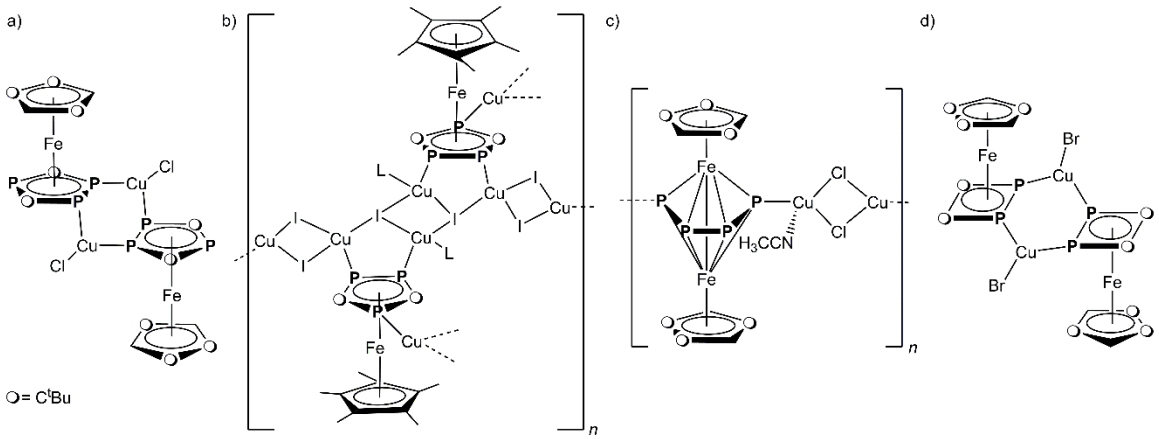

Figure 1.16 Selected coordination products of triphosphaferrocenes (type **F**) and CuX (X = Cl, Br, I).

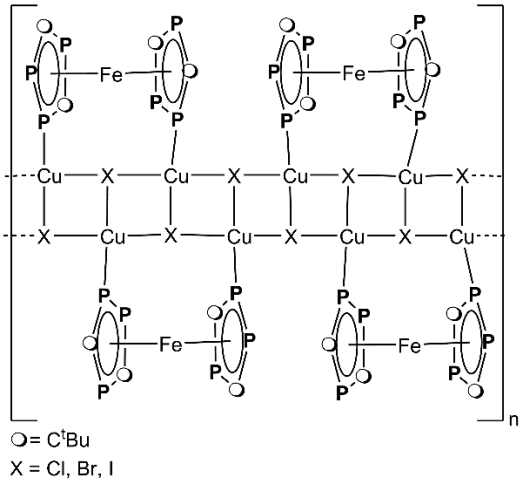

Figure 1.17 1D ladder-like polymer by a type **I** complex.

On the other hand, the hexaphosphaferrocene of type **I**, which displays the phosphorus-richest ferrocene analogue, builds up either oligomeric or 1D polymeric coordination compounds, always with ladder-like motifs (*Figure 1.17*).

The most astonishing building block among all phosphaferrocenes is type **H**, especially its Cp* derivative [Cp*Fe(η^5-P_5)] (**H-1**).[77f] First investigations regarding its coordination behavior towards coinage metal salts allowed the isolation of 1D and 2D polymers with well-known $\{Cu_2X_2\}$ (X = Cl, Br, I) four-membered and $\{Cu_2P_4\}$ six-membered rings (*Figure 1.18*).[79] In the case of CuCl, a 1,2-coordination of the P_5 ring is present, whereas in the bromide and iodide derivatives the coordination of a further P atom (1,2,4-coordination) leads to a 2D network.

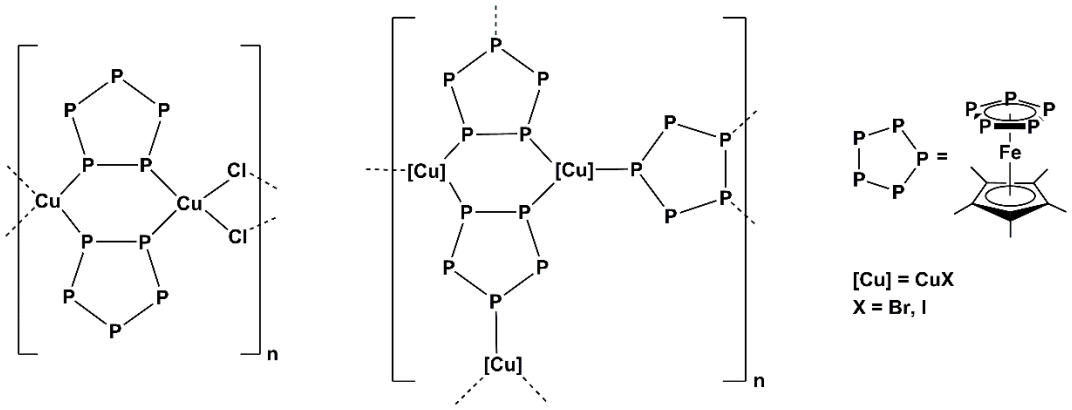

Figure 1.18 1D und 2D polymers consisting of **H-1** and CuX (X = Cl, Br, I).

However, two phosphorus atoms still remain uncoordinated and a closer look to the self-assembly processes finally led to the isolation of the supramolecule $[Cp^*Fe(\eta^5\text{-}P_5)]@[\{Cp^*Fe(\eta^5\text{-}P_5)\}_{12}(CuBr)_{25}(CH_3CN)_{10}]$ containing a 1,2,3,4,5-coordinated pentaphosphaferrocene (*Figure 1.20*a).[80] Due to the preferred tetrahedral coordination environment of copper in combination with the five-fold symmetry of the *cyclo*-P_5 ligand no polymer, but rather a ball-shaped sphere is formed. The formed cavity incorporates one molecule of **H-1**, and therefore the application of this system in host-guest chemistry has quickly been recognized. Appropriate template molecules which have so far successfully been incorporated into a pentaphosphaferrocene-based supramolecule are: $[Cp^*Fe(\eta^5\text{-}P_5)]$ (*Figure 1.20*a),[80,81] C_{60} (*Figure 1.20*c),[82] *o*-$C_2B_{10}H_{12}$ (*Figure 1.20*b),[83] $[FeCp_2]$ (same host as in *Figure 1.20*b),[84] $[(CpCr)_2(\mu,\eta^{5:5}\text{-}As_5)]$ (*Figure 1.20*d),[84] $[CpCr(\eta^5\text{-}As_5)]$ (*Figure 1.20*e),[84] As_4 (*Figure 1.20*f)[85] and P_4 (same host as in *Figure 1.20*f).[85]

Table 1.1 Selected characteristics of host molecules derived from $[Cp^*Fe(\eta^5\text{-}P_5)]$ (**H-1**).

	80-vertex ball	90-vertex ball	99-vertex ball	100-vertex sphere
Host	$(\mathbf{H\text{-}1})_{12}(CuX)_{20}$	$(\mathbf{H\text{-}1})_{12}(CuX)_{25}(CH_3CN)_{10}$	$(\mathbf{H\text{-}1})_{13}(CuCl)_{26}(H_2O)_2(CH_3CN)_9$	$(\mathbf{H\text{-}1})_{10}(CuI)_{30}(CH_3CN)_6$
Halide X	Cl, Br	Cl, Br	Cl	I
Atoms (scaffold)	60 P, 20 Cu	60 P, 25 Cu, 5 X	65 P, 26 Cu, 8 Cl	40 P, 30 Cu, 30 I
Vertices (scaffold)	80	90	99	100
Outer size	2.1 nm	~ 2.3 nm	2.3 nm	2.1 x 3.3 nm
Inner cavity	0.8 nm	1.0 x 1.3 nm	1.4 nm	0.5 nm
Guests	*o*-$C_2B_{10}H_{12}$, $[FeCp_2]$, $[CpCr(\eta^5\text{-}As_5)]$	$[Cp^*Fe(\eta^5\text{-}P_5)]$, $[(CpCr)_2(\mu,\eta^{5:5}\text{-}As_5)]$	C_{60}	P_4, As_4
See Figure	*Figure 1.20*b,e	*Figure 1.20*a,d	*Figure 1.20*c	*Figure 1.20*f
See References	[83], [84]	[80], [81], [84]	[82]	[85]

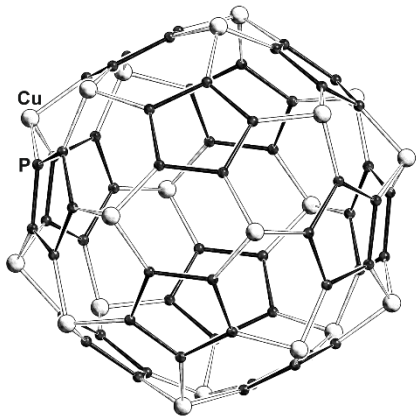

Figure 1.19 Scaffold of the 80-vertex ball.

The corresponding host molecules differ in the number of **H-1** and CuX moieties as well as in their linkage pattern. Therefore, different sizes and shapes result, each appropriate for the respective template. An overview of selected characteristics of these nano-sized supramolecules is given in *Table 1.1*.

A particular highlight is the ball-shaped sphere $[\{Cp^*Fe(\eta^5\text{-}P_5)\}_{12}(CuX)_{20}]$ (X = Cl, Br):[83,84] The 80-vertex scaffold is solely constructed by 12 five-membered (P_5) and 30 six-membered rings (Cu_2P_4) obeying the isolated-pentagon rule and showing icosahedral symmetry, hence it displays a carbon-free I_h-C_{80} analogue (*Figure 1.19*). Due to an additional $\{Cu(CH_3CN)_2X\}_5$ 'belt' (X = Cl, Br) the 90-vertex ball is slightly bigger while retaining fullerene topology.[80,81,84] On the other hand, the biggest supramolecules, the 99-vertex ball[82] and 100-vertex sphere,[85] show a differently linked scaffold and are comparable to fullerenes only to a certain extent. The cavity of the latter cuboid-shaped sphere is divided into two halves by an extended {CuI} framework, hence it provides only minor space (0.5 nm) for guest molecules (P_4, As_4), which appear to be disordered over these two voids.

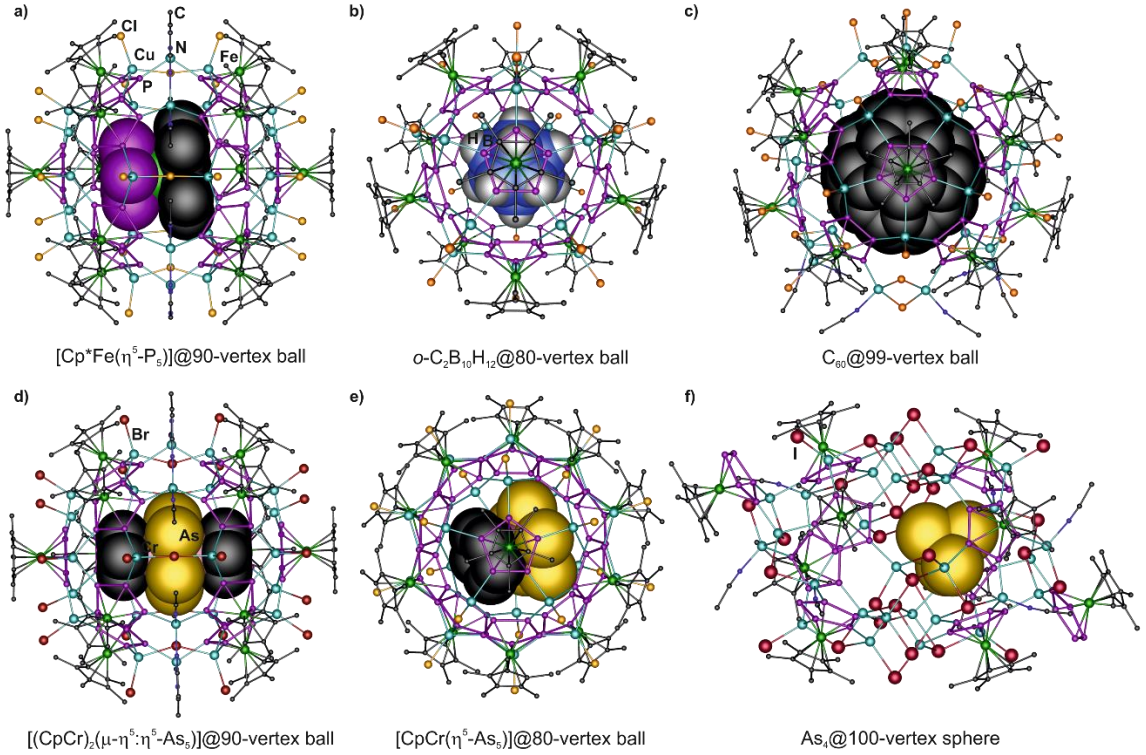

Figure 1.20 Selected molecular structures of spherical supramolecules consisting of **H-1** and CuX (X = Cl, Br, I). H atoms, solvent molecules and minor parts of disorder are omitted for clarity. The incorporated molecules are highlighted by the space-filling model.

The described self-assembly processes are all very sensitive to parameters such as solvent, concentration, template and molar ratio of **H-1**:CuX. As an example for the latter determinant the use of a deficit of CuCl can be briefly mentioned, whereas in the previously described examples at least two equivalents of CuCl were used. In this case, not only a novel polymeric product, but also an unprecedented nano-capsule with outer dimensions of 3.0 x 2.3 nm can be isolated.[86] It consists of two half shells, which are held together merely by weak dispersion interactions in the solid state. Due to the elongated scaffolds (1.5 x 0.8 nm) two molecules of **H-1** are encapsulated (instead of one in the 90-vertex ball).

One potential application of these host-guest systems is demonstrated by the use of $[(CpCr)_2(\mu,\eta^{5:5}\text{-}As_5)]$ as a template.[84] With CuBr it is incorporated into the 90-vertex ball, whereas the chloride salt surprisingly allowed the isolation of the smaller 80-vertex sphere with an enclosed molecule of $[CpCr(\eta^5\text{-}As_5)]$. Hence, a fragmentation of the triple decker complex occurred, revealing the unprecedented 16 VE sandwich complex $[CpCr(\eta^5\text{-}As_5)]$ as a guest. Therefore, pentaphosphaferrocene-based host-guest systems might be used not only for the stabilization but also for the generation of novel and/or labile complexes.

Furthermore, the influence of the Cp^R ligand of the pentaphosphaferrocenes **H** has also been studied: Reactions of the pentabenzyl derivative $[Cp^{Bn}Fe(\eta^5\text{-}P_5)]$ (Cp^{Bn} = $\eta^5\text{-}C_5(CH_2C_6H_5)_5$; **H-2**)[77c] with CuX (X = Cl, Br) show similar results at first glance and allowed the isolation of the isostructural 80-vertex ball $[(\textbf{H-2})_{12}(CuX)_{20}]$.[87] On the contrary to **H-1**, no template is needed for its formation, the voids are occupied by solvent molecules and the assembly to polymeric products is not observed. Furthermore, also porous spheres $[(\textbf{H-2})_{12}(CuX)_{20\text{-}n}]$ ($n \leq 4.6$) and the tetrahedral-shaped supramolecule $[(\textbf{H-2})_{12}(CuBr)_{51}(CH_3CN)_8]$ with an outer diameter of 3.6 nm are formed. Due to the benzyl ligands the products show a good solubility in CH_2Cl_2, hence the reversible rearrangement as well as the encapsulation and subsequent release of ferrocene could be investigated.

A drastical increase of the sterical demand of the Cp^R ligand by the use of $[Cp^{BIG}Fe(\eta^5\text{-}P_5)]$ (Cp^{BIG} = $\eta^5\text{-}C_5(4\text{-}^nBuC_6H_4)_5$; **H-3**) allows for the formation of an even more giant supramolecule, which is constructed onion-like from several layers and exhibits analogy to the icosahedral *I*-C_{140} fullerene.[88]

This exceptional position of the pentaphosphaferrocene **H** and the aggregation to fullerene-like supramolecules can be traced back to the five-fold symmetric P_5 ligand. Only two groups recently introduced other five-fold-connected planar nodes: Williams and coworkers report on ferrocene derivatives containing the pentakis(4-pyridyl)cyclopentadienyl[89] and pentakis(1-methylpyrazole)cyclopentadienyl[90] ligand, respectively (*Figure 1.21*a,b). Both the former in combination with $[Cu(CH_3CN)_4][PF_6]$ and the latter with a dirhodium(II) tetracarboxylate derivative,

are capable of the formation of fullerene-like spheres of the type $[(metal)_{30}(ligand)_{12}]$, yet structural characterization remain to be seen.

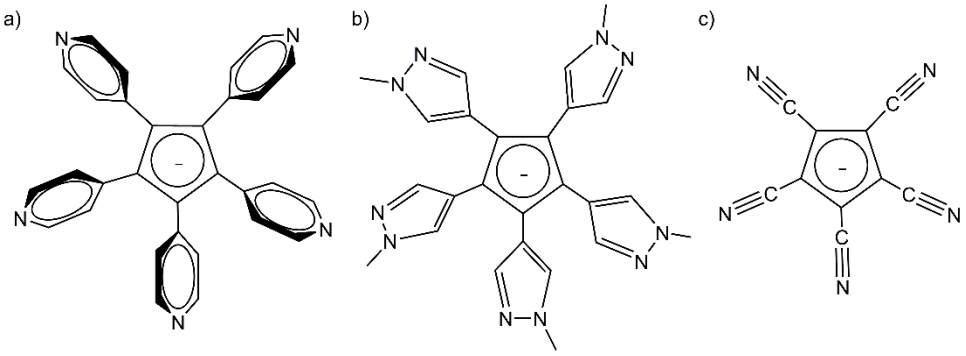

Figure 1.21 Five-fold-connected planar nodes.

On the other hand, the group of Wright succeeded in the construction of a three-dimensional MOF based on fullerene-like units of the pentacyanocyclopentadienyl ligand $[C_5(CN)_5]^-$ and sodium cations (*Figure 1.21*c, *Figure 1.22*).[91]

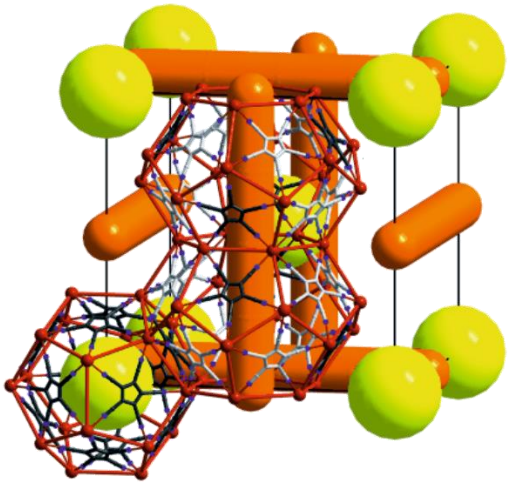

Figure 1.22 Schematic representation of the fullerene-type MOF obtained by Williams *et al.*; voids are illustrated by yellow spheres and orange bars. The figure is reproduced with permission of John Wiley & Sons from Ref. [91b], license number 3637011506236.

Surprisingly, also the self-assembly process of CuCl with the P_n ligand complex $[Cp''Ta(CO)_2(\eta^4\text{-}P_4)]$ (*Figure 1.13*, type **D**; Cp'' = $\eta^5\text{-}C_5H_3{}^tBu_2$) containing a four-membered ring, builds up a discrete spherical supramolecule.[92] Its scaffold consists of 32 atoms arranged in alternating four-membered (P_4) and six-membered (Cu_2P_4) rings, hence it shows structural analogy to non-classical fullerenes with variable ring sizes (*Figure 1.23*).[93]

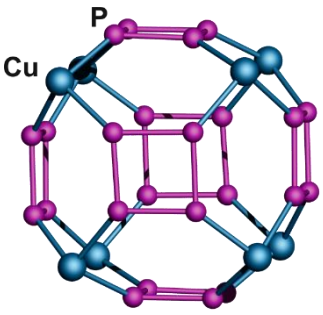

Figure 1.23 32-vertex scaffold of the type **D** containing sphere.

1.6 References

[1] J. M. Lehn, *Science* 1993, *260*, 1762.

[2] D. J. Cram, *Angew. Chem.* 1988, *100*, 1041.

[3] C. J. Pedersen, *Angew. Chem.* 1988, *100*, 1053.

[4] J. M. Lehn, *Angew. Chem.* 1988, *100*, 91.

[5] J. W. Steed, D. R. Turner, K. J. Wallace, *Core Concepts in Supramolecular Chemistry and Nanochemistry*, John Wiley & Sons, Ltd, 2007.

[6] a) E. C. Constable, *Pure Appl. Chem.* 1996, *68*, 253; b) E. C. Constable, A. M. W. Cargill Thompson, *Supramol. Chem.* 1994, *4*, 95.

[7] J. M. Lehn, A. Rigault, J. Siegel, J. Harrowfield, B. Chevrier, D. Moras, *Proc. Natl. Acad. Sci. U. S. A.* 1987, *84*, 2565.

[8] J. C. Bailar, *Prep. Inorg. React.* 1964, *1*, 1.

[9] S. R. Batten, N. R. Champness, X.-M. Chen, J. Garcia-Martinez, S. Kitagawa, L. Öhrström, M. O'Keeffe, S. M. Paik, J. Reedijk, *Pure Appl. Chem.* 2013, *85*, 1715.

[10] a) L. Chen, Q. Chen, M. Wu, F. Jiang, M. Hong, *Acc. Chem. Res.* 2015, *48*, 201; b) E. C. Constable, *Coord. Chem. Rev.* 2008, *252*, 842; c) A. Y. Robin, K. M. Fromm, *Coord. Chem. Rev.* 2006, *250*, 2127; d) S. Kitagawa, R. Kitaura, S.-i. Noro, *Angew. Chem. Int. Ed.* 2004, *43*, 2334; e) G. F. Swiegers, T. J. Malefetse, *Chem. Rev.* 2000, *100*, 3483.

[11] a) E. J. Mensforth, M. R. Hill, S. R. Batten, *Inorg. Chim. Acta* 2013, *403*, 9; b) M. Wen, M. Munakata, Y. Suenaga, T. Kuroda-Sowa, M. Maekawa, S. G. Yan, *Inorg. Chim. Acta* 2001, *322*, 133; c) K. Sugimoto, T. Kuroda-Sowa, M. Munakata, M. Maekawa, *Chem. Commun.* 1999, 455.

[12] F. Hung-Low, K. K. Klausmeyer, *Inorg. Chim. Acta* 2008, *361*, 1298.

[13] S. Kitagawa, M. Munakata, T. Tanimura, *Inorg. Chem.* 1992, *31*, 1714.

[14] H.-C. Zhou, J. R. Long, O. M. Yaghi, *Chem. Rev.* 2012, *112*, 673; b) J. L. C. Rowsell, O. M. Yaghi, *Angew. Chem. Int. Ed.* 2005, *44*, 4670; c) A. C. Sudik, A. R. Millward, N. W. Ockwig, A. P. Cote, J. Kim, O. M. Yaghi, *J. Am. Chem. Soc.* 2005, *127*, 7110; d) J. L. C. Rowsell, O. M. Yaghi, *Microporous Mesoporous Mater.* 2004, *73*, 3.

[15] a) M. P. Suh, H. J. Park, T. K. Prasad, D.-W. Lim, *Chem. Rev.* 2012, *112*, 782; b) K. Sumida, D. L. Rogow, J. A. Mason, T. M. McDonald, E. D. Bloch, Z. R. Herm, T.-H. Bae, J. R. Long, *Chem. Rev.* 2012, *112*, 724; c) J.-R. Li, R. J. Kuppler, H.-C. Zhou, *Chem. Soc. Rev.* 2009, *38*, 1477.

[16] B. Chen, S. Xiang, G. Qian, *Acc. Chem. Res.* 2010, *43*, 1115.

[17] L. E. Kreno, K. Leong, O. K. Farha, M. Allendorf, R. P. Van Duyne, J. T. Hupp, *Chem. Rev.* 2012, *112*, 1105.

[18] M. D. Allendorf, C. A. Bauer, R. K. Bhakta, R. J. T. Houk, *Chem. Soc. Rev.* 2009, *38*, 1330.

[19] a) M. Yoon, R. Srirambalaji, K. Kim, *Chem. Rev.* 2012, *112*, 1196; b) J. Y. Lee, O. K. Farha, J. Roberts, K. A. Scheidt, S. B. T. Nguyen, J. T. Hupp, *Chem. Soc. Rev.* 2009, *38*, 1450.

[20] Y. Inokuma, S. Yoshioka, J. Ariyoshi, T. Arai, Y. Hitora, K. Takada, S. Matsunaga, K. Rissanen, M. Fujita, *Nature* 2013, *495*, 461.

[21] H. Li, M. Eddaoudi, M. O'Keeffe, O. M. Yaghi, *Nature* 1999, *402*, 276.

[22] O. M. Yaghi, G. Li, H. Li, *Nature* 1995, *378*, 703.

[23] N. L. Rosi, J. Eckert, M. Eddaoudi, D. T. Vodak, J. Kim, M. O'Keeffe, O. M. Yaghi, *Science* 2003, *300*, 1127.

[24] a) D. Ajami, J. Rebek, *Acc. Chem. Res.* 2013, *46*, 990; b) K. Tiefenbacher, D. Ajami, J. Rebek, *Angew. Chem. Int. Ed.* 2011, *50*, 11805.

[25] a) P. Mal, B. Breiner, K. Rissanen, J. R. Nitschke, *Science* 2009, *324*, 1697; b) G. Steinfeld, V. Lozan, H.-J. Krüger, B. Kersting, *Angew. Chem. Int. Ed.* 2009, *48*, 1954; c) S. Sato, J. Iida, K. Suzuki, M. Kawano, T. Ozeki, M. Fujita, *Science* 2006, *313*, 1273.

[26] a) C. J. Hastings, M. D. Pluth, R. G. Bergman, K. N. Raymond, *J. Am. Chem. Soc*. 2010, *132*, 6938; b) M. D. Pluth, R. G. Bergman, K. N. Raymond, *Science* 2007, *316*, 85; c) M. D. Pluth, R. G. Bergman, K. N. Raymond, *Angew. Chem. Int. Ed.* 2007, *46*, 8587; d) M. Yoshizawa, M. Tamura, M. Fujita, *Science* 2006, *312*, 251.

[27] a) S. Zarra, D. M. Wood, D. A. Roberts, J. R. Nitschke, *Chem. Soc. Rev.* 2015, *44*, 419; b) W. Meng, A. B. League, T. K. Ronson, J. K. Clegg, W. C. Isley, D. Semrouni, L. Gagliardi, C. J. Cramer, J. R. Nitschke, *J. Am. Chem. Soc.* 2014, *136*, 3972; c) N. J. Young, B. P. Hay, *Chem Commun* 2013, *49*, 1354; d) J. S. Mugridge, R. G. Bergman, K. N. Raymond, *J. Am. Chem. Soc.* 2012, *134*, 2057; e) R. W. Saalfrank, A. Scheurer, *Top. Curr. Chem.* 2012, *319*, 125; f) Z. Laughrey, B. C. Gibb, *Chem. Soc. Rev.* 2011, *40*, 363; g) S. J. Dalgarno, N. P. Power, J. L. Atwood, *Coord. Chem. Rev.* 2008, *252*, 825.

[28] a) Y. Inokuma, M. Kawano, M. Fujita, *Nat. Chem.* 2011, *3*, 349; b) Q.-F. Sun, J. Iwasa, D. Ogawa, Y. Ishido, S. Sato, T. Ozeki, Y. Sei, K. Yamaguchi, M. Fujita, *Science* 2010, *328*, 1144; c) J. K. Klosterman, M. Iwamura, T. Tahara, M. Fujita, *J. Am. Chem. Soc.* 2009, *131*, 9478; d) S. Sato, Y. Ishido, M. Fujita, *J. Am. Chem. Soc.* 2009, *131*, 6064; e) M. Yoshizawa, J. K. Klosterman, M. Fujita, *Angew. Chem. Int. Ed.* 2009, *48*, 3418; f) M. Fujita, M. Tominaga, A. Hori, B. Therrien, *Acc. Chem. Res.* 2005, *38*, 369.

[29] a) S. Li, J. Huang, F. Zhou, T. R. Cook, X. Yan, Y. Ye, B. Zhu, B. Zheng, P. J. Stang, *J. Am. Chem. Soc.* 2014, *136*, 5908; b) V. Vajpayee, Y. H. Song, T. R. Cook, H. Kim, Y. Lee, P. J. Stang, K.-W. Chi, *J. Am. Chem. Soc.* 2011, *133*, 19646.

[30] a) M. D. Wise, J. J. Holstein, P. Pattison, C. Besnard, E. Solari, R. Scopelliti, G. Bricogne, K. Severin, *Chem. Sci.* 2015, *6*, 1004; b) K. Severin, *Chem. Commun.* 2006, 3859.

[31] a) M. C. Jahnke, F. E. Hahn, *Coord. Chem. Rev.* 2015, *293-294*, 95; b) Y.-F. Han, G.-X. Jin, F. E. Hahn, *J. Am. Chem. Soc.* 2013, *135*, 9263; c) M. Schmidtendorf, T. Pape, F. E. Hahn, *Angew. Chem. Int. Ed.* 2012, *51*, 2195.

[32] J. J. Berzelius, *Poggendorffs Ann. Phys. Chem.* 1826, *6*, 380.

[33] M. T. Pope, A. Mueller, *Angew. Chem.* 1991, *103*, 56.

[34] a) A. Mueller, P. Gouzerh, *Chem. Eur. J.* 2014, *20*, 4862; b) A. Mueller, P. Gouzerh, *Chem. Soc. Rev.* 2012, *41*, 7431; c) D.-L. Long, R. Tsunashima, L. Cronin, *Angew. Chem. Int. Ed.* 2010, *49*, 1736.

[35] a) A. Mueller, B. Botar, S. K. Das, H. Boegge, M. Schmidtmann, A. Merca, *Polyhedron* 2004, *23*, 2381; b) A. Müller, E. Beckmann, H. Bögge, M. Schmidtmann, A. Dress, *Angew. Chem. Int. Ed.* 2002, *41*, 1162.

[36] C. Anson, A. Eichhöfer, I. Issac, D. Fenske, O. Fuhr, P. Sevillano, C. Persau, D. Stalke, J. Zhang, *Angew. Chem. Int. Ed.* 2008, *47*, 1326.

[37] a) O. Fuhr, S. Dehnen, D. Fenske, *Chem. Soc. Rev.* 2013, *42*, 1871; b) J. F. Corrigan, O. Fuhr, D. Fenske, *Adv. Mater.* 2009, *21*, 1867.

[38] P. D. Jadzinsky, G. Calero, C. J. Ackerson, D. A. Bushnell, R. D. Kornberg, *Science* 2007, *318*, 430.

[39] A. Dass, S. Theivendran, P. R. Nimmala, C. Kumara, V. R. Jupally, A. Fortunelli, L. Sementa, G. Barcaro, X. Zuo, B. C. Noll, *J. Am. Chem. Soc.* 2015, *137*, 4610.

[40] a) H. Schnoeckel, A. Schnepf, *Aluminium and Gallium Clusters*, John Wiley & Sons Ltd., 2011, pp. 402; b) H. Schnöckel, A. Schnepf, R. L. Whetten, C. Schenk, P. Henke, *Z. Anorg. Allg. Chem.* 2011, *637*, 15; c) J. Vollet, J. R. Hartig, H. Schnöckel, *Angew. Chem. Int. Ed.* 2004, *43*, 3186; d) A. Schnepf, B. Jee, H. Schnöckel, E. Weckert, A. Meents, D. Luebbert, E. Herrling, B. Pilawa, *Inorg. Chem.* 2003, *42*, 7731; e) A. Schnepf, H. Schnöckel, *Angew. Chem. Int. Ed.* 2001, *40*, 712.

[41] a) T. F. Faessler, *Struct. Bond*. 2011, *140*, 91; b) S. Scharfe, F. Kraus, S. Stegmaier, A. Schier, T. F. Faessler, *Angew. Chem. Int. Ed.* 2011, *50*, 3630.

[42] N. T. Tran, D. R. Powell, L. F. Dahl, *Angew. Chem*. 2000, *112*, 4287.

[43] H. W. Kroto, J. R. Heath, S. C. O'Brien, R. F. Curl, R. E. Smalley, *Nature* 1985, *318*, 162.

[44] H. Kroto, *Angew. Chem. Int. Ed. Engl.* 1997, *36*, 1579.

[45] R. F. Curl, *Angew. Chem. Int. Ed. Engl.* 1997, *36*, 1567.

[46] R. E. Smalley, *Angew. Chem. Int. Ed. Engl.* 1997, *36*, 1595.

[47] a) P. A. Thrower, *Carbon* 1999, *37*, 1677; b) D. A. Bochvar, E. G. Gal'pern, *Dokl. Akad. Nauk SSSR* 1973, *209*, 610.

[48] a) M. S. Dresselhaus, G. Dresselhaus, P. C. Eklund, *Science of Fullerenes and Carbon Nanotubes*, Academic Press, 1996; b) P. W. Fowler, D. E. Manolopoulos, *An Atlas of Fullerenes*, Clarendon Press, 1995.

[49] a) F. Beer, A. Gugel, K. Martin, J. Rader, K. Mullen, *J. Mater. Chem.* 1997, *7*, 1327; b) H. Shinohara, H. Sato, Y. Saito, M. Takayama, A. Izuoka, T. Sugawara, *J. Phys. Chem.* 1991, *95*, 8449.

[50] S. Yang, T. Wei, E. Kemnitz, S. I. Troyanov, *Chem. Asian J.* 2014, *9*, 79.

[51] B. Q. Mercado, A. Jiang, H. Yang, Z. Wang, H. Jin, Z. Liu, M. M. Olmstead, A. L. Balch, *Angew. Chem. Int. Ed.* 2009, *48*, 9114.

[52] S. Stevenson, G. Rice, T. Glass, K. Harich, F. Cromer, M. R. Jordan, J. Craft, E. Hadju, R. Bible, M. M. Olmstead, K. Maitra, A. J. Fisher, A. L. Balch, H. C. Dorn, *Nature* 1999, *402*, 898.

[53] a) M. Saunders, H. A. Jimenez-Vazquez, R. J. Cross, S. Mroczkowski, M. L. Gross, D. E. Giblin, R. J. Poreda, *J. Am. Chem. Soc.* 1994, *116*, 2193; b) M. Saunders, H. A. Jimenez-Vazquez, R. J. Cross, R. J. Poreda, *Science* 1993, *259*, 1428.

[54] K. Komatsu, M. Murata, Y. Murata, *Science* 2005, *307*, 238.

[55] K. Kurotobi, Y. Murata, *Science* 2011, *333*, 613.

[56] I. Haiduc, F. T. Edelmann, *Supramolecular Organometallic Chemistry*, Wiley-VCH, 2007.

[57] H. Suzuki, Y. Yamamoto, N. Tajima, K. Tatsumi, *Chem. Commun.* 2000, 1801.

[58] F. E. Hahn, C. Radloff, T. Pape, A. Hepp, *Organometallics* 2008, *27*, 6408.

[59] M. J. Almond, M. P. Beer, M. G. B. Drew, D. A. Rice, *J. Organomet. Chem.* 1991, *421*, 129.

[60] a) D. Braga, S. L. Giaffreda, F. Grepioni, A. Pettersen, L. Maini, M. Curzi, M. Polito, *Dalton Trans.* 2006, 1249; b) D. Braga, S. L. Giaffreda, F. Grepioni, A. Pettersen, L. Maini, M. Curzi, M. Polito, *Dalton Trans.* 2006, 1249; c) D. Braga, M. Polito, D. D'Addario, E. Tagliavini, D. M. Proserpio, F. Grepioni, J. W. Steed, *Organometallics* 2003, *22*, 4532.

[61] a) T. Fukino, H. Joo, Y. Hisada, M. Obana, H. Yamagishi, T. Hikima, M. Takata, N. Fujita, T. Aida, *Science* 2014, *344*, 499; b) Z. M. Hudson, I. Manners, *Science* 2014, *344*, 482.

[62] F. P. Schmidtchen, M. Berger, *Chem. Rev.* 1997, *97*, 1609.

[63] P. D. Beer, *Acc. Chem. Res.* 1998, *31*, 71.

[64] a) M. Caporali, L. Gonsalvi, A. Rossin, M. Peruzzini, *Chem. Rev.* 2010, *110*, 4178; b) B. M. Cossairt, N. A. Piro, C. C. Cummins, *Chem. Rev.* 2010, *110*, 4164; c) M. Scheer, G. b. Balázs, A. Seitz, *Chem. Rev.* 2010, *110*, 4236; d) F. Mathey, *J. Organomet. Chem.* 2002, *646*, 15.

[65] a) M. Scheer, *Dalton Trans.* 2008, 4372; b) M. Peruzzini, R. R. Abdreimova, Y. Budnikova, A. Romerosa, O. J. Scherer, H. Sitzmann, *J. Organomet. Chem.* 2004, *689*, 4319; c) O. J. Scherer, S. Weigel, G. Wolmershäuser, *Chem. Eur. J.* 1998, *4*, 1910.

[66] a) M. Fleischmann, C. Heindl, M. Seidl, G. Balázs, A. V. Virovets, E. V. Peresypkina, M. Tsunoda, F. P. Gabbaï, M. Scheer, *Angew. Chem. Int. Ed.* 2012, *51*, 9918; b) O. J. Scherer, J. Schwalb, H. Sitzmann, *Inorg. Synth.* 1990, *27*, 224; c) O. J. Scherer, H. Sitzmann, G. Wolmershäuser, *Angew. Chem.* 1985, *97*, 358; d) O. J. Scherer, H. Sitzmann, G. Wolmershäuser, *J. Organomet. Chem.* 1984, *268*, C9.

[67] a) M. Scheer, L. Gregoriades, J. Bai, M. Sierka, G. Brunklaus, H. Eckert, *Chem. Eur. J.* 2005, *11*, 2163; b) J. Bai, E. Leiner, M. Scheer, *Angew. Chem. Int. Ed.* 2002, *41*, 783.

[68] M. Scheer, L. J. Gregoriades, M. Zabel, J. Bai, I. Krossing, G. Brunklaus, H. Eckert, *Chem. Eur. J.* 2008, *14*, 282.

[69] B. Attenberger, S. Welsch, M. Zabel, E. Peresypkina, M. Scheer, *Angew. Chem. Int. Ed.* 2011, *50*, 11516.

[70] L. J. Gregoriades, B. K. Wegley, M. Sierka, E. Brunner, C. Groeger, E. V. Peresypkina, A. V. Virovets, M. Zabel, M. Scheer, *Chem. Asian J.* 2009, *4*, 1578.

[71] F. Dielmann, Doctoral Thesis, *Universität Regensburg*, 2011.

[72] L. J. Gregoriades, Doctoral Thesis, *Universität Regensburg*, 2006.

[73] a) C. S. J. Callaghan, P. B. Hitchcock, J. F. Nixon, *J. Organomet. Chem.* 1999, *584*, 87; b) G. Recker, *Z. Anorg. Allg. Chem.* 1976, *423*, 242.

[74] R. Bartsch, P. B. Hitchcock, J. F. Nixon, *Chem. Commun.* 1987, 1146.

[75] R. Bartsch, P. B. Hitchcock, J. F. Nixon, *J. Organomet. Chem.* 1988, *340*, C37.

[76] A. S. Ionkin, W. J. Marshall, B. M. Fish, A. A. Marchione, L. A. Howe, F. Davidson, C. N. McEwen, *Eur. J. Inorg. Chem.* 2008, 2386.

[77] a) M. Fleischmann, J. S. Jones, F. P. Gabbai, M. Scheer, *Chem. Sci.* 2015, *6*, 132; b) S. Heinl, G. Balázs, M. Scheer, *Phosphorus, Sulfur Silicon Relat. Elem.* 2014, *189*, 924; c) F. Dielmann, R. Merkle, S. Heinl, M. Scheer, *Z. Naturforsch.* 2009, *64*, 3; d) O. J. Scherer, T. Hilt, G. Wolmershäuser, *Organometallics* 1998, *17*, 4110; e) O. J. Scherer, T. Brück, G. Wolmershäuser, *Chem. Ber.* 1988, *121*, 935; f) O. J. Scherer, T. Brück, *Angew. Chem.* 1987, *99*, 59.

[78] a) S. Deng, C. Schwarzmaier, M. Zabel, J. F. Nixon, M. Bodensteiner, E. V. Peresypkina, G. Balázs, M. Scheer, *Eur. J. Inorg. Chem.* 2011, 2991; b) A. Schindler, G. Balázs, M. Zabel, C. Groeger, R. Kalbitzer, M. Scheer, *C. R. Chim.* 2010, *13*, 1241; c) S. Deng, C. Schwarzmaier, U. Vogel, M. Zabel, J. F. Nixon, M. Scheer, *Eur. J. Inorg. Chem.* 2008, 4870.

[79] J. Bai, A. V. Virovets, M. Scheer, *Angew. Chem. Int. Ed.* 2002, *41*, 1737.

[80] J. Bai, A. V. Virovets, M. Scheer, *Science* 2003, *300*, 781.

[81] a) M. Scheer, A. Schindler, J. Bai, B. P. Johnson, R. Merkle, R. Winter, A. V. Virovets, E. V. Peresypkina, V. A. Blatov, M. Sierka, H. Eckert, *Chem. Eur. J.* 2010, *16*, 2092; b) M. Scheer, J. Bai, B. P. Johnson, R. Merkle, A. V. Virovets, C. E. Anson, *Eur. J. Inorg. Chem.* 2005, 4023.

[82] M. Scheer, A. Schindler, R. Merkle, B. P. Johnson, M. Linseis, R. Winter, C. E. Anson, A. V. Virovets, *J. Am. Chem. Soc.* 2007, *129*, 13386.

[83] a) E. V. Peresypkina, C. Heindl, A. Schindler, M. Bodensteiner, A. V. Virovets, M. Scheer, *Z. Kristallogr.* 2014, *229*, 735; b) M. Scheer, A. Schindler, C. Groeger, A. V. Virovets, E. V. Peresypkina, *Angew. Chem. Int. Ed.* 2009, *48*, 5046.

[84] A. Schindler, C. Heindl, G. Balázs, C. Groeger, A. V. Virovets, E. V. Peresypkina, M. Scheer, *Chem. Eur. J.* 2012, *18*, 829.

[85] C. Schwarzmaier, A. Schindler, C. Heindl, S. Scheuermayer, E. V. Peresypkina, A. V. Virovets, M. Neumeier, R. Gschwind, M. Scheer, *Angew. Chem. Int. Ed.* 2013, *52*, 10663.

[86] S. Welsch, C. Groeger, M. Sierka, M. Scheer, *Angew. Chem. Int. Ed.* 2011, *50*, 1435.

[87] F. Dielmann, M. Fleischmann, C. Heindl, E. V. Peresypkina, A. V. Virovets, R. M. Gschwind, M. Scheer, *Chem. Eur. J.* 2015, *21*, 6208.

[88] S. Heinl, E. V. Peresypkina, A. V. Virovets, M. Scheer, *Angew. Chem. Int. Ed.* 2015, submitted.

[89] O. Oms, T. Jarrosson, L. H. Tong, A. Vaccaro, G. Bernardinelli, A. F. Williams, *Chem. Eur. J.* 2009, *15*, 5012.

[90] L. H. Tong, L. Guenee, A. F. Williams, *Inorg. Chem.* 2011, *50*, 2450.

[91] a) R. J. Less, T. C. Wilson, B. Guan, M. McPartlin, A. Steiner, P. T. Wood, D. S. Wright, *Eur. J. Inorg. Chem.* 2013, 1161; b) J. Bacsa, R. J. Less, H. E. Skelton, Z. Soracevic, A. Steiner, T. C. Wilson, P. T. Wood, D. S. Wright, *Angew. Chem. Int. Ed.* 2011, *50*, 8279.

[92] B. P. Johnson, F. Dielmann, G. Balázs, M. Sierka, M. Scheer, *Angew. Chem. Int. Ed.* 2006, *45*, 2473.

[93] R. L. Murry, D. L. Strout, G. K. Odom, G. E. Scuseria, *Nature* 1993, *366*, 665.

2. Research Objectives

As it was demonstrated in the introducing chapter 1.5, the coordination behavior of 1,2,4-triphosphaferrocenes [$Cp^RFe(\eta^5\text{-}P_3C_2R'_2)$] strongly depends on the substitution pattern of the Cp^R ligand (Cp^R = Cp, Cp*, Cp'''). Thus, the variation of the R' groups in the phospholyl ligand should have an even greater impact on the reactivity, since they are situated directly beside the phosphorus atoms available for a coordination. However, reactions with Cu(I) halides have so far been restricted to [$Cp^RFe(\eta^5\text{-}P_3C_2{}^tBu_2)$].

In addition, going to the heavier homologue, 1,2,4-triarsolyl ligands are not known in literature, though the one-pot-approach applied by the group of Ionkin seems promising for their synthesis (*cf*. chapter 1.5). Thus, the objectives are as follows:

- Variation (Enhancement as well as decrease of the sterical demand) of the R' group in 1,2,4-$(P_3C_2R'_2)^-$ ligands and investigation of the coordination and reaction behavior of the corresponding phosphaferrocenes towards Cu(I) halides
- Screening of the transferability of the mentioned one-pot-synthesis for 1,2,4-triphospholyl ligands to the arsenic derivative

It was also shown that the pentaphosphaferrocenes [$Cp^RFe(\eta^5\text{-}P_5)$] ($Cp^R$ = Cp*, Cp^{Bn}) in combination with Cu(I) halides display excellent building blocks for the formation of neutral nano-sized supramolecules. In addition, they are capable of the encapsulation and therefore sometimes stabilization of small molecules. Based on these results, research objectives for this work are:

- Variation of the Cu source, stoichiometry and template with the aim of the synthesis of novel supramolecules regarding different shapes (balls and capsules), topologies (within and beyond fullerene topology) and overall charges (neutral and charged)
- Studies of the required properties of the template molecules to be incorporated in pentaphosphaferrocene-based spheres, such as size, symmetry and presence of Cp ligands
- Use of electron-rich and -poor sandwich complexes as template to investigate the influence of their redox potential
- Investigations on the potential fragmentation of triple decker complexes

3. A *cyclo*-P_6 Ligand Complex for the Formation of Planar 2D Layers

C. Heindl, E. V. Peresypkina, A. V. Virovets, D. Lüdeker, G. Brunklaus and M. Scheer

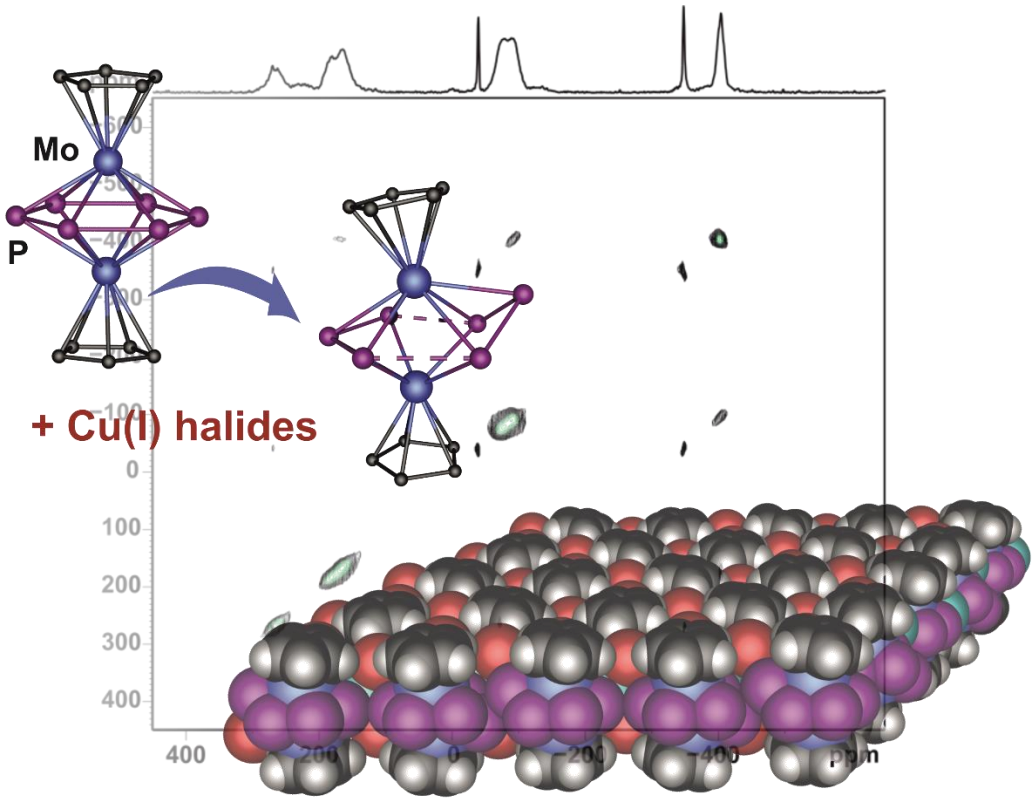

Abstract:

The all-phosphorus analogue of benzene, stabilized as a middle deck in triple decker complexes, displays a promising building block for the formation of graphene-like sheet structures. Herein, we report on the self-assembly of $[(CpMo)_2(\mu,\eta^{6:6}\text{-}P_6)]$ (**1**) with CuX (X = Br, I) revealing the unprecedented 2D networks $[\{(CpMo)_2P_6\}(CuBr)_4]_n$ (**2**) and $[\{(CpMo)_2P_6\}(CuI)_2]_n$ (**3**), respectively. X-ray structural analyses exhibit a unique deformation of the previously planar *cyclo*-P_6 ligand. This includes bending of one P atom in an 'envelope' conformation as well as a bisallylic distortion. Despite this, **2** and **3** form absolutely planar layers. Both polymers were furthermore analyzed by $^{31}P\{^1H\}$ magic angle spinning (MAS) NMR spectroscopy revealing signals corresponding to six non-equivalent phosphorus sites. A reliable peak assignment is achieved by 2D correlation spectra as well as DFT chemical shift computations.

3.1 Introduction

Tailored synthesis of inorganic analogues of organic molecules comprises a fascinating area of fundamental research. Following the so-called isolobal principle,[1] substitution of methine moieties by phosphorus atoms appears quite promising. And in fact, 2016 marks the 50th anniversary of the first successful synthesis of a phosphabenzene in which one CH unit is replaced by a P atom,[2] thereby setting the stage for the ultimate goal: the preparation of carbon-free hexaphosphabenzene. Since then, many theoretical studies with respect to its aromaticity were reported that outlined the instability of a free *cyclo*-P_6 unit.[3] Nevertheless, its detection in an inert stabilizing matrix at low temperature might be feasible so that the challenge still persists. Another synthetic approach demonstrated by the Scherer group includes stabilization of the P_6 ring *via* coordination to transition metals, thus affording a triple decker complex $[(Cp^*Mo)_2(\mu,\eta^{6:6}\text{-}P_6)]$ ($Cp^* = \eta^5\text{-}C_5Me_5$) bearing a planar P_6 middle deck for the first time (*Figure 3.1*).[4] Triple decker complexes containing the *cyclo*-P_6 unit could also be obtained for vanadium,[5] tungsten[5] and niobium,[6] respectively. Quite recently, the sandwich complex $[(CpMo)_2(\mu,\eta^{6:6}\text{-}P_6)]$ (**1**) with the parent Cp ligands was synthesized and characterized.[7] In case of the Mo and W complexes the *cyclo*-P_6 ring reveals a perfect D_{6h} symmetry, whereas V and Nb derivatives exhibit a slight bisallylic distortion.[6a] Notably, the middle deck in $[(Cp^*Ti)_2(\mu,\eta^{3:3}\text{-}P_6)]$ has a chair conformation (*Figure 3.1*).[8]

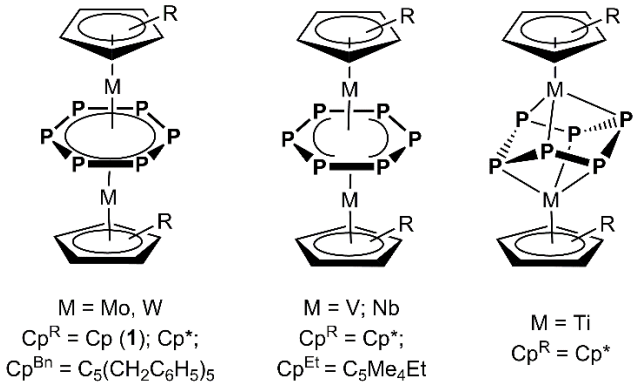

Figure 3.1 Triple decker complexes containing a *cyclo*-P_6 middle deck.

In contrast to benzene, the presence of lone pairs at the phosphorus atoms converts these triple decker complexes into excellent building blocks for supramolecular chemistry. Particularly intriguing, since one may envision graphene-like honeycomb networks resulting from reactions with Lewis acidic metal salts.

In our group, Cu(I) halides have been widely applied for linkage of unsubstituted P_n complexes[9] und thus also for $[(Cp^RMo)_2(\mu,\eta^{6:6}\text{-}P_6)]$ (Cp^R = Cp*, Cp^{Bn} = $\eta^5\text{-}C_5(CH_2C_6H_5)_5$). Here, three one-

dimensional coordination polymers are obtained with the intact *cyclo*-P_6 ligand in a 1,2,3,4-coordination mode (*Figure 3.2*, type **D**)[10] as well as a two-dimensional network *via* coordination of five or even six P atoms to copper, though forming non-planar corrugated sheets.[11]

Concerning the parent compound **1**, except for rather weak interactions of the P_6 unit with a mercury trimer [(*o*-$C_6F_4Hg)_3$] yielding a 'super-sandwich' structure,[7] the corresponding subsequent chemistry utilizing its coordination properties is unknown to date.

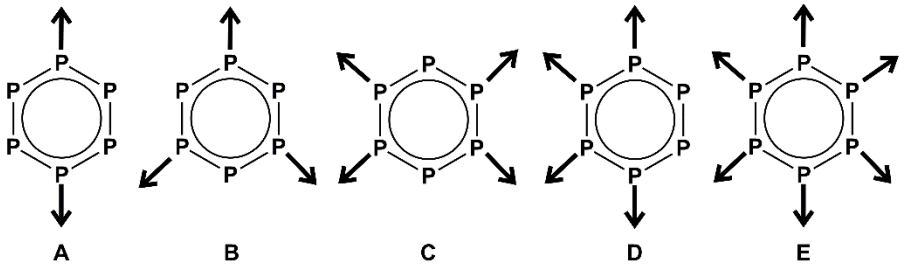

Figure 3.2 Possible coordination modes of a *cyclo*-P_6 ligand.

The P_6 unit offers competitive coordination sites (*Figure 3.2*) and one is faced with some problems. A considerable variety of connectivity renders a growth of single crystals suitable for X-ray analysis challenging. Indeed, twinned or layered crystals may also be encountered but particularly occur in the case of Cp rings. The obtained polymeric products are often insoluble and at times form microcrystalline powders so that X-ray diffraction analysis is crucial for a determination of the exact coordination pattern. Modern solid state NMR provides complementary information including the number of independent molecules in the unit cell, intermolecular distances or connectivity, the spatial proximity of constituent moieties and even orientation relations. Hence, it is a very powerful tool for structure determination, particularly in case of powdered compounds ("NMR crystallography").[12]

Herein, we report the coordination properties of the parent triple decker complex **1** towards CuX (X = Br, I) revealing unprecedented 2D networks and distortion of the P_6 middle deck. All polymers were characterized by X-ray diffraction analysis as well as 1D $^{31}P\{^1H\}$ magic-angle spinning (MAS) NMR where the peak assignment is based on the analysis of 2D ^{31}P-^{31}P MAS NMR correlation spectra and (split basis set) density functional theory (DFT) ^{31}P chemical shift computations.

3.2 Results and Discussion

When a colorless solution of CuX (X = Br I) in CH_3CN is layered onto an orange-brown solution of **1** in CH_2Cl_2 or toluene, an immediate color change to grey-black at the phase boundary occurs. During the diffusion process, a black powder precipitates and small black crystallites are formed. The products are insoluble in hexane, toluene, CH_2Cl_2, CH_3CN or thf, but possess a good solubility

in pyridine, though at expense of a fragmentation of the compounds. This is evidenced by the singlet peak at δ = -351.5 ppm in the corresponding $^{31}P\{^1H\}$ solution NMR spectra (in pyridine-d_5) of the black microcrystalline solid and precipitate attributed to pristine **1**. Therefore, quite an effort was made to successfully derive suitable conditions for crystallization of the coordination products, applying a variety of different solvent mixtures and dilution conditions (see experimental part).

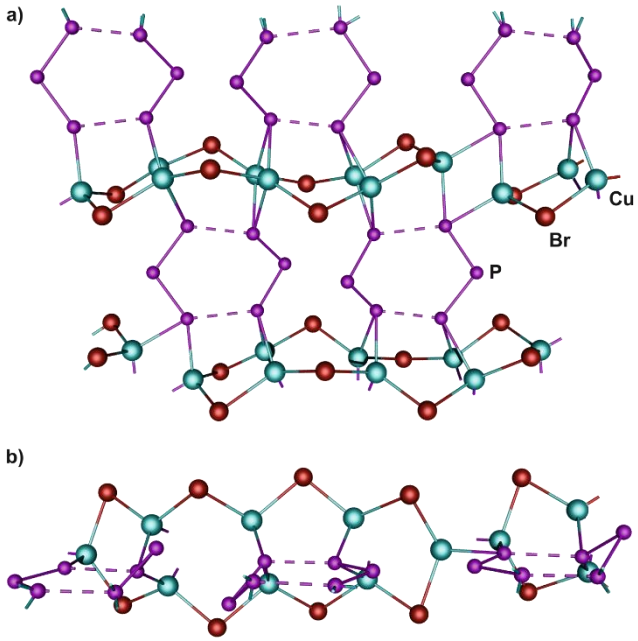

Figure 3.3 Section of the 2D polymeric network **2**. {CpMo} units and minor disordered fragments are omitted for clarity; a) top view; b) side view.

In the presence of CuBr, the polymer $[\{(CpMo)_2(\mu,\eta^{3:3:1:1:1:1}\text{-}P_3)(\mu,\eta^{3:2:1:1:1:1}\text{-}P_3)\}Cu_4(\mu\text{-}Br)_4]_n$ (**2**) crystallizes as black plates in the centrosymmetric triclinic space group $P\bar{1}$. Its structural analysis reveals a two-dimensional network with a *cyclo*-P_6 middle deck in 1,2,4,5-coordination mode (*Figure 3.2*, type **C**; *Figure 3.3*). Each of the four P atoms coordinates two Cu atoms forming $\{Cu_2P_2\}$ four-membered rings. Taking into account the μ-Br ligands, contorted five-membered $\{P_2Cu_2Br\}$ rings become also visible (*Figure 3.3*a). A distinctive feature in **2** is the distortion of the *cyclo*-P_6 deck which is no longer planar.

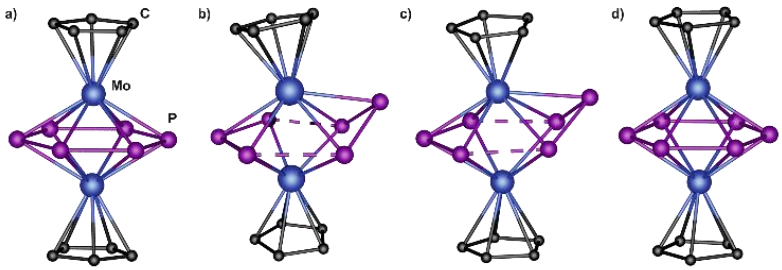

Figure 3.4 Comparison of the distortion of the P_6 ring in a) **1**; b) **2**; c) **3a**; d) **3b**.

The side view illustrates that one P atom is bent out of the plane by 1.141(3) Å and therefore solely coordinated to one molybdenum atom with a bond length of 2.652(3) Å (*Figure 3.4*b). In comparison to the other Mo-P distances (2.400(2) Å – 2.657(3) Å) this bond appears rather stretched. Furthermore, the P_6 ring shows a significant bisallylic distortion where the P_3 ligands are separated by 2.652(3) Å and 2.444(3) Å, respectively. The remaining P-P bond lengths are 2.168(4) Å and 2.162(4) Å for one P_3 ligand and 2.138(3) Å and 2.136(5) Å for the other (containing the 'envelope' P atom). Thus, the bond lengths are in between a single and double bond,[13] and even shorter than in complex **1** ($P\text{-}P_{average}$: 2.177(2) Å).[7] The distortion of the whole unit leads the Cp ligands to be inclined by 9.26° compared to a parallel arrangement in **1**.

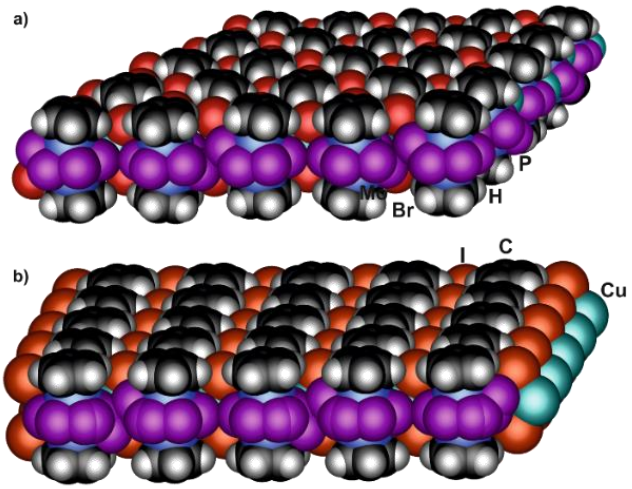

Figure 3.5 Space-filling representation of a section of a) **2** and b) **3** forming a planar layer.

Notably, the geometry is unique for P_6 middle decks, most likely resulting from the coordination to Cu. Though the vanadium and niobium derivatives also show a bis-allylic system, the P_6-rings remain planar (*Figure 3.1*). Furthermore, no chair-like conformation is present in **2**, hampering comparison to the titanium complex (*Figure 3.1*). Despite this distorted linking pattern compound **2** forms planar layers (*Figure 3.5*).

In the presence of CuI the compound $[\{(CpMo)_2(\mu,\eta^{3:3:1:1}\text{-}P_3)(\mu,\eta^{3:2:1:1}\text{-}P_3)\}_{0.84}\{(CpMo)_2(\mu,\eta^{6:6:1:1:1:1}\text{-}P_6)\}_{0.16}Cu_2(\mu\text{-}I)_2]_n$ (**3**) is obtained, crystallizing as black plates in the monoclinic space group *C*2/*m*. Its structure is comprised of a two-dimensional polymer with a 1,2,4,5-coordination mode of the middle deck (*Figure 3.2* type **C**, *Figure 3.6*), comparable to **2**. In this case, unlike the Br derivative, each P atom is bound to *one* copper atom, which in turn forms $\{Cu_2P_4\}$ six-membered and $\{Cu(\mu\text{-}I)\}_2$ four-membered rings, resulting in a characteristic tetrahedral environment for Cu. Hence, the Cu halide framework is much less extended than in **2**. The *cyclo*-P_6 rings, however, appear to be disordered exhibiting two distinct coordination modes: $[\{(CpMo)_2(\mu\text{-},\eta^{3:3:1:1}\text{-}P_3)(\mu,\eta^{3:2:1:1}\text{-}P_3)\}Cu_2(\mu\text{-}I)_2]_n$ (**3a**, *Figure 3.6*a,b) and $[\{(CpMo)_2(\mu,\eta^{6:6:1:1:1:1}\text{-}P_6)\}Cu_2(\mu\text{-}I)_2]$ (**3b**, *Figure 3.6*c,d) with corresponding occupancy factors of 0.84 and 0.16, respectively.

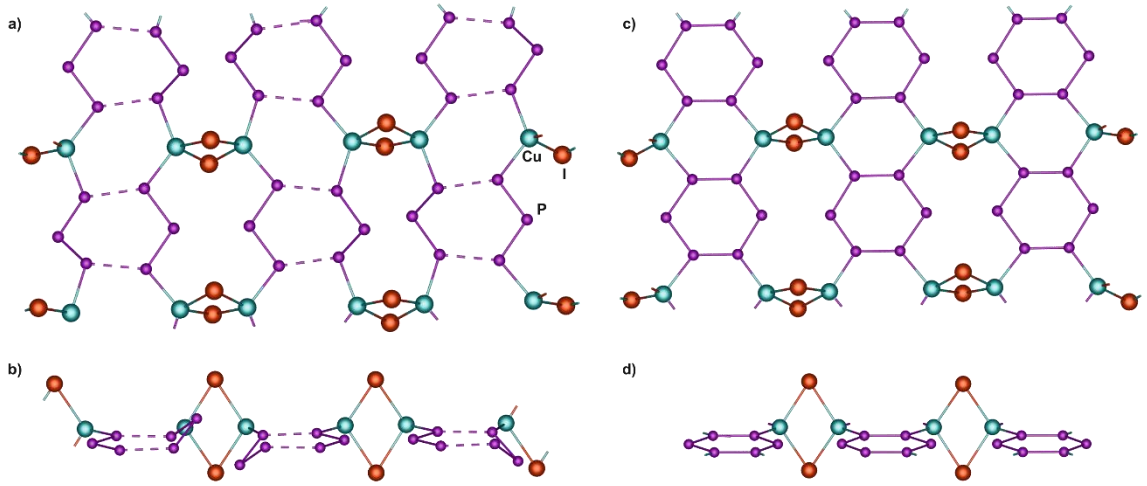

Figure 3.6 a) Section of the 2D polymeric network with all P_6 ligands showing the geometry and coordination mode of **3a** (84%). {CpMo} units are omitted for clarity; top view; b) side view; c) section of the 2D polymeric network with all P_6 ligands showing the geometry and coordination mode of **3b** (16%). {CpMo} units are omitted for clarity; top view; d) side view.

The middle deck in **3a** shows the same bisallylic distortion as in **2** but has more uniform distances of 2.563(8) Å and 2.544(8) Å between the P_3 ligands (*Figure 3.4*c). The bending of one P atom out of plane by 1.113(9) Å is somewhat less distinctive but in a comparable range as in **2**, though the Cp ligands retain their parallel arrangement in **3a**. The bent phosphorus atom is additionally disordered over the mirror plane with an occupancy factor of 0.42 each. The distance between molybdenum and this 'out-of-plane' phosphorus atom (2.683(8) Å) is the longest among all Mo-P bond lengths (2.434(4) Å – 2.598(4) Å), but possible uncertainties caused by the disorder should also be kept in mind. Again, the remaining P-P bond lengths ($\eta^{3:3:1:1}$-P_3: 2.127(7) Å, 2.132(7) Å; $\eta^{3:2:1:1}$-P_3: 2.151(9) Å, 2.147(10) Å) are shortened compared to the pristine complex **1**.

Surprisingly, with an occupancy factor of 0.16 the intact *cyclo*-P_6 middle deck is present (**3b**, *Figure 3.4*d, *Figure 3.6*c,d). It is located on a mirror plane and therefore perfectly planar. In comparison to **1** and in analogy to **2** and **3a**, the coordination to Cu leads to a shortening of the P-P bond lengths, which is most significant for P_{coord}-P_{coord} with values of 2.00(3) Å and 2.01(4) Å, respectively (P-P_{coord}: 2.03(3) Å – 2.132(7) Å).

The question whether the bent (**3a**) and planar (**3b**) *cyclo*-P_6 middle decks occur within the same layer or the layers comprising the same middle decks form with different probability cannot be answered using structural data solely. On the other hand, the same coordination mode to Cu, as well as a lack of structural effects (e.g. superstructural ordering), favor the hypothesis of mixed layers in **3**. As in **2**, absolutely planar sheet-like structures are also formed in **3** (*Figure 3.5*b).

Compared to the above mentioned 1D and 2D coordination polymers containing $[(Cp^RMo)_2(\mu,\eta^{6:6}\text{-}P_6)]$ (Cp^R = Cp*, Cp^{Bn}) which maintain the planarity of the middle decks, the coordination mode as well as the distortion of the *cyclo*-P_6 ligand in **2** and **3** are unique.

Furthermore, the only 2D network constructed by the Cp* derivative and CuCl forms corrugated sheets, whereas the layers in **2** and **3** are planar.

Since the considered polymer networks are insoluble in common solvents and fragmentation is observed in pyridine, $^{31}P\{^1H\}$ MAS NMR spectra of both compounds (**2** and **3**) were recorded. Even though the ^{31}P chemical shifts occur over a rather large range of values, the spread of observed signals over a range of around 700 ppm is quite remarkable. In order to achieve a sufficient spectral resolution while allowing for quantitative interpretation of the acquired spectra, the conflicting demands of the significant ^{31}P chemical shift anisotropy and line-broadening contributions from ^{31}P-$^{63,65}Cu$ dipolar couplings have to be considered. Hence, the $^{31}P\{^1H\}$ MAS NMR spectra of **2** and **3** were recorded at fast MAS and a magnetic field of 4.7 T rather than at the also available field of 11.7 T.

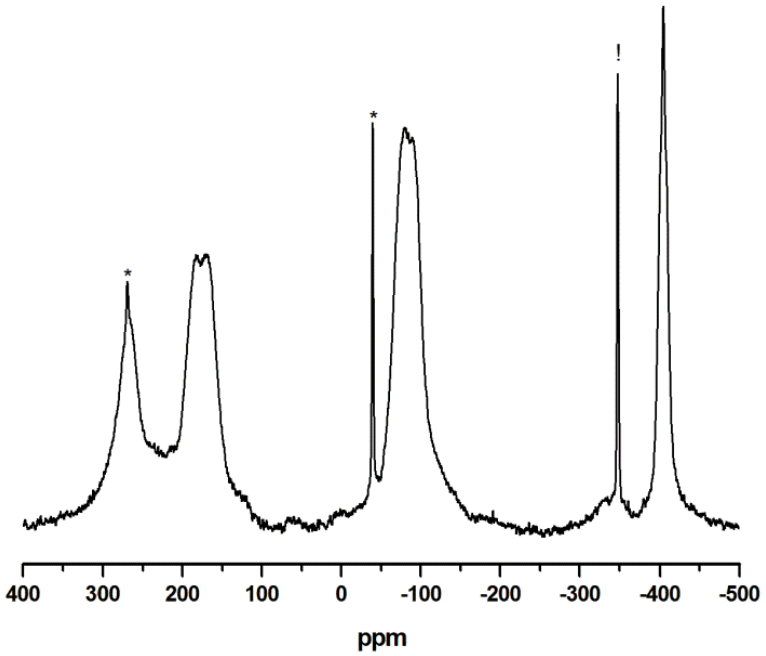

Figure 3.7 The ^{31}P MAS NMR spectrum of **2** (acquired at 81.02 MHz and 25 kHz MAS). A sharp peak (marked with !) at -347.4 ppm indicates residual **1** while the signals marked with asterisks are spinning sidebands.

The $^{31}P\{^1H\}$ MAS NMR spectrum of **2** (*Figure 3.7*) at first glance exhibits four rather broad peaks and a sharp peak at -347.4 ppm with spinning sidebands (marked with asterisks). The latter signal can readily be attributed to residual **1**, whereas an assignment of the other signals reflecting the P_6 unit is not straightforward. The corresponding isotropic chemical shifts however could be unambiguously identified from the diagonal peaks in a 2D ^{31}P-^{31}P correlation spectrum of **2** with radiofrequency-driven dipolar recoupling (RFDR) applied during a short mixing time (*Figure 3.8*).[14]

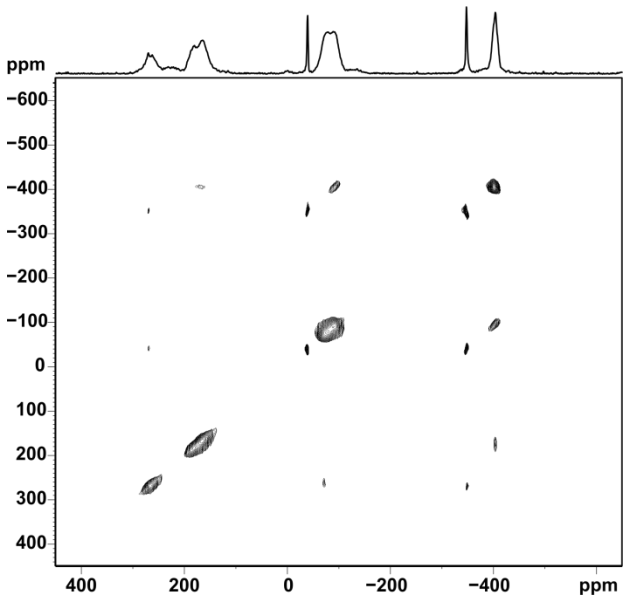

Figure 3.8 2D ^{31}P- ^{31}P RFDR MAS NMR spectrum of **2** (acquired at 81.02 MHz and 25 kHz MAS at a short mixing time of 320 µs). The peaks in the diagonal (marked in green) reflect the isotropic chemical shifts of the phosphorus sites that are not readily accessible from the 1D ^{31}P MAS NMR spectrum of **2**.

In good agreement with the six independent phosphorus sites identified in the crystal structure of **2** the RFDR spectrum (*Figure 3.8*) indicated signals at 268.3 ppm, 185.6 ppm, 164.7 ppm, -74.9 ppm, -91.4 ppm and -403.8 ppm, respectively, where the subsequent line-shape analysis revealed a 1:1:1:1:1:1 peak area distribution and an impurity fraction of 5% (sharp signal of **1**). A cutout of **2** (see *Figure 3.9*) was subjected to a split basis set DFT chemical shift computation with PBE1PBE / cc-pVQZ[15] level for ^{31}P and used for assignment (for labelling see *Figure 3.9*). It is apparent that a comparable coordination of the considered phosphorus atoms by copper or molybdenum atoms results in rather similar ^{31}P chemical shifts yielding the following peak assignment: δ = 268.3 (P13; DFT: δ = 337 ppm), 185.6 (P15; DFT: δ = 235 ppm), 164.7 (P11; DFT: δ = 166 ppm), -74.9 (P14; DFT: δ = -18 ppm), -91.4 (P12; DFT: δ = -26 ppm) and -403.8 ppm (P16; DFT: δ = -480 ppm).

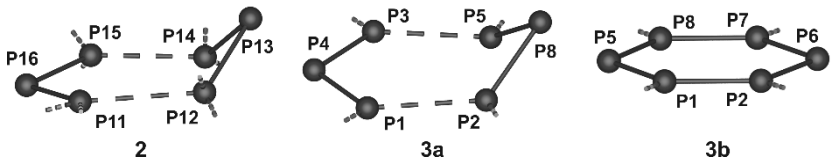

Figure 3.9 Site labelling of the P_6 ligands in **2**, **3a** and **3b** as subjected to ^{31}P DFT chemical shift computation.

In contrast, the ^{31}P MAS NMR spectrum of **3** (*Figure 3.10*) is clearly in agreement with the presence of different coordination modes of the *cyclo*-P_6 unit as documented by the larger spread of signals compared to **2**, thus yielding gaussian-type peaks at δ = 283.4, 270.3, 114.4, 35.9, -22.3, -37.6 ppm as well as -345 and -653 ppm. Though at this stage unambiguous spectral fitting could not be achieved, in part due to residual **1**, ^{31}P DFT chemical shift computations at PBE1PBE/cc-pVQZ level of theory based on representative structure cutouts of **3a** and **3b** (for labelling see *Figure 3.9*)

indicated that the constituents of the P_6 unit in **3b** resonate between δ = -350 ppm and -520 ppm. Hence, they are significantly shifted towards more negative values (P2/P7 DFT: δ = -353 ppm, P1/P8 DFT: δ = -394 ppm; P5 DFT: δ = -455 ppm, P6 DFT: δ = -519 ppm). In the case of **3a**, phosphorus sites are computed at δ = 234 (P3), 234 (P2), 227 (P8), 11 (P5), -30 (P1) and -368 ppm (P4), respectively, which is more comparable to **2**, thereby reflecting a similar distortion of the P_6 unit in **3a** (see *Figure 3.4*).

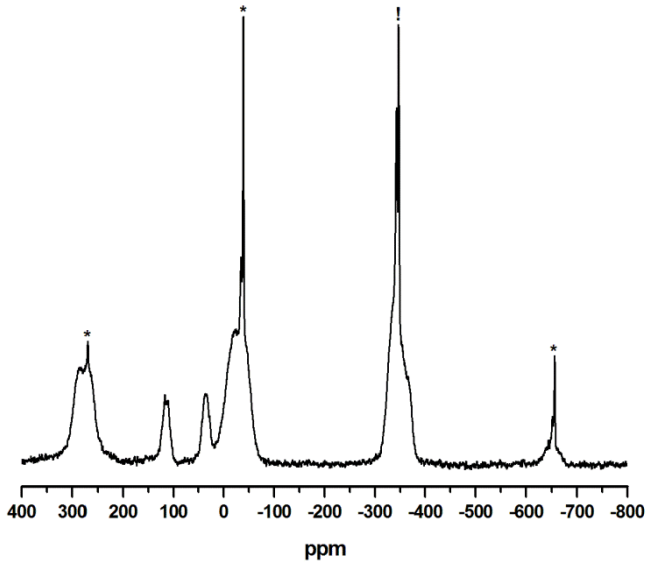

Figure 3.10 The ^{31}P MAS NMR spectrum of **3** (acquired at 81.02 MHz and 25 kHz MAS). A sharp peak (marked with !) at -346.7 ppm likely indicates residual **1** while signals marked with asterisks are spinning sidebands; the additional sharp peak at -342.9 ppm may be attributed to a further impurity. In summary, the overall signal fraction of the sharp peaks is approximately 12%.

Nevertheless, further impact of local coordination including bond lengths, torsion angles or even the orientation of the {CpMo} units on the local electron density distribution at the distinct phosphorus sites in **2** and **3** is evident, rendering ^{31}P MAS NMR a sensitive probe for structure analysis of such compounds.

In summary, the first coordination polymers **2** and **3** containing the parent triple decker complex **1** are obtained by the self-assembly with CuX (X = Br, I). Their structures reveal two-dimensional polymers with the *cyclo*-P_6 middle deck in a 1,2,4,5-coordination mode to copper. Resembling graphene-like sheets, the hereby formed layers are absolutely planar, which is unique for this type of complex. Surprisingly, the coordination profoundly affects the geometry of the P_6 unit of **1** as evidenced by a significant bisallylic distortion and 'envelope' conformation of one phosphorus atom in both polymers. Due to insolubility of **2** and **3**, they were comprehensively characterized by 1D and 2D ^{31}P{^{1}H} MAS NMR spectroscopy. The obtained signals are spread over a remarkable range of more than 900 ppm and correspond to six independent phosphorus atoms, being consistent with the distorted P_6 moiety. In addition, DFT chemical shift computations allow a reliable assignment of the signals.

3.3 Experimental Part

General Remarks:

All reactions were performed under an inert atmosphere of dry nitrogen or argon with standard vacuum, Schlenk and glove-box techniques. Solvents were purified, dried and degassed prior to use by standard procedures. $[(CpMo)_2(\mu,\eta^{6:6}\text{-}P_6)]$ was synthesized following the reported procedure.[7] Commercially available chemicals (CuBr, CuI) were used without further purification. Solution NMR spectra were recorded on a Bruker Avance 300 spectrometer. The corresponding ESI-MS spectra were acquired on a ThermoQuest Finnigan MAT TSQ 7000 mass spectrometer, whereas elemental analyses were performed on a Vario EL III apparatus.

The $^{31}P\{^1H\}$ MAS NMR spectra of **2** and **3** were recorded at 4.7 T (^{31}P resonance at 81.02 MHz) and 25 kHz MAS using a Bruker Avance III 200 spectrometer and a Bruker 2.5 mm MAS NMR probe accumulating 2048 scans at a relaxation delay of 90 s and SPINAL64 high power proton decoupling. All pulse lengths were adjusted with respect to a radio-frequency field strength of 100 kHz (that is, $\pi/2$ pulses of 2.5 µs). In order to avoid severe baseline distortions, the rotor-synchronized Hahn spin echo sequence was applied (with echo delays of a rotor period (τ_R = 40 µs), corrected for finite pulse durations). The signal (FID of 32k points) was sampled with a dwell time of 0.5 µs and zero-filled to 128k points prior to processing. Spectral fitting was performed with DMFit.[16] All DFT PBE1PBE computations (with 6-311G(d,p) (for H, C, O), cc-pVQZ (for P), LANL2DZ (for Mo, Cu, Br, I) were done with and as implemented in the gaussian09 software package.[17] The obtained ^{31}P chemical shielding σ was "translated" into chemical shifts δ with respect to H_3PO_4 [$\delta_{standard}$ = 0 ppm; $\sigma_{standard}$(cc-pVQZ) = 349.5809 ppm] using the expression $\delta_{sample} = \sigma_{sample} - \sigma_{standard} + \delta_{standard}$.

Synthesis of $[\{(CpMo)_2(\mu,\eta^{3:3:1:1:1:1}\text{-}P_3)(\mu,\eta^{3:2:1:1:1:1}\text{-}P_3)\}Cu_4(\mu\text{-}Br)_4]_n$ (2)

In a big Schlenk tube a bright orange-brown solution of $[(CpMo)_2(\mu,\eta^{6:6}\text{-}P_6)]$ (100 mg, 0.20 mmol) in CH_2Cl_2 (100 mL) is carefully layered first with a solvent mixture of CH_2Cl_2/CH_3CN (2/1, 20 mL), then with a colorless solution of CuBr (186 mg, 1.30 mmol) in CH_3CN (50 mL). Already after one day the formation of small black crystals of **2** at the phase boundary, sometimes in addition to red plates of $[(CpMo)_2(\mu,\eta^{6:6}\text{-}P_6)]$ can be observed. After complete diffusion the mother liquor is decanted and the crystals are washed with CH_2Cl_2 to remove residues of the starting material $[(CpMo)_2(\mu,\eta^{6:6}\text{-}P_6)]$. Afterwards, the crystals are washed with hexane (3 x 15 mL) and dried *in vacuo*. Of course, the synthesis of **2** can also be down-scaled to a few mg of the starting materials and accordingly a few mL of solvents. Crystals suitable for X-ray structural analysis can be obtained by layering a solution of **2** (4 mg, 0.008 mmol) in CH_2Cl_2 (5 mL) first with a solvent mixture of CH_2Cl_2/CH_3CN (2/1, 2 mL),

afterwards with a solution of CuBr (7 mg, 0.05 mmol) in the same solvent mixture of CH_2Cl_2/CH_3CN (2/1, 5 mL) in a thin Schlenk tube.

Analytical Data of **2**:

Yield: 105 mg (0.05 mmol, 53%)

^{1}H NMR (pyridine-d_5): δ [ppm] = 2.55 (s, $(CpMo)_2P_6$).

^{31}P{^{1}H} NMR (pyridine-d_5): δ [ppm] = -351.60 (s, $(CpMo)_2P_6$).

Positive ion ESI-MS (pyridine): *m/z* (%) = 935.5 $[\{(CpMo)_2P_6\}Cu_3Br_2(C_5H_5N)]^+$, 899.5 $[\{(CpMo)_2P_6\}Cu_3Br_2(CH_3CN)]^+$, 858.5 $[\{(CpMo)_2P_6\}Cu_3Br_2]^+$, 795.6 $[\{(CpMo)_2P_6\}Cu_2Br(C_5H_5N)]^+$, 776.9 $[\{(CpMo)_2P_6\}Cu(C_5H_5N)_2(CH_3CN)]^+$, 729.9 $[\{(CpMo)_2P_6\}Cu(C_5H_5N)_2]^+$, 711.9 $[\{(CpMo)_2P_6\}Cu_2Br]^+$, 649.7 $[\{(CpMo)_2P_6\}Cu(C_5H_5N)]^+$, 508.6 (6) $[Cu_3Br_2(C_5H_5N)_2]^+$, 364.7 $[Cu_2Br(C_5H_5N)_2]^+$, 220.9 (100) $[Cu(C_5H_5N)_2]^+$, 182.9 (60) $[Cu(C_5H_5N)(CH_3CN)]^+$.

Negative ion ESI-MS (pyridine): *m/z* (%) = 796.2 (4) $[Cu_5Br_6]^-$, 654.3 (3) $[Cu_4Br_5]^-$, 510.4 (4) $[Cu_3Br_4]^-$, 366.4 (27) $[Cu_2Br_3]^-$, 222.5 (100) $[CuBr_2]^-$.

Elemental analysis: Calculated (%) for $[\{(CpMo)_2P_6\}(CuBr)_4]$ (1082 g/mol): C 11.10, H 0.93; found: C 11.19, H 0.98.

Synthesis of $[\{(CpMo)_2(\mu,\eta^{3:3:1:1}\text{-}P_3)(\mu,\eta^{3:2:1:1}\text{-}P_3)\}_{0.84}\{(CpMo)_2(\mu,\eta^{6:6:1:1:1:1}\text{-}P_6)\}_{0.16}Cu_2(\mu\text{-}I)_2]_n$ (3)

In a big Schlenk tube a bright orange-brown solution of $[(CpMo)_2(\mu,\eta^{6:6}\text{-}P_6)]$ (90 mg, 0.18 mmol) in CH_2Cl_2 (120 mL) is carefully layered first with a solvent mixture of CH_2Cl_2/CH_3CN (2/1, 20 mL), then with a colorless solution of CuI (203 mg, 1.07 mmol) in CH_3CN (60 mL). Already after one day the formation of small black crystals of **3** at the phase boundary (in addition to red plates of $[(CpMo)_2(\mu,\eta^{6:6}\text{-}P_6)]$) can be observed. After complete diffusion the mother liquor is decanted and the crystals are washed several times with CH_2Cl_2 to remove $[(CpMo)_2(\mu,\eta^{6:6}\text{-}P_6)]$. As soon as the CH_2Cl_2 solution is absolutely colorless, the crystals are washed with a toluene/hexane mixture and dried *in vacuo*. Of course, the synthesis of **3** can also be down-scaled to a few mg of the starting materials and accordingly a few mL of solvents. Crystals suitable for X-ray structural analysis can be obtained, when a solution of $[(CpMo)_2(\mu,\eta^{6:6}\text{-}P_6)]$ (4 mg, 0.008 mmol) in toluene (5 mL) is layered with a solution of CuI (8 mg, 0.04 mmol) in a solvent mixture of CH_2Cl_2 (5 mL) and CH_3CN (1 mL) in a thin Schlenk tube.

Analytical Data of **3**:

Yield: 75 mg (0.084 mmol, 47%)

^{1}H NMR (pyridine-d_5): δ [ppm] = 2.53 (s, $(CpMo)_2P_6$)

^{31}P{^{1}H} NMR (pyridine-d_5): δ [ppm] = -351.51 (s, $(CpMo)_2P_6$)

Positive ion ESI-MS (pyridine): *m/z* (%) = 952.4 $[\{(CpMo)_2P_6\}Cu_3I_2]^+$, 841.7 $[\{(CpMo)_2P_6\}Cu_2I(C_5H_5N)]^+$, 760.9 $[\{(CpMo)_2P_6\}Cu_2I]^+$, 729.9 $[\{(CpMo)_2P_6\}Cu(C_5H_5N)_2]^+$, 649.8 $[\{(CpMo)_2P_6\}Cu(C_5H_5N)]^+$, 410.7 (3) $[Cu_2I(C_5H_5N)_2]^+$, 220.9 (100) $[Cu(C_5H_5N)_2]^+$, 182.9 (54) $[Cu(C_5H_5N)(CH_3CN)]^+$

Negative ion ESI-MS (pyridine): *m/z* (%) = 506.5 (5) $[Cu_2I_3]^-$, 316.6 (100) $[CuI_2]^-$, 126.7 (54) $[I]^-$

Elemental analysis: Calculated (%) for $[\{(CpMo)_2P_6\}(CuI)_2]$ (889 g/mol): C 13.51, H 1.13; found: C 12.58, H 1.15.

3.4 Crystallographic Details

Crystals of **2** and **3** were taken from a Schlenk flask under a stream of argon and immediately covered with mineral oil or perfluorinated Fomblin® mineral oil to prevent decomposition. X-ray diffraction studies of **2** and **3** faced many challenges, since the crystals are very small in size and systematically twinned owing to their layered structure. Therefore the single crystals chosen for measurement were very small and had low diffraction power, hence the collection of data at high theta angles required high exposure times.

The data for **2** were collected on an Agilent Technologies SuperNova diffractometer equipped with Eos CCD detector and an Enhanced Ultra MoK_α sealed tube (λ = 0.71073 Å) using 0.5° ω scans. The data for **3** were collected on an Agilent Technologies diffractometer equipped with Titan^{S2} CCD detector and a SuperNova CuK_α microfocus source (λ = 1.54178 Å) using 0.5° ω scans. All measurements were performed at 123 K. The structures were solved by direct methods with *SHELX97*.[18] The structures were refined by full-matrix least-squares method against $|F|^2$ in anisotropic approximation using *SHELXL97* or the multiprocessor and variable memory version *SHELXL2013*. All non-hydrogen atoms were refined anisotropically, while the hydrogen atoms were refined riding on pivot atoms.

In the polymer **2**, the copper atoms are disordered over two close positions. The corresponding occupancies were refined with equated U_{iso} to give the 0.6/0.4 and 0.85/0.15 values for Cu(1) and Cu(3) positions, respectively. The further refinement was performed with fixed occupancies in anisotropic approximation.

The middle deck in **3** comprises planar *cyclo*-P_6 and $P_3\cdots P_3$ moieties disordered in a 0.16 and 0.84 ratio. In addition, the 'out-of-plane' P atom belonging to the major component is disordered over the mirror plane. Three of the 'in-plane' P atoms coincide for both ligands. A SADI restraint was used on two P-P distances involving the minor component to bring them into a reasonable range. Because of the high absorption (μ = 41.72), the residual density peaks reach 3.25 eA^{-3} and displacement parameters of light carbon atoms are affected.

Table 3.1 Experimental details for **2** and **3**.

Crystal Data	**2**	**3**
Chemical formula	$C_{10}H_{10}Br_4Cu_4Mo_2P_6$	$C_{10}H_{10}Cu_2I_2Mo_2P_6$
M_r	1081.68	888.76
Crystal system, space group	triclinic, $P\bar{1}$	monoclinic, $C2/m$
Temperature (K)	123(1)	123
a, b, c (Å)	8.1892(4), 10.3010(5), 13.5161(6)	10.3181(5), 18.553(1), 10.3364(5)
α, β, γ (°)	77.009(4), 86.788(4), 67.230(4)	90, 92.952(5), 90
V (Å^3)	1023.80(9)	1976.08(19)
Z	2	4
F(000)	1000	1632
Radiation type	Mo K_α	Cu K_α
μ (mm^{-1})	13.54	41.72
Crystal color and shape	black plate	black plate
Crystal size (mm)	0.28 × 0.07 × 0.01	0.13 × 0.06 × 0.01
Data collection		
Diffractometer	SuperNova, Single source at offset, Eos diffractometer	SuperNova, Titan^{S2} diffractometer
Absorption correction	analytical	gaussian
T_{min}, T_{max}	0.198,0.894	0.065, 0.674
No. of measured, independent and observed [$I > 2\sigma(I)$] reflections	13687, 8496, 6645	5332, 1968, 1471
R_{int}	0.060	0.073
$(\sin\theta/\lambda)_{max}$ (Å^{-1})	0.703	0.624
Range of h, k, l	h = -11→11, k = -13→14, l = -18→18	h = -12→11, k = -23→21, l = -9→12
Refinement		
$R[F^2 > 2\sigma(F^2)]$, $wR(F^2)$, S	0.060, 0.165, 1.04	0.068, 0.182, 1.00
No. of reflections	8496	1968
No. of parameters	254	124
No. of restraints	92	1
H-atom treatment	H-atom parameters constrained	H-atom parameters constrained
$\Delta\rangle_{max}$, $\Delta\rangle_{min}$ (e Å^{-3})	1.92, -2.60	3.25, -2.06

3.5 Author Contributions

- The syntheses and characterization of **2** and **3** were performed by Claudia Heindl
- X-ray structural analyses of **2** and **3** were performed by Dr. Eugenia V. Peresypkina, Dr. Alexander V. Virovets and Claudia Heindl

- The manuscript (introduction, results and discussion, experimental part; including figures and graphical abstract) was written by Claudia Heindl; with the following exceptions:
- The section 'crystallographic details' was written by Dr. Eugenia V. Peresypkina
- The MAS NMR investigations and DFT computations on **2** and **3** as well as their description and figures were performed by David Lüdeker and PD Dr. Gunther Brunklaus.

3.6 References

[1] R. Hoffmann, *Angew. Chem. Int. Ed.* 1982, *21*, 711.

[2] G. Maerkl, *Angew. Chem.* 1966, *78*, 907.

[3] a) T. N. Minh, A. F. Hegarty, *J. Chem. Soc., Chem. Commun.* 1986, 383; b) S. Nagase, K. Ito, *Chem. Phys. Lett.* 1986, *126*, 43; c) D. S. Warren, B. M. Gimarc, *J. Am. Chem. Soc.* 1992, *114*, 5378; d) P. v. R. Schleyer, H. Jiao, N. J. R. van Eikema Hommes, V. G. Malkin, O. Malkina, *J. Am. Chem. Soc.* 1997, *119*, 12669; e) S. Sakai, *J. Phys. Chem. A* 2002, *106*, 10370; f) J. J. Engelberts, R. W. A. Havenith, J. H. Van Lenthe, L. W. Jenneskens, P. W. Fowler, *Inorg. Chem.* 2005, *44*, 5266; g) S. C. A. H. Pierrefixe, F. M. Bickelhaupt, *Aust. J. Chem.* 2008, *61*, 209.

[4] O. J. Scherer, H. Sitzmann, G. Wolmershäuser, *Angew. Chem.* 1985, *97*, 358.

[5] O. J. Scherer, J. Schwalb, H. Swarowsky, G. Wolmershäuser, W. Kaim, R. Gross, *Chem. Ber.* 1988, *121*, 443.

[6] a) O. J. Scherer, J. Vondung, G. Wolmershäuser, *Angew. Chem.* 1989, *101*, 1395; b) A. C. Reddy, E. D. Jemmis, O. J. Scherer, R. Winter, G. Heckmann, G. Wolmershäuser, *Organometallics* 1992, *11*, 3894.

[7] M. Fleischmann, C. Heindl, M. Seidl, G. Balázs, A. V. Virovets, E. V. Peresypkina, M. Tsunoda, F. P. Gabbaï, M. Scheer, *Angew. Chem. Int. Ed.* 2012, *51*, 9918.

[8] O. J. Scherer, H. Swarowsky, G. Wolmershäuser, W. Kaim, S. Kohlmann, *Angew. Chem.* 1987, *99*, 1178.

[9] a) F. Dielmann, C. Heindl, F. Hastreiter, E. V. Peresypkina, A. V. Virovets, R. M. Gschwind, M. Scheer, *Angew. Chem. Int. Ed.* 2014, *53*, 13605; b) B. P. Johnson, F. Dielmann, G. Balázs, M. Sierka, M. Scheer, *Angew. Chem. Int. Ed.* 2006, *45*, 2473; c) M. Scheer, L. Gregoriades, J. Bai, M. Sierka, G. Brunklaus, H. Eckert, *Chem. Eur. J.* 2005, *11*, 2163; d) J. Bai, A. V. Virovets, M. Scheer, *Science* 2003, *300*, 781.

[10] F. Dielmann, Dissertation thesis (Universität Regensburg) 2011.

[11] L. Gregoriades, Dissertation thesis (Universität Regensburg) 2006.

[12] a) D. Luedeker, G. Brunklaus, *Solid State Nucl. Magn. Reson.* 2015, *65*, 29; b) T. Wiegand, D. Luedeker, G. Brunklaus, K. Bussmann, G. Kehr, G. Erker, H. Eckert, *Dalton Trans.* 2014, *43*, 12639; c) M. Khan, V. Enkelmann, G. Brunklaus, *J. Org. Chem.* 2009, *74*, 2261.

[13] a) P. Pyykkö, M. Atsumi, *Chem. Eur. J.* 2009, *15*, 186; b) P. Pyykkö, M. Atsumi, *Chem. Eur. J.* 2009, *15*, 12770.

[14] A. E. Bennett, C. M. Rienstra, J. M. Griffiths, W. Zhen, P. T. Lansbury, R. G. Griffin, *J. Chem. Phys.* 1998, *108*, 9463.

[15] a) C. Adamo, V. Barone, *J. Chem. Phys.* 1999, *110*, 6158; b) D. E. Woon, T. H. Dunning, *J. Chem. Phys.* 1993, *98*, 1358.

[16] D. Massiot, F. Fayon, M. Capron, I. King, S. Le Calvé, B. Alonso, J. O. Durand, B. Bujoli, Z. Gan, G. Hoatson, *Magn. Reson. Chem.* 2002, *40*, 70.

[17] Gaussian 09, Revision A.02., M. J. Frisch, G. W. Trucks, H. B. Schlegel, G. E. Scuseria, M. A. Robb, J. R. Cheeseman, G. Scalmani, V. Barone, B. Mennucci, G. A. Petersson, H. Nakatsuji, M. Caricato, X. Li, H. P. Hratchian, A. F. Izmaylov, J. Bloino, G. Zheng, J. L. Sonnenberg, M. Hada, M. Ehara, K. Toyota, R. Fukuda, J. Hasegawa, M. Ishida, T. Nakajima, Y. Honda, O. Kitao, H. Nakai, T. Vreven, J. A. Montgomery, Jr., J. E. Peralta, F. Ogliaro, M. Bearpark, J. J. Heyd, E. Brothers, K. N. Kudin, V. N. Staroverov, R. Kobayashi, J. Normand, K. Raghavachari, A. Rendell, J. C. Burant, S. S. Iyengar, J. Tomasi, M. Cossi, N. Rega, J. M. Millam, M. Klene, J. E. Knox, J. B. Cross, V. Bakken, C. Adamo, J. Jaramillo, R. Gomperts, R. E. Stratmann, O. Yazyev, A. J. Austin, R. Cammi, C. Pomelli, J. W. Ochterski, R. L. Martin, K. Morokuma, V. G. Zakrzewski, G. A. Voth, P. Salvador, J. J. Dannenberg, S. Dapprich, A. D. Daniels, O. Farkas, J. B. Foresman, J. V. Ortiz, J. Cioslowski, D. J. Fox, gaussian, Inc., Wallingford CT, (2009).

[18] G. M. Sheldrick. *Acta Cryst. sect. C* 2015, *C71*, 3.

4. Unexpected Fragmentations of Triphosphaferrocene – Formation of Supramolecular Assemblies Containing the (1,2,4-$P_3C_2Mes_2$)$^-$ Ligand

C. Heindl, A. Kuntz, E. V. Peresypkina, A. V. Virovets, M. Zabel, D. Lüdeker, G. Brunklaus, M. Scheer, *Dalton Trans.* 2015, *44*, 6502-6509. Reproduced by permission of The Royal Society of Chemistry, which can be viewed online.

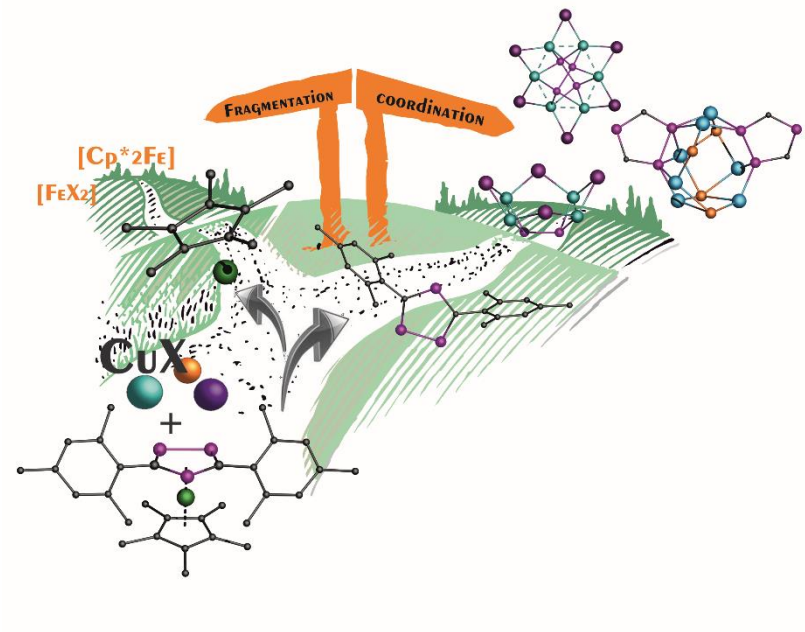

Abstract:

While reacting the sterically demanding triphosphaferrocene [Cp*Fe(η^5-$P_3C_2Mes_2$)] (**1**) with Cu(I) halides, the sandwich complex undergoes an unprecedented fragmentation into decamethylferrocene, FeX_2 (X = Cl, Br, I) and [$P_3C_2Mes_2$]$^-$ units. Subsequently, these phospholyl ligands act as versatile, negatively charged building blocks for the formation of supramolecular aggregates representing monomeric, dimeric and polymeric (1D and 2D) coordination compounds. They all bear rather non-typical structural motifs within the large varieties of the copper halide chemistry. Beside the X-ray structural analyses, the obtained assemblies were also characterized in solution in which they undergo fragmentation and re-aggregation processes.

4.1 Introduction

Ferrocene [Fe(η^5-C_5H_5)$_2$] is one of the fundamental molecules in organometallic chemistry and until now the flood of publications devoted to its chemical properties does not stop. Apart from its use as a reference redox system (Fc/Fc^+),[1] chiral ferrocene-based ligands represent important classes of auxiliaries in asymmetric homogeneous catalysis.[2] Based on the isolobal principle the substitution of one up to six methine moieties by phosphorus atoms is possible, which gives rise to the class of phosphaferrocenes.[3] These 18 VE sandwich complexes turned out to be very stable and, in contrast to ferrocene, the lone pairs of the P atoms enable them to be excellent building blocks in coordination and supramolecular chemistry.[4] Therefore new perspectives for the synthesis of phosphorus-based oligomers and polymers open up.

For the aggregation of these organometallic moieties we have broadly used Cu(I) halides.[5] To combine the central role of copper in catalysis[6] with the potential of phosphaferrocenes in this area,[3b] it is of special interest to accumulate copper halides by phosphaferrocenes. For such a purpose the 1,2,4-triphosphaferrocenes [Cp^{R}Fe(η^5-$P_3C_2{}^tBu_2$)] (Cp^R = Cp, Cp*, Cp'''; Cp* = C_5Me_5; Cp''' = $C_5H_2{}^tBu_3$) with three possible coordination sites is suited very well. Recently, we have shown that their coordination behavior strongly depend on the steric demand of the adjacent Cp^R ring and the nature of the halide.[7]

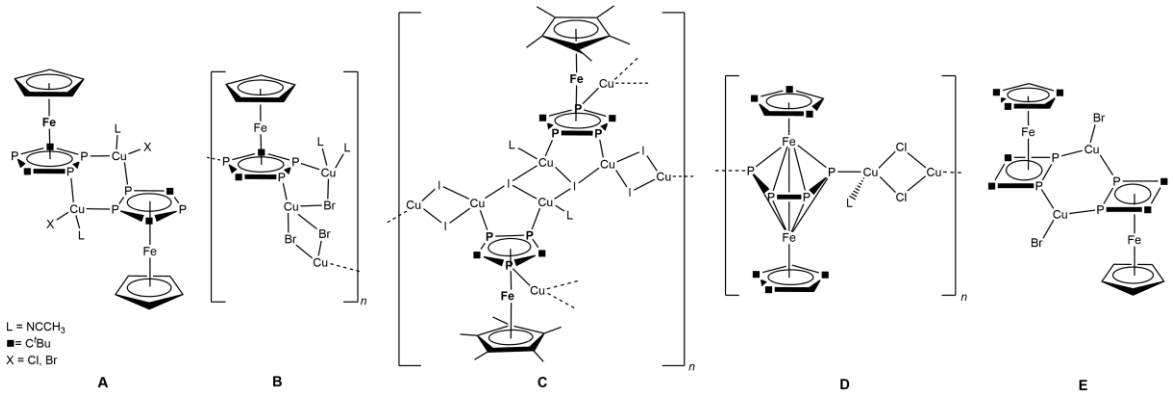

Figure 4.1 Selected coordination compounds of triphosphaferrocenes [Cp^{R}Fe(η^5-$P_3C_2{}^tBu_2$)] (Cp^R = Cp, Cp*, Cp''') and Cu(I) halides.

A selection of the obtained structural motifs is shown in *Figure 4.1*. Using less bulky Cp^R ligands (Cp^R = Cp, Cp*) the coordination of two or even three phosphorus atoms leads to the formation of dimeric (**A**) and polymeric compounds (**B** and **C**).[7a,b] However, the use of Cp''' entails a much higher steric demand of the triphosphaferrocene, hence different products could be obtained. Beside the formation of a complex similar to **A**, two unexpected fragmentation reactions of the $P_3C_2{}^tBu_2$ ring took place. Treating [Cp'''Fe(η^5-$P_3C_2{}^tBu_2$)] with an excess of CuCl a polymeric chain containing the triple decker moieties [(FeCp''')$_2$(μ,$\eta^{4:4}$-P_4)] is formed (**D**).[7c] In **D**, formally a C_2P moiety was replaced

by two phosphorus atoms. In contrast, in the resulting diphosphacyclobutadiene ring in **E** a formal elimination of a P atom occurred.[7a]

Since the substitution pattern of the Cp^R ligand seems to play a determining role, the question arises, whether a change of the steric demand of the triphospholyl ligand itself would cause consequences. Hence, instead of the *tert*-butyl groups, we decided to use [Cp*Fe{η^5-(1,2,4-$P_3C_2Mes_2$)}] (Mes = 2,4,6-trimethylphenyl) (**1**)[8] with two sterically even more demanding mesityl groups next to the phosphorus atoms and explore its coordination behavior towards Cu(I) halides.

Herein we report on the unexpected fragmentation of **1** by the reaction with CuX (X = Cl, Br, I) yielding a large diversity of unprecedented coordination compounds and show the usefulness of the formed $[P_3C_2Mes_2]^-$ five-membered ring as a building block for extended structures in:
$[(\mu,\eta^{1:2:2}\text{-}P_3C_2Mes_2)(\mu,\eta^{1:3:3}\text{-}P_3C_2Mes_2)\{Cu_7(CH_3CN)_7(\mu_4\text{-}X)(\mu_3\text{-}X)_2(\mu\text{-}X)\}\{Cu_2(\mu_2\text{-}X)_2X\}\{Cu(CH_3CN)(\mu_2\text{-}X)\}]_2 \cdot 6\ CH_3CN$ (**2** · 6 CH_3CN: X = Cl, **3** · 6 CH_3CN: X = Br),
$[(\mu,\eta^{1:2:3}\text{-}P_3C_2Mes_2)_2\{Cu(CH_3CN)\}_6(\mu\text{-}Br)_2(\mu_3\text{-}Br)_2\{Cu(CH_3CN)_2Br\}_2] \cdot CH_3CN$ (**4a** · CH_3CN),
$[(\mu,\eta^{1:1:2}\text{-}P_3C_2Mes_2)_3(\mu,\eta^{1:2:3}\text{-}P_3C_2Mes_2)\{Cu_5(CH_3CN)_5(\mu_2\text{-}Br)\}\{Cu(CH_3CN)_2CuBr_2\}_2\{Cu(CH_3CN)_2\}]_n[CuBr_2]_n \cdot 2\ CH_3CN$ (**5** · 2 CH_3CN),
$[(\mu,\eta^{1:2:2}\text{-}P_3C_2Mes_2)\{Cu(CH_3CN)(\mu\text{-}I)\}_4\{Cu(CH_3CN)_3\}] \cdot 0.5\ C_7H_8 \cdot 2.5\ CH_3CN$ (**6** · 0.5 C_7H_8 · 2.5 CH_3CN),
$[(\mu,\eta^{1:2:2}\text{-}P_3C_2Mes_2)Cu_7(CH_3CN)_4(\mu_4\text{-}I)_2(\mu_3\text{-}I)_2(\mu\text{-}I)_2]_n \cdot 2\ C_7H_8$ (**7** · 2 C_7H_8),
$[(\mu,\eta^{1:3:3}\text{-}P_3C_2Mes_2)\{Cu(CH_3CN)_3\}_2\{Cu(\mu\text{-}I)\}_6] \cdot 0.5\ CH_2Cl_2 \cdot 3\ CH_3CN$ (**8** · 0.5 CH_2Cl_2 · 3 CH_3CN) and
$[Cp^*Fe(CH_3CN)_3]_n[(\mu,\eta^{1:3:3}\text{-}P_3C_2Mes_2)_2\{Cu(CH_3CN)_2\}\{Cu(\mu\text{-}I)\}_6]_n \cdot 0.6\ CH_2Cl_2$ (**9** · 0.6 CH_2Cl_2).

4.2 Results and Discussion

Coordination behavior of 1 towards Cu(I) halides – Unexpected Fragmentation

The self-assembly process of **1** and CuX (X = Cl, Br, I) leads to different coordination compounds depending on the conditions applied. Surprisingly, the building block **1** always underwent cleavage. Out of the fragmentation products, only the 1,2,4-triphospholyl ligand remains in the isolated products, hence the $[Cp^*Fe]^+$ unit must have been split off. These fragments together with remaining halide anions might initially form the dimeric complex $[Cp^*Fe(\mu\text{-}X)]_2$ (X = Cl, Br, I), which displays a known intermediate and can even be isolated, when Cp^R ligands with a higher steric demand are used.[9] Since this compound is coordinatively unsaturated, it, in all probability, dissociates into $[Cp^*_2Fe]$ and $FeBr_2$. To support this assumption, the reaction mixtures were analyzed by ^{1}H NMR spectroscopy and mass spectrometry. In fact, a singlet at 1.64 ppm in the ^{1}H NMR spectra can be assigned for $[Cp^*_2Fe]$ and the EI mass spectra display peaks corresponding to

decamethylferrocene as well. In addition, the negative ion ESI mass spectra of the mother liquors exhibit peaks for $[FeCl_3]^-$ and $[FeBr_3]^-$, respectively.

Among the stable phosphaferrocenes the rather uncommon fragmentations are related to the cleavage of C-P bonds in the phospholyl ligands (**D** and **E**). Hence, the unexpected instability of **1** is unique and can most likely be attributed to the influence of the bulky mesityl ligand. This is confirmed by the existence of a stable $[P_3C_2Mes^*_2]$ (Mes* = 2,4,6-tri-*tert*-butylphenyl) radical, reported by Ionkin et al, by using the similar, sterically even more demanding Mes* moiety.[10]

Solid-State Characterization of the Coordination Compounds

All isolated coordination compounds contain the remaining negatively charged $[P_3C_2Mes_2]^-$ unit as a building block. So far, the cyclic 1,2,4-triphospholyl ligand was mainly used for the synthesis of (half-)sandwich complexes.[11] Its coordination behavior towards Lewis acids, especially coinage metal salts, has rather been neglected, although interesting coordination modes to gold centers have been observed by the reaction with $[(PPh_3)AuCl]$ and $[(PEt_3)AuCl]$, respectively.[12] However concerning Cu, to the best of our knowledge, only two reactions are known: Nixon *et al.* treated $K[P_3C_2{}^tBu_2]$ with Cu_2I_2 in presence of PMe_3, yielding the binuclear complexes $[\{P_3C_2{}^tBu_2\}\{Cu(PMe_3)_2\}_2I]$ and $[\{P_3C_2{}^tBu_2\}_2\{Cu(PMe_3)_2\}_2]$.[12b] Zenneck *et al.* succeeded in the synthesis of the versatile $[\{\eta^5\text{-}(P_3C_2{}^tBu_2)\}Cu(PPh_3)]$ complex.[13]

In general, Cu(I) halides display versatile building blocks in coordination chemistry, and therefore a large variety of different coordination compounds can be obtained. Since the structural motifs differ when different halides are used, they will be described separately.

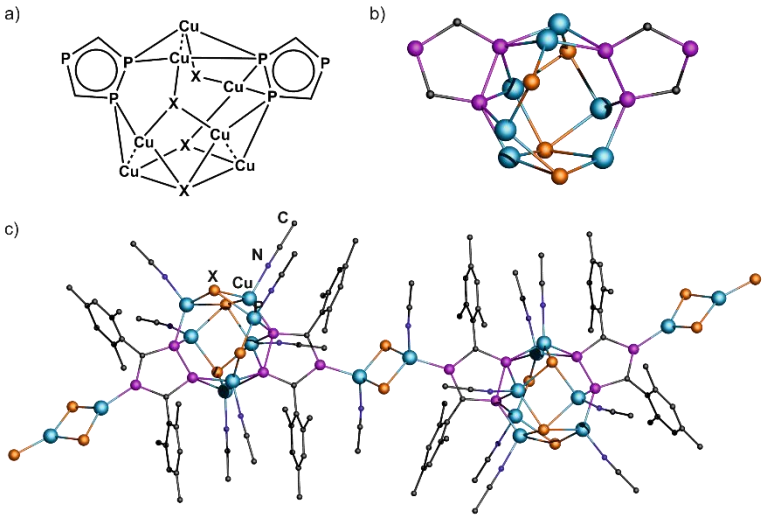

Figure 4.2 a) 'Cage' motif in **2** · 6 CH_3CN (X = Cl) and **3** · 6 CH_3CN (X = Br); b) section of the molecular structure of **2** · 6 CH_3CN illustrating the 'cage' motif; c) molecular structure of the dimer of **2** · 6 CH_3CN. H atoms and solvent molecules are omitted for clarity.

CuCl-containing Compound (2)

The reaction of **1** with CuCl selectively leads to the formation of the dimeric complex $[(\mu,\eta^{1:2:2}\text{-}P_3C_2Mes_2)(\mu,\eta^{1:3:3}\text{-}P_3C_2Mes_2)\{Cu_7(CH_3CN)_7(\mu_4\text{-}Cl)(\mu_3\text{-}Cl)_2(\mu\text{-}Cl)\}\{Cu_2(\mu_2\text{-}Cl)_2Cl\}\{Cu(CH_3CN)(\mu_2\text{-}Cl)\}]_2$ (**2**), which can be isolated as solvate **2** · 6 CH_3CN in quantitative yields (*Figure 4.2c*).

Compound **2** · 6 CH_3CN displays a dimer of two central $\{(P_3C_2Mes_2)_2Cu_7Cl_4\}$ cages (*Figure 4.2*a,b), which are bridged by a $\{Cu(CH_3CN)\}_2Cl_2$ four-membered ring formed by tetrahedrally coordinated copper ions. The unique P atom of the peripheral $P_3C_2Mes_2$ fragment is additionally coordinated at each side of the dimer by a terminal Cu_2Cl_3 fragment, in which the threefold-coordinated copper ions are in a triangular planar environment. In total, four $[P_3C_2Mes_2]^-$ rings and 16 Cl^- balance the positive charge of 20 Cu^+. The central structural motif can be described as an unprecedented cage of 15 inorganic atoms (4 P, 7 Cu, 4 Cl), consisting of one Cu ion and three Cu_2 dimers (2.546(1) Å - 2.617(1) Å), connected by a μ_2-Cl, two μ_3-Cl and one μ_4-Cl (2.303(1) Å – 2.840(1) Å). The unique phosphorus atom of the $[P_3C_2Mes_2]^-$ ligand is η^1-coordinated to copper (2.173(1) Å – 2.153(1) Å). On the other hand, the adjacent P atoms each show a η^2- and η^3-coordination with longer Cu–P distances to two Cu_2 dimers and two Cu_2 dimers and one unique Cu ion, respectively. The Cu-P distances involving Cu_2 dimers (2.221(1) Å – 2.406(1) Å) are systematically shorter than those to the unique Cu ion (2.419(1) Å – 2.501(1) Å) (see *Table 4.1*). The P_3C_2 rings of the phospholyl ligands are planar (deviation 0.01°) with the mesityl ligands rotated by 82.6° and 72.6° at the peripheral phospholyl rings and of 89.1° and 79.9° in the central ones, respectively. Thus, the rotation is much more distinctive than in **1** (46.07(1)° and 40.85(1)°, respectively),[8] most likely due to the absence of a Cp* ligand.

CuBr-containing Compounds (3-5)

Diffusion of a CH_3CN solution of CuBr into a CH_2Cl_2 solution of **1** leads to the crystallization of three different coordination compounds depending on the conditions applied: $[(\mu,\eta^{1:2:2}\text{-}P_3C_2Mes_2)(\mu,\eta^{1:3:3}\text{-}P_3C_2Mes_2)\{Cu_7(CH_3CN)_7(\mu_4\text{-}Br)(\mu_3\text{-}Br)_2(\mu\text{-}Br)\}\{Cu_2(\mu_2\text{-}Br)_2Br\}\{Cu(CH_3CN)(\mu_2\text{-}Br)\}]_2$ · 6 CH_3CN (**3** · 6 CH_3CN), $[(\mu,\eta^{1:2:3}\text{-}P_3C_2Mes_2)_2\{Cu(CH_3CN)\}_6(\mu_2\text{-}Br)_2(\mu_3\text{-}Br)_2\{Cu(CH_3CN)_2Br\}_2]$ · CH_3CN (**4a** · CH_3CN) and $[(\mu,\eta^{1:1:2}\text{-}P_3C_2Mes_2)_3(\mu,\eta^{1:2:3}\text{-}P_3C_2Mes_2)\{Cu_5(CH_3CN)_5(\mu_2\text{-}Br)\}\{Cu(CH_3CN)_2CuBr_2\}_2\{Cu(CH_3CN)_2\}]_n[CuBr_2]_n$ · 2 CH_3CN (**5** · 2 CH_3CN). If a molar ratio of **1**:CuBr = 1:2 is used, compound **5** · 2 CH_3CN is formed selectively, which is in agreement with the stoichiometric ratio of $(P_3C_2Mes_2)$:Cu = 1:2 in **5** · 2 CH_3CN. Excess of CuBr (1:5 or 1:10) therefore enables the assembly to **3** and **4**. However, since the ratio $(P_3C_2Mes_2)$:Cu is the same in **3** and **4** (1:5), a selective synthesis is rather difficult. Nonetheless a preferred crystallization of **4** · CH_3CN is achieved by applying more diluted and pure CH_3CN

solutions, while the use of more concentrated and CH_2Cl_2/CH_3CN solvent mixtures favors the crystallization of **3** · 6 CH_3CN. Compound **3** · 6 CH_3CN is isostructural to the Cl derivative **2** · 6 CH_3CN (*Figure 4.2*). The bond distances in **3** · 6 CH_3CN remain in a similar range despite the presence of the larger halogen anion (see *Table 4.1*).

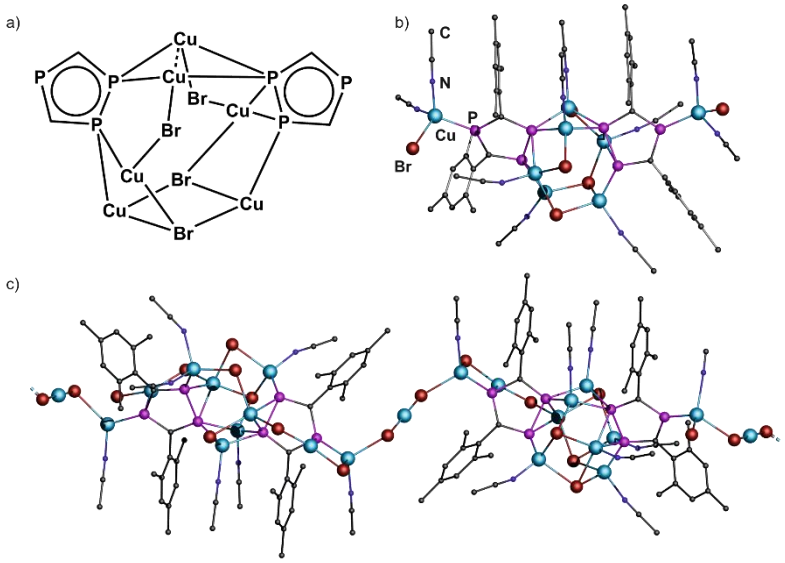

Figure 4.3 a) 'Cage' motif in **4a** · CH_3CN; b) molecular structure of **4a** · CH_3CN; c) section of the polymeric structure of **4b** · CH_3CN. H atoms and solvent molecules are omitted for clarity.

Surprisingly, the X-ray structural analysis of **4** · CH_3CN reveals a solid solution of different compounds attended with partial occupancies and complex disorder of the Cu, Br and CH_3CN positions. The monomeric compound $[(\mu,\eta^{1:2:3}\text{-}P_3C_2Mes_2)_2\{Cu(CH_3CN)\}_6(\mu_2\text{-}Br)_2(\mu_3\text{-}Br)_2\{Cu(CH_3CN)_2Br\}_2]$ (**4a** · CH_3CN) displays the structural fragment with major occupation (70%) (*Figure 4.3*b). The central cage motif in **4a** · CH_3CN is structurally related to those of the dimer **3** · 6 CH_3CN with one missing $\{Cu(CH_3CN)\}$ unit to give a formally neutral $\{(P_3C_2Mes_2)_2Cu_6Br_4\}$ cage (*Figure 4.3*a). This difference influences the connectivity and bond lengths, hence the Br ions connect the Cu ions in a μ_2-(2 Br) or a μ_3-fashion (2 Br) (2.431(1) Å – 2.592(1) Å), respectively. The coordination mode of the adjacent P atoms to Cu is also different, one is η^2-, the other η^3-coordinated within a more extensive range of the distances (2.202(2) Å – 2.521(2) Å). In **4a** · CH_3CN only one Cu_2 dimer is present with a distance of 2.533(1) Å compared to three dimers in **3**. The unique phosphorus atoms each coordinate a $\{Cu(CH_3CN)_2Br\}$ unit instead of the Cu_2Br_3 unit in **3** · 6 CH_3CN. Other similar structural fragments of the solid solution **4** · CH_3CN with minor occupation factors are possible, among them even the polymeric compound $[(P_3C_2Mes_2)_2Cu_{11}Br_9(MeCN)_7]_x$ (**4b** · CH_3CN) (occupation factor 10%) containing a linear coordinated Cu (Cu-Br: 2.226(4) Å) (*Figure 4.3*c) co-exists.

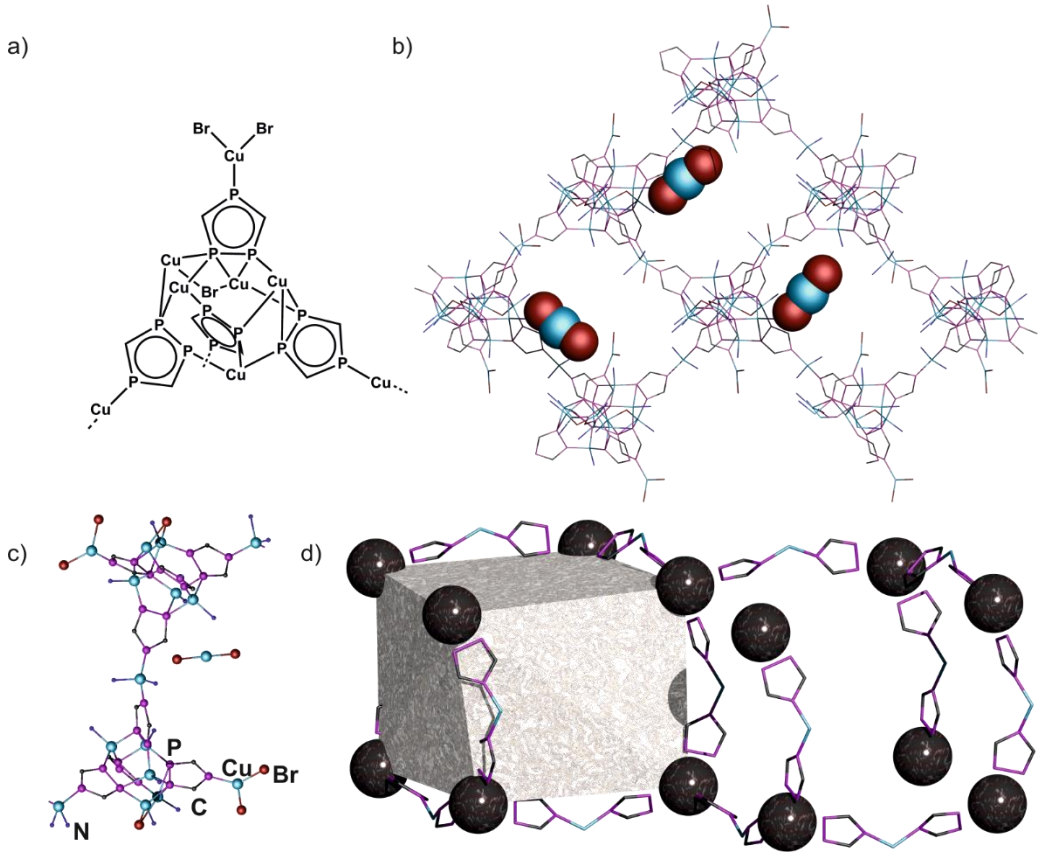

Figure 4.4 a) 'Cage' motif in **5** · 2 CH_3CN; b) section of the polymeric structure of **5** · 2 CH_3CN illustrating the mesh-like structure (view along the crystallographic *a* axis). The anions are displayed in the space-filling model, the network in 'wires and sticks'. H atoms, mesityl ligands and solvent molecules are omitted for clarity; c) repeating unit in **5** · 2 CH_3CN. H atoms, mesityl ligands and solvent molecules are omitted for clarity; d) schematic representation of the cube-like arrangement of a single layer in **5** · 2 CH_3CN.

Whereas with CuCl the used molar ratio does not influence the product formation, with CuBr **5** · 2 CH_3CN can be obtained selectively and reproducible, when less than five equivalents of CuBr are used. Its structural analysis reveals a 2D network, which is rather astonishing in consideration of the bulky mesityl substituents. A totally different cage motif again demonstrates the versatility of the phospholyl ligand and CuBr in coordination chemistry. The central core contains four [$P_3C_2Mes_2$] units (*Figure 4.4*a), whose adjacent P atoms coordinate two Cu_2 dimers (2.527(2) Å – 2.663(2) Å) and one single Cu in either an η^1- (3 P; 2.239(2) Å – 2.282(2) Å), η^2- (4 P; 2.282(2) Å – 2.538(2) Å) or an η^3- (1 P; 2.331(2) Å – 2.469(2) Å) coordination mode. In addition, one Br bridges two Cu atoms with a distance of 2.295(2) Å – 2.350(2) Å, resulting in a distorted tetrahedral environment for these Cu. One of the four unique P atoms is linked to a terminal {$CuBr_2$} unit with a trigonal planar Cu, which blocks further growth into this direction, while the other three coordinate a {$Cu(CH_3CN)_2$} unit, whereby polymerization is enabled. The repeating unit (two 'cages' plus the linking and terminal moieties) therefore consists of eight [$P_3C_2Mes_2$]$^-$, six Br^- and 15 Cu^+. Its remaining charge is balanced by a linear dibromocuprate counter ion [$CuBr_2$]$^-$ (*Figure 4.4*c). The 2D

network of **5** · 2 CH_3CN can be described as a sheet-like structure with porous layers. A single layer consists of 'cubes' out of four repeating units stringing together (*Figure 4.4*d). Since in one direction polymerization is hindered due to the terminal {$CuBr_2$} unit, four edges per cube are absent. The view along the crystallographic *a* axis illustrates the resulting mesh-like structure (*Figure 4.4*b). However, these meshes display no empty voids, but are occupied by the mesityl ligands and the counterion.

CuI-containing Compounds (6-9)

By combining **1** and CuI, products with two different very rare structural motifs of CuI units can be realized: the 'crown' (*Figure 4.5*a) and the 'hexagram' motif (*Figure 4.7*a). Both are found either in a monomeric coordination compound or in a 1D polymer: [(μ,$\eta^{1:2:2}$-$P_3C_2Mes_2$){Cu(CH_3CN)(μ_2-I)}$_4${Cu(CH_3CN)$_3$}] · 0.5 C_7H_8 · 2.5 CH_3CN (**6** · 0.5 C_7H_8 · 2.5 CH_3CN), [(μ,$\eta^{1:2:2}$-$P_3C_2Mes_2$)Cu_7(CH_3CN)$_4$(μ_4-I)$_2$(μ_3-I)$_2$(μ_2-I)$_2$]$_n$ · 2 C_7H_8 (**7** · 2 C_7H_8), [(μ,$\eta^{1:3:3}$-$P_3C_2Mes_2$){Cu(CH_3CN)$_3$}$_2${Cu(μ_2-I)}$_6$] · 0.5 CH_2Cl_2 · 3 CH_3CN (**8** · 0.5 CH_2Cl_2 · 3 CH_3CN) and [Cp*Fe(CH_3CN)$_3$]$_n$[(μ,$\eta^{1:3:3}$-$P_3C_2Mes_2$)$_2${Cu(CH_3CN)$_2$}{Cu(μ_2-I)}$_6$]$_n$ · 0.6 CH_2Cl_2 (**9** · 0.6 CH_2Cl_2).

A controlled and selective synthesis of one specific compound is a big challenge due to similar molar ratios in the products ($P_3C_2Mes_2$:Cu = 1:5, 1:7, 1:8 and 1:7 in **6**, **7**, **8** and **9**, respectively). However, it has never occurred that products with different structural motifs crystallize out of one sample. Hence, either the crystallization of one single compound or of mixtures of **6** · 0.5 C_7H_8 · 2.5 CH_3CN and **7** · 2 C_7H_8 or **8** · 0.5 CH_2Cl_2 · 3 CH_3CN and **9** · 0.6 CH_2Cl_2 can be obtained, respectively. Furthermore, the crystallization of solely **7** (polymer) is obtained when a pure CH_3CN solution is used. On the other hand, pure **6** · 0.5 C_7H_8 · 2.5 CH_3CN (monomer) crystallizes by applying CH_2Cl_2/CH_3CN solvent mixtures or more diluted conditions, which has been proved reproducible. Additionally an excess of **1** is conducive, since in **6** · 0.5 C_7H_8 · 2.5 CH_3CN the lowest Cu content is present. Unfortunately, the formation of **9** has only been observed on very rare occasions together with **8** · 0.5 CH_2Cl_2 · 3 CH_3CN. Several attempts to reproduce this compound only resulted in the selective isolation of **8** · 0.5 CH_2Cl_2 · 3 CH_3CN, independent of the solvents and crystallization procedures.

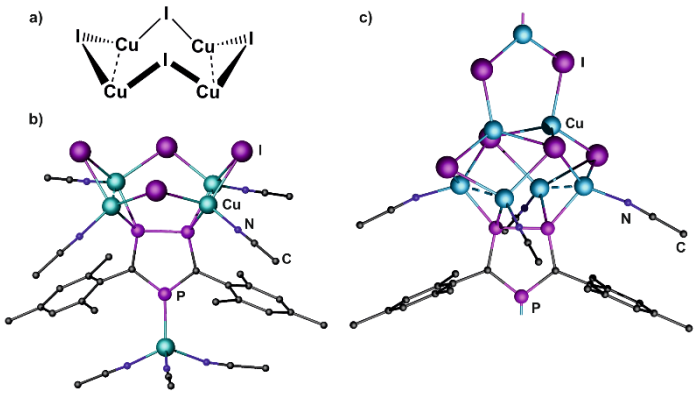

Figure 4.5 a) 'Crown' structural motif in **6** · 0.5 C_7H_8 · 2.5 CH_3CN and **7** · 2 C_7H_8; b) molecular structure of **6** · 0.5 C_7H_8 · 2.5 CH_3CN; c) repeating unit of the polymeric structure of **7**. H atoms and the minor position of the disordered mesityl ligand are omitted for clarity.

The 'crown' motif in **6** · 0.5 C_7H_8 · 2.5 CH_3CN consists of an eight-membered $\{Cu_4I_4\}$ ring which is significantly distorted by the presence of two opposed Cu_2 dimers (2.556(1) Å – 2.561(1) Å) which are separated by 4.030(1) Å – 4.032(1) Å one from another (*Figure 4.5*b). The copper atoms of each dimer are coordinated by the adjacent P atoms of the phospholyl ligands (2.292(1) Å – 2.313(1) Å). In contrast, the third P atom again shows a η^1-coordination to a single Cu ion revealing a shorter bond length of 2.217(1) Å, as it was observed in the previous discussed compounds (for a comparison of selected bond lengths see *Table 4.1*). The tetrahedral coordination of Cu is accomplished by CH_3CN ligands. The presence of five Cu^+, four I^- and one $[P_3C_2Mes_2]^-$ ligand affords charge balance.

By formally replacing three CH_3CN ligands at the terminal Cu ion by two CuI fragments, **6** serves as repeating unit for the 1D polymer **7** · 2 C_7H_8 (*Figure 4.5*c, *Figure 4.6*). The geometry of the 'crown' fragment retains similar Cu-P (2.235(2) Å – 2.428(3) Å) and Cu-I distances (2.657(2) Å – 2.864(2) Å), but the Cu···Cu separations became significantly more uniform, 2.688(2) Å and 3.664(2) Å (*Table 4.1*), respectively. To bridge these units, an additional five-membered $\{Cu_3I_2\}$ ring is formed, and another Cu_2 dimer (Cu···Cu 2.876(1) Å) coordinates an iodide of the 'crown'. In **7**, the iodine atoms do not bridge only two Cu ions as in **6** · 0.5 C_7H_8 · 2.5 CH_3CN, but show a μ_3- and μ_4-coordination mode, respectively. A neutral coordination polymer results, since the repeating unit contains seven Cu^+, six I^- and one $[P_3C_2Mes_2]^-$ ligand. The rotation of the mesityl ligands with respect to the phospholyl plane is comparable to **2** · 6 CH_3CN with angles of 89.5° in **7** · 2 C_7H_8 and 84.1° and 83.8° in **6** · 0.5 C_7H_8 · 2.5 CH_3CN, respectively.

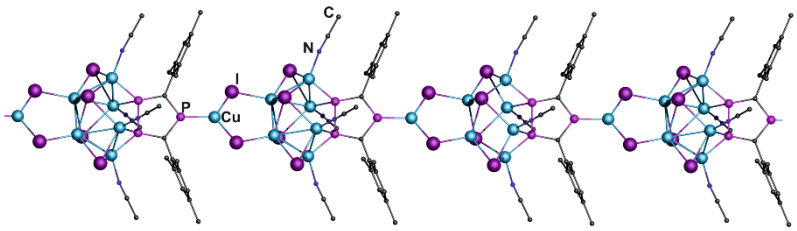

Figure 4.6 Section of the polymeric structure of **7** · 2 C_7H_8. H atoms, disorder and solvent molecules are omitted for clarity.

The $\{Cu_4I_4\}$ 'crown' motif in **6** and **7** is uncommon, since this number of CuI units usually prefers a cubane- or step-like arrangement.[14] Its formation was only observed once by Sugimoto *et al.* and in this case the copper ions are coordinated by sulfur atoms.[15]

Among the large variety of CuX (X = Cl, Br, I) coordination compounds in the literature, only one example is known for the 'hexagram' structural motif: $[\{(triphos)\text{-}CoP_3\}_2\{CuBr\}_6]$ (triphos = $MeC(CH_2PPh_2)_3$).[16] Hence, **8** and **9** represent the first examples with an iodine-containing hexagonal core.

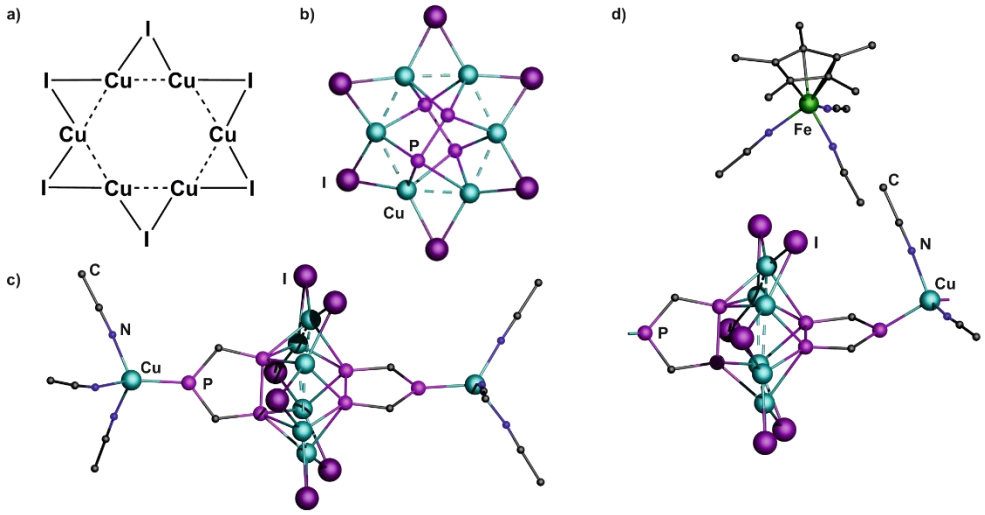

Figure 4.7 a) 'Hexagram' structural motif in **8** · 0.5 CH_2Cl_2 · 3 CH_3CN and **9** · 0.6 CH_2Cl_2; b) section of the molecular structure of **8** · 0.5 CH_2Cl_2 · 3 CH_3CN (top view) illustrating the 'hexagram' motif; c) molecular structure of **8** · 0.5 CH_2Cl_2 · 3 CH_3CN; d) repeating unit of the polymeric structure of **9** · 0.6 CH_2Cl_2. H atoms, mesityl ligands and solvent molecules are omitted for clarity.

The central almost planar Cu_6 ring (deviation 0.12 Å) is coordinated by two phospholyl ligands, which are rotated to each other by 66.6° (*Figure 4.7*b). Each of the adjacent P atoms shows a η^3-coordination mode towards Cu with bond lengths of 2.304(4) Å – 2.820(4) Å. As in the case of the Cu_2 dimers in **2**-**7**, Cu···Cu interactions may be considered in **8** · 0.5 CH_2Cl_2 · 3 CH_3CN as well, since the Cu···Cu distances are in the range of 2.471(3) – 2.553(3) Å.[17] Six I^- ions bridge these edges in a μ_2-fashion (2.550(2) – 2.627(2) Å) so that a distorted 'hexagram' structural motif is formed. This

core structure is completed by two terminal {Cu(CH_3CN)$_3$} units, which are coordinated by the remaining P atoms (*Figure 4.7*c). With eight Cu^+, six I^- and two $[P_3C_2Mes_2]^-$ ligands **8** · 0.5 CH_2Cl_2 · 3 CH_3CN also displays a neutral molecular complex.

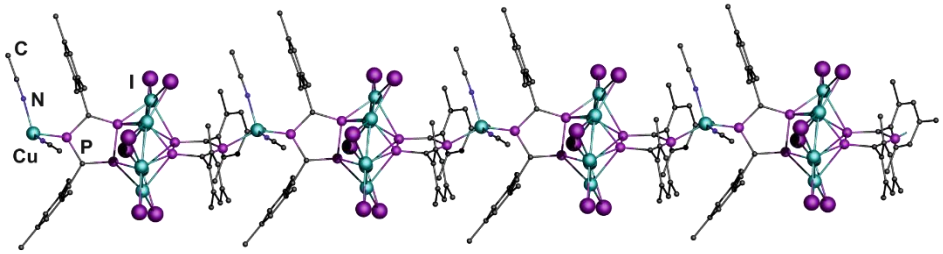

Figure 4.8 Section of the anionic polymeric structure of **9**. H atoms and minor disordered components are omitted for clarity.

Removing formally one {Cu(CH_3CN)$_3$} unit and CH_3CN ligand from different sides of the molecular complex **8**, the resulting complex forms the negatively charged repeating unit of the 1D polymer **9** · 0.6 CH_2Cl_2 without significant changes concerning the 'hexagram' motif (*Figure 4.7*d, *Figure 4.8*). The Cu-Cu and Cu-I bond lengths vary in ranges of 2.454(2) Å – 2.535(2) Å and 2.537(1) Å – 2.617(1) Å, respectively. The Cu-P bonds are slightly shorter within the range of 2.251(2) Å –2.778(2) Å (for a comparison of selected bond lengths see *Table 4.1*). Surprisingly, [Cp*Fe(CH_3CN)$_3$]$^+$ turned out to act as counter ion, which is known as an extremely water-sensitive complex with very labile acetonitrile ligands.[18] Hence, another reaction pathway of the [Cp*Fe]$^+$ cation aforesaid becomes apparent in this case, namely the accomplishment of the free coordination sites by acetonitrile ligands.

Table 4.1 Selected bond lengths [Å] of **2-9**. Ranges of bond lengths are given whenever more than one bond is present in the asymmetric unit.

	X	Cu···Cu	Cu-P_{unique}	Cu_{dimer}-P	Cu_{unique}-P	Cu-X
2	Cl	2.564(1) – 2.617(1)	2.153(1) – 2.173(1)	2.221(1) – 2.406(1)	2.419(1) – 2.501(1)	2.303(1) – 2.840(1)
3	Br	2.531(1) – 2.599(1)	2.169(2) – 2.189(2)	2.230(2) – 2.386(2)	2.420(2) – 2.514(2)	2.291(1) – 2.660(1)
4a	Br	2.533(1)	2.219(2)	2.202(2) – 2.521(2)	2.202(2) – 2.521(2)	2.431(1) – 2.592(1)
5	Br	2.527(2) – 2.663(2)	2.239(2) – 2.282(2)	2.239(2) – 2.538(2)	2.266(3) – 2.373(3)	2.295(2) – 2.350(2)
6	I	2.556(1) – 2.561(1)	2.217(1)	2.292(1) – 2.313(1)	-	2.633(1) – 2.694(1)
7	I	2.688(2) – 2.876(1)	2.191(3)	2.235(2) – 2.428(3)	-	2.657(2) – 2.864(2)
8	I	2.471(3) – 2.553(3)	2.202(4) – 2.218(4)	2.304(4) – 2.820(4)	-	2.550(2) – 2.627(2)

9	I	2.454(2) – 2.535(2)	2.256(2)	2.251(2) – 2.778(2)	-	2.537(1) – 2.617(1)

Spectroscopic characterization of the products

All obtained compounds **2**-**9** are completely insoluble in non-polar solvents like *n*-hexane or toluene as well as in more polar solvents like CH_2Cl_2 and Et_2O. But they all show solubility in CH_3CN up to a certain degree, which enables their characterization in solution by NMR spectroscopy as well as by mass spectrometry. The solubility decreases when going to the heavier halides, but the lowest solubility is found for **5** due to its 2D polymeric structure (characterization in solution by ^1H and mass spectrometry only). The $^{31}P\{^1H\}$ NMR spectrum of **3** in CD_3CN shows four very broad signals at δ = 136, 160, 204 and 217 ppm with integral ratios of 4:6:3:2. The broadening of the signals implies that the coordination of the P atoms to Cu (nuclear spin I = 3/2) is still present in solution. Compared to **1** (δ = 73.2 ppm),[8] the signals show a strong downfield shift, though this comparison is hampered, since no coordination to Fe is present in the product. In contrast, the signals of **3** are shifted to higher field when compared to the free phospholyl ligand in $K[P_3C_2Mes_2]$ (δ = 261.7 and 266.4 ppm).[8] This is in agreement with the observations made for other coordination compounds starting from different P_n ligand complexes and Cu(I) halides.[19] However, to explain the integral ratios of the observed signals, one must assume the presence of two different compounds in solution. In addition, the $^{31}P\{^1H\}$ NMR spectrum of freshly dissolved crystals of pure **4** · CH_3CN surprisingly looks exactly the same with minimal differences in the integral ratio (δ = 135, 160, 205 and 217 ppm with integral ratios of 4:5:2.5:2). Since elemental analyses confirm the purity of the respective products, these results imply dynamic dis- and re-assembly behavior in solution.

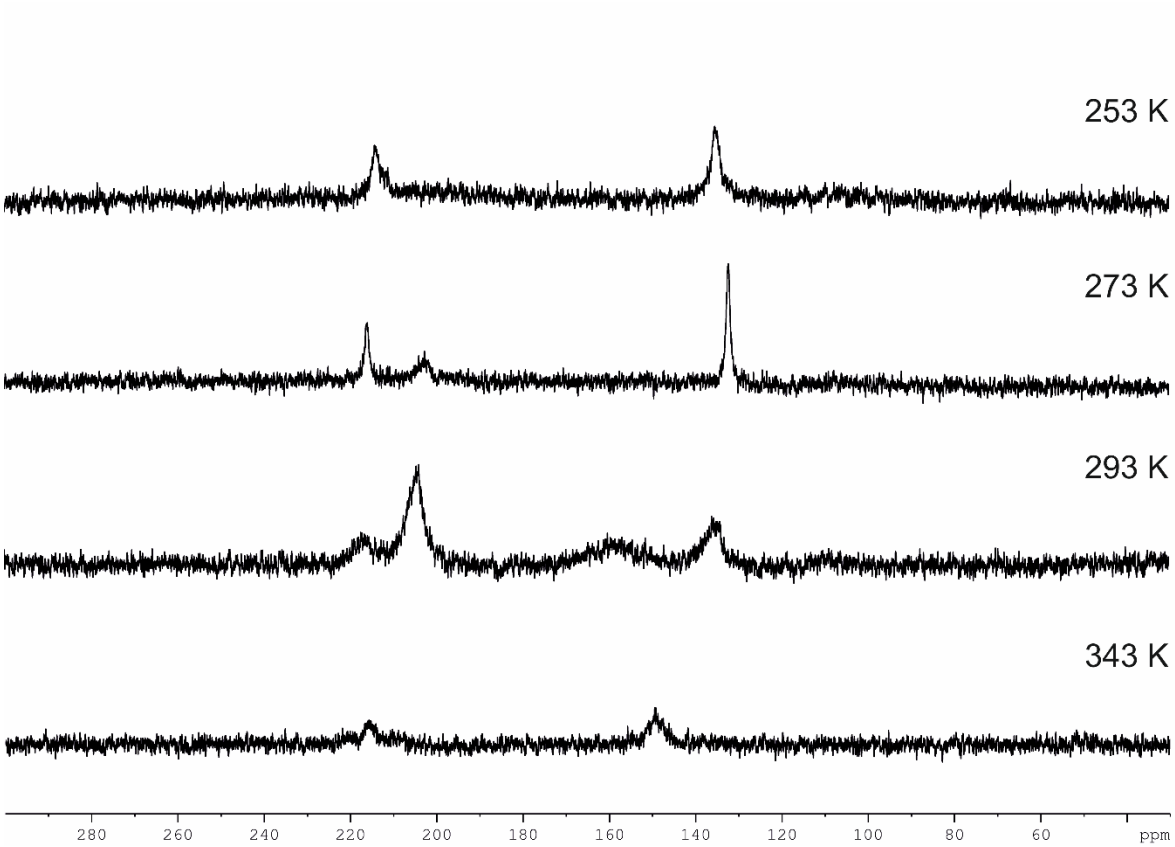

Figure 4.9 VT $^{31}P\{^1H\}$ NMR of freshly dissolved crystals of **3**.

In addition, for a plausible assignment variable temperature $^{31}P\{^1H\}$ NMR spectra of crystals of **3** · 6 CH_3CN were recorded (*Figure 4.9*). Upon cooling to 273 K the outer signals at δ = 135 and 217 ppm get sharpened and increase by intensity. In contrast, the intensity of the inner signals at δ = 160 and 204 ppm decrease and the signals vanish completely upon further cooling to 253 K. The opposite effect, namely the disappearance of the outer signals, is monitored when the sample is heated to 343 K. Therefore the inner signals can be attributed to a rather small, monomeric unit, since its formation requires bond dissociations, which are forced by higher temperatures. In contrast, cooling favors the existence of larger aggregates, hence the outer signals are assigned to dimeric or oligomeric coordination compounds. The values for the integral ratios are in accordance with this, each group being 2:1 for the adjacent and the unique P atoms, respectively. These dynamic processes are further confirmed by mass spectrometry. In the received positive ion ESI spectra many different fragments from $[\{P_3C_2Mes_2\}Cu_5Br_3\{CH_3CN\}]^+$ up to $[\{P_3C_2Mes_2\}_4Cu_{17}Br_{12}]^+$ can be identified.

The behavior in solution does not depend on the used halide, since the same observations were made for compounds **2** and **6**-**9**. Interestingly, the $^{31}P\{^1H\}$ NMR spectrum of dissolved crystals of **2** also looks similar like compound **3**, but after many attempts no second compound could be isolated, most probably due to the preferred crystallization of **2**.

Furthermore, it should be noted that in the $^{31}P\{^1H\}$ NMR spectra of the CuI-containing assemblies **6**-**9** the signals exhibit the same chemical shift like **2**-**4** despite their different structural motifs in the solid state: 'crown' (**6**,**7**) and 'hexagram' (**8**,**9**) motif compared to the 'cage' motif (**2**-**4**). However, the quality of the received spectra is initially quite poor caused by the low solubility so that the extremely broad signals start to disappear into the noise through coordination to Cu. Similar association processes in solution can again be proposed by means of the ESI mass spectra, which show peaks at higher mass numbers than the molecular weight in the solid state. For example, in the spectrum of the monomeric compound **6** the fragment $[\{P_3C_2Mes_2\}_4Cu_{11}I_6]^+$ is observed.

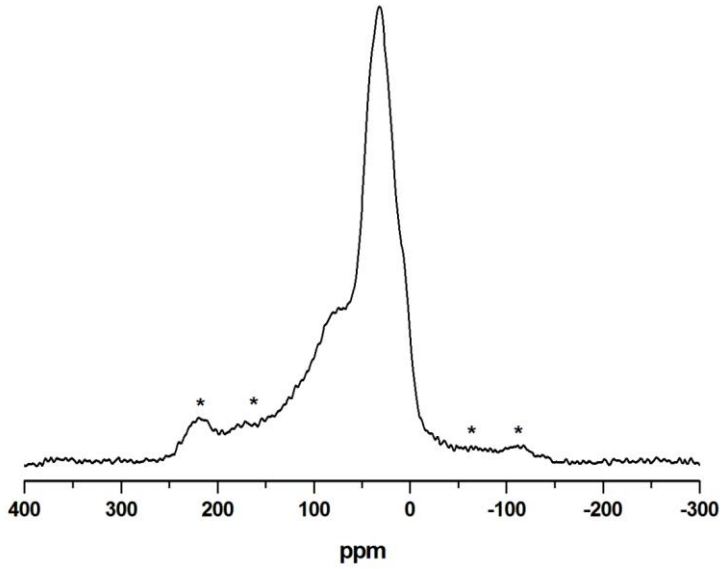

Figure 4.10 $^{31}P\{^1H\}$ MAS NMR spectrum of **6**, recorded at 202.48 MHz (11.7 T) and 29762 Hz MAS using a commercially available Bruker 2.5 mm HXY triple-resonance probe. The data were obtained using a rotor-synchronized Hahn-Echo (t_R = 33.6µs), 8196 scans were acquired at a relaxation delay of 10s and a rf-field strength of 100 kHz (π/2-pulse of 2.5µs). Spinning sidebands are marked with asterisks.

Due to its limited solubility, ^{31}P and ^{65}Cu MAS NMR spectra were acquired for compound **6**. Despite the rather high spinning frequency of 30 kHz, the $^{31}P\{^1H\}$ MAS NMR spectrum of **6** exhibits two broad featureless signals at 31.8 and 82.6 ppm with an integrated area ratio of about 2 : 1 in good agreement with the molecular structure of **6** (*Figure 4.10*). In comparison to reported data of copper-coordinated phosphorus cage compounds,[20] all peaks are noticeably shifted to lower ppm values, reminiscent of $Cu_3P_3I_2$ in which the polymeric phosphorus tube is coordinated by more flexible copper iodide ligands.[21] The presence of spinning sidebands in the ^{31}P MAS NMR spectrum indicates substantial ^{31}P chemical shift anisotropy typically observed in cases of locally distorted symmetry, e.g. imposed by the various ligands coordinated to phosphorus atoms. Any lineshape splitting due to ^{31}P-$^{63,65}Cu$ heteronuclear scalar interactions (*J*-couplings) could not be resolved at the applied magnetic fields (4.7 and 11.7 T), most likely owing to ^{31}P-$^{63,65}Cu$ residual dipolar

couplings.[22] The ^{65}Cu MAS NMR spectrum of **6** (*Figure 4.11*) is dominated by a gaussian-shaped peak at 5.5 ppm, where the estimated quadrupolar coupling constant of $C_Q \approx 0.9$ MHz is comparable the coupling constant determined for purified solid copper(I) iodide, reflecting reasonable local symmetry such as tetrahedral coordination. Therefore, this peak is tentatively attributed to the copper atom coordinated to the single phosphorus atom rather than the P_2-'dumbbell'. In contrast, the copper atoms comprising the highly distorted 'crown' motif are attributed to the weak featureless shoulders recognized in the region around -23 ppm.

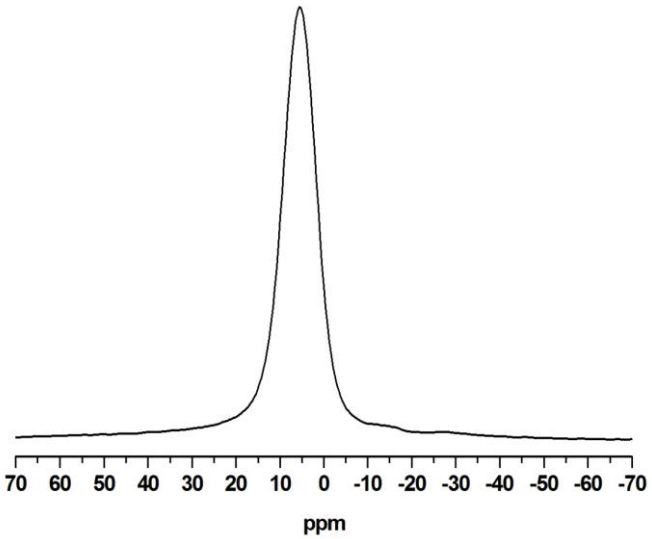

Figure 4.11 ^{65}Cu MAS NMR spectrum of **6**, acquired at 142.02 MHz (11.7 T) and 20 kHz MAS using a commercially available Bruker 2.5 mm HXY triple-resonance probe averaging 189.000 Scans at a relaxation delay of 100 ms and a $\pi/12$-pulse of 0.5 µs (rf-field strength of 83.3 kHz).

Conclusions

In summary, we reported on an unexpected fragmentation of otherwise very stable phosphaferrocenes by reaction with Cu(I) halides. The observed splitting of [Cp*Fe(η^5-$P_3C_2Mes_2$)] (**1**) into a [Cp*Fe]$^+$ and a [P_3C_2Mes]$^-$ unit can most likely be attributed to the bulky mesityl ligands. While the [Cp*Fe]$^+$ fragment reacts independently, the self-assembly processes of the remaining phospholyl ligands and CuX (X = Cl, Br, I) lead to the formation of a large variety of coordination compounds, among them monomeric, dimeric as well as 1D and 2D polymeric aggregates. The obtained structural motifs represent novel 'cages' composed by P, Cu and X atoms (X = Cl, Br), a very seldom appearing Cu_4I_4 'crown' and a Cu_6I_6 'hexagram' yet unknown for CuI systems. All obtained products show dynamic dissociation and association behavior in solution, which turns the so far rather neglected 1,2,4-triphospholyl ligand into an interesting and attractive ligand in coordination chemistry. It remains to be investigated further, whether the salt K[$P_3C_2Mes_2$] can also be used as a building block in metallosupramolecular chemistry.

4.3 Experimental Part

General Remarks:

All reactions were performed under an inert atmosphere of dry nitrogen or argon with standard vacuum, Schlenk and glove-box techniques. Solvents were purified, dried and degassed prior to use by standard procedures. [Cp*Fe(η^5-$P_3C_2Mes_2$)] was synthesized following the reported procedure.[8] Commercially available chemicals (CuCl, CuBr, CuI) were used without further purification. Solution NMR spectra were recorded on a Bruker Avance 300 or 400 spectrometer. The corresponding ESI-MS spectra were acquired on a ThermoQuest Finnigan MAT TSQ 7000 mass spectrometer, whereas elemental analyses were performed on a Vario EL III apparatus.

Synthesis of [(μ,$\eta^{1:2:2}$-$P_3C_2Mes_2$)(μ,$\eta^{1:3:3}$-$P_3C_2Mes_2$){$Cu_7(CH_3CN)_7(\mu_4\text{-}Cl)(\mu_3\text{-}Cl)_2(\mu\text{-}Cl)$}{$Cu_2(\mu_2\text{-}Cl)_2Cl$}{$Cu(CH_3CN)(\mu_2\text{-}Cl)$}]$_2$ (2)

In a thin Schlenk tube a solution of [Cp*Fe(η^5-$P_3C_2Mes_2$)] (30 mg, 0.06 mmol) in toluene (6 mL) is layered with a solution of CuCl (11 mg, 0.11 mmol) in CH_3CN (5 mL). After complete diffusion the solution is filtered and concentrated to 5 mL. Within a few weeks at room temperature red crystals of **2** · 6 CH_3CN can be obtained. The mother liquor is decanted, the crystals are washed with hexane (3 x 5 mL) and dried *in vacuo*.

Analytical data of **2**:

Yield: 12 mg (0.0058 mmol, 96%)

^{1}H NMR (CD_3CN): δ [ppm] = 2.06 (s, 6H, *o*-CH_3), 2.24 (s, 3H, *p*-CH_3), 6.88 (s, 2H, *aryl*-H).

^{13}C{^{1}H} NMR (CD_3CN): δ [ppm] = 20.97 (*o*-CH_3), 21.96 (*p*-CH_3), 127.96 (*aryl*-CH), 134.89 (*aryl*-$\underline{C}CH_3$), 135.92 (*aryl*-$\underline{C}CH_3$), 137.12 (*aryl*-C).

^{31}P{^{1}H} NMR (CD_3CN): δ [ppm] = 123.6 (br), 155.0 (br), 209.0 (br), 216.0 (br).

Positive ion ESI-MS (Et_2O/CH_3CN): *m/z* (%) = 2036.0 [{$P_3C_2Mes_2$}$_4Cu_8Cl_3$]$^+$, 1937.1 [{$P_3C_2Mes_2$}$_4Cu_7Cl_2$]$^+$, 1837.2 [{$P_3C_2Mes_2$}$_4Cu_6Cl$]$^+$, 1739.2 [{$P_3C_2Mes_2$}$_4Cu_5$]$^+$, 1616.7 [{$P_3C_2Mes_2$}$_3Cu_7Cl_3$]$^+$, 1516.9 [{$P_3C_2Mes_2$}$_3Cu_6Cl_2$]$^+$, 1419.1 [{$P_3C_2Mes_2$}$_3Cu_5Cl$]$^+$, 1319.1 [{$P_3C_2Mes_2$}$_3Cu_4$]$^+$, 1198.7 [{$P_3C_2Mes_2$}$_2Cu_6Cl_3$]$^+$, 1154.9 [{$P_3C_2Mes_2$}$_2Cu_4Cl${Et_2O}{CH_3CN}$_2$]$^+$, 1055.0 [{$P_3C_2Mes_2$}$_2Cu_3${Et_2O}{CH_3CN}$_2$]$^+$, 901.1 [{$P_3C_2Mes_2$}Cu_5Cl_3{CH_3CN}$_3$]$^+$, 801.2 [{$P_3C_2Mes_2$}Cu_4Cl_2{CH_3CN}$_3$]$^+$, 703.3 (100) [{$P_3C_2Mes_2$}Cu_3Cl{CH_3CN}$_3$]$^+$, 469.2 [Cu_3Cl_2{CH_3CN}$_3$]$^+$, 374.1 [Cu_3Cl_2{Et_2O}{CH_3CN}]$^+$, 333.0 [Cu_3Cl_2{Et_2O}]$^+$..

Negative ion ESI-MS (Et_2O/CH_3CN): *m/z* (%) = 894.2 [Cu_7Cl_8{CH_2Cl_2}{CH_3CN}$_2$]$^-$, 866.2 [Cu_8Cl_9{CH_3CN}]$^-$, 796.1 [Cu_6Cl_7{CH_2Cl_2}{CH_3CN}$_2$]$^-$, 766.3 [Cu_7Cl_8{CH_3CN}]$^-$, 740.3 [Cu_6Cl_7{Et_2O}{CH_3CN}]$^-$, 668.2 [Cu_6Cl_7{CH_3CN}]$^-$, 640.4 [Cu_5Cl_6{Et_2O}{CH_3CN}]$^-$, 612.3

$[Cu_5Cl_6\{CH_3CN\}_2]^-$, 584.3 $[Cu_4Cl_5\{Et_2O\}\{CH_3CN\}_2]^-$, 542.5 $[Cu_3Cl_4\{CH_2Cl_2\}\{CH_3CN\}_3]^-$, 514.4 $[Cu_4Cl_5\{CH_3CN\}_2]^-$, 486.5 $[Cu_3Cl_4\{Et_2O\}\{CH_3CN\}_2]^-$, 414.5 $[Cu_3Cl_4\{CH_3CN\}_2]^-$, 386.4 $[Cu_2Cl_3\{Et_2O\}\{CH_3CN\}_2]^-$, 360.4 $[Cu_4Cl_3]^-$, 288.5 $[CuCl_2\{Et_2O\}\{CH_3CN\}_2]^-$, 232.6 $[Cu_2Cl_3]^-$, 134.6 (100) $[CuCl_2]^-$.

Elemental analysis: Calculated (%) for $[(P_3C_2Mes_2)_4Cl_{16}Cu_{20}(CH_3CN)_{11}]$ (3712.9 g/mol): C 32.99, H 3.28, N 4.15; found: C 32.02, H 3.37, N 4.55.

Analytical data of the mother liquor of **2** (after 2 hours of stirring):

Positive ion ESI-MS (CH_2Cl_2/CH_3CN): *m/z* (%) = 2099.2 $[\{Cp^*Fe(P_3C_2Mes_2)\}_3Cu_5Cl_4]^+$, 1999.4 $[\{Cp^*Fe(P_3C_2Mes_2)\}_3Cu_4Cl_3]^+$, 1899.3 $[\{Cp^*Fe(P_3C_2Mes_2)\}_3Cu_3Cl_2]^+$, 1801.5 $[\{Cp^*Fe(P_3C_2Mes_2)\}_3Cu_2Cl]^+$, 1353.2 $[\{Cp^*Fe(P_3C_2Mes_2)\}_2Cu_3Cl_2]^+$, 1255.4 $[\{Cp^*Fe(P_3C_2Mes_2)\}_2Cu_2Cl]^+$, 1155.4 $[\{Cp^*Fe(P_3C_2Mes_2)\}_2Cu]^+$, 650.1 (100) $[\{Cp^*Fe(P_3C_2Mes_2)\}Cu\{CH_3CN\}]^+$, 546.1 $[Cp^*Fe(P_3C_2Mes_2)]^+$.

Negative ion ESI-MS (CH_2Cl_2/CH_3CN): *m/z* (%) = 332.5 $[Cu_3Cl_4]^-$, 232.6 (100) $[Cu_3Cl_4]^-$, 160.7 $[FeCl_3]^-$, 134.7 $[CuCl_2]^-$.

EI-MS (70 eV): 326.2 (100) $[Cp^*_2Fe]$.

Synthesis of $[(\mu,\eta^{1:2:2}\text{-}P_3C_2Mes_2)(\mu,\eta^{1:3:3}\text{-}P_3C_2Mes_2)\{Cu_7(CH_3CN)_7(\mu_4\text{-}Br)(\mu_3\text{-}Br)_2(\mu\text{-}Br)\}\{Cu_2(\mu_2\text{-}Br)_2Br\}\{Cu(CH_3CN)(\mu_2\text{-}Br)\}]_2$ (3)

In a thin Schlenk tube a solution of $[Cp^*Fe(\eta^5\text{-}P_3C_2Mes_2)]$ (25 mg, 0.05 mmol) in CH_2Cl_2 (8 mL) is layered with a solution of CuBr (33 mg, 0.23 mmol) in CH_3CN (20 mL). After complete diffusion the solution is concentrated to 15 mL and layered with Et_2O. While storing at 8°C, the formation of bright red plates of **3** · 6 CH_3CN can be observed. After complete diffusion the slightly turbid mother liquor is decanted, the crystals are washed with hexane (3 x 5 mL) and dried *in vacuo*.

Analytical data of **3**:

Yield: 28 mg (0.007 mmol, crystalline, 56% referred to $[Cp^*Fe(\eta^5\text{-}P_3C_2Mes_2)]$)

^{1}H NMR (CD_3CN): δ [ppm] = 1.95 (s, CH_3CN), 2.04 (s, 6H, *o*-CH_3), 2.14 (s, 6H, *o*-CH_3), 2.26 (s, 6H, *p*-CH_3), 6.90 (s, 4H, *aryl*-H).

^{13}C{^{1}H} NMR (CD_3CN): δ [ppm] = 21.11 (*p*-CH_3), 22.82 (*o*-CH_3), 128.60 (*aryl*-CH), 136.91 (*aryl*-$\underline{C}CH_3$), 138.31 (*aryl*-$\underline{C}CH_3$).

^{31}P{^{1}H} NMR (CD_3CN): δ [ppm] = 136.0 (br, (**3**)-2P), 160.2 (br, (**4**)-1P), 203.9 (br, (**4**)-2P), 217.3 (br, (**3**)-1P).

Positive ion ESI-MS (CH_3CN): *m/z* (%) = 2455.0 $[\{P_3C_2Mes_2\}_4Cu_{10}Br_5]^+$, 2313.1 $[\{P_3C_2Mes_2\}_4Cu_9Br_4]^+$, 2169.2 $[\{P_3C_2Mes_2\}_4Cu_8Br_3]^+$, 2025.2 $[\{P_3C_2Mes_2\}_4Cu_7Br_2]^+$, 1881.4 $[\{P_3C_2Mes_2\}_4Cu_6Br_1]^+$, 1748.9 $[\{P_3C_2Mes_2\}_3Cu_7Br_3]^+$, 1648.1 $[\{P_3C_2Mes_2\}_3Cu_6Br_2\{CH_3CN\}]^+$, 1607.0 $[\{P_3C_2Mes_2\}_3Cu_6Br_2]^+$, 1506.2 $[\{P_3C_2Mes_2\}_3Cu_5Br\{CH_3CN\}]^+$, 1474.7 $[\{P_3C_2Mes_2\}_2Cu_7Br_4]^+$, 1463.3 $[\{P_3C_2Mes_2\}_3Cu_5Br]^+$, 1330.8 $[\{P_3C_2Mes_2\}_2Cu_6Br_3]^+$, 1319.3 $[\{P_3C_2Mes_2\}_3Cu_4]^+$, 1230.0 $[\{P_3C_2Mes_2\}_2Cu_5Br_2\{CH_3CN\}]^+$, 1188.9 $[\{P_3C_2Mes_2\}_2Cu_5Br_2]^+$, 1127.2 $[\{P_3C_2Mes_2\}_2Cu_4Br\{CH_3CN\}_2]^+$, 1097.6 $[\{P_3C_2Mes_2\}Cu_6Br_4\{CH_3CN\}]^+$, 1054.5 $[\{P_3C_2Mes_2\}_2Cu_4Br]^+$, 953.7 $[\{P_3C_2Mes_2\}Cu_5Br_3\{CH_3CN\}]^+$, 144.9 (100) $[Cu\{CH_3CN\}_2]^+$.

Negative ion ESI-MS (CH_3CN): *m/z* (%) = 798.2 $[Cu_5Br_6]^-$, 654.4 $[Cu_4Br_5]^-$, 510.5 $[Cu_3Br_4]^-$, 366.4 $[Cu_2Br_3]^-$, 222.5 (100) $[CuBr_2]^-$.

Synthesis of $[(\mu,\eta^{1:2:3}\text{-}P_3C_2Mes_2)_2Cu_{9.33}Br_{7.33}(CH_3CN)_{8.5}]$ (4)

In a thin Schlenk tube a solution of $[Cp^*Fe(\eta^5\text{-}P_3C_2Mes_2)]$ (50 mg, 0.09 mmol) in CH_2Cl_2 (5 mL) is layered with a solution of CuBr (129 mg, 0.9 mmol) in CH_3CN (5 mL). During diffusion the formation of small orange-red plates of **4** · CH_3CN and a small amount of bright yellow plates of $[Cu(CH_3CN)Br]_n$ (identification by unit cell parameters and comparison with CCDC data base) due to the excess of CuBr can be observed. After complete diffusion the slightly turbid mother liquor is decanted, the crystals are washed with hexane (3 x 5 mL) dried *in vacuo*. The small amount of big bright plates of $[Cu(CH_3CN)Br]_n$ can easily be removed mechanically under the microscope to give pure **4**.

Analytical data of **4**:

Yield: 85 mg (0.041 mmol, crystalline, 92% referred to $[Cp^*Fe(\eta^5\text{-}P_3C_2Mes_2)]$)

^{1}H NMR (CD_3CN): δ [ppm] = 1.95 (s, CH_3CN), 2.04 (s, 6H, *o*-CH_3), 2.14 (s, 6H, *o*-CH_3), 2.26 (s, 6H, *p*-CH_3), 6.90 (s, 4H, *aryl*-H).

^{13}C{^{1}H} NMR (CD_3CN): δ [ppm] = 21.11 (*p*-CH_3), 22.82 (*o*-CH_3), 128.60 (*aryl*-CH), 136.91 (*aryl*-$\underline{C}CH_3$), 138.31 (*aryl*-$\underline{C}CH_3$).

^{31}P{^{1}H} NMR (CD_3CN): δ [ppm] = 136.0 (br, (**3**)-2P), 160.2 (br, (**4**)-1P), 203.9 (br, (**4**)-2P), 217.3 (br, (**3**)-1P).

Positive ion ESI-MS (CH_3CN): *m/z* (%) = 3438.2 $[\{P_3C_2Mes_2\}_4Cu_{17}Br_{12}]^+$, 3293.4 $[\{P_3C_2Mes_2\}_4Cu_{16}Br_{11}]^+$, 3163.0 $[\{P_3C_2Mes_2\}_4Cu_{15}Br_{10}]^+$, 3019.1 $[\{P_3C_2Mes_2\}_4Cu_{14}Br_9]^+$, 2873.1 $[\{P_3C_2Mes_2\}_4Cu_{13}Br_8]^+$, 2733.1 $[\{P_3C_2Mes_2\}_4Cu_{12}Br_7]^+$, 2591.2 $[\{P_3C_2Mes_2\}_4Cu_{11}Br_6]^+$, 2457.2 $[\{P_3C_2Mes_2\}_4Cu_{10}Br_5]^+$, 2313.0 $[\{P_3C_2Mes_2\}_4Cu_9Br_4]^+$, 2169.1 $[\{P_3C_2Mes_2\}_4Cu_8Br_3]^+$, 2025.1 $[\{P_3C_2Mes_2\}_4Cu_7Br_2]^+$, 1881.3 (100) $[\{P_3C_2Mes_2\}_4Cu_6Br_1]^+$, 1739.4 $[\{P_3C_2Mes_2\}_4Cu_5]^+$, 1647.9 $[\{P_3C_2Mes_2\}_3Cu_6Br_2\{CH_3CN\}]^+$, 1607.1 $[\{P_3C_2Mes_2\}_3Cu_6Br_2]^+$, 1504.2 $[\{P_3C_2Mes_2\}_3Cu_5Br\{CH_3CN\}]^+$, 1463.0 $[\{P_3C_2Mes_2\}_3Cu_5Br]^+$, 1328.6 $[\{P_3C_2Mes_2\}_2Cu_6Br_3]^+$, 1319.2 $[\{P_3C_2Mes_2\}_3Cu_4]^+$, 1230.0 $[\{P_3C_2Mes_2\}_2Cu_5Br_2\{CH_3CN\}]^+$, 1188.9 $[\{P_3C_2Mes_2\}_2Cu_5Br_2]^+$, 1126.8 $[\{P_3C_2Mes_2\}_2Cu_4Br\{CH_3CN\}]^+$.

Negative ion ESI-MS (CH_3CN): *m/z* (%) = 510.3 $[Cu_3Br_4]^-$, 366.5 $[Cu_2Br_3]^-$, 294.5 $[FeBr_3]^-$, 222.7 (100) $[CuBr_2]^-$.

Elemental analysis: Calculated (%) for $[(P_3C_2Mes_2)_2Cu_{9.3}Br_{7.3}(CH_3CN)_3]$ (2053.9 g/mol): C 28.07, H 2.75, N 2.73; found: C 27.64, H 2.96, N 3.28.

Analytical data of the mother liquor of **4**:

Positive ion ESI-MS (CH_2Cl_2/CH_3CN): *m/z* (%) = 326.1 (100) $[Cp^*_2Fe]^+$, 273.0 $[Cp^*Fe\{CH_3CN\}_2]^+$, 232.1 $[Cp^*Fe\{CH_3CN\}]^+$.

Negative ion ESI-MS (CH_2Cl_2/CH_3CN): *m/z* (%) = 798.2 $[Cu_5Br_6]^-$, 741.0 $[Fe_3Br_7O]^-$, 726.3 $[Fe_3Br_7]^-$, 654.4 $[Cu_4Br_5]^-$, 510.4 $[Cu_3Br_4]^-$, 375.4 $[FeBr_4]^-$, 366.4 $[Cu_2Br_3]^-$, 294.5 (100) $[FeBr_3]^-$, 222.5 $[CuBr_2]^-$.

EI-MS (70 eV): 326.2 $[Cp^*_2Fe]$.

After 5 minutes of stirring:

^{1}H NMR (CD_2Cl_2/CD_3CN): δ [ppm] = 1.61 (s, 15H, Cp*), 2.21 (s, 6H, *p*-CH_3), 2.74 (s, 12H, *o*-CH_3), 6.91 (s, 4H, *aryl*-H).

After 4 hours of stirring:

^{1}H NMR (CD_2Cl_2/CD_3CN): δ [ppm] = 1.60 (s, 15H, Cp*), 1.69 (s, Cp^*_2Fe), 2.21 (s, 6H, *p*-CH_3), 2.75 (s, 12H, *o*-CH_3), 6.92 (s, 4H, *aryl*-H).

Synthesis of $[(\mu,\eta^{1:1:2}\text{-}P_3C_2Mes_2)_3(\mu,\eta^{1:2:3}\text{-}P_3C_2Mes_2)\{Cu_5(CH_3CN)_5(\mu_2\text{-}Br)\}\{Cu(CH_3CN)_2CuBr_2\}_2\{Cu(CH_3CN)_2\}]_n[CuBr_2]_n$ (5)

In a thin Schlenk tube a solution of $[Cp^*Fe(\eta^5\text{-}P_3C_2Mes_2)]$ (25 mg, 0.05 mmol) in CH_2Cl_2 (8 mL) is layered with a solution of CuBr (22 mg, 0.15 mmol) in CH_3CN (20 mL). After complete diffusion the solution is concentrated to 15 mL and layered with Et_2O. Already during the diffusion process the formation of red crystals of **5** · 2 CH_3CN can be observed. After complete diffusion the slightly turbid mother liquor is decanted, the crystals are washed with hexane (3 x 5 mL) and dried *in vacuo*.

Analytical data of **5**:

Yield: 30 mg (0.006 mmol, crystalline, 96% referred to $[Cp^*Fe(\eta^5\text{-}P_3C_2Mes_2)]$)

^{1}H NMR (CD_3CN): δ [ppm] = 1.95 (s, CH_3CN), 2.02 (s, 12H, *o*-CH_3), 2.25 (s, 6H, *p*-CH_3), 5.44 (s, CH_2Cl_2), 6.87 (s, 4H, *aryl*-H).

Positive ion ESI-MS (CH_3CN): *m/z* (%) = 2171.2 $[\{P_3C_2Mes_2\}_4Cu_8Br_3]^+$, 2025.3 $[\{P_3C_2Mes_2\}_4Cu_7Br_2]^+$, 1881.4 $[\{P_3C_2Mes_2\}_4Cu_6Br]^+$, 1739.4 $[\{P_3C_2Mes_2\}_4Cu_5]^+$, 1646.4 $[\{P_3C_2Mes_2\}_3Cu_6Br_2\{CH_3CN\}]^+$, 1319.1 $[\{P_3C_2Mes_2\}_3Cu_4]^+$, 1014.1 $[\{P_3C_2Mes_2\}_4Cu_7Br\{CH_3CN\}_2]^{2+}$, 993.2 $[\{P_3C_2Mes_2\}_4Cu_7Br\{CH_3CN\}]^{2+}$,

985.3[{$P_3C_2Mes_2$}$_2$$Cu_{11}Br_2${$CH_3CN$}]$^{2+}$, 973.0 [{$P_3C_2Mes_2$}$_4$$Cu_7Br]^{2+}$, 963.3 [{$P_3C_2Mes_2$}$_4$$Cu_6${$CH_3CN$}$_3$]$^{2+}$, 942.2 [{$P_3C_2Mes_2$}$_4$$Cu_6${$CH_3CN$}$_2$]$^{2+}$, 920.6 [{$P_3C_2Mes_2$}$_4$$Cu_6${$CH_3CN$}]$^{2+}$, 901.2 [{$P_3C_2Mes_2$}$_4$$Cu_6]^{2+}$.

Negative ion ESI-MS (CH_3CN): *m/z* (%) = 304.6 (100) $[Cu_2Br_2O]^-$, 222.7 $[CuBr_2]^-$.

Elemental analysis: Calculated (%) for $[(P_3C_2Mes_2)_8Cu_{16}Br_8(CH_3CN)_7(CH_2Cl_2)_3]$ (5040.7 g/mol): C 42.18, H 4.06, N 1.95; found: C 41.99, H 4.03, N 2.02.

Synthesis of [(μ,η$^{1:2:2}$-$P_3C_2Mes_2$){Cu(CH_3CN)(μ-I)}$_4${Cu(CH_3CN)$_3$}] (6)

A solution of [Cp*Fe(η^5-$P_3C_2Mes_2$)] (110 mg, 0.2 mmol) in CH_2Cl_2 (5 mL) is added to a solution of CuI (50 mg, 0.26 mmol) in CH_3CN (25 mL). After stirring the reaction mixture for 2 h, it is filtered (the residual solid still contains [Cp*Fe(η^5-$P_3C_2Mes_2$)], since an excess was used) and layered with Et_2O. After complete diffusion at -28°C red plates of **6** · 0.5 C_7H_8 · 2.5 CH_3CN can be obtained. The mother liquor is decanted, the crystals are washed with hexane (3 x 5 mL) and dried *in vacuo*. By concentrating the mother liquor and storing at -28 °C, a second crop of crystals can be obtained.

Analytical data of **6**:

Yield: 40 mg (0.031 mmol, crystalline, 59% referred to CuI)

^{1}H NMR (CD_3CN): *δ* [ppm] = 1.95 (s, CH_3CN), 2.04 (s, 3H, *p*-CH_3), 2.13 (s, 3H, *p*-CH_3), 2.22 (s, 6H, *o*-CH_3), 2.27 (s, 6H, *o*-CH_3), 6.90 (s, 4H, *aryl*-H).

^{13}C{^{1}H} NMR (CD_3CN): *δ* [ppm] = 21.1 (s, CH_3), 23.5 (s, CH_3), 26.2 (s, CH_3), 128.7 (s, *aryl*-C), 136.9 (s, *aryl*-C), 138.4 (s, *aryl*-C).

^{31}P{^{1}H} NMR (CD_3CN): *δ* [ppm] = 134 (br), 153 (br), 205 (br), 224 (br).

Positive ion ESI-MS (CH_3CN): *m/z* = 2883.2 [{$P_3C_2Mes_2$}$_4$$Cu_{11}I_6]^+$, 2878.2 [{$P_3C_2Mes_2$}$_3$$Cu_{12}I_8]^+$, 2691.5 [{$P_3C_2Mes_2$}$_4$$Cu_{10}I_5]^+$, 2650.4 [{$P_3C_2Mes_2$}$_3$$Cu_{11}I_7]^+$, 2500.1 [{$P_3C_2Mes_2$}$_4$$Cu_9I_4]^+$, 2463.1 [{$P_3C_2Mes_2$}$_3$$Cu_{10}I_6]^+$, 2424.7 [{$P_3C_2Mes_2$}$_2$$Cu_{11}I_8]^+$, 2312.7 [{$P_3C_2Mes_2$}$_3$$Cu_{12}I_8]^+$, 2273.0 [{$P_3C_2Mes_2$}$_3$$Cu_9I_5]^+$, 2234.7 [{$P_3C_2Mes_2$}$_2$$Cu_{10}I_7]^+$, 2119.7 [{$P_3C_2Mes_2$}$_4$$Cu_7I_2]^+$, 2081.2 [{$P_3C_2Mes_2$}$_3$$Cu_8I_4]^+$, 2042.9 [{$P_3C_2Mes_2$}$_2$$Cu_9I_6]^+$, 1929.1 [{$P_3C_2Mes_2$}$_4$$Cu_6I]^+$, 1890.8 [{$P_3C_2Mes_2$}$_3$$Cu_7I_3]^+$, 1742.0 [{$P_3C_2Mes_2$}$_4$$Cu_5]^+$, 1700.9 [{$P_3C_2Mes_2$}$_3$$Cu_6I_2]^+$, 1661.8 [{$P_3C_2Mes_2$}$_2$$Cu_7I_4]^+$, 1511.0 [{$P_3C_2Mes_2$}$_3$$Cu_5I]^+$, 1472.4 [{$P_3C_2Mes_2$}$_2$$Cu_6I_3]^+$, 1321.6 [{$P_3C_2Mes_2$}$_3$$Cu_4]^+$, 1285.2 [{$P_3C_2Mes_2$}$_2$$Cu_5I_2]^+$, 1242.2 [{$P_3C_2Mes_2$}$Cu_6I_4]^+$, 1172.8 [{$P_3C_2Mes_2$}$_2$$Cu_4I${$CH_3CN$}$_2$]$^+$, 1131.8 [{$P_3C_2Mes_2$}$_2$$Cu_4I${$CH_3CN$}]$^+$, 1090.8 [{$P_3C_2Mes_2$}$_2$$Cu_4I]^+$, 1052.4 [{$P_3C_2Mes_2$}$Cu_5I_3]^+$.

Negative ion ESI-MS (CH_3CN): *m/z* (%) = 1270.1 $[Cu_6I_7]^-$, 1078.2 $[Cu_5I_6]^-$, 888.3 $[Cu_4I_5]^-$, 698.5 $[Cu_3I_4]^-$, 506.6 $[Cu_2I_3]^-$, 316.8 (100) $[CuI_2]^-$.

Elemental analysis: Calculated (%) for [($P_3C_2Mes_2$)Cu_5I_4(CH_3CN)$_3$] (1303.8 g/mol): C 23.96, H 2.40, N 3.22; found: C 23.96, H 2.50, N 3.28.

Synthesis of $[(\mu,\eta^{1:2:2}\text{-}P_3C_2Mes_2)Cu_7(CH_3CN)_4(\mu_4\text{-}I)_2(\mu_3\text{-}I)_2(\mu\text{-}I)_2]_n$ (7)

In a schlenk tube a solution of $[Cp^*Fe(\eta^5\text{-}P_3C_2Mes_2)]$ (28 mg, 0.05 mmol) in CH_2Cl_2 (10 mL) is layered with a solution of CuI (35 mg, 0.18 mmol) in CH_3CN (10 mL). After complete diffusion the solution is filtered, concentrated to 3 mL and layered onto a toluene solution (10 mL) in a thin schlenk tube. During diffusion the formation of yellow crystals of **7** · 2 C_7H_8 can be observed. The mother liquor is decanted, the crystals are washed with hexane (3 x 5 mL) and dried *in vacuo*.

Analytical data of **7**:

Yield: 18 mg (0.01 mmol, crystalline, 41% referred to CuI)

^{1}H NMR (CD_3CN): δ [ppm] = 1.95 (s, CH_3CN), 2.26 (s, br, 18H, CH_3), 6.92 (s, 4H, *aryl*-H).

$^{31}P\{^1H\}$ NMR (CD_3CN): δ [ppm] = 137.2 (br), 222.6 (br).

Negative ion ESI-MS (dme/CH_3CN): *m/z* (%) = 2108.7 $[\{P_3C_2Mes_2\}_2Cu_8I_7]^-$, 1957.0 $[\{P_3C_2Mes_2\}_2Cu_7I_6\{CH_3CN\}]^-$, 1916.7 $[\{P_3C_2Mes_2\}_2Cu_7I_6]^-$, 1726.9 $[\{P_3C_2Mes_2\}_2Cu_6I_5]^-$, 1536.8 $[\{P_3C_2Mes_2\}_2Cu_5I_4]^-$, 1498.6 $[\{P_3C_2Mes_2\}Cu_6I_6]^-$, 1344.9 $[\{P_3C_2Mes_2\}_2Cu_4I_3]^-$, 1306.6 $[\{P_3C_2Mes_2\}Cu_5I_5]^-$, 1116.7 $[\{P_3C_2Mes_2\}Cu_4I_4]^-$, 1268.2 $[Cu_6I_7]^-$, 1078.2 $[Cu_5I_6]^-$, 888.3 $[Cu_4I_5]^-$, 698.5 $[Cu_3I_4]^-$, 506.6 $[Cu_2I_3]^-$, 316.8 (100) $[CuI_2]^-$.

Elemental analysis: Calculated (%) for $[(P_3C_2Mes_2)Cu_7I_6(CH_3CN)_2$*1.5 $C_7H_8]$ (1782 g/mol): C 23.26, H 2.26, N 1.57; found: C 23.58, H 2.45, N 1.58.

Synthesis of $[(\mu,\eta^{1:3:3}\text{-}P_3C_2Mes_2)\{Cu(CH_3CN)_3\}_2\{Cu(\mu\text{-}I)\}_6]$ (8) and $[Cp^*Fe(CH_3CN)_3]_n[(\mu,\eta^{1:3:3}\text{-}P_3C_2Mes_2)_2\{Cu(CH_3CN)_2\}\{Cu(\mu\text{-}I)\}_6]_n$ (9)

In a thin schlenk tube a solution of $[Cp^*Fe(\eta^5\text{-}P_3C_2Mes_2)]$ (25 mg, 0.046 mmol) in CH_2Cl_2 (8 mL) is layered with a solution of CuI (44 mg, 0.23 mmol) in CH_3CN (20 mL). After complete diffusion the solution is filtered, concentrated to 15 mL and layered with Et_2O (15 mL). During diffusion the formation of orange-red plates of **8** · 0.5 CH_2Cl_2 · 3 CH_3CN and uniquely of red rods of **9** · 0.6 CH_2Cl_2 can be observed. The mother liquor is decanted, the crystals are washed with hexane (3 x 5 mL) and dried *in vacuo*.

Analytical data of **8** and **9**:

Yield: 28 mg (In the event, only **8** is present: 0.013 mmol, crystalline, 45% referred to CuI; in the event, only **9** is present: 0.011 mmol, crystalline, 35% referred to CuI; a calculation of the ratio of **8** and **9** cannot be made, since one compound is molecular (**8**), the other one polymeric (**9**).

^{1}H NMR (CD_3CN): δ [ppm] = 1.95 (s, CH_3CN), 2.04 (s, 3H, *p*-CH_3), 2.13 (s, 12H, *o*-CH_3), 2.20 (s, 6H, *o*-CH_3), 2.26 (s, 6H, *p*-CH_3), 6.90 (s, br, 6H, *aryl*-H).

$^{31}P\{^1H\}$ NMR (CD_3CN): δ [ppm] = 135 (br), 206 (br), 223 (br).

Positive ion ESI-MS (CH_3CN): *m/z* (%) = 2693.1 $[\{P_3C_2Mes_2\}_4Cu_{10}I_5]^+$, 2501.1 $[\{P_3C_2Mes_2\}_4Cu_9I_4]^+$, 2464.7 $[\{P_3C_2Mes_2\}_3Cu_{10}I_6]^+$, 2311.3 $[\{P_3C_2Mes_2\}_4Cu_8I_3]^+$, 2119.3 $[\{P_3C_2Mes_2\}_4Cu_7I_2]^+$, 2082.9 $[\{P_3C_2Mes_2\}_3Cu_8I_4]^+$, 1929.4 $[\{P_3C_2Mes_2\}_4Cu_6I]^+$, 1891.0 $[\{P_3C_2Mes_2\}_3Cu_7I_3]^+$, 1742.2 $[\{P_3C_2Mes_2\}_4Cu_5]^+$, 1699.1 $[\{P_3C_2Mes_2\}_3Cu_6I_2]^+$, 1662.8 $[\{P_3C_2Mes_2\}_2Cu_7I_4]^+$, 1550.1 $[\{P_3C_2Mes_2\}_3Cu_5I\{CH_3CN\}]^+$, 1511.1 $[\{P_3C_2Mes_2\}_3Cu_5I]^+$, 1472.9 $[\{P_3C_2Mes_2\}_2Cu_6I_3]^+$, 1322.0 $[\{P_3C_2Mes_2\}_3Cu_4]^+$, 1283.6 $[\{P_3C_2Mes_2\}_2Cu_5I_2]^+$, 1173.1 $[\{P_3C_2Mes_2\}_2Cu_4I\{CH_3CN\}_2]^+$, 1132.0 $[\{P_3C_2Mes_2\}_2Cu_4I\{CH_3CN\}]^+$, 1093.7 $[\{P_3C_2Mes_2\}_2Cu_4I]^+$, 996.1 $[\{P_3C_2Mes_2\}_4Cu_7I]^{2+}$, 901.1 $[\{P_3C_2Mes_2\}_4Cu_6]^{2+}$, 144.9 $[Cu\{CH_3CN\}_2]^+$.

Negative ion ESI-MS (CH_3CN): *m/z* (%) = 2944.9 $[\{P_3C_2Mes_2\}_4Cu_{10}I_7]^-$, 2908.5 $[\{P_3C_2Mes_2\}_3Cu_{11}I_9]^-$, 2867.8 $[\{P_3C_2Mes_2\}_2Cu_{12}I_{11}]^-$, 2759.2 $[\{P_3C_2Mes_2\}_4Cu_9I_6]^-$, 2720.5 $[\{P_3C_2Mes_2\}_3Cu_{10}I_8]^-$, 2678.4 $[\{P_3C_2Mes_2\}_2Cu_{11}I_{10}]^-$, 2563.1 $[\{P_3C_2Mes_2\}_4Cu_8I_5]^-$, 2524.7 $[\{P_3C_2Mes_2\}_3Cu_9I_7]^-$, 2488.3 $[\{P_3C_2Mes_2\}_2Cu_{10}I_9]^-$, 2374.3 $[\{P_3C_2Mes_2\}_4Cu_7I_4]^-$, 2335.1 $[\{P_3C_2Mes_2\}_3Cu_8I_6]^-$, 2298.4 $[\{P_3C_2Mes_2\}_2Cu_9I_8]^-$, 2260.1 $[\{P_3C_2Mes_2\}Cu_{10}I_{10}]^-$, 2145.0 $[\{P_3C_2Mes_2\}_3Cu_7I_5]^-$, 2108.6 $[\{P_3C_2Mes_2\}_2Cu_8I_7]^-$, 2068.1 $[\{P_3C_2Mes_2\}Cu_9I_9]^-$, 1954.9 $[\{P_3C_2Mes_2\}_3Cu_6I_4]^-$, 1916.8 $[\{P_3C_2Mes_2\}_2Cu_7I_6]^-$, 1878.3 $[\{P_3C_2Mes_2\}Cu_8I_8]^-$, 1767.1 $[\{P_3C_2Mes_2\}_3Cu_5I_3]^-$, 1726.7 $[\{P_3C_2Mes_2\}_2Cu_6I_5]^-$, 1688.3 $[\{P_3C_2Mes_2\}Cu_7I_7]^-$, 1650.0 $[Cu_8I_9]^-$, 1534.8 $[\{P_3C_2Mes_2\}_2Cu_5I_4]^-$, 1498.5 $[\{P_3C_2Mes_2\}Cu_6I_6]^-$, 1460.1 $[Cu_7I_8]^-$, 1346.9 $[\{P_3C_2Mes_2\}_2Cu_4I_3]^-$, 1306.6 $[\{P_3C_2Mes_2\}Cu_5I_5]^-$, 1270.2 $[Cu_6I_7]^-$, 1116.7 $[\{P_3C_2Mes_2\}Cu_4I_4]^-$, 1078.3 $[Cu_5I_6]^-$, 888.4 $[Cu_4I_5]^-$, 698.5 $[Cu_3I_4]^-$, 506.6 $[Cu_2I_3]^-$, 316.6 (100) $[CuI_2]^-$.

Analytical data of **8**:

Positive ion ESI-MS (CH_3CN): *m/z* (%) = 2693.1 $[\{P_3C_2Mes_2\}_4Cu_{10}I_5]^+$, 2501.1 $[\{P_3C_2Mes_2\}_4Cu_9I_4]^+$, 2462.7 $[\{P_3C_2Mes_2\}_3Cu_{10}I_6]^+$, 2311.2 $[\{P_3C_2Mes_2\}_4Cu_8I_3]^+$, 2274.7 $[\{P_3C_2Mes_2\}_3Cu_9I_5]^+$, 2119.2 $[\{P_3C_2Mes_2\}_4Cu_7I_2]^+$, 2082.8 $[\{P_3C_2Mes_2\}_3Cu_8I_4]^+$, 1929.4 $[\{P_3C_2Mes_2\}_4Cu_6I]^+$, 1891.0 $[\{P_3C_2Mes_2\}_3Cu_7I_3]^+$, 1740.1 $[\{P_3C_2Mes_2\}_4Cu_5]^+$, 1701.0 $[\{P_3C_2Mes_2\}_3Cu_6I_2]^+$, 1662.6 $[\{P_3C_2Mes_2\}_2Cu_7I_4]^+$, 1550.0 $[\{P_3C_2Mes_2\}_3Cu_5I\{CH_3CN\}]^+$, 1511.1 $[\{P_3C_2Mes_2\}_3Cu_5I]^+$, 1472.8 $[\{P_3C_2Mes_2\}_2Cu_6I_3]^+$, 1322.0 $[\{P_3C_2Mes_2\}_3Cu_4]^+$, 1283.6 $[\{P_3C_2Mes_2\}_2Cu_5I_2]^+$, 1173.0 $[\{P_3C_2Mes_2\}_2Cu_4I\{CH_3CN\}_2]^+$, 1131.9 $[\{P_3C_2Mes_2\}_2Cu_4I\{CH_3CN\}]^+$, 1093.0 $[\{P_3C_2Mes_2\}_2Cu_4I]^+$, 996.2 $[\{P_3C_2Mes_2\}_4Cu_7I]^{2+}$, 901.2 $[\{P_3C_2Mes_2\}_4Cu_6]^{2+}$.

Negative ion ESI-MS (CH_3CN): *m/z* (%) = 2562.5 $[\{P_3C_2Mes_2\}_4Cu_8I_5]^-$, 2528.7 $[\{P_3C_2Mes_2\}_3Cu_9I_7]^-$, 2490.2 $[\{P_3C_2Mes_2\}_2Cu_{10}I_9]^-$, 2373.2 $[\{P_3C_2Mes_2\}_4Cu_7I_4]^-$, 2334.9 $[\{P_3C_2Mes_2\}_3Cu_8I_6]^-$, 2296.4 $[\{P_3C_2Mes_2\}_2Cu_9I_8]^-$, 2144.7 $[\{P_3C_2Mes_2\}_3Cu_7I_5]^-$, 2106.7 $[\{P_3C_2Mes_2\}_2Cu_8I_7]^-$, 2070.2 $[\{P_3C_2Mes_2\}Cu_9I_9]^-$, 1954.9 $[\{P_3C_2Mes_2\}_3Cu_6I_4]^-$, 1916.5 $[\{P_3C_2Mes_2\}_2Cu_7I_6]^-$, 1878.3 $[\{P_3C_2Mes_2\}Cu_8I_8]^-$, 1841.8 $[Cu_9I_{10}]^-$, 1765.0 $[\{P_3C_2Mes_2\}_3Cu_5I_3]^-$, 1726.7 $[\{P_3C_2Mes_2\}_2Cu_6I_5]^-$, 1688.3 $[\{P_3C_2Mes_2\}Cu_7I_7]^-$, 1651.8 $[Cu_8I_9]^-$, 1534.7 $[\{P_3C_2Mes_2\}_2Cu_5I_4]^-$, 1498.3 $[\{P_3C_2Mes_2\}Cu_6I_6]^-$, 1460.1 $[Cu_7I_8]^-$, 1306.5 $[\{P_3C_2Mes_2\}Cu_5I_5]^-$,

1270.1 $[Cu_6I_7]^-$, 1116.6 $[\{P_3C_2Mes_2\}Cu_4I_4]^-$, 1078.2 $[Cu_5I_6]^-$, 888.5 $[Cu_4I_5]^-$, 698.5 $[Cu_3I_4]^-$, 506.6 $[Cu_2I_3]^-$, 316.6 (100) $[CuI_2]^-$.

Elemental analysis: Calculated (%) for $[(P_3C_2Mes_2)_2Cu_8I_6(CH_3CN)_4]$ (2145 g/mol): C 26.88, H 2.63, N 2.61; found: C 26.59, H 2.69, N 2.70.

Analytical data of the mother liquor of **8** and **9**:

Positive ion ESI-MS (CH_2Cl_2/CH_3CN): *m/z* (%) = 526.7 (100) $[Cu_3I_2\{CH_3CN\}_2]^+$, 432.1 $[Cp^*FeCu\{CH_3CN\}]^+$, 389.2 $[Cp^*FeCu]^+$, 334.7 $[Cu_2I\{CH_3CN\}_2]^+$, 326.1 (90) $[Cp^*_2Fe]^+$.

Negative ion ESI-MS (CH_2Cl_2/CH_3CN): *m/z* (%) = 2411.5 $[Cu_{12}I_{13}]^-$, 2219.4 $[Cu_{11}I_{12}]^-$, 2031.6 $[Cu_{10}I_{11}]^-$, 1841.6 $[Cu_9I_{10}]^-$, 1649.8 $[Cu_8I_9]^-$, 1459.9 $[Cu_7I_8]^-$, 1270.1 $[Cu_6I_7]^-$, 1078.2 $[Cu_5I_6]^-$, 888.3 $[Cu_4I_5]^-$, 698.5 $[Cu_3I_4]^-$, 506.6 $[Cu_2I_3]^-$, 380.6 $[I_3]^-$, 316.7 (100) $[CuI_2]^-$.

4.4 Crystallographic Details

Crystals of **2-9** were taken from a Schlenk tube under a stream of argon and covered with mineral oil. The single crystal was taken to the pre-centered goniometer head with CryoMount® and directly attached to the diffractometer into a stream of cold nitrogen. The data for **2** · 6 CH_3CN, **6** · 0.5 C_7H_8 · 2.5 CH_3CN, **7** · 2 C_7H_8 and **8** · 0.5 CH_2Cl_2 · 3 CH_3CN were collected on an Agilent Technologies Gemini R-Ultra diffractometer equipped with Ruby CCD detector and an Enhanced Ultra CuK_α sealed tube (λ = 1.54178 Å) using 1° ω scans. The data for **3** · 6 CH_3CN, **4** · CH_3CN, **5** · 2 CH_3CN were collected on an Agilent Technologies diffractometer equipped with a Titan^{S2} CCD detector and a SuperNova CuK_α microfocus source using 1° ω scans. The data for **9** · 0.6 CH_2Cl_2 were collected on an Agilent Technologies diffractometer equipped with an Atlas CCD detector and a SuperNova CuK_α microfocus source using 1° ω scans. All measurements were performed at 123 K. Crystallographic data and details of the diffraction experiments are given in *Table 4.2 – Table 4.5*. The structures of **2-9** were solved by direct methods with *SIR97*,[23] *SHELX97* or *SHELX2013*.[24] The structures were refined by full-matrix least-squares method against $|F|^2$ in anisotropic approximation using *SHELXL97* or the multiprocessor and variable memory version *SHELXL2013*. All non-hydrogen atoms were refined anisotropically, whereas the hydrogen atoms were refined riding on pivot atoms.

The crystal structure of **4** · CH_3CN is severely disordered. The displacement parameters of the heavy atoms were set equal to U_{iso} = 0.05 A^{-2}, subsequently the occupancy factors were refined. Their resulting values were fixed and the refinement of the displacement parameters was performed. The model was checked to be non-contradictory. For this reason the occupancy factors

of each disordered part of the structure were analyzed to give no contradictions with the occupancy factors of conflicting disordered components. The occupancy factors of all atoms in the environment of copper atoms were checked to be in agreement with the occupancy factors and coordination polyhedra of the copper atoms. The missing CH_3CN molecules were found from the difference electron density map. Several solvent CH_3CN molecules are also disordered.

The crystal of **5** · 2 CH_3CN appeared to be a racemic twin (ratio 0.64(2)/0.34(2)) in the space group *Pc*. The structure possesses disorder of the heavy part. To refine the occupancies of these heavy atoms, their isotropic displacement parameters were fixed at 0.05 A^{-2}. The refined values were fixed and the displacement parameters were also refined. The linear counter anion $[CuBr_2]^-$ is disordered over at least two positions with high displacement parameters. On one hand, no residual density was found to correspond to any position of another anion (for example, disordered Br^-) that would allow to reduce the occupancy factors for the $[CuBr_2]^-$ anion. On the other hand, further split of the Cu and Br positions did not give a satisfactory geometry of the anion. Therefore the disorder of the anion over two positions of the same relative weight was accepted as the only possibility to reach charge balance.

In **6** · 0.5 C_7H_8 · 2.5 CH_3CN one of the mesityl ligands and one of the coordinated MeCN group are disordered over two positions with a ratio of 0.5/0.5 and 0.45/0.55, respectively. Solvated MeCN and toluene molecules in **6** · 0.5 C_7H_8 · 2.5 CH_3CN are disordered each over two close positions with the same ratio of 0.5/0.5. In **8** · 0.5 CH_2Cl_2 · 3 CH_3CN and **9** · 0.6 CH_2Cl_2 solvated CH_2Cl_2 molecules partly (0.5 and 0.6) occupy their positions.

CIF files with comprehensive information on the details of the diffraction experiments and full tables of bond lengths and angles for **2-9** are deposited in Cambridge Crystallographic Data Center under the deposition codes CCDC 1043724 - CCDC 1043731, respectively.

Table 4.2 Experimental details for compounds **2** and **3.**

Crystal Data	**2** · 6 CH_3CN	**3** · 6 CH_3CN
CCDC Codes	CCDC 1043724	CCDC 1043726
Chemical formula	$C_{112}H_{136}Cl_{16}Cu_{20}N_{16}P_{12}$·6($C_2H_3N$)	$C_{112}H_{136}Br_{16}Cu_{20}N_{16}P_{12}$·6($C_2H_3N$)
M_r	2081.17	4873.69
Crystal system, space group	triclinic, *P*$\bar{1}$	triclinic, *P*$\bar{1}$
Temperature (K)	173	123
a, *b*, *c* (Å)	14.7230(11), 16.4433(8), 17.7704(9)	14.7655 (4),16.7179(5), 17.9266(5)
α, β, γ (°)	89.990(4), 83.485(5), 71.708(5)	90.321(2), 96.606(2), 108.593(2)
V ($Å^3$)	4055.5(4)	4162.1(2)
Z	1	1

F(000)	2084	2372
Radiation type	Cu K_α	Cu K_α
μ (mm^{-1})	6.68	8.65
Crystal color and shape	orange-red plate	orange block
Crystal size (mm)	0.15 × 0.10 × 0.04	0.13 × 0.07 × 0.04
Data collection		
Diffractometer	Oxford Diffraction Gemini Ultra diffractometer	SuperNova, Titan^{S2} diffractometer
Absorption correction	multi-scan	gaussian
T_{min}, T_{max}	0.569, 1.000	0.627, 0.826
No. of measured, independent and observed [$I > 2\sigma(I)$] reflections	24323, 12422, 9915	25708, 15945, 11431
R_{int}	0.030	0.051
$(\sin\theta/\lambda)_{max}$ ($Å^{-1}$)	0.574	0.625
Range of *h*, *k*, *l*	*h* = -16→16, *k* = -18→14, *l* = -20→20	*h* = -18→17, *k* = -20→15, *l* = -20→22
Refinement		
$R[F^2 > 2\sigma(F^2)]$, $wR(F^2)$, *S*	0.044, 0.127, 1.05	0.048, 0.125, 0.92
No. of reflections	12422	15945
No. of parameters	897	897
H-atom treatment	H-atom parameters constrained	H-atom parameters constrained
$\Delta\rangle_{max}$, $\Delta\rangle_{min}$ (e $Å^{-3}$)	1.20, -0.65	2.47, -1.56

Table 4.3 Experimental details for compounds **4** and **5.**

Crystal Data	**4** · CH_3CN	**5** · 2 CH_3CN
CCDC Codes	CCDC 1043725	CCDC 1043727
Chemical formula	$C_{59}H_{72.50}Br_{7.33}Cu_{9.33}N_{9.50}P_6$	$C_{196}H_{230}Br_8Cu_{16}N_{18}P_{24}$
M_r	2279.51	5237.17
Crystal system, space group	monoclinic, *C*2/*c*	monoclinic, *Pc*
Temperature (K)	123	123
a, *b*, *c* (Å)	30.3248(7), 16.9395(4), 16.0657(3)	26.6111(4), 20.1860(2), 23.5404(3)
α, β, γ (°)	90, 102.218(2), 90	90, 102.911(2), 90
V ($Å^3$)	8065.8(3)	12325.5(3)
Z	4	2
F(000)	4441	5272
Radiation type	Cu K_α	Cu K_α
μ (mm^{-1})	8.32	4.80
Crystal color and shape	orange plate	orange prism
Crystal size (mm)	0.14 × 0.12 × 0.06	0.25 × 0.13 × 0.04

Data collection		
Diffractometer	Supernova, Titan^{S2} diffractometer	Supernova, Titan^{S2} diffractometer
Absorption correction	gaussian	gaussian
T_{min}, T_{max}	0.361, 0.658	0.415, 0.833
No. of measured, independent and observed [$I > 2\sigma(I)$] reflections	23524, 8030, 6220	80558, 38117, 33313
R_{int}	0.063	0.032
$(\sin\theta/\lambda)_{max}$ (Å^{-1})	0.624	0.621
Range of h, k, l	h = -37→35, k = -21→19, l = -18→19	h = -25→32, k = -24→24, l = -26→29
Refinement		
$R[F^2 > 2\sigma(F^2)]$, $wR(F^2)$, S	0.062, 0.175, 0.97	0.059, 0.158, 1.02
No. of reflections	8030	38117
No. of parameters	517	2350
H-atom treatment	H-atom parameters constrained	H-atom parameters constrained
$\Delta\rangle_{max}$, $\Delta\rangle_{min}$ (e Å^{-3})	2.15, -0.78	1.23, -0.67

Table 4.4 Experimental details for compounds **6** and **7**.

Crystal Data	**6** · 0.5 C_7H_8 · 2.5 CH_3CN	**7** · 2 C_7H_8
CCDC Codes	CCDC 1043728	CCDC 1043729
Chemical formula	$C_{34}H_{43}Cu_5I_4N_7P_3$·0.5($C_7H_8$)·2.5($C_2H_3N$)	$C_{49}H_{57}Cu_7I_6N_4P_3$
M_r	1616.67	2001.07
Crystal system, space group	triclinic, $P\bar{1}$	monoclinic, $C2/c$
Temperature (K)	123	123
a, b, c (Å)	13.4384(3), 14.3484(2), 15.5780(4)	31.3947(18), 12.7194(5), 16.5419(8)
α, β, γ (°)	83.695(2), 77.946(2), 80.480(2)	90, 109.401(6), 90
V (Å^3)	2888.2(1)	6230.5(6)
Z	2	4
F(000)	1556	3780
Radiation type	Cu K_α	Cu K_α
μ (mm^{-1})	19.88	26.92
Crystal color and shape	red elongated plate	yellow needle
Crystal size (mm)	0.20 × 0.11 × 0.04	0.24 × 0.04 × 0.04
Data collection		
Diffractometer	Xcalibur, Ruby, Gemini ultra diffractometer	Xcalibur, Ruby, Gemini ultra diffractometer
Absorption correction	gaussian	analytical
T_{min}, T_{max}	0.080, 0.521	0.178, 0.550

No. of measured, independent and observed [$I > 2\sigma(I)$] reflections	31867, 10141, 9195	15147, 5489, 4289
R_{int}	0.027	0.043
$(\sin\theta/\lambda)_{max}$ (Å^{-1})	0.596	0.597
Range of h, k, l	h = -15→15, k = -16→12, l = -18→18	h = -37→33, k = -13→15, l = -12→19
Refinement		
$R[F^2 > 2\sigma(F^2)]$, $wR(F^2)$, S	0.026, 0.069, 1.05	0.044, 0.114, 1.01
No. of reflections	10141	5489
No. of parameters	688	324
H-atom treatment	H-atom parameters constrained	H-atom parameters constrained
$\Delta\rangle_{max}$, $\Delta\rangle_{min}$ (e Å^{-3})	0.98, -2.12	2.84, -1.34

Table 4.5 Experimental details for compounds **8** and **9**.

Crystal Data	**8** · 0.5 CH_2Cl_2 · 3 CH_3CN	**9** · 0.6 CH_2Cl_2
CCDC Codes	CCDC 1043730	CCDC 1043731
Chemical formula	$C_{58.50}H_{72}ClCu_8I_6N_9P_6$	$C_{60.6}H_{75.2}Cl_{1.2}Cu_7FeI_6N_5P_6$
M_r	2392.24	2364.12
Crystal system, space group	monoclinic, $C2/c$	monoclinic, $P2_1/n$
Temperature (K)	123	123
a, b, c (Å)	48.744(3), 12.3812(5), 30.1538(19)	12.5667(6), 29.445(1), 21.734(1)
α, β, γ (°)	90, 117.951(9), 90	90, 90.144(5), 90
V (Å^3)	16075(2)	8042.3(7)
Z	8	4
F(000)	9144	4525
Radiation type	Cu K_α	Cu K_α
μ (mm^{-1})	22.11	23.26
Crystal color and shape	red plate	red rod
Crystal size (mm)	0.27 × 0.18 × 0.03	0.29 × 0.13 × 0.03
Data collection		
Diffractometer	Xcalibur, Ruby, Gemini ultra diffractometer	SuperNova, Single source at offset, Atlas diffractometer
Absorption correction	analytical	analytical
T_{min}, T_{max}	0.055, 0.556	0.069, 0.540
No. of measured, independent and observed [$I > 2\sigma(I)$] reflections	60525, 14144, 6817	27532, 15888, 12704
R_{int}	0.170	0.049
$(\sin\theta/\lambda)_{max}$ (Å^{-1})	0.596	0.628
Range of h, k, l	h = -56→57, k = -14→14, l = -35→19	h = -10→15, k = -35→35, l = -26→27

Refinement		
$R[F^2 > 2\sigma(F^2)]$, $wR(F^2)$, S	0.067, 0.171, 0.79	0.047, 0.163, 1.05
No. of reflections	14144	15888
No. of parameters	815	815
No. of restraints	1	0
H-atom treatment	H-atom parameters constrained	H-atom parameters constrained
$\Delta\rangle_{max}$, $\Delta\rangle_{min}$ (e Å^{-3})	3.19, -1.48	2.05, -1.89

4.5 Author Contributions

- The synthesis and characterization of compound **2** were performed by Dr. Andrea Kuntz and are also part of her dissertation thesis (University of Regensburg, 2010)
- The syntheses and characterization of compounds **3 – 9** were performed by Claudia Heindl
- X-ray structural analysis of **2** was performed by Dr. Manfred Zabel
- X-ray structural analyses of **3 – 9** were performed by Dr. Eugenia V. Peresypkina, Dr. Alexander V. Virovets and Claudia Heindl
- The manuscript (introduction, results and discussion, experimental part; including figures and graphical abstract) was written by Claudia Heindl with the following exceptions:
- The section 'crystallographic details' was written by Dr. Eugenia V. Peresypkina
- MAS NMR investigations of **6** and their description within the manuscript were performed by David Lüdeker and PD Dr. Gunther Brunklaus

4.6 References

[1] a) G. Gritzner, J. Kuta, *Pure Appl. Chem.* 1984, *56*, 461; b) N. G. Connelly, W. E. Geiger, *Chem. Rev.* 1996, *96*, 877.

[2] A. Togni, in *Metallocenes: Synthesis - Reactivity - Applications*, Volume 11 (Eds.: A. Togni, R. Halterman), WILEY-VCH, 1998, pp. 685–718.

[3] a) F. Mathey, *J. Organomet. Chem.* 2002, *646*, 15; b) L. Weber, *Angew. Chem. Int. Ed.* 2002, *41*, 563.

[4] a) C. Mueller, R. Bartsch, A. Fischer, P. G. Jones, R. Schmutzler, *J. Organomet. Chem.* 1996, *512*, 141; b) M. M. Al-Ktaifani, P. B. Hitchcock, J. F. Nixon, *J. Organomet. Chem.* 2008, *693*, 611; c) C. Mueller, R. Bartsch, A. Fischer, P. G. Jones, *Polyhedron* 1993, *12*, 1383. d) M. H. A. Benvenutti, P. B. Hitchcock, J. F. Nixon, M. D. Vargas, *Chem. Commun.* 1996, 441.

[5] a) A. Schindler, M. Zabel, J. F. Nixon, M. Scheer, *Z. Naturforsch.* **2009**, *64*, 1429; b) C. Schwarzmaier, A. Schindler, C. Heindl, S. Scheuermayer, E. V. Peresypkina, A. V. Virovets, M. Neumeier, R. Gschwind, M. Scheer, *Angew. Chem. Int. Ed.* **2013**, *52*, 10896; c) A. Schindler, C. Heindl, G. Balázs, C. Groeger, A. V. Virovets, E. V. Peresypkina, M. Scheer, *Chem. Eur. J.* **2012**, *18*, 829; d) F. Dielmann, A. Schindler, S. Scheuermayer, J. Bai, R. Merkle, M. Zabel, A. V. Virovets, E. V. Peresypkina, G. Brunklaus, H. Eckert, M. Scheer, *Chem. Eur. J.* **2012**, *18*, 1168; e) M. Scheer, *Dalton Trans.* **2008**, 4372.

[6] a) O. Daugulis, H.-Q. Do, D. Shabashov, *Acc. Chem. Res.* **2009**, *42*, 1074; b) C. Zhang, C. Tang, N. Jiao, *Chem. Soc. Rev.* **2012**, *41*, 3464; c) D. M. D'Souza, T. J. J. Mueller, *Chem. Soc. Rev.* **2007**, *36*, 1095.

[7] a) S. Deng, C. Schwarzmaier, M. Zabel, J. F. Nixon, M. Bodensteiner, E. V. Peresypkina, G. Balázs, M. Scheer, *Eur. J. Inorg. Chem.* **2011**, 2991; b) A. Schindler, G. Balázs, M. Zabel, C. Groeger, R. Kalbitzer, M. Scheer, *C. R. Chim.* **2010**, *13*, 1241; c) S. Deng, C. Schwarzmaier, U. Vogel, M. Zabel, J. F. Nixon, M. Scheer, *Eur. J. Inorg. Chem.* **2008**, 4870.

[8] C. Heindl, A. Schindler, M. Bodensteiner, E. V. Peresypkina, A. V. Virovets, M. Scheer, *Phosphorus, Sulfur Silicon and Relat. Elem.* **2015**, *190*, 397.

[9] a) Y. Li, Y. Li, B. Wang, Y. Luo, D. Yang, P. Tong, J. Zhao, L. Luo, Y. Zhou, S. Chen, F. Cheng, J. Qu, *Nat. Chem.* **2013**, *5*, 320; b) M. Wallasch, G. Wolmershäuser, H. Sitzmann, *Angew. Chem. Int. Ed.* **2005**, *44*, 2597; c) H. Sitzmann, T. Dezember, W. Kaim, F. Baumann, D. Stalke, J. Kärcher, E. Dormann, H. Winter, C. Wachter, M. Kelemen, *Angew. Chem. Int. Ed.* **1996**, *35*, 2872; d) M. D. Walter, J. Grunenberg, P. S. White, *Chem. Sci.* **2011**, *2*, 2120.

[10] A. S. Ionkin, W. J. Marshall, B. M. Fish, A. A. Marchione, L. A. Howe, F. Davidson, C. N. McEwen, *Eur. J. Inorg. Chem.* **2008**, 2386.

[11] a) R. Bartsch, P. B. Hitchcock, J. F. Nixon, *J. Organomet. Chem.* **1988**, *340,* C37; b) R. Bartsch, P. B. Hitchcock, J. F. Nixon, *J. Organomet. Chem.* **1988**, *356*, C1; c) P. B. Hitchcock, J. F. Nixon, R. M. Matos, *J. Organomet. Chem.* **1995**, *490*, 155; d) F. G. N. Cloke, J. R. Hanks, P. B. Hitchcock, J. F. Nixon, *Chem. Commun.* **1999**, 1731; e) F. Mathey, *J. Organomet. Chem.* **2002**, *646*, 15; f) G. K. B. Clentsmith, F. G. N. Cloke, M. D. Francis, J. R. Hanks, P. B. Hitchcock, J. F. Nixon, *J. Organomet. Chem.* **2008**, *693*, 2287.

[12] a) M. Hofmann, F. W. Heinemann, U. Zenneck, *J. Organomet. Chem.* **2002**, *643-644*, 357; b) M. M. Al-Ktaifani, P. B. Hitchcock, J. F. Nixon, *J. Organomet. Chem.* **2003**, *665*, 101.

[13] F. W. Heinemann, M. Zeller, U. Zenneck, *Organometallics* **2004**, *23*, 1689.

[14] R. Peng, M. Li, D. Li, *Coord. Chem. Rev.* **2010**, *254*, 1.

[15] K. Sugimoto, T. Kuroda-Sowa, M. Munakata, M. Maekawa, *Chem. Commun.* **1999**, 455.

[16] F. Cecconi, C. A. Ghilardi, S. Midollini, A. Orlandini, *J. Chem. Soc., Chem. Commun.* 1982, 229.

[17] a) C.-M. Che, S.-W. Lai, *Coord. Chem. Rev.* 2005, *249*, 1296; b) M. Jansen, *Angew. Chem.* 1987, *99*, 1136.

[18] a) D. Catheline, D. Astruc, *Organometallics* 1984, *3*, 1094; b) D. Catheline, D. Astruc, *J. Organomet. Chem.* 1983, *248*, C9.

[19] a) F. Dielmann, A. Schindler, S. Scheuermayer, J. Bai, R. Merkle, M. Zabel, A. V. Virovets, E. V. Peresypkina, G. Brunklaus, H. Eckert, M. Scheer, *Chem. Eur. J.* 2012, *18*, 1168; b) E.-M. Rummel, M. Eckhardt, M. Bodensteiner, E. V. Peresypkina, W. Kremer, C. Groeger, M. Scheer, *Eur. J. Inorg. Chem.* 2014, 1625.

[20] a) G. Brunklaus, J. C. C. Chan, H. Eckert, S. Reiser, T. Nilges, A. Pfitzner, *Phys. Chem. Chem. Phys.* 2003, *17*, 3768; b) S. Reiser, G. Brunklaus, J. H. Hong, J. C. C. Chan, H. Eckert, A. Pfitzner, *Chem. Eur. J.* 2002, *8*, 4228.

[21] a) A. Pfitzner, M. F. Braeu, J. Zweck, G. Brunklaus, H. Eckert, *Angew. Chem. Int. Ed.* 2004, *43*, 4228; b) G. Brunklaus, J. C. C. Chan, H. Eckert, *Z. Phys. Chem.* 2003, *217*, 1627.

[22] a) S. E. Ashbrook, J. McManus, M. J. Thrippelton, S. Wimperis, *Prog. Nucl. Magn. Reson. Spec.* 2009, *55*, 160; b) B. Thomas, S. Paasch, S. Steuernagel, K. Eichele, *Solid State Nucl. Magn. Reson.* 2001, *20*, 108.

[23] G. Sheldrick, *Acta Cryst. sect. A* 2008, *64,* 112.

[24] A. Altomare, M. C. Burla, M. Camalli, G. L. Cascarano, C. Giacovazzo, A. Guagliardi, A. G. G. Moliterni, G. Polidori, R. Spagna, *J. Appl. Cryst.* 1999, *32*, 115.

5. 1,2,4-Triphospholyl Anions – Versatile Building Blocks for the Formation of 1D, 2D and 3D Assemblies

C. Heindl, E. V. Peresypkina, A. V. Virovets, V. Y. Komarov, M. Scheer, *Dalton Trans.* **2015**, *44*, 10245-10252.

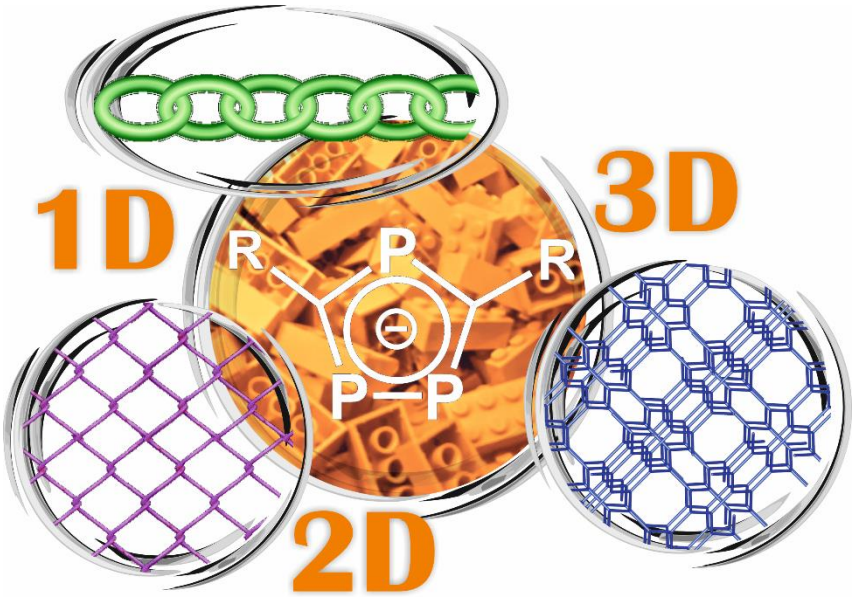

Abstract:

The potential of $K[P_3C_2R_2]$ (R = ^{t}Bu, Mes) as building blocks in metallosupramolecular chemistry was investigated and self-assembly processes with Cu(I) halides result in the formation of a large variety of unprecedented one-, two- and even three-dimensional aggregates. The 3D networks show an interesting topological similarity to allotropes of carbon: diamond and the theoretically proposed polybenzene. Furthermore, the negative charge of the phospholyl ligand favors the generation of cationic Cu_aX_b (a > b, X = Cl, Br, I) assemblies, a challenging area within the well-studied coordination chemistry of CuX units. In addition, the 1D strands were also characterized in solution, revealing that oligomeric units are present.

5.1 Introduction

Self-assembly processes and metal-organic frameworks (MOFs) became indispensable principles in supramolecular and coordination chemistry as well as in crystal engineering.[1] The spontaneous organization of small building blocks to large assemblies by non-covalent interactions is not only of fundamental interest, but also suited for the development of new materials with defined and tunable properties. Especially the involvement of coordinative bonds in metallosupramolecular chemistry offers numerous benefits, since they are relatively strong, but often weak enough to show dynamic behavior. The variety of the used ligands is large, however, the nature of the donor atoms is mostly limited to oxygen, nitrogen or sulphur. So far phosphorus as donor atom played only a minor role, opening a field of broad perspectives. A selection of building blocks based on phosphorus as donor atom is displayed in *Figure 5.1*.

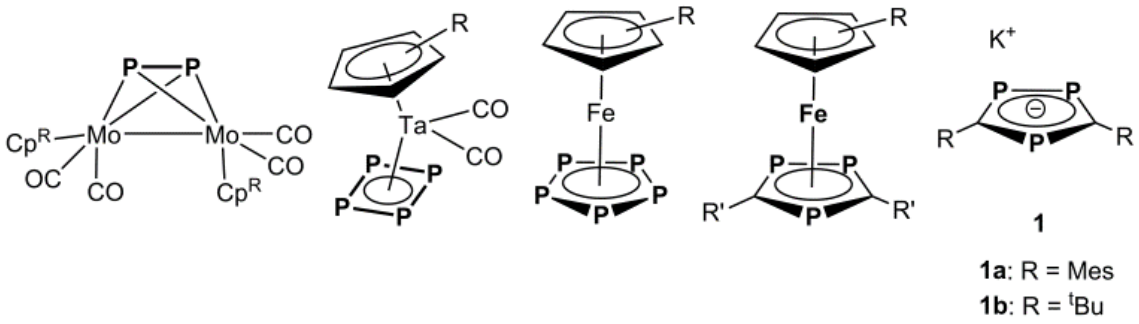

Figure 5.1 Selected building blocks for metallosupramolecular chemistry based on phosphorus as donor atom.

Especially phosphaferrocenes and CuX (X = Cl, Br, I) turned out to be a great combination for the construction of monomeric,[2] oligomeric,[3] polymeric[3,4] and even spherical[5] coordination compounds. This vast abundance of results can be partially traced back to the variability and flexibility of the coordination behavior of Cu halides.[6] Despite this, two aspects still display challenging areas: Firstly, though innumerable neutral and anionic aggregates are reported in literature, cationic Cu_aX_b (a > b) assemblies occur only sporadically. Secondly, the formation of 1D strands or 2D networks is well known, though the isolation of 3D assemblies with phosphorus as donor atom was only possible in very rare cases. To the best of our knowledge, the only examples of 3D aggregates are built up by inorganic cage molecules[7] or an organic linker containing a PPh_3 group.[8] However, especially in view of future usage such as gas storage and catalytic activities, three-dimensional aggregates seem to be the most promising candidates.

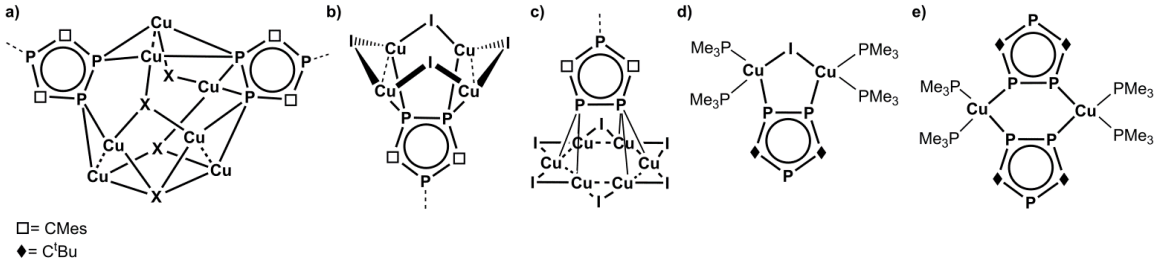

Figure 5.2 Selected coordination compounds containing triphospholyl ligands and Cu(I) halides.

Recently we reported on an unexpected fragmentation of the triphosphaferrocene [Cp*Fe(η^5-$P_3C_2Mes_2$)] (Cp* = η^5-C_5Me_5, Mes = 2,4,6-trimethylphenyl) into $[Cp^*Fe]^+$ and $[P_3C_2Mes_2]^-$ moieties, when reacting it with CuX (X = Cl, Br, I).[9] The remaining phospholyl ligands $[P_3C_2Mes_2]^-$ serve as building blocks for a variety of coordination compounds with rare or even novel structural motifs (*Figure 5.2*a-c). Due to the negative charge of this ligand, a buildup of cationic Cu_aX_b (a > b) aggregates is predetermined. Since the synthesis of [Cp*Fe(η^5-$P_3C_2Mes_2$)] starts from K[$P_3C_2Mes_2$] (**1a**), $FeBr_2$ and LiCp*,[10] the question arose, if the detour of its synthesis and subsequent fragmentation can be avoided. Therefore, we were interested in the suitability of K[$P_3C_2Mes_2$] itself as a building block. In the literature, the use of 1,2,4-triphospholyl salts Q[$P_3C_2R_2$] (Q = Li, K; R = Mes, ^{t}Bu, Ph) was primarily made for the preparation of the sandwich complexes tri- and hexaphosphametallocenes[11] or for coupling reactions resulting in phosphorus rich cage compounds.[12] Investigations concerning its coordination chemistry towards coinage metal salts are rare and mostly started not from its potassium or lithium salts, but by its neutral trimethylstannyl-triphosphole derivatives.[13] Only Nixon *et al.* treated K[$P_3C_2{}^tBu_2$] with Et_3PAuCl and Cu_2I_2/PMe_3, respectively, and obtained monomeric (for Cu see: *Figure 5.2*d) or dimeric products (for Cu see: *Figure 5.2*e).[14] In these reactions the presence of the ligands PEt_3 and PMe_3, respectively, impedes further aggregation.

Herein we report on the self-assembly process of K[$P_3C_2Mes_2$] (**1a**) with CuX (X = Cl, Br, I) yielding the monomeric compounds [(μ,$\eta^{1:2:2}$-$P_3C_2Mes_2$){Cu(CH_3CN)(μ_2-I)}$_4${Cu(CH_3CN)$_3$}] and [(μ,$\eta^{1:3:3}$-$P_3C_2Mes_2$)$_2${Cu(CH_3CN)$_3$}$_2${Cu(μ_2-I)}$_6$], the 3D network **2** as well as the 1D polymers **3**, **4**, **5**, **6**. Furthermore, by using the ^{t}Bu derivative K[$P_3C_2{}^tBu_2$] (**1b**) the 1D polymer **7**, the 3D aggregates **8** and **9** and the 2D network of **10** could be isolated:

[(μ,$\eta^{1:1:2}$-$P_3C_2Mes_2$)$_2${Cu(CH_3CN)}$_2${Cu(CH_3CN)$_2$}]^+_n[Cl]^-_n (**2**)

[(μ,$\eta^{1:2:2}$-$P_3C_2Mes_2$){Cu(CH_3CN)(μ_2-Cl)}$_4${K(μ_2-dme)}{Cu(CH_3CN)$_{0.5}$(μ_2-Cl)}]$_n$ (**3**)

[(μ,$\eta^{1:2:2}$-$P_3C_2Mes_2$){Cu(CH_3CN)(μ_2-Br)}$_4${K(μ_2-thf)}{Cu(μ_2-Br)}]$_n$ (**4**)

[(μ,$\eta^{1:2:2}$-$P_3C_2Mes_2$){Cu(CH_3CN)(μ_2-I)}$_2${Cu(CH_3CN)(μ_3-I)}$_2$Cu]$_n$ (**5**)

[(μ,$\eta^{1:2:2}$-$P_3C_2Mes_2$){Cu(CH_3CN)(μ_3-I)}$_2${Cu(CH_3CN)(μ_4-I)}$_2$Cu$_2${Cu(CH_3CN)}(μ_3-I)(μ_2-I)]$_n$ (**6**)

[(μ,$\eta^{1:2:2}$-$P_3C_2{}^tBu_2$)($CuCl$)$_3$(μ_3-Cl)$_2${Cu(CH_3CN)}$_3${Cu(μ_2-Cl)}{Cu(CH_3CN)$_3$}$_2$]$_n$ (**7**)

$[(P_3C_2{}^tBu_2)_3Cu_{9.85}Cl_{6.85}(CH_3CN)_{1.9}]_n$ (**8**)

$[(P_3C_2{}^tBu_2)_3Cu_{10.1}Br_{7.1}(CH_3CN)_{1.2}]_n$ (**9**)

$[K(thf)_6]_n[(\mu,\eta^{1:3:3}\text{-}P_3C_2{}^tBu_2)_2\{Cu_3(\mu_2\text{-}I)_2\}_2\{Cu(\mu_2\text{-}I)_2\}]_n$ (**10**)

5.2 Results and Discussion

Reactions of $K[P_3C_2R_2]$ (**1**; **1a**: R = Mes; **1b**: R = ^{t}Bu) with CuX (X = Cl, Br, I) were carried out by two different approaches: a yellow to orange solution of **1** in thf or dme can either be layered with a colorless solution of CuX in CH_3CN or both solutions are stirred together. In all cases an immediate color change to deep red can be observed. Depending on the presence and amount of CH_3CN, concentration, molar ratio, crystallization conditions and the R group in the phospholyl ligand, a variety of different products can be isolated (for R = Mes, see *Scheme 5.1*; for R = ^{t}Bu, see *Scheme 5.2*), even with the same halide. In these cases the compounds generally crystallize separately and not as mixtures, therefore a selective synthesis is possible in most instances (for detailed conditions see below and experimental part). In doing so, the stoichiometric amount of CuX is the most significant factor for a directed synthesis, as it can be seen in *Scheme 5.1* and *Scheme 5.2*.

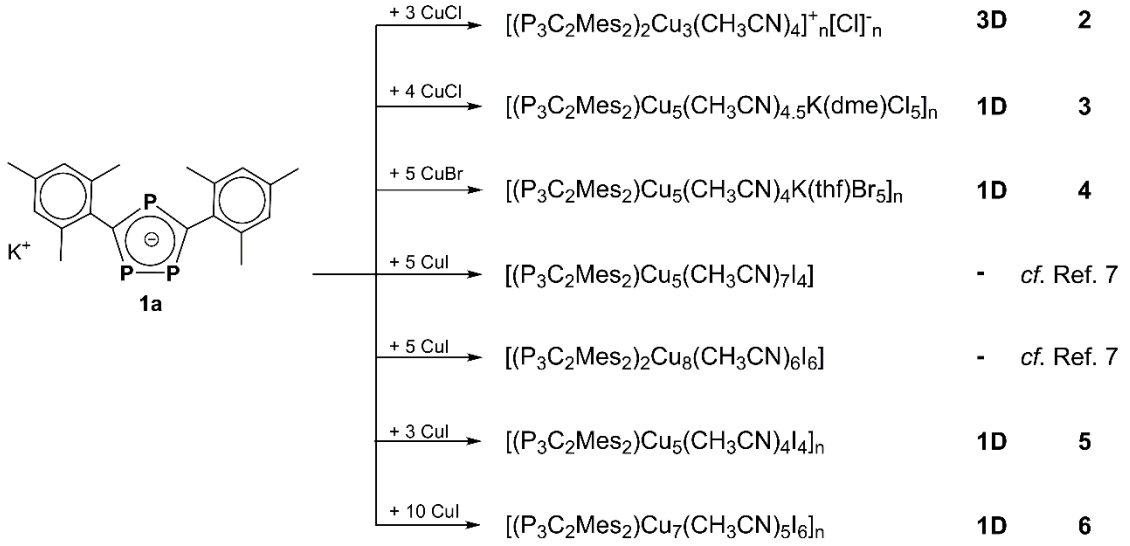

Scheme 5.1 Reactions of **1a** with CuX (X = Cl, Br, I).

Since several coordination compounds containing **1a** exist due to the fragmentation of $[Cp^*Fe(\eta^5\text{-}P_3C_2Mes_2)]$,[9] the question arises, if they can also be synthesized using **1a** as starting material. Indeed, with CuI two known products can be obtained. Both are monomeric compounds, the first with a $\{Cu_4I_4\}$ unit forming a crown-like structural motif (*Figure 5.2*b), the other with a $\{Cu_6I_6\}$ six-point star-like arrangement, which is coordinated by one phospholyl ligand from each side (*Figure 5.2*c). But surprisingly, these two represent the only previously observed examples. In

fact, a great pool of novel coordination polymers with different structural motifs is obtained and is described in the following.

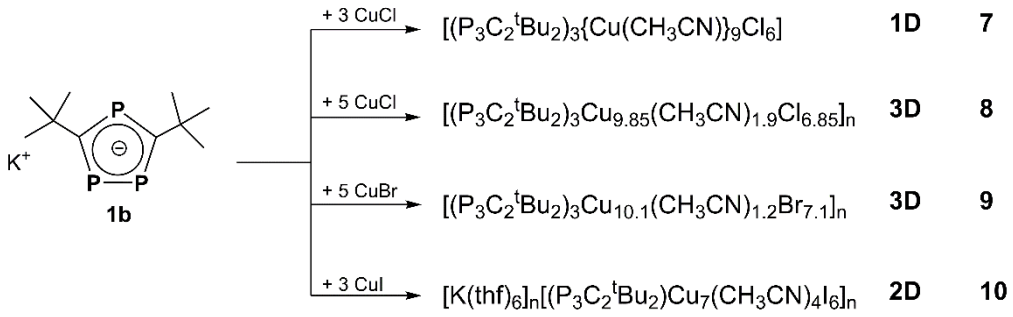

Scheme 5.2 Reactions of **1b** with CuX (X = Cl, Br, I).

One common feature among them is the coordination of all three phosphorus atoms of the triphospholyl ring to form polymeric aggregates. Furthermore, CuCl and CuBr tend to form isotypical compounds (*cf.* compound **3** and **4** and **7** and **8**, respectively), whereas CuI-containing frameworks often differ in their structural motif. Another determining factor is the substitution pattern in the phospholyl ligand. The sterically demanding Mes ligand almost exclusively leads to the formation of 1D strands with compound **2** as an exceptional case. In contrast, smaller ^{t}Bu groups allow the aggregation in all directions. In addition, compounds **2**-**9** show short X···H (X = Cl, Br, I) distances ($< \Sigma_{vdW\text{-}radii}$) with methyl groups of acetonitrile and the R group of **1** (R = Mes, ^{t}Bu) and therefore weak interactions within the chain or layer as well as between them are indicated. Henceforth, the obtained products are described in relation to their dimensionality.

One-dimensional polymers (3-7)

The mesityl group in **1a** exhibits a high steric demand, so that an aggregation in one direction is feasible and preferred. Surprisingly, most of the products (**3**-**6**) show the structural motif of an eight membered $\{Cu_4X_4\}$ ring. Its distortion and close Cu···Cu contacts lead to a crown-like arrangement (*Figure 5.2*b and *Figure 5.3*, left). This is so far only known for X = I[9,15] and here it is rather unusual, since $\{Cu_4I_4\}$ units tend to form heterocubanes or ladders.[6]

Hence, **3** and **4** display the first examples for the Cl- and Br-derivative of this structural motif, respectively. Compound **3** can be isolated as yellow-orange prisms in good yields (57%), compound **4** as yellow-orange blocks in very good yields (88%). Both crystallize as solvates in monoclinic space groups (**3**: $P2_1/n$, **4**: $C2/m$) and display isotypical compounds (*Figure 5.3*a-d). The Cu_2-dimers in the formed crown show a distance of 2.545(1) Å and 2.553(1) Å for **3** and 2.548(1) Å for **4**. They are coordinated by the adjacent P atoms of **1a** with bond lengths of 2.274(1) Å – 2.296(1) Å in **3** and 2.280(1) Å – 2.294(1) Å in **4**, respectively. The halides additionally interact with a potassium centered above the 'crown' (K···Cl: 3.080(2) Å – 3.179(2) Å; K···Br: 3.210(1) Å – 3.344(1) Å). The

coordination sphere is completed by two additional thf (in **3**) or dme (in **4**) molecules. These solvent ligands exhibit a bridging coordination mode and therefore connect two $\{(P_3C_2Mes_2)(Cu_4X_4)\}$ units. The aggregation is accomplished by a $\{Cu_2X_2\}$ four-membered ring, which is coordinated by isolated P atoms of **1a** from each side. These four-membered rings are severely disordered over two (in **3**) up to eight (in **4**) positions around the direction of the chain. In some positions the Cu atoms are additionally coordinated by CH_3CN, therefore some of them show a trigonal, some a tetrahedral environment.

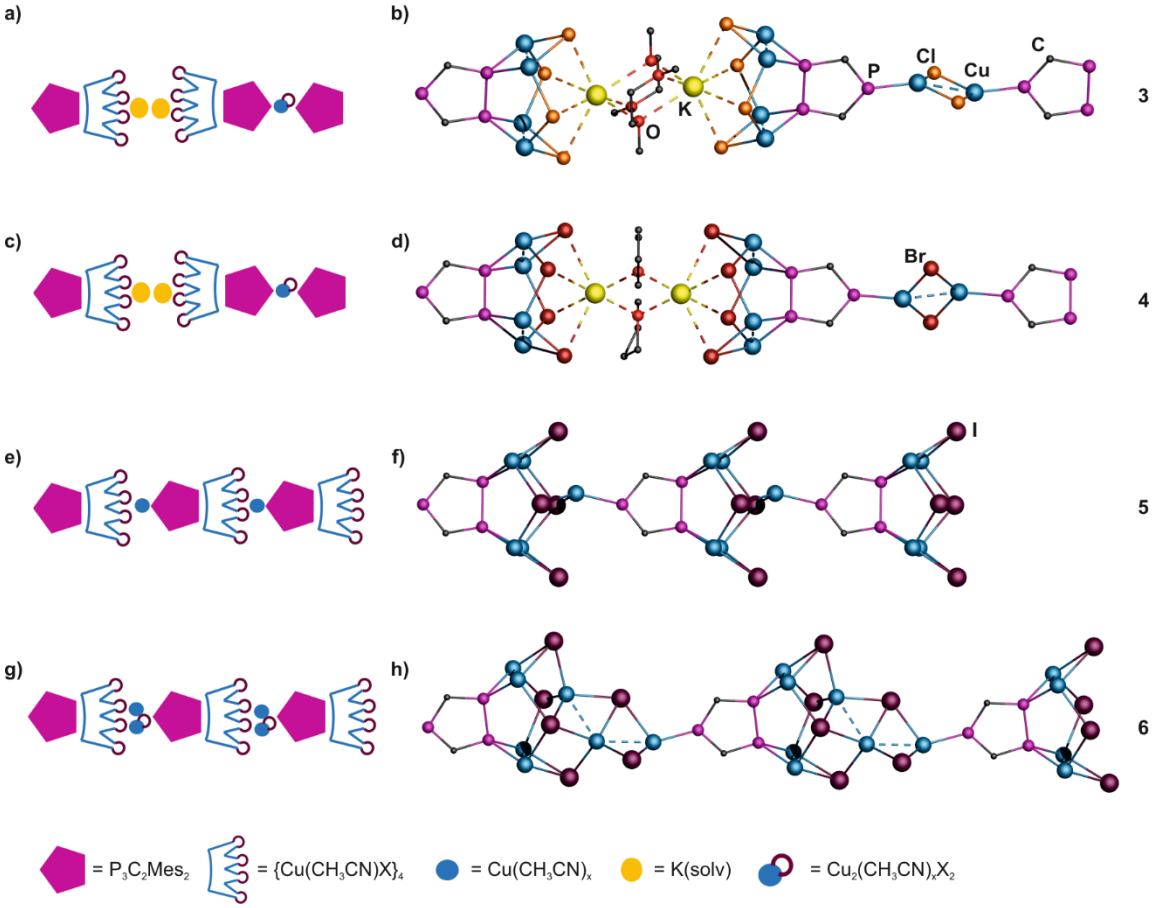

Figure 5.3 Left: schematic representations of the structures of a) **3**; c) **4**; e) **5** and g) **6**; right: sections of the polymeric structures of b) **3**; d) **4**; f) **5** and h) **6**. Mesityl and CH_3CN ligands, H atoms, solvents and minor positions of disordered groups are omitted for clarity.

Using CuI, two slightly different 1D polymers (**5**, **6**) were isolated (*Figure 5.3*e-h). Compound **5** crystallizes as red-brown blocks in the tetragonal space group *P*4/*n*, compound **6** as orange lath-shaped crystals in the triclinic space group *P*$\bar{1}$. The $\{Cu_4I_4\}$ arrangement is similar to **3** and **4** with close Cu···Cu distances (**5**: 2.541(4) Å; **6**: 2.523(2) Å) and Cu-P bond lengths (**5**: 2.277(5) Å – 2.319(6) Å; **6**: 2.285(2) Å – 2.319(2) Å). In **5**, this unit is polymerized into a 1D chain by one additional Cu, coordinated by the isolated P atom of **1a** (P-Cu 2.249(6) Å) and two I-tips of the 'crown' (*Figure 5.3*e,f).

The diffraction pattern of **5** shows quite strong diffuse scattering (see crystallographic details) caused by correlated disorder of the $\{Cu_5I_4(CH_3CN)_4(P_3C_2Mes_2)\}$ repeating units within the polymeric chain. Our attempts to model this effect allowed us to suppose that there is the strong negative correlation (alternation of repeating units' rotations) within the polymeric chains together with a weaker negative correlation between neighboring chains.

In contrast, in **6** a $\{Cu_3I_2\}$ fragment serves as linkage between the top of the crown and the third P atom of the phospholyl ligand (P-Cu 2.214(2) Å) (*Figure 5.3*g,h). The formation of **5** and **6** is remarkable, since the reaction of $[Cp^*Fe(\eta^5\text{-}P_3C_2Mes_2)]$ and CuI also gives a 1D polymer containing the same structural motif, but polymerized *via* a $\{Cu_3I_2\}$ five-membered ring.[9] So, these results again demonstrate the structural variability of the Cu(I) halides, especially of CuI. The orientation of **1a** in **5** and **6** is the same along the chain, while in **3** and **4** they show an alternating orientation. Note, that the Cu_aI_b assembly is positively charged in both polymers, namely $[Cu_5I_4]^+$ in **5** and $[Cu_7I_6]^+$ in **6**. Thus, these examples expand the small and unexplored area of cationic Cu_aX_b clusters. The reason for their formation can be traced back to the use of the negatively charged triphospholyl ligand. This approach was also used in two other examples, in which anionic triazolate and tetrazolate linking units were used, respectively.[16]

Summing up the results of the reaction of **1a** with CuI, four different coordination compounds are obtained. Fortunately, a selective synthesis can be controlled mainly by stoichiometry. For example, an excess of copper iodide (**1a**:Cu = 1:10) leads to the crystallization of solely compound **6**, which is in agreement with the highest molar ratio of Cu in **6** (**1a**:Cu = 1:7). In contrast, the monomeric compound with the Cu_6 star-like arrangement (*Figure 5.2*c) contains the lowest molar ratio of Cu (**1a**:Cu = 1:4) and can therefore be obtained, when less equivalents of CuI are used. Unfortunately, all attempts to reproduce polymer **5** failed, most likely due to the preferred crystallization of its monomeric derivative (*Figure 5.2*b) with the ame molar ratio (**1a**:Cu = 1:5). Also the variation of concentration and solvent were not successful in this case.

Going from **1a** to **1b**, with CuCl the 1D polymer **7** crystallizes as orange plates in the monoclinic space group $P2_1/m$. It reveals a different structural motif than the other one-dimensional 'crown' polymers (*Figure 5.4*). Due to the lower steric demand of the ^{t}Bu group, the arrangement of three phospholyl rings close to each other is possible. They are connected by three Cu_2-dimers (Cu···Cu 2.482(1) Å – 2.496(1) Å), which form a triangular prism (P-Cu 2.325(1) Å – 2.361(1) Å). The prism is capped by two μ_3-Cl with μ_3-Cl-Cu 2.390(1) Å – 2.441(1) Å bond lengths. Each Cu atom is additionally coordinated by either Cl^- or CH_3CN moieties to reach a tetrahedral environment. Two of these three halides are terminal (η^1-Cl-Cu 2.231(1) Å), while the third coordinates another copper atom (μ_2-Cl-Cu 2.279(2) Å – 2.300(2) Å), which is in turn bound to an isolated P atom of **1b**. The remaining P

atoms of the other two ligands prevent polymerization in other directions by coordination of terminal {Cu(CH$_3$CN)$_3$} units (Cu-P 2.191(2) Å). Therefore, compound **7** displays a 1D polymer. The central assembly with 7 Cu$^+$ and 6 Cl$^-$ can be regarded as an isomeric unit to the assembly in **6** and is another unprecedented example of a cationic Cu$_a$X$_b$ unit.

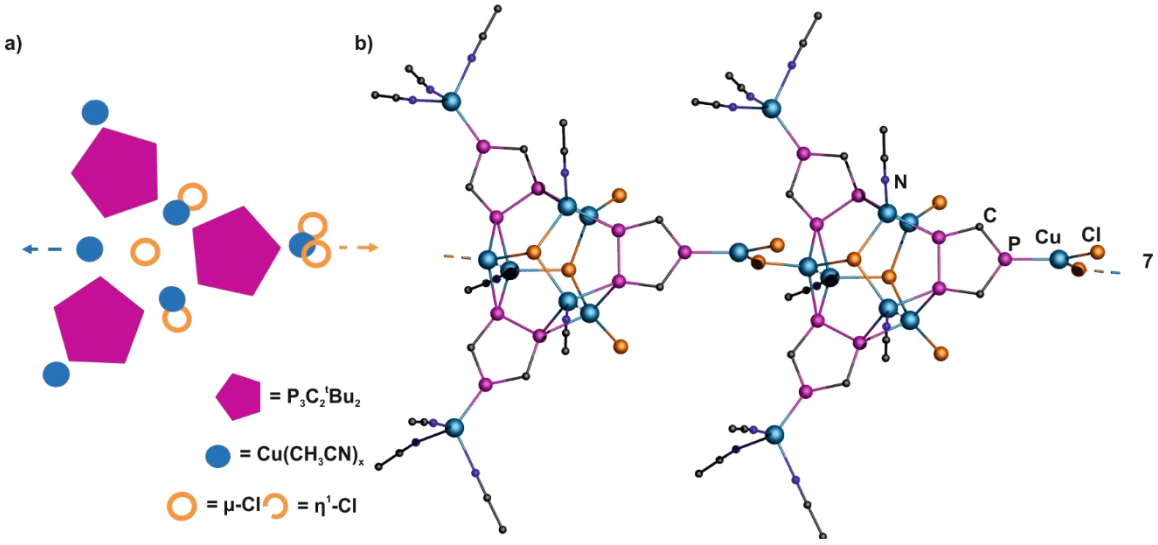

Figure 5.4 a) Schematic representation of the structure of **7**; b) section of the polymeric structure of **7**. ^{t}Bu ligands, H atoms, solvents and minor positions of disordered CH$_3$CN are omitted for clarity.

Two-dimensional assembly (10)

Starting from **1b** and CuI as building blocks occasionally the 2D network **10** can be isolated. Compound **10** crystallizes as dark red brown blocks in the orthorhombic space group *Pbcn*. In **10**, a central Cu$_5$-ring with Cu···Cu distances in the range from 2.540(4) Å – 2.796(4) Å is coordinated from each side by two units of **1b**, which are perpendicular to each other (Cu-P 2.256(5) Å – 2.564(5) Å) (*Figure 5.5*a,b). Four Cu atoms are part of two Cu$_3$I$_2$-rings, a building unit, which also occurs in **8** and **9** (see below). The coordination sphere of the remaining Cu is saturated by two μ$_2$-I ligands (Cu-I 2.483(3) Å – 2.650(3) Å), hence a tetrahedral environment results for each copper atom.

Aggregation takes place by the coordination of the isolated P atom of **1b** to the isolated Cu atom of the perpendicular {Cu$_3$I$_2$} ring *via* a relatively short Cu-P bond of 2.215(5) Å. Through the propagation in four directions within the layer a mesh-like structure is formed (*Figure 5.5*c). Furthermore, **10** also displays an unprecedented representative of a cationic copper halide aggregate, since 7 Cu$^+$ and 6 I$^-$ are present in the repeating unit. In total, the combination with two units of **1b** even leads to an anionic assembly, which is balanced by K(thf)$_6^+$ cations embedded in the mashes and separating the layers from each other. Together with the ^{t}Bu groups of **1b** the meshes do not provide free space. Due to the alternating arrangement of cationic and anionic 'layers' no short I···H distances can be found in the crystal structure of **10**.

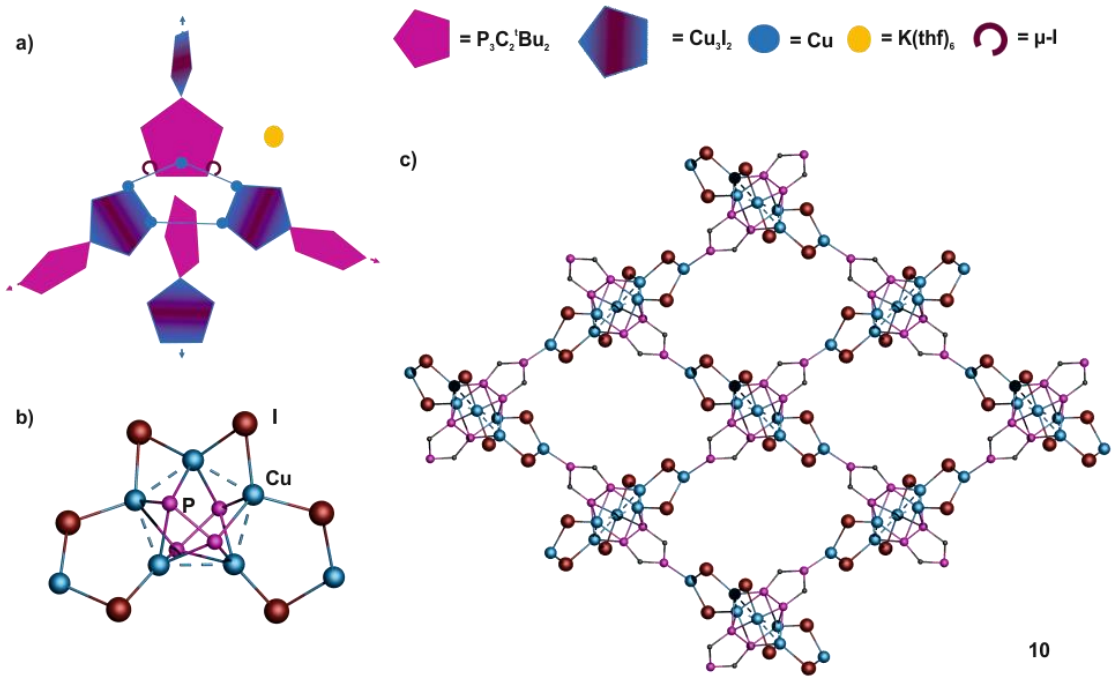

Figure 5.5 a) Schematic representation of the structure of **10**; b) core motif of **10**; c) section of the 4-connected anionic polymer network of **10**. ^{t}Bu and CH_3CN ligands, H atoms, solvents and counterions are omitted for clarity.

Three-dimensional networks (2, 8, 9)

Surprisingly, from the reaction of **1a** with CuCl as a second product also the 3D polymer **2** can be isolated, despite the sterically demanding Mes group. Since they differ significantly in their Cu content, a directed synthesis is enabled by stoichiometric control. More than three equivalents CuCl lead to the formation of **3** (**1a**:Cu = 1:5), whereas three or less equivalents of CuCl result in the crystallization of **2** (**1a**:Cu = 1:1.5).

Compound **2** crystallizes as red blocks in the tetragonal space group $I\bar{4}2d$. The repeating unit contains four phospholyl ligands **1a**, whose adjacent P atoms are connected *via* two Cu_2 dimers (Cu···Cu 2.555(2) Å; P-Cu 2.181(4) – 2.503(5) Å) (*Figure 5.6*a-c). Hence, this is the only assembly, whose central core structure does not include a halide and is built up only by **1a** and Cu units. The linkage of the remaining P atoms of the phospholyl rings by $Cu(CH_3CN)_2$ leads to a polymeric structure. Charge balance is afforded by the presence of an uncoordinated Cl^- per repeating unit (4 **1a**$^-$, 5 Cu^+, 1 Cl^-).

In addition, this core acts as a tetrahedral node and induces a propagation in the other two dimensions, resulting in a 3D network (*Figure 5.6*e-f). Analysis with TOPOS 4.0 reveals that its net topology can be assigned to the **dia** type (*Figure 5.6*d).[17] Hence, it shows topological similarity with diamond, which gives this net its name.

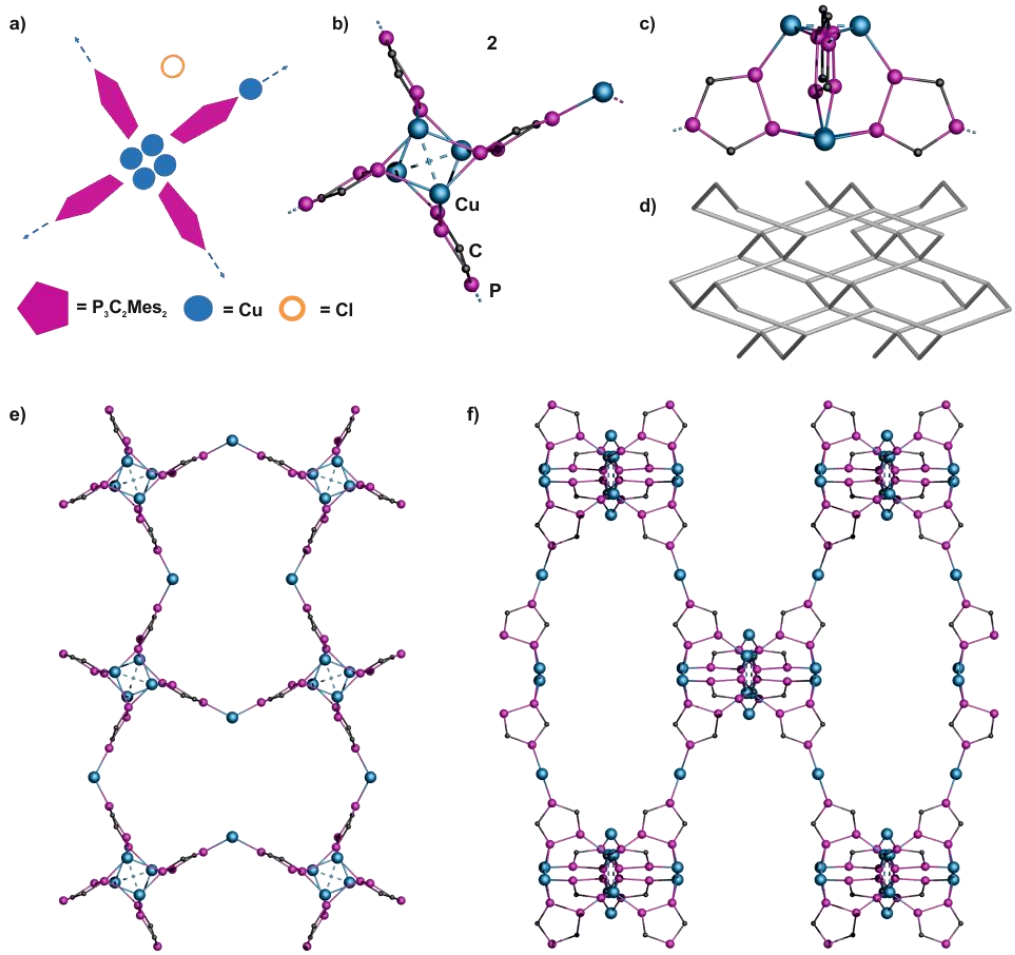

Figure 5.6 a) Schematic representation of the structure of **2**; b) central structural motif of **2** (top view); c) central motif of **2** (lateral view) illustrating the tetrahedral nodes; d) fragment of the **dia** net; e)-f) sections of the cationic polymer network of **2**. View along the e) *c* axis, f) *a* axis. Mes and CH_3CN ligands, H atoms, counterions and solvents are omitted for clarity.

Also with R = ^{t}Bu in **1b** the formation of three-dimensional networks is observed. When a solution of **1b** in dme is layered with a solution of CuX (X = Cl, Br), at the phase boundary the formation of big dark red blocks of **8** (X = Cl) and **9** (X = Br), respectively, can be observed already after one day. Both compounds are isotypical and crystallize in the cubic space group $F\bar{4}3c$.

However, their core structures turned out to be severely disordered. The crystal structure of **9** is more ordered, therefore it will be described first. The central structural motif of **9** contains three Cu_2-dimers and the adjacent P atoms of three units of **1b**, which are arranged according to a distorted hexagonal $\{P_6Cu_6\}$ prism (Cu···Cu 2.694(1) Å – 2.783(2) Å; Cu-P 2.298(2) Å – 2.620(2) Å) (*Figure 5.7*a-c). This prism is capped by copper on one side and by a CuBr unit on the other one. In addition, each Cu_2-dimer is a component of a $\{Cu_3Br_2\}$ five-membered ring (similarly to **10**). This description is the case for 87% of **9**, whereas in its minor part (13%) the μ_3-Br coordinates an additional $\{Cu(CH_3CN)_3\}$ unit, and some Br positions are replaced by acetonitrile ligands. In **8**, the

disorder is similar and the major part remains the same as in **9**. However, different occupation factors and additional Cu deficiencies make its description more complicated (see crystallographic section). In total, the differences in the occupation factors of the disordered fragments for **8** and **9** and the requirement of a charge balance lead to the sum formulae $[(P_3C_2{}^tBu_2)_3Cu_{9.85}Cl_{6.85}(CH_3CN)_{1.9}]_n$ for **8** and $[(P_3C_2{}^tBu_2)_3Cu_{10.1}Br_{7.1}(CH_3CN)_{1.2}]_n$ for **9**.

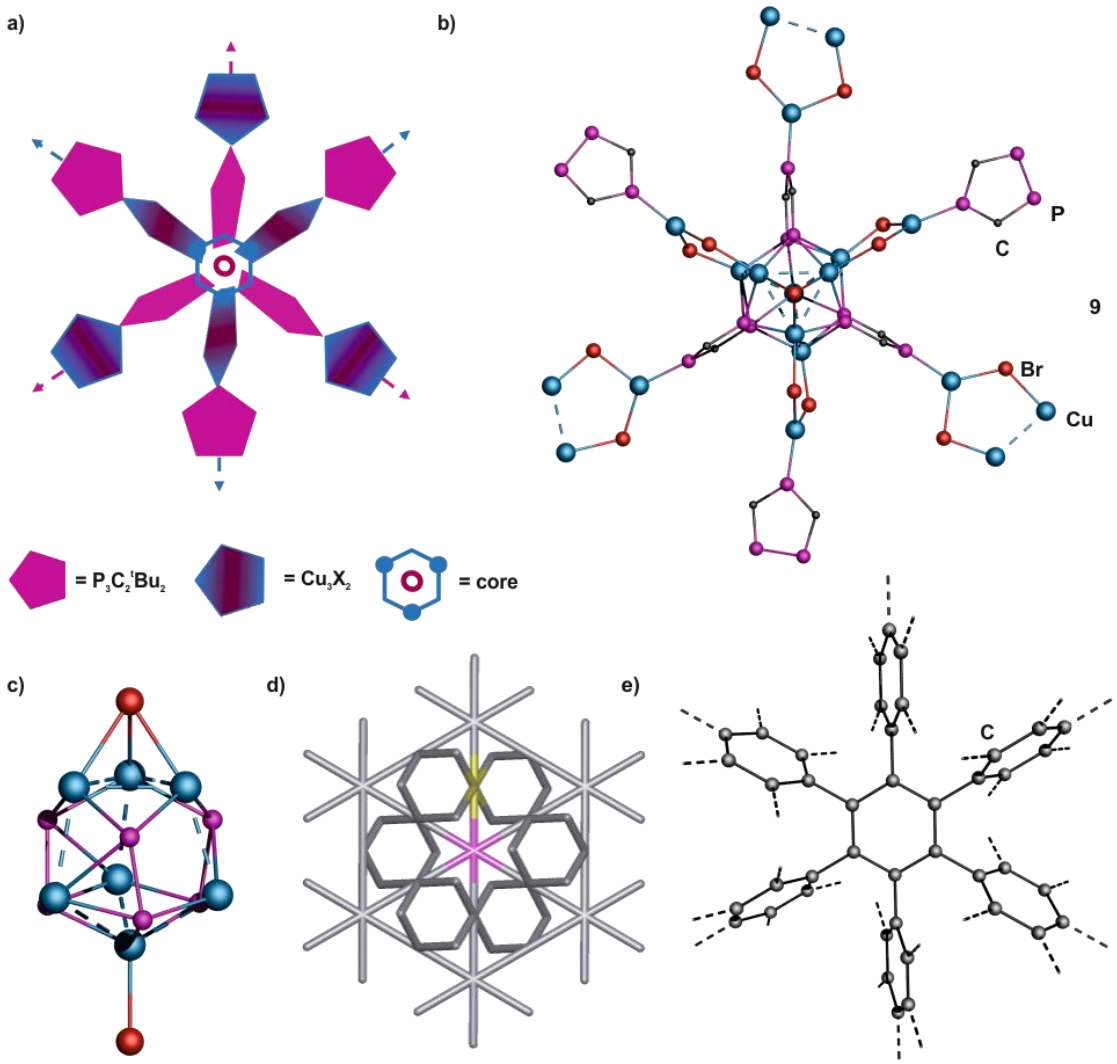

Figure 5.7 a) Schematic representation of the structure of **8** and **9**; b) section of the polymeric structure of **9**. ^{t}Bu and CH_3CN ligands, H atoms, solvents and minor positions of disordered fragments are omitted for clarity; c) major part of the central core motif in **9** (87%); d) fragment of the **hxg** net with mutually tilted 6-connected nodes marked in magenta and yellow; e) section of the polymeric structure of polybenzene (simulated).

Interestingly, the core of both compounds **8** and **9** is proceeded stellar-like to give a 6-connected 3D network (*Figure 5.7*a,b). It demonstrates topological similarity with one of the theoretically possible allotropes of carbon, so-called polybenzene or cubic graphite (*Figure 5.7*e). The polybenzene structure can be derived from a benzene molecule if every hydrogen atom is replaced by a phenyl ring, in which every hydrogen atom is in turn replaced by a phenyl ring, *etc* (*Figure 5.7*e).[18,19] This structure was first predicted by Gibson *et al.* in 1946.[20] Calculations based on first-

principles molecular dynamics showed that this carbon allotrope should be quite stable, but so far no synthetic approach was found.[19]

If one treats the phenyl ring as a 'node' of the framework, the resulting 6-connected 3D net belongs to the **hxg** topological type (*Figure 5.7*d),[17,21] the same as the found 3D framework in **8** and **9** irrespective of any disorder. Eight other crystal structures of coordination polymers retain the same topological type. In these complexes $\{M_3(\mu_3\text{-}O)\}^{4+}$ or $\{M_3(\mu_3\text{-}OH)\}^{5+}$ units (M^{2+} = Cu^{2+}, Ni^{2+}) are joint to each other by N-heterocyclic bridging ligands like 1,2,4-triazolate,[22] 5-(4-pyridyl)tetrazolate,[23] or pyrazole-4-carboxylate.[24] Interestingly, all structures crystallize or are described in cubic space groups, *i.e.* $Fd\bar{3}c$ ($\{M_3(\mu_3\text{-}O)\}$- or $\{M_3(\mu_3\text{-}OH)\}$-based polymers), $Pn\bar{3}m$ (polybenzene) and $F\bar{4}3c$ (**8** and **9**).

Whereas crystals of **2** decompose rapidly in air, the crystals of **8** and **9** turned out to be extremely stable. They were kept in air during two years, intriguingly without losing crystallinity. A repeated elemental analysis of **9** and X-ray diffraction experiments of **8** and **9**, respectively, proved the identical composition and excluded oxidation.

Since the combination of CuCl and **1b** leads to two different compounds (**7** and **8**), the conditions of a directed synthesis were investigated. In this case the used method turned out to be of importance. Since **7** is soluble, it can be isolated from stirring experiments, while diffusion methods exclusively lead to the crystallization of the completely insoluble polymer **8**. As a supporting factor, a higher molar ratio is used for the synthesis of **8** (**1b**:Cu = 1:5).

Characterization in solution

All received compounds are insoluble in common solvents like hexane, toluene, Et_2O, thf, dme and CH_2Cl_2. Only the 1D polymers (**3**-**7**) are soluble in CH_3CN to give yellow to deep red solutions. If a coordination to Cu (nuclear spin I = 3/2) is still present in solution one would expect two broad signals in the corresponding $^{31}P\{^1H\}$ NMR spectra. This is the case for **6** and **7**. The signals of **6** appear at δ = 136 and 222 ppm with the integral ratio of 2:1 for the adjacent and the isolated P atoms of the phospholyl ring, respectively. In comparison with the salt **1a** (δ = 261.7 ppm (t, 1 P) and 266.4 ppm (d, 2 P)), both signals are shifted to higher field. Interestingly, the adjacent phosphorus atoms show a much more intensive shift (130 ppm) than the isolated one (40 ppm) so that the order of the signals is inverted. In contrast, the signals of the adjacent P atoms of **1b** (δ = 246.3 ppm (d, 2 P)) are shifted to a higher field than the isolated one (δ = 254.9 ppm (t, 1 P)), which is reversed compared to **1a**. However, in **7** this trend does not occur and the signals of **7** (δ = 137 (2 P) and 264 (1 P) ppm) appear in the same order like in the spectra of **1a** and **6**. Hence, the signal of the isolated

phosphorus shows a slight downfield shift of 11 ppm, whereas the signal of the adjacent P atoms is strongly upfield shifted by 109 ppm.

In contrast, the $^{31}P\{^{1}H\}$ NMR spectrum of **3** shows only one small broad signal at 205 ppm, so Cu remains coordinated to the phospholyl ligand in solution. The lack of a second signal might be a hint of the equivalence of the P atoms. However, a more likely reason is the disappearance of the other signal below the noise floor due to its broadness, since the quality of the spectrum is due to the bad solubility already quite poor.

Surprisingly, the $^{31}P\{^{1}H\}$ NMR spectrum of the isotypical compound **4** shows three signals. Due to the identical shift the signal at δ = 138 ppm it can be assigned to the isolated P atom of the phospholyl ligand. The other two signals appear at 204 and 217 ppm, respectively. This indicates the presence of two different species in the ratio of 3:1. The signals might be attributed to a smaller, monomeric and a larger, oligomeric unit. Similar depolymerization processes were also observed for other phospholyl-based polymers.[9]

The exact size of the aggregate in solution cannot be derived from the NMR spectra, though hints for at least oligomeric units are also given by mass spectrometry. The corresponding cationic ESI mass spectra show fragments up to $[(P_3C_2Mes_2)_4Cu_{11}Cl_6]^+$, $[(P_3C_2Mes_2)_4Cu_{10}Br_5]^+$, $[(P_3C_2Mes_2)_4Cu_{10}I_5]^+$ and $[(P_3C_2{}^tBu_2)_7Cu_{16}Cl_8]^+$, respectively.

The 2D and 3D networks are insoluble even in CH_3CN. However, its analysis by ESI mass spectrometry was able for **2** and **9** after sonication, which leads to a degradation of the 3D network. The corresponding spectra look almost the same like the above mentioned ones with $[(P_3C_2Mes_2)_5Cu_8Cl_2]^+$ as the biggest fragment for **2** and $[(P_3C_2{}^tBu_2)_7Cu_{17}Br_9]^+$ for **9**.

Furthermore, solutions of the polymeric compounds **2**, **4**, **7**-**9** and the monomeric compound $[(P_3C_2Mes_2)\{Cu(CH_3CN)(\mu_2\text{-}I)\}_4\{Cu(CH_3CN)_3\}]$ (marked as **1a**Cu_5I_4) in CH_3CN were analyzed by UV-vis spectroscopy (*Figure 5.8*; performed by Dr. Hirsch, University of Regensburg). The solubility of the 3D polymer **9** is too poor, even for UV-vis spectroscopy analysis, therefore no absorption could be detected. All other compounds show several partially overlapping absorption bands. The spectra of $[(P_3C_2Mes_2)\{Cu(CH_3CN)(\mu_2\text{-}I)\}_4\{Cu(CH_3CN)_3\}]$, the bromine-containing 1D polymer **4** and the chlorine-containing 3D polymer **2** all show an absorption band at λ = 532 nm, responsible for the red color of the respective solution. In contrast, the solutions of the 1D chain **7** and the 3D network **8** are yellow. Therefore no relation between absorption and dimensionality or the present halide of the polymeric scaffolds can be drawn, respectively. However, a relationship between absorption and the R group of the phospholyl group is indicated, since $[(P_3C_2Mes_2)\{Cu(CH_3CN)(\mu_2\text{-}I)\}_4\{Cu(CH_3CN)_3\}]$, **4** and **2** all contain the mesityl substituted building

block **1a**, whereas **7** and **8** are built up by the ^{t}Bu derivative **1b**. Moreover, these results are in agreement with the depolymerization processes in donor solvents like CH_3CN as discussed above.

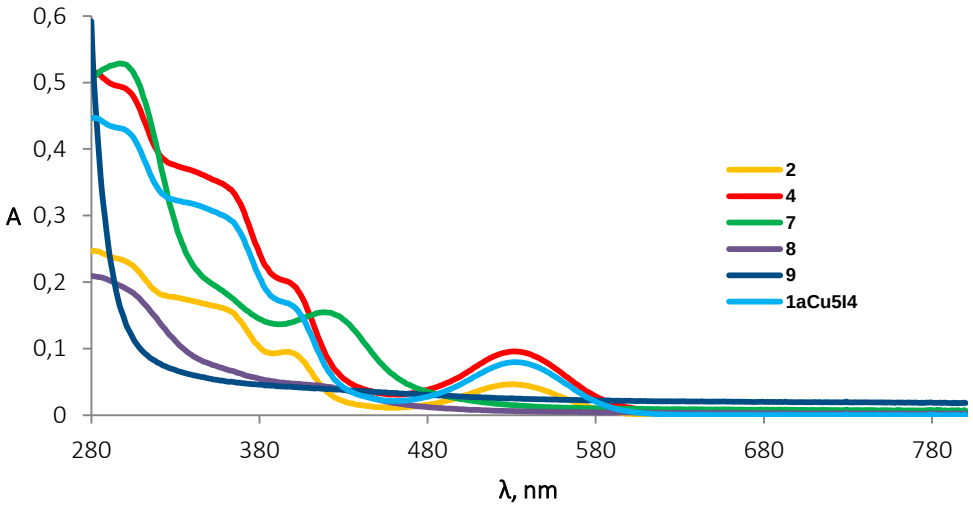

Figure 5.8 UV-vis spectra of **2**, **4**, **7-9** and $[(P_3C_2Mes_2)\{Cu(CH_3CN)(\mu_2\text{-}I)\}_4\{Cu(CH_3CN)_3\}]$ (marked as **1a**Cu_5I_4) in CH_3CN.

Conclusions

In summary, the triphospholyl ligands **1a** and **1b** were introduced as building blocks in supramolecular chemistry. The self-assembly processes with CuX (X = Cl, Br, I) lead to the formation of unprecedented polymeric networks. The negative charge of the cyclic ligand favors the aggregation of cationic Cu_aX_b (a > b) assemblies, which occurred so far only rarely. The 1D strands in **3**-**6** show a rather uncommon crown-like arrangement. The 2D network of **10** is comparable with a wire-mesh. Even the selective synthesis of three-dimensional aggregates is possible, all of them exhibiting an interesting structure. The net of **2** reveals tetrahedral nodes and a resulting **dia**-topology and is therefore related to diamond. On the other hand, the star-like build-up of compounds **8** and **9** can be assigned to the **hxg**-topology, hence it shows structural analogy to 'polybenzene'. This allotrope of carbon is proposed to be quite stable, however could not be synthesized so far. The results nicely demonstrate the potential of the triphospholyl ligands in supramolecular chemistry, especially for the formation of MOF-like assemblies.

5.3 Experimental Part

General Remarks:

All reactions were performed under an inert atmosphere of dry nitrogen or argon with standard vacuum, Schlenk and glove-box techniques. Solvents were purified, dried and degassed prior to use by standard procedures. $K[P_3C_2Mes_2]$[10] and $K[P_3C_2{}^{t}Bu_2]$[25] were synthesized following reported

procedures. Commercially available chemicals (CuCl, CuBr, CuI) were used without further purification. Solution NMR spectra were recorded on a Bruker Avance 300 or 400 spectrometer. The corresponding ESI-MS spectra were acquired on a ThermoQuest Finnigan MAT TSQ 7000 mass spectrometer and elemental analyses were performed on a Vario EL III apparatus.

Synthesis of $[(\mu,\eta^{1:1:2}\text{-}P_3C_2Mes_2)_2\{Cu(CH_3CN)\}_2\{Cu(CH_3CN)_2\}]^+_n[Cl]^-_n$ (2)

In a Schlenk tube a solution of $K[P_3C_2Mes_2]$ (66 mg, 0.17 mmol) in dme (10 mL) is layered with a solution of CuCl (50 mg, 0.5 mmol) in CH_3CN (10 mL). At the phase boundary a color change to deep red can be observed. After complete diffusion and precipitation of a beige powder the red solution is decanted. While storing at 8°C, the formation of red rods of **2** can be observed within a few days. The mother liquor is decanted, the crystals are washed with hexane (3 x 5 mL) and dried *in vacuo*. By concentrating the mother liquor and layering with Et_2O, a second crop of crystals can be obtained.

Analytical data of **2**:

Yield: 40 mg (0.34 mmol, 20%)

^{1}H NMR (CD_3CN): δ [ppm] = 2.02 (s, 3H, *o*-CH_3), 2.11 (s, 3H, *o*-CH_3), 2.25 (s, 3H, *p*-CH_3), 3.28 (s, ($C\underline{H}_3OCH_2)_2$), 3.45 (s, ($CH_3OC\underline{H}_2)_2$), 6.88 (s, 2H, *aryl*-H).

Positive ion ESI-MS (CH_3CN): *m/z* = 2356.7 $[\{P_3C_2Mes_2\}_5Cu_8Cl_2]^+$, 2257.6 $[\{P_3C_2Mes_2\}_5Cu_7Cl]^+$, 2036.4 $[\{P_3C_2Mes_2\}_4Cu_8Cl_3]^+$, 1936.6 $[\{P_3C_2Mes_2\}_4Cu_7Cl_2]^+$, 1837.6 $[\{P_3C_2Mes_2\}_4Cu_6Cl]^+$, 1739.6 $[\{P_3C_2Mes_2\}_4Cu_5]^+$, 1517.3 $[\{P_3C_2Mes_2\}_3Cu_6Cl_2]^+$, 1419.2 $[\{P_3C_2Mes_2\}_3Cu_5Cl]^+$, 1319.3 $[\{P_3C_2Mes_2\}_3Cu_4]^+$, 998.9 $[\{P_3C_2Mes_2\}_2Cu_4Cl]^+$, 901.2 $[\{P_3C_2Mes_2\}_4Cu_6]^{2+}$.

Negative ion ESI-MS (CH_3CN): *m/z* (%) = 232.6 $[Cu_2Cl_3]^-$, 134.8 (100) $[CuCl_2]^-$.

Synthesis of $[(\mu,\eta^{1:2:2}\text{-}P_3C_2Mes_2)\{Cu(CH_3CN)(\mu_2\text{-}Cl)\}_4\{K(\mu_2\text{-}dme)\}\{Cu(CH_3CN)_{0.5}(\mu_2\text{-}Cl)\}]_n$ (3)

In a Schlenk tube a solution of $K[P_3C_2Mes_2]$ (50 mg, 0.12 mmol) in dme (9 mL) is first layered with a solvent mixture of dme and CH_3CN (1:1; 3 mL), afterwards with a solution of CuCl (51 mg, 0.52 mmol) in CH_3CN (12 mL). After complete diffusion and precipitation of a beige powder the red solution is filtered and concentrated to 5 mL. While storing at -28°C the formation of yellow prisms of **3** can be observed within a few days. The mother liquor is decanted, the crystals are washed with hexane (3 x 5 mL) and dried *in vacuo*. By concentrating the mother liquor, a second crop of crystals can be obtained.

Analytical data of **3**:

Yield: 66 mg (0.068 mmol, 57%)

^{1}H NMR (CD_3CN): δ [ppm] = 1.95 (s, CH_3CN), 2.03 (s, 3H, *o*-CH_3), 2.19 (s, 3H, *o*-CH_3), 2.26 (s, 3H, *p*-CH_3), 6.90 (s, 2H, *aryl*-H).

^{31}P{^{1}H} NMR (mother liquor, C_6D_6 capillary): δ [ppm] = 31.3 (br), 117.7 (br), 218.3 (br).

Positive ion ESI-MS (CH_3CN): *m/z* = 2333.9 $[\{P_3C_2Mes_2\}_4Cu_{11}Cl_6]^+$, 2232.7 $[\{P_3C_2Mes_2\}_4Cu_{10}Cl_5]^+$, 2134.4 $[\{P_3C_2Mes_2\}_4Cu_9Cl_4]^+$, 2035.2 $[\{P_3C_2Mes_2\}_4Cu_8Cl_3]^+$, 1978.5 $[\{P_3C_2Mes_2\}_4Cu_7Cl_2\{CH_3CN\}]^+$, 1937.1 $[\{P_3C_2Mes_2\}_4Cu_7Cl_2]^+$, 1837.2 $[\{P_3C_2Mes_2\}_4Cu_6Cl]^+$, 1738.5 $[\{P_3C_2Mes_2\}_4Cu_5]^+$, 1617.1 $[\{P_3C_2Mes_2\}_3Cu_7Cl_3]^+$, 1419.4 $[\{P_3C_2Mes_2\}_3Cu_5Cl]^+$, 1319.0 $[\{P_3C_2Mes_2\}_3Cu_4]^+$, 1198.8 $[\{P_3C_2Mes_2\}_2Cu_6Cl_3]^+$, 1139.8 $[\{P_3C_2Mes_2\}_2Cu_5Cl_2\{CH_3CN\}]^+$, 1098.8 $[\{P_3C_2Mes_2\}_2Cu_5Cl_2]^+$, 991.7 $[\{P_3C_2Mes_2\}_4Cu_7Cl\{CH_3CN\}_2]^{2+}$, 970.7 $[\{P_3C_2Mes_2\}_4Cu_7Cl\{CH_3CN\}]^{2+}$, 950.7 $[\{P_3C_2Mes_2\}_4Cu_7Cl]^{2+}$, 901.2 $[\{P_3C_2Mes_2\}_4Cu_6]^{2+}$

Negative ion ESI-MS (CH_3CN): *m/z* (%) = 530.4 $[Cu_5Cl_6]^-$, 232.8 $[Cu_2Cl_3]^-$, 135.0 (100) $[CuCl_2]^-$

Elemental analysis: Calculated (%) for $[(P_3C_2Mes_2)Cl_5Cu_5K(CH_3CN)(dme)_{0.5}]$ (976 g/mol): C 29.55, H 3.10, N 1.44; found: C 29.12, H 3.29, N 1.83.

Synthesis of $[(\mu,\eta^{1:2:2}\text{-}P_3C_2Mes_2)\{Cu(CH_3CN)(\mu_2\text{-}Br)\}_4\{K(\mu_2\text{-}thf)\}\{Cu(\mu_2\text{-}Br)\}]_n$ (4)

In a Schlenk tube a solution of $K[P_3C_2Mes_2]$ (50 mg, 0.12 mmol) in dme (9 mL) is first layered with a solvent mixture of dme and CH_3CN (1:1; 3 mL), afterwards with a solution of CuBr (93 mg, 0.52 mmol) in CH_3CN (12 mL). After complete diffusion and precipitation of a beige powder the red solution is stored at -28°C. Within one day the formation of yellow-orange blocks of **4** can be observed. The mother liquor is decanted, the crystals are washed with hexane (3 x 5 mL) and thf (2 x 8 mL) and dried *in vacuo*. By concentrating the mother liquor and storing it at -28°C, a second crop of crystals can be obtained. **4** can also be synthesized by using thf instead of dme, however due to the lower solubility of $K[P_3C_2Mes_2]$ in thf a larger amount is needed (20 mL).

Analytical data of **4**:

Yield: 145 mg (0.106 mmol, 88%)

^{1}H NMR (CD_3CN): δ [ppm] = 1.79 (m, thf), 1.95 (s, CH_3CN), 2.04 (s, 3H, *o*-CH_3), 2.11 (s, 3H, *o*-CH_3), 2.26 (s, 3H, *p*-CH_3), 3.63 (m, thf) 6.89 (s, 2H, *aryl*-H).

^{31}P{^{1}H} NMR (CD_3CN): δ [ppm] = 137.9 (br), 204.3 (br), 216.8 (br).

Positive ion ESI-MS (CH_3CN): *m/z* = 2457.8 $[\{P_3C_2Mes_2\}_4Cu_{10}Br_5]^+$, 2313.5 $[\{P_3C_2Mes_2\}_4Cu_9Br_4]^+$, 2169.1 $[\{P_3C_2Mes_2\}_4Cu_8Br_3]^+$, 2025.2 $[\{P_3C_2Mes_2\}_4Cu_7Br_2]^+$, 1881.4 $[\{P_3C_2Mes_2\}_4Cu_6Br_1]^+$, 1749.0 $[\{P_3C_2Mes_2\}_3Cu_7Br_3]^+$, 1738.6 $[\{P_3C_2Mes_2\}_4Cu_5]^+$, 1474.5 $[\{P_3C_2Mes_2\}_4Cu_{14}Br_8]^{2+}$, 1423.6 $[\{P_3C_2Mes_2\}_4Cu_{13}Br_7\{CH_3CN\}]^{2+}$, 1373.9 $[\{P_3C_2Mes_2\}_4Cu_{12}Br_6\{CH_3CN\}_2]^{2+}$, 1302.0 $[\{P_3C_2Mes_2\}_4Cu_{11}Br_5\{CH_3CN\}_2]^{2+}$, 1280 $[\{P_3C_2Mes_2\}_4Cu_{11}Br_5\{CH_3CN\}]^{2+}$, 1259 $[\{P_3C_2Mes_2\}_4Cu_{11}Br_5]^{2+}$, 1229.5 $[\{P_3C_2Mes_2\}_4Cu_{10}Br_4\{CH_3CN\}_2]^{2+}$, 1208 $[\{P_3C_2Mes_2\}_4Cu_{10}Br_4\{CH_3CN\}]^{2+}$, 1187.6

$[\{P_3C_2Mes_2\}_4Cu_{10}Br_4]^{2+}$, 1156.8 $[\{P_3C_2Mes_2\}_4Cu_9Br_3\{CH_3CN\}_2]^{2+}$, 1107.1 $[\{P_3C_2Mes_2\}_4Cu_8Br_2\{CH_3CN\}_3]^{2+}$, 1086.1 $[\{P_3C_2Mes_2\}_4Cu_8Br_2\{CH_3CN\}_2]^{2+}$, 1063.4 $[\{P_3C_2Mes_2\}_4Cu_8Br_2\{CH_3CN\}]^{2+}$, 1013.7 $[\{P_3C_2Mes_2\}_4Cu_7Br\{CH_3CN\}_2]^{2+}$, 993.4 $[\{P_3C_2Mes_2\}_4Cu_7Br\{CH_3CN\}]^{2+}$, 973 $[\{P_3C_2Mes_2\}_4Cu_7Br]^{2+}$.

Negative ion ESI-MS (CH_3CN): *m/z* = 796.2 $[Cu_5Br_6]^-$, 654.5 $[Cu_4Br_5]^-$, 508.5 $[Cu_3Br_4]^-$, 366.7 $[Cu_2Br_3]^-$, 222.8 $[CuBr_2]^-$.

Elemental analysis: Calculated (%) for $[(P_3C_2Mes_2)Br_5Cu_5K(CH_3CN)_3(dme)_{1.5}]$ (1370 g/mol): C 28.05, H 3.38, Br 29.16, N 3.07; found: C 27.52, H 3.20, Br 29.20, N 3.24.

Elemental analysis (after drying *in vacuo* for several hours): Calculated (%) for $[(P_3C_2Mes_2)Br_5Cu_5K(CH_3CN)]$ (1153 g/mol): C 22.92, H 2.19, N 1.22; found: C 22.57, H 2.53, N 1.34.

Synthesis of $[(\mu,\eta^{1:2:2}\text{-}P_3C_2Mes_2)\{Cu(CH_3CN)(\mu_2\text{-}I)\}_4\{Cu(CH_3CN)_3\}]$

In a Schlenk tube a solution of $K[P_3C_2Mes_2]$ (50 mg, 0.12 mmol) in dme (9 mL) is first layered with a solvent mixture of dme and CH_3CN (1:1; 3 mL), afterwards with a solution of CuI (123 mg, 0.52 mmol) in CH_3CN (12 mL). After complete diffusion and precipitation of a beige powder the red solution is filtered and concentrated to 10 mL. While storing at -28°C the formation of small orange polyhedrons of $[(\mu,\eta^{1:2:2}\text{-}P_3C_2Mes_2)\{Cu(CH_3CN)(\mu_2\text{-}I)\}_4\{Cu(CH_3CN)_3\}]$ is observed. The mother liquor is decanted, the crystals are washed with pentane (3 x 5 mL) and dried *in vacuo*. By concentrating the mother liquor to 2 mL and storing it at -28°C, a second crop of crystals can be obtained, which is isolated in the same way as before. $[(\mu,\eta^{1:2:2}\text{-}P_3C_2Mes_2)\{Cu(CH_3CN)(\mu_2\text{-}I)\}_4\{Cu(CH_3CN)_3\}]$ can also be synthesized by using thf instead of dme, however due to the lower solubility of $K[P_3C_2Mes_2]$ in thf a larger volume is needed (20 mL).

$[(\mu,\eta^{1:2:2}\text{-}P_3C_2Mes_2)\{Cu(CH_3CN)(\mu_2\text{-}I)\}_4\{Cu(CH_3CN)_3\}]$ can also be synthesized by using $[Cp^*Fe(\eta^5\text{-}P_3C_2Mes_2)]$ as starting material.[9]

Analytical data of $[(\mu,\eta^{1:2:2}\text{-}P_3C_2Mes_2)\{Cu(CH_3CN)(\mu_2\text{-}I)\}_4\{Cu(CH_3CN)_3\}]$:

Yield: 55 mg (0.042 mmol, crystalline, 40% referred to CuI)

^{1}H NMR (CD_3CN): δ [ppm] = 1.95 (s, CH_3CN), 2.04 (s, 3H, *p*-CH_3), 2.13 (s, 3H, *p*-CH_3), 2.22 (s, 6H, *o*-CH_3), 2.27 (s, 6H, *o*-CH_3), 6.90 (s, 4H, *aryl*-H).

^{13}C{^{1}H} NMR (CD_3CN): δ [ppm] = 21.1 (s, CH_3), 23.5 (s, CH_3), 26.2 (s, CH_3), 128.7 (s, *aryl*-C), 136.9 (s, *aryl*-C), 138.4 (s, *aryl*-C).

^{31}P{^{1}H} NMR (CD_3CN): δ [ppm] = 134 (br), 153 (br), 205 (br), 224 (br).

Positive ion ESI-MS (CH_3CN): *m/z* (%) = 2883.2 $[\{P_3C_2Mes_2\}_4Cu_{11}I_6]^+$, 2878.2 $[\{P_3C_2Mes_2\}_3Cu_{12}I_8]^+$, 2691.5 $[\{P_3C_2Mes_2\}_4Cu_{10}I_5]^+$, 2650.4 $[\{P_3C_2Mes_2\}_3Cu_{11}I_7]^+$, 2500.1 $[\{P_3C_2Mes_2\}_4Cu_9I_4]^+$, 2463.1 $[\{P_3C_2Mes_2\}_3Cu_{10}I_6]^+$, 2424.7 $[\{P_3C_2Mes_2\}_2Cu_{11}I_8]^+$, 2312.7 $[\{P_3C_2Mes_2\}_3Cu_{12}I_8]^+$, 2273.0

$[\{P_3C_2Mes_2\}_3Cu_9I_5]^+$, 2234.7 $[\{P_3C_2Mes_2\}_2Cu_{10}I_7]^+$, 2119.7 $[\{P_3C_2Mes_2\}_4Cu_7I_2]^+$, 2081.2 $[\{P_3C_2Mes_2\}_3Cu_8I_4]^+$, 2042.9 $[\{P_3C_2Mes_2\}_2Cu_9I_6]^+$, 1929.1 $[\{P_3C_2Mes_2\}_4Cu_6I]^+$, 1890.8 $[\{P_3C_2Mes_2\}_3Cu_7I_3]^+$, 1742.0 $[\{P_3C_2Mes_2\}_4Cu_5]^+$, 1700.9 $[\{P_3C_2Mes_2\}_3Cu_6I_2]^+$, 1661.8 $[\{P_3C_2Mes_2\}_2Cu_7I_4]^+$, 1511.0 $[\{P_3C_2Mes_2\}_3Cu_5I]^+$, 1472.4 $[\{P_3C_2Mes_2\}_2Cu_6I_3]^+$, 1321.6 $[\{P_3C_2Mes_2\}_3Cu_4]^+$, 1285.2 $[\{P_3C_2Mes_2\}_2Cu_5I_2]^+$, 1242.2 $[\{P_3C_2Mes_2\}Cu_6I_4]^+$, 1172.8 $[\{P_3C_2Mes_2\}_2Cu_4I\{CH_3CN\}_2]^+$, 1131.8 $[\{P_3C_2Mes_2\}_2Cu_4I\{CH_3CN\}]^+$, 1090.8 $[\{P_3C_2Mes_2\}_2Cu_4I]^+$, 1052.4 $[\{P_3C_2Mes_2\}Cu_5I_3]^+$.

Negative ion ESI-MS (CH_3CN): *m/z* (%) = 1270.1 $[Cu_6I_7]^-$, 1078.2 $[Cu_5I_6]^-$, 888.3 $[Cu_4I_5]^-$, 698.5 $[Cu_3I_4]^-$, 506.6 $[Cu_2I_3]^-$, 316.8 (100) $[CuI_2]^-$.

Elemental analysis: Calculated (%) for $[(P_3C_2Mes_2)Cu_5I_4(CH_3CN)_3]$ (1304 g/mol): C 23.96, H 2.40, N 3.22; found: C 23.96, H 2.50, N 3.28.

Synthesis of $[(\mu,\eta^{1:3:3}\text{-}P_3C_2Mes_2)_2\{Cu(CH_3CN)_3\}_2\{Cu(\mu_2\text{-}I)\}_6]$

In a Schlenk tube $K[P_3C_2Mes_2]$ (80 mg, 0.2 mmol) and CuI (190 mg, 1.0 mmol) are dissolved in a solvent mixture of dme (15 mL) and CH_3CN (3 mL). An immediate color change to deep red and turbidity can be observed. The solution is stirred for ten hours. After filtration the solvent of the red solution is removed *in vacuo*. The red solid is dissolved in a solvent mixture of CH_3CN (ca. 8 mL) and CH_2Cl_2 (ca. 8 mL), again filtered and layered with Et_2O. While storing at 8°C, the formation of crystals of $[(\mu,\eta^{1:3:3}\text{-}P_3C_2Mes_2)_2\{Cu(CH_3CN)_3\}_2\{Cu(\mu_2\text{-}I)\}_6]$ is observed. The mother liquor is decanted, the crystals are washed with hexane (3 x 5 mL) and dried *in vacuo*.

$[(\mu,\eta^{1:3:3}\text{-}P_3C_2Mes_2)_2\{Cu(CH_3CN)_3\}_2\{Cu(\mu_2\text{-}I)\}_6]$ can also be synthesized by using $[Cp^*Fe(\eta^5\text{-}P_3C_2Mes_2)]$ as starting material.[9]

Analytical data of $[(\mu,\eta^{1:3:3}\text{-}P_3C_2Mes_2)_2\{Cu(CH_3CN)_3\}_2\{Cu(\mu_2\text{-}I)\}_6]$:

Yield: 45 mg (0.021 mmol, crystalline, 17% referred to CuI)

^{1}H NMR (CD_3CN): δ [ppm] = 1.95 (s, CH_3CN), 2.04 (s, 3H, *p*-CH_3), 2.13 (s, 12H, *o*-CH_3), 2.20 (s, 6H, *o*-CH_3), 2.26 (s, 6H, *p*-CH_3), 6.90 (s, br, 6H, *aryl*-H).

^{31}P{^{1}H} NMR (CD_3CN): δ [ppm] = 135 (br), 206 (br), 223 (br).

Positive ion ESI-MS (CH_3CN): *m/z* = 2693.1 $[\{P_3C_2Mes_2\}_4Cu_{10}I_5]^+$, 2501.1 $[\{P_3C_2Mes_2\}_4Cu_9I_4]^+$, 2462.7 $[\{P_3C_2Mes_2\}_3Cu_{10}I_6]^+$, 2311.2 $[\{P_3C_2Mes_2\}_4Cu_8I_3]^+$, 2274.7 $[\{P_3C_2Mes_2\}_3Cu_9I_5]^+$, 2119.2 $[\{P_3C_2Mes_2\}_4Cu_7I_2]^+$, 2082.8 $[\{P_3C_2Mes_2\}_3Cu_8I_4]^+$, 1929.4 $[\{P_3C_2Mes_2\}_4Cu_6I]^+$, 1891.0 $[\{P_3C_2Mes_2\}_3Cu_7I_3]^+$, 1740.1 $[\{P_3C_2Mes_2\}_4Cu_5]^+$, 1701.0 $[\{P_3C_2Mes_2\}_3Cu_6I_2]^+$, 1662.6 $[\{P_3C_2Mes_2\}_2Cu_7I_4]^+$, 1550.0 $[\{P_3C_2Mes_2\}_3Cu_5I\{CH_3CN\}]^+$, 1511.1 $[\{P_3C_2Mes_2\}_3Cu_5I]^+$, 1472.8 $[\{P_3C_2Mes_2\}_2Cu_6I_3]^+$, 1322.0 $[\{P_3C_2Mes_2\}_3Cu_4]^+$, 1283.6 $[\{P_3C_2Mes_2\}_2Cu_5I_2]^+$, 1173.0

$[\{P_3C_2Mes_2\}_2Cu_4I\{CH_3CN\}_2]^+$, 1131.9 $[\{P_3C_2Mes_2\}_2Cu_4I\{CH_3CN\}]^+$, 1093.0 $[\{P_3C_2Mes_2\}_2Cu_4I]^+$, 996.2 $[\{P_3C_2Mes_2\}_4Cu_7I]^{2+}$, 901.2 $[\{P_3C_2Mes_2\}_4Cu_6]^{2+}$.

Negative ion ESI-MS (CH_3CN): *m/z* (%) = 2562.5 $[\{P_3C_2Mes_2\}_4Cu_8I_5]^-$, 2528.7 $[\{P_3C_2Mes_2\}_3Cu_9I_7]^-$, 2490.2 $[\{P_3C_2Mes_2\}_2Cu_{10}I_9]^-$, 2373.2 $[\{P_3C_2Mes_2\}_4Cu_7I_4]^-$, 2334.9 $[\{P_3C_2Mes_2\}_3Cu_8I_6]^-$, 2296.4 $[\{P_3C_2Mes_2\}_2Cu_9I_8]^-$, 2144.7 $[\{P_3C_2Mes_2\}_3Cu_7I_5]^-$, 2106.7 $[\{P_3C_2Mes_2\}_2Cu_8I_7]^-$, 2070.2 $[\{P_3C_2Mes_2\}Cu_9I_9]^-$, 1954.9 $[\{P_3C_2Mes_2\}_3Cu_6I_4]^-$, 1916.5 $[\{P_3C_2Mes_2\}_2Cu_7I_6]^-$, 1878.3 $[\{P_3C_2Mes_2\}Cu_8I_8]^-$, 1841.8 $[Cu_9I_{10}]^-$, 1765.0 $[\{P_3C_2Mes_2\}_3Cu_5I_3]^-$, 1726.7 $[\{P_3C_2Mes_2\}_2Cu_6I_5]^-$, 1688.3 $[\{P_3C_2Mes_2\}Cu_7I_7]^-$, 1651.8 $[Cu_8I_9]^-$, 1534.7 $[\{P_3C_2Mes_2\}_2Cu_5I_4]^-$, 1498.3 $[\{P_3C_2Mes_2\}Cu_6I_6]^-$, 1460.1 $[Cu_7I_8]^-$, 1306.5 $[\{P_3C_2Mes_2\}Cu_5I_5]^-$, 1270.1 $[Cu_6I_7]^-$, 1116.6 $[\{P_3C_2Mes_2\}Cu_4I_4]^-$, 1078.2 $[Cu_5I_6]^-$, 888.5 $[Cu_4I_5]^-$, 698.5 $[Cu_3I_4]^-$, 506.6 $[Cu_2I_3]^-$, 316.6 (100) $[CuI_2]^-$.

Elemental analysis: Calculated (%) for $[(P_3C_2Mes_2)_2Cu_8I_6(CH_3CN)_4]$ (2145 g/mol): C 26.88, H 2.63, N 2.61; found: C 26.59, H 2.69, N 2.70.

Synthesis of $[(\mu,\eta^{1:2:2}\text{-}P_3C_2Mes_2)\{Cu(CH_3CN)(\mu_2\text{-}I)\}_2\{Cu(CH_3CN)(\mu_3\text{-}I)\}_2Cu]_n$ (5)

In a Schlenk tube a solution of $K[P_3C_2Mes_2]$ (16 mg, 0.042 mmol) in dme (5 mL) is layered with a solution of CuI (25 mg, 0.13 mmol) in CH_3CN (5 mL). After complete diffusion the red solution is concentrated to 5 mL and layered with hexane. The formation of small red-brown blocks of **5** at the phase boundary could be observed once. The mother liquor was decanted, the crystals were washed with hexane (3 x 5 mL) and dried *in vacuo*. Attempts to reproduce **5** failed every time.

Analytical data of **5**:

Yield: a few crystals (< 5%)

Positive ion ESI-MS (CH_3CN): *m/z* (%) = 2692.5 $[\{P_3C_2Mes_2\}_4Cu_{10}I_5]^+$, 2500.6 $[\{P_3C_2Mes_2\}_4Cu_9I_4]^+$, 2309.5 $[\{P_3C_2Mes_2\}_4Cu_8I_3]^+$, 2119.5 $[\{P_3C_2Mes_2\}_4Cu_7I_2]^+$, 2079.1 $[\{P_3C_2Mes_2\}_3Cu_8I_4]^+$, 1929.4 $[\{P_3C_2Mes_2\}_4Cu_6I]^+$, 1891.0 $[\{P_3C_2Mes_2\}_3Cu_7I_3]^+$, 1739.6 $[\{P_3C_2Mes_2\}_4Cu_5]^+$, 1700.9 $[\{P_3C_2Mes_2\}_3Cu_6I_2]^+$, 1552.1 $[\{P_3C_2Mes_2\}_3Cu_5I\{CH_3CN\}]^+$, 1511.1 $[\{P_3C_2Mes_2\}_3Cu_5I]^+$, 1472.6 $[\{P_3C_2Mes_2\}_2Cu_6I_3]^+$, 1319.2 (100) $[\{P_3C_2Mes_2\}_3Cu_4]^+$, 1172.8 $[\{P_3C_2Mes_2\}_2Cu_4I\{CH_3CN\}_2]^+$, 1131.9 $[\{P_3C_2Mes_2\}_2Cu_4I\{CH_3CN\}]^+$, 1090.9 $[\{P_3C_2Mes_2\}_2Cu_4I]^+$, 901.0 $[\{P_3C_2Mes_2\}_4Cu_6]^{2+}$.

Negative ion ESI-MS (CH_3CN): *m/z* (%) = 888.4 $[Cu_4I_5]^-$, 698.5 $[Cu_3I_4]^-$, 506.6 $[Cu_2I_3]^-$, 316.8 (100) $[CuI_2]^-$.

Synthesis of $[(\mu,\eta^{1:2:2}\text{-}P_3C_2Mes_2)\{Cu(CH_3CN)(\mu_3\text{-}I)\}_2\{Cu(CH_3CN)(\mu_4\text{-}I)\}_2Cu_2\{Cu(CH_3CN)\}(\mu_3\text{-}I)(\mu_2\text{-}I)]_n$ (6)

A solution of $K[P_3C_2Mes_2]$ (33 mg, 0.084 mmol) in dme (15 mL) is added to a solution of CuI (160 mg, 0.84 mmol) in CH_3CN (15 mL), whereby the solution turned deep red. It was stirred for three hours, filtered and layered with Et_2O. After several months at r.t., orange crystals of **6** at the upper

level have formed. The mother liquor was decanted, the crystals were washed with hexane (3 x 5 mL) and dried *in vacuo*.

Analytical data of **6**:

Yield: 86 mg (0.05 mmol, crystalline, 60%)

^{1}H NMR (CD_3CN): δ [ppm] = 1.11 (t, Et_2O), 1.95 (s, CH_3CN), 2.26 (s, 6H, *o*-CH_3), 2.28 (s, 3H, *p*-CH_3), 3.28 (s, dme), 3.41 (q, Et_2O), 3.44 (s, dme), 6.93 (s, 2H, *aryl*-H).

^{31}P{^{1}H} NMR (CD_3CN): δ [ppm] = 136 (br, 2P), 222 (br, 1P).

Negative ion ESI-MS (dme, CH_3CN, Et_2O): *m/z* (%) = 888.3 $[Cu_4I_5]^-$, 698.4 $[Cu_3I_4]^-$, 506.6 $[Cu_2I_3]^-$, 316.7 (100) $[CuI_2]^-$.

Elemental analysis: Calculated (%) for $[(P_3C_2Mes_2)I_7Cu_6(CH_3CN)_4]$ (1816 g/mol): C 19.84, H 2.05, N 3.08; found: C 20.92, H 2.20, N 3.16.

Synthesis of $[(\mu,\eta^{1:2:2}\text{-}P_3C_2{}^tBu_2)(CuCl)_3(\mu_3\text{-}Cl)_2\{Cu(CH_3CN)\}_3\{Cu(\mu_2\text{-}Cl)\}\{Cu(CH_3CN)_3\}_2]_n$ (7)

A solution of $K[P_3C_2{}^tBu_2]$ (50 mg, 0.18 mmol) in dme (10 mL) is added to a solution of CuCl (55 mg, 0.56 mmol) in CH_3CN (10 mL). Within one minute the color changes from yellow to orange up to red and becomes turbid after 30 minutes of stirring. After two hours the reaction mixture is filtered, the solvent removed *in vacuo* and the red solid dissolved in as less as possible CH_3CN. Upon cooling, the formation of neon orange plates of **7** is observed. The mother liquor is decanted, the crystals are washed with hexane (3 x 5 mL) and dried *in vacuo*.

Analytical data of **7**:

Yield: 65 mg (0.044 mmol, 73% referred to $K[P_3C_2{}^tBu_2]$)

^{1}H NMR (CD_3CN): δ [ppm] = 1.77 (s, ^{t}Bu), 1.99 (s, CH_3CN).

^{31}P{^{1}H} NMR (CD_3CN): δ [ppm] = 136.7 (br, 2P), 264.8 (br, 1P).

Positive ion ESI-MS (CH_3CN): *m/z* (%) = 2918.8 $[\{P_3C_2{}^tBu_2\}_7Cu_{16}Cl_8]^+$, 2821.0 $[\{P_3C_2{}^tBu_2\}_7Cu_{15}Cl_7]^+$, 2725.0 $[\{P_3C_2{}^tBu_2\}_7Cu_{14}Cl_6]^+$, 2621.2 $[\{P_3C_2{}^tBu_2\}_6Cu_{15}Cl_8]^+$, 2523.0 $[\{P_3C_2{}^tBu_2\}_6Cu_{14}Cl_7]^+$, 2425.0 $[\{P_3C_2{}^tBu_2\}_5Cu_{15}Cl_9]^+$, 2327.0 $[\{P_3C_2{}^tBu_2\}_5Cu_{14}Cl_8]^+$, 2227.1 $[\{P_3C_2{}^tBu_2\}_5Cu_{13}Cl_7]^+$, 2129.0 $[\{P_3C_2{}^tBu_2\}_5Cu_{12}Cl_6]^+$, 2030.9 $[\{P_3C_2{}^tBu_2\}_5Cu_{11}Cl_5]^+$, 1935.0 $[\{P_3C_2{}^tBu_2\}_4Cu_{12}Cl_7]^+$, 1835.0 $[\{P_3C_2{}^tBu_2\}_4Cu_{11}Cl_6]^+$, 1185.9 $[\{P_3C_2{}^tBu_2\}_3Cu_6Cl_2\{CH_3CN\}]^+$, 1144.9 $[\{P_3C_2{}^tBu_2\}_3Cu_6Cl_2]^+$, 1046.9 $[\{P_3C_2{}^tBu_2\}_3Cu_5Cl]^+$, 947.1 (100) $[\{P_3C_2{}^tBu_2\}_3Cu_4]^+$.

Negative ion ESI-MS (CH_3CN): *m/z* = 2988.3 $[\{P_3C_2{}^tBu_2\}_7Cu_{18}Cl_{13}]^{2-}$, 2891.1 $[\{P_3C_2{}^tBu_2\}_7Cu_{17}Cl_{12}]^{2-}$, 2792.8 $[\{P_3C_2{}^tBu_2\}_6Cu_{16}Cl_{11}]^-$, 2694.8 $[\{P_3C_2{}^tBu_2\}_6Cu_{15}Cl_{10}]^-$, 2595.0 $[\{P_3C_2{}^tBu_2\}_6Cu_{14}Cl_9]^-$, 2498.9 $[\{P_3C_2{}^tBu_2\}_5Cu_{15}Cl_{11}]^-$, 2398.9 $[\{P_3C_2{}^tBu_2\}_5Cu_{14}Cl_{10}]^-$, 2298.9 $[\{P_3C_2{}^tBu_2\}_5Cu_{13}Cl_9]^-$, 2201.0 $[\{P_3C_2{}^tBu_2\}_4Cu_{14}Cl_{11}]^-$, 2102.9 $[\{P_3C_2{}^tBu_2\}_4Cu_{13}Cl_{10}]^-$, 2004.9 $[\{P_3C_2{}^tBu_2\}_3Cu_{14}Cl_{12}]^-$, 1906.8 $[\{P_3C_2{}^tBu_2\}_3Cu_{13}Cl_{11}]^-$, 1806.8 $[\{P_3C_2{}^tBu_2\}_3Cu_{12}Cl_{10}]^-$, 1708.9 $[\{P_3C_2{}^tBu_2\}_3Cu_{11}Cl_9]^-$, 1610.9

$[\{P_3C_2{}^tBu_2\}_3Cu_{10}Cl_8]^-$, 1512.9 $[\{P_3C_2{}^tBu_2\}_2Cu_{11}Cl_{10}]^-$, 1412.7 $[\{P_3C_2{}^tBu_2\}_2Cu_{10}Cl_9]^-$, 1314.8 $[\{P_3C_2{}^tBu_2\}_2Cu_9Cl_8]^-$, 1216.6 $[\{P_3C_2{}^tBu_2\}_2Cu_8Cl_7]^-$, 1118.6 $[\{P_3C_2{}^tBu_2\}_2Cu_7Cl_6]^-$, 1020.7 $[\{P_3C_2{}^tBu_2\}Cu_8Cl_8]^-$, 920.7 $[\{P_3C_2{}^tBu_2\}Cu_7Cl_7]^-$, 822.6 $[\{P_3C_2{}^tBu_2\}Cu_6Cl_6]^-$, 724.6 $[\{P_3C_2{}^tBu_2\}Cu_5Cl_5]^-$, 624.8 $[\{P_3C_2{}^tBu_2\}Cu_4Cl_4]^-$, 528.7 $[\{P_3C_2{}^tBu_2\}Cu_3Cl_3]^-$, 428.9 $[\{P_3C_2{}^tBu_2\}Cu_2Cl_2]^-$, 328.9 $[\{P_3C_2{}^tBu_2\}CuCl]^-$, 232.7 $[Cu_2Cl_3]^-$.

Elemental analysis: Calculated (%) for $[(P_3C_2{}^tBu_2)_3Cl_6Cu_9(CH_3CN)_2]$ (1560 g/mol): C 26.17, H 3.88, N 1.80; found: C 26.02, H 3.74, N 1.73.

Synthesis of $[(P_3C_2{}^tBu_2)_3Cu_{9.85}Cl_{6.85}(CH_3CN)_{1.9}]_n$ (8)

In a Schlenk tube a solution of $K[P_3C_2{}^tBu_2]$ (30 mg, 0.11 mmol) in dme (15 mL) is layered with a solution of CuCl (55 mg, 0.55 mmol) in CH_3CN (10 mL). Already after several hours the formation of big dark red blocks of **8** at the red phase boundary is observed. After complete diffusion the colorless mother liquor is decanted, the crystals are washed with hexane (3 x 5 mL) and dried *in vacuo*.

Analytical data of **8**:

Yield: 56 mg (0.031 mmol, 85% referred to $K[P_3C_2{}^tBu_2]$)

Negative ion ESI-MS (mother liquor, dme/CH_3CN): *m/z* (%) = 232.6 $[Cu_2Cl_3]^-$, 134.7 $[CuCl_2]^-$.

Elemental analysis: Calculated (%) for $[(P_3C_2{}^tBu_2)_3Cl_7Cu_{10}(CH_3CN)_3(C_4H_{10}O_2)]$ (1790 g/mol): C 26.83, H 4.11, Cl 13.86, N 2.35; found: C 26.61, H 4.00, Cl 13.84, N 2.51.

Synthesis of $[(P_3C_2{}^tBu_2)_3Cu_{10.1}Br_{7.1}(CH_3CN)_{1.2}]_n$ (9)

In a Schlenk tube a solution of $K[P_3C_2{}^tBu_2]$ (30 mg, 0.11 mmol) in dme (15 mL) is layered with a solution of CuBr (80 mg, 0.55 mmol) in CH_3CN (10 mL). Already after several hours the formation of big dark red blocks of **9** at the red phase boundary is observed. After complete diffusion the colorless mother liquor is decanted, the crystals are washed with hexane (3 x 5 mL) and dried *in vacuo*.

Analytical data of **9**:

Yield: 50 mg (0.024 mmol, 65% referred to $K[P_3C_2{}^tBu_2]$)

Positive ion ESI-MS (thf/CH_3CN): *m/z* = 3415.1 $[\{P_3C_2{}^tBu_2\}_7Cu_{17}Br_9]^+$, 3267.9 $[\{P_3C_2{}^tBu_2\}_7Cu_{16}Br_8]^+$, 3123.8 $[\{P_3C_2{}^tBu_2\}_6Cu_{16}Br_9]^+$, 2979.9 $[\{P_3C_2{}^tBu_2\}_6Cu_{15}Br_8]^+$, 2834.7 $[\{P_3C_2{}^tBu_2\}_6Cu_{14}Br_7]^+$, 2688.8 $[\{P_3C_2{}^tBu_2\}_6Cu_{13}Br_6]^+$, 2541.2 $[\{P_3C_2{}^tBu_2\}_5Cu_{13}Br_7]^+$, 2399.3 $[\{P_3C_2{}^tBu_2\}_5Cu_{12}Br_6]^+$, 2253.1 $[\{P_3C_2{}^tBu_2\}_5Cu_{11}Br_5]^+$, 1672.9 $[\{P_3C_2{}^tBu_2\}_4Cu_8Br_3]^+$, 1526.5 $[\{P_3C_2{}^tBu_2\}_4Cu_7Br_2]^+$, 1385.1 $[\{P_3C_2{}^tBu_2\}_4Cu_6Br]^+$, 1234.8 $[\{P_3C_2{}^tBu_2\}_3Cu_6Br_2]^+$, 1090.9 $[\{P_3C_2{}^tBu_2\}_3Cu_5Br]^+$, 947.0 $[\{P_3C_2{}^tBu_2\}_3Cu_4]^+$.

Negative ion ESI-MS (thf/CH_3CN): *m/z* = 3419.3 $[\{P_3C_2{}^tBu_2\}_5Cu_{18}Br_{14}]^-$, 3281.9 $[\{P_3C_2{}^tBu_2\}_6Cu_{16}Br_{11}]^-$, 3136.0 $[\{P_3C_2{}^tBu_2\}_6Cu_{15}Br_{10}]^-$, 2993.8 $[\{P_3C_2{}^tBu_2\}_6Cu_{14}Br_9]^-$, 2843.2 $[\{P_3C_2{}^tBu_2\}_5Cu_{14}Br_{10}]^-$, 2701.4 $[\{P_3C_2{}^tBu_2\}_5Cu_{13}Br_9]^-$, 2557.1 $[\{P_3C_2{}^tBu_2\}_4Cu_{13}Br_{10}]^-$, 2409.0 $[\{P_3C_2{}^tBu_2\}_4Cu_{12}Br_9]^-$, 2262.9 $[\{P_3C_2{}^tBu_2\}_4Cu_8Br_{11}]^-$, 2114.8 $[\{P_3C_2{}^tBu_2\}_3Cu_{11}Br_9]^-$, 1968.5 $[\{P_3C_2{}^tBu_2\}_3Cu_{10}Br_8]^-$, 1826.3 $[\{P_3C_2{}^tBu_2\}_3Cu_9Br_7]^-$, 1680.5 $[\{P_3C_2{}^tBu_2\}_3Cu_8Br_6]^-$, 1538.6 $[\{P_3C_2{}^tBu_2\}_3Cu_7Br_5]^-$, 1386.3 $[\{P_3C_2{}^tBu_2\}_2Cu_7Br_6]^-$, 1242.4 $[\{P_3C_2{}^tBu_2\}_2Cu_6Br_5]^-$, 1092.3 $[\{P_3C_2{}^tBu_2\}Cu_6Br_6]^-$, 519.0 $[\{P_3C_2{}^tBu_2\}Cu_2Br_2]^-$, 366.7 $[Cu_2Br_3]^-$, 222.9 $[CuBr_2]^-$.

Negative ion ESI-MS (mother liquor, dme/CH_3CN): *m/z* (%) = 366.4 $[Cu_2Br_3]^-$, 222.6 $[CuBr_2]^-$.

Elemental analysis: Calculated (%) for $[(P_3C_2{}^tBu_2)_3Br_7Cu_{10}(CH_3CN)_3]$ (2011 g/mol): C 21.50, H 3.16, Br 27.81, N 2.09; found: C 21.89, H 3.45, Br 26.73, N 1.65.

Elemental analysis (after two years in air): Calculated (%) for $[(P_3C_2{}^tBu_2)_3Br_7Cu_{10}(CH_3CN)]$ (1929 g/mol): C 19.92, H 2.98, N 0.73; found: C 19.83, H 3.48, N 0.92.

Synthesis of $[K(thf)_6]_n[(\mu,\eta^{1:3:3}\text{-}P_3C_2{}^tBu_2)_2\{Cu_3(\mu_2\text{-}I)_2\}_2\{Cu(\mu_2\text{-}I)_2\}]_n$ (10)

In a Schlenk tube $K[P_3C_2{}^tBu_2]$ (50 mg, 0.18 mmol) and CuI (105 mg, 0.55 mmol) are dissolved in thf (12 mL). An immediate color change to deep red is observed. The solution is stirred for 2 hours, before the solvent is removed *in vacuo*. The red solid is dissolved in as less CH_3CN as possible and layered onto toluene. After complete diffusion the mother liquor is almost colorless and dark red blocks of **10** have formed. The mother liquor is decanted, the crystals are washed with toluene (3 x 5 mL) and dried *in vacuo*. Attempts to reproduce **10** were successful only once.

Analytical data of **10**:

Yield: 13 mg (0.006 mmol, 8% referred to CuI)

Negative ion ESI-MS (CH_3CN): *m/z* (%) = 1078.1 $[Cu_5I_6]^-$, 888.3 $[Cu_4I_5]^-$, 698.5 $[Cu_3I_4]^-$, 506.6 $[Cu_2I_3]^-$, 316.7 (100) $[CuI_2]^-$.

5.4 Crystallographic Details

The data for **6** were collected on an Agilent Technologies diffractometer equipped with Titan^{S2} CCD detector and a SuperNova CuK_α microfocus source using 1° ω scans. The data for **2**, **3, 4**, **5, 9** were collected using 1° ω scans and for **7, 8** and **10** using 0.5° ω scans on an Agilent Technologies diffractometer equipped with Atlas CCD detector and a SuperNova CuK_α microfocus source. Crystallographic data and details of the diffraction experiments are given in *Table 5.1 – Table 5.5*. The structures of **2-8**, **10** were solved by direct methods with *SIR97*,[26] *SHELX97* or *SHELX2013*.[27] The structures were refined by full-matrix least-squares method against $|F|^2$ in anisotropic approximation using either *SHELXL97* or the multiprocessor and variable memory version

SHELXL2013. All non-hydrogen atoms were refined anisotropically, while the hydrogen atoms were refined riding on pivot atoms.

2: The structure was refined as an inversion twin with batch components 0.8(1)/0.2(1). We faced with unexplainably large displacement parameters for almost all atoms even at T = 123 K and quite bad quality factors in **2** despite the signs for a good experiment, clear symmetry and a chemically reasonable structure of the complex. Despite this, only positions of two adjacent P atoms of the phospholyl ligands were split with the probability 0.7/0.3. The outer sphere counter anion Cl^- is disordered over six close positions and therefore was refined in an isotropic approximation. The solvent molecules and one of the coordinated MeCN molecules are disordered over 2 and 3 positions, respectively. They were refined with geometric restraints.

3: The CuCl and Cu(MeCN)Cl fragments of the $\{Cu_2Cl_2\}$ bridges in **3** are disordered (1:1) over several close positions, probably because of a mixed trigonally and tetrahedrally coordinated Cu. The coordinated to K^+ and solvated dme molecules as well as the solvated MeCN molecules are disordered.

4: In **4**, the $\{Cu_2Br_2\}$ fragment is disordered around the direction of the chain so that there are three close positions of the Cu atom in the independent part. The corresponding Br atoms are disordered over total eight positions. The Cu and Br atoms have occupancies less than 0.2 and were therefore refined in an isotropic approximation. The residual electron density peaks of more than 2 $e \cdot A^{-3}$ can only be avoided if the disorder of the Cu_2Br_2 fragment is described with such a high number of the split positions. The main factors that favor the disorder are presumably: 1) a high steric demand of two Mes groups, which screen the disordered fragment and allow it to re-orientate freely in the resulted cavity, and 2) the choice between a trigonal and tetrahedral coordination environment of Cu that in some of the disordered positions they are additionally coordinated by a MeCN molecule. The solvent MeCN molecules and thf molecules coordinated to K^+ counter cation are disordered over two positions and were treated with some geometrical restraints.

5: The diffraction pattern of the crystal of **5** was featured by diffuse scattering that is described below. The effect is strongly related to the disorder of the repeating units over 4-axis.

6: In **6**, one of the MeCN molecules coordinated to copper is disordered over two close positions. Solvated MeCN and Et_2O molecules were refined as 0.5 and 0.4 molecular occupancies, and their positions partly overlap. The hexane molecule is disordered over the inversion center.

7: In **7**, the Cl atoms of the bridging $\{Cu_6Cl_5(P_3C_2{}^tBu_2)_3\}$ fragments are disordered over three close positions. One MeCN molecule coordinated to copper is disordered over two positions. Solvated MeCN is severely disordered in the inter-chain cavities.

8 and **9**: Compound **8** and **9** are isotypical, and the model of **9** was used for the refinement of **8**. The similar structures however differ in details. In the Cl analogue the copper atom and the Cl atom bonded to it are disordered over two positions, while in the Br analogue it is ordered. This difference leads to a variation of the polymeric chain structure. Another Cu atom belonging to the $Cu(MeCN)_3$ fragment occupies the position with different probability refined to 0.25 for the Cl and to 0.1 for the Br analogues, respectively. In both structures the Cu atoms in the Cu(2) position are bonded with X(2) (X = Cl, Br) that has less occupancy than Cu(2). We supposed that the environment of Cu(2) is most probably completed by a coordinated MeCN molecule (minor content of 0.183 or 0.133, respectively) that was not located in the mixed X/MeCN positions because of the proximity to the heavy X = Cl or Br atoms. The undetermined MeCN was nevertheless included into the final structural formula.

According to the Cambridge Structural Database, at least four crystal structures are known, where a MeCN ligand is coordinated in a monodentate-bridging mode to two Cu atoms. Three of them are complexes of Cu^+ with N- and P-donor atom ligands and one is a complex of Cu^{2+}. Two Cu-μ-N distances in $[Cu(dpme)_2(\mu\text{-}NCMe)(NCMe)_2]ClO_4 \cdot MeCN$ of 2.29 and 2.32 Å, are close to the Cu-X(2) distances in **8** and **9**.[28] The atomic coordinates of the $\{Cu_2(\mu\text{-}NCMe)\}$ fragment were used to model a possible MeCN bridging ligand with coinciding positions of X(2) and N atoms. The analysis of the interatomic distances involving the atoms of the modelled MeCN proves that the corresponding cavity in both crystal structures is large enough to allow this ligand to occupy the mixed ligand X/MeCN position.

10: In **10**, four of six thf molecules in the $K(thf)_6^+$ cation are conformationally disordered over two positions. The solvated thf molecule is disordered in the space between polymeric layers.

CIF files with comprehensive information on the details of the diffraction experiments and full tables of bond lengths and angles for **2-10** are deposited in Cambridge Crystallographic Data Center under the deposition codes CCDC-1056476 - CCDC-1056484, respectively. The topological features of the 3D polymers were performed using TOPOSPro.[17]

Table 5.1 Experimental details for compounds **2** and **3**.

Crystal Data	2	3
CCDC Codes	CCDC-1056476	CCDC-1056477
Chemical formula	$C_{48}H_{56}ClCu_3N_4P_6 \cdot 0.6(CH_3CN)$	$C_{39}H_{57.50}Cl_5Cu_5KN_6O_{3.50}P_3$
M_r	1125.49	1293.37
Crystal system, space group	tetragonal, $I\bar{4}2d$	monoclinic, $P2_1/n$
Temperature (K)	123	150
a, b, c (Å)	25.9670(2), 25.9670(2), 17.9760(2)	13.5753(3), 26.0211(6), 15.6295(4)

α, β, γ (°)	90, 90, 90	90, 97.061(2), 90
V (Å^3)	12120.9(2)	5479.2(2)
Z	8	4
F(000)	4634	2622
Radiation type	Cu K_α	Cu K_α
μ (mm^{-1})	3.38	6.22
Crystal color and shape	red prism	yellow prism
Crystal size (mm)	0.18 × 0.13 × 0.03	0.11 × 0.05 × 0.04
Data collection		
Diffractometer	SuperNova, Single source at offset, Atlas diffractometer	SuperNova, Single source at offset, Atlas diffractometer
Absorption correction	gaussian	gaussian
T_{min}, T_{max}	0.648, 0.893	0.601, 0.778
No. of measured, independent and observed [$I > 2\sigma(I)$] reflections	13152, 5757, 4063	20040, 10599, 6315
R_{int}	0.022	0.041
$(\sin\theta/\lambda)_{max}$ (Å^{-1})	0.622	0.622
Refinement		
$R[F^2 > 2\sigma(F^2)]$, $wR(F^2)$, S	0.095, 0.260, 1.05	0.044, 0.108, 0.88
No. of reflections	5757	10599
No. of parameters	353	608
No. of restraints	12	-
H-atom treatment	H-atom parameters constrained	H-atom parameters constrained
$\Delta\rangle_{max}$, $\Delta\rangle_{min}$ (e Å^{-3})	1.86, -0.54	0.57, -0.43

Table 5.2 Experimental details for compounds **4** and **5**.

Crystal Data	4	5
CCDC Codes	CCDC-1056478	CCDC-1056479
Chemical formula	$C_{34.60}H_{45.90}Br_5Cu_5KN_{5.30}OP_3$	$C_{28}H_{34}Cu_5I_4N_4P_3$
M_r	1401.32	1344.80
Crystal system, space group	monoclinic, $C2/m$	tetragonal, $P4/n$
Temperature (K)	123	123
a, b, c (Å)	19.5159(3), 25.8364(4), 13.6766(2)	15.5501(2), 15.5501(2), 9.3497(2)
α, β, γ (°)	90, 127.405(1), 90	90, 90, 90
V (Å^3)	5477.93(16)	2260.81(8)
Z	4	2
F(000)	2730	1264
Radiation type	Cu K_α	Cu K_α
μ (mm^{-1})	8.16	25.21
Crystal color and shape	yellow-orange block	red-brown block

Crystal size (mm)	0.09 × 0.06 × 0.04	0.08 × 0.06 × 0.03
Data collection		
Diffractometer	SuperNova, Single source at offset, Atlas diffractometer	SuperNova, Single source at offset, Atlas diffractometer
Absorption correction	analytical	gaussian
T_{min}, T_{max}	0.569, 0.761	0.354, 0.540
No. of measured, independent and observed [$I > 2\sigma(I)$] reflections	34635, 5576, 4748	5373, 2050, 1615
R_{int}	0.030	0.035
$(\sin\theta/\lambda)_{max}$ (Å^{-1})	0.623	0.605
Refinement		
$R[F^2 > 2\sigma(F^2)]$, $wR(F^2)$, S	0.043, 0.139, 1.11	0.076, 0.220, 1.06
No. of reflections	5576	2050
No. of parameters	312	193
No. of restraints	-	-
H-atom treatment	H-atom parameters constrained	H-atom parameters not refined
$\Delta\rangle_{max}$, $\Delta\rangle_{min}$ (e Å^{-3})	1.80, -0.79	1.69, -1.24

Table 5.3 Experimental details for compounds **6** and **7**.

Crystal Data	6	7
CCDC Codes	CCDC-1056480	CCDC-1056481
Chemical formula	$C_{35.6}H_{49.5}Cu_7I_6N_{5.5}O_{0.4}P_3$	$C_{64.20}H_{105.30}Cl_6Cu_9N_{17.10}P_9$
M_r	1860.00	2180.05
Crystal system, space group	triclinic, $P\bar{1}$	monoclinic, $P2_1/m$
Temperature (K)	123	123
a, b, c (Å)	11.926(1), 12.3005(7), 20.889(1)	13.1219(2), 27.5544(6), 13.9810(4)
α, β, γ (°)	79.096(5), 89.381(5), 64.029(7)	90, 95.626(2), 90
V (Å^3)	2696.1(3)	5030.7(2)
Z	2	2
F(000)	1742	2216
Radiation type	Cu K_α	Cu K_α
μ (mm^{-1})	31.04	5.18
Crystal color and shape	orange lath	orange plate
Crystal size (mm)	0.24 × 0.09 × 0.05	0.12 × 0.09 × 0.04
Data collection		
Diffractometer	SuperNova, Titan^{S2} diffractometer	SuperNova, Single source at offset, Atlas diffractometer
Absorption correction	gaussian	analytical
T_{min}, T_{max}	0.093, 0.550	0.693, 0.857
No. of measured, independent	16228, 10356, 8315	17849, 9906, 7571

and observed [$I > 2\sigma(I)$] reflections		
R_{int}	0.049	0.032
$(\sin\theta/\lambda)_{max}$ (Å^{-1})	0.624	0.623
Refinement		
$R[F^2 > 2\sigma(F^2)]$, $wR(F^2)$, S	0.051, 0.142, 1.01	0.047, 0.143, 1.03
No. of reflections	10356	9906
No. of parameters	534	569
No. of restraints	12	0
H-atom treatment	H-atom parameters constrained	H-atom parameters constrained
$\Delta\rangle_{max}$, $\Delta\rangle_{min}$ (e Å^{-3})	2.46, -2.62	0.96, -0.62

Table 5.4 Experimental details for compounds **8** and **9**.

Crystal Data	**8**	**9**
CCDC Codes	CCDC-1056482	CCDC-1056483
Chemical formula	$C_{33.8}H_{59.67}Cl_{6.85}Cu_{9.85}N_{1.9}P_9$	$C_{33.13}H_{58.7}Br_{7.10}Cu_{10.10}P_9N_{1.57}$
M_r	1640.10	1966.89
Crystal system, space group	cubic, $F\bar{4}3c$	cubic, $F\bar{4}3c$
Temperature (K)	123	123
a, b, c (Å)	35.5021(1), 35.5021(1), 35.5021(1)	35.7790(1), 35.7790(1), 35.7790(1)
α, β, γ (°)	90, 90, 90	90, 90, 90
V (Å^3)	44746.8(4)	45802.0(4)
Z	32	32
F(000)	26011	30236
Radiation type	Cu K_α	Cu K_α
μ (mm^{-1})	9.651	12.383
Crystal color and shape	dark red block	dark red block
Crystal size (mm)	0.19 × 0.14 × 0.13	0.18 × 0.16 × 0.10
Data collection		
Diffractometer	SuperNova, Single source at offset, Atlas diffractometer	SuperNova, Single source at offset, Atlas diffractometer
Absorption correction	gaussian	analytical
T_{min}, T_{max}	0.325, 0.508	0.211, 0.427
No. of measured, independent and observed [$I > 2\sigma(I)$] reflections	48284, 3910, 3826	91270, 3957, 3934
R_{int}	0.031	0.024
$(\sin\theta/\lambda)_{max}$ (Å^{-1})	0.630	0.627
Refinement		
$R[F^2 > 2\sigma(F^2)]$, $wR(F^2)$, S	0.046, 0.132, 1.07	0.030, 0.0875, 1.069
No. of reflections	3910	3957
No. of parameters	207	197

H-atom treatment	H-atom parameters constrained	H-atom parameters constrained
$\Delta\rangle_{max}$, $\Delta\rangle_{min}$ (e Å^{-3})	2.14, -0.95	1.50, -1.25
Absolute structure parameter	0.020(13)	-0.027(5)

Table 5.5 Experimental details for compound **10**.

Crystal Data	10
CCDC Code	CCDC-1056484
Chemical formula	$C_{46}H_{88}Cu_7I_6KO_{6.50}P_6$
M_r	2176.26
Crystal system, space group	orthorhombic, *Pbcn*
Temperature (K)	123
a, *b*, *c* (Å)	13.3881(3), 29.8918(6), 18.0577(3)
α, β, γ (°)	90, 90, 90
V (Å^3)	7226.6(2)
Z	4
F(000)	4184
Radiation type	Cu K_α
μ (mm^{-1})	24.429
Crystal color and shape	dark brown block
Crystal size (mm)	0.24 × 0.20 × 0.12
Data collection	
Diffractometer	SuperNova, Single source at offset, Atlas diffractometer
Absorption correction	gaussian
T_{min}, T_{max}	0.033, 0.211
No. of measured, independent and observed [$I > 2\sigma(I)$] reflections	34111, 7067, 6829
R_{int}	0.095
$(\sin\theta/\lambda)_{max}$ (Å^{-1})	0.622
Refinement	
$R[F^2 > 2\sigma(F^2)]$, $wR(F^2)$, S	0.080, 0.2173, 1.097
No. of reflections	7067
No. of parameters	338
H-atom treatment	H-atom parameters constrained
$\Delta\rangle_{max}$, $\Delta\rangle_{min}$ (e Å^{-3})	2.14, -1.13

Diffuse Scattering in 5 (analyzed by Vladislav Yu. Komarov)

The diffraction pattern of **5** shows quite strong diffuse scattering that is visible even during the routine diffraction experiment. The diffraction pattern in the reciprocal space reconstructed with

CrysAlisPro (Agilent Technologies) software shows that in addition to the Braggs peaks, two types of diffuse spots appear.

The diffuse spots of the first type lie on the planes perpendicular to *c** with the *l* = integer, near to the points where *h* and *k* values are both half-integer. If *h* or *k* is integer, the diffuse scattering in the planes is not observed. It is also true for the area near to the systematically absent Bragg reflections with *hk*0, *h+k=2n+1* (due to the presence of the glide plane *n*⊥*c*). The spots of this type have quite a complex shape with two close maximums. The distribution of the diffuse scattering intensity is quite narrow but noticeably wider than those for the Bragg peaks (*Figure 5.9*c-e). The spots of the first types are observed up to high *l* values (*Figure 5.10*).

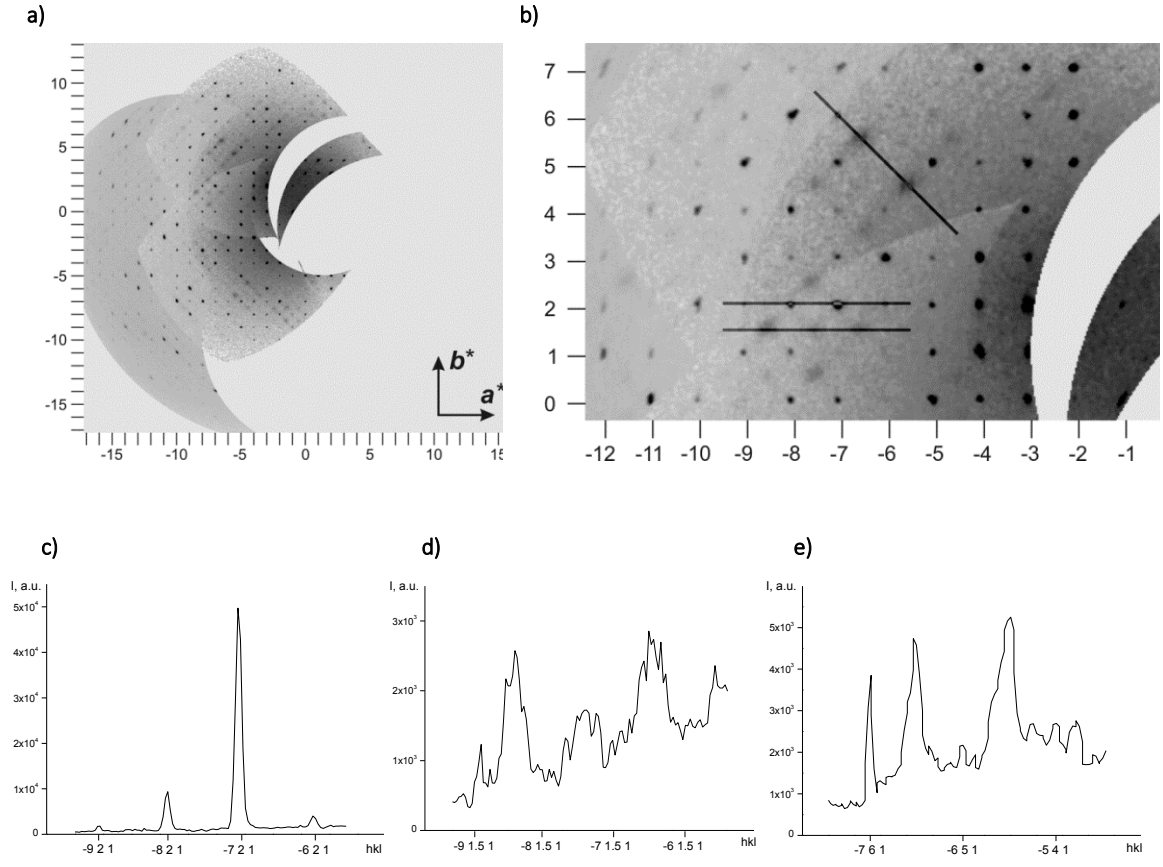

Figure 5.9 The reconstruction of *hk*1 section showing diffuse spots of the first type: a) general view; b) close view; c)-e) intensity profile along the highlited rows at b).

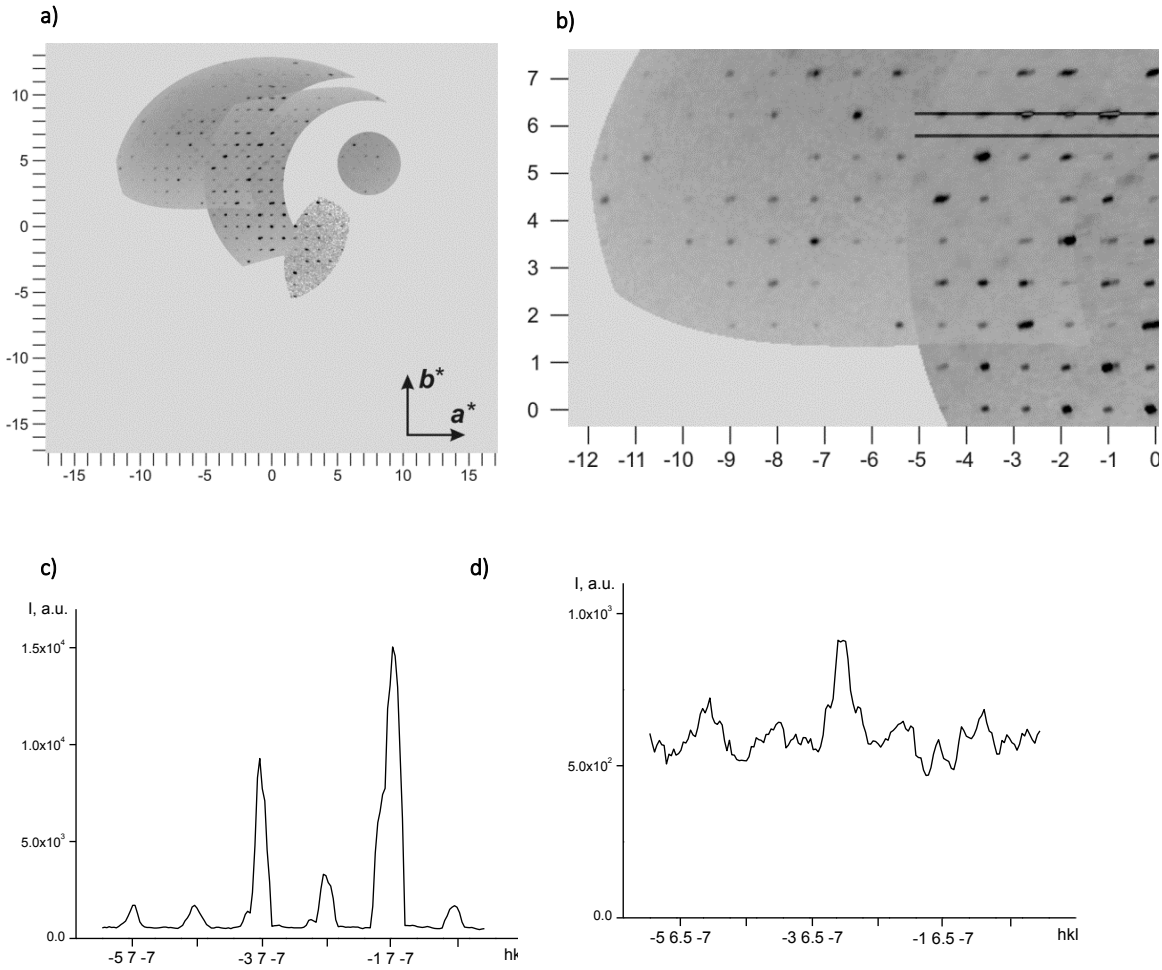

Figure 5.10 The reconstruction of the *hk*-7 section: a) general view; b) close view; c)-d) intensity profiles along the highlited rows at b).

The spots of the second type are cross-shaped and lie on the planes perpendicular to *c**, but on the contrary, with the *half-integer l* and near to the points with *integer h* and *k* values (*Figure 5.11*). These spots are observed for the whole range $-10.5 \leq l \leq 7.5$. The 'arms' of the 'crosses' are directed along *a*±b** diagonals. The reconstruction of the detailed profile for these spots appeared to be impossible due to the artefacts resulting from the wide ω-scans taken during a routine diffraction experiment.

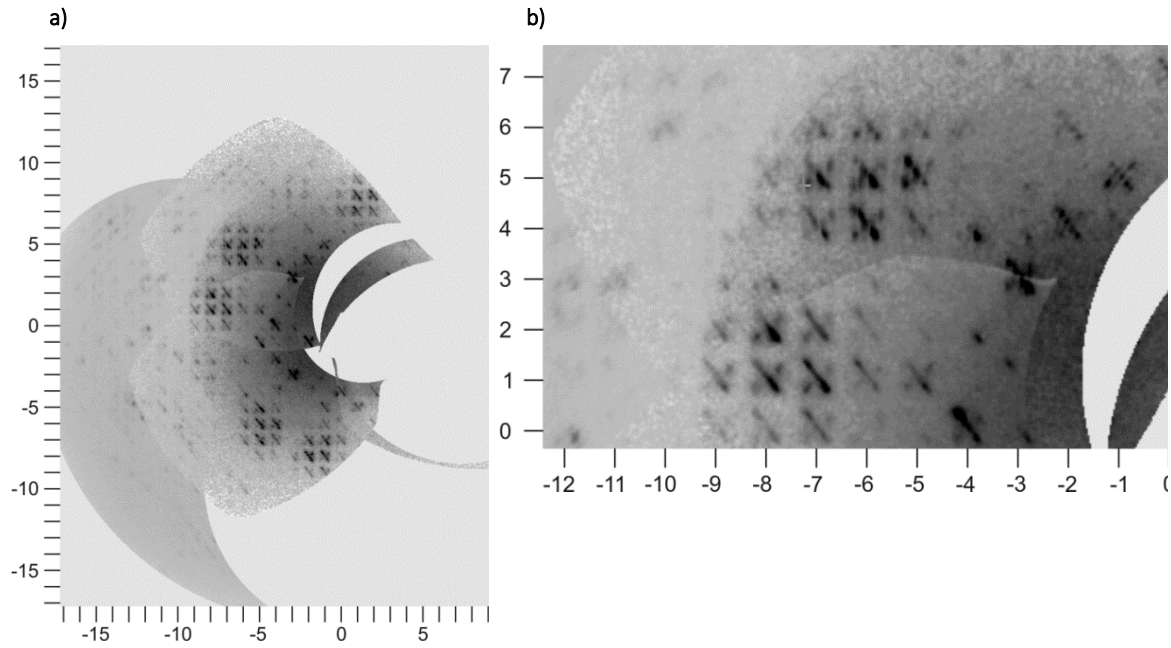

Figure 5.11 The reconstruction of the *hk*0.5 diffraction section: a) general view; b) close view.

The symmetry of the diffuse scattering spots of both types is in a good agreement with the symmetry of the Bragg diffraction (point group 4/*m*).

The diffuse scattering obviously originates from the disorder of the polymeric chains and/or $\{Cu_5I_4(MeCN)_4(P_3C_2Mes_2)\}$ repeating units by 90° rotation around the 4-fold axis parallel to ***c***. At that, each orientation of the $\{Cu_5I_4(MeCN)_4(P_3C_2Mes_2)\}$ repeating unit may require a preferable orientation either of the units of the neighboring chains or within the single chain due to the sterical hindering between the bulky Mes groups. Therefore, there is a correlation between the neighboring orientations despite their equal probability in the averaged crystal structure imposed by the 4-fold axis.

The correct reduction of diffuse intensities for the modelling of the real crystal would require special diffraction techniques (using a strong monochromatic radiation source, noise-free detector *etc*.). The data from a routine structural determination we possess are obviously not enough to make final conclusions. Nevertheless, preliminary consideration shows that we can propose two possible disorder models. One model assumes coexistence of differently oriented chains, but the orientation of all repeating units in every chain is identical. Another more complicated model assumes that the repeating units of the same chain can be rotated around the Cu-P bond in respect to each other. The results of preliminary calculations prove that only the latter model, sophisticated with local relaxation of atomic groups, explains the presence of both types of the diffuse scattering spots. Qualitatively the best result corresponds to the models where the orientation of the closest repeating units alternate both within the polymeric chain and, less strictly, between them.

5.5 Author Contributions

- The syntheses and characterization of the compounds **3**, **4**, **6** – **10** were performed by Claudia Heindl within the scope of this thesis
- The syntheses and characterization of the compounds **2** and **5** were performed by Claudia Heindl within the scope of the degree thesis (University of Regensburg, 2010)
- X-ray structural analyses were performed by Dr. Eugenia V. Peresypkina, Dr. Alexander V. Virovets and Claudia Heindl
- The manuscript (introduction, results and discussion, experimental part; including figures and graphical abstract) was written by Claudia Heindl with the following exceptions:
- The section 'crystallographic details' was written by Dr. Alexander V. Virovets and Dr. Vladislav Yu. Komarov (section: diffuse scattering) and Dr. Eugenia V. Peresypkina

5.6 References

[1] a) S. I. Stupp, L. C. Palmer, *Chem. Mater.* 2014, *26*, 507; b) N. Lanigan, X. Wang, *Chem. Commun.* 2013, *49*, 8133; c) R. W. Saalfrank, A. Scheurer, *Top Curr Chem* 2012, *319*, 125; d) S. J. Dalgarno, *Annu. Rep. Prog. Chem., Sect. B: Org. Chem.* 2010, *106*, 197; e) M. Mastalerz, *Angew. Chem. Int. Ed.* 2010, *49*, 5042; f) T. H. Rehm, C. Schmuck, *Chem. Soc. Rev.* 2010, *39*, 3597; g) J.-M. Lehn, *Proceedings of the National Academy of Sciences* 2002, *99*, 4763; h) F. A. Cotton, C. Lin, C. A. Murillo, *Acc. Chem. Res.* 2001, *34*, 759.

[2] S. Deng, C. Schwarzmaier, M. Zabel, J. F. Nixon, A. Y. Timoshkin, M. Scheer, *Organometallics* 2009, *28*, 1075.

[3] a) S. Deng, C. Schwarzmaier, M. Zabel, J. F. Nixon, M. Bodensteiner, E. V. Peresypkina, G. Balázs, M. Scheer, *Eur. J. Inorg. Chem.* 2011, 2991; b) A. Schindler, G. Balázs, M. Zabel, C. Groeger, R. Kalbitzer, M. Scheer, *C. R. Chim.* 2010, *13*, 1241; c) A. Schindler, M. Zabel, J. F. Nixon, M. Scheer, *Z. Naturforsch.* 2009, *64*, 1429; d) S. Deng, C. Schwarzmaier, U. Vogel, M. Zabel, J. F. Nixon, M. Scheer, *Eur. J. Inorg. Chem.* 2008, 4870.

[4] a) S. Deng, C. Schwarzmaier, C. Eichhorn, O. Scherer, G. Wolmershauser, M. Zabel, M. Scheer, *Chem. Commun.* 2008, 4064; b) J. Bai, A. V. Virovets, M. Scheer, *Angew. Chem. Int. Ed.* 2002, *41*, 1737.

[5] a) F. Dielmann, M. Fleischmann, C. Heindl, E. V. Peresypkina, A. V. Virovets, R. M. Gschwind, M. Scheer, *Chem. Eur. J.* 2015, *21*, 6208; b) F. Dielmann, C. Heindl, F. Hastreiter, E. V. Peresypkina, A. V. Virovets, R. M. Gschwind, M. Scheer, *Angew. Chem. Int. Ed.* 2014, *53*,

13605; c) C. Schwarzmaier, A. Schindler, C. Heindl, S. Scheuermayer, E. V. Peresypkina, A. V. Virovets, M. Neumeier, R. Gschwind M. Scheer, *Angew. Chem. Int. Ed.* 2013, *52*, 10896; d) A. Schindler, C. Heindl, G. Balázs, C. Groeger, A. V. Virovets, E. V. Peresypkina; M. Scheer, *Chem. Eur. J.* 2012, *18*, 829; e) S. Welsch, C. Groeger, M. Sierka, M. Scheer, *Angew. Chem. Int. Ed.* 2011, *50*, 1435; f) M. Scheer, A. Schindler, J. Bai, B. P. Johnson, R. Merkle, R. Winter, A. V. Virovets, E. V. Peresypkina, V. A. Blatov, M. Sierka, H. Eckert, *Chem. Eur. J.* 2010, *16*, 2092; g) M. Scheer, A. Schindler, C. Groeger, A. V. Virovets, E. V. Peresypkina, *Angew. Chem. Int. Ed.* 2009, *48*, 5046; h) M. Scheer, A. Schindler, R. Merkle, B. P. Johnson, M. Linseis, R. Winter, C. E. Anson, A. V. Virovets, *J. Am. Chem. Soc.* 2007, *129*, 13386; i) M. Scheer, J. Bai, B. P. Johnson, R. Merkle, A. V. Virovets, C. E. Anson, *Eur. J. Inorg. Chem.* 2005, 4023; j) J. Bai, A. V. Virovets, M. Scheer, *Science* 2003, *300*, 781.

[6] R. Peng, M. Li, D. Li, *Coord. Chem. Rev.* 2010, *254*, 1.

[7] a) P. Schwarz, J. Wachter, M. Zabel, *Inorg. Chem.* 2011, *50*, 12692; b) P. Schwarz, J. Wachter, M. Zabel, *Inorg. Chem.* 2011, *50*, 8477; c) A. Biegerl, C. Groeger, H. R. Kalbitzer, A. Pfitzner, J. Wachter, R. Weihrich, M. Zabel, *J. Solid State Chem.* 2011, *184*, 1719; d) A. Biegerl, E. Brunner, C. Groeger, M. Scheer, J. Wachter, M. Zabel, *Chem. Eur. J.* 2007, *13*, 9270.

[8] C.-Z. Mei, X.-Y. Hu, G.-R. Yang, K.-H. Li, W.-W. Shan, *Z. Naturforsch.* 2012, *67*, 951.

[9] C. Heindl, A. Kuntz, E. V. Peresypkina, A. V. Virovets, M. Zabel, D. Luedeker, G. Brunklaus, M. Scheer, *Dalton Trans.* 2015, *44*, 6502.

[10] C. Heindl, A. Schindler, M. Bodensteiner, E. V. Peresypkina, A. V. Virovets, M. Scheer, *Phosphorus, Sulfur Silicon Relat. Elem.* 2015, *190*, 397.

[11] a) G. K. B. Clentsmith, F. G. N. Cloke, M. D. Francis, J. R. Hanks, P. B. Hitchcock, J. F. Nixon, *J. Organomet. Chem.* 2008, *693*, 2287; b) T. Clark, A. Elvers, F. W. Heinemann, M. Hennemann, M. Zeller, U. Zenneck, *Angew. Chem. Int. Ed.* 2000, *39*, 2087; c) C. S. J. Callaghan, P. B. Hitchcock, J. F. Nixon, *J. Organomet. Chem.* 1999, *584*, 87; d) P. B. Hitchcock, J. F. Nixon, R. M. Matos, *J. Organomet. Chem.* 1995, *490*, 155; e) R. Bartsch, P. B. Hitchcock, J. F. Nixon, *J. Organomet. Chem.* 1989, *373*, C17; f) R. Bartsch, P. B. Hitchcock, J. F. Nixon, *J. Organomet. Chem.* 1988, *340*, C37; g) R. Bartsch, P. B. Hitchcock, J. F. Nixon, *J. Organomet. Chem.* 1988, *356*, C1.

[12] a) M. M. Al-Ktaifani, W. Bauer, U. Bergstrasser, B. Breit, M. D. Francis, F. W. Heinemann, P. B. Hitchcock, A. Mack, J. F. Nixon, H. Pritzkow, M. Regitz, M. Zeller, U. Zenneck, *Chem. Eur. J.* 2002, *8*, 2622; b) M. M. Al-Ktaifani, D. P. Chapman, M. D. Francis, P. B. Hitchcock, J. F. Nixon, L. Nyulaszi, *Angew. Chem. Int. Ed.* 2001, *40*, 3474; c) R. Bartsch, P. B. Hitchcock, J. F. Nixon, *J. Organomet. Chem.* 1989, *375*, C31.

[13] a) F. W. Heinemann, M. Zeller, U. Zenneck, *Organometallics* 2004, *23*, 1689; b) M. Hofmann, F. W. Heinemann, U. Zenneck, *J. Organomet. Chem.* 2002, *643*, 357.

[14] M. M. Al-Ktaifani, P. B. Hitchcock, J. F. Nixon, *J. Organomet. Chem.* 2003, *665*, 101.

[15] K. Sugimoto, T. Kuroda-Sowa, M. Munakata, M. Maekawa, *Chem. Commun.* 1999, 455.

[16] a) M. Li, Z. Li, D. Li, *Chem. Commun.* 2008, 3390; b) J.-P. Zhang, Y.-Y. Lin, X.-C. Huang, X.-M. Chen, *J. Am. Chem. Soc.* 2005, *127*, 5495.

[17] a) V. A. Blatov, A. P. Shevchenko, D. M. Proserpio, *Cryst. Growth Des.* 2014, *14*, 3576; b) M. O'Keeffe, M. A. Peskov, S. J. Ramsden, O. M. Yaghi, *Accts. Chem. Res.* 2008, *41*, 1782, http://rcsr.anu.edu.au.

[18] a) X. Shen, D. M. Ho, R. A. Pascal, Jr., *Org. Lett.* 2003, *5*, 369; b) A. J. Berresheim, M. Mueller, K. Muellen, *Chem. Rev.* 1999, *99*, 1747.

[19] M. O'Keeffe, G. Adams, O. Sankey, *Phys. Rev. Lett.* 1992, *68*, 2325.

[20] J. Gibson, M. Holohan, H. L. Riley, *J. Chem. Soc.* 1946, 456.

[21] O. Delgado Friedrichs, M. O'Keeffe, O. M. Yaghi, *Acta Cryst. sect. A* 2003, *A59*, 515.

[22] a) T. Yamada, G. Maruta, S. Takeda, *Chem. Commun.* 2011, *47*, 653; b) W. Ouellette, A. V. Prosvirin, J. Valeich, K. R. Dunbar, J. Zubieta, *Inorg. Chem.* 2007, *46*, 9067; c) W. Ouellette, M. H. Yu, C. J. O'Connor, D. Hagrman, J. Zubieta, *Angew. Chem. Int. Ed.* 2006, *45*, 3497; d) Q.-G. Zhai, C.-Z. Lu, S.-M. Chen, X.-J. Xu, W.-B. Yang, *Cryst. Growth Des.* 2006, *6*, 1393; e) B. Ding, L. Yi, P. Cheng, D.-Z. Liao, S.-P. Yan, *Inorg. Chem.* 2006, *45*, 5799.

[23] W. Ouellette, H. Liu, C. J. O'Connor, J. Zubieta, *Inorg. Chem.* 2009, *48*, 4655.

[24] E. Quartapelle Procopio, F. Linares, C. Montoro, V. Colombo, A. Maspero, E. Barea, J. A. R. Navarro, *Angew. Chem. Int. Ed.* 2010, *49*, 7308.

[25] C. S. J. Callaghan, P. B. Hitchcock, J. F. Nixon, *J. Organomet. Chem.* 1999, *584*, 87.

[26] G. M. Sheldrick, *Acta Cryst. sect. C* 2015, *C71*, 3.

[27] A. Altomare, M. C. Burla, M. Camalli, G. L. Cascarano, C. Giacovazzo, A. Guagliardi, A. G. G. Moliterni, G. Polidori, R. Spagna, *J. Appl. Cryst.* 1999, *32*, 115.

[28] X.-L. Li, X.-G. Meng, S.-P. Xu, *Chin. J. Struct. Chem.*, 2009, *28*, 1619.

6. A Breakthrough in Arsolyl Chemistry – Synthesis and Structural Characterization of the First Tetraarsolyl Ring

C. Heindl, E. V. Peresypkina, A. V. Virovets, M. Scheer

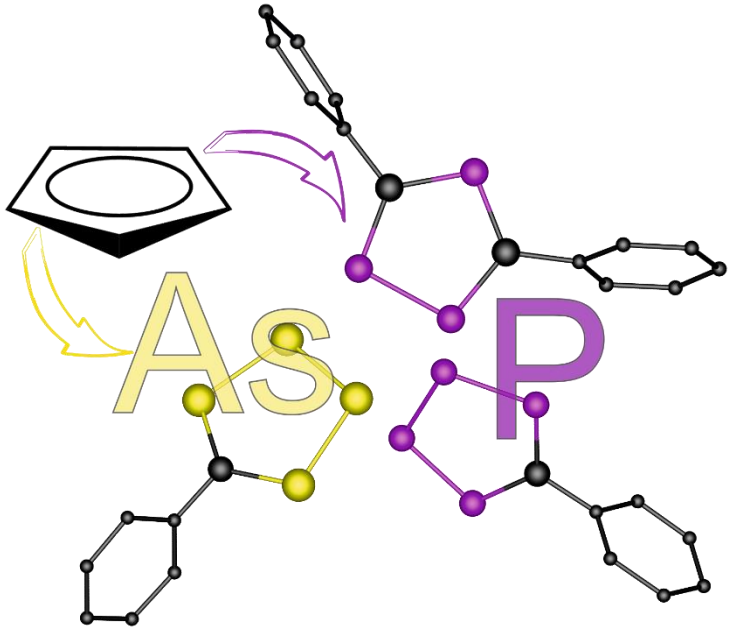

Abstract:

The synthesis of inorganic analogues of the cyclopentadienyl anion Cp^- displays a fascinating as well as challenging field of current research. The replacement of methine moieties by phosphorus is well investigated for the synthesis of mono-, 1,2,4-tri- and pentaphospholyl ligands. On the other hand, arsenic derivatives are far less aware and 1,2,4-triarsolyl and tetraarsolyl salts are not known at all. Herein, we report on the synthesis of $Cs[E_3C_2(trip)_2]$ (**1a**: E = P; **1b**: E = As; trip = 2,4,6-tri-*iso*-propylphenyl) and $Cs[E_4C(trip)]$ (**2a**: E = P; **2b**: E = As). Thereby compound **1b** represents the first 1,2,4-triarsolyl ligand and **2b** the first tetraarsolyl ligand. All salts are obtained *via* a one-pot synthesis using $E(SiMe_3)_3$, 2,4,6-tri-*iso*-propylbenzoyl chloride and CsF. The products **1a**·$2C_4H_8O_2$, **2a**·Et_2O and **2b**·$3C_4H_8O_2$ could be characterized by X-ray structural analysis revealing planar heterocycles. Noteworthy, compound **2a**·Et_2O displays the second tetraphospholyl ligand, which was yet structurally characterized.

6.1 Introduction

According to the noble lecture of Roald Hoffmann in 1981,[1] the isolobal analogy builds bridges between organometallic, organic and inorganic chemistry. Until today, the substitution of CH_x (x = 1, 2, 3) moieties by heteroatoms is of special interest in fundamental chemistry. Especially the incorporation of group 15 elements in aromatic molecules is a fascinating area. For example, the replacement of methine groups in the cyclopentadienyl anion Cp^- by phosphorus or arsenic leads to the class of phospholyl and arsolyl rings $[E_n(CR)_{5-n}]$ (E = P, As), respectively (*Figure 6.1*).

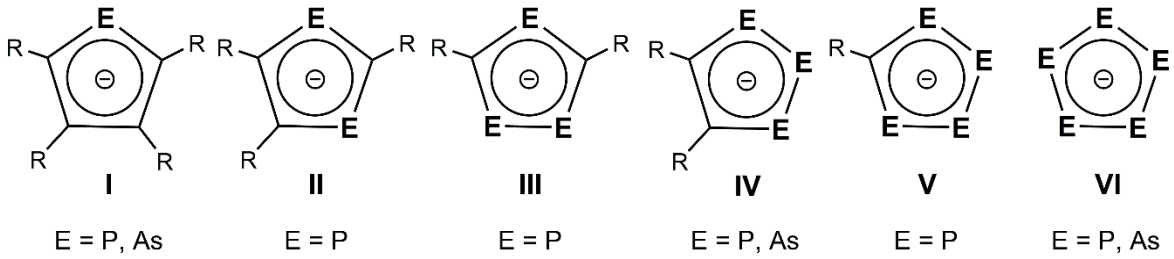

Figure 6.1 Selected types of phospholyl (E = P) and arsolyl (E = As) rings; below: existing derivatives.

In this field, the mono-substituted derivatives **I** are well known and intensively studied for both P and As.[2] The all-pnictogen analogue **VI** can mostly be obtained in metallocenes and triple decker complexes by co-thermolysis of the molecular allotropes P_4 and As_4, respectively, with transition metal complexes.[3] The entirely substituent-free ring P_5^- is far more difficult to handle, though it is persistent in solution.[4] Recently, Cummins *et al.* were able to synthesize the sodium salt of the free diphosphatriazolate anion $P_2N_3^-$.[5] On the other hand, numerous investigations for the 1,2,4-triphospholyl ligand **III**[6] and at least a few for the 1,3-diphospholyl derivative **II** have been reported,[6f,7] whereby their syntheses mostly start either from phosphaalkenes or –alkynes. Though, due to the lower stability of As-C multiple bonds, compounds of type **II** and **III** are not yet known for the heavier homologue arsenic. Analog synthetic approaches only result in the formation of the $[As(C^tBu)]_4$ cubane.[8] Merely the mixed heterocycle $[AsP_2(C^tBu)_2]^-$ is known,[9] whose structural characterization was only successful after coordination to a $W(CO)_5$ fragment in $[CpFe\{AsP_2(C^tBu)_2\}W(CO)_5]$.[10] A completely different approach is needed for the synthesis of the also very rare 1,2,3-isomers **IV**: the reaction of alkynes either with P_4 butterfly complexes[11] or with the Zintl anions $[E_7]^{3-}$ (E = P, As).[12] The latter route yields the only example known of a 1,2,3-arsolyl ligand. The lowest number of publications can be found for the derivative **V**, not known at all for E = As and only two structurally characterized derivatives for E = P.[6b,13] Particularly interesting, Ionkin *et al.* introduced a three-component reaction of CsF, $P(SiMe_3)_3$ and 2,4,6-tri-*tert*-butylbenzoyl chloride yielding a mixture of $Cs[1,2,4\text{-}P_3C_2Mes^*_2]$ and $Cs[P_4CMes^*]$ (Mes* = 2,4,6-tri-*tert*-butylphenyl), both stabilized by bulky supermesityl groups.[6b] Since no intermediates have to be isolated using this one-pot reaction, this strategy seems auspicious for the transfer to the arsenic-

analogue. Furthermore, to avoid the extensive synthesis of the supermesityl ligand, we were interested in the portability of this synthetic route to slightly smaller R groups, such as the tri-*iso*-propylphenyl (trip) derivative.

Herein we report on the synthesis of $Cs[E_3C_2(trip)_2]$ (**1a**: E = P; **1b**: E = As; trip = 2,4,6-tri-*iso*-propylphenyl) and $Cs[E_4C(trip)]$ (**2a**: E = P; **2b**: E = As). Thereby compound **1b** displays the first 1,2,4-triarsolyl ligand and **2b** the first tetraarsolyl ligand, both closing significant gaps in the row of arsenic containing analogues of the cyclopentadienyl anion. Furthermore, the salts **1a**·$2C_4H_8O_2$, **2a**·Et_2O and **2b**·$3C_4H_8O_2$ could also be characterized by X-ray structural analysis.

6.2 Results and Discussion

Following the synthetic route for the preparation of $Cs[P_3C_2Mes^*_2]$ and $Cs[P_4CMes^*]$, 2,4,6-tri-*iso*-propylbenzoyl chloride bearing the smaller trip substituent was reacted with $P(SiMe_3)_3$ and CsF in 1,4-dioxane (*Scheme 6.1*). Already while combining the reagents the colorless solutions get yellow-orange and when refluxing a darkening to deep red and turbidity are observed.

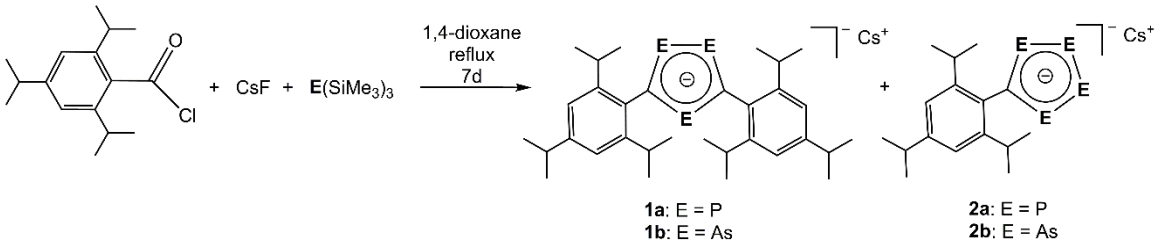

Scheme 6.1 Synthesis of **1a** and **1b** and **2a** and **2b**, respectively.

The reaction progress can easily be monitored by NMR spectroscopy. After one day, the $^{31}P\{^1H\}$ NMR spectrum of the reaction mixture shows three main signals corresponding to $P(SiMe_3)_3$, **1a** and **2a** in the ratio 2:2:1. In the corresponding spectrum after three days of reflux the ratio is determined to be 1.1:1.8:1. After seven days of reflux the intensity of the signal of $P(SiMe_3)_3$ still decreases, however signals that can be assigned to by-products according to reference [6b] appear. The ratio **1a**:**2a** = 1.8:1 remains constant at this stage. After filtration of the hot solution, separation of **1a** and **2a** is achieved by fractional crystallization, since the solubility of **2a** containing only one trip ligand in dioxane is lower compared to **1a** (for details see experimental part). *Via* this method, pure **1a** (third crop of crystals) and pure **2a** (first crop of crystals) can be isolated in yields of 15% and 4%, respectively. Taking also the second crop of crystals consisting of a mixture of both into account, the yield amounts to 16% for **1a** and 12% for **2a**, respectively. These display usual values for this kind of chemistry. However, this separation procedure is very sensitive to the concentration, temperature and diffusion time, hence often recrystallization is required.

Both compounds **1a** and **2a** are well soluble in donor solvents like dioxane, dme, CH_3CN and thf and only poorly soluble in nonpolar solvents like toluene and hexane. The $^{31}P\{^1H\}$ spectrum of **1a** in thf-d_8 shows a triplet at δ = 273.9 ppm for the isolated P atom in the ring and a dublet at δ = 270.5 ppm for the adjacent P atoms with an integral ratio of 1:2 ($^2J_{PP}$ = 38 Hz). In comparison with $Cs[P_3C_2Mes^*_2]$ the first mentioned signal is therefore slightly upfield-shifted (δ = 287.6 ppm), whereas the latter shows a small shift to lower field (δ = 267.9 ppm). In the ^1H NMR spectrum of **1a** two sets of signals of the trip ligand are observed (see experimental part). In the $^{31}P\{^1H\}$ NMR spectrum of **2a** in thf-d_8 mulitplets characteristic for an AA'MM' spin system at δ = 372.8 and 366.0 ppm with respective coupling constants of $^1J_{AA'}$ = 488.2 Hz, $^2J_{AM'}$ = -1.6 Hz, $^3J_{MM'}$ = 52.0 Hz and $^1J_{AM}$ = 492.0 Hz (simulated values, for experimental and simulated spectra see *Figure 6.2*) are obtained. The same trend is observed, namely the upfield shift of the former and the downfield shift of the latter multiplet in comparison with the bulkier Cs[P_4CMes*] ligand (δ = 386.5 and 341.6 ppm). Both anions, $[P_3C_2(trip)_2]^-$ and $[P_4C(trip)]^-$, can also be detected in the negative ion ESI-MS spectrum.

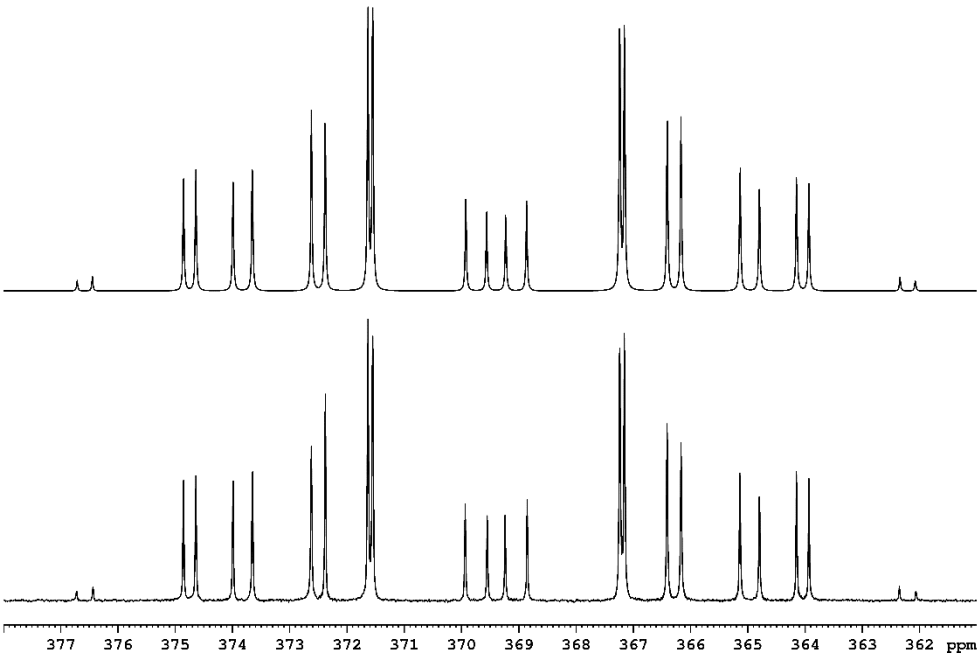

Figure 6.2 $^{31}P\{^1H\}$ NMR spectrum of **2a**: simulated (top) and experimental (below).

Due to the successful transfer of this one-pot synthesis, published by Ionkin et al, to the trip substituent, it has subsequently applied to $As(SiMe_3)_3$ as starting material. Hereby, the addition of CsF to a solution of $As(SiMe_3)_3$ in 1,4-dioxane immediately leads to a very dark, almost black slurry suspension. After adding a solution of tri-*iso*-propylbenzoyl chloride in the same solvent and refluxing for 1.5 hours the color of the reaction mixture changed to deep red, as it was observed in the synthesis of **1a** and **2a**. In the ^1H NMR spectrum of the reaction mixture several overlapping sets of the trip ligand (one big and some smaller ones) as well as of the protons of $As(SiMe_3)_3$ are

recorded, hence a reliable statement of the ratio cannot be made. After six days of reflux the same work-up strategy like for the phosphorus derivatives **1a** and **2a** was performed, and in fact, several crops of crystals were obtained (for details see experimental part). Unfortunately, a fractional crystallization of **1b** and **2b** was only partially successful in this case. Pure **1b** cannot be obtained and **2b** contains very minor impurities of **1b** (see experimental part). The majority of the first crop of crystals consists of yellow rods, whose X-ray structural characterization reveals the first tetraarsolyl ligand **2b** (see below). In addition, a small amount of a beige microcrystalline powder is also obtained. Subsequently, the mother liquor is decanted and the solid (crystals and powder) dissolved in CD_3CN. The main signals in the recorded ^1H NMR spectrum were assigned to the trip ligand of **2b** considering almost identical chemical shifts for **2a**. In addition, two small sets of signals (intensity 10%) for the trip ligand with an integral ratio of 1:1 appear, though partially overlapping. These indicate the presence of the triarsolyl ligand **1b**. A further clear hint is the negative ion ESI-MS spectrum of every crop of crystals, which always shows peaks at *m/z* = 514.9 and 655.2, that can be assigned to $[As_4C(trip)]^-$ and $[As_3C_2(trip)_2]^-$, respectively. Taking this molar ratio (determined by ^1H NMR: 10% of **1b**, 90% of **2b**) in account, the yield of the isolated crystals amounts to 33%, which is even slightly better than in the phosphorus derivatives.

Hence it can be stated, that the one-pot-route described above can also be transferred for the synthesis of a tri- and tetraarsolyl ligand, though with **2b** as main product besides a small amount of **1b**.

Compound **1a**·$2C_4H_8O_2$ crystallizes as yellow prisms in the triclinic space group $P\bar{1}$. Its structural analysis reveals a perfectly planar (deviation 0.009(2) Å) five-membered P_3C_2-ring with P-C and P-P distances of 1.733(3) Å – 1.743(3) Å and 2.108(1) Å, respectively (*Figure 6.3*a). Both values are in the middle range between a single and a double bond,[14] corroborating the belief of aromaticity of these systems. The cesium cation shows a η^1-coordination to two dioxane molecules (3.039(2) Å – 3.100(3) Å), respectively, and Cs···H interactions with the ^{i}Pr ligands of both the corresponding and the adjacent ring (3.265(1) Å – 3.709(1) Å). Surprisingly, it is also η^6-coordinated by a phenyl ring of the trip ligand with distances of 3.304(1) Å and 3.298(1) Å. This could not be observed in the Mes* derivative.[6b] Furthermore, short P-Cs distances to the isolated phosphorus atom of the ring (3.795(1) Å and 3.809(1) Å) as well as to a P atom of the P_2 'dumbbell' of the neighboring anion (3.623(1) Å and 3.634(1) Å) can also be observed. This high coordination number of Cs leads to a 2D polymeric structure of this salt, whereas it is described as a 1D chain in $Cs[P_3C_2Mes^*_2]$.[6b]

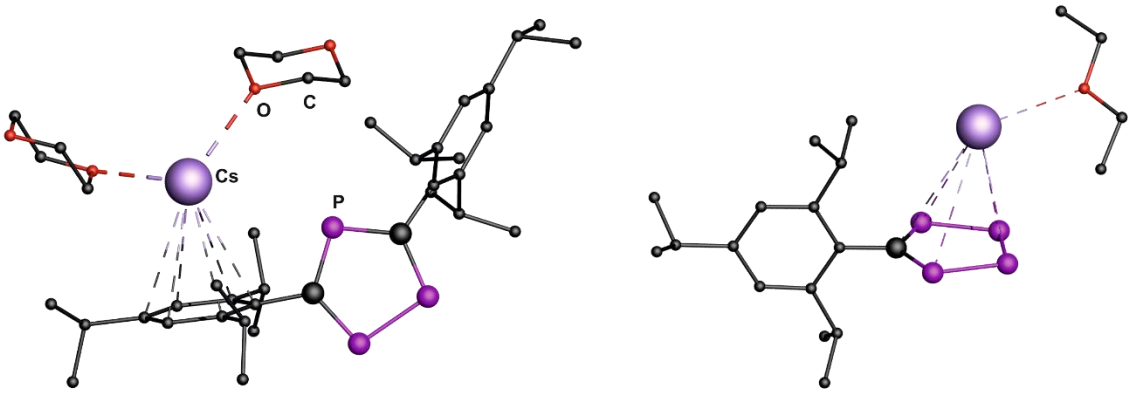

Figure 6.3 Section of the structure of **1a**·$2C_4H_8O_2$ (left) and **2a**·$C_4H_{10}O$ (right). Hydrogen atoms and minor positions of disorder are omitted for clarity.

In contrast, the same crystallization procedure for **2a** only leads to crystals of insufficient quality for X-ray structural analysis. Gratifyingly, cooling a solution of **2a** in Et_2O turned out to be expedient. Using this method, compound **2a** crystallized in the monoclinic space group *C*2/*c* as Et_2O solvate. The central motif is a five-membered planar P_4C ring that shows a slightly stronger deviation of 0.024(3) Å than the P_3C_2 ligand in **1a**·$2C_4H_8O_2$ (*Figure 6.3*b). Compared to **1a**·$2C_4H_8O_2$, the P-P distances in **2a**·Et_2O are slightly shorter (2.087(3) Å – 2.102(3) Å), whereas the P-C bond lengths are somewhat elongated (1.742(7) Å – 1.753(7) Å). The coordination sphere of Cs is different, in **2a**·Et_2O it includes a η^1-coordination of the 1,4-dioxane ligand (3.042(5) – 3.075(6) Å) and of a P atom (3.651(2) Å – 3.695(2) Å), respectively, as well as short distances to three hydrogens of one ^{i}Pr ligand (3.051(1) Å – 3.459(1) Å). Furthermore, in contrast to the η^6-coordination to the phenyl ring in **1a**·$2C_4H_8O_2$, in **2a**·Et_2O a η^5-coordination to the central *cyclo*-P_4C moiety is obtained (3.591(1) Å – 3.683(1) Å). Such a η^5-interaction can be also found in $[Cp_3Cs_2]^-$,[15] however not in the cesium salts of the phospholyl derivatives obtained by Ionkin *et al.*[6b] Similarly to **1a**·$2C_4H_8O_2$, the tendency of Cs^+ to form polymeric aggregates can also be observed in **2a**·Et_2O in form of 2D layers in the solid state. Besides Cs[P_4CMes*], compound **2a**·Et_2O displays the second example of a structurally characterized tetraphospholyl salt. Interesting to note, that the group of Baudler alone reported evidence of $[P_4CH]^-$, yet only based on NMR spectroscopic hints.[16]

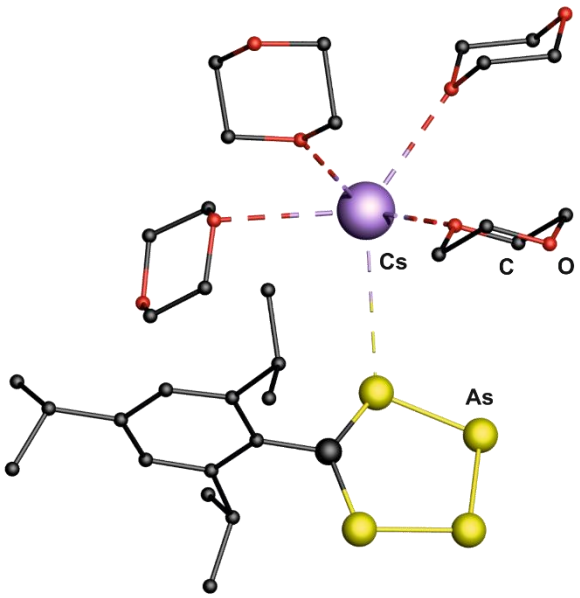

Figure 6.4 Section of the structure of **2b**·$3C_4H_8O_2$. Hydrogens are omitted for clarity.

Yellow needles of **2b**·$3C_4H_8O_2$ can be obtained by cooling down a hot solution of **2b** in dioxane. Compound **2b**·$3C_4H_8O_2$ crystallizes in the triclinic space group $P\bar{1}$ and its X-ray structural analysis reveals a planar As_4C ring with a similar deviation value of 0.022(3) Å compared to **2a**·Et_2O (0.024(3) Å) (*Figure 6.4*). Nearly equal As-C bond lengths of 1.857(14) Å and 1.859(16) Å are found, whereas the As-As distances can be subdivided in two longer ones (2.310(2) Å and 2.311(2) Å) and one shorter value of 2.287(3) Å for the bond opposite to the carbon atom. Compared to the *cyclo*-As_5 ligand in [$Cp^{Et}Fe(\eta^5$-$As_5)$] (Cp^{Et} = C_5Me_4Et)[3c] the average As-As bond length of 2.327(6) Å is longer than the corresponding distances in **2b**·$3C_4H_8O_2$. However, all As-As and As-C distances in **2b**·$3C_4H_8O_2$ are between a single and a double bond.[14] Again, the Cs cation shows a different environment, in **2b**·$3C_4H_8O_2$ it coordinates four dioxane ligands (3.025(9) – 3.152(9) Å) and shows one relatively short As-Cs contact of 3.873(2) Å. In **2b**·$3C_4H_8O_2$, two dioxane molecules bridge two Cs cations and therefore polymerization again in two directions is found in the solid state.

In summary, a one-pot-synthesis applied by the group of Ionkin for the synthesis of Cs[1,2,4-$P_3C_2Mes^*_2$] and Cs[P_4CMes^*] was successfully transferred to the slightly smaller 2,4,6-tri-*iso*-propylphenyl (trip) ligand. The cesium salts of the 1,2,4-triphospholyl ligand (**1a**) as well as the tetraphospholyl ligand (**2a**) can be isolated as dioxane solvates. Astonishingly, this synthetic approach is also applicable for the synthesis of the respective arsenic derivatives Cs[1,2,4-$As_3C_2(trip)_2$] (**1b**) and Cs[$As_4C(trip)$] (**2b**). Compounds **1b** and **2b** display the first representatives of a 1,2,4-triarsolyl and a tetraarsolyl ligand, respectively. Compounds **1a**, **2a** as well as **2b** could also be structurally characterized revealing planar rings. The cesium cations show interactions with a phenyl ring of **1a**, the *cyclo*-P_4C unit of **2a** and an arsenic atom of **2b**, respectively. In combination with bridging dioxane ligands a two-dimensional polymer-like structure is found in all crystals.

6.3 Experimental Part

General Remarks

All reactions were performed under an inert atmosphere of dry nitrogen or argon with standard vacuum, Schlenk and glove-box techniques. Solvents were purified, dried and degassed prior to use by standard procedures. $P(SiMe_3)_3$ was synthesized following the reported procedure.[17] $As(SiMe_3)_3$ was kindly provided by Eva-Maria Rummel, University of Regensburg. Commercially available chemicals (2,4,6-tri-*iso*-propylbenzoyl chloride, CsF) were used without further purification. Solution NMR spectra were recorded on a Bruker Avance 300 or 400 spectrometer. The corresponding ESI-MS spectra were acquired on a ThermoQuest Finnigan MAT TSQ 7000 mass spectrometer. Elemental analyses were performed on a Vario EL III apparatus.

Synthesis of $Cs[P_3C_2(trip)_2]$ (1a) and $Cs[P_4C(trip)]$ (2a)

$P(SiMe_3)_3$ (5.2 g, 20.6 mmol) is dissolved in 1,4-dioxane (80 mL), afterwards a suspension of CsF (9.4 g, 61 mmol) in 1,4-dioxane (30 mL) and a solution of 2,4,6-tri-*iso*-propylbenzoyl chloride (5.5 g, 20.6 mmol) in 1,4-dioxane (30 mL) is added. Thereby a color change from the colorless solutions to yellow-orange can be observed. The reaction mixture is refluxed for seven days, whereby the solution gets deep red and turbid. Generally, the refluxing time should last at least seven days but no longer than ten days. At the end, the hot solution is filtered and the products can be separated by fractional crystallization of the red solution. The first crop of crystals is obtained by cooling the warm solution to r.t. and storage at r.t. for two days, containing solely $Cs[P_4C(trip)]$ (trip = 2,4,6-tri-*iso*-propylphenyl). The second crop of crystals is obtained by layering the mother liquor with hexane and storage at 8°C, containing mainly $Cs[P_3C_2(trip)_2]$ (92%) and a small amount of $Cs[P_4C(trip)]$ (8%). For the third crop of crystals the solvent of the mother liquor is removed, the residue dissolved in Et_2O and stored at 8°C. This crop finally contains solely $Cs[P_3C_2(trip)_2]$. Depending on the amount of solvent at the beginning, the amount of hexane and the diffusion time, the ratios can differ significantly and to get pure $Cs[P_4C(trip)]$ and $Cs[P_3C_2(trip)_2]$, respectively, recrystallization is often required. Generally, the isolation of pure $Cs[P_3C_2(trip)_2]$ is more challenging than of $Cs[P_4C(trip)]$.

Analytical data of **1a**:

Yield: 658 mg (0.8 mmol, 16% referred to $P(SiMe_3)_3$)

^{1}H NMR (thf-d_8): δ [ppm] = 1.03 (d, $^3J_{HH}$ = 6.9 Hz, 12H, Me_{ortho}), 1.07 (d, $^3J_{HH}$ = 6.9 Hz, 12H, Me_{ortho}), 1.13 (d, $^3J_{HH}$ = 6.9 Hz, 6H, Me_{para}), 1.27 (d, $^3J_{H\text{-}H}$ = 6.9 Hz, 6H, Me_{para}), 2.87 – 3.45 (m, $CH_{Methine}$), 3.56 (s, 8H, dioxane), 6.9 – 7.3 (br, 4H, CH_{aryl}).

^{31}P{^{1}H} NMR (thf-d_8): δ [ppm] = 270.48 (d, $^2J_{PP}$ = 38 Hz, 2P, **1a**), 273.86 (t, $^2J_{PP}$ = 38 Hz, 1P, **1a**).

^{31}P NMR (thf-d_8): δ [ppm] = 270.5 (d, $^2J_{PP}$ = 38 Hz, 2P, **1a**), 273.9 (t, $^2J_{PP}$ = 38 Hz, 1P, **1a**).

Negative ion ESI-MS (dme, second crop of crystals): *m/z* (%) = 523.3 (80) $[P_3C_2(trip)_2]^-$, 339.0 (100) $[P_4C(trip)]^-$

Positive ion ESI-MS (dme, second crop of crystals): *m/z* (%) = 300.6 (12) $[Cs_2Cl]^+$, 222.7 (28) $[Cs(dme)]^+$, 132.6 (100) $[Cs]^+$

Elemental analysis: Calculated (%) for $[(C_{32}H_{46}CsP_3)(C_{16}H_{23}CsP_4)_2(C_4H_8O_2)]$ (second crop of crystals) (1689 g/mol): C 48.36, H 5.97; found: 48.29, H 6.14.

Analytical data of **2a**:

Yield: 442 mg (0.8 mmol, 12% referred to $P(SiMe_3)_3$)

^{1}H NMR (thf-d_8): δ [ppm] = 1.03 (d, $^3J_{HH}$ = 7 Hz, 12H, Me_{ortho}), 1.12 (t, 0.25 Et_2O), 1.29 (d, $^3J_{HH}$ = 7 Hz, 6H, Me_{para}), 2.90 (sept, $^3J_{HH}$ = 7 Hz, 3H, $CH_{Methine}$), 3.39 (q, 0.25 Et_2O), 6.97 (s, 2H, CH_{aryl}).

^{13}C{^{1}H} NMR (thf-d_8): δ [ppm] = 15.55 (s, Et_2O), 30.72 (s, CH_3), 35.24 (s, CH), 120.17 (s, C_{meta}), 145.77 (s, C_{ortho}), 147.37 (t, $^2J_{PC}$ = 4.3 Hz, C_{ipso}).

^{31}P{^{1}H} NMR (thf-d_8): δ [ppm] = 366.0 (m, 2 P, P_A(**2a**) and $P_{A'}$(**2a**)); 372.8 (m, 2 P, P_M(**2a**) and $P_{M'}$(**2a**)); $^1J_{A\text{-}A'}$ = 488.2 Hz, $^2J_{A\text{-}M'}$ = -1.6 Hz, $^3J_{M\text{-}M'}$ = 52.0 Hz, $^1J_{A\text{-}M}$ = 492.0 Hz (simulated values).

Negative ion ESI-MS (dme, second crop of crystals): *m/z* (%) = 523.3 (80) $[P_3C_2(trip)_2]^-$, 339.0 (100) $[P_4C(trip)]^-$

Positive ion ESI-MS (dme, second crop of crystals): *m/z* (%) = 300.6 (12) $[Cs_2Cl]^+$, 222.7 (28) $[Cs(dme)]^+$, 132.6 (100) $[Cs]^+$

Elemental analysis: Calculated (%) for [Cs[P_4C(trip)]·dme] (recrystallized from dme) (562.3 g/mol): C 42.72, H 5.92; found: C 42.45, H 5.91.

Synthesis of $Cs[As_3C_2(trip)_2]$ (1b) and $Cs[As_4C(trip)]$ (2b)

$As(SiMe_3)_3$ (3.3 g, 11.6 mmol) is dissolved in 1,4-dioxane (40 mL), afterwards solid CsF (5.2 g, 34.2 mmol) and a solution of 2,4,6-tri-*iso*-propylbenzoyl chloride (3.1 g, 11.6 mmol) in 1,4-dioxane (30 mL) is added. Thereby, the color darkens from the colorless solutions to almost black. The reaction mixture is refluxed for six days, whereby the solution gets first greenish and after 1.5 h deep red and turbid. At the end the hot red solution is filtered, cooled to r.t. and stored at r.t. for two days. Thereby, yellow rods of $Cs[As_4C(trip)]$ crystallize, accompanied by the precipitation of a small amount of a beige powder, which is attributed to $Cs[As_3C_2(trip)_2]$. A second crop of microcrystalline powder is obtained by layering the mother liquor with hexane (100 mL) and storage at 8°C, containing $Cs[As_3C_2(trip)_2]$ and $Cs[As_4C(trip)]$. Pure $Cs[As_3C_2(trip)_2]$ unfortunately cannot be obtained by following crystallization procedures, since other by-products, as mentioned by Ionkin *et al.*,[6b] also crystallize.

Analytical data of **1b** and **2b**:

Yield: 850 mg (~1.01 mmol for a 10% **1b** / 90% **2b** mixture; 33% referred to $As(SiMe_3)_3$)

^{1}H NMR (CD_3CN): δ [ppm] = 1.03 (d, $^3J_{HH}$ = 6.9 Hz, 12H, As_4C: Me_{ortho}), 1.08 – 1.25 (m, 4H, 0.1 As_3C_2: Me), 1.30 (d, $^3J_{HH}$ = 6.9 Hz, 6H, As_4C: Me_{para}), 2.75 – 2.90 (m, 0.2H, 0.1 As_3C_2: CH_{para}), 2.92 (sept, $^3J_{HH}$ = 6.9 Hz, 1H, As_4C: CH_{para}), 3.11 (sept, $^3J_{HH}$ = 6.9 Hz, 2H, As_4C: CH_{ortho}), 3.4 – 3.5 (m, 0.2H, 0.1 As_3C_2: CH_{ortho}), 3.59 (s, 20H, 2.5 dioxane), 6.88 (s, 0.2H, 0.1 As_3C_2: CH_{aryl}), 6.93 (s, 0.2H, 0.1 As_3C_2: CH_{aryl}), 7.06 (s, 2H, As_4C: CH_{aryl}).

$^{13}C\{^1H\}$ NMR (CD_3CN): δ [ppm] = 24.61 (s, Me_{para}), 24.76 (s, Me_{ortho}), 31.09 (s, CH_{ortho}), 35.10 (s, CH_{para}), 120.84 (s, C_{meta}), 142.35 (s, C_{para}), 146.10 (s, C_{ortho}),147.00 (s, C_{ipso}), 246.29 (s, As_4C).

Negative ion ESI-MS (dme): *m/z* (%) = 655.2 (10) $[As_3C_2(trip)_2]^-$, 514.9 (100) $[As_4C(trip)]^-$

Positive ion ESI-MS (dme): *m/z* (%) = 300.6 $[Cs_2Cl]^+$, 222.7 $[Cs(dme)]^+$, 132.7 $[Cs]^+$

Elemental analysis (first crop of crystals): Calculated (%) for $Cs[As_4C(trip)]*2.5\ C_4H_8O_2$ (868.2 g/mol): C 35.97, H 4.99; found: C 35.91, H 4.90.

Elemental analysis (second crop of crystals): Calculated (%) for $Cs[As_4C(trip)]*2C_4H_8O_2$ (33%) / $Cs[As_3C_2(trip)_2]*2C_4H_8O_2$ (67%): C 45.17, H 6.38; found: C 45.01, H 5.77.

6.4 Crystallographic Details

Crystals of **1a, 2a, 2b** were taken from a Schlenk flask under a stream of argon and immediately covered with mineral oil or perfluorinated Fomblin® mineral oil to prevent both decomposition and a loss of solvent. The quickly chosen single crystals covered by a drop of the oil were taken to the pre-centered goniometer head with CryoMount® and directly attached to the diffractometer into a stream of cold nitrogen.

The data for **1a** were collected on an Agilent Technologies Gemini R-Ultra diffractometer equipped with an Atlas^{S2} CCD detector and an Enhanced Ultra CuK_α sealed tube (λ = 1.54178 Å) using 0.5° ω scans. The data for **2a** and **2b** were collected on an Agilent Technologies diffractometer equipped with a Titan^{S2} CCD detector and a SuperNova CuK_α microfocus source using 1° ω scans. All measurements were performed at 123 K.

In **2a**, the structure demonstrates an unusual disorder. The minor positions, 4% for Cs(1a), 8% for P(11a)-P(14a) and 6% for P(21a)-P(24a) found in the residual density map correspond to the structure reflected by a *pseudo* mirror plane at (*x*, 0, *z*). The mirror plane would result in combination with the symmetry elements of the *C*2/*c* space group to a shortening of the *c* lattice constant by two times and the presence of a *pseudo* body-centered lattice together with a base-centered *C* lattice. This results in partial weakening of all reflections with $l=2n+1$ and, in combination with the *C* lattice systematic absences that require $h+k=2n+1$, with $h+k+l=2n+1$. In

other words, in minority of the unit cells the *c* glide plane at (*x*, 0, *z*) is violated resulting in opposite 'conflicting' positions of some repeating units in the polymeric chain. The corresponding carbon atoms of the *cyclo*-P_4C ligand were not located due to their negligible contribution to the diffraction pattern.

The structure of **2b** was refined as triclinic, but twinned by *pseudo* merohedry (twin matrix: -1 0 0, 0 1 0, 0 0 -1) with twin batches 0.471(2)/0.529(2). In the absence of the systematic absences corresponding to the screw axes and glide planes, an appropriate model in the monoclinic crystal system was found in none of *P*2, *Pm* or *P*2/*m* space groups. One of the dioxane molecules coordinated by Cs^+ is disordered over two positions with a 0.62/0.38 ratio.

All structures were solved by direct methods with *SHELX97*.[18] The structures were refined by full-matrix least-squares method against $|F|^2$ in anisotropic approximation using *SHELXL97* or the multiprocessor and variable memory version *SHELXL2013*. All non-hydrogen atoms were refined anisotropically, while the hydrogen atoms were refined riding on pivot atoms.

Crystallographic data and details of the diffraction experiments are given in *Table 6.1* and *Table 6.2*.

Table 6.1 Experimental details for compounds **1a** and **2a**.

Crystal Data	1a	2a
Chemical formula	$C_{40}H_{62}CsO_4P_3$	$C_{20}H_{33}CsOP_4$
M_r	832.71	546.25
Crystal system, space group	triclinic, $P\bar{1}$	monoclinic, *C*2/*c*
Temperature (K)	123	123
a, *b*, *c* (Å)	9.6771(1), 17.7961(2), 25.4269(2)	35.062(3), 12.138(6), 25.020(2)
α, β, γ (°)	101.716(1), 93.984(1), 90.146(1)	90, 109.079(8), 90
V (Å^3)	4276.67(8)	10062.7(12)
Z	4	16
F(000)	1736	4416
Radiation type	Cu K_α	Cu K_α
μ (mm^{-1})	8.08	13.92
Crystal color and shape	yellow prism	yellow prism
Crystal size (mm)	0.33 × 0.14 × 0.11	0.16 × 0.11 × 0.08
Data collection		
Diffractometer	Xcalibur, Atlas, Gemini ultra diffractometer	SuperNova, TitanS2 diffractometer
Absorption correction	analytical	gaussian
T_{min}, T_{max}	0.263, 0.516	0.263, 0.537
No. of measured, independent and observed [$I > 2\sigma(I)$] reflections	62019, 15048, 12701	17082, 9685, 6574
R_{int}	0.035	0.071

$(\sin\theta/\lambda)_{max}$ (Å^{-1})	0.597	0.624
Range of h, k, l	h = -11→9, k = -21→20, l = -30→30	h = -29→43, k = -10→14, l = -30→29
Refinement		
$R[F^2 > 2\sigma(F^2)]$, $wR(F^2)$, S	0.035, 0.088, 1.02	0.062, 0.160, 0.98
No. of reflections	15048	9685
No. of parameters	933	521
No. of restraints	0	0
H-atom treatment	H atoms treated by a mixture of independent and constrained refinement	H-atom parameters constrained
$\Delta\rangle_{max}$, $\Delta\rangle_{min}$ (e Å^{-3})	2.01, -0.85	2.59, -1.54

Table 6.2 Experimental details for compound **2b**.

Crystal Data	2b
Chemical formula	$C_{28}H_{47}As_4CsO_6$
M_r	912.24
Crystal system, space group	triclinic, $P\bar{1}$
Temperature (K)	123
a, b, c (Å)	8.791(1), 10.148(1), 19.728(1)
α, β, γ (°)	89.937(6), 84.598(8), 89.93(1)
V (Å^3)	1752.1(3)
Z	2
F(000)	900
Radiation type	Cu K_α
μ (mm^{-1})	12.75
Crystal color and shape	yellow needle
Crystal size (mm)	0.56 × 0.05 × 0.03
Data collection	
Diffractometer	SuperNova, Titan^{S2} diffractometer
Absorption correction	gaussian
T_{min}, T_{max}	0.092, 0.740
No. of measured, independent and observed [$I > 2\sigma(I)$] reflections	10331, 6685, 4851
R_{int}	0.064
$(\sin\theta/\lambda)_{max}$ (Å^{-1})	0.624
Range of h, k, l	h = -10→8, k = -11→12, l = -24→24
Refinement	
$R[F^2 > 2\sigma(F^2)]$, $wR(F^2)$, S	0.071, 0.201, 1.01

No. of reflections	6685
No. of parameters	355
No. of restraints	0
H-atom treatment	H-atom parameters constrained
$\Delta\rangle_{max}$, $\Delta\rangle_{min}$ (e Å^{-3})	1.81, -2.37

6.5 Author Contributions

- The syntheses and characterization of all compounds were performed by Claudia Heindl
- X-ray structural analyses were performed together by Dr. Eugenia V. Peresypkina, Dr. Alexander V. Virovets and Claudia Heindl
- The manuscript (introduction, results and discussion, experimental part; including figures and graphical abstract) was written by Claudia Heindl; with the following exception:
- The section 'crystallographic details' was written by Dr. Eugenia V. Peresypkina

6.6 References

[1] R. Hoffmann, *Angew. Chem. Int. Ed.* 1982, *21*, 711.

[2] a) P. Le Floch, *Coord. Chem. Rev.* 2006, *250*, 627; b) M. Westerhausen, M. W. Ossberger, P. Mayer, H. Piotrowski, H. Noeth, *Organometallics* 2004, *23*, 3417; c) F. Nief, D. Turcitu, L. Ricard, *Chem. Commun.* 2002, 1646; d) F. Mathey, *Coord. Chem. Rev.* 1994, *137*, 1; e) S. C. Sendlinger, B. S. Haggerty, A. L. Rheingold, K. H. Theopold, *Chem. Ber.* 1991, *124*, 2453; f) A. J. Ashe, III, S. Mahmoud, C. Elschenbroich, M. Wuensch, *Angew. Chem.* 1987, *99*, 249; g) G. Thiollet, F. Mathey, R. Poilblanc, *Inorg. Chim. Acta* 1979, *32*, L67; h) F. Mathey, A. Mitschler, R. Weiss, *J. Am. Chem. Soc.* 1977, *99*, 3537; i) E. H. Braye, I. Caplier, R. Saussez, *Tetrahedron* 1971, *27*, 5523.

[3] a) F. Dielmann, R. Merkle, S. Heinl, M. Scheer, *Z. Naturforsch.* 2009, *64*, 3; b) E. Urnežius, W. W. Brennessel, C. J. Cramer, J. E. Ellis, P. v. R. Schleyer, *Science* 2002, *295*, 832; c) O. J. Scherer, C. Blath, G. Wolmershäuser, *J. Organomet. Chem.* 1990, *387*, C21; d) M. Baudler, S. Akpapoglou, D. Ouzounis, F. Wasgestian, B. Meinigke, H. Budzikiewicz, H. Münster, *Angew. Chem.* 1988, *100*, 288; e) O. J. Scherer, T. Brück, *Angew. Chem.* 1987, *99*, 59; f) O. J. Scherer, J. Schwalb, G. Wolmershäuser, W. Kaim, R. Groß, *Angew. Chem.* 1986, *98*, 349.

[4] M. Baudler, S. Akpapoglou, D. Ouzounis, F. Wasgestian, B. Meinigke, H. Budzikiewicz, H. Münster, *Angew. Chem.* 1988, *100*, 288.

[5] A. Velian, C. C. Cummins, *Science* 2015, *348*, 1001.

[6] a) C. Heindl, A. Schindler, M. Bodensteiner, E. V. Peresypkina, A. V. Virovets, M. Scheer, *Phosphorus Sulfur Silicon Relat. Elem.* **2014**, *190*, 397; b) A. S. Ionkin, W. J. Marshall, B. M. Fish, A. A. Marchione, L. A. Howe, F. Davidson, C. N. McEwen, *Eur. J. Inorg. Chem.* **2008**, 2386; c) G. K. B. Clentsmith, F. G. N. Cloke, M. D. Francis, J. R. Hanks, P. B. Hitchcock, J. F. Nixon, *J. Organomet. Chem.* **2008**, *693*, 2287; d) F. G. N. Cloke, J. R. Hanks, P. B. Hitchcock, J. F. Nixon, *Chem. Commun.* **1999**, 1731; e) R. Bartsch, P. B. Hitchcock, J. F. Nixon, *J. Organomet. Chem.* **1988**, *340*, C37; f) R. Bartsch, P. B. Hitchcock, J. F. Nixon, *Chem. Commun.* **1987**, 1146.

[7] a) R. Bartsch, J. F. Nixon, *J. Organomet. Chem.* **1991**, *415*, C15; b) R. Bartsch, P. B. Hitchcock, J. F. Nixon, *J. Chem. Soc., Chem. Commun.* **1990**, 472.

[8] P. B. Hitchcock, J. A. Johnson, J. F. Nixon, *Angew. Chem.* **1993**, *105*, 86; *Angew. Chem. Int. Ed. Engl.* **1993**, *32*, 83.

[9] a) J. F. Nixon, *Phosphorus, Sulfur Silicon Relat. Elem.* **1994**, *93-94*, 87; b) R. Bartsch, P. B. Hitchcock, J. A. Johnson, R. M. Matos, J. F. Nixon, *Phosphorus, Sulfur Silicon Relat. Elem.* **1993**, *77*, 45.

[10] S. S. Al-Juaid, P. B. Hitchcock, J. A. Johnson, J. F. Nixon, *J. Organomet. Chem.* **1994**, *480*, 45.

[11] a) S. Deng, C. Schwarzmaier, C. Eichhorn, O. Scherer, G. Wolmershauser, M. Zabel, M. Scheer, *Chem. Commun.* **2008**, 4064; b) O. J. Scherer, T. Hilt, G. Wolmershäuser, *Angew. Chem. Int. Ed.* **2000**, *39*, 1425.

[12] a) R. S. P. Turbervill, A. R. Jupp, P. S. B. McCullough, D. Ergocmen, J. M. Goicoechea, *Organometallics* **2013**, *32*, 2234; b) R. S. P. Turbervill, J. M. Goicoechea, *Chem. Commun.* **2012**, *48*, 6100.

[13] M. Scheer, S. Deng, O. J. Scherer, M. Sierka, *Angew. Chem. Int. Ed.* **2005**, *44*, 3755.

[14] a) P. Pyykkö, M. Atsumi, *Chem. Eur. J.* **2009**, *15*, 186; b) P. Pyykkö, M. Atsumi, *Chem. Eur. J.* **2009**, *15*, 12770.

[15] S. Harder, *Coord. Chem. Rev.* **1998**, *176*, 17.

[16] M. Baudler, D. Duester, D. Ouzounis, *Z. Anorg. Allg. Chem.* **1987**, *544*, 87.

[17] G. Becker, G. Gutekunst, H. J. Wessely, *Z. Anorg. Allg. Chem.* **1980**, *462*, 113.

[18] G. M. Sheldrick, *Acta Cryst. sect. C* **2015**, *C71*, 3.

7. First Coordination Polymers Based on 1,3-Diphosphaferrocenes and 1,1',2,3',4-Pentaphosphaferrocenes

C. Heindl, E. V. Peresypkina, S. Reisinger, C. Schwarzmaier, L. Rummel, A. V. Virovets, M. Scheer, *Eur. J. Inorg. Chem.* 2015, accepted.

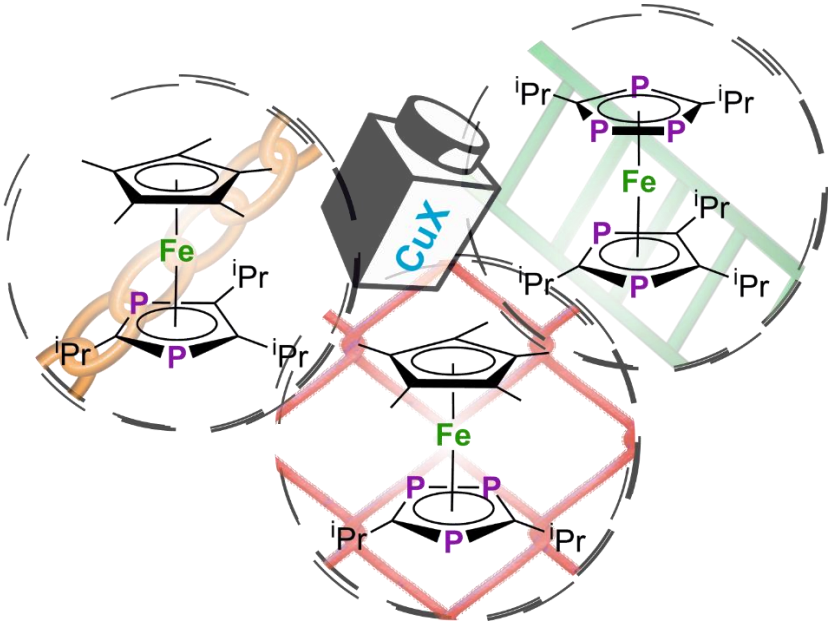

Abstract:

Phosphaferrocenes in combination with coinage metal salts proved to be excellent building blocks in supramolecular chemistry for the build-up of oligomeric and polymeric assemblies. The synthesis of a series of novel phosphaferrocenes containing the 1,3-$P_2C_3{}^iPr_3$ and/or the 1,2,4-$P_3C_2{}^iPr_2$ ligand is described herein. The self-assembly processes of the 1,3-diphospha-, 1,2,4-triphospha- and the 1,1',2,3',4-pentaphosphaferrocenes with Cu(I) halides respectively, lead to the formation of one- or two-dimensional polymers: Using [Cp*Fe(η^5-$P_2C_3iPr_3$)], infinite chains are formed, whereas with [(η^5-$P_3C_2{}^iPr_2$)Fe(η^5-$P_2C_3{}^iPr_3$)] 1D ladder-like structures are obtained. These coordination products represent the first polymers containing such a di- and pentaphosphaferrocene, respectively. On the other hand, the use of [Cp*Fe(η^5-$P_3C_2{}^iPr_2$)] leads to the construction of 2D networks with intact sandwich complexes, which is rather uncommon for this class of complexes.

7.1 Introduction

2016 marks the 50th anniversary of the 2,4,6-triphenyl-phosphabenzene and until now the fundamental interest in main group heterocycles is unabated.[1] Due to the isolobal principle the formal substitution of methine moieties of aromatic rings (e.g. benzene, cyclopentadienide) by substituent-free phosphorus atoms is possible. The resulting derivatives of Cp^- are also capable of acting as η^5-ligands for the synthesis of sandwich complexes, classified as phosphametallocenes. Among them, the phosphaferrocenes containing iron and one up to six P atoms are the most popular representatives. First labeled as 'laboratory curiosity',[2] their widespread potential in catalysis and supramolecular chemistry soon was recognized. Contrary to their all-carbon analogue, the lone pairs of the phosphorus atoms turn them into excellent building blocks towards Lewis acidic metal salts. Our group especially uses Cu(I) halides to introduce the prevailing role of copper in catalysis into this class of compounds. Furthermore, they show a high versatility in the self-assembly processes with phosphaferrocenes as it has been demonstrated by our group.

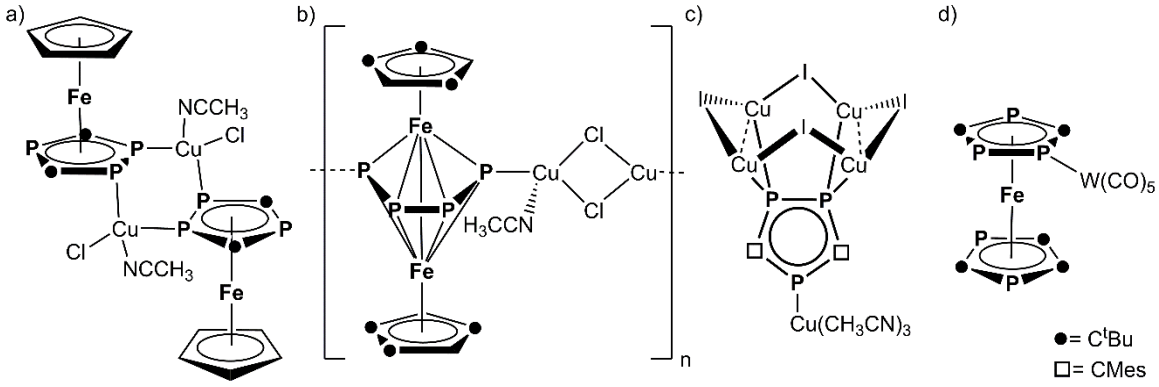

Figure 7.1 Selected examples of coordination products of a)-c) 1,2,4-triphosphaferrocenes with Cu(I) halides; d) a 1,1',2,3',4-pentaphosphaferrocene with a $\{W(CO)_5\}$ fragment.

The 1,2,3,4,5-pentaphosphaferrocene $[Cp^*Fe(\eta^5\text{-}P_5)]$ ($Cp^* = \eta^5\text{-}C_5Me_5$), for instance, is capable of building up either polymeric[3] or, depending on the applied conditions, even spherical coordination compounds.[4] As a matter of course, these sensitive self-assembly processes also depend on the substitution pattern of the phosphaferrocenes. Especially 1,2,4-triphosphaferrocenes $[Cp^RFe(\eta^5\text{-}P_3C_2R'_2)]$ (Cp^R = Cp, Cp*, Cp'''; Cp''' = $\eta^5\text{-}C_5H_2{}^tBu_3$; R' = ^{t}Bu, Ph, Mes) have been synthesized and studied extensively concerning their coordination potential (*Figure 7.1*a-c).[5] Thereby, special attention is paid to the influence of the substitution pattern on the coordination behavior towards Cu(I) halides. For example, the 1,2,4-triphosphaferrocenes $[Cp^RFe(\eta^5\text{-}P_3C_2{}^tBu_2)]$ (Cp^R = Cp, Cp*) form dimeric (*Figure 7.1*a) and oligomeric products with stoichiometric amounts of CuX (X = Cl, Br, I) and in one case a two-dimensional polymer using an excess of CuI.[6] The latter example surprisingly displays the only coordination polymer containing an intact 1,2,4-triphosphaferrocene complex. On the other hand, an astonishing fragmentation and

rearrangement process to a tetraphosphabutadiene ligand can be observed with the Cp''' derivative [Cp'''Fe(η^5-$P_3C_2{}^tBu_2$)] (*Figure 7.1*b).[7]

Furthermore, it turned out that especially the R' group at the phospholyl ligand profoundly affects its reactivity. Thus, the enhancement of the steric bulk at the phospholyl ring results in a completely different reactivity: The combination of the mesityl substituted phosphaferrocene [Cp*Fe(η^5-$P_3C_2Mes_2$)] with CuX (X= Cl, Br, I) particularly entails the fragmentation of the sandwich complex. The split-off $[P_3C_2Mes_2]^-$ ligand serves as building block for the formation of oligomeric and polymeric assemblies (*Figure 7.1*c).[8] Encouraged by these results we are interested in a further modification of the R' group in the phospholyl ligand. Since especially the reduction of the steric bulk has been neglected so far, the smaller ^{i}Pr substituent moved into focus.

The common synthetic route for the preparation of $[P_3C_2R'_2]^-$ starts from the corresponding phosphaalkene[5d] or phosphaalkyne[9] and is accompanied by the formation of $[P_2C_3R'_3]^-$ as a byproduct (*Scheme 7.1*).

Concerning the ^{i}Pr group, Nixon et al. already reacted a mixture of the phosphaalkynes ^{i}PrC≡P and ^{t}BuC≡P with sodium, resulting in the formation of nine differently substituted 1,3-di- and 1,2,4-triphospholyl ligands.[9]

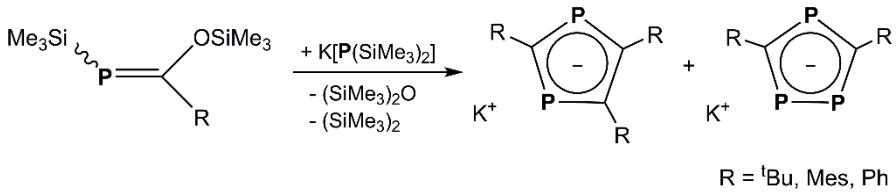

Scheme 7.1 An usual synthesis of 1,3-di- and 1,2,4-triphospholyl moieties.

Though several derivatives of 1,3-diphospholyl ligands were synthesized by this method, no comprehensive coordination studies involving these heterocycles are known in literature. Only a few phosphaferrocenes are structurally characterized: two 1,3-diphosphaferrocenes [Cp^RFe(η^5-$P_2C_3R'_3$)],[5f,10], four 1,1',3,3'-tetraphosphaferrocenes [(η^5-$P_2C_3R'_3$)$_2$Fe][11] and one 1,1',2,3',4-pentaphosphaferrocene [(η^5-$P_3C_2{}^tBu_2$)Fe(η^5-$P_2C_3{}^tBu_3$)].[12] In addition, the latter sandwich complex has only been used for coordination of a {$W(CO)_5$} fragment (*Figure* 7.1d)[13] and a ligand transfer reaction.[14] Furthermore, the group of Nixon describe mass spectrometric evidence of the ^{i}Pr derivatives of these three phosphaferrocene derivatives among a mixture of more than 20 different sandwich complexes.[9]

Considering the stage of reports, it is further obvious that no supramolecular assemblies based on phosphaferrocenes containing a 1,3-diphospholyl ligand are known.

Herein we report on the straightforward synthesis and characterization of a series of partly hitherto unknown phosphaferrocenes containing the ^{i}Pr substituted phospholyl ligands 1,3-[$P_2C_3{}^{i}Pr_3$] and 1,2,4-[$P_3C_2{}^{i}Pr_2$].

Among these sandwich complexes, the 1,3-di-, 1,2,4-tri- and 1,1',2,3',4-pentaphosphaferrocene were also used as building blocks in combination with Cu(I) halides, respectively. Thereby, reactions with the 1,2,4-triphosphaferrocene allow the isolation of novel 2D polymeric networks. On the other hand, the use of [(η^5-$P_2C_3R'_3$)$_2$Fe] and [(η^5-$P_3C_2{}^{t}Bu_2$)Fe(η^5-$P_2C_3{}^{t}Bu_3$)], respectively, leads to the formation of 1D chains, which display the first coordination polymers containing this type of a di- and pentaphosphaferrocene, respectively.

7.2 Results and Discussion

Synthesis and Characterization of the Phosphaferrocenes

The preparation of the phospholyl ligands K[$P_2C_3{}^{i}Pr_3$] (**1a**) and K[$P_3C_2{}^{i}Pr_2$] (**1b**) was carried out analogously to the ^{t}Bu derivative[15] starting from the corresponding phosphaalkene $Me_3SiO(^{i}Pr)C{=}P(SiMe_3)$[16] and $KP(SiMe_3)_2$ (*cf. Scheme 7.1* for R = ^{i}Pr).[17] In contrast, Nixon *et al.* reacted the phosphaalkyne with elemental sodium to obtain the sodium derivatives of **1a** and **1b** among other products.[9] Interestingly, the product distribution of **1a** and **1b** turned out to be temperature-sensitive. According to $^{31}P\{^{1}H\}$ NMR spectroscopy after 1d of heating at 50 °C the ratio **1a**:**1b** is about 1:1. After isolation of this first crop of product the remaining mother liquor was heated a further day in favor of the formation of **1b** (**1a**:**1b** = 0.75:1). When the reaction mixture is finally refluxed at 100 °C, the last crop of the isolated off-white powder solely contains the triphospholyl salt **1b**. Therefore a selective synthesis at least of **1b** is feasible, even though more time-consuming. Since both salts are needed for the subsequent reaction, the initial solution is heated to 75 °C for three days instead to give **1a** and **1b** in a rough 1:1 ratio.

The $^{31}P\{^{1}H\}$ NMR spectrum of the isolated product in thf-d_8 shows a singlet at δ = 159.58 ppm, which can be assigned to **1a** (for a comparison to Na[$P_2C_3{}^{i}Pr_3$]: δ = 155.0 ppm).[9]

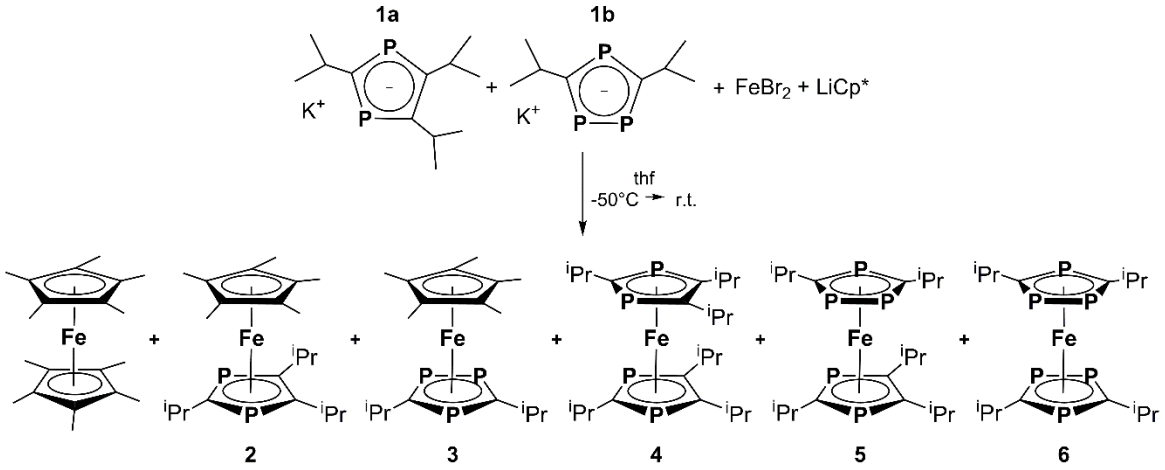

Scheme 7.2 Synthesis of the phosphaferrocenes **2-6**.

Surprisingly, for **1b** a doublet of doublet at δ = 247.6 ppm ($^2J_{PP}$ = 51.6 and 45.1 Hz) and *pseudo*-doublet (δ = 244.7 ppm) with a merged coupling constant of $^2J_{PP}$ = 49.0 Hz and a distinctive roof effect of the signals is obtained for the isolated and the adjacent phosphorus atoms, respectively. For a comparison, previously reported derivatives $[1,2,4\text{-}P_3C_2R_2]^-$ all show a (slightly low-field shifted) doublet and triplet with a similar coupling constant (R = Mes:[5a] δ = 266.4, 261.7 ppm, $^2J_{PP}$ = 38 Hz; R = Ph,[15a] δ = 274.4, 253.9 ppm, $^2J_{PP}$ = 43 Hz; R = ^{t}Bu:[15b] δ = 256, 248 ppm, $^2J_{PP}$ = 49 Hz). For $Na[P_3C_2{}^iPr_2]$, a slight high-field shift compared to **1b** is observed (δ = 241.6 and 246.6 ppm, $^2J_{PP}$ = 48 Hz).[9]

For the subsequent synthesis of the novel 1,3-diphosphaferrocene [Cp*Fe(η^5-$P_2C_3iPr_3$)] (**2**) and the 1,2,4-triphosphaferrocene [Cp*Fe(η^5-$P_3C_2{}^iPr_2$)] (**3**) we also referred to the established strategy of the ^{t}Bu derivative.[5k] For this, solutions of $FeBr_2$(dme) and LiCp* in thf were added to a mixture of **1a** and **1b** in thf at -50°C resulting in an immediate color change from orange to deep reddish brown (*Scheme 7.2*). $^{31}P\{^1H\}$ NMR spectroscopic investigations of the crude reaction mixture reveal signals corresponding to **2** and **3**, but also signals of small amounts of by-products. These include $[Cp^*{}_2Fe]$, the 1,1',3,3'-tetraphosphaferrocene [(η^5-$P_2C_3{}^iPr_3$)$_2$Fe] (**4**), the 1,1',2,3',4-pentaphosphaferrocene [(η^5-$P_3C_2{}^iPr_2$)Fe(η^5-$P_2C_3{}^iPr_3$)] (**5**), as well as the 1,1',2,2',4,4'-hexaphosphaferrocene [(η^5-$P_3C_2{}^iPr_2$)$_2$Fe] (**6**). The sandwich complexes **5** and **6** are already reported on, though only characterized by mass spectrometry in a mixture of more than 20 phosphaferrocenes.[9]

A separation of the phosphaferrocenes is enabled by an elaborate column chromatographic work-up. Using hexane, a yellow band of $[Cp^*{}_2Fe]$, followed by a green fraction of a mixture of **4**, **5** and **6** is eluted. With a slightly more polar eluent (hexane/toluene = 10/1) a red band of a mixture of **2** and **3** is obtained. For the isolation of the pure phosphaferrocenes a further column

chromatographic work-up of the green and red fraction, respectively, is necessary (see experimental part). By this way, analytically pure **2**, **3** and **5** are obtained.

All phosphaferrocenes were identified by their characteristical chemical shifts and multiplicity in the ^{1}H and $^{31}P\{^{1}H\}$ NMR spectra. Compared to **1a** and **1b**, the P atoms show a significant high field shift of more than 100 ppm in the corresponding $^{31}P\{^{1}H\}$ NMR spectra, which is an usual trend in phosphaferrocene chemistry.[5a,f,12,18] In contrast to **1b** and in analogy to known 1,2,4-triphospholyl derivatives, the P_3C_2 rings all show a doublet and a triplet for the isolated and adjacent phosphorus atoms upon coordination to iron, respectively ($^{2}J_{PP}$ = 43.8 Hz in **3**, 42.0 Hz in **5** and 38.0 Hz in **6**). On the other hand, a singlet is obtained for the P_2C_3 ligands. In addition, multiplets, ranging from δ = 2.2 – 3.1 ppm can be assigned to the methine groups in the ^{1}H NMR spectra, whereas all methyl groups show doublets ($^{3}J_{HH}$ = 6.1 – 6.7 Hz) with chemical shifts between 1.0 – 1.7 ppm (for a detailed assignment see experimental part). In ferrocenes containing **1a**, two sets of signals are observed for the CH units (integral ratio: 1:2) and three for the CH_3 groups (1:1:1). For the **1b** ligands in **3**, **5** and **6**, respectively, one multiplet (CH) and two doublets (CH_3) per ring are obtained.

Furthermore, in the FD mass spectra the molecular ion peaks can be observed for all complexes **2**-**6**, though with very low intensity for **4**.

In addition, the structures of **2**, **4** and **5** were confirmed by X-ray structural analyses (see below).

Table 7.1 $^{31}P\{^{1}H\}$ chemical shifts δ [ppm] of **2** – **5** in C_6D_6 at r.t. and of **6** in CD_2Cl_2 at 193 K.

	δ [ppm] (P_2C_3)	δ [ppm] (P_3C_2)	$^{2}J_{PP}$ [Hz]
1a	161.4 (s)		
1b		247.6 (dd), 244.7 (*pseudo*-d)	51.6, 45.1, 49.0
2	-2.8 (s)	-	-
3	-	29.7 (t), 49.6 (d)	43.8
4	6.7 (s)	-	-
5	15.0 (s)	46.9 (t), 53.7 (d)	42.0
6	-	46.2 (d), 69.3 (t)	38.0

Molecular structures of 2, 4 and 5

Crystals of **2**, **4** and **5** suitable for X-ray structural analysis can be obtained by layering a toluene solution of the respective phosphaferrocene with CH_3CN and storing at -28 °C. Compound **2** crystallizes in the monoclinic space group $P2_1/c$, compound **4** in the triclinic space group $P\bar{1}$ and **5** crystallizes in three monoclinic polymorphic modifications ($P2_1$, $P2_1/n$, for details see crystallographic section). All molecular structures can be described as sandwich complexes with η^5-coordinated ligands in an eclipsed conformation. The tetraphosphaferrocene **4** forms the most 'perfect' sandwich complex with an interplanar angle of 0.27(5)° and the angle $(P_2C_3{}^{i}Pr_3)_{centroid}$-Fe-

$(P_2C_3{}^iPr_3)_{centroid}$ being 179.84(2)°. These distortions are slightly more distinctive in **2** (3.33(7)° and 177.09(3)°) and **5** (3.57(7)° and 177.25(3)°), respectively.

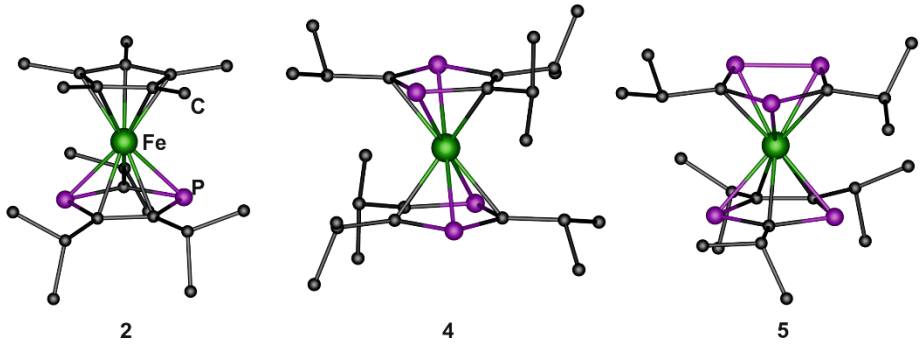

Figure 7.2 Molecular structures of the phosphaferrocenes **2**, **4** and **5**. H atoms are omitted for clarity.

Within the coordinated di- and triphospholyl rings, all bond lengths range quite accurately between a single and a double bond confirming the aromaticity of this ligand (*Table 7.2*; covalent radii: C-C: 1.50 Å; C-P: 1.86 Å; P-P: 2.22 Å; C=C: 1.34 Å; C=P: 1.69 Å; P=P: 2.04 Å).[19]

Table 7.2 Selected bond lengths [Å] within the phospholyl rings in **2**, **4**, **5**, **5'** and **5''**. Ranges of bond lengths are given whenever more than one bond is present in the asymmetric unit.

	ligand	P-P	P-C	C-C
2	P_2C_3	-	1.761(2) – 1.784(2)	1.424(2) – 1.426(3)
4	P_2C_3	-	1.770(2) – 1.789(2)	1.425(3) – 1.430(3)
5	P_2C_3	-	1.759(5) – 1.790(6)	1.438(7) – 1.440(7)
	P_3C_2	2.121(2) – 2.134(2)	1.746(5) – 1.777(5)	-
5'	P_2C_3	-	1.763(1) – 1.786(1)	1.419(2)
	P_3C_2	2.126(1)	1.759(2) – 1.769(2)	-
5''	P_2C_3	-	1.756(3) – 1.794(3)	1.441(4) – 1.445(3)
	P_3C_2	2.119(1) – 2.121(1)	1.761(3) – 1.772(3)	-

Diphosphaferrocene 2 as building block

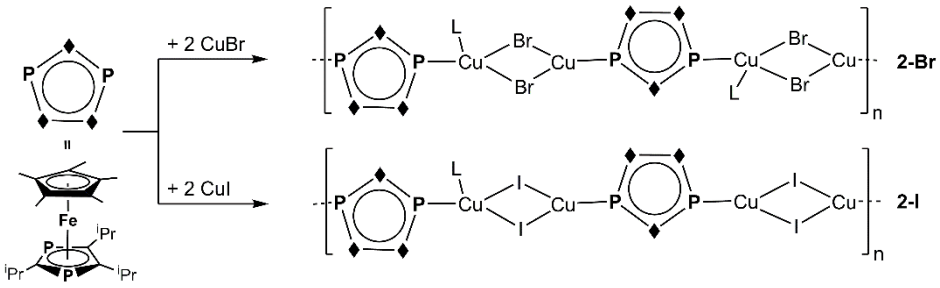

Scheme 7.3 1,3-Diphosphaferrocene-derived coordination polymers **2-Br** and **2-I**.

Although 1,3-diphosphaferrocenes are known since 1990,[10] it has not been applied for the formation of supramolecular assemblies yet. However, the separated and therefore opposite positions of the phosphorus atoms in the ring are predestinated for the build-up of one-

dimensional coordination polymers. Hence, diffusion experiments of **2** with CuX (X = Br, I) were carried out leading to the crystallization of $[\{Cp^*Fe(\mu_3,\eta^{5:1:1}\text{-}P_2C_3{}^iPr_3)\}Cu_2(\mu\text{-}Br)_2(CH_3CN)]_n\cdot 0.75(CH_3CN)$ (**2-Br**) and $[\{Cp^*Fe(\mu_3,\eta^{5:1:1}\text{-}P_2C_3{}^iPr_3)\}Cu_2(\mu\text{-}I)_2(CH_3CN)_{0.5}]_n\cdot 0.5(CH_3CN)$ (**2-I**), respectively (*Scheme 7.3*).

Compound **2-Br** crystallizes as orange platelets in the monoclinic space group *C*2/c, whereas **2-I** crystallizes in the orthorhombic space group $P2_12_12_1$. The X-ray structural analyses reveal that in both products, **2-Br** and **2-I**, one-dimensional chains are formed by moieties of **2** linked *via* $\{Cu_2(\mu\text{-}X)_2\}$ four-membered rings (*Figure 7.3*).

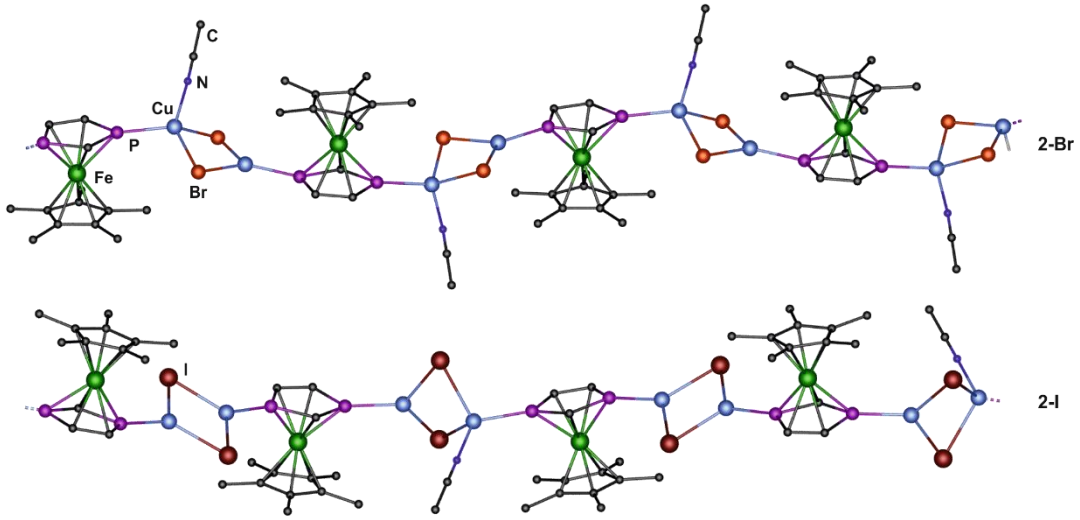

Figure 7.3 Section of the polymeric structures of **2-Br** and **2-I**. ^{i}Pr ligands and H atoms are omitted for clarity.

The bending of the strands is caused by the position of the phosphorus atoms within the P_2C_3 five-membered ring and the tetrahedral coordination environment of some of the copper ions. The latter makes the difference between the iodine and the bromine derivative: At first, they differ in their amount of acetonitrile ligands, whose coordination leads to an expansion of the environment of copper from trigonal planar to tetrahedral. In **2-Br**, every second Cu atom is affected and thus, all $\{Cu_2(\mu\text{-}Br)_2(CH_3CN)\}$ rings are similar. On the contrary, the iodine derivative **2-I** contains less acetonitrile ligands and only every fourth Cu atom is coordinated. Consequently, the $\{Cu_2(\mu\text{-}I)_2\}$ and $\{Cu_2(\mu\text{-}I)_2(CH_3CN)\}$ units are perpendicular to each other. This results in a different undulation of the chains. Furthermore, the phosphaferrocene units in **2-Br** are orientated upwards and downwards in alternation. In contrast, this change in direction is obtained only after every second moiety of **2** in **2-I** (*Figure 7.3*). This coordination motif of $\{Cu_2(\mu\text{-}X)_2\}$ rings is known and has already been observed for several assemblies,[20] also with P_n ligand complexes.[3,21]

Once crystallized, both compounds are insoluble in common solvents, therefore a characterization in solution could not be carried out. Merely, the still slightly yellow-orange mother liquor can be used for NMR spectroscopic and mass spectrometric investigations. Thereby, in the

anionic ESI spectra only peaks assigned to copper halide fragments up to $[Cu_5Br_6]^-$ for **2-Br** and $[Cu_4I_5]^-$ for **2-I** are obtained. On the contrary, the cationic ESI spectra show peaks for ferrocene-containing fragments with the largest at *m/z* = 1043.3 ($[\{Cp^*Fe(P_2C_3{}^iPr_3)\}_2Cu_2Br]^+$) for **2-Br** and at *m/z* = 712.0 ($[\{Cp^*Fe(P_2C_3{}^iPr_3)\}Cu_2I(CH_3CN)]^+$) for **2-I**. In the $^{31}P\{^1H\}$ NMR spectra of the mother liquors of **2-Br** and **2-I** small singlets for the P_2C_3 ligand at δ = 14.3 and 15.9 ppm are observed, respectively. Since no significant broadening of the signal due to the coordination of the P atoms to Cu (nuclear spin *I* = 3/2) is recognizable, it can most likely be attributed to the free complex **2**.

Triphosphaferrocene 3 as building block

To study the influence of the smaller ^{i}Pr substituents in comparison to the Mes and ^{t}Bu derivatives, also the 1,2,4-triphosphaferrocene **3** was used for consecutive reactions. Layering experiments of **3** with CuX (X = Cl, Br) lead to the formation of the 2D polymeric compounds $[\{Cp^*Fe(\mu_4,\eta^{5:1:1:1}\text{-}P_3C_2{}^iPr_2)\}Cu_2(\mu\text{-}Cl)_2]_n$ (**3-Cl**) and $[\{Cp^*Fe(\mu_4,\eta^{5:1:1:1}\text{-}P_3C_2{}^iPr_2)\}Cu_2(\mu\text{-}Br)_2]_n{\cdot}0.15C_7H_8$ (**3-Br**), respectively (*Scheme 7.4*).

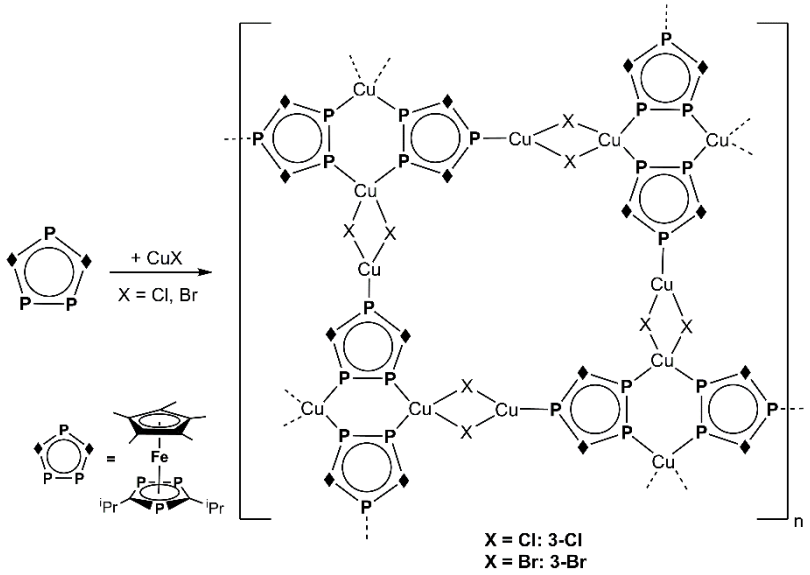

Scheme 7.4 1,2,4-Triphosphaferrocene-derived coordination polymers **3-Cl** and **3-Br**.

Both crystallize as isomorphous compounds in the monoclinic space group $P2_1/c$. In addition, compound **3-Cl** turned out to be polymorphous crystallizing also in the orthorhombic space group *Pbca* (**3-Cl'**, for details see crystallographic part). The X-ray structural analyses reveal two-dimensional networks with a mesh-like construction (*Figure 7.4*). Similarly to **2-X** (X = Br, I), the phosphaferrocenes are linked by four-membered $\{Cu_2(\mu\text{-}X)_2\}$ rings. However, in **3-Cl** and **3-Br** the presence and coordination of three P atoms lead to the extension of the polymer in two dimensions (*Figure 7.4*).

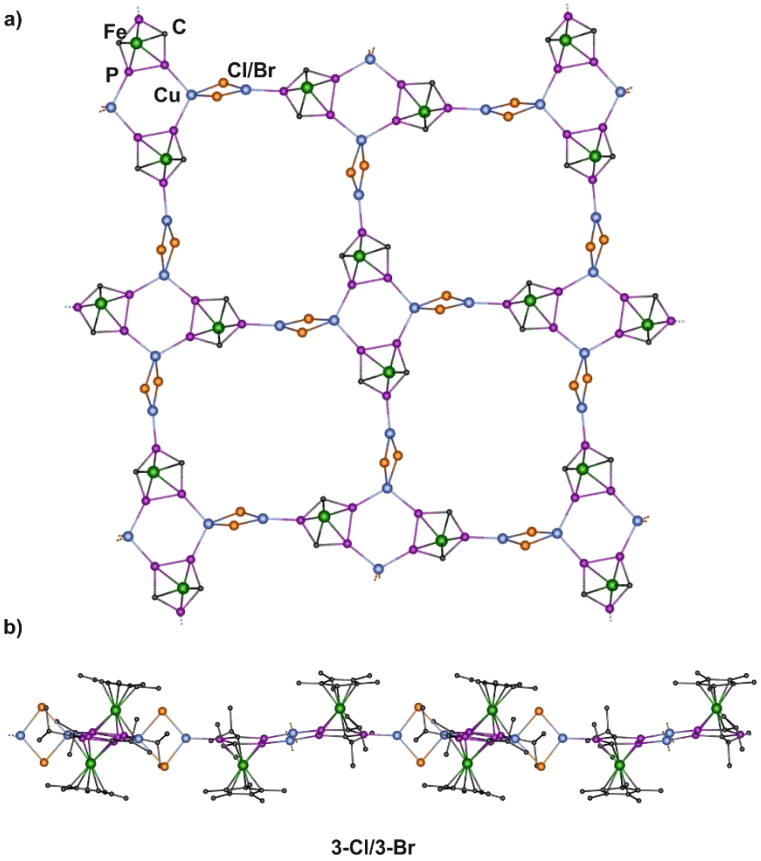

Figure 7.4 Section of the polymeric structures of **3-Cl** and **3-Br**: a) top view, Cp* and ^{i}Pr ligands are omitted for clarity; b) side view, H atoms are omitted for clarity.

Noteworthy, all copper ions attached to the isolated P atom of the P_3C_2 ring show a trigonal planar environment, whereas any other Cu is tetrahedrally coordinated. Again, contiguous phosphaferrocene units in **3-Cl** and **3-Br** are orientated upwards and downwards (*Figure 7.4*b). The meshes therefore form layers separated by the Cp* ligands and, in the case of **3-Br**, provide enough space for a solvent molecule embedded between these layers.

Remarkably, **3-Cl** and **3-Br** display the first polymeric compounds containing triphosphaferrocenes and CuX (X = Cl, Br) despite many trials. Previous findings all demonstrate that either fragmentation reactions of the phosphaferrocene occur[7,8] or dimeric[6a] and oligomeric[6b] compounds are formed. Only the use of CuI yields a coordination polymer in combination with [Cp*Fe(η^5-$P_3C_2{}^{t}Bu_2$)].[6b] A meaningful comparison can be drawn to pentaphosphaferrocene containing polymers bearing the *cyclo*-P_5 unit in a 1,2,4-coordination mode. This type is known for all halides in the 2D networks [{Cp*Fe(μ_4,$\eta^{5:1:1:1}$-P_5)}(CuX)]$_n$ (X = Cl, Br, I). In these, the structural motif differs and the P atoms are linked *via* simple {CuX} units in contrast to {$Cu_2(\mu$-$X)_2$} (X = Cl, Br) rings in **3-Cl** and **3-Br**, respectively.

Since already the one-dimensional polymers **2-Br** and **2-I** are insoluble, it is not surprising that also the 2D networks **3-Cl** and **3-Br** cannot be dissolved in any common solvent. Nonetheless, the

mother liquors are still slightly colored, hence they were analyzed by ESI mass spectrometry and $^{31}P\{^{1}H\}$ NMR spectroscopy. However, for the Cl-derivative no signal in the respective NMR spectrum can be obtained, whereas in the $^{31}P\{^{1}H\}$ NMR spectrum of the mother liquor of **3-Br** small signals of the P_3C_2 ligand at δ = 11.4 ppm (d, $^{2}J_{PP}$ = 46 Hz, 2P) and δ = 22.7 ppm (t, $^{2}J_{PP}$ = 46 Hz, 1P) are observed, again most probably belonging to the free complex **3**. Similarly to **2-Br** and **2-I**, in the anionic ESI spectra $[Cu_{n-1}X_n]^-$ units are detected with n ≤ 4 for X = Cl and n ≤ 6 for X = Br. The largest peaks in the cationic ESI spectra at *m/z* = 1541.4 and 1573.5 are assigned to $[\{Cp^*Fe(P_3C_2{}^iPr_2)\}_3Cu_4Cl_3]^+$ and $[\{Cp^*Fe(P_3C_2{}^iPr_2)\}_2Cu_6Br_5]^+$, respectively (for smaller fragments see experimental part).

Pentaphosphaferrocene 5 as building block

Since no supramolecular assemblies containing pentaphosphaferrocenes of the type $[(\eta^5\text{-}P_3C_2R_2)Fe(\eta^5\text{-}P_2C_3R_3)]$ are mentioned in literature, also the reactivity of **5** towards Cu(I) halides has been investigated. Diffusion experiments of solutions of **5** in CH_2Cl_2 or toluene and CuX (X = Br, I) in CH_3CN lead to the formation of green prisms of $[\{(\mu_3,\eta^{5:1:1}\text{-}P_3C_2{}^iPr_2)Fe(\mu,\eta^{5:1}\text{-}P_2C_3{}^iPr_3)\}Cu_3(\mu\text{-}Br)(\mu_3\text{-}Br)(\mu_4\text{-}Br)]_n{\cdot}0.5C_7H_8$ (**5-Br**) and of strongly intergrown plates of $[\{(\mu,\eta^{5:1}\text{-}P_3C_2{}^iPr_2)Fe(\mu,\eta^{5:1}\text{-}P_2C_3{}^iPr_3)\}Cu_2(\mu_3\text{-}I)_2]_n$ (**5-I**), respectively (Scheme 7.5).

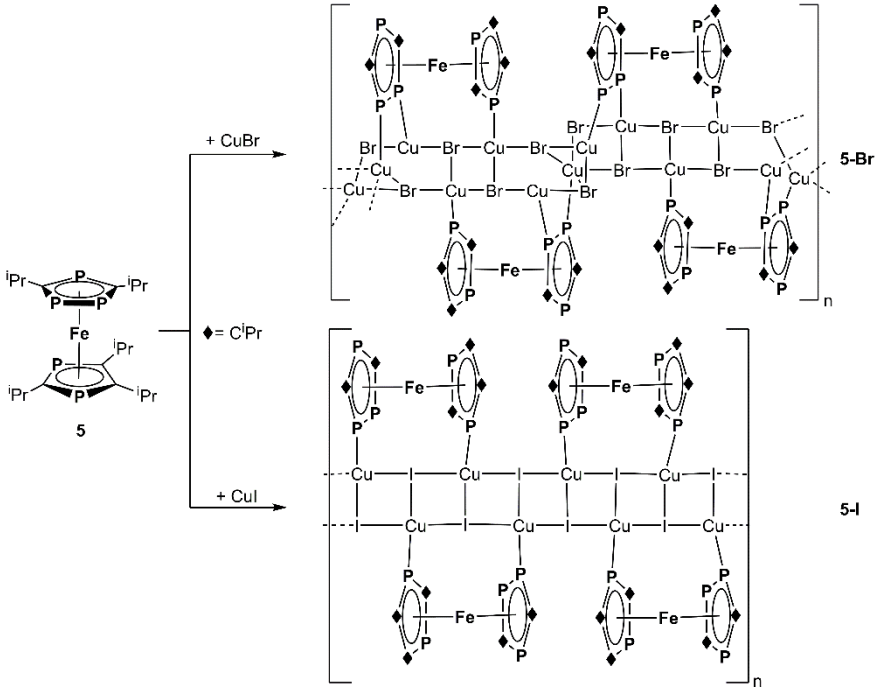

Scheme 7.5 1,1',2,3',4-Pentaphosphaferrocene-derived coordination polymers **5-Br** and **5-I**.

Due to the simpler structure **5-I** will be described first. It crystallizes in the monoclinic space group $P2_1/n$ and displays a 1D linear polymer formed by a {CuI} double strand with the sandwich complex **5** acting as a 1,1'-chelating ligand (*Figure 7.5* right). The regular structure of this ladder is

formed by iodine atoms, all comprising a μ_3 coordination mode, and tetrahedrally coordinated Cu atoms.

The 1D polymer **5-Br** crystallizes as solvate in the triclinic space group *P*$\bar{1}$ and shows a similar ladder-like scaffold. The moieties of **5** also act as chelating ligands, though the coordination *via* three P atoms (two from the tri- and one from the diphospholyl ligand) leads to a 1,2,1'-connectivity. As a consequence, the {CuBr} double strand is bent at the positions of the triphospholyl ligand and a stair-like arrangement results with the bromide ligands in a μ-, μ_3- or even μ_4-fashion.

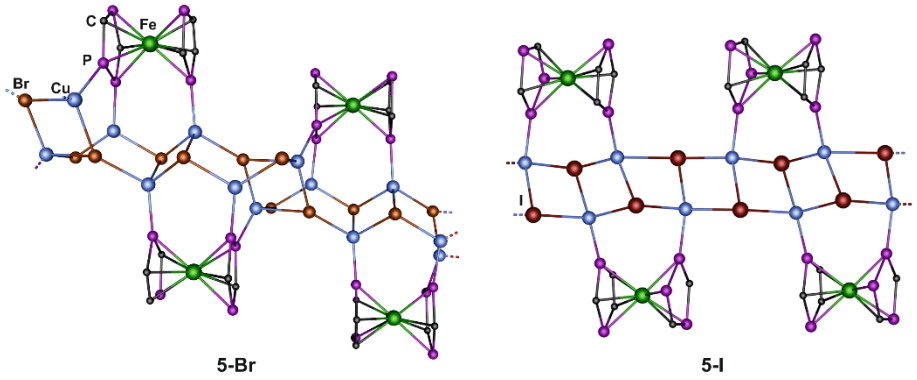

Figure 7.5 Section of the polymeric structures of **5-Br** (left) and **5-I** (right). ^{i}Pr ligands and solvent molecules are omitted for clarity.

Similar structural motifs are already known for the hexaphosphaferrocene containing polymers $[\{Fe(\mu,\eta^{5:1}\text{-}P_3C_2{}^{t}Bu_2)_2\}\{Cu(\mu_3\text{-}X)\}_2]_x$ (X = Cl, Br, I) and $[\{Fe(\mu,\eta^{5:1}\text{-}P_3C_2{}^{t}Bu_2)\ (\mu_3,\eta^{5:1:1}\text{-}P_3C_2{}^{t}Bu_2)\}Cu_3(\mu\text{-}I)(\mu_3\text{-}I)_2(CH_3CN)]_x$.[22] In these products, the sterically demanding ^{t}Bu groups lead to a sinusoidal distortion of the strands, which cannot be observed in **5-Br** and **5-I**.

The characterization of the polymers **5-Br** and **5-I** in solution is again limited to the mother liquor. This time, only in the $^{31}P\{^{1}H\}$ NMR spectrum corresponding to **5-I** signals are obtained, which can be assigned to the free complex **5**. Yet, they are slightly highfield-shifted (δ = 9.5 ppm (s, 2 P, P_2C_3), 30.8 ppm (d, $^{2}J_{P\text{-}P}$ = 43.2 Hz, 2 P, P_3C_2), 46.9 (t, $^{2}J_{P\text{-}P}$ = 43.6 Hz, 1 P, P_3C_2)). In the anionic as well as cationic ESI mass spectra of this solution a variety of different fragments is detected (for details see experimental part). Among them, the largest peak appears at *m/z* 1078.3 for $[Cu_5I_6]^-$ and 1796.9 for $[\{(P_2C_3{}^{i}Pr_2)Fe(P_3C_2{}^{i}Pr_2)\}_2Cu_5I_4]^+$, respectively.

Conclusions

In conclusion, the di- and triphospholyl salts **1a/b** bearing rather small ^{i}Pr groups were synthesized starting from the phosphaalkene. By the subsequent reaction with Fe(II) bromide and LiCp* a series of partially novel phosphaferrocenes **2**-**6** could be synthesized containing two, three, four, five or six phosphorus atoms.

Since no supramolecular assemblies are known neither for a 1,3-diphospha- nor for a 1,1',2,3',4-pentaphosphaferrocene, their coordination behavior towards Cu(I) halides has been studied. As a result, both building blocks form one-dimensional polymers, yet with different structures. Whereas with **2** infinite chains (**2-Br**, **2-I**) are obtained, the self-assembly of **5** with CuX (X = Br, I) leads to ladder-like structural motifs (**5-Br**, **5-I**) with **5** acting as a chelating ligand. The obtained products therefore represent the first polymers containing 1,3-di- and 1,1',2,3',4-pentaphosphaferrocenes, respectively.

Furthermore, previous results have shown that 1,2,4-triphosphaferrocenes tend to form di- and oligomeric products with intact sandwich complexes or, on the other hand, polymeric products, though with fragmented and/or rearranged moieties of the building block. On the contrary, using the ^{i}Pr-substituted derivative **3**, the isolation of the 2D networks **3-Cl** and **3-Br** is possible. Both compounds contain intact units of **3** and therefore display the second and third representative of a triphosphaferrocene-based polymer, respectively. Furthermore, they show an unprecedented mesh-like structure.

7.3 Experimental Part

General Remarks:

All reactions were performed under an inert atmosphere of dry nitrogen or argon with standard vacuum, Schlenk and glove-box techniques. Solvents were purified, dried and degassed prior to use by standard procedures. $Me_3SiO(^{i}Pr)C{=}P(SiMe_3)$,[16] $K[P(SiMe_3)_2]$[17] and $[FeBr_2(dme)]$[23] were synthesized following the reported procedures. Commercially available chemicals (CuCl, CuBr, CuI) were used without further purification. Solution NMR spectra were recorded on a Bruker Avance 300 or 400 spectrometer. The corresponding ESI-MS spectra were recorded on a ThermoQuest Finnigan MAT TSQ 7000 mass spectrometer, whereas EI-MS and FD-MS spectra were measured on a Finnigan MAT 95 mass spectrometer. Elemental analyses were performed on a Vario EL III apparatus.

Synthesis of $K[P_2C_3{}^{i}Pr_3]$ (1a) and $K[P_3C_2{}^{i}Pr_2]$ (1b)

A suspension of $K[P(SiMe_3)_2]$ (2.40 g, 0.11 mol) in a mixture of toluene (20 mL) and Et_2O (10 mL) is added to a solution of the phosphaalkene $Me_3SiO(^{i}Pr)C{=}P(SiMe_3)$ (5.5 g, 0.022 mol) in toluene (10 mL). An immediate color change from yellow to orange-red is observed. The reaction mixture is heated to 75 °C for three days. After cooling to r.t. the off-white powder is filtered, washed with toluene (2 × 10 mL) and dried *in vacuo* to give **1a** and **1b** in a 1:1 mixture.

Yield: 1.35 g (5.32 mmol, 48%, molar ratio **1a**:**1b** = 1:1)

Analytical data of **1a**:

^{1}H NMR (thf-d_8): δ [ppm] = 1.33 (d, $^{3}J_{HH}$ = 6.8 Hz, 12 H, CH_3-adjacent), 1.37 (d, $^{3}J_{HH}$ = 6.8 Hz, 6 H, CH_3-isolated), 3.28 (m, 2 H, CH-adjacent), 3.44 (m, 1 H, CH-isolated).

^{31}P{^{1}H} NMR (thf-d_8): δ [ppm] = 161.44 (s, 2 P).

Analytical data of **1b**:

^{1}H NMR (thf-d_8): δ [ppm] = 1.43 (d, $^{3}J_{HH}$ = 6.8 Hz, 12 H, CH_3), 3.79 (m, 2 H, CH).

^{31}P{^{1}H} NMR (thf-d_8): δ [ppm] = 247.60 (dd, $^{2}J_{PP}$ = 51.6 Hz, 45.1 Hz, 1 P, P-isolated), 244.72 (*pseudo*-d, $^{2}J_{PP}$ = 49.0 Hz, 2 P, P-adjacent).

Synthesis of the phosphaferrocenes [Cp*Fe(η^5-$P_2C_3{}^{i}Pr_3$)] (2), [Cp*Fe(η^5-$P_3C_2{}^{i}Pr_2$)] (3), [(η^5-$P_2C_3{}^{i}Pr_3$)$_2$Fe] (4), [(η^5-$P_3C_2{}^{i}Pr_2$)Fe(η^5-$P_2C_3{}^{i}Pr_3$)] (5) and [(η^5-$P_3C_2{}^{i}Pr_2$)$_2$Fe] (6)

[$FeBr_2$(dme)] (2.0 g, 6.5 mmol) and a mixture of **1a** and **1b** (ratio: 1/1, 1.7 g, 6.5 mmol) is dissolved in thf (200 mL) at -40 °C resulting in an immediate color change from yellow-orange to dark red. A suspension of LiCp* (930 mg, 6.5 mmol) in thf (50 mL) is added subsequently. The reaction mixture is warmed up to r.t. and the solvent is removed under reduced pressure. Afterwards the residue is dissolved in toluene, filtered through celite and the solvent is again removed. The solid is adsorbed on silica and loaded onto a column filled with silica (50 cm x 3 cm). Using hexane as eluent, a yellow band of [Cp*$_2$Fe] can be eluted, followed by a green fraction containing the hexaphosphaferrocene **6**, the pentaphosphaferrocene (**5**) and the tetraphosphaferrocene (**4**) (70 mg, ~3%, calculated by means of the average molar weight). Switching to a hexane/toluene mixture (10/1) a red band of the triphosphaferrocene **3** and the diphosphaferrocene **2** (440 mg, ~17%, calculated by means of the average molar weight) can be eluted. To separate **2** and **3** or **4**, **5**, and **6**, respectively, the solvent of the respective fraction is removed and a further chromatographic work-up is needed (50 cm x 3 cm). Unfortunately, the products cannot be eluted as separate bands, therefore several fractions have to be collected. The first fraction gives pure **2**, the last pure **3** and the ones in-between mixtures with different molar ratios. Furthermore, an elemental analysis could not be carried out, since the phosphaferrocenes are oily solids at r.t. and the crystals, obtained at lower temperature, start melting when warmed to r.t. Therefore, standard solutions were prepared for consecutive reactions.

Analytical data of **2**/**3**:

Yield: 440 mg (17%): integral ratios from ^{31}P{^{1}H} NMR (C_6D_6): 50% **2**, 50% **3**.

Analytical data of **2**:

^{1}H NMR (C_6D_6): δ [ppm] = 1.16 (d, $^3J_{HH}$ = 6.1 Hz, 6H, ^{i}Pr-CH_3), 1.24 (d, $^3J_{HH}$ = 6.2 Hz, 6H, ^{i}Pr-CH_3), 1.60 (d, $^3J_{HH}$ = 6.2 Hz, 6H, ^{i}Pr-CH_3), 1.70 (s, 15H, Cp*-CH_3), 2.26 (m, br, 1H, iPr-CH), 2.38 (m, br, 2H, iPr-CH).

^{31}P{^{1}H} NMR (C_6D_6): δ [ppm] = -2.84 (s, 2P).

FD-MS (toluene): 418.2 (M^+).

Analytical data of **3**:

^{1}H NMR (C_6D_6): δ [ppm] = 1.32 (d, $^3J_{HH}$ = 6.6 Hz, 6H, ^{i}Pr-CH_3), 1.43 (d, $^3J_{HH}$ = 6.5 Hz, 6H, ^{i}Pr-CH_3), 1.62 (s, 15H, Cp*-CH_3), 2.72 (m, br, 2H, iPr-CH).

^{31}P{^{1}H} NMR (C_6D_6): δ [ppm] = 29.69 (t, $^2J_{PP}$ = 43.8 Hz, 1P, $P_{isolated}$), 49.63 (d, $^2J_{PP}$ = 43.8 Hz, 2P, $P_{adjacent}$).

FD-MS (toluene): 394.3 (M^+).

Analytical data of **4**/**5**/**6**:

Yield: 70 mg: integral ratios from ^{31}P{^{1}H} NMR (C_6D_6):, 57% **5**, 39% **6** and 4% **4**.

Analytical data of **4**:

^{31}P{^{1}H} NMR (C_6D_6): δ [ppm] = 6.7 (s, br, 4P).

FD-MS (hexane): 510.2 (M^+).

Analytical data of of **5**:

^{1}H NMR (C_6D_6): δ [ppm] = 1.04 (d, $^3J_{HH}$ = 6.7 Hz, 6H, ^{i}Pr-CH_3), 1.23 (d, $^3J_{HH}$ = 6.7 Hz, 6H, ^{i}Pr-CH_3), 1.45 (d, $^3J_{HH}$ = 6.7 Hz, 6H, ^{i}Pr-CH_3), 1.54 (d, $^3J_{HH}$ = 6.7 Hz, 6H, ^{i}Pr-CH_3), 1.72 (d, $^3J_{HH}$ = 6.7 Hz, 6H, ^{i}Pr-CH_3), 2.46 (m, br, 2H, ^{i}Pr-CH), 2.59 (m, br, 1H, ^{i}Pr-CH), 3.12 (m, br, 2H, ^{i}Pr-CH).

^{31}P{^{1}H} NMR (C_6D_6): δ [ppm] = 15.00 (s, 2P, P_2C_3), 46.90 (t, $^2J_{PP}$ = 42.0 Hz, 1P, $P_{isolated}$), 53.68 (d, $^2J_{PP}$ = 42.0 Hz, 2P, $P_{adjacent}$).

FD-MS (hexane): 486.1 (M^+).

Analytical data of **6**:

^{1}H NMR (C_6D_6): δ [ppm] = 1.29 (d, $^3J_{HH}$ = 6.7 Hz, 12H, ^{i}Pr-CH_3), 1.36 (d, $^3J_{HH}$ = 6.7 Hz, 12H, ^{i}Pr-CH_3), 2.91 (m, br, 4H, ^{i}Pr-CH).

^{31}P{^{1}H} NMR (C_6D_6): δ [ppm] = 51.3 (m, br, 2P, $P_{adjacent}$), 68.7 (m, br, 1P, $P_{isolated}$).

^{31}P{^{1}H} NMR (CD_2Cl_2, 193K): δ [ppm] = 46.22 (d, $^2J_{PP}$ = 34 Hz, 2P, $P_{adjacent}$), 69.28 (t, $^2J_{PP}$ = 38 Hz, 1P, $P_{isolated}$).

FD-MS (hexane): 462.0 (M^+).

Synthesis of [{Cp*Fe(μ_3,$\eta^{5:1:1}$-$P_2C_3{}^iPr_3$)}Cu_2(μ-Br)$_2$(CH_3CN)]$_n$ (2-Br)

A solution of CuBr (24 mg, 0.16 mmol) in 1 mL acetonitrile is layered onto a solution of **2** (35 mg, 0.08 mmol) in 0.5 mL toluene in a thin schlenk tube. After diffusion, small orange platelets of **2-Br**

are formed. The mother liquor is decanted and the crystals are washed with CH_2Cl_2, then dried *in vacuo*.

Analytical data of **2-Br**:

Yield: 5 mg (6.7 µmol, 8%).

$^{31}P\{^1H\}$ NMR (C_6D_6 capillary, mother liquor): δ [ppm] = 14.26 (s, P_2C_3).

Positive ion ESI-MS (mother liquor, toluene/CH_3CN): *m/z* (%) = 1043.3 $[\{Cp^*Fe(P_2C_3{}^iPr_3)\}_2Cu_2Br]^+$, 899.3 $[\{Cp^*Fe(P_2C_3{}^iPr_3)\}_2Cu]^+$, 326.1 (100) $[Cp^*{}_2Fe]^+$.

Negative ion ESI-MS (mother liquor, toluene/CH_3CN): *m/z* (%) = 798.3 $[Cu_5Br_6]^-$, 652.4 $[Cu_4Br_5]^-$, 510.4 $[Cu_3Br_4]^-$, 366.5 (100) $[Cu_2Br_3]^-$, 222.7 $[CuBr_2]^-$.

Elemental analysis: Calculated (%) for $[\{Cp^*Fe(\eta^5\text{-}P_2C_3{}^iPr_3)\}Cu_2Br_2(CH_3CN)_{1.5}]$ (766.8 g/mol): C 39.16, H 5.32, N 2.74; found: C 39.38, H 5.43, N 2.59.

Synthesis of $[\{Cp^*Fe(\mu_3,\eta^{5:1:1}\text{-}P_2C_3{}^iPr_3)\}Cu_2(\mu\text{-}I)_2(CH_3CN)_{0.5}]_n$ (2-I)

A solution of CuI (32 mg, 0.17 mmol) in 6 mL acetonitrile is layered onto a solution of **2** (35 mg, 0.08 mmol) in 3 mL toluene in a thin schlenk tube. After diffusion, small orange platelets of **2-I** are formed. The mother liquor is decanted and the crystals are washed with CH_2Cl_2, then dried *in vacuo*.

Analytical data of **2-I**:

Yield: 7 mg (8.8 µmol, 10%).

$^{31}P\{^1H\}$ NMR (C_6D_6 capillary, mother liquor): δ [ppm] = 15.95 (s, P_2C_3).

Positive ion ESI-MS (mother liquor, toluene/CH_3CN): *m/z* (%) = 712.0 $[\{Cp^*Fe(P_2C_3{}^iPr_3)\}Cu_2I(CH_3CN)]^+$, 522.1 $[\{Cp^*Fe(P_2C_3{}^iPr_3)\}Cu(CH_3CN)]^+$, 326.1 (100) $[Cp^*{}_2Fe]^+$.

Negative ion ESI-MS (mother liquor, toluene/CH_3CN): *m/z* (%) = 888.4 $[Cu_4I_5]^-$, 698.5 $[Cu_3I_4]^-$, 506.6 $[Cu_2I_3]^-$, 316.6 (100) $[CuI_2]^-$.

Elemental analysis: Calculated (%) for $[\{Cp^*Fe(\eta^5\text{-}P_2C_3{}^iPr_3)\}Cu_2I_2]$ (799.2 g/mol): C 33.06, H 4.54; found: C 33.76, H 4.63.

Synthesis of $[\{Cp^*Fe(\mu_4,\eta^{5:1:1:1}\text{-}P_3C_2{}^iPr_2)\}Cu_2(\mu\text{-}Cl)_2]_n$ (3-Cl)

A colorless solution of CuCl (30 mg, 0.30 mmol) in 3 mL acetonitrile is layered onto a red solution of **3** (36 mg, 0.09 mmol) in 2 mL toluene in a thin schlenk tube. Thereby, the phase boundary turns orange and overnight small orange crystals of **3-Cl** are formed. After complete diffusion, the mother liquor is decanted and the crystals are washed with a hexane/toluene (3/1) mixture (3 x 3 mL), then dried *in vacuo*.

Analytical data of **3-Cl**:

Yield: 17 mg (0.03 mmol, 33%).

$^{31}P\{^{1}H\}$ NMR (C_6D_6 capillary, mother liquor): δ [ppm] = no signal detectable.

Positive ion ESI-MS (mother liquor, toluene/CH_3CN): *m/z* = 1541.4 $[\{Cp^*Fe(P_3C_2{}^iPr_2)\}_3Cu_4Cl_3]^+$, 1441.4 $[\{Cp^*Fe(P_3C_2{}^iPr_2)\}_3Cu_3Cl_2]^+$, 1384.4 $[\{Cp^*Fe(P_3C_2{}^iPr_2)\}_3Cu_2Cl(CH_3CN)]^+$, 1341.7 $[\{Cp^*Fe(P_3C_2{}^iPr_2)\}_3Cu_2Cl]^+$, 1541.4 $[\{Cp^*Fe(P_3C_2{}^iPr_2)\}_3Cu_4Cl_3]^+$.

Negative ion ESI-MS (mother liquor, toluene/CH_3CN): *m/z* (%) = 332.5 (5) $[Cu_3Cl_4]^-$, 232.7 (100) $[Cu_2Cl_3]^-$, 134.7 (20) $[CuCl_2]^-$.

Elemental analysis: Calculated (%) for $[\{Cp^*Fe(\eta^5\text{-}P_3C_2{}^iPr_2)\}Cu_2Cl_2]$ (592.2 g/mol): C 36.51, H 4.94; found: C 37.51, H 5.03.

Synthesis of $[\{Cp^*Fe(\mu_4,\eta^{5:1:1:1}\text{-}P_3C_2{}^iPr_2)\}Cu_2(\mu\text{-}Br)_2]_n$ (3-Br)

A colorless solution of CuBr (40 mg, 0.28 mmol) in 3 mL acetonitrile is layered onto a red solution of **3** (36 mg, 0.09 mmol) in 2 mL toluene in a thin schlenk tube. Thereby, the phase boundary turns orange and overnight a colorless precipitate is formed. Within a week, small orange crystals of **3-Br** are formed. The mother liquor is decanted and the crystals are washed with a hexane/toluene (3/1) mixture (3 x 3 mL) and CH_3CN to remove precipitated CuBr, then dried *in vacuo*.

Analytical data of **3-Br**:

Yield: 27 mg (0.04 mmol, 44%).

$^{31}P\{^{1}H\}$ NMR (C_6D_6 capillary, mother liquor): δ [ppm] = 11.38 (d, $^2J_{PP}$ = 46 Hz, 2P, $P_{adjacent}$), 22.71 (t, $^2J_{PP}$ = 46 Hz, 1P, $P_{isolated}$).

Positive ion ESI-MS (mother liquor, toluene/CH_3CN): *m/z* = 1573.5 $[\{Cp^*Fe(P_3C_2{}^iPr_2)\}_2Cu_6Br_5]^+$, 1507.6 $[\{Cp^*Fe(P_3C_2{}^iPr_2)\}Cu_8Br_7(CH_3CN)]^+$, 1431.4 $[\{Cp^*Fe(P_3C_2{}^iPr_2)\}_2Cu_5Br_4]^+$, 1356.6 $[\{Cp^*Fe(P_3C_2{}^iPr_2)\}Cu_7Br_6(CH_3CN)]^+$, 1283.4 $[\{Cp^*Fe(P_3C_2{}^iPr_2)\}_2Cu_4Br_3]^+$, 1209.6 $[\{Cp^*Fe(P_3C_2{}^iPr_2)\}Cu_6Br_5(CH_3CN)]^+$, 1135.5 $[\{Cp^*Fe(P_3C_2{}^iPr_2)\}_2Cu_3Br_2]^+$, 985.3 $[\{Cp^*Fe(P_3C_2{}^iPr_2)\}_2Cu_2Br]^+$.

Negative ion ESI-MS (mother liquor, toluene/CH_3CN): *m/z* (%) = 798.1 (3) $[Cu_5Br_6]^-$, 654.2 (3) $[Cu_4Br_5]^-$, 510.4 (18) $[Cu_3Br_4]^-$, 366.3 (100) $[Cu_2Br_3]^-$, 222.5 (42) $[CuBr_2]^-$.

Elemental analysis: Calculated (%) for $[\{Cp^*Fe(\eta^5\text{-}P_3C_2{}^iPr_2)\}Cu_2Br_2(CH_3CN)_{0.1}(C_7H_8)_{0.1}]$ (694.4 g/mol): C 32.69, H 4.37, N 0.20; found: C 32.84, H 4.29, N 0.3.

Synthesis of $[\{(\mu_3,\eta^{5:1:1}\text{-}P_3C_2{}^iPr_2)Fe(\mu,\eta^{5:1}\text{-}P_2C_3{}^iPr_3)\}Cu_3(\mu\text{-}Br)(\mu_3\text{-}Br)(\mu_4\text{-}Br)]_n$ (5-Br)

A colorless solution of CuBr (34 mg, 0.24 mmol) in 3 mL acetonitrile is layered onto a green solution of **5** (23 mg, 0.05 mmol) in 3 mL CH_2Cl_2 in a thin schlenk tube. Thereby, no significant color change at the phase boundary can be observed. After diffusion, the reaction mixture is again

layered with toluene. Within a few days, green prism of **5-Br** are formed. The mother liquor is decanted and the crystals are washed with hexane (3 x 3 mL) and dried *in vacuo*.

Analytical data of **5-Br**:

Yield: 24 mg (0.025 mmol, 50%).

$^{31}P\{^1H\}$ NMR (mother liquor, C_6D_6 capillary): δ [ppm] = no signal detectable.

Negative ion ESI-MS (mother liquor, CH_2Cl_2/CH_3CN): *m/z* (%) = 510.4 (15) $[Cu_3Br_4]^-$, 366.4 (100) $[Cu_2Br_3]^-$, 222.5 (37) $[CuBr_2]^-$.

Elemental analysis: Calculated (%) for $[\{(\eta^5\text{-}P_3C_2{}^iPr_2)Fe(\eta^5\text{-}P_2C_3{}^iPr_3)\}Cu_3Br_3(C_7H_8)_{0.5}]$; (962.7 g/mol): C 29.32, H 4.08; found: C 29.46, H 4.11.

Synthesis of $[\{(\mu,\eta^{5:1}\text{-}P_3C_2{}^iPr_2)Fe(\mu,\eta^{5:1}\text{-}P_2C_3{}^iPr_3)\}Cu_2(\mu_3\text{-}I)_2]_n$ (5-I)

A colorless solution of CuI (45 mg, 0.24 mmol) in 3 mL acetonitrile is layered onto a green solution of **5** (23 mg, 0.05 mmol) in 3 mL CH_2Cl_2 in a very thin schlenk tube. Thereby, no significant color change at the phase boundary can be observed. Within two weeks, green-brown intergrown plates of **5-I** are formed. The mother liquor is decanted, the crystals are washed with hexane (3 x 3 mL) and dried *in vacuo*.

Analytical data of **5-I**:

Yield: 16 mg (0.018 mmol, 37%).

$^{31}P\{^1H\}$ NMR (mother liquor, C_6D_6 capillary): δ [ppm] = 9.45 (s, 2P, P_2C_3), 30.75 (d, $^2J_{PP}$ = 43.2 Hz, 2P, $P_{adjacent}$), 46.88 (t, $^2J_{PP}$ = 43.6 Hz, 1P, $P_{isolated}$).

Positive ion ESI-MS (mother liquor, CH_2Cl_2/CH_3CN): *m/z* (%) = 1796.9 $[\{(P_2C_3{}^iPr_2)Fe(P_3C_2{}^iPr_2)\}_2Cu_5I_4]^+$, 1690.2 $[\{(P_2C_3{}^iPr_2)Fe(P_3C_2{}^iPr_2)\}Cu_7I_6]^+$, 1628.8 $[\{(P_2C_3{}^iPr_2)Fe(P_3C_2{}^iPr_2)\}Cu_6I_5(CH_3CN)(CH_2Cl_2)]^+$, 1587.9 $[\{(P_2C_3{}^iPr_2)Fe(P_3C_2{}^iPr_2)\}Cu_6I_5(CH_2Cl_2)]^+$, 1606.9 $[\{(P_2C_3{}^iPr_2)Fe(P_3C_2{}^iPr_2)\}_2Cu_4I_3]^+$, 1543.9 $[\{(P_2C_3{}^iPr_2)Fe(P_3C_2{}^iPr_2)\}Cu_6I_5(CH_3CN)]^+$, 1500.6 $[\{(P_2C_3{}^iPr_2)Fe(P_3C_2{}^iPr_2)\}Cu_6I_5]^+$, 1437.2 $[\{(P_2C_3{}^iPr_2)Fe(P_3C_2{}^iPr_2)\}Cu_5I_4(CH_3CN)_3]^+$, 1417.1 $[\{(P_2C_3{}^iPr_2)Fe(P_3C_2{}^iPr_2)\}_2Cu_3I_2]^+$, 1395.9 $[\{(P_2C_3{}^iPr_2)Fe(P_3C_2{}^iPr_2)\}Cu_5I_4(CH_3CN)_2]^+$, 1288.2 $[\{(P_2C_3{}^iPr_2)Fe(P_3C_2{}^iPr_2)\}Cu_4I_3(CH_2Cl_2)_2]^+$, 1247.1 $[\{(P_2C_3{}^iPr_2)Fe(P_3C_2{}^iPr_2)\}Cu_4I_3(CH_3CN)(CH_2Cl_2)]^+$, 1227.1 $[\{(P_2C_3{}^iPr_2)Fe(P_3C_2{}^iPr_2)\}_2Cu_2I_1]^+$, 1206.1 $[\{(P_2C_3{}^iPr_2)Fe(P_3C_2{}^iPr_2)\}Cu_4I_3(CH_2Cl_2)]^+$, 1120.6 $[\{(P_2C_3{}^iPr_2)Fe(P_3C_2{}^iPr_2)\}Cu_4I_3]^+$.

Negative ion ESI-MS (mother liquor, CH_2Cl_2/CH_3CN): *m/z* (%) = 1078.3 (8) $[Cu_5I_6]^-$, 888.4 (14) $[Cu_4I_5]^-$, 698.4 (47) $[Cu_3I_4]^-$, 506.5 (78) $[Cu_2I_3]^-$, 316.6 (100) $[CuI_2]^-$.

Elemental analysis: Calculated (%) for $[\{(\eta^5\text{-}P_3C_2{}^iPr_2)Fe(\eta^5\text{-}P_2C_3{}^iPr_3)\}Cu_2I_2]$; (867.1 g/mol): C 27.70, H 4.07; found: C 27.78, H 4.02.

7.4 Crystallographic Details

All structures were solved by direct methods with *SHELX97*.[24] The structures were refined by full-matrix least-squares method against $|F|^2$ in anisotropic approximation using *SHELXL97* or the multiprocessor and variable memory version *SHELXL2013*. All non-hydrogen atoms were refined anisotropically, while the hydrogen atoms were refined riding on pivot atoms.

Crystals of **2-I** and **5** proved to be inversion twins crystallizing in chiral $P2_12_12_1$ and $P2_1$ space groups, respectively. The corresponding twin batches were refined as 0.593(3)/0.407(3) and 0.888(5)/0.112(5).

The pentaphosphaferrocene crystallized in three monoclinic polymorphic modifications as **5**, **5'** and **5''**.

A *pseudo*symmetry was detected by PLATON in the crystal structure of **4** as an inversion center. Taking into account that the structure is triclinic an additional symmetry element can end up only in a smaller unit cell. Indexation of the diffraction pattern gives the reported unit cell, but analysis of the spatial distribution of the strongest reflections shows a three times smaller possible subcell, and a = 8.659, b = 8.880, c = 9.644, α = 79.29, β = 78.02, γ = 61.70. The transformation matrix from the subcell to the large unit cell is (0 1 -1, 1 -1 -1, -1 0 -1). Our attempt to solve and refine the structure in the subcell returned half of the molecule as an independent part and R_1 = 0.037, however with flattened a.d.p. ellipsoids of the carbon atoms belonging to the methyl groups. The comparison of the a.d.p. ellipsoids in two independent molecules in the large unit cell with those in the subcell allows us to conclude that the superstructural effects originate from a conformational flexibility of the ^{i}Pr groups.

A *B*-centering was detected by PLATON in the crystal structure of **2**. However, the I/σ for the reflections that violate this *B*-centering is still high, 14.5, compared to mean I/σ=32.8. Two independent molecules that could be related by *b* translation would coincide except for two ^{i}Pr groups.

In **2-I** one of the ^{i}Pr groups of the P_2C_3 ring is disordered with a relative weight refined to 0.6/0.4 over two close positions, whose atoms were not possible to refine anisotropically for this reason. In both structures, **3-Br** and **5-Br**, solvated toluene molecules are disordered in a similar fashion over an inversion center so that the Me group of one position overlaps with the 4-carbon of a benzyl ring of the other. The carbon atoms of the toluene were refined in an isotropic approximation. The atoms of the coinciding positions were refined with equated displacement parameters. Since the overall molecular occupancy is 0.3 for **3-Br**, the geometry of the molecule was refined with geometrical restraints. In **2-Br** one of the solvated MeCN molecule has a molecular occupancy of 0.5 and is disordered over the center of symmetry. It was refined in an isotropic approximation.

The crystals of **5-I** were systematically twinned as stack of plates. For this reason a very thin crystal was chosen for the measurement. Nevertheless, the twinning could not be completely avoided that resulted in high K and R_{int} values. The number of carbon atoms was refined with restrained anisotropic displacement parameters.

Crystallographic data and details of the diffraction experiments are given in *Table 7.3* – *Table 7.8*.

Table 7.3 Experimental details for compounds **2** and **4**.

Crystal Data	**2**	**4**
Chemical formula	$C_{22}H_{36}FeP_2$	$C_{24}H_{42}FeP_4$
M_r	418.30	510.31
Crystal system, space group	monoclinic, $P2_1/c$	triclinic, $P\bar{1}$
Temperature (K)	123	123
a, b, c (Å)	9.1532(2), 33.9928(5), 14.0171(2)	11.8344(3), 13.0807(4), 14.2363(4)
α, β, γ (°)	90, 90.330(1), 90	67.789(3), 69.866(3), 77.591(2)
V (Å^3)	4361.25(13)	1906.47(11)
Z	8	3
F(000)	1792	816
Radiation type	Cu K_α	Cu K_α
μ (mm^{-1})	6.93	7.19
Crystal color and shape	orange plate	red-brown block
Crystal size (mm)	0.47 × 0.24 × 0.06	0.29 × 0.21 × 0.19
Data collection		
Diffractometer	SuperNova, Single source at offset, Atlas diffractometer	Xcalibur, Ruby, Gemini ultra diffractometer
Absorption correction	gaussian	analytical
T_{min}, T_{max}	0.226, 0.677	0.296, 0.430
No. of measured, independent and observed [$I > 2\sigma(I)$] reflections	44567, 8422, 7502	23628, 6639, 5013
R_{int}	0.047	0.029
$(\sin\theta/\lambda)_{max}$ (Å^{-1})	0.624	0.595
Range of h, k, l	h = -10→11, k = -42→41, l = -17→17	h = -14→14, k = -15→15, l = -16→16
Refinement		
$R[F^2 > 2\sigma(F^2)]$, $wR(F^2)$, S	0.037, 0.106, 1.04	0.030, 0.079, 0.90
No. of reflections	8422	6639
No. of parameters	473	394
No. of restraints	0	0
H-atom treatment	H-atom parameters constrained	H-atom parameters constrained

$\Delta\rangle_{max}$, $\Delta\rangle_{min}$ (e Å^{-3})	0.71, -0.47	0.44, -0.38

Table 7.4 Experimental details for compounds **5** and **5'**.

Crystal Data	5	5'
Chemical formula	$C_{20}H_{35}FeP_5$	$C_{20}H_{35}FeP_5$
M_r	486.18	486.18
Crystal system, space group	monoclinic, $P2_1$	monoclinic, $P2_1/n$
Temperature (K)	123	123
a, *b*, *c* (Å)	9.6056(1), 16.9567(2), 14.3763(2)	9.5449(1), 15.9135(2), 15.1917(1)
α, β, γ (°)	90, 92.825(1), 90	90, 94.664(1), 90
V (Å^3)	2338.76(5)	2299.87(4)
Z	4	4
F(000)	1024	1024
Radiation type	Cu K_α	Cu K_α
μ (mm^{-1})	8.42	8.56
Crystal color and shape	green block	green plate
Crystal size (mm)	0.19 × 0.09 × 0.08	0.22 × 0.14 × 0.04
Data collection		
Diffractometer	Xcalibur, Ruby, Gemini ultra diffractometer	SuperNova, Titan^{S2} diffractometer
Absorption correction	analytical	gaussian
T_{min}, T_{max}	0.412, 0.655	0.317, 0.732
No. of measured, independent and observed [$I > 2\sigma(I)$] reflections	14958, 7064, 6636	24371, 4626, 4258
R_{int}	0.027	0.054
$(\sin\theta/\lambda)_{max}$ (Å^{-1})	0.595	0.624
Range of h, k, l	h = -9→11, k = -19→20, l = -17→17	h = -11→11, k = -18→19, l = -18→18
Refinement		
$R[F^2 > 2\sigma(F^2)]$, $wR(F^2)$, S	0.036, 0.097, 1.11	0.026, 0.069, 0.99
No. of reflections	7064	4626
No. of parameters	470	245
No. of restraints	1	0
H-atom treatment	H-atom parameters constrained	H-atom parameters constrained
$\Delta\rangle_{max}$, $\Delta\rangle_{min}$ (e Å^{-3})	0.86, -0.33	0.49, -0.45

Table 7.5 Experimental details for compounds **5''** and **2-Br**.

Crystal Data	5''	2-Br
Chemical formula	$C_{20}H_{35}FeP_5$	$C_{24}H_{39}Br_2Cu_2FeNP_2{\cdot}0.75(CH_3CN)$

M_r	486.18	777.04
Crystal system, space group	monoclinic, $P2_1/n$	monoclinic, $C2/c$
Temperature (K)	126	123
a, b, c (Å)	13.6464(4), 12.1784(2), 28.7527(8)	25.4093(5), 19.3055(2), 15.7888(3)
α, β, γ (°)	90, 90.183(2), 90	90, 126.781(3) , 90
V (Å^3)	4778.4(2)	6203.2(3)
Z	8	8
F(000)	2048	3124
Radiation type	Cu K_α	Cu K_α
μ (mm^{-1})	8.25	9.39
Crystal color and shape	green rod	yellow plate
Crystal size (mm)	0.36 × 0.03 × 0.03	0.15 × 0.05 × 0.04
Data collection		
Diffractometer	Xcalibur, Atlas[S2], Gemini ultra diffractometer	Xcalibur, Atlas, Gemini ultra diffractometer
Absorption correction	analytical	analytical
T_{min}, T_{max}	0.282, 0.824	0.382, 0.706
No. of measured, independent and observed [$I > 2\sigma(I)$] reflections	19437, 8317, 5864	49844, 5508, 4644
R_{int}	0.042	0.040
$(\sin\theta/\lambda)_{max}$ (Å^{-1})	0.596	0.597
Range of h, k, l	h = -16→12, k = -13→14, l = -34→30	h = -30→30, k = -22→22, l = -18→18
Refinement		
$R[F^2 > 2\sigma(F^2)]$, $wR(F^2)$, S	0.029, 0.055, 0.80	0.029, 0.075, 1.05
No. of reflections	8317	5508
No. of parameters	489	328
No. of restraints	0	1
H-atom treatment	H atoms treated by a mixture of independent and constrained refinement	H-atom parameters constrained
$\Delta\rangle_{max}$, $\Delta\rangle_{min}$ (e Å^{-3})	0.64, -0.31	0.97, -0.48

Table 7.6 Experimental details for compounds **2-I** and **3-Cl**.

Crystal Data	2-I	3-Cl
Chemical formula	$C_{24}H_{39}Cu_2FeI_2NP_2$	$C_{18}H_{29}Cl_2Cu_2FeP_3$
M_r	840.23	592.15
Crystal system, space group	orthorhombic, $P2_12_12_1$	orthorhombic, *Pbca*
Temperature (K)	123	123
a, b, c (Å)	11.1640(2), 14.2254(2), 37.2743(4)	16.6294(3), 16.8479(3), 16.9793(3)

α, β, γ (°)	90, 90, 90	90, 90, 90
V (Å^3)	5919.62(15)	4757.10(15)
Z	8	8
F(000)	3280	2400
Radiation type	Cu K_α	Cu K_α
μ (mm^{-1})	23.04	10.21
Crystal color and shape	yellow plate	red prism
Crystal size (mm)	0.19 × 0.16 × 0.04	0.23 × 0.19 × 0.10
Data collection		
Diffractometer	Xcalibur, Atlas, Gemini ultra diffractometer	SuperNova, Titan^{S2} diffractometer
Absorption correction	analytical	gaussian
T_{min}, T_{max}	0.055, 0.424	0.189, 0.433
No. of measured, independent and observed [$I > 2\sigma(I)$] reflections	97078, 10506, 9981	10725, 4622, 3815
R_{int}	0.042	0.034
$(\sin\theta/\lambda)_{max}$ (Å^{-1})	0.597	0.624
Range of h, k, l	*h* = -12→13, *k* = -16→16, *l* = -44→44	*h* = -20→16, *k* = -8→20, *l* = -18→20
Refinement		
$R[F^2 > 2\sigma(F^2)]$, $wR(F^2)$, *S*	0.019, 0.047, 1.03	0.035, 0.088, 0.95
No. of reflections	10506	4622
No. of parameters	601	244
No. of restraints	0	0
H-atom treatment	H-atom parameters constrained	H-atom parameters constrained
$\Delta\rangle_{max}$, $\Delta\rangle_{min}$ (e Å^{-3})	0.87, -0.62	0.74, -0.65

Table 7.7 Experimental details for compounds **3-Cl'** and **3-Br**.

Crystal Data	3-Cl'	3-Br
Chemical formula	$C_{18}H_{29}Cl_2Cu_2FeP_3$	$C_{18}H_{29}Br_2Cu_2FeP_3 \cdot 0.15(C_7H_8)$
M_r	592.15	694.89
Crystal system, space group	monoclinic, $P2_1/c$	monoclinic, $P2_1/c$
Temperature (K)	123	123
a, *b*, *c* (Å)	8.4412(1), 16.8393(2), 17.2062(2)	8.6057(1), 16.8865(1), 17.7057(1)
α, β, γ (°)	90, 100.823(1), 90	90, 99.799(1), 90
V (Å^3)	2402.25(5)	2535.46(4)
Z	4	4
F(000)	1200	1374
Radiation type	Cu K_α	Cu K_α
μ (mm^{-1})	10.77	11.95

Crystal color and shape	red cube	purple prism
Crystal size (mm)	0.10 × 0.09 × 0.07	0.15 × 0.12 × 0.10
Data collection		
Diffractometer	SuperNova, Titan^{S2} diffractometer	Xcalibur, Atlas^{S2}, Gemini ultra diffractometer
Absorption correction	gaussian	analytical
T_{min}, T_{max}	0.403, 0.562	0.254, 0.433
No. of measured, independent and observed [$I > 2\sigma(I)$] reflections	23102, 4828, 4271	37615, 4485, 4298
R_{int}	0.049	0.028
$(\sin\theta/\lambda)_{max}$ (Å^{-1})	0.624	0.596
Range of h, k, l	h = -10→10, k = -20→20, l = -20→21	h = -9→10, k = -20→20, l = -21→21
Refinement		
$R[F^2 > 2\sigma(F^2)]$, $wR(F^2)$, S	0.029, 0.074, 0.98	0.023, 0.054, 1.07
No. of reflections	4828	4485
No. of parameters	244	259
No. of restraints	0	1
H-atom treatment	H-atom parameters constrained	H-atom parameters constrained
$\Delta\rangle_{max}$, $\Delta\rangle_{min}$ (e Å^{-3})	0.41, -0.73	0.58, -0.39

Table 7.8 Experimental details for compounds **5-Br** and **5-I**.

Crystal Data	5-Br	5-I
Chemical formula	$C_{20}H_{35}Br_3Cu_3FeP_5{\cdot}0.5(C_7H_8)$	$C_{20}H_{35}Cu_2FeI_2P_5$
M_r	962.59	867.06
Crystal system, space group	triclinic, $P\bar{1}$	monoclinic, $P2_1/n$
Temperature (K)	123	123
a, b, c (Å)	9.5046(2), 10.6841(2), 16.5146(2)	8.9909(3), 31.866(1), 48.048(2)
α, β, γ (°)	76.978(1), 78.518(1), 85.863(1)	90, 93.688(3), 90
V (Å^3)	1600.55(5)	13737.1(9)
Z	2	20
F(000)	946	8400
Radiation type	Cu K_α	Cu K_α
μ (mm^{-1})	12.61	26.43
Crystal color and shape	green prism	green-brown plate
Crystal size (mm)	0.19 × 0.08 × 0.07	0.08 × 0.04 × 0.02
Data collection		
Diffractometer	Xcalibur, Atlas^{S2}, Gemini ultra diffractometer	SuperNova, Titan^{S2} diffractometer
Absorption correction	analytical	gaussian
T_{min}, T_{max}	0.212, 0.533	0.302, 0.669

No. of measured, independent and observed [$I > 2\sigma(I)$] reflections	16570, 5643, 5219	84747, 27095, 11532
R_{int}	0.021	0.115
$(\sin\theta/\lambda)_{max}$ (Å^{-1})	0.596	0.624
Range of h, k, l	h = -11→11, k = -12→12, l = -16→19	h = -8→10, k = -34→39, l = -57→57
Refinement		
$R[F^2 > 2\sigma(F^2)]$, $wR(F^2)$, S	0.020, 0.049, 1.05	0.060, 0.148, 0.78
No. of reflections	5643	27095
No. of parameters	325	1401
No. of restraints	0	102
H-atom treatment	H-atom parameters constrained	H-atom parameters constrained
$\Delta\rangle_{max}$, $\Delta\rangle_{min}$ (e Å^{-3})	0.68, -0.45	1.92, -1.79

7.5 Author Contributions

- The synthesis and characterization of **1a/b** was mainly performed by Dr. Christoph Schwarzmaier
- The syntheses and characterization of the phosphaferrocenes **2**, **3**, **4**, **5** and **6**, as well as the polymeric products **3-Cl**, **3-Br**, **5-Br** and **5-I** were performed by Claudia Heindl
- The syntheses and characterization of the polymeric products **2-Br** and **2-I** were performed by Dr. Sabine Reisinger and are also part of her dissertation thesis (University of Regensburg, **2014**)
- X-ray structural analyses of **2**, **4**, **5**, **5'**, **5''**, **3-Cl**, **3-Cl'**, **3-Br**, **5-Br** and **5-I** were performed by Dr. Eugenia V. Peresypkina, Dr. Alexander V. Virovets and Claudia Heindl
- X-ray structural analyses and refinements of **2-Br** and **2-I** were performed together by Dr. Eugenia V. Peresypkina, Dr. Alexander V. Virovets and Dr. Sabine Reisinger
- The manuscript (introduction, results and discussion, experimental part; including figures and graphical abstract) was written by Claudia Heindl; with the following exception:
- The section 'crystallographic details' was written by Dr. Eugenia V. Peresypkina
- Some syntheses and characterization were carried out by Lena Rummel in the course of her bachelor thesis under the supervision of Claudia Heindl

7.6 References

[1] G. Maerkl, *Angew. Chem.* **1966**, *78*, 907.

[2] L. Weber, *Angew. Chem., Int. Ed.* **2002**, *41*, 563.

[3] J. Bai, A. V. Virovets, M. Scheer, *Angew. Chem. Int. Ed.* **2002**, *41*, 1737.

[4] a) C. Schwarzmaier, A. Schindler, C. Heindl, S. Scheuermayer, E. V. Peresypkina, A. V. Virovets, M. Neumeier, R. Gschwind, M. Scheer, *Angew. Chem. Int. Ed.* 2013, *52*, 10896; b) J. Bai, A. V. Virovets, M. Scheer, *Science* 2003, *300*, 781.

[5] a) C. Heindl, A. Schindler, M. Bodensteiner, E. V. Peresypkina, A. V. Virovets, M. Scheer, *Phosphorus, Sulfur Silicon Relat. Elem*. 2015, *190*, 397; b) M. M. Al-Ktaifani, P. B. Hitchcock, J. F. Nixon, *J. Organomet. Chem.* 2008, *693*, 611; M. Scheer, c) S. Deng, O. J. Scherer, M. Sierka, *Angew. Chem. Int. Ed.* 2005, *44*, 3755; d) C. S. J. Callaghan, P. B. Hitchcock, J. F. Nixon, *J. Organomet. Chem.* 1999, *584*, 87; e) M. H. A. Benvenutti, P. B. Hitchcock, J. F. Nixon, M. D. Vargas, *Chem. Commun.* 1996, 441; f) C. Müller, R. Bartsch, A. Fischer, P. G. Jones, R. Schmutzler, *J. Organomet. Chem*. 1996, *512*, 141; g) M. H. A. Benvenutti, P. B. Hitchcock, J. F. Nixon, M. D. Vargas, *J. Chem. Soc., Dalton Trans.* 1996, 739; h) C. Mueller, R. Bartsch, A. Fischer, P. G. Jones, *Polyhedron* 1993, *12*, 1383; i) C. Müller, R. Bartsch, A. Fischer, P. G. Jones, *J. Organomet. Chem*. 1993, *453*, C16; j) R. Bartsch, A. Gelessus, J. F. Nixon, P. B. Hitchcock, *J. Organomet. Chem*. 1992, *430*, C10; k) R. Bartsch, P. B. Hitchcock, J. F. Nixon, *J. Organomet. Chem.* 1988, *340*, C37.

[6] a) S. Deng, C. Schwarzmaier, M. Zabel, J. F. Nixon, M. Bodensteiner, E. V. Peresypkina, G. Balázs, M. Scheer, *Eur. J. Inorg. Chem.* 2011, 2991; b) A. Schindler, G. Balázs, M. Zabel, C. Groeger, R. Kalbitzer, M. Scheer, *C. R. Chim.* 2010, *13*, 1241.

[7] S. Deng, C. Schwarzmaier, U. Vogel, M. Zabel, J. F. Nixon, M. Scheer, *Eur. J. Inorg. Chem.* 2008, 4870.

[8] C. Heindl, A. Kuntz, E. V. Peresypkina, A. V. Virovets, M. Zabel, D. Luedeker, G. Brunklaus, M. Scheer, *Dalton Trans.* 2015, *44*, 6502.

[9] R. Bartsch, J. F. Nixon, *J. Organomet. Chem.* 1991, *415*, C15.

[10] N. Maigrot, L. Ricard, C. Charrier, F. Mathey, *Angew. Chem., Int. Ed.* 1990, *29*, 534.

[11] a) N. Maigrot, M. L. Sierra, C. Charrier, L. Ricard, F. Mathey, *Polyhedron* 1992, *11*, 601; b) M. L. Sierra, N. Maigrot, C. Charrier, L. Ricard, F. Mathey, *Organometallics* 1992, *11*, 459.

[12] a) R. Bartsch, P. B. Hitchcock, J. F. Nixon, *Chem. Commun.* 1987, 1146; b) M. Driess, D. Hu, H. Pritzkow, H. Schaeufele, U. Zenneck, M. Regitz, W. Roesch, *J. Organomet. Chem.* 1987, *334*, C35.

[13] R. Bartsch, A. Gelessus, P. B. Hitchcock, J. F. Nixon, *J. Organomet. Chem.* 1992, *430*, C10.

[14] D. Boehm, F. Heinemann, D. Hu, S. Kummer, U. Zenneck, *Collect. Czech. Chem. Commun.* 1997, *62*, 309.

[15] a) C. S. J. Callaghan, P. B. Hitchcock, J. F. Nixon, *J. Organomet. Chem.* 1999, *584*, 87; b) G. Becker, W. Becker, R. Knebl, H. Schmidt, U. Weeber, M. Westerhausen, *Nova Acta Leopold.* 1985, *59*, 55.

[16] W. Roesch, U. Vogelbacher, T. Allspach, M. Regitz, *J. Organomet. Chem.* 1986, *306*, 39.

[17] F. Uhlig, R. Hummeltenberg, *J. Organomet. Chem.* 1993, *452*, C9.

[18] D. Heift, Z. Benko, H. Gruetzmacher, *Chem. Eur. J.* 2014, *20*, 11326.

[19] a) P. Pyykkö, M. Atsumi, *Chem. Eur. J.* 2009, *15*, 12770; b) P. Pyykkö, M. Atsumi, *Chem. Eur. J.* 2009, *15*, 186.

[20] R. Peng, M. Li, D. Li, *Coord. Chem. Rev.* 2010, *254*, 1.

[21] M. Scheer, *Dalton Trans.* 2008, 4372.

[22] A. Schindler, M. Zabel, J. F. Nixon, M. Scheer, *Z. Naturforsch.* 2009, *64*, 1429.

[23] Deng, S. Diploma thesis, University of Karlsruhe (Karlsruhe), 2002.

[24] G. M. Sheldrick. *Acta Cryst. sect. C* 2015, *C71*, 3.

8. Novel Polymeric Aggregates of Pentaphosphaferrocenes and Monocationic Coinage Metal Salts

Synthesis of $[\{Cp^*Fe(\eta^5\text{-}P_5)\}\{Cu(GaCl_4)\}_2]_n$ and $[\{Cp^{BIG}Fe(\eta^5\text{-}P_5)\}Ag]_n[Al(OC(CF_3)_3)_4]_n$

C. Heindl, S. Heinl, D. Lüdeker, G. Brunklaus, W. Kremer, M. Scheer, *Inorg. Chim. Acta* **2014**, *422*, 218-223. Reprinted with Permission of ‚Elsevier': License number: 3621900365623; May 04, 2015

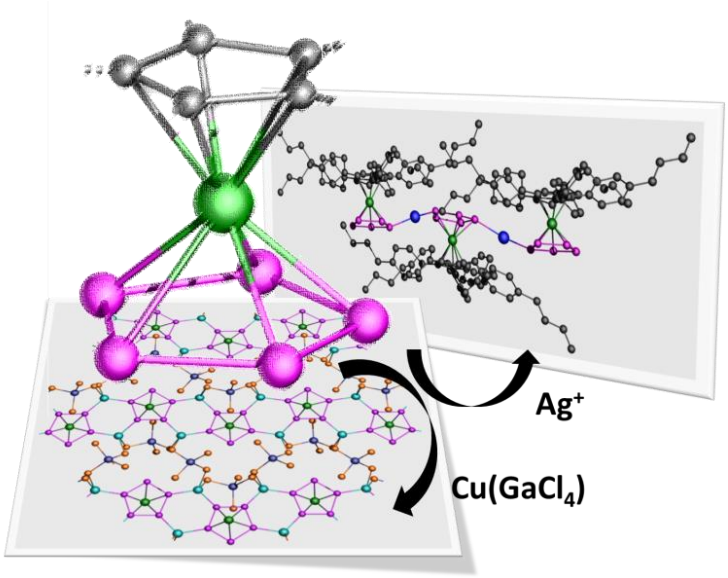

Abstract:

The reaction of pentaphosphaferrocenes $[Cp^RFe(\eta^5\text{-}P_5)]$ (Cp^R = Cp* = $\eta^5\text{-}C_5Me_5$, Cp^{BIG} = $\eta^5\text{-}C_5(4\text{-}^nBuC_6H_4)$) with monocationic salts of copper and silver leads to the formation of $[\{Cp^*Fe(\eta^5\text{-}P_5)\}\{Cu(GaCl_4)\}_2]_n$ (**2**) and $[\{Cp^{BIG}Fe(\eta^5\text{-}P_5)\}Ag]_n[Al\{OC(CF_3)_3\}_4]_n$ (**3**), respectively, representing the rare structural motifs of a 1,2,3,4- or a 1,3-coordination mode of the *cyclo*-P_5 unit. Both the 2D network as well as the 1D polymer are obtained from self-assembly processes and characterized by X-ray structure analysis. Compound **2** exemplifies a sheet-like structure, whose layers are linked by short Cl···H-contacts, whereas the structure of **3** is comprised of cationic strands, whose positive charge is balanced by the weakly coordinating anion $[Al\{OC(CF_3)_3\}_4]$. Dissociative properties of both polymeric complexes are compared by solution and solid state NMR spectroscopy.

8.1 Introduction

The isolobal analogy between phosphorus atoms and methine groups opened up an interesting class of organometallic compounds: the phosphaferrocenes. The most exciting representative is probably pentaphosphaferrocene [Cp*Fe(η^5-P_5)] (Cp* = η^5-C_5Me_5) (**1a**) exhibiting a *cyclo*-P_5-ring.[1] In contrast to ferrocenes [$Cp^R{}_2Fe$], the lone pairs of the P atoms in **1a** turns them into excellent building blocks for coordination and supramolecular chemistry. This field was so far dominated by N- and O-donor ligands as bridging units between metal centers.[2] However, our group showed, that bare phosphorus ligands are in no way inferior.[3] Especially in combination with monocationic coinage metal salts, the versatile coordination behavior of **1a** is demonstrated.[4] The products of its self-assembly processes with CuX (X = Cl, Br, I) range from 1D and 2D polymers[4c,h,j] to spherical supramolecules with fullerene-like topology.[4a,b,d-g,i]

Changing from CuX, containing a coordinated halogen ligand, to Ag[Al{$OC(CF_3)_3$}$_4$], bearing a weakly coordinating anion, a novel coordination motif (1,2,3-coordination mode in [{Cp*Fe(η^5-P_5)}Ag]$_n$[Al{$OC(CF_3)_3$}$_4$]$_n$) and a dynamic oligomerization behavior in solution of the resulting polymer were obtained.[4h] These findings demonstrate the influence of the used counter anion. Hence we were interested in the coordination chemistry of **1a** towards Cu($GaCl_4$), whose tetrachlorogallate anion can form both: ion-contacted[5] as well as ion-separated[6] complexes.

Although the self-assembly process of the pentaphosphaferrocene proved to be versatile and very sensitive to all supposable parameters, the study of the steric influence of the Cp^R ring was neglected so far. Thus, we introduced the sterically much more demanding Cp^{BIG} (Cp^{BIG} = η^5-$C_5(4\text{-}^nBuC_6H_4)$) ligand and examined the coordination behavior of [Cp^{BIG}Fe(η^5-P_5)][7] (**1b**) towards Ag[Al{$OC(CF_3)_3$}$_4$].

Herein we report on the synthesis of two new polymeric coordination compounds with monocationic coinage metal salts: [{Cp*Fe(η^5-P_5)}{Cu($GaCl_4$)}$_2$]$_n$ (**2**) and [{Cp^{BIG}Fe(η^5-P_5)}Ag]$_n$[Al{$OC(CF_3)_3$}$_4$]$_n$ (**3**).

8.2 Results and Discussion

Upon diffusion of a toluene solution of **1a** into a CH_2Cl_2 solution of Cu($GaCl_4$) the crystallization of yellow rods of the two-dimensional coordination network [{Cp*Fe(η^5-P_5)}{Cu($GaCl_4$)}$_2$]$_n$ (**2**) can be obtained in quantitative yields (*Figure* 8.1).

The repeating unit of **2** contains **1a** and Cu($GaCl_4$) in a 1:2 molar ratio, in which the tetrachlorogallate anion is part of the polymeric framework and coordinates to Cu, resulting in a neutral coordination compound.

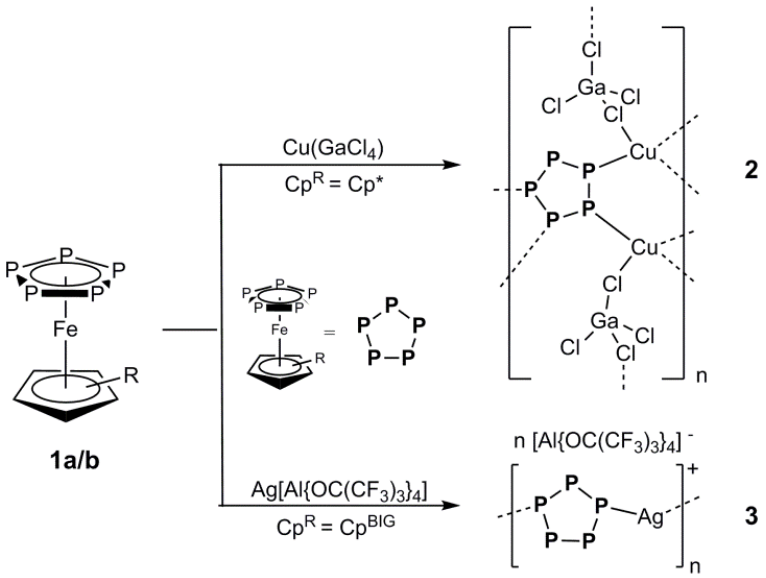

Figure 8.1 Reaction of $[Cp^RFe(\eta^5\text{-}P_5)]$ (**1a**: Cp^R = Cp*; **1b**: $Cp^R = Cp^{BIG}$) with $Cu(GaCl_4)$ and $Ag[Al\{OC(CF_3)_3\}_4]$, respectively. The polymeric compounds are represented by their repeating units.

The structure of **2** was elucidated by X-ray structural analysis (*Figure 8.2*). It reveals an unusual 1,2,3,4 coordination mode of each P_5 ring, which was only observed once in a CuI-containing polymer.[4c] The Cu^I cations show a distorted tetrahedral environment with angles ranging from 87.72(3)° to 116.94(3)°, which is typical for copper in the oxidation state +1.[8] They are coordinated by two P atoms and two Cl atoms from $GaCl_4$ and form six-membered $\{Cu_2P_4\}$ rings between the *cyclo*-P_5 units. In contrast, the Cl atoms occur in two coordination modes: half of them are only coordinated to Ga and therefore terminal, the other two bridge Ga and Cu yielding seven-membered $\{P_2Cu_2Cl_2Ga\}$ rings. Concerning the bond lengths, the Cl-Ga distances for μ_2-Cl atoms (2.39 Å) are longer than the corresponding ones for terminal halides (2.14 Å).

The network can be described as a 2D sheet structure, whose single layers are limited by the terminal Cl and the Cp* ligands from **1a**. They in turn are orientated alternating upwards and downwards the layer (*Figure 8.3*). The shortest gap between the layers is the distance between terminal Cl ligands and the H atoms from the Cp* units. It constitutes 2.780(1) Å and therefore goes below the sum of the van-der-Waals-radii of Cl and H (2.95 Å),[9] indicating the presence of hydrogen bonds (*Figure 8.4*).

Most likely due to formation of the 2D network, compound **2** is rather insoluble in common solvents though its slight solubility in CH_3CN is accompanied by fragmentation. Hence, the corresponding $^{31}P\{^1H\}$ and ^1H NMR spectra of **2** in CD_3CN merely exhibit one sharp singlet at 143.4 ppm and 1.45 ppm, respectively, reflecting shifts similar to those observed for free **1a**.[1]

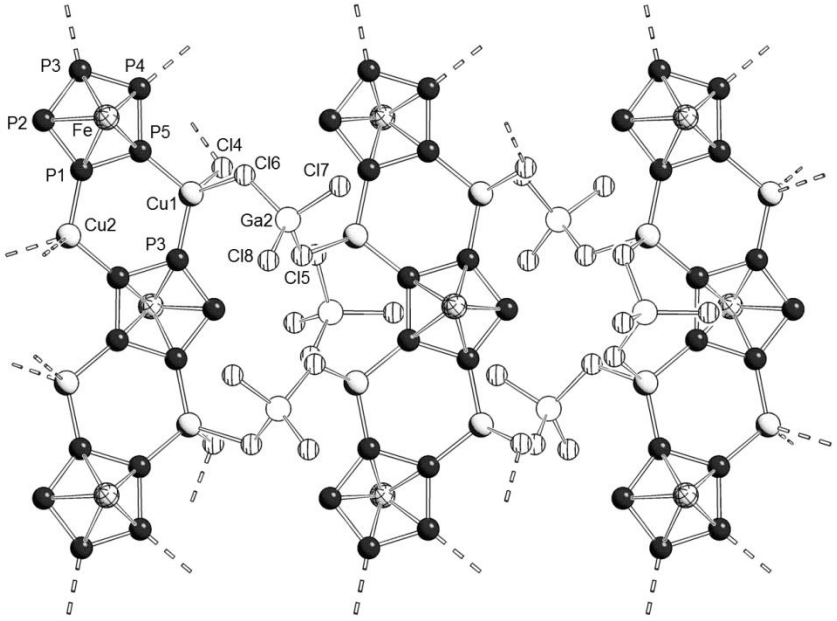

Figure 8.2 Section of the polymeric network of **2** in the crystal. For clarity reasons the C and H atoms are omitted. In case of disorder only the main part is shown. Selected bond lengths [Å] and angles [°]: P1-P2 2.1145(11), P2-P3 2.1120(11), P3-P4 2.0996(11), P4-P5 2.1028(11), P1-P5 2.1019(11), P1-Cu2 2.2611(9), P5-Cu1 2.2777(9), Cu1-Cl4 2.4055(9), Cu1-Cl6 2.3687(9), Ga2-Cl5 2.2049(10), Ga2-Cl6 2.2149(9), Ga2-Cl7 2.118(4), Ga2-Cl8 2.1494(10), P1-P2-P3 104.14(4), P2-P3-P4 110.64(5), P3-P4-P5 107.21(5), P1-P5-P4 106.86(5), P2-P1-P5 110.743(5), P4-P5-Cu1 128.55(4), P1-P5-Cu1 123.89(4), P5-P1-Cu2 117.98(4), P5-Cu1-Cl4 110.35(3), P3-Cu1-Cl4 110.82(3), P5-Cu1-P3 116.94(3), Cl6-Cu1-Cl4 87.72(3), Cl6-Cu1-P3 115.51(3), Cl6-Cu1-P5 111.75(3), Ga2-Cl6-Cu1 119.06(4), Cl8-Ga2-Cl5 105.58(4), Cl5-Ga2-Cl7 117.5(1), Cl7-Ga2-Cl6 106.2(1), Cl7-Ga2-Cl8 113.8(1), Cl6-Ga2-Cl8 109.31(4), Cl6-Ga2-Cl5 103.92(3).

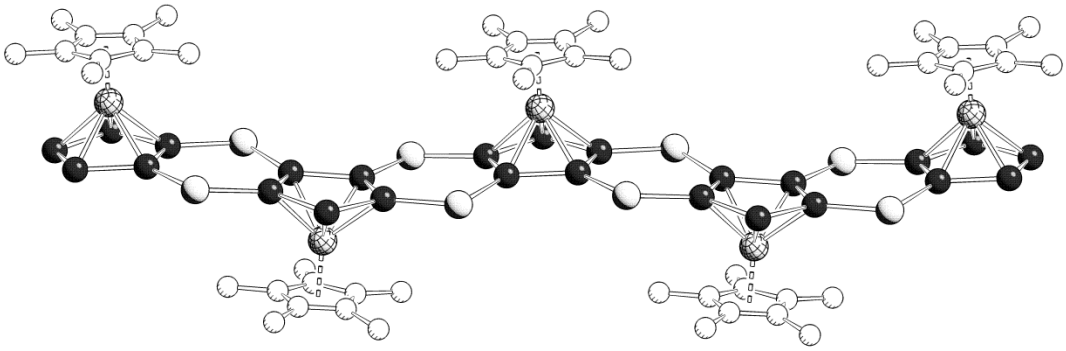

Figure 8.3 Section of **2** illustrating the alternating orientation of the Cp* ligands. For clarity reasons the Ga, Cl and H atoms are omitted.

The positive ion ESI mass spectrum of **2** also displays signals corresponding to small complex fragments up to the cation $[(Cp^*FeP_5)_2Cu_3Cl_2]^+$ while the single peak in the negative ion ESI mass spectrum corresponds to $(GaCl_4)^-$.

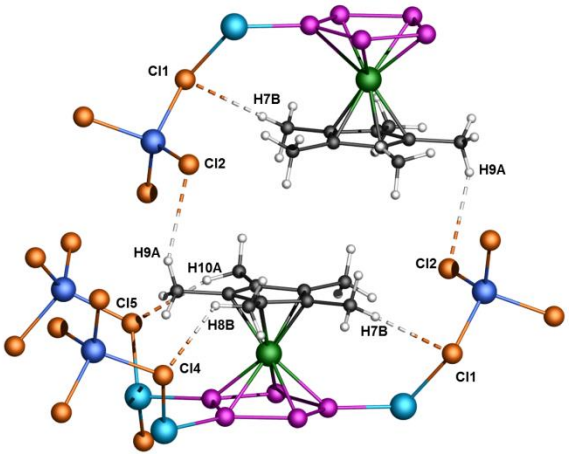

Figure 8.4 Section of **2** showing short Cl–H distances. Selected bond lengths [Å]: H9A-Cl2 2.8609(8), H7B-Cl1 2.7986(8), H8B-Cl4 2.6998(8), H10A-Cl5 2.6219(15).

In addition, compound **2** was further examined by multinuclear solid state NMR spectroscopy (*Figure 8.6*). The major peak at 1.98 ppm in its ^{1}H magic-angle spinning (MAS) NMR spectrum represents the methyl groups of Cp* units that are partially involved in hydrogen-bonding to Cl ligands while a peak at 7.18 ppm (area 4.5%) can be attributed to residual toluene from the solvent diffusion reaction (*Figure 8.5*).

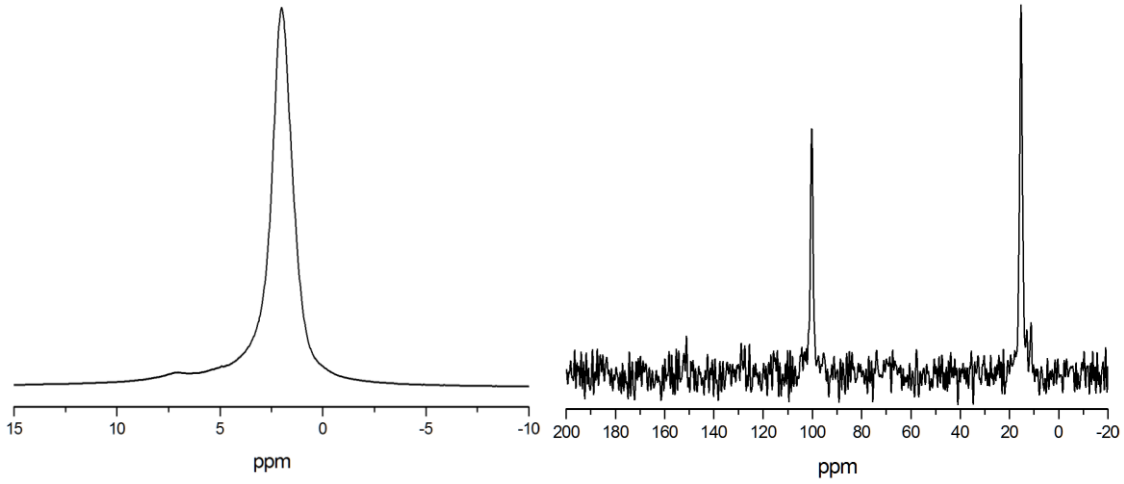

Figure 8.5 left: Rotor-synchronized ^{1}H MAS NMR spectrum of **2** at 298 K, acquired at 500.18 MHz (11.7 T) and 30 kHz MAS using a commercially available Bruker 2.5 mm HXY triple-resonance probe averaging 16 scans at a relaxation delay of 50s; right: ^{13}C{^{1}H} CPMAS NMR spectrum of **2** at 298 K, recorded at 125.78 MHz (11.7 T) and 25 kHz MAS using a commercially available Bruker 2.5 mm HXY triple-resonance probe with a contact time of 4ms while accumulating 512 scans at a relaxation delay of 10s.

Note that the ^{13}C{^{1}H} cross-polarization MAS NMR spectrum of **2** (*Figure 8.5*) shows two main resonances at 15.3 ppm (methyl groups) and 100.2 ppm (Cp* ring) irrespective of the alternating arrangement, as expected in the likely presence of molecular (rotational) dynamics, though the two minor peaks at 11.2 ppm and 12.9 ppm, respectively, could be either indicative of hydrogen-bonding or of impurities.

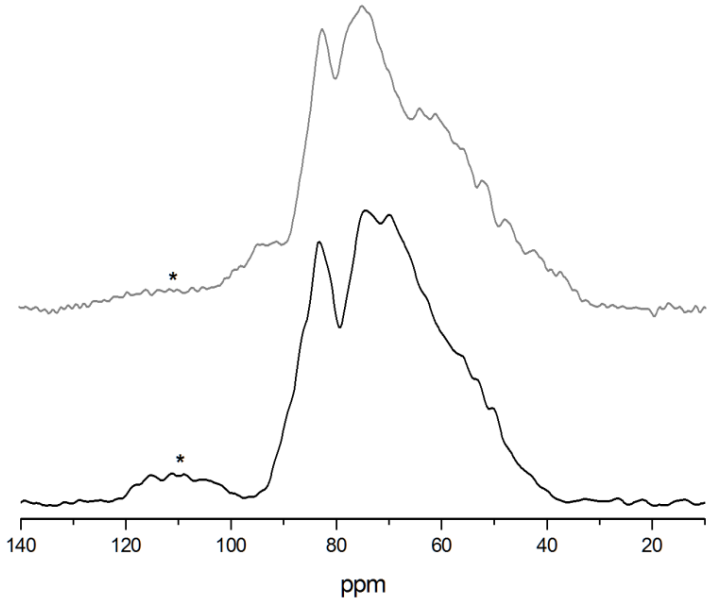

Figure 8.6 $^{31}P\{^{1}H\}$ MAS NMR spectra of **2** at 298 K at 7.0 T (top) and 11.7 T (bottom), each acquired at 30 kHz MAS. The presence of rather strong ^{31}P-$^{63,65}Cu$ interactions is revealed by a spread of intensities and signal broadening at the lower magnetic field. The signal marked with an asterisk arises from an impurity.

In contrast, the $^{31}P\{^{1}H\}$ MAS NMR spectra of **2** recorded at two different magnetic fields (7.0 T & 11.7 T) are rather crowded reflecting the presence of line-broadening effects such as residual dipolar couplings[10] due to significant $^{63,65}Cu$ and $^{35,37}Cl$ quadrupolar interactions imposed by a distorted tetrahedral coordination of both the Cu^{I} cations and tetrachlorogallate anions (*Figure 8.6*). Unlike a more favorable case,[11] the expected multiplet fine structure from either ^{31}P-^{31}P and/or ^{31}P-$^{63,65}Cu$ indirect spin-spin couplings is obscured and compared to the 1D polymer of $[\{CpFe(\eta^{5:1:1}\text{-}P_5)\}CuCl]_n$,[4c] all peaks are shifted to lower ppm values, rendering peak assignment difficult. Nevertheless, it appears reasonable to attribute the signal at 83 ppm to the crystallographic P2 site that solely is not coordinated to Cu^{I} cations (reminiscent of $[\{CpFe(\eta^{5:1:1}\text{-}P_5)\}CuBr]_n$).[4c] The rather similar sites P1 and P5 are tentatively assigned to the signal centered at about 70 ppm while P3 and P4 are estimated at less than 60 ppm, which is in agreement with a preliminary DFT ^{31}P chemical shift computation of the *cyclo*-P_5 ring moiety.

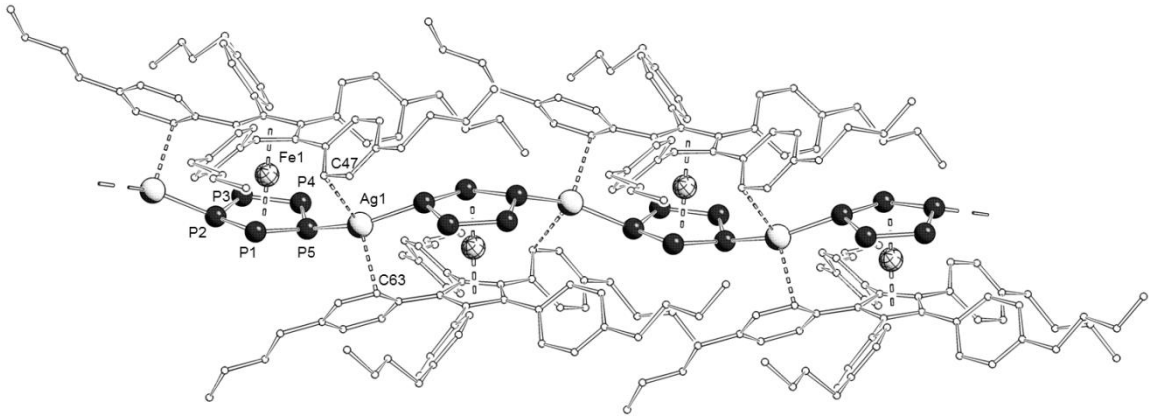

Figure 8.7 Section of the polymer chain $[\{(Cp^{BIG}Fe(\eta^5\text{-}P_5)\}Ag]_n^{n+}$ in **3** in the crystal. For clarity reasons the C atoms are shown in 'wire-or-stick' model and H atoms and $[Al\{OC(CF_3)_3\}_4]$ counter anions are omitted. Selected bond lengths [Å] and angles [°]: P1-P2 2.101(3), P2-P3 2.117(3), P3-P4 2.101(3), P4-P5 2.102(3), P1-P5 2.107(3), Ag1-P2 2.443(2), Ag1-P5 2.454(2), Ag1-C47 2.618(8), Ag1-C63 2.730(9), Ag1-$P_{5,plane}$ 0.8032(6), P1-P2-P3 111.6(1), P2-P3-P4 105.9(1), P3-P4-P5 107.0(1), P1-P5-P4 111.4(1), P2-P1-P5 103.1(1), P2-Ag1-P5 149.78(7), P2-Ag1-C47 108.8(2), P2-Ag1-C63 93.6(2), P5-Ag1-C47 91.3(2), P5-Ag1-C63 95.4(2), C47-Ag1-C63 120.1(3), Ag1-P2-P1 111.0(1), Ag1-P2-P3 129.0(1), Ag1-P5-P1 125.0(1), Ag1-P5-P4 115.5(1), Ag1-P5-$P_{5\text{-plane}}$ 20.72(6).

The diffusion of $[Cp^{BIG}Fe(\eta^5\text{-}P_5)]$ (**1b**) solutions (hexane/CH_2Cl_2) into CH_2Cl_2 solutions of $[\{Ag(CH_2Cl_2)\}Al\{OC(CF_3)_3\}_4]$ results in the formation and crystallization of green bars of the one-dimensional polymer $[\{Cp^{BIG}Fe(\eta^5\text{-}P_5)\}Ag]_n[Al\{OC(CF_3)_3\}_4]_n$ (**3**) (*Figure 8.7*). Notably, the repeating unit can be described as 1:1 adduct of the two starting materials, but with CH_2Cl_2 elimination from the silver salt. In contrast, we have shown recentl that the sterically less demanding pentaphosphaferrocene moiety **1a** forms a 1D polymer $[\{Cp^*Fe(\eta^5\text{-}P_5)\}_2Ag]_n[Al\{OC(CF_3)_3\}_4]_n$ (**4**) containing a 2:1 ratio of **1a** and Ag^+.[4h] A similar arrangement of four molecules **1b** around silver cations is prevented by the bulkiness of the Cp^{BIG} ligand.

The bright green needle shaped crystals were analyzed by X-ray diffraction. The Ag^I cations are coordinated by two molecules of **1b** and each *cyclo*-P_5 ligand coordinates in a 1,3-coordination mode to two Ag ions. Each Ag^+ is additionally coordinated by two *ortho*-C atoms from the phenyl groups from the Cp^{BIG} ligands with Ag–C distances of 2.618(8) Å and 2.730(9) Å. Compared to already known compounds with Ag-π interactions with phenyl groups, the contacts in **3** are in the upper region of distance.[12] The coordination of two P and two C atoms results in a heavily distorted tetrahedral environment for the Ag atoms. The angles on the Ag centers range from 91.3(2)° to 149.78(7)°, illustrating the distortion from an ideal tetrahedron (109.5°). Alternatively it can be seen as linear complex where the Ag^+ is deflected from linearity due to Ag-π interactions. The Ag atom is moved out of the $P_{5\text{-plane}}$ by 0.8032(6) Å (Ag1-P5-$P_{5\text{-plane}}$ 20.72(6)°) while the counterions are located in the dimples formed by the Cp^{BIG} ligands on the opposite site to the iron atoms.

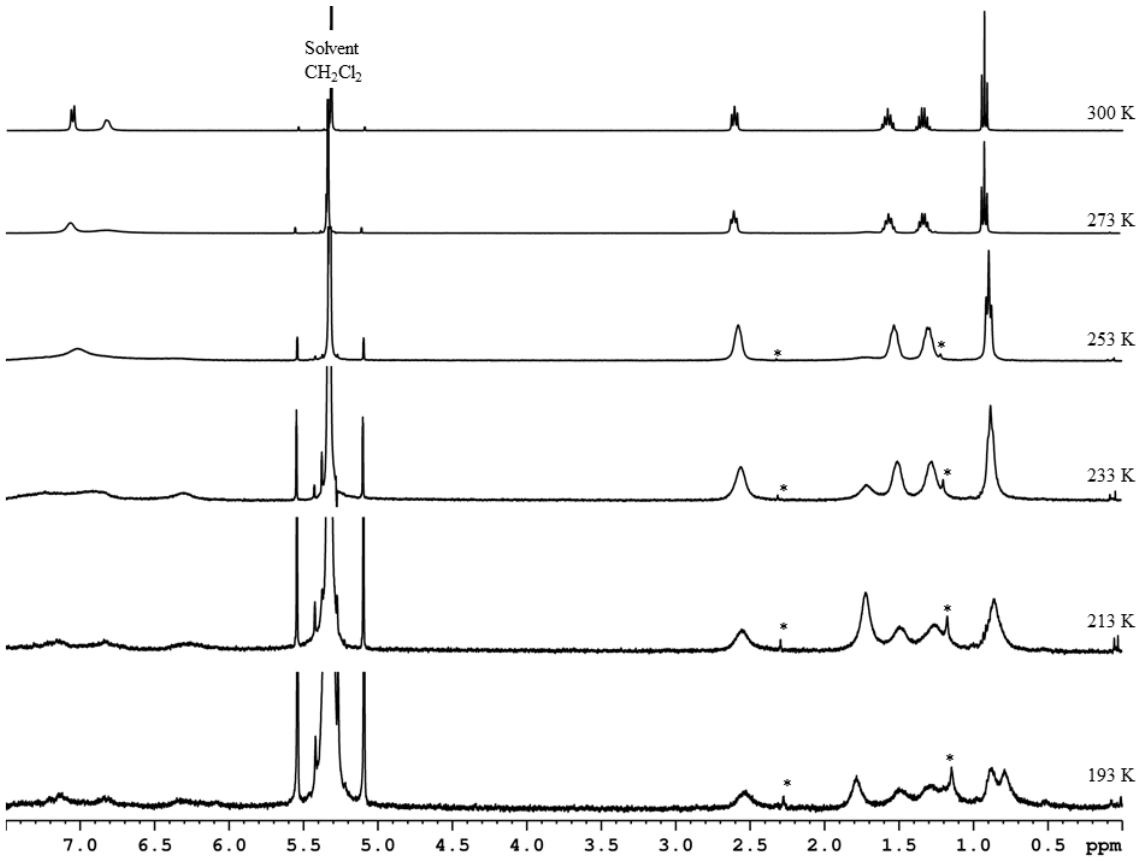

Figure 8.8 ^{1}H NMR spectra of **3** in CH_2Cl_2 at various temperatures. Intensities drop down at lower T why a higher magnification is used. Signal marked with an asterisk arise from small impurities.

Compound **3** is well soluble in CH_2Cl_2 and thf but insoluble in hexane. The $^{31}P\{^{1}H\}$ NMR spectrum of **3** in CH_2Cl_2 shows only one very broad signal at δ = 135 ppm ($\omega_{1/2} \approx 4000$ Hz), therefore NMR investigations at various temperatures were carried out. Cooling the sample leads to an additional broadening of the signal and at 253 K even no signal can be detected. Further cooling does not lead to observable changes. A highly fluxional behavior in solution is also described for **4**.[4h] However, the dynamic processes of **3** are much slower, which is the reason, that at r.t. no sharp singlet is observed like in the case of **4**. This can be explained by the coordination of one P and one C atom to Ag^{+}, which effectively results in a chelate-like ligand.

The ^{1}H NMR spectrum of **3** at r.t. shows one set of signals for a Cp^{BIG} ligand (*Figure 8.8*). Four sharp signals with the appropriate multiplicity in the aliphatic region for the ^{n}Bu groups are found (δ = 0.93, 1.34, 1.58 and 2.61 ppm). Two further signals are observed in the aromatic region for the phenyl groups, one broaden singlet at δ = 6.83 ppm and one doublet at δ = 7.06 ppm ($^{3}J_{HH}$ = 8.4 Hz). The observation of only one distinct set of signals is an indication for the fragmentation of the polymeric chain in solution as well as for an almost free rotation of the Cp^{BIG} ligand. The broadened signal at δ = 6.83 ppm most likely reflects interactions between the Ag^{+} ions and the π-systems of the phenyl groups, thus indicating that **1b** remains coordinated to silver even in solution. This is

indeed evident from the ESI mass spectrum (CH_2Cl_2/CH_3CN) with the three major peaks attributed to either $[(Cp^{BIG}FeP_5)_2Ag]^+$, $[(Cp^{BIG}FeP_5)Ag(CH_3CN)]^+$ and $[(Cp^{BIG}FeP_5)Ag]^+$, respectively. As anticipated, all signals in the ^1H NMR spectra get broader upon cooling, combined with an intensity decrease. At 253 K the signal at δ = 6.83 ppm is not observed anymore and two new signals at δ = 1.71 and 6.30 ppm arise. When reaching 233 K, the signal at δ = 7.06 ppm splits into two signals at δ = 6.9 and 7.2 ppm, respectively, while even the signal of the methyl groups at δ = 0.93 ppm splits into two at 193 K. The relative integral ratio of the signal at δ = 1.71 and 2.61 ppm changes in favor of the signal at δ = 1.71 ppm (at 193 K: 1.15:1). These observations suggest a rather hindered Cp^{BIG} rotation at low temperatures, even though pronounced aggregation/polymerization or intensity losses due to precipitation could also occur. Hence, the effective concentration of **3** in solution is lowered.

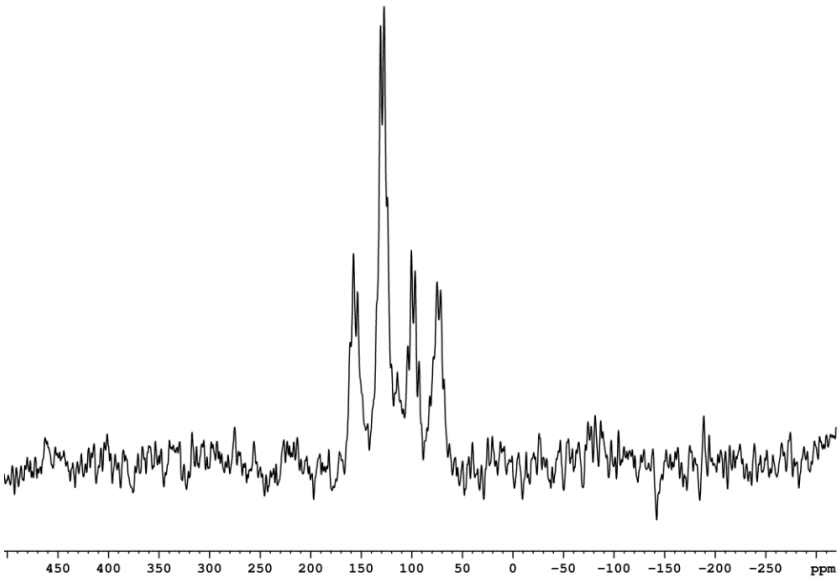

Figure 8.9 $^{31}P\{^1H\}$ MAS NMR spectrum of **3** at 298 K.

The $^{31}P\{^1H\}$ MAS NMR spectrum of **3** shows four multiplets at δ = 73.4, 98.8, 129.3 and 157.6 ppm, respectively, in a 1:1:2:1 integral ratio, reflecting the *cyclo*-P_5 moiety (*Figure 8.9*). Though an absolute assignment of the signals is not possible at this stage, it appears reasonable to attribute the two Ag^+ coordinated sites P2 and P5 to the peak at δ = 129.3 ppm.

In summary, we presented the synthesis and characterization of two novel polymeric coordination compounds with mono-cationic coinage metal salts: $[\{Cp^*Fe(\eta^5\text{-}P_5)\}\{Cu(GaCl_4)\}_2]_n$ (**2**) and $[\{Cp^{BIG}Fe(\eta^5\text{-}P_5)\}Ag]_n[Al\{OC(CF_3)_3\}_4]_n$ (**3**), in which the respective 1,2,3,4- and 1,3-coordination modes of both P_5 ligands is rather uncommon. In combination with pentaphosphaferrocene **1a** the versatile counterion $(GaCl_4)^-$ prefers coordination to Cu and a 2D network with sheet-like structure is formed. Using the sterically much more demanding Cp^{BIG} structural motifs, which were realized with Cp*, cannot be formed due to the space requirements of **1b**. Hence, the formation of a

hitherto unknown 1D polymer is observed. Its positive charges are balanced by rather weakly coordinating anions $[Al\{OC(CF_3)_3\}_4]$, which separate the strands from each other. Since in both cases at least partial depolymerization was found in solution, the compounds were additionally characterized by solid state NMR spectroscopy.

8.3 Experimental Part

General Remarks:

All experiments were carried out under an atmosphere of dry argon or nitrogen using glovebox and Schlenk techniques. Solvents were purified, dried and degassed prior to use. $[Cp^*Fe(\eta^5\text{-}P_5)]$,[1] $Cu(GaCl_4)$,[5b,13] $[\{Ag(CH_2Cl_2)\}Al\{OC(CF_3)_3\}_4]$[14] and $[Cp^{BIG}Fe(\eta^5\text{-}P_5)]$[7] were prepared according to literature procedure. The NMR spectra were measured on a Bruker Avance 300, 400 or 600 spectrometer. The solid state NMR spectra of **2** were measured on a Bruker Avance III 300 and Avance 500 spectrometer. The solid state NMR spectra of **3** were measured on a Bruker Avance 300. ESI-MS spectra were measured on a ThermoQuest Finnigan MAT TSQ 7000 mass spectrometer. The elemental analyses were determined on a Vario EL III apparatus.

Synthesis of $[\{Cp^*Fe(\eta^5\text{-}P_5)\}\{Cu(GaCl_4)\}_2]_n$ (2):

A turbid colorless solution of $Cu(GaCl_4)$ (80 mg, 290 µmol) in CH_2Cl_2 (12 mL) is layered with a green solution of $[Cp^*Fe(\eta^5\text{-}P_5)]$ (**1a**) (50 mg, 145 µmol) in toluene (10 mL) in a long thin Schlenk tube. The phase boundary colors yellow, the turbid solution turns clear and crystal growth of **2** can be obtained within one day. After complete diffusion the mother liquor is decanted. The yellow-golden needles are washed with hexane and CH_2Cl_2 and dried *in vacuo*.

Yield: 119 mg (133 µmol, 92%)

^{1}H NMR (CD_3CN): δ [ppm] = 1.45 (s, Cp*).

$^{31}P\{^1H\}$ NMR (CD_3CN): δ [ppm] = 143.4 (s, P_5).

Positive ion ESI-MS (CH_2Cl_2): *m/z* (%) = 952.6 (1) $[\{Cp^*Fe(\eta^5\text{-}P_5)\}_2Cu_3Cl_2]^+$, 854.7 (4) $[\{Cp^*Fe(\eta^5\text{-}P_5)\}_2Cu_2Cl]^+$, 754.8 (100) $[\{Cp^*Fe(\eta^5\text{-}P_5)\}_2Cu]^+$, 449.9 (52) $[\{Cp^*Fe(\eta^5\text{-}P_5)\}Cu(CH_3CN)]^+$), 408.9 (5) $[\{Cp^*Fe(\eta^5\text{-}P_5)\}Cu]^+$.

Negative ion ESI-MS (CH_2Cl_2): *m/z* (%) = 210.8 (100) $[GaCl_4]^-$.

Elemental analysis: Calculated (%) for $[C_{10}H_{15}Cl_8Cu_2FeGa_2P_5]$ (896 g/mol): C 13.40, H 1.69; found: C 13.61, H 2.19.

Synthesis of $[\{Cp^{BIG}Fe(\eta^5\text{-}P_5)\}Ag]_n[Al\{OC(CF_3)_3\}_4]_n$ (3):

A solution of [{Ag(CH_2Cl_2)}Al{$OC(CF_3)_3$}$_4$] (163 mg, 140 µmol) in CH_2Cl_2 (2 mL) is layered with a solution of [$Cp^{BIG}Fe(\eta^5\text{-}P_5)$] (60 mg, 64 µmol) in a mixture of hexane (3 mL) and CH_2Cl_2 (1 mL). After complete diffusion bright green needle shaped crystals are obtained. The mother liquor is decanted and the crystals are washed with hexane and dried *in vacuo*. The crystals are covered with a brownish amorphous substance, which could not be removed even not by recrystallization.

Yield: 56 mg (28 µmol, 43%)

^{1}H NMR (CD_2Cl_2): δ [ppm] = 0.93 (t, $^3J_{HH}$ = 7.4 Hz, 15H, ^{n}Bu), 1.34 (sext, $^3J_{HH}$ = 7.4 Hz, 10H, ^{n}Bu), 1.58 (m, 10H, ^{n}Bu), 2.61 (t, $^3J_{HH}$ = 7.8 Hz, 10H, ^{n}Bu), 6.83 (s-br, $\omega_{1/2}$ = 18 Hz, 10H, Ph), 7.06 (d, $^3J_{HH}$ = 8.4 Hz, 10H, Ph).

^{31}P{^{1}H} NMR (CD_2Cl_2): δ [ppm] = 135 (very broad, $\omega_{1/2} \approx$ 4000 Hz).

^{31}P{^{1}H} MAS NMR: δ [ppm] = 73.4 (m, 1P), 98.8 (m, 1P), 129.3 (m, 2P), 157.6 (m, 1P).

^{19}F{^{1}H} NMR (CD_2Cl_2): δ [ppm] = -75.59 (s).

Positive ion ESI-MS (CH_3CN/CH_2Cl_2): *m/z* (%) = 1981.5 (40) [$(Cp^{BIG}FeP_5)_2Ag]^+$, 1084.4 (100) [$(Cp^{BIG}FeP_5)Ag(CH_3CN)]^+$, 1043.4 (38) [$(Cp^{BIG}FeP_5)Ag]^+$.

Negative ion ESI-MS (CH_3CN/CH_2Cl_2): *m/z* (%) = 967.1 (100) [Al{$OC(CF_3)_3$}$_4$]$^-$.

Elemental analysis: Calculated (%) for [$C_{71}H_{65}AgAlF_{36}FeO_4P_5$] (2012 g/mol): C 42.39, H 3.26; found: C 40.48, H 3.17.

8.4 Crystallographic Details

The structures were solved by direct methods of the program SIR-92 (for **2**)[15] or chargeflipping methods with the program Superflip (for **3**)[16] and refined with the least square method on F^2 employing SHELXL-97[17] with anisotropic displacements for non-H atoms. Hydrogen atoms were located in idealized positions and refined isotropically according to the riding model. The crystal structure of compound **3** was refined as an inversion twin.

CCDC-993425 (**2**) and CCDC-993426 (**3**) contain the supplementary crystallographic data for this paper. These data can be obtained free of charge at www.ccdc.cam.ac.uk/conts/retrieving.html (or from the Cambridge Crystallographic Data Center, 12 Union Road, Cambridge CB2 1EZ, UK; Fax: + 44-1223-336-033; e-mail: deposit@ccdc.cam.ac.uk).

Table 8.1 Experimental details for compound **2** and **3**.

Crystal data	2	3
CCDC Code	CCDC-993425	CCDC-993426
Chemical formula	$C_{10}H_{15}Cl_8Cu_2FeGa_2P_5$	$C_{71}H_{65}AgAlF_{36}FeO_4P_5$
M_r	2011.78	2011.78
Crystal system, space group	orthorhombic, *Pbca*	orthorhombic, *Pna*2$_1$

Temperature (K)	123	123
a, *b*, *c* (Å)	19.6453(2), 12.6984(1), 21.3504(3)	31.4504(5), 17.9259(3), 14.7931(2)
α, β, γ (°)	90, 90, 90	90, 90, 90
V (Å^3)	5326.15(10)	8340.0(2)
Z	8	4
F(000)	3456	4032
Radiation type	Cu K_α	Cu K_α
μ (mm^{-1})	18.556	5.438
Crystal color and shape	yellow rod	pale green bar
Crystal size (mm)	0.4842 × 0.0632 × 0.0337	0.2590 × 0.0670 × 0.0324
Data collection		
Diffractometer	SuperNova, Single source at offset, Atlas diffractometer	SuperNova, Single source at offset, Atlas diffractometer
Absorption correction	analytical	analytical
T_{min}, T_{max}	0.126, 0.641	0.379, 0.841
No. of measured, independent and observed [$I > 2\sigma(I)$] reflections	28148, 5253, 4601	60877, 14463, 12920
R_{int}	0.0517	0.0675
Range of *h*, *k*, *l*	*h* = -24→24, *k* = -15→15, *l* = -25→21	*h* = -37→39, *k* = -22→21, *l* = -16→18
Refinement		
$R[F^2 > 2\sigma(F^2)]$, $wR(F^2)$, *S*	0.031, 0.085, 0.996	0.0741, 0.2080, 1.105
No. of reflections	5253	14463
No. of parameters	276	1088
No. of restraints	0	51
H-atom treatment	H-atom parameters constrained	H-atom parameters constrained
$\Delta\rangle_{max}$, $\Delta\rangle_{min}$ (e Å^{-3})	0.84/-0.75	2.37/ -0.71
Flack parameter[18]		0.273(7)

8.5 Author Contributions

- The synthesis and characterization (including X-ray structural analysis, excluding MAS NMR investigations) of compound **2** was performed by Claudia Heindl
- The synthesis and characterization (including X-ray structural analysis, excluding MAS NMR investigations) of compound **3** was performed by Dr. Sebastian Heinl
- The manuscript (including figures and graphical abstract) was written by Claudia Heindl with the following exceptions:
- The discussion of compound **3** (including figures) was written by Dr. Sebastian Heinl

- MAS NMR investigations of **2** and their description were performed by David Lüdeker and PD Dr. Gunther Brunklaus
- MAS NMR investigations of **3** were performed by Prof. Werner Kremer
- This chapter is also part of the dissertation thesis of Dr. Sebastian Heinl (University of Regensburg, 2014)

8.6 References

[1] O. J. Scherer, T. Brück, *Angew. Chem.* **1987**, *99*, 59.

[2] a) E. C. Constable, C. E. Housecroft, *Chem. Soc. Rev.* **2013**, *42*, 1429; b) P. J. Lusby, *Annu. Rep. Prog. Chem., Sect. A: Inorg. Chem.* **2013**, *109*, 254; c) Y. E. Alexeev, B. I. Kharisov, T. C. H. García, A. D. Garnovskii, *Coord. Chem. Rev.* **2010**, *254*, 794.

[3] a) M. Scheer, *Dalton Trans.* **2008**, 4372; b) E.-M. Rummel, M. Eckhardt, M. Bodensteiner, E. V. Peresypkina, W. Kremer, C. Groeger, M. Scheer, *Eur. J. Inorg. Chem.* **2014**, 1625; c) B. Attenberger, S. Welsch, M. Zabel, E. Peresypkina, M. Scheer, *Angew. Chem. Int. Ed.* **2011**, *50*, 11516; d) L. J. Gregoriades, B. K. Wegley, M. Sierka, E. Brunner, C. Groeger, E. V. Peresypkina, A. V. Virovets, M. Zabel, M. Scheer, *Chem. Asian J.* **2009**, *4*, 1578.

[4] a) C. Schwarzmaier, A. Schindler, C. Heindl, S. Scheuermayer, E. V. Peresypkina, A. V. Virovets, M. Neumeier, R. Gschwind, M. Scheer, *Angew. Chem. Int. Ed.* **2013**, *52*, 10896; b) A. Schindler, C. Heindl, G. Balázs, C. Groeger, A. V. Virovets, E. V. Peresypkina, M. Scheer, *Chem. Eur. J.* **2012**, *18*, 829; c) F. Dielmann, A. Schindler, S. Scheuermayer, J. Bai, R. Merkle, M. Zabel, A. V. Virovets, E. V. Peresypkina, G. Brunklaus, H. Eckert, M. Scheer, *Chem. Eur. J.* **2012**, *18*, 1168; d) S. Welsch, C. Groeger, M. Sierka, M. Scheer, *Angew. Chem. Int. Ed.* **2011**, *50*, 1435; e) M. Scheer, A. Schindler, J. Bai, B. P. Johnson, R. Merkle, R. Winter, A. V. Virovets, E. V. Peresypkina, V. A. Blatov, M. Sierka, H. Eckert, *Chem. Eur. J.* **2010**, *16*, 2092; f) M. Scheer, A. Schindler, C. Groeger, A. V. Virovets, E. V. Peresypkina, *Angew. Chem. Int. Ed.* **2009**, *48*, 5046; g) M. Scheer, A. Schindler, R. Merkle, B. P. Johnson, M. Linseis, R. Winter, C. E. Anson, A. V. Virovets, *J. Am. Chem. Soc.* **2007**, *129*, 13386; h) M. Scheer, L. J. Gregoriades, A. V. Virovets, W. Kunz, R. Neueder, I. Krossing, *Angew. Chem. Int. Ed.* **2006**, *45*, 5689; i) J. Bai, A. V. Virovets, M. Scheer, *Science* **2003**, *300*, 781; j) J. Bai, A. V. Virovets, M. Scheer, *Angew. Chem. Int. Ed.* **2002**, *41*, 1737.

[5] a) L. C. Forfar, T. J. Clark, M. Green, S. M. Mansell, C. A. Russell, R. A. Sanguramath, J. M. Slattery, *Chem. Commun.* **2012**, *48*, 1970; b) H. Schmidbaur, W. Bublak, B. Huber, G. Reber, G. Müller, *Angew. Chem. Int. Ed.* **1986**, *25*, 1089.

[6] H. V. Ly, M. Parvez, R. Roesler, *Inorg. Chem.* 2006, *45*, 345.

[7] S. Heinl, G. Balázs, M. Scheer, *Phosphorus, Sulfur Silicon Relat. Elem*. 2014, *189*, 924.

[8] R. Peng, M. Li, D. Li, *Coord. Chem. Rev.* 2010, *254*, 1.

[9] www.webelements.com (26.02.2014)

[10] a) S. E. Ashbrook, J. McManus, M. J. Thrippelton, S. Wimperis, *Prog. Nucl. Magn. Reson. Spec.* 2009, *55*, 160; b) B. Thomas, S. Paasch, S. Steuernagel, K. Eichele, *Solid State Nucl. Magn. Reson.* 2001, *20*, 108.

[11] G. Brunklaus, J. C. C. Chan, H. Eckert, S. Reiser, T. Nilges, A. Pfitzner, *Phys. Chem. Chem. Phys.* 2003, *17*, 3768.

[12] The Ag–C distances roughly range between 2.45 Å and 2.85 Å based on CCDC structural database search.

[13] This compound was in-house available.

[14] I. Krossing, Chem*. Eur. J.* 2001, *7*, 490.

[15] A. Altomare, M. C. Burla, M. Camalli, G.L. Cascarano, C. Giacovazzo, A. Guagliardi, A. G. G. Moliterni, G. Polidori, R. Spagna, *J. Appl. Cryst.* 1999, *32*, 115.

[16] L. Palatinus, G. Chapuis, *J. Appl. Cryst.* 2007, *40*, 786.

[17] G. M. Sheldrick, *Acta Cryst. sect. A* 2008, A64, 112.

[18] H.D. Flack, *Acta Cryst. sect. A* 1983, A39, 876.

9. Diversity of Novel Hosts in Response to Cationic and Reactive Templates

C. Heindl, E. V. Peresypkina, A. V. Virovets, M. Scheer

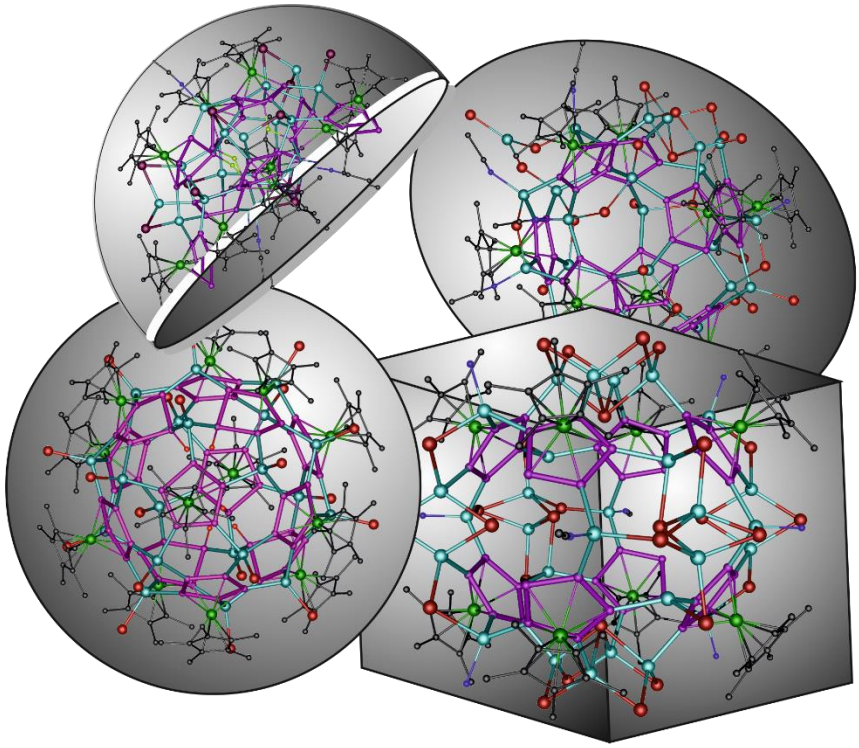

Abstract:

Pentaphosphaferrocene [Cp*Fe(η^5-P_5)] (**1a**) displays an excellent building block for the template-directed synthesis of spherical supramolecules. Herein, the self-assembly of **1a** with Cu(I) and Cu(II) halides in the presence of labile sandwich complexes, such as [$FeCp_2$][PF_6], [$CoCp_2$][PF_6], [$CoCp_2$] and [$Cr(C_6H_6)_2$] is reported. Their oxidation or reduction capacity, respectively, does not inhibit their template impact and for the first time cationic metallocenes ([$CoCp_2$]$^+$, [$Cr(C_6H_6)_2$]$^+$) are enclosed in organometallic host molecules. Furthermore, the flexibility and diversity of Cu halides in combination with **1a** is once again demonstrated, since unprecedented supramolecules are formed: For example, the involvement of six units of **1a** leads to two different spheres, which are arranged *via* the vertices of either a cube or of a square antiprism, respectively. On the other hand, a hemispherical-shaped scaffold is constructed by nine moieties of **1a**. To balance the positive charge of the guest molecules, anionic hosts are formed for the first time.

9.1 Introduction

The self-assembly of DNA strands or enzyme-substrate-interactions demonstrate that supramolecular chemistry is at least as old as humanity itself. During the last decades, this field of chemistry was successfully implemented in non-biological systems for the synthesis of large assemblies constructed by small building blocks *via* the self-assembly approach.[1] Particularly intriguing is the synthesis of discrete spheres, which can act as container for small molecules or ions.[2] Within this area, coordinative bonds turned out to be a powerful tool for the rational design of novel cages or capsules, largely with di- or tridentate N, O or S donor ligands as connecting moieties.[2,3]

In this manner, we have recently introduced pentaphosphaferrocenes [$Cp^RFe(\eta^5\text{-}P_5)$] (**1a**: Cp^R = Cp^* = $\eta^5\text{-}C_5Me_5$; **1b**: Cp^R = Cp^{Et} = $\eta^5\text{-}C_5Me_4Et$; **1c**: Cp^R = Cp^{Bn} = $\eta^5\text{-}C_5(CH_2C_6H_5)_5$; **1d**: Cp^R = Cp^{BIG} = $\eta^5\text{-}C_5(4\text{-}^nBuC_6H_4)_5$) in combination with Cu(I) halides capable of the formation of neutral nano-sized supramolecules with and beyond fullerene-like topology (*Figure 9.1*).[4] With phosphorus as donating element and a five-fold symmetry, the *cyclo*-P_5 ligand in **1a-d** ranks an outstanding position among the huge variety of building blocks. Notably, the received spheres are prime examples of template-directed syntheses and the flexible coordination behavior of CuX (X = Cl, Br, I) as well as of the P_5 ring gives rise to the adaptability of this system. Accordingly, different sizes of the templates lead to the formation of different supramolecules exhibiting template specific cavities (*Figure 9.1*).

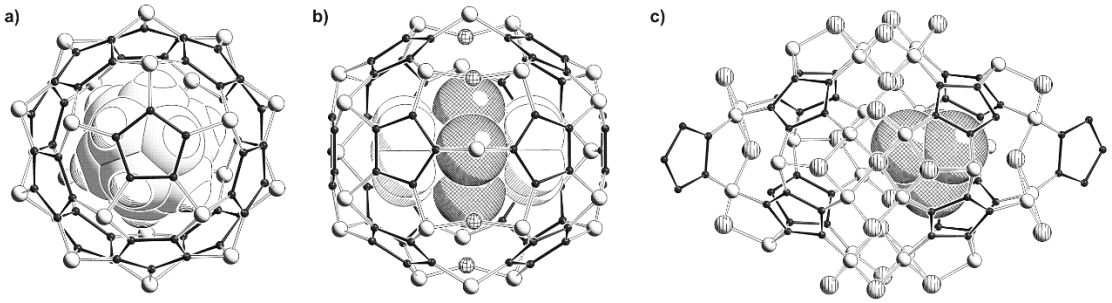

Figure 9.1 Selected scaffolds of spherical supramolecules composed by **1a**: a) 80-vertex scaffold incorporating *o*-carborane; b) 90-vertex scaffold incorporating [$(CpCr)_2(\mu,\eta^{5:5}\text{-}As_5)$]; c) 100-vertex scaffold incorporating P_4.

Comparing the template properties, not only the incorporation of stable molecules e.g. ferrocene,[4d] *o*-carborane[4g] (*Figure 9.1*a) and C_{60}[4h] succeeded, but also otherwise labile species like white phosphorus and yellow arsenic molecules could be stabilized by enclosure in a supramolecular host (*Figure 9.1*c).[4c] To expand the scope of application, we were interested in the variation of two further properties of the possible guest molecules. So far all incorporated molecules are neutral compounds, which are compatible with the neutral hosts. Hence, the

question arises, whether charged templates such as $[FeCp_2][PF_6]$ or $[CoCp_2][PF_6]$ can also be used for a template-directed formation of supramolecules.

$[MCp_2]^+$ cations can be included into cavities of various organic cavitands like calixarenes,[5] thiacalixarenes,[6] pilararenes,[7] cyclodextrines[8] and cucurbiturils.[9] Salts of $[CoCp_2]^+$ can also intercalate in some layered inorganic compounds, like $MoPS_3$ or $FePS_3$,[10] layered sulphides and selenides[11] or mesoporous niobium oxide.[12] To the best of our knowledge, there are no examples of inclusion of $[MCp_2]^+$ cations into cavities inside inorganic or organometallic molecules.

Furthermore, even though labile species (e.g. As_4, P_4) turned out to be appropriate guests for pentaphosphaferrocene-derived supramolecules, they have never shown reactivity towards the building blocks. Yet, particularly Cu in the oxidation state +1 is known for its redox activity. This fact caused our interest in the practicability of reducing agents such as $[CoCp_2]$ or $[Cr(C_6H_6)_2]$ as guests.

Herein we report on the template-controlled self-assembly processes of $[Cp^*Fe(\eta^5\text{-}P_5)]$ (**1a**) and CuX (X = Br, I) and $CuBr_2$, respectively, in presence of either $[FeCp_2][PF_6]$, $[CoCp_2][PF_6]$, $[CoCp_2]$ or $[Cr(C_6H_6)_2]$ as templates. Some self-assembly processes include oxidation or reduction of the template and subsequent incorporation of the cationic sandwich complex in an inorganic host for the first time. Thereby different supramolecules are obtained, some of which exhibiting unprecedented scaffolds and shapes:

$[FeCp_2]@[\{Cp^*Fe(\eta^5\text{-}P_5)\}_{12}(CuBr)_{17.3}]$ (**3**),

$[CoCp_2]^+@[\{Cp^*Fe(\eta^5\text{-}P_5)\}_8Cu_{24.25}Br_{28.25}(CH_3CN)_6]^{4-}\cdot 3[CoCp_2]^+$ (**4**),

$[\{Cp^*Fe(\eta^5\text{-}P_5)\}_9\{Cp^*Fe(\eta^4\text{-}P_5OH)\}_3(CuBr)_{20}]^{3-}\cdot 3[CoCp_2]^+$ (**5**),

$\{[Cp_2Co]^+@[\{Cp^*Fe(\eta^5\text{-}P_5)\}Cu_{24.4}I_{26.4}(CH_3CN)_8]^{2-}\}\{[Cp_2Co]^+@[\{Cp^*Fe(\eta^5\text{-}P_5)\}_8Cu_{28}I_{28}(CH_3CN)_{9.8}]\}$ (**6**),

$[\{Cp^*Fe(\eta^5\text{-}P_5)\}_3\{(Cp^*Fe(\eta^4\text{-}P_5))_2O\}_3Cu_{16}I_{10}(CH_3CN)_7]\cdot 3.9CH_3CN$ (**7**) and

$[Cr(C_6H_6)_2]^+_{0.6}@[\{Cp^*Fe(\eta^5\text{-}P_5)\}_{12}Cu_{17.925}Br_{18.525}]$ (**8**).

9.2 Results and Discussion

Since ferrocene is known as an appropriate guest molecule for fullerene-like hosts, the choice of a cationic template fell on the ferricinium cation $[FeCp_2]^+$. When a solution of **1a** in CH_2Cl_2 is layered carefully with a solution of $[FeCp_2][PF_6]$ and CuBr in acetonitrile, the formation of brown plates of the 2D polymer $[(\mathbf{1a})CuBr]_n$[13] (**2a**) and big dark blocks of $[FeCp_2]@[\{Cp^*Fe(\eta^5\text{-}P_5)\}_{12}(CuBr)_{17.3}]$ (**3**) at the phase boundary can be observed already after one day. The X-ray structural analysis of **3**, crystallizing in the trigonal space group $R\bar{3}$, reveals a supramolecule constructed by 12 *cyclo*-P_5 ligands and 30 $\{Cu_2P_4\}$ hexagons resembling the I_h-C_{80} fullerene topology (*Figure 9.2*). Due to CuBr vacancies, the ideal scaffold of 20 CuBr units is reduced to an average of

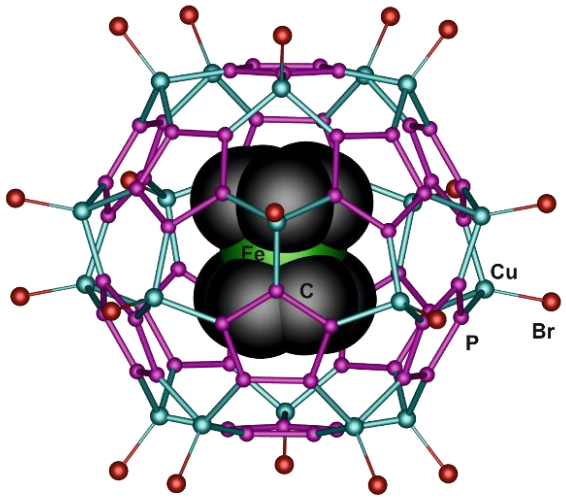

Figure 9.2 Molecular structure of **3**. {Cp*Fe} ligands, minor parts of disorder and solvent molecules are omitted for clarity. The template is shown in the space-filling model.

17.6 moieties in **3**.[14] This idealized 80-vertex host molecule containing CuBr already appeared once when *o*-carborane is encapsulated (*Figure 9.1*a).[15] Furthermore, the well-known Cl derivative of this sphere is capable of the trapping of several templates such as *o*-carborane,[4g] $[CpCr(\eta^5\text{-}As_5)]$[4d] and $[FeCp_2]$,[4d] though crystallizing in the cubic crystal system. Also in **3**, one molecule of the sandwich complex is found within the cavity of the host. Surprisingly, no $[PF_6]^-$ or an additional Br^- as counterion is present, obviously the neutral metallocene is encapsulated. Diamagnetic ferrocene and the paramagnetic ferricinium cation can easily be distinguished by EPR and NMR spectroscopy. The absence of a signal in the EPR spectrum and the presence of a signal in the ^1H NMR spectrum (δ = 4.16 ppm) give evidence of the incorporation of neutral ferrocene. The reduction of $[FeCp_2]^+$ to $[FeCp_2]$ is most probably enabled by oxidizing Cu^+ to Cu^{2+}.

Hence, for the incorporation of a cation a more stable complex might be required. Therefore, the 18 valence electron complex $[CoCp_2][PF_6]$ was used as template. Applying the same conditions as before, the formation of brown plates of **2a** and smaller reddish crystals of $[CoCp_2]^+$@$[\{Cp^*Fe(\eta^5\text{-}P_5)\}_8Cu_{24.25}Br_{28.25}(CH_3CN)_6]^{4-}\cdot 3[CoCp_2]^+$ (**4**) can be observed after a few days. The X-ray structural analysis of **4** reveals an unprecedented supramolecule beyond the fullerene topology. It contains eight molecules of **1a**, which are arranged by the vertices of a square antiprism (*Figure 9.4*a). This overall number of P_5 units in a sphere is exceptional, since the fullerene-like species mostly contain 12 *cyclo*-P_5 ligands.[4] Strictly speaking, there is only one example, $C_6H_4Cl_2$@$[\{Cp^*Fe(\eta^5\text{-}P_5)\}_8(CuI)_{28}(CH_3CN)_{10}]$, which unfortunately has been observed only once.[16] Another CuI-containing example is known with 10 P_5 rings, two of which are 'terminal' ligands and the remaining eight construct a cube-like scaffold (*Figure 9.1*c).[4c]

The CuBr scaffold in **4** consists of a middle belt, which is completed from above and below by a bowl-like $\{Cu_4Br_5\}^-$ fragment, respectively (*Figure 9.3*). This bowl-motif is also part of a CuI-containing supramolecule (*Figure 9.1*c).[4c] The severely disordered middle belt in **4** has a summarized composition of $Cu_{16.25}Br_{18.25}(CH_3CN)_6$. It can further be split up into anionic $\{Cu_2(\mu_3\text{-}$

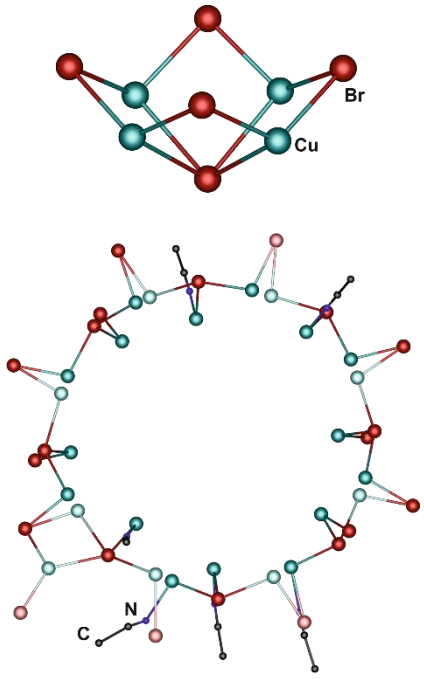

Figure 9.3 Bowl-like $\{Cu_4Br_5\}^-$ fragment (top) and middle ring (bottom) of the scaffold of **4**. Minor parts of disorder are displayed in brighter color.

Br)$Br_2\}^-$, neutral $\{Cu_2(\mu_3\text{-}Br)Br(CH_3CN)\}$ and cationic $\{Cu_2(\mu_3\text{-}Br)(CH_3CN)_2\}^+$ fragments with partial occupancies of some Cu and Br positions (*Figure 9.3*). In total (middle belt plus two 'bowls'), a sum formula of $[\{Cp^*Fe(\eta^5\text{-}P_5)\}_8Cu_{24.25}Br_{28.25}(CH_3CN)_6]^{4-}$ results for the inorganic host. The negative charge is balanced by four $[CoCp_2]^+$ cations. Three of them are located in the outer sphere; the fourth one exactly fits into the cavity of the supramolecule (*Figure 9.4*a). Hence, the building blocks **1a** and CuBr adapt to the cationic template by forming an unprecedented anionic host, which displays the first inorganic assembly incorporating $[Cp_2M]^+$.

Encouraged by this result, we were interested in the potential of neutral $[CoCp_2]$ as a template. For this purpose, a dark green solution of **1a** and $CoCp_2$ (molar ratio **1a**:$CoCp_2$ = 3:1) in CH_2Cl_2 is layered with a solution of CuBr in CH_3CN. In doing so, the formation of a metallic mirror can be observed, most likely of Cu^0. Nonetheless, after some days besides the formation of bright brown plates of the 2D polymer **2a**[13] also small red plates can be observed. The X-ray structural analysis of these plates reveals the same charged sphere **4**, as it has been observed using $[CoCp_2][PF_6]$. Having 19 valence electrons, $[CoCp_2]$ displays a strong and widely used reducing agent. Hence, Cu^+ is reduced by the metallocene to give elemental Cu and the hereby formed $[CoCp_2]^+$ is again incorporated to give **4** in 51% crystalline yield.

To avoid the loss of copper during this reaction, CuBr was exchanged by its corresponding Cu(II) salt. And in fact, the self-assembly process again leads to the formation of small plates of **4** after reduction of Cu(II) to Cu(I). Unfortunately, the yield could not be increased by this method, since the polymeric by-product **2a**[13] is also formed during this reaction.

These results nicely demonstrate the suitability of $[CoCp_2]^+$ as template, since the novel supramolecule **4** is formed in all three systems: **1a**/$[CoCp_2][PF_6]$/CuBr, **1a**/$[CoCp_2]$/CuBr and **1a**/$[CoCp_2]$/$CuBr_2$.

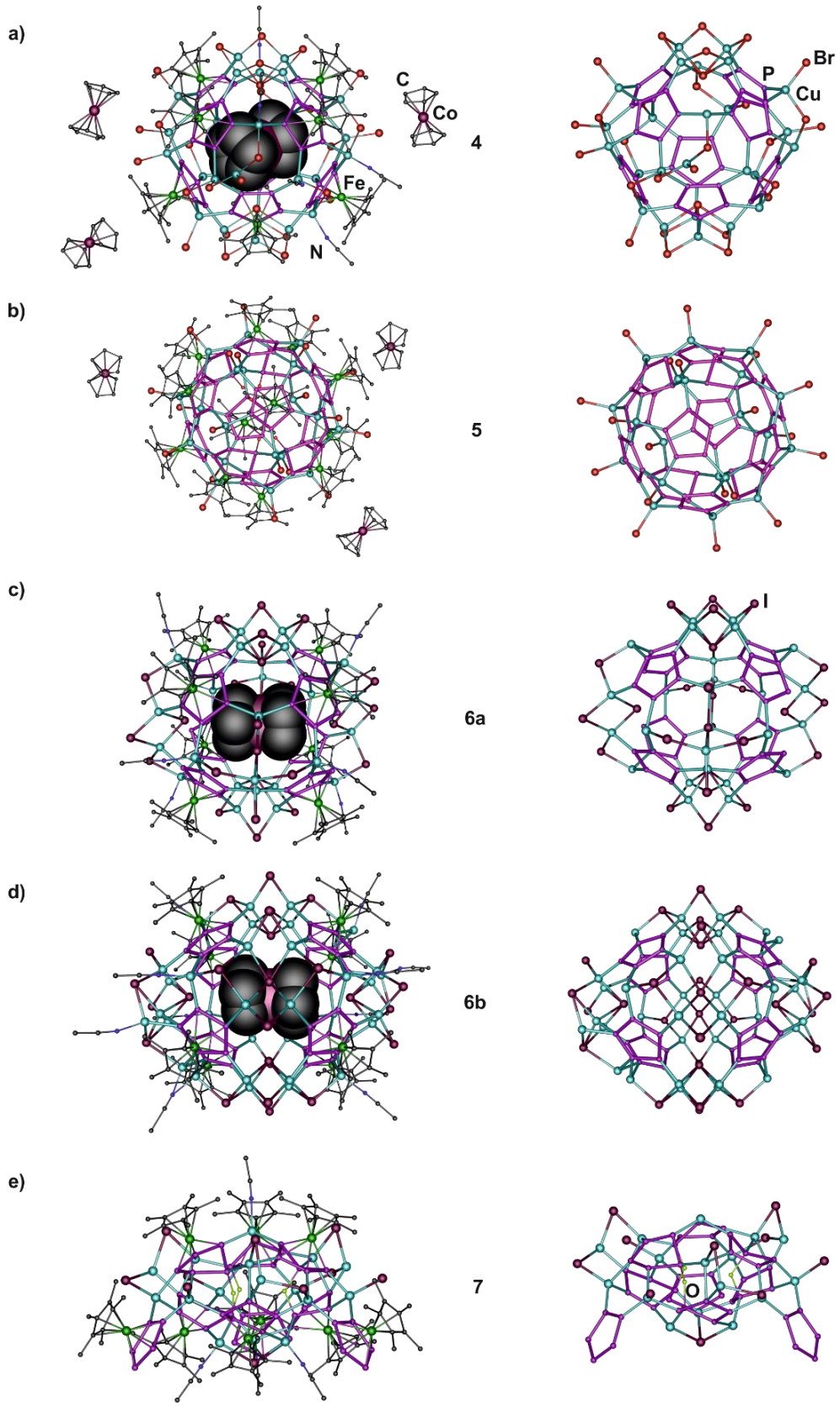

Figure 9.4. Scaffolds (right) and complete molecular structures (left) of the obtained supramolecules with $[CoCp_2]/[CoCp_2][PF_6]$ as template: a) **4**; b) **5**; c) **6a**; d) **6b**; e) **7**. Hydrogen atoms, minor parts of disorder and solvent molecules are omitted for clarity. Incorporated templates are displayed in the space-filling model.

However, in rare cases, a different crystalline phase (**5**) was found in the reaction mixture, which crystallizes as very small black blocks in the trigonal space group *R*$\bar{3}$m. Its molecular structure reveals the 80-vertex nanoball $[\{Cp^*Fe(\eta^5\text{-}P_5)\}_9\{Cp^*Fe(\eta^4\text{-}P_5OH)\}_3(CuBr)_{20}]^{3-}\cdot 3[CoCp_2]^+$ (**5**) constructed by 12 molecules of **1a** and 20 CuBr units (*Figure 9.4*b). This host molecule resembles the known I_h-C_{80} analogue (*Figure 9.1*a), which has been observed several times, e.g. in **3**.[4] However, the special feature of **5** is an envelope conformation of three *cyclo*-P_5 units, in which one P atom is displaced out of the plane by roughly 1.1 Å (*Figure 9.5*a). It is additionally coordinated by a monoatomic substituent. The residual electron density and the bond lengths most likely assign it to be an oxygen atom of a hydroxyl group. This ligand might derive from traces of water in the solvent, since compound **5** cannot be reproduced, when accurately dried solvent (H_2O content < 10 ppm) is used. Furthermore, **5** can be synthesized, when additional H_2O is added to the reaction mixture, which supports this assumption. As a result, these $[Cp^*Fe(\eta^4\text{-}P_5OH)]$ building blocks bear a negative charge,[17] which is balanced by three $[CoCp_2]^+$ located in the outer sphere of the nanoball (*Figure 9.4*b). Furthermore, the $[Cp^*Fe(\eta^4\text{-}P_5OH)]$ moieties require more space, making the encapsulation of the template or of solvent molecules impossible.

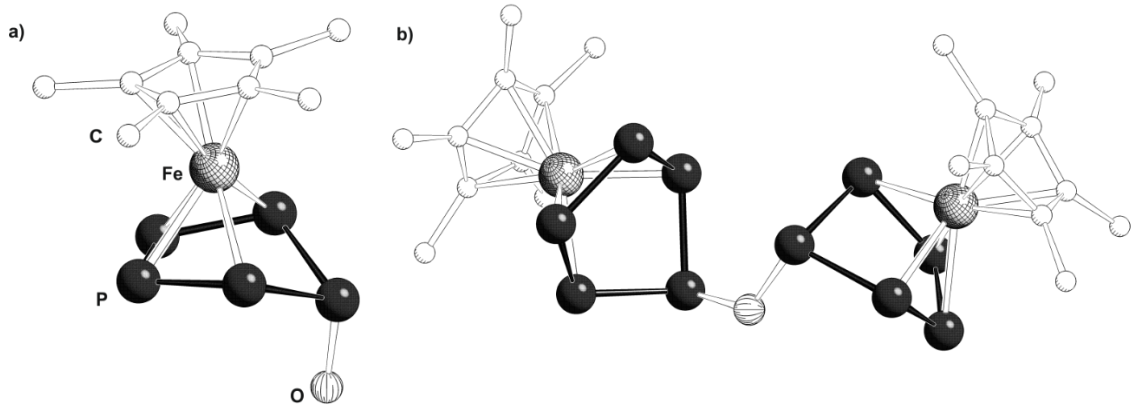

Figure 9.5 Envelope conformation of some *cyclo*-P_5 rings in a) **5** and b) **7**.

On the other hand, the analogous reaction route using CuI leads to the growth of brown plates of the polymer $[(\mathbf{1a})CuI]_n$ (**2b**)[13] and small red blocks of $\{[Cp_2Co]^+@[\{Cp^*Fe(\eta^5\text{-}P_5)\}_8\{Cu_4I_5\}_2\{Cu_2I_4\}_4\{CuI\}_{0.4}\{Cu(CH_3CN)\}_8]^{2-}\}\{[Cp_2Co]^+@[\{Cp^*Fe(\eta^5\text{-}P_5)\}_8\{Cu_4I_5\}_{2.6}\{Cu_2I_4\}_2\{Cu_4I_5(CH_3CN)\}_{1.8}\{Cu(CH_3CN)\}_8]\}$ (**6**) at the phase boundary. Compound **6** crystallizes in the monoclinic space group $P2_1/c$. Its structure reveals two different supramolecular hosts, the anionic host molecule $[\{Cp^*Fe(\eta^5\text{-}P_5)\}_8\{Cu_4I_5\}_2\{Cu_2I_4\}_4\{CuI\}_{0.4}\{Cu(CH_3CN)\}_8]^{2-}$ (**6a**) (*Figure 9.4*c) and the neutral host sphere $[\{Cp^*Fe(\eta^5\text{-}P_5)\}_8\{Cu_4I_5\}_{2.6}\{Cu_2I_4\}_2\{Cu_4I_5(CH_3CN)\}_{1.8}\{Cu(CH_3CN)\}_8]$ (**6b**) (*Figure 9.4*d). Both consist of eight units of **1a**, four of them in a 1,2,3,4,5- and the other four in a 1,2,3,4-coordination mode of the *cyclo*-P_5 ligand. The mutual arrangement of the **1a** moieties in the supramolecule is reminiscent of a cube similarly to the previously mentioned CuI-containing

supramolecule (*Figure 9.1*c).[4c] The extended CuI-framework can be represented for clarity as different fragments. In **6a**, four $\{Cu_2I_4\}^{2-}$ fragments appear as two different structural isomers and are linked by additional $\{Cu(CH_3CN)\}^+$ groups and partly occupied {CuI} units. From above and below the sphere is completed by bowl-like $\{Cu_4I_5\}^-$ fragments as it is observed in **4** and a supramolecule containing ten P_5 units (also see *Figure 9.3* top).[4c] Hence, for the host **6a** the simplified formula $[(\mathbf{1a})_8Cu_{24.4}I_{26.4}(CH_3CN)\}_8]^{2-}$ with a 91-vertex scaffold results (*Figure 9.4*c right). Its elongated cavity ranges from 4.9 Å in width and 6.7 Å in length and therefore perfectly suits for the encapsulation of a cobaltocenium cation, which has a length of 6.6 Å. This leads to a total charge of -1 for $[CoCp_2]^+$@**6a** (host: -2, guest: +1). In **6b**, instead of some $\{Cu_2I_4\}^{2-}$ fragments a bowl-like $\{Cu_4I_5\}^-$ and $\{Cu_4I_5(CH_3CN)\}$ fragments prevail to construct a neutral 96-vertex scaffold of the sum formula $[(\mathbf{1a})_8(Cu_{28}I_{28}(CH_3CN)_{9.8}]$ (*Figure 9.4*d right). The inner diameter (4.9 Å × 7.1 Å) is once more large enough for the encapsulation of a small molecule. Hence, again one $[CoCp_2]^+$ is incorporated which results in a total charge of +1 for this host-guest complex $[CoCp_2]^+$@**6b** (host: 0, guest: +1). Thus, it balances the negative charge of $[CoCp_2]^+$@**6a**. Compound **6** can therefore be described as ion pair $[(CoCp_2)^+$@**6b**$]^+[(CoCp_2)^+$@**6a**$]^-$. The outer diameter reach values of 2.67 nm for **6a** and 2.99 nm for **6b**, respectively. For a comparison, the 80- and 90-vertex nanoballs (*Figure 9.1*a,b) have a size of 2.2 nm, respectively, whereas fullerene C_{60} amounts less than 1 nm.

In analogy to the formation of **5**, also with CuI once a different crystalline phase, namely $[\{Cp^*Fe(\eta^5\text{-}P_5)\}_3\{(Cp^*Fe(\eta^4\text{-}P_5))_2O\}_3Cu_{16}I_{10}(CH_3CN)_7]\cdot 3.9CH_3CN$ (**7**) could be obtained when synthesizing **6**. Compound **7** crystallizes in the monoclinic space group $P2_1/c$ and its X-ray structural analysis shows a further unprecedented supramolecule of hemispherical, lens-like shape (*Figure 9.4*e). It contains nine pentaphosphaferrocene ligands, whereas six of them show an envelope conformation of the P_5 ring, as it is observed in **5**. The 'out-of-plane' phosphorus atom also bears a monoatomic substituent, which is analogously attributed to be an oxygen atom. Unfortunately, all attempts to reproduce **7** failed, even when additional H_2O is added to the solvent, hence the assignment of this light atom to oxygen is not unambigious. In contrast to **5**, this substituent is not terminal, but bridges two opposed $[Cp^*Fe(\eta^4\text{-}P_5)]$ units to give three $[\{Cp^*Fe(\eta^4\text{-}P_5)\}_2O]^{2-}$ moieties per supramolecule (*Figure 9.5*b). These bent P_5 rings still show a 1,2,3,4,5-coordination mode, whereas the remaining three units of **1a** bearing planar P_5 ligands show a 1,2-coordination mode. The scaffold furthermore contains 16 tetrahedrally coordinated Cu^+ and 10 I^-, either as terminal or bridging (μ_2 or μ_3) ligand. In total, the supramolecule is neutral (3 $[\{Cp^*Fe(\eta^4\text{-}P_5)\}_2O]^{2-}$, 10 I^-, 16 Cu^+). Due to the interconnected *cyclo*-P_5 ligands, compound **7** does not provide any accessible cavity, hence no encapsulation of the template can be observed. The outer size amounts to 2.48 nm × 1.65 nm.

Encouraged by these diverse results another redox-active sandwich complex, namely $[Cr(C_6H_6)_2]$, was tested for its suitability. In an analogous manner, a dark green solution of **1a** and $[Cr(C_6H_6)_2]$ in CH_2Cl_2 is layered with a colorless solution of CuBr in CH_3CN. Similarly to the synthesis of **4**, already after several minutes a metallic mirror at the phase boundary can be observed. Thus, one can again assume the oxidation of the template and reduction of the Cu(I) cations to elemental Cu. Nevertheless, besides plates of **2a** also small blocks of $[Cr(C_6H_6)_2]^+_{0.6}$@$[\{Cp^*Fe(\eta^5\text{-}P_5)\}_{12}Cu_{17.925}Br_{18.525}]$ (**8**) are obtained after complete diffusion. Compound **8** crystallizes in the trigonal space group $R\bar{3}$ and its structure shows the already mentioned fullerene-like 80-vertex supramolecule (*cf.* compound **3**) with incorporated $[Cr(C_6H_6)_2]^+$, which shows an occupancy factor of 0.6 and is therefore present in 60% of the supramolecules. As in **3**, the idealized $[\{Cp^*Fe(\eta^5\text{-}P_5)\}_{12}Cu_{20}Br_{20}]$ host molecule of **8** exhibits CuBr vacancies resulting in porous $[\{Cp^*Fe(\eta^5\text{-}P_5)\}_{12}Cu_{17.925}Br_{18.525}]$ spheres. Due to charge balance requirements of the cationic guest $[Cr(C_6H_6)_2]^+$ the overall site occupancy factors of Cu (17.925) are less than the ones of Br (18.525). The positive charge of the $[Cr(C_6H_6)_2]^+$ guest is verified by the absence of a signal in the ^1H NMR spectrum and the presence of a signal in the EPR spectrum (see below). As in the case for cobaltocene, compound **8** can also be synthesized using $CuBr_2$ instead of the Cu(I) salt. Due to the reduction of Cu(II) to Cu(I), the precipitation of Cu^0 is avoided in this case.

All obtained supramolecular compounds **4-8** are insoluble in common solvents like hexane, toluene, Et_2O and thf. In some cases they show a very little solubility in CH_3CN, CH_2Cl_2 or mixtures of these solvents, enabling a mass spectrometric characterization (for the full analysis see experimental part). Hereby, fragments up to $[\{Cp^*Fe(\eta^5\text{-}P_5)\}_2Cu_3Br_2]^+$ (at *m/z* = 1040.5) for **8** and even $[\{Cp^*Fe(\eta^5\text{-}P_5)\}_3Cu_7Br_6]^+$ (at *m/z* = 1962.3) for **3** appear in the corresponding ESI spectra. Furthermore, this method is also well-suited for the detection of the template, although no conclusion about its charge can be made. Exemplarily, in the cationic ESI mass spectrum of **5**, a peak at *m/z* = 189.0 corresponding to $[CoCp_2]^+$ is observed.

In addition, all products show solubility in pyridine, however accompanied by fragmentation of the host. This is evidenced by both the ^1H and $^{31}P\{^1H\}$ NMR spectra, which only show signals corresponding to the non-coordinated building block **1a.** As an example, for dissolved crystals of **3** a sharp singlet at δ = 143.5 ppm in the $^{31}P\{^1H\}$ NMR spectrum (*cyclo*-P_5) and a singlet at δ = 1.34 ppm in the ^1H NMR spectrum (Cp* ligand) is obtained. An automatic consequence is the release of the template, which also can be detected by NMR or EPR spectroscopy as well as mass spectrometry. Thus, in the ^1H NMR spectrum of **3** a singlet at δ = 4.16 ppm is assigned to the Cp ligands of ferrocene (literature:[18] δ = 4.04 ppm). On the other hand, the guest cations can easily

be detected in the corresponding cationic ESI MS spectra of **4** and **6** ($[CoCp_2]^+$) as well as of **8** ($[Cr(C_6H_6)_2]^+$), respectively.

Evidences for an unpaired electron are gained by EPR spectroscopy. In the respective EPR spectra of **3**, **4** and **6** no signal can be detected, which is in agreement with the presence of the neutral 18 VE complex $[FeCp_2]$ in **3** as well as the cationic 18 VE complex $[CoCp_2]^+$ in **4** and **6**. On the other hand, since the 17 VE sandwich complex $[Cr(C_6H_6)_2]^+$ is supposed to be incorporated in the host molecule of **8**, the unpaired electron should be detectable in the EPR spectrum of **8**. And in fact, a solution of **8** in pyridine is EPR active revealing a signal with a <g> value of 1.9721, which is similar to the one observed in the spectrum of $K[Cr(C_6H_6)_2]$ in dme (<g> = 1.9859) (*Figure 9.6*).[19] In addition, hyperfine splitting is caused by 12 equivalent protons as it is known for $[Cr(C_6H_6)_2]^+$.[19]

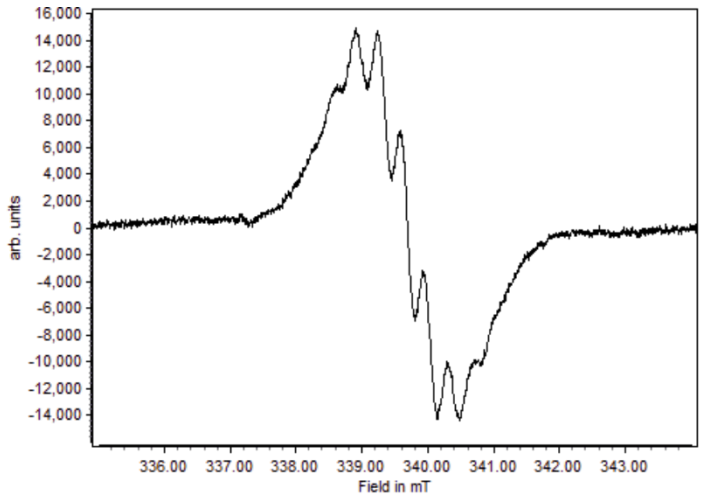

Figure 9.6 EPR spectrum of **8** (9.44 GHz, pyridine) at r.t.

In summary, the versatility and flexibility of host molecules, which consist of **1a** and CuX (X = Br, I), is demonstrated. Even reducing agents, such as $[CoCp_2]$ and $[Cr(C_6H_6)_2]$, as well as the oxidant $[FeCp_2][PF_6]$ do not inhibit the formation of supramolecules. On the converse, they mostly are incorporated after their oxidation and reduction, respectively. Three resulting spheres are reminiscent of the I_h-C_{80} topology (Compounds **3**, **5** and **8**). One of them (**5**) shows an envelope conformation of the *cyclo*-P_5 ligand, the latter (**8**) bears a negative charge due to diverse Cu and Br vacancies. Furthermore, supramolecules with unprecedented scaffolds were isolated and structurally characterized. Thereby, different numbers of **1a** moieties lead to different shapes, for example a hemisphere-like one bearing nine P_5 ligands (Compound **7**). On the other hand, eight units of **1a** are arranged *via* the vertices of a square antiprism (Compound **4**) and a cube (Compound **6**), respectively. Furthermore, the host molecules act as counterions for the cationic guest molecules and bear a negative charge of up to -4 in **4**. Remarkably, the host-guest complexes **5**, **6** and **8** display the first inorganic spheres incorporating $[MCp_2]^+$.

9.3 Experimental Part

General Remarks

All reactions were performed under an inert atmosphere of dry nitrogen or argon with standard vacuum, Schlenk and glove-box techniques. Solvents were purified, dried and degassed prior to use by standard procedures. [Cp*Fe(η^5-P_5)],[20] [Cp_2Fe][PF_6],[21,22] [Cp_2Co],[22,23] [Cp_2Co][PF_6][22,24] and [$(C_6H_6)_2Cr$][22,25] were synthesized following reported procedures. Commercially available chemicals (CuBr, $CuBr_2$, CuI) were used without further purification. Solution NMR spectra were recorded on a Bruker Avance 300 or 400 spectrometer. The corresponding ESI-MS spectra were acquired on a ThermoQuest Finnigan MAT TSQ 7000 mass spectrometer and EI-MS spectra were measured on a Finnigan MAT 95 mass spectrometer. Elemental analyses were performed on a Vario EL III apparatus. The X-Band EPR measurements were carried out with a MiniScope MS400 device with a frequency of 9.5 GHz and rectangular resonator TE102 of Magnettech GmbH.

Synthesis of $[FeCp_2]_{1-x}$@[{Cp*Fe(η^5-P_5)}$_{12}$($CuBr)_{20-n}$] (3)

In a Schlenk tube a green solution of [Cp*Fe(η^5-P_5)] (50 mg, 0.145 mmol) in CH_2Cl_2 (12 mL) is layered with a blue solution of CuBr (42 mg, 0.29 mmol) and [Cp_2Fe][PF_6] (30 mg, 0.09 mmol) in CH_3CN (12 mL). Thereby, the phase boundary turns yellow-brownish. Already after one day at the phase boundary the formation of black rhombohedra of **3** (yet only sporadically) and of brownish plates of **2a**[13] (as the main product) at the bottom can be observed. After complete diffusion the mother liquor is decanted, the crystals are washed with hexane (2 x 10 mL) and with CH_3CN (2 x 10 mL) to remove residues of [Cp_2Fe][PF_6] and dried *in vacuo*.

Analytical data of a mixture of **3** and **2a**:

Yield: 70 mg

^{1}H NMR (pyridine-d_5): δ [ppm] = 1.34 (s, [Cp*Fe(η^5-P_5)]), 4.16 (s, $FeCp_2$).

^{31}P{^{1}H} NMR (pyridine-d_5): δ [ppm] = 143.5 (s, [Cp*Fe(η^5-P_5)]).

^{19}F{^{1}H} NMR (pyridine-d_5): no signal.

Positive ion ESI-MS (CH_2Cl_2): *m/z* (%) = 1962.3 [{Cp*Fe(η^5-P_5)}$_3$$Cu_7Br_6$]$^+$, 1818.1 [{Cp*Fe($\eta^5$-$P_5$)}$_3$$Cu_6Br_5$]$^+$, 1678.0 [{Cp*Fe($\eta^5$-$P_5$)}$_3$$Cu_5Br_4$]$^+$, 1531.9 [{Cp*Fe($\eta^5$-$P_5$)}$_3$$Cu_4Br_3$]$^+$, 1471.8 [{Cp*Fe($\eta^5$-$P_5$)}$_2$$Cu_6Br_5$]$^+$, 1388.4 [{Cp*Fe($\eta^5$-$P_5$)}$_3$$Cu_3Br_2$]$^+$, 1330.5 [{Cp*Fe($\eta^5$-$P_5$)}$_2$$Cu_5Br_4$]$^+$, 1184.3 [{Cp*Fe($\eta^5$-$P_5$)}$_2$$Cu_4Br_3$]$^+$, 1042.4 [{Cp*Fe($\eta^5$-$P_5$)}$_2$$Cu_3Br_2$]$^+$, 898.6 [{Cp*Fe($\eta^5$-$P_5$)}$_2$$Cu_2Br$]$^+$, 754.7 [{Cp*Fe($\eta^5$-$P_5$)}$_2$Cu]$^+$, 593.5 [{Cp*Fe($\eta^5$-$P_5$)}$Cu_2Br${$CH_3CN$}]$^+$, 449.7 [{Cp*Fe($\eta^5$-$P_5$)}Cu{$CH_3CN$}]$^+$, 408.6 [{Cp*Fe($\eta^5$-$P_5$)}Cu]$^+$.

Negative ion ESI-MS (CH_2Cl_2): *m/z* (%) = 796.1 [Cu_5Br_6]$^-$, 652.3 [Cu_4Br_5]$^-$, 510.4 [Cu_3Br_4]$^-$, 366.4 [Cu_2Br_3]$^-$, 222.6 [$CuBr_2$]$^-$.

EI-MS (70 eV): 345.9 [Cp*Fe(η^5-P_5)], 283.9 [{Cp*Fe(η^5-P_5)}-P_2], 186.0 [Cp_2Fe].

Elemental analysis: Calculated (%) for [{Cp*Fe(η^5-P_5)}$_{12}$$Cu_{18}$$Br_{18}$($FeCp_2$)] (6919 g/mol): C 22.57, H 2.77; calculated (%) for [{Cp*Fe(η^5-P_5)}CuBr]$_n$ (489.4 g/mol): C 24.54, H 3.09; found: C 24.50, H 2.98.

Analytical data of the mother liquor of **3**:

$^{31}P\{^1H\}$ NMR (C_6D_6 capillary): δ [ppm] = -143.57 (*pseudo*-t, $^1J_{PF}$ = 708 Hz, $[PF_6]^-$).

$^{19}F\{^1H\}$ NMR (C_6D_6 capillary): δ [ppm] = -72.7 (d, $^1J_{PF}$ = 708 Hz, $[PF_6]^-$).

Synthesis of $[CoCp_2]^+$@[{Cp*Fe(η^5-P_5)}$_8$$Cu_{24.25}$$Br_{28.25}$($CH_3CN$)$_6$]$^{4-}$·3$[CoCp_2]^+$ (4)

Method A: In a Schlenk tube a green solution of [Cp*Fe(η^5-P_5)] (50 mg, 0.145 mmol) in CH_2Cl_2 (12 mL) is layered with a yellow solution of CuBr (83 mg, 0.58 mmol) and [Cp_2Co][PF_6] (30 mg, 0.09 mmol) in CH_3CN (12 mL). In doing so, the phase boundary turns yellow-brownish. After one day the formation of big red-black rhombohedra of **4** (at and above the phase boundary) and a small amount of brownish plates of **2a**[13] (at the bottom) can be observed. After complete diffusion the mother liquor is decanted, the crystals are washed with hexane (2 x 10 mL) and CH_3CN (2 x 10 mL) to remove residues of [Cp_2Co][PF_6] and dried *in vacuo*. The only way to get pure **4** is to grab the crystals of the Schlenk wall (and not from the ground) with a spatula and quickly dip it into a Schlenk tube with hexane. However, the yield of pure **4** is always underestimated, since bigger crystals of **4** fall to the bottom due to their higher weight and are not isolated using this method.

Method B: In a Schlenk tube a dark green solution of [Cp*Fe(η^5-P_5)] (50 mg, 0.145 mmol) and [Cp_2Co] (10 mg, 0.053 mmol) in CH_2Cl_2 (12 mL) is layered with a green solution of $CuBr_2$ (130 mg, 0.58 mmol) in CH_3CN (14 mL). Thereby the phase boundary turns slightly yellow-brownish. After one day the formation of small crystals of **4** (at and above the phase boundary) and of brownish plates of **2a**[13] (at the bottom) can be observed. After complete diffusion the mother liquor is decanted, the crystals are washed with hexane (2 x 10 mL) and dried *in vacuo*.

Method C: In a Schlenk tube a dark green solution of [Cp*Fe(η^5-P_5)] (50 mg, 0.145 mmol) and [Cp_2Co] (10 mg, 0.053 mmol) in CH_2Cl_2 (12 mL) is layered with a colorless solution of CuBr (84 mg, 0.59 mmol) in CH_3CN (14 mL). Thereby, the phase boundary turns yellow-brownish. After one day the formation of small plates of **4** and of brown plates of **2a**[13] can be observed. After complete diffusion the mother liquor is decanted, the crystals are washed with hexane (3 x 10 mL) and dried *in vacuo*.

Analytical data of **4**:

Yield: Method A: 62 mg (8.4 µmol, 46%); method B: 40 mg (5.4 µmol, 30%); method C: 68 mg (9.2 µmol, 51%)

^{1}H NMR (pyridine-d_5): δ [ppm] = 1.25 (s, [Cp*Fe(η^5-P_5)]).

^{31}P{^{1}H} NMR (pyridine-d_5): δ [ppm] = 147.65 (s, [Cp*Fe(η^5-P_5)]).

^{19}F{^{1}H} NMR (pyridine-d_5): no signal.

Positive ion ESI-MS (pyridine): *m/z* (%) = 1075.7 [{Cp*Fe(η^5-P_5)}$Cu_4Br_3(C_5H_5N)_3]^+$, 998.6 [{Cp*Fe(η^5-P_5)}$Cu_4Br_3(C_5H_5N)_2]^+$, 933.8 [{Cp*Fe(η^5-P_5)}$Cu_3Br_2(C_5H_5N)_3]^+$, 710.8 [{Cp*Fe(η^5-P_5)}$Cu_2Br(C_5H_5N)_2]^+$, 631.8 [{Cp*Fe(η^5-P_5)}$Cu_2Br(C_5H_5N)]^+$, 487.9 [{Cp*Fe(η^5-P_5)}$Cu(C_5H_5N)]^+$, 220.9 $[Cu(C_5H_5N)_2]^+$, 188.9 $[CoCp_2]^+$.

Negative ion ESI-MS (pyridine): *m/z* (%) = 366.5 $[Cu_2Br_3]^-$, 222.6 $[CuBr_2]^-$.

Elemental analysis: Calculated (%) for [{Cp*Fe(η^5-P_5)}$_8Cu_{24}Br_{28}(CoCp_2)_4(CH_3CN)_3$] (7410 g/mol): C 20.42, H 2.30, N 0.57; found: C 21.56, H 2.64, N 0.43.

Analytical Data of the mother liquor of **4**:

^{31}P{^{1}H} NMR (C_6D_6 capillary): δ [ppm] = -143.56 (*pseudo*-q, $^{1}J_{PF}$ = 708 Hz, $[PF_6]^-$).

^{19}F{^{1}H} NMR (C_6D_6 capillary): δ [ppm] = -72.7 (d, $^{1}J_{PF}$ = 708 Hz, $[PF_6]^-$).

Positive ion ESI-MS (CH_2Cl_2/CH_3CN): *m/z* (%) = 523.0 $[(CoCp_2)_2(PF_6)]^+$, 188.9 $[CoCp_2]^+$

Negative ion ESI-MS (CH_2Cl_2/CH_3CN): *m/z* (%) = 478.9 $[(CoCp_2)(PF_6)_2]^-$, 144.7 $[PF_6]^-$

Synthesis of [{Cp*Fe(η^5-P_5)}$_9${Cp*Fe(η^4-P_5OH)}$_3$(CuBr)$_{20}$]$^{3-}$·3[$CoCp_2$]$^+$ (5)

In a Schlenk tube a dark green solution of [Cp*Fe(η^5-P_5)] (30 mg, 0.087 mmol) and [Cp_2Co] (15 mg, 0.080 mmol) in toluene (10 mL) is layered with a colorless solution of CuBr (25 mg, 0.174 mmol) in CH_3CN (10 mL). Thereby, the phase boundary turns yellow-brownish. During diffusion, the formation of small black crystals of **5** at and above the phase boundary, brown plates of **2a**[13] at the bottom and a black precipitate can be observed. After complete diffusion the mother liquor is decanted, the crystals are washed with hexane (3 x 5 mL) and toluene (2 x 10 mL) to remove residues of [Cp_2Co] and dried *in vacuo*. The only way to get pure **5** is to grab the crystals of the Schlenk wall (and not from the ground) with a spatula and quickly dip it into a Schlenk tube with hexane. However, the yield of pure **5** is always underestimated, since bigger crystals of **5** fall to the bottom due to their higher weight and are not isolated using this method. Compound **5** cannot be reproduced, when accurately dried solvent (H_2O content < 10 ppm) is used. On the contrary, addition of a small amount of H_2O to the solvent, leads to the formation of **5**.

Analytical data of **5**:

Yield: 5 mg (0.65 µmol, 9%)

^{1}H NMR (pyridine-d_5): δ [ppm] = 1.32 (s, [Cp*Fe(η^5-P_5)]).

^{31}P{^{1}H} NMR (pyridine-d_5): δ [ppm] = 152.4 (s, [Cp*Fe(η^5-P_5)]).

^{31}P NMR (pyridine-d_5): δ [ppm] = 152.4 (s, [Cp*Fe(η^5-P_5)]).

Positive ion ESI-MS (CH_3CN): *m/z* (%) = 189.0 (100) $[Cp_2Co]^+$

Negative ion ESI-MS (CH_3CN): *m/z* (%) = 521.8 (100) $[Cu_5Br_7]^{2-}$

EI-MS (70 eV): 345.9 [Cp*Fe(η^5-P_5)], 284.0 [{Cp*Fe(η^5-P_5)}-P_2], 189.0 [Cp_2Co].

Raman [cm^{-1}] : 467 (P-P), 1107 (P-O), 1420 cm^{-1} (C-C); 2904 cm^{-1} (C-H_3)

Elemental analysis: Calculated (%) for [{Cp*Fe(η^5-P_5)}$_9${Cp*Fe(η^4-P_5OH)}$_3$($CuBr)_{20}$($CoCp_2)_3$] (7639 g/mol): C 23.59, H 2.81; found: C 23.05, H 2.93.

Synthesis of {[$Cp_2Co]^+$@[{Cp*Fe(η^5-P_5)}$Cu_{24.4}I_{26.4}(CH_3CN)_8]^{2-}$}{[$Cp_2Co]^+$@[{Cp*Fe($\eta^5$-$P_5$)}$_8Cu_{28}I_{28}(CH_3CN)_{9.8}$]} (6)

In a Schlenk tube a dark green solution of [Cp*Fe(η^5-P_5)] (50 mg, 0.145 mmol) and [Cp_2Co] (10 mg, 0.053 mmol) in CH_2Cl_2 (12 mL) is layered with a colorless solution of CuI (110 mg, 0.58 mmol) in CH_3CN (13 mL). Thereby, the phase boundary turns yellow-brownish. During diffusion, the formation of small red blocks of **6** and a small amount of plates of **2b**[13] can be observed. After complete diffusion the mother liquor is decanted, the crystals are washed with hexane (2 x 10 mL) and dried *in vacuo*.

Analytical data of **6**:

Yield: 35 mg (4.3 µmol, 24%)

^{1}H NMR (pyridine-d_5): δ [ppm] = 1.33 (s, [Cp*Fe(η^5-P_5)]), 5.72 (s, $[CoCp_2]^+$).

^{31}P{^{1}H} NMR (pyridine-d_5): δ [ppm] = 145.1 (s, [Cp*Fe(η^5-P_5)]).

^{31}P NMR (pyridine-d_5): δ [ppm] = 145.0 (s, [Cp*Fe(η^5-P_5)]).

Positive ion ESI-MS (pyridine): *m/z* (%) = 756.9 [{Cp*Fe(η^5-P_5)}$Cu_2I(C_5H_5N)_2]^+$, 678.0 [{Cp*Fe(η^5-P_5)}$Cu_2I_2(C_5H_5N)]^+$, 600.7 [{Cp*Fe(η^5-P_5)}$Cu_2I]^+$, 487.8 [{Cp*Fe(η^5-P_5)}$Cu(C_5H_5N)]^+$, 220.9 (100) $[Cu(C_5H_5N)_2]^+$, 188.9 $[CoCp_2]^+$.

Negative ion ESI-MS (pyridine): *m/z* (%) = 316.6 (100) $[CuI_2]^-$.

Elemental analysis: Calculated (%) for [{Cp*Fe(η^5-P_5)}$_8Cu_{26}I_{27}$($CoCp_2$)($CH_3CN)_3$] (8158 g/mol): C 14.13, H 1.72, N 0.52; found: C 16.56, H 2.12, N 0.44. The higher C and H content can be attributed to small impurities of [Cp*Fe(η^5-P_5)(CuI)]$_n$ (C 22.39, H 2.82).

Analytical data of the mother liquor of **6**:

Positive ion ESI-MS (CH_2Cl_2/CH_3CN): *m/z* (%) = 2913.7 $[Cu_{16}I_{15}]^+$, 2725.8 $[Cu_{15}I_{14}]^+$, 2534.0 $[Cu_{14}I_{13}]^+$, 2446.0 $[Cu_{14}I_{12}Cl]^+$, 2346.1 $[Cu_{13}I_{12}]^+$, 2154.1 $[Cu_{12}I_{11}]^+$, 2064.1 $[Cu_{12}I_{10}Cl]^+$, 1964.4 $[Cu_{11}I_{10}]^+$, 1872.1 $[Cu_{11}I_9Cl]^+$, 1774.1 $[Cu_{10}I_9]^+$, 1628.8 $[Cu_9I_8\{CH_3CN\}]^+$, 1582.4 $[Cu_9I_8]^+$, 1436.9 $[Cu_8I_7\{CH_3CN\}]^+$, 1394.0 $[Cu_8I_7]^+$, 1288.1 $[Cu_7I_6\{CH_3CN\}_2]^+$, 1247.1 $[Cu_7I_6\{CH_3CN\}]^+$, 1206.1 $[Cu_7I_6]^+$, 1096.3 $[Cu_6I_5\{CH_3CN\}_2]^+$, 1055.3 $[Cu_6I_5\{CH_3CN\}]^+$, 1016.1 $[Cu_6I_5]^+$, 537.0 $[\{Cp^*Fe(\eta^5\text{-}P_5)\}CuI]^+$, 188.8 (100) $[Cp_2Co]^+$.

Negative ion ESI-MS (CH_2Cl_2/CH_3CN): *m/z* (%) = 1080.3 $[Cu_5I_6]^-$, 888.4 $[Cu_4I_5]^-$, 698.5 $[Cu_3I_4]^-$, 506.6 $[Cu_2I_3]^-$, 316.6 (100) $[CuI_2]^-$.

Synthesis of $[\{Cp^*Fe(\eta^5\text{-}P_5)\}_3\{(Cp^*Fe(\eta^4\text{-}P_5))_2O\}_3Cu_{16}I_{10}(CH_3CN)_7]\cdot 3.9CH_3CN$ (7)

In a Schlenk tube a dark green solution of $[Cp^*Fe(\eta^5\text{-}P_5)]$ (30 mg, 0.087 mmol) and $[Cp_2Co]$ (15 mg, 0.080 mmol) in toluene (10 mL) is layered with a colorless solution of CuI (33 mg, 0.174 mmol) in CH_3CN (10 mL). Thereby the phase boundary turns yellow-brownish. Already after one day the formation of small plates of **2b**[13] and once of small black crystals of **7** accompanied by the precipitation of a black powder can be observed. After complete diffusion the mother liquor is decanted, the crystals are washed with hexane (3 x 5 mL) and dried *in vacuo*. Unfortunately, all attempts to reproduce **7** failed, therefore no analytical data can be provided.

Analytical data of **7**:

Yield: 6 mg (1.1 µmol, 11%)

Synthesis of $[Cr(C_6H_6)_2]^+@[\{Cp^*Fe(\eta^5\text{-}P_5)\}_{12}Cu_{19-n}Br_{20-n}]$ (8)

Method A: In a Schlenk tube a dark greenish solution of $[Cp^*Fe(\eta^5\text{-}P_5)]$ (50 mg, 0.145 mmol) and $[Cr(C_6H_6)_2]$ (5 mg, 0.024 mmol) in CH_2Cl_2 (12 mL) is layered with a colorless solution of CuBr (52 mg, 0.36 mmol) in CH_3CN (12 mL). In doing so, the phase boundary turns yellow-brownish. Already after one day the formation of big red-black rhombohedra of **8** (at and above the phase boundary) and a small amount of plates of **2a**[13] (at the bottom) can be observed. After complete diffusion the mother liquor is decanted, the crystals are washed with hexane (2 x 10 mL) and toluene (2 x 10 mL) to remove residues of $[Cr(C_6H_6)_2]$ and dried *in vacuo*. The only way to get pure **8** is to grab the crystals of the Schlenk wall (and not from the ground) with a spatula and quickly dip it into a Schlenk tube with hexane. However, the yield of pure **8** is always underestimated, since bigger crystals of **8** fall to the ground due to their higher weight and are not isolated using this method.

Method B: In a Schlenk tube a dark green solution of $[Cp^*Fe(\eta^5\text{-}P_5)]$ (50 mg, 0.145 mmol) and $[Cr(C_6H_6)_2]$ (30 mg, 0.073 mmol) in CH_2Cl_2 (20 mL) is layered with a solvent mixture of CH_2Cl_2 and

CH_3CN (2:1, 3 mL) and afterwards with a green solution of $CuBr_2$ (65 mg, 0.29 mmol) in CH_3CN (20 mL). Thereby, the phase boundary turns slightly yellow-brownish. The formation of small dark crystals of **8** (at and above the phase boundary) and of brownish plates of **2a**[13] (at the bottom) can be observed. After complete diffusion the mother liquor is decanted, the crystals are washed with pentane (3 x 5 mL) and toluene (3 x 5 mL) and dried *in vacuo*.

Analytical data of **8**:

Yield: 31 mg (4.6 µmol, 38%)

^{1}H NMR (pyridine-d_5): δ [ppm] = 1.29 (s, [Cp*Fe(η^5-P_5)]).

^{31}P{^{1}H} NMR (pyridine-d_5): δ [ppm] = 150.19 (s, [Cp*Fe(η^5-P_5)]).

Positive ion ESI-MS (CH_2Cl_2): *m/z* (%) = 1040.5 [{Cp*Fe(η^5-P_5)}$_2$$Cu_3Br_2$]$^+$, 898.6 [{Cp*Fe($\eta^5$-$P_5$)}$_2$$Cu_2Br$]$^+$, 754.7 [{Cp*Fe($\eta^5$-$P_5$)}$_2$Cu]$^+$, 593.7 [{Cp*Fe($\eta^5$-$P_5$)}$Cu_2Br${$CH_3CN$}]$^+$, 449.8 [{Cp*Fe($\eta^5$-$P_5$)}Cu{$CH_3CN$}]$^+$, 408.8 [{Cp*Fe($\eta^5$-$P_5$)}Cu]$^+$, 208.1 [Cr($C_6H_6$)$_2$]$^+$.

Negative ion ESI-MS (CH_2Cl_2): *m/z* (%) = 654.2 [Cu_4Br_5]$^-$, 510.4 [Cu_3Br_4]$^-$, 366.4 [Cu_2Br_3]$^-$, 222.6 [$CuBr_2$]$^-$.

EI-MS (70 eV): 345.9 [Cp*Fe(η^5-P_5)], 283.9 [{Cp*Fe(η^5-P_5)}-P_2].

Elemental analysis: Calculated (%) for [{Cp*Fe(η^5-P_5)}$_{12}$$Cu_{16}Br_{17}${Cr($C_6H_6$)$_2$}] (6735 g/mol): C 23.54, H 2.87; found: C 23.78, H 3.09.

9.4 Crystallographic Details

Crystals of **3-8** were taken from a Schlenk flask under a stream of argon and immediately covered with mineral oil or perfluorinated Fomblin® mineral oil to prevent both decomposition and a loss of solvent. The quickly chosen single crystals covered by a drop of the oil were taken to the pre-centered goniometer head with CryoMount® and directly attached to the diffractometer into a stream of cold nitrogen. X-ray diffraction studies faced many challenges, since the crystals have relatively small size and decompose rapidly losing solvent molecules. The diffraction power of crystals was very low, and the collection of data at high theta angles required high exposure times.

The data for **3**, **4**, **6**, **8** were collected on an Agilent Technologies diffractometer equipped with a Titan^{S2} CCD detector and a SuperNova CuK_α microfocus source using 0.5° ω scans. The data for **5** and **7** were collected on an Agilent Technologies diffractometer equipped with an Atlas CCD detector and a SuperNova CuK_α microfocus source using 1° ω scans. Crystallographic data and details of the diffraction experiments are given in *Table 9.1 – Table 9.3*. The structures were solved by direct methods with *SIR97*,[26] *SHELX97* or *SHELX2013*.[27] The structures were refined by full-matrix least-squares method against $|F|^2$ in anisotropic approximation using *SHELXL97* or the

multiprocessor and variable memory version *SHELXL2013*. All non-hydrogen atoms were refined anisotropically, while the hydrogen atoms were refined riding on pivot atoms.

In every supramolecule of **4** and **6** some positions of CuBr and CuI, respectively, are partly vacant indicated by enlarged displacement parameters. The occupancies for these positions were refined with fixed isotropic U_{iso} similar to the average U_{iso} (usually 0.03-0.04) for the fully occupied heavy atoms in the corresponding structure. The constraints on the Cu and Br displacement parameters were then removed and anisotropic approximation was used for the further refinement.

Some solvent molecules in **4** and **6** could be located from the difference Fourier map. The solvent molecules in most cases are disordered and their molecular occupancy factors were refined using the FVAR instruction of SHELX with isotropic displacement parameters fixed at $U_{iso} = 0.05$. The resulting occupancies were fixed and the C and N atoms with occupancy more than 0.5 were refined anisotropically. Most dichloromethane molecules in **4** and **6** were refined with restraint geometry. The restraints were removed at the final stage of the refinement if possible. Due to the disorder the solvent content is generally underestimated.

The outer sphere and encapsulated cobaltocenium cations in **4** and **6** occupy either a general position or an inversion center. All encapsulated $[Cp_2Co]^+$ are disordered over the inversion center. Each position was located using geometry constraints for the Cp rings. The molecular occupancy factors for each Cp ring were refined with fixed displacement parameters. At the end stages of the refinement the geometrical constraints were removed.

Table 9.1 Experimental details for compounds **3** (* = preliminary data),[28] and **4** (final data).

Crystal Data	3	4
Chemical formula	$(FeC_{10}H_{10})\cdot C_{120}H_{180}Br_{17.3}Cu_{17.3}Fe_{12}P_{60}$*	$C_{132}H_{178}Br_{28.25}Cu_{24.25}Fe_8N_6P_{40}\cdot 4(C_{10}H_{10}Co)\cdot 3.7(CH_2Cl_2)\cdot 5.55(CH_3CN)$
M_r	7206.38*	8110.50
Crystal system, space group	trigonal, $R\bar{3}$	triclinic, $P\bar{1}$
Temperature (K)	123	123
a, *b*, *c* (Å)	42.2701(5), 42.2701(5), 52.0744(5)	20.4315(4), 21.5102(5), 32.8727(5)
α, β, γ (°)	90, 90, 120	77.781(2), 86.624(1), 73.247(2)
V (Å^3)	80579(2)	13520.5(5)
Z	12	2
F(000)	> 42937	7795
Radiation type	Cu K_α	Cu K_α
μ (mm^{-1})	> 15.502	15.14
Crystal color and shape	black rhombohedron	red rhombic plate
Crystal size (mm)	0.35 x 0.15 x 0.12	0.15 × 0.12 × 0.08
Data collection		

Diffractometer	SuperNova, Titan^{S2} diffractometer	SuperNova, Titan^{S2} diffractometer
Absorption correction	gaussian	gaussian
T_{min}, T_{max}	0.081, 0.366	0.215, 0.439
No. of measured, independent and observed [$I > 2\sigma(I)$] reflections	171006,36072, 26859	103026, 51708, 36255
R_{int}	0.077	0.067
$(\sin \theta/\lambda)_{max}$ (Å^{-1})		0.625
Range of h, k, l	h = -45→51, k = -52→51, l = -64→64	h = -20→24, k = -25→26, l = -39→38
Refinement	*	
$R[F^2 > 2\sigma(F^2)]$, $wR(F^2)$, S	0.0641, 0.1973, 0.991	0.065, 0.191, 1.02
No. of reflections	36072	51708
No. of parameters	1731	2555
No. of restraints	7	14
H-atom treatment	H-atom parameters constrained	H-atom parameters constrained
$\Delta\rangle_{max}$, $\Delta\rangle_{min}$ (e Å^{-3})	4.644, -3.815	2.75, -1.53

Table 9.2 Experimental details for compounds **5** (* = preliminary data)[28] and **6** (final data).

Crystal Data	**5**	**6**
Chemical formula	$C_{120}H_{180}Br_{20}Cu_{20}Fe_{12}P_{60}O_6 \cdot 3(C_{10}H_{10}Co)$*	$C_{238.20}H_{350.70}Cl_{13.60}Co_2Cu_{52.40}Fe_{16}I_{54.40}N_{25.70}P_{80}$
M_r	8251.07*	17778. 83
Crystal system, space group	trigonal, $R\bar{3}m$	monoclinic, $P2_1/c$
Temperature (K)	123	123
a, b, c (Å)	23.5383(7), 23.5383(7), 50.568(1)	32.5420(4), 22.9579(2), 33.3552(3)
α, β, γ (°)	90, 90, 120	90, 94.500(1), 90
V (Å^3)	24264(2)	24842.7(4)
Z	3	2
F(000)	> 11600	16528
Radiation type	Cu K_α	Cu K_α
μ (mm^{-1})	> 13.29	36.40
Crystal color and shape	black block	brown parallelepiped
Crystal size (mm)	0.08 x 0.08 x 0.12	0.28 × 0.14 × 0.12
Data collection		
Diffractometer	SuperNova, Single source at offset, Atlas diffractometer	SuperNova, Titan^{S2} diffractometer
Absorption correction	multi-Scan	gaussian
T_{min}, T_{max}	0.519, 1.000	0.059, 0.270
No. of measured, independent	54631, 4904, 3189	100258, 47905, 30234

and observed [$I > 2\sigma(I)$] reflections		
R_{int}	0.034	0.078
$(\sin\theta/\lambda)_{max}$ (Å^{-1})		0.624
Range of h, k, l	h = -19→24, k = -29→13, l = -61→56	h = -39→33, k = -28→20, l = -41→40
Refinement	*	
$R[F^2 > 2\sigma(F^2)]$, $wR(F^2)$, S	0.081, 0.322, 1.12	0.066, 0.169, 0.94
No. of reflections	4904	47905
No. of parameters	333	2374
No. of restraints	0	19
H-atom treatment	H-atom parameters constrained	H-atom parameters constrained
$\Delta\rangle_{max}$, $\Delta\rangle_{min}$ (e Å^{-3})	0.193, -0.616	2.34, -3.54

Table 9.3 Experimental details for compounds **7** (final data) and **8** (* = preliminary data).[28]

Crystal Data	**7**	**8**
Chemical formula	$C_{140.85}H_{200.90}Cu_{16}Fe_9I_{10}N_{10.90}O_3P_{45}$	$(CrC_{12}H_{12})_{0.6}\cdot C_{120}H_{180}Br_{18.525}Cu_{17.925}Fe_{12}P_{60}$*
M_r	6276.76	6895.54*
Crystal system, space group	monoclinic, $P2_1/c$	trigonal, $R\bar{3}$
Temperature (K)	123	123
a, b, c (Å)	26.7047(7), 20.9464(4), 43.226(1)	42.2851(3), 42.2851(3), 52.2327(6)
α, β, γ (°)	90, 105.997(3), 90	90, 90, 120
V (Å^3)	23242.7(9)	80881(1)
Z	4	12
F(000)	12197	
Radiation type	Cu K_α	Cu K_α
μ (mm^{-1})	20.10	14.98
Crystal color and shape	black plate	black rhombohedron
Crystal size (mm)	0.65 × 0.12 × 0.03	0.24 x 0.15 x 0.12
Data collection		
Diffractometer	SuperNova, Single source at offset, Atlas diffractometer	SuperNova, Titan^{S2} diffractometer
Absorption correction	gaussian	gaussian
T_{min}, T_{max}	0.035, 0.596	0.258, 0.460
No. of measured, independent and observed [$I > 2\sigma(I)$] reflections	93079, 43976, 34163	112146 34722, 27512
R_{int}	0.052	0.057
$(\sin\theta/\lambda)_{max}$ (Å^{-1})	0.624	
Range of h, k, l	h = -33→31, k = -23→24, l = -44→53	h = -45→51, k = -49→40, l = -61→60

Refinement		*
$R[F^2 > 2\sigma(F^2)]$, $wR(F^2)$, S	0.062, 0.174, 1.02	0.063, 0.205, 0.872
No. of reflections	43976	27512
No. of parameters	2297	1746
No. of restraints	11	1
H-atom treatment	H atoms treated by a mixture of independent and constrained refinement	H-atom parameters constrained
$\Delta\rangle_{max}$, $\Delta\rangle_{min}$ (e Å^{-3})	1.83, -4.51	1.383,-2.132

9.5 Author Contributions

- The syntheses and characterization of the compounds **3, 4, 6** and **8** were performed by Claudia Heindl within the scope of this thesis
- The syntheses and characterization of the compounds **5** and **7** were performed by Claudia Heindl within the scope of the degree thesis (University of Regensburg, **2010**)
- X-ray structural analyses of **3-8** were performed together by Dr. Eugenia V. Peresypkina, Dr. Alexander V. Virovets and Claudia Heindl
- The manuscript (introduction, results and discussion, experimental part; including figures and graphical abstract) was written by Claudia Heindl; with the following exception:
- The section 'crystallographic details' for completed refinements was written by Dr. Eugenia V. Peresypkina

9.6 References

[1] a) S. I. Stupp, L. C. Palmer, *Chem. Mater.* **2014**, *26*, 507; b) N. Lanigan, X. Wang, *Chem. Commun.* **2013**, *49*, 8133; c) R. W. Saalfrank, A. Scheurer, *Top Curr Chem* **2012**, *319*, 125; d) S. J. Dalgarno, *Annu. Rep. Prog. Chem., Sect. B: Org. Chem.* **2010**, *106*, 197; e) M. Mastalerz, *Angew. Chem. Int. Ed.* **2010**, *49*, 5042; f) T. H. Rehm, C. Schmuck, *Chem. Soc. Rev.* **2010**, *39*, 3597; g) J.-M. Lehn, *Proc. Natl. Acad. Sci. U.S.A.* **2002**, *99*, 4763; h) F. A. Cotton, C. Lin, C. A. Murillo, *Acc. Chem. Res.* **2001**, *34*, 759.

[2] a) A. Mueller, P. Gouzerh, *Chem. Eur. J.* **2014**, *20*, 4862; b) S. Mukherjee, P. S. Mukherjee, *Chem. Commun.* **2014**, *50*, 2239; c) W. Meng, J. K. Clegg, J. R. Nitschke, *Angew. Chem. Int. Ed.* **2012**, *51*, 1881; d) Z. Laughrey, B. C. Gibb, *Chem. Soc. Rev.* **2011**, *40*, 363; e) B. Breiner, J. K. Clegg, J. R. Nitschke, *Chem. Sci.* **2011**, *2*, 51; f) Y. Inokuma, M. Kawano, M. Fujita, *Nat. Chem.*

2011, *3*, 349; g) P. Jin, S. J. Dalgarno, J. L. Atwood, *Coord. Chem. Rev.* 2010, *254*, 1760; h) M. Yoshizawa, J. K. Klosterman, M. Fujita, *Angew. Chem. Int. Ed.* 2009, *48*, 3418; i) T. S. Koblenz, J. Wassenaar, J. N. H. Reek, *Chem. Soc. Rev.* 2008, *37*, 247; j) S. J. Dalgarno, N. P. Power, J. L. Atwood, *Coord. Chem. Rev.* 2008, *252*, 825; k) C. Schmuck, *Angew. Chem. Int. Ed.* 2007, *46*, 5830; l) B. J. Holliday, C. A. Mirkin, *Angew. Chem. Int. Ed.* 2001, *40*, 2022; m) T. Heinz, D. M. Rudkevich, J. Rebek, Jr., *Nature* 1998, *394*, 764.

[3] a) N. J. Young, B. P. Hay, *Chem Commun* 2013, *49*, 1354; b) L. F. Lindoy, K.-M. Park, S. S. Lee, *Chem. Soc. Rev.* 2013, *42*, 1713; c) M. Schmidtendorf, T. Pape, F. E. Hahn, *Angew. Chem. Int. Ed.* 2012, *51*, 2195; d) S. R. Seidel, P. J. Stang, *Acc. Chem. Res.* 2002, *35*, 972.

[4] a) F. Dielmann, M. Fleischmann, C. Heindl, E. V. Peresypkina, A. V. Virovets, R. M. Gschwind, M. Scheer, *Chem. Eur. J.* 2015, *21*, 6208; b) S. Heinl, E. V. Peresypkina, A. V. Virovets, M. Scheer, *Angew. Chem. Int. Ed.* 2015, submitted; c) C. Schwarzmaier, A. Schindler, C. Heindl, S. Scheuermayer, E. V. Peresypkina, A. V. Virovets, M. Neumeier, R. Gschwind, M. Scheer, *Angew. Chem. Int. Ed.* 2013, *52*, 10896; d) A. Schindler, C. Heindl, G. Balázs, C. Groeger, A. V. Virovets, E. V. Peresypkina, M. Scheer, *Chem. Eur. J.* 2012, *18*, 829; e) S. Welsch, C. Groeger, M. Sierka, M. Scheer, *Angew. Chem. Int. Ed.* 2011, *50*, 1435; f) M. Scheer, A. Schindler, J. Bai, B. P. Johnson, R. Merkle, R. Winter, A. V. Virovets, E. V. Peresypkina, V. A. Blatov, M. Sierka, H. Eckert, *Chem. Eur. J.* 2010, *16*, 2092; g) M. Scheer, A. Schindler, C. Groeger, A. V. Virovets, E. V. Peresypkina, *Angew. Chem. Int. Ed.* 2009, *48*, 5046; h) M. Scheer, A. Schindler, R. Merkle, B. P. Johnson, M. Linseis, R. Winter, C. E. Anson, A. V. Virovets, *J. Am. Chem. Soc.* 2007, *129*, 13386; i) M. Scheer, J. Bai, B. P. Johnson, R. Merkle, A. V. Virovets, C. E. Anson, *Eur. J. Inorg. Chem.* 2005, 4023; j) J. Bai, A. V. Virovets, M. Scheer, *Science* 2003, *300*, 781.

[5] a) A. V. Mossine, H. Kumari, D. A. Fowler, A. K. Maerz, S. R. Kline, C. L. Barnes, J. L. Atwood, *Isr. J. Chem.* 2011, *51*, 840; b) V. Rudzevich, O. Kasyan, A. Drapailo, M. Bolte, D. Schollmeyer, V. Bohmer, *Chem. Asian J.* 2010, *5*, 1347; c) P. D. Beer, A. D. Keefe, A. M. Z. Slawin, D. J. Williams, *J. Chem. Soc., Dalton Trans.* 1990, 3675; d) Y. Wang, A. E. Kaifer, *Chem. Commun.* 1998, 1457.

[6] L. Frish, M. O. Vysotsky, V. Boehmer, Y. Cohen, *Org. Biomol. Chem.* 2003, *1*, 2011.

[7] W. Xia, X.-Y. Hu, Y. Chen, C. Lin, L. Wang, *Chem. Commun.* 2013, *49*, 5085.

[8] a) A. U. Moozyckine, J. L. Bookham, M. E. Deary, D. M. Davies, *J. Chem. Soc., Perkin Trans. 2* 2001, 1858; b) B. Klingert, G. Rihs, *J. Chem. Soc., Dalton Trans.* 1991, 2749.

[9] a) A. E. Kaifer, *Acc. Chem. Res.* 2014, *47*, 2160; b) S. Gadde, A. E. Kaifer, *Curr. Org. Chem.* 2011, *15*, 27.

[10] a) H. Sakai, T. Yamazaki, N. Machida, T. Shigematsu, S. Nasu, *Mol. Cryst. Liq. Cryst. Sci. Technol., Sect. A* 2000, *341*, 105; b) J. S. O. Evans, D. O'Hare, R. Clement, *J. Am. Chem. Soc.* 1995, *117*, 4595.

[11] a) A. N. Titov, O. N. Suvorova, S. Y. Ketkov, S. G. Titova, A. I. Merentsov, *Phys. Solid State* 2006, *48*, 1466; b) L. Hernan, J. Morales, L. Sanchez, J. Santos, E. Rodriguez-Castellon, J. L. Martinez, *Chem. Mater.* 2000, *12*, 3792; c) A. Ibarz, E. Ruiz, S. Alvarez, *J. Chem. Soc., Dalton Trans.* 2000, 1463.

[12] S. Murray, M. Trudeau, D. M. Antonelli, *Adv. Mater.* 2000, *12*, 1339.

[13] J. Bai, A. V. Virovets, M. Scheer, *Angew. Chem. Int. Ed.* 2002, *41*, 1737.

[14] For a more detailed discussion of these vacancies see: a) chapter 10; b) chapter 11; c) Ref. [4a].

[15] E. V. Peresypkina, C. Heindl, A. Schindler, M. Bodensteiner, A. V. Virovets, M. Scheer, *Z. Kristallogr.* 2014, *229*, 735.

[16] S. Reisinger, Dissertation thesis (Universität Regensburg) 2014.

[17] a) E. Maedl, M. V. Butovskii, G. Balázs, E. V. Peresypkina, A. V. Virovets, M. Seidl, M. Scheer, *Angew. Chem. Int. Ed.* 2014, *53*, 7643; b) M. V. Butovskiy, G. Balázs, M. Bodensteiner, E. V. Peresypkina, A. V. Virovets, J. Sutter, M. Scheer, *Angew. Chem. Int. Ed.* 2013, *52*, 2972.

[18] L. Phillips, F. Separovic, M. J. Aroney. *New J. Chem.* 2003, *27*, 381.

[19] C. Elschenbroich, E. Bilger, J. Koch, J. Weber, *J. Am. Chem. Soc.* 1984, *106*, 4297.

[20] O. J. Scherer, T. Brück, *Angew. Chem.* 1987, *99*, 59.

[21] A. N. Nesmeyanov, R. B. Materikova, I. R. Lyatifov, T. K. Kurbanov, N. S. Kochetkova, *J. Organomet. Chem.* 1978, *145*, 241.

[22] This compound was in-house available.

[23] J. F. Cordes, *Chem. Ber.* 1962, *95*, 3084.

[24] J. E. Sheats, M. D. Rausch, *J. Org. Chem.* 1970, *35*, 3245.

[25] E. O. Fischer, *Inorg. Synth.* 1960, *6*, 132.

[26] G. M. Sheldrick, *Acta Cryst. sect. C* 2015, *C71*, 3.

[27] A. Altomare, M. C. Burla, M. Camalli, G. L. Cascarano, C. Giacovazzo, A. Guagliardi, A. G. G. Moliterni, G. Polidori, R. Spagna, *J. Appl. Cryst.* 1999, *32*, 115.

[28] Please note: Due to the uncompleted refinement, not all parameters (e.g. F(000)) can be stated and some given parameters, such as μ, R_{int}, as well as the sum formula have to be treated as temporarily values and may change at a later stage.

10. The Missing Parent Compound [(C5H5)Fe(η5-P5)]: Synthesis, Characterization and Coordination Behavior

C. Heindl, E. V. Peresypkina, G. Balázs, E. Mädl, A. V. Virovets, M. Scheer

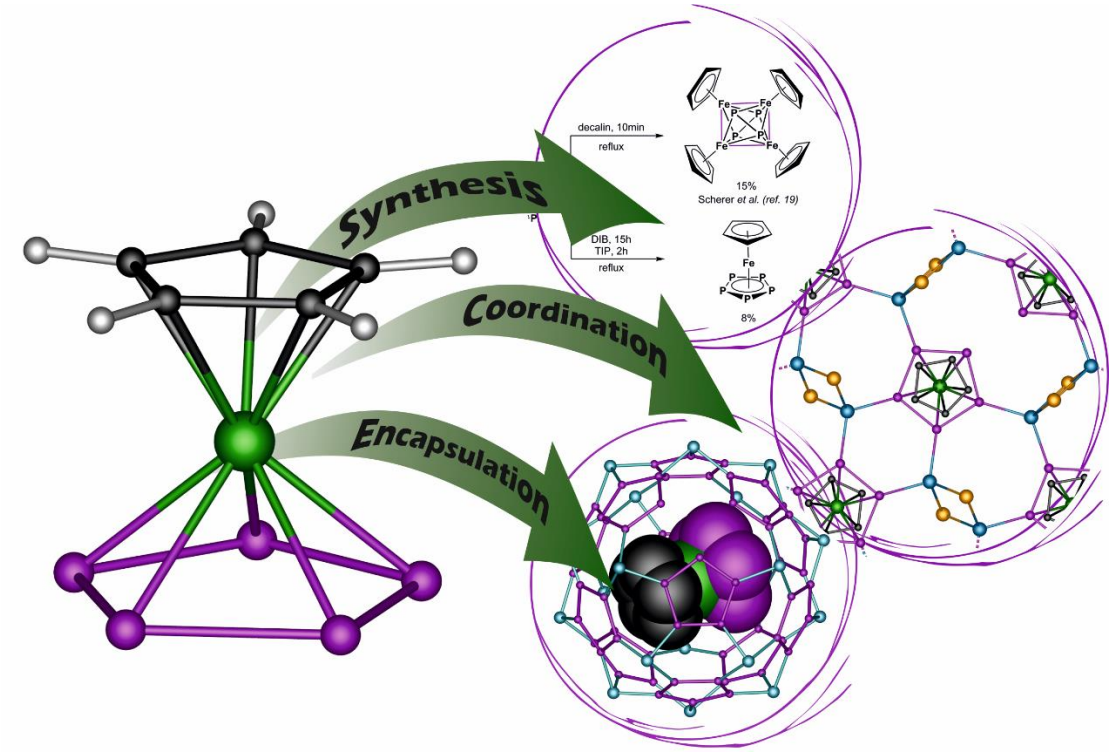

Abstract:

The so far missing parent compound of the pentaphosphaferrocenes [CpFe(η5-P5)] (**1b**) was synthesized by the thermolysis of [CpFe(CO)2]2 with P4 using the very high-boiling solvent diisopropylbenzene. Its comprehensive characterization by, *inter alia*, NMR spectroscopy, single crystal X-ray structure analysis, cyclic voltammetry and DFT computations is described herein. Moreover, its coordination behavior towards Cu(I) halides is explored, revealing the unprecedented 2D polymeric networks [{CpFe(η5:1:1:1:1-P5)}Cu2(μ-X)2]n (**2a**: X = Cl, **2b**: X = Br) and [{CpFe(η5:1:1-P5)}Cu(μ-I)]n (**3**) and even the first *cyclo*-P5 containing 3D polymer [{CpFe(η5:1:1-P5)}Cu(μ-I)]n (**4**). In addition, the sandwich complex **1b** can also be incorporated in nano-sized supramolecules based on [Cp*Fe(η5-P5)] (**1a**) and CuX (X = Cl, Br, I): [CpFe(η5-P5)]@[{Cp*Fe(η5-P5)}12(CuX)20-n] (**5a**: X = Cl, n = 2.4; **5b**: X = Br, n = 2.4; **5c**: X = I, n = 0.95). Hereby, in the case of CuI, the formation of the fullerene-like sphere **5c** is observed for the first time.

10.1 Introduction

The establishment of organometallic chemistry as a distinct subfield is to a large extent owed to the discovery and structure determination of the ferrocene molecule [Fe(η^5-C$_5$H$_5$)$_2$] in 1951.[1] Finally, E.O. Fischer and G. Wilkinson were honoured for this pioneering work by the award of the Noble Prize in 1973.[2] Beside its application as a reference redox system (Fc/Fc$^+$),[3] ferrocene derivatives play an important role e.g. in asymmetric catalysis,[4] polymer chemistry[5] and for magnetic materials.[6] These derivatives do not only vary in their functionalization pattern, but also in the substitution of methine moieties by isolobal hetero atoms. The introduction of phosphorus atoms into the cyclopentadienyl ligand affords the class of phosphaferrocenes.[7]

Among them the pentaphosphaferrocene [Cp*Fe(η^5-P$_5$)] (Cp* = C$_5$Me$_5$) (**1a**), containing a *cyclo*-P$_5$ ligand, is of special interest. Firstly published in 1987 by Scherer *et al.*,[8] it has become an important building block in supramolecular and coordination chemistry,[9] especially for the formation of 1D and 2D polymers.[10]

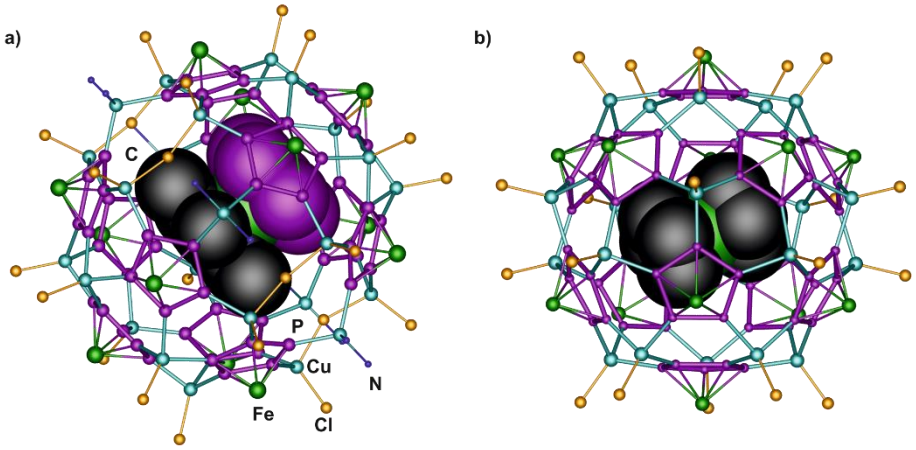

Figure 10.1 Fullerene-like spheres based on **1a** and CuCl: a) 90-vertex supramolecule incorporating **1a**; b) 80-vertex supramolecule incorporating [FeCp$_2$].

Certainly, from extra interest is its ability to act as a building block for the formation of spherical supramolecules with fullerene topology by the self-assembly with CuX (X = Cl, Br, I).[11] Furthermore, these spheres can encapsulate molecules like compound **1a** itself (*Figure 10.1*a),[11e,h,i] ferrocene (*Figure 10.1*b),[11c] *o*-carborane[11a,f] and C$_{60}$.[11g] These reactions turned out to be very sensitive to many parameters like stochiometry, solvent, concentration and the used halide. Hence, also the nature of the Cp^R ligand in the pentaphosphaferrocene should profoundly affect the coordination behavior. Due to its simple synthesis (*Scheme 10.1*) a huge variety of pentaphosphaferrocenes is known with Cp^R = Cp^{Et} = η^5-C$_5$Me$_4$Et;[12] Cp' = η^5-C$_5$H$_4$^{t}Bu;[13] Cp'' = η^5-C$_5$H$_3$^{t}Bu$_2$;[13] Cp''' = η^5-C$_5$H$_2$^{t}Bu$_3$;[14] Cp^{Bn} = η^5-C$_5$(CH$_2$Ph)$_5$;[15] Cp^S = η^5-C$_5$Me$_4$C$_2$H$_4$SMe;[15] Cp^{BIG} = η^5-C$_5$(4-^{n}BuC$_6$H$_4$)$_5$.[16]

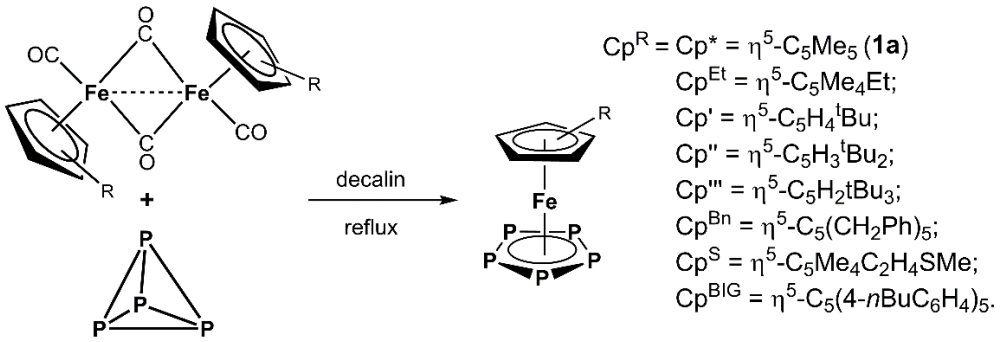

Scheme 10.1 General procedure for the synthesis of pentaphosphaferrocenes.

In view of the large variety of Cp^R substituted pentaphosphaferrocenes, it is astonishing that the parent compound [CpFe(η^5-P_5)] (**1b**) with an unsubstituted Cp ligand was never reported. Certainly especially this sandwich complex is of great interest as building block itself as well as guest for the encapsulation in fullerene-like supramolecules.

Although several detailed DFT computational studies predict **1b** to be stable,[17] its synthesis remained an insuperable challenge. One reason might be that the use of decalin as solvent does not lead to the formation of **1b**, but to a tetranuclear iron cluster (*Scheme 10.2*).[18] However, recently we have shown that by using a higher-boiling solvent triple decker complexes can be obtained in much better yields than earlier reported procedures and the hitherto unknown parent compound [$(CpMo)_2(\mu,\eta^{6:6}$-$P_6)$] could also be synthesized.[19]

Herein we report on the synthesis and comprehensive characterization of the parent compound [CpFe(η^5-P_5)] (**1b**). In order to compare its coordination behavior with substituted pentaphosphaferrocenes, the reactivity towards Cu(I) halides was studied. Among the obtained products the first 3D polymer in *cyclo*-P_5 coordination chemistry is described. Furthermore, we describe its ability to act as a template for the formation of inorganic nano-sized spheres.

10.2 Results and Discussion

Synthesis and Characterization of 1b

For the synthesis of all aforesaid pentaphosphaferrocenes the same route is applied (*Scheme 10.1*). Thermolysis of $[Cp^RFe(CO)_2]_2$ with P_4 in decalin and subsequent chromatographic work-up affords the desired complex as a green solid. However, transferring this strategy to the Cp derivative the tetranuclear iron cluster $[(CpFe)_4(P_2)_2]$ is obtained exclusively (*Scheme 10.2*).[18]

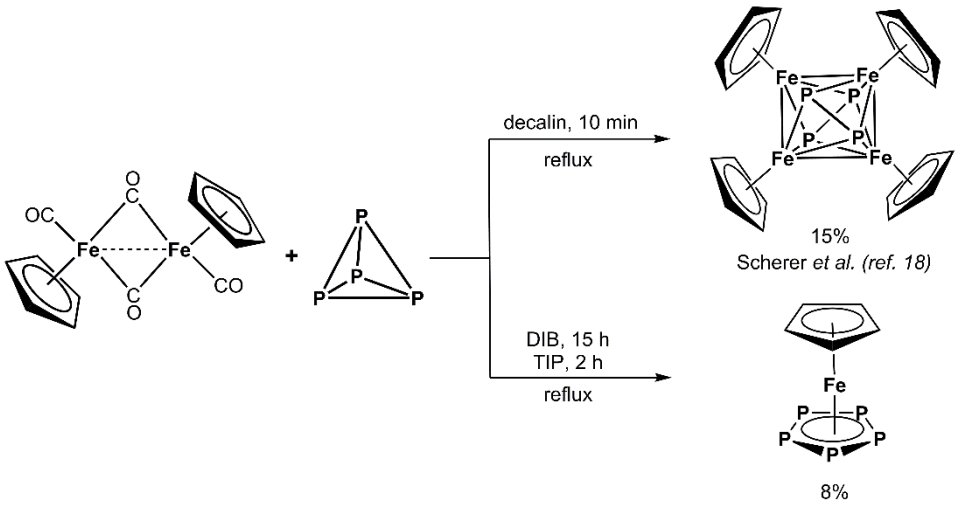

Scheme 10.2 Thermolysis reaction of $[CpFe(CO)_2]_2$ with P_4.

Since thermal decompositions per se depend on the applied temperature, $[CpFe(CO)_2]_2$ was allowed to react with P_4 in 1,3-diisopropylbenzene with an even higher boiling point (DIB, bp = 203 °C; decalin: bp = 187-196 °C). Gratifyingly, this small temperature discrepancy most likely was the decisive factor and the unsubstituted parent compound **1b** could be obtained as solely product according to $^{31}P\{^1H\}$ NMR spectroscopy (*Scheme 10.2*). However, also an influence of the aromatic character of this solvent cannot be precluded. Compound **1b** is purified by chromatographic workup to give a green powder in 8% yield. To investigate, whether the yield can be enhanced by a further increase of the temperature, the reaction was performed in 1,3,5-triisopropylbenzene (TIP, bp = 232-236 °C). In fact, **1b** can be isolated after a significantly reduced reaction time of 2 hours, though the yield remains constant.

Complex **1b** is rather poorly soluble in aliphatic solvents like *n*-hexane, moderately soluble in toluene and CH_2Cl_2 and insoluble in CH_3CN. As expected, the ^1H NMR spectrum of **1b** shows one singlet at δ = 3.39 ppm, which is upfield shifted compared to $[FeCp_2]$ (δ = 4.04 ppm).[20] In the $^{31}P\{^1H\}$ NMR spectrum one singlet appears at δ = 169.5 ppm and therefore reveals the equivalence of the P atoms. The signal exhibits one of the farthest downfield shift among the pentaphosphaferrocene complexes (signals range from δ = 152.8 ppm for $[Cp^{Et}Fe(\eta^5\text{-}P_5)]$[12] to δ = 173.6 for $[Cp^{BIG}Fe(\eta^5\text{-}P_5)]$[16]), therefore the shift does not go hand-in-hand with the steric bulk, as previously assumed.[15,16] Furthermore, complex **1b** sublimes at 80 °C/10^{-3} mbar, just as **1a**.[8]

By layering a CH_2Cl_2 solution of **1b** with CH_3CN in a thin schlenk tube, **1b** crystallizes as green prisms in the monoclinic space group $P2_1/m$. Its molecular structure reveals a sandwich complex with η^5-coordinated rings in a perfect eclipsed conformation, which is in accordance with all theoretical predictions (*Figure 10.2*).[17] In contrast, due to the steric demand of the methyl substitutents the Cp* derivative **1a** deviates from the eclipsed conformation by 11.6(1)°.[10b] The interplanar angle of **1b** is close to zero (0.56(8)°) and the angle $Cp_{(centroid)}\text{-}Fe\text{-}P_{5(centroid)}$ of 179.87(4),

both reveal a perfect sandwich complex almost free of distortion. The molecule **1b** lies in a mirror plane (C_s point symmetry) that bisects both Cp and P_5 rings (*Figure 10.2*) similarly to Cp_2Ru,[21] Cp_2Os[22] and the low-temperature orthorhombic modification of Cp_2Fe.[23] In contrast to ferrocene,[23] **1b** demonstrates no phase transition in the temperature range 123 K – 298 K. The diffraction experiment of a green block of **1b** showed only increased thermal motion at room temperature. A comparison of selected bond lengths of **1b** with optimized geometries based on DFT computations as well as with experimental data of **1a** (at 123 K) is given in *Table 10.1*. It can be stated, that all predicted values are in part significantly longer than the experimentally observed ones. Furthermore, π-stacking interactions are present, since the **1b** molecules are arranged into chains (along the *c* axis) *via* Cp···*cyclo*-P_5 interactions with interplanar distances of 3.71 Å or 3.78 Å at T = 123 K or r.t., respectively.

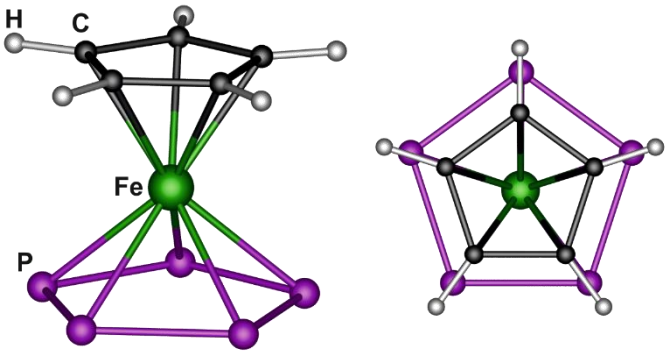

Figure 10.2 Molecular structure of **1b** in the crystal (side and top view).

Table 10.1 Selected bond lengths and reported DFT optimized geometries of **1b** at 123 K (l.t.), **1b** at 298 K (r.t.) and **1a**, respectively.

Bond lengths / Å	Fe-Cp^R (centroid)	Fe-P_5 (centroid)	P-$P_{average}$
1b	1.693(1) l.t. 1.698(1) r.t.	1.536(1) l.t. 1.536(1) r.t.	2.113(3) l.t. 2.10(1) r.t.
Katsyuba *et al.*[17a]	1.706	1.623	2.148
Padma Malar[17b]	1.705	1.624	2.148
Frenking *et al.*[17c]	1.716	1.599	2.163
Frison *et al.*[17d]	1.695	1.578	2.137
This work	1.712	1.585	2.127
1a[10b]	1.720(1)	1.535(1)	2.120(2)

Winter *et al.* investigated the interesting redox behavior of the Cp* substituted derivative **1a** and stated a one electron oxidation and reduction, which is reversible at high scan rates.[24] However, the resulting complexes are not stable and readily dimerize to give $[\mathbf{1a}_2]^{2+}$ and $[\mathbf{1a}_2]^{2-}$, respectively. Their proposed structures were finally confirmed experimentally by our group.[25] For a comparison, electrochemical investigations were also performed for **1b** (*Figure 10.3*). Cyclic

voltammetry data at a sweep rate of 0.1 Vs^{-1} reveal an irreversible oxidation at a peak potential of 0.8 V (0.6 V for **1a**). On the contrary to **1a**, no coupled cathodic signal, which might be attributed to a dimeric species, appears. Most likely its stabilization by the sterically more demanding Cp* ligand is crucial, therefore it cannot be observed for **1b**. However, the reduction behavior of **1b** is in line with the results for **1a**. A reduction wave at a peak potential of -1.86 (-2.05 V for **1a**) as well as the corresponding anodic signal at -1.20 V (-1.34 V for **1a**) constitute a chemically reversible couple.

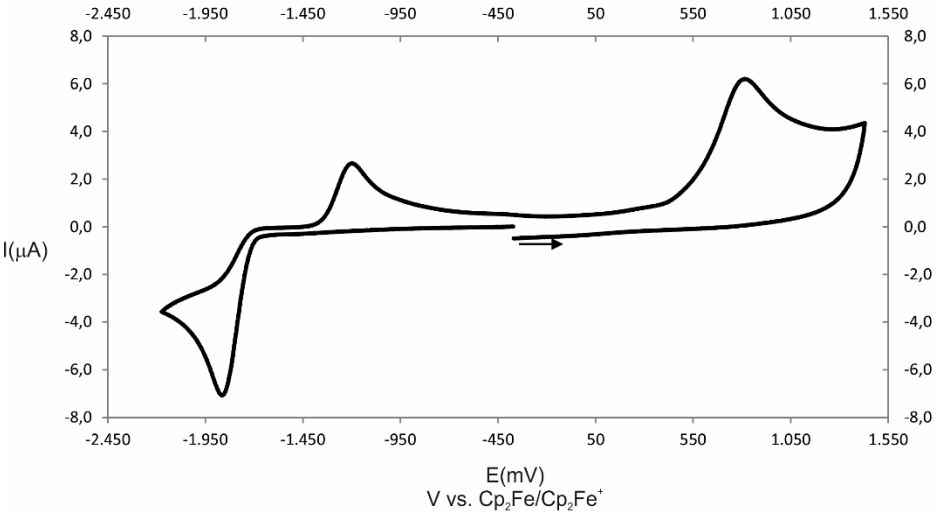

Figure 10.3 Cyclic voltammogram of **1b** in $CH_2Cl_2/^nBu_4NPF_6$ solution at r.t. and v = 0.1 Vs^{-1}.

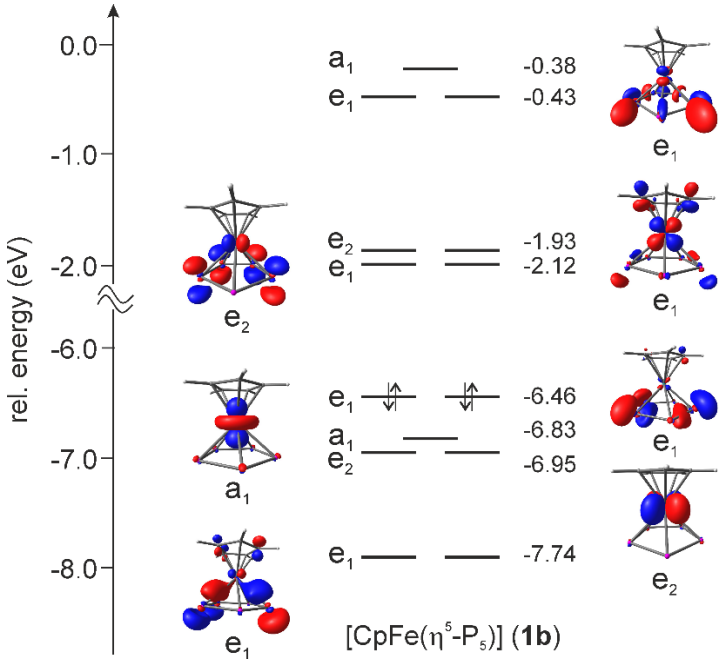

Figure 10.4 Energy level diagram for **1b** calculated at the B3LYP/6-31++G(3df,3pd) level of theory.

DFT computations[26] on the electronic structure of **1b** show the expected orbital ordering, which resemble that of **1a**[27] (*Figure 10.4*). Comparing it with **1a**, in **1b** the Highest Occupied Molecular Orbital (HOMO) as well as the Lowest Unoccupied Molecular Orbital (LUMO) lie slightly lower in energy than in **1a** rendering **1b** a weaker donor though a better acceptor (*Figure 10.5*). The HOMO-

LUMO gap in **1b** is 4.34 eV, whereas in **1a** it is 4.48 eV. The difference in the relative energy of the frontier orbitals in **1a** and **1b** is in line with the results of the CV measurements.

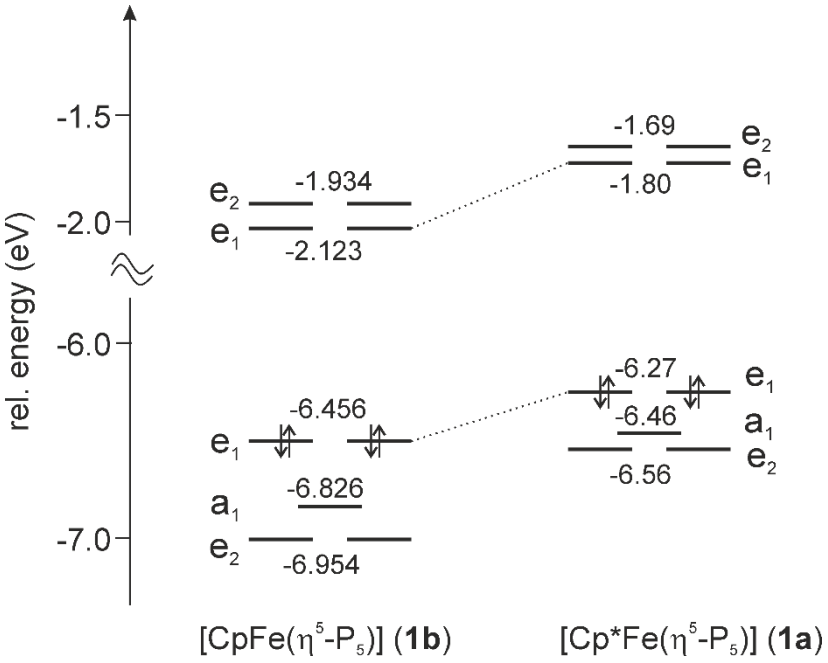

Figure 10.5 Comparative energy level diagram of **1a** and **1b**.

Coordination Behavior of 1b towards Cu(I) Halides

Due to the lone pairs on the P_5 ring in combination with its outstanding five-fold symmetry pentaphosphaferrocenes represent excellent building blocks in supramolecular chemistry. Hence, the coordination behavior of **1b** towards Cu(I) halides was investigated (*Scheme 10.3*). Therefore, a green solution of **1b** in CH_2Cl_2 or toluene is layered with a colorless solution of CuX (X = Cl, Br, I) in CH_3CN in a very thin schlenk tube. Hereby, the phase boundary turns yellow-orange and small crystals of $[\{CpFe(\eta^{5:1:1:1:1}\text{-}P_5)\}Cu_2(\mu\text{-}X)_2]_n$ (**2a**: X = Cl, **2b**: X = Br), $[\{CpFe(\eta^{5:1:1}\text{-}P_5)\}Cu(\mu\text{-}I)]_n$ (**3**) and $[\{CpFe(\eta^{5:1:1}\text{-}P_5)\}Cu(\mu\text{-}I)]_n$ (**4**), respectively, start to grow already after a few hours. Due to the same (in-)solubility, the polymers **3** and **4** cannot be separated. Unfortunately, also a selective synthesis is not feasible, since they contain the same molar ratio of **1b** and CuI.

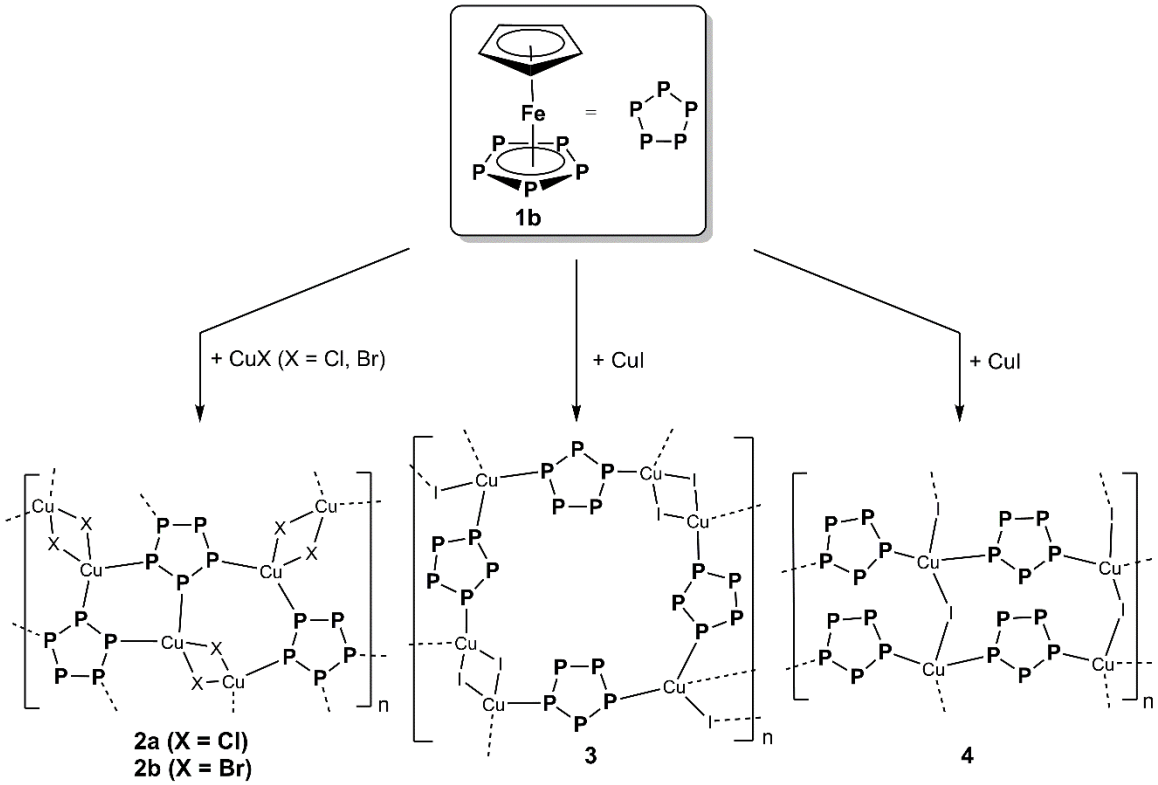

Scheme 10.3 Coordination behavior of **1b** towards Cu(I) halides.

Compounds **2a** and **2b** are isostructural and crystallize as very thin orange plates in the triclinic space group *P*$\bar{1}$. X-ray structural analyses reveal 2D polymers with a 1,2,3,4-coordination mode of the *cyclo*-P_5 ligand (*Figure 10.6*a). The coordination of four P atoms of the ring occurred before in three previous examples, namely $[\{Cp^RFe(\eta^5\text{-}P_5)\}(CuI)_3]_n$ (Cp^R = Cp*, Cp^{Bn})[10c,28] and $[\{Cp^*Fe(\eta^5\text{-}P_5)\}\{Cu(GaCl_4)\}_2]_n$.[10d] However, **2a** and **2b** differ from these examples in its connectivity and show an unprecedented structural motif. In addition to $\{Cu_2P_4\}$ hexagons and $\{Cu_2X_2\}$ squares also seven-membered $\{Cu_3P_4\}$ rings are present. This linking pattern forms a planar 2D sheet structure with an alternating upwards and downwards orientation of the {CpFe} fragments. Noteworthy, they now deviate from the eclipsed conformation to the *cyclo*-P_5 unit by ~14°. Interestingly, **2a**,**b** represent a novel layer topology with 3-coordinated Cu^+ and 4-coordinated **1b** units serving as nodes and halide spacers (see crystallographic section).[29]

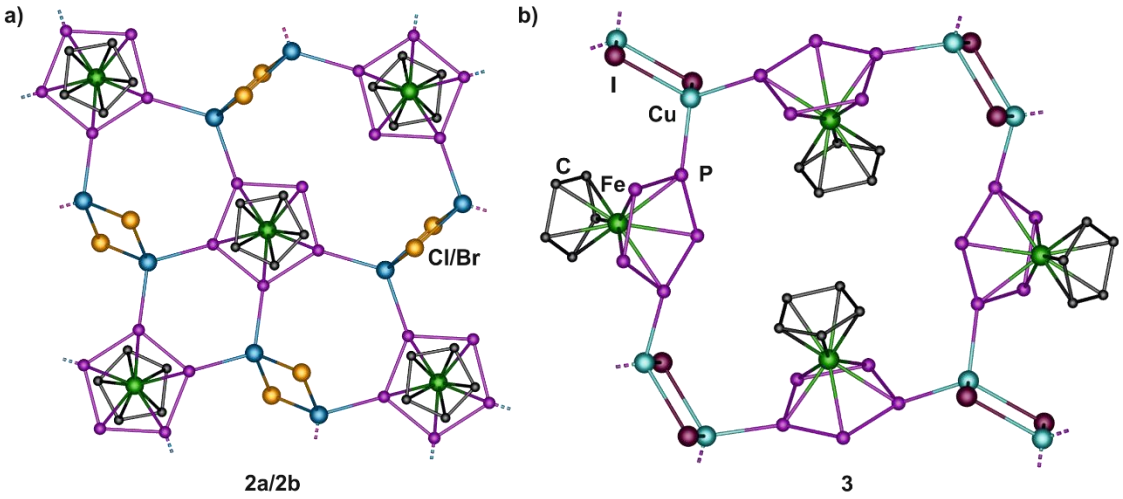

Figure 10.6 Sections of the 2D polymeric structures of a) **2a**/**2b** and b) **3**. Hydrogen atoms are omitted for clarity.

Compound **3** crystallizes in the monoclinic space group $P2_1/c$. Its 2D polymeric network consists of connected rectangles of **1b** and four-membered Cu_2I_2 rings (*Figure 10.6*b). Two of the four {FeCp} units at a time per rectangle are orientated towards each other. The *cyclo*-P_5 moieties show a 1,3-coordination mode, which has been unknown for pentaphosphaferrocenes for a long time. Recently, we were able to obtain two examples, $[\{Cp^*Fe(\eta^5\text{-}P_5)\}(CuI)]_n$[10c] and $[\{Cp^{BIG}Fe(\eta^5\text{-}P_5)\}Ag]_n[Al\{OC(CF_3)_3\}_4]_n$,[10d] both forming infinite chain 1D polymers. On the contrary, **3** forms two-dimensional layers. When the bridging iodine atoms and the 1,3-coordinated **1b** molecules are treated as spacers and the Cu atoms as nodes of the polymeric structure, the honeycomb **hcb** topology of the layer becomes evident.[29,30]

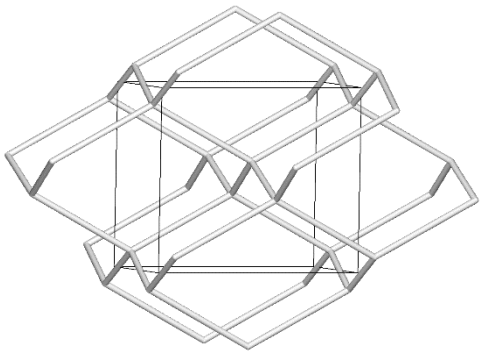

Figure 10.7 **dia** topology in **4**.

Compound **4** crystallizes as red prisms in the orthorhombic space group $Pna2_1$. Remarkably, its polymeric structure is extended in all three dimensions. This is astonishing, since all obtained pentaphosphaferrocene-based polymers are either 1D or 2D.[10] A 3D polymer has never been observed so far. Two P atoms per P_5 ring are connected to Cu, resulting in a 1,3-coordination mode as it is observed in **3** (*Figure 10.8*). A further commonality with **3** is the tetrahedral environment of Cu, the bridging coordination of iodide as well as the same sum formula of $[\{CpFe(\eta^5\text{-}P_5)\}Cu(\mu\text{-}I)]_n$. In contrast to **3**, no $\{Cu_2I_2\}$ rings but infinite {CuI} zigzag chains are formed in **4** (*Figure 10.8*). Its net topology can be assigned to the **dia** type[29,31] which is well-known from diamond (*Figure 10.7*).

Among these polymers, π-stacking interactions, similar to the ones found in **1b**, do not appear. Despite rather short interlayer distances of 3.22 Å in **2a** and 3.27 Å in **2b**, the layers are mutually

shifted and do not afford a direct contact of the π-systems. In both **3** and **4** the π-systems are not parallel, and all contacts involving P atoms are within the range of van der Waals interactions.

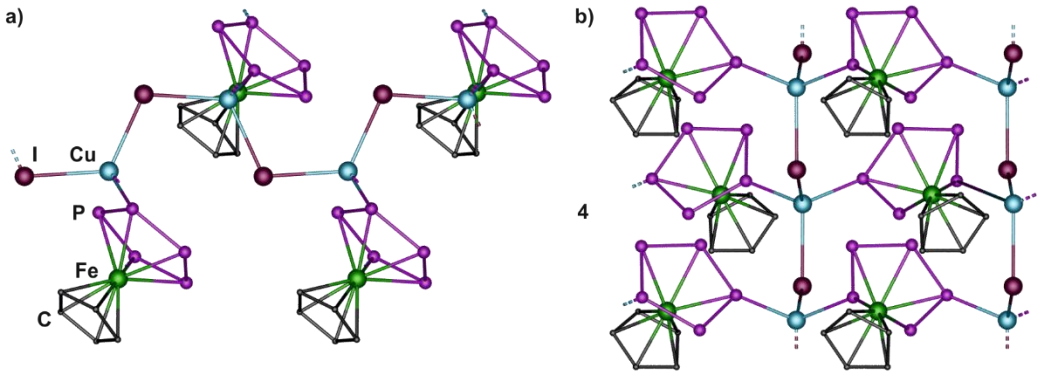

Figure 10.8 Sections of the 3D polymeric structure of **4**: view along the crystallographic a) *a* axis and b) *b* axis. Hydrogen atoms are omitted for clarity.

All four coordination polymers are insoluble in common solvents like hexane, toluene, CH_2Cl_2, CH_3CN, Et_2O and thf. Merely in pyridine they can be dissolved, though accompanied by complete fragmentation. Hence in the ^{1}H and $^{31}P\{^{1}H\}$ NMR spectrum, respectively, only the singlet for **1b** can be detected.

Inclusion of 1b in Fullerene-like Spheres

Compound **1b** not only represents an interesting building unit, but is also excellently suited for the encapsulation into pentaphosphaferrocene-based supramolecules. Recently, we were able to show, that ferrocene [$FeCp_2$] can be incorporated in an 80-vertex sphere consisting of 12 molecules of **1a** and 20 CuCl units.[11c] The scaffold only consists of five- (P_5) and six-membered (Cu_2P_4) rings and therefore shows I_h-C_{80} fullerene topology. Also pentaphosphaferrocene **1a** itself acts as a template and is enclosed by a 90-vertex supramolecule.[11e,h,i] This sphere exhibits a slightly larger scaffold due to the larger size of **1a**. For a vivid comparison, one can imagine the 80-vertex ball divided into two equal half shells and a [{$Cu(CH_3CN)_2$}$_5X_5$] (X = Cl, Br) belt inserted between them. Since the size of **1b** is in between, the question arises, which host will be the preferred one.

To investigate this, a dark green solution of **1a** and **1b** in CH_2Cl_2 (molar ratio **1a**:**1b** = 9:1) is layered with a colorless solution of CuX (X = Cl, Br, I), respectively. Remarkably, in all three reactions black rhombohedra of [$CpFe(\eta^5\text{-}P_5)$]@[{$Cp^*Fe(\eta^5\text{-}P_5)$}$_{12}$$(CuX)_{20\text{-}n}$] (**5a**: X = Cl, n = 2.4; **5b**: X = Br, n = 2.4; **5c**: X = I, n = 0.95) are formed. All three compounds are isostructural and crystallize in the trigonal space group $R\bar{3}$. In their structures one molecule of **1b** is incorporated into the aforesaid smaller 80-vertex nanoball regardless of the halide used (*Figure 10.9*). Noteworthy, **5c** displays the

first fullerene-analogue containing iodide. All previous attempts resulted in the formation of polymeric products. Merely two P_5-based supramolecules with CuI are known, however both without fullerene topology.[11b,28]

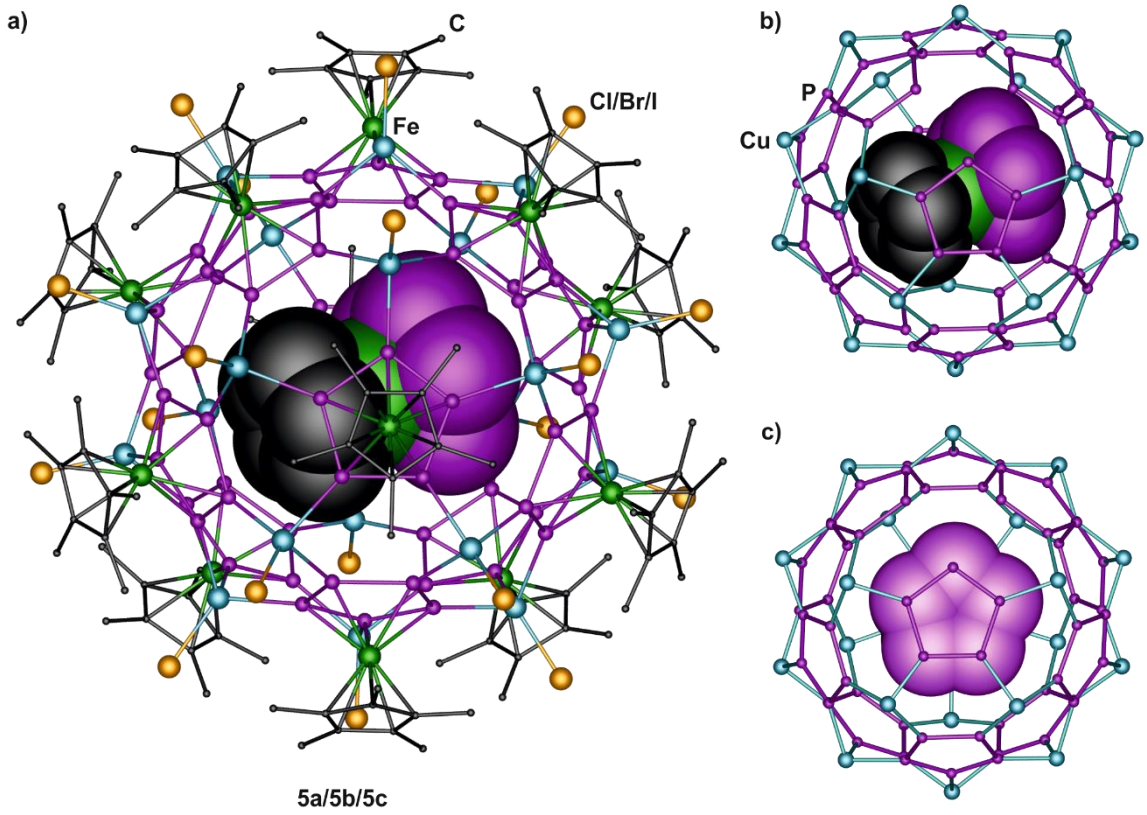

Figure 10.9 a) Molecular structures of **5a-c** in the crystals. Hydrogen atoms, minor position of disordered guest molecules are omitted for clarity; b) partly vacant inorganic scaffold of the supramolecules with incorporated **1b**; c) illustration of the π-π-interactions between the P_5 ligands.

The host molecules in **5a-c** consist of 12 moieties of **1a**, which show a 1,2,3,4,5-coordination mode to copper. The complete 80-vertex scaffold would contain 20 CuX (X = Cl, Br, I) units forming 30 $\{Cu_2P_4\}$ six-membered rings. However, in all three spherical compounds the scaffold exhibits some number of CuX vacancies. In a similar way, this phenomenon was observed for the same system with *o*-carborane as a guest.[11a] As a consequence, the ideal number of 20 in the $Cu_{20}P_{60}$ scaffold is reduced per supramolecule to 17.6 for **5a** and **5b** and 19.05 for **5c** (*Figure 10.9*b). Some solvent CH_2Cl_2 molecules point into the vacant holes that can cause a partial ordering of vacancies and a change of the structural type from cubic[11f] to rhombohedral.[11a] Another consequence of these 'holes' for the adjacent *cyclo*-P_5 ligands is the reduction of the five-fold mode to a 1,2,3,4-coordination to copper.

The outer diameter of all three supramolecules is 2.12 nm and does not depend on the halide used, since the Cp* ligands protrude furthest. The inner diameters are determined by the distance between opposite *cyclo*-P_5 ligands and are therefore also identical with a value of 0.77 nm. These

dimensions are in good agreement with previously obtained 80-vertex spheres.[11a,c,f] Furthermore, the spherical cavity shows the appropriate size for one molecule **1b** (0.70 x 0.67 nm).

The guest molecule is present in each cavity of the supramolecules **5a-c** as indicated by the occupancy factors of the Fe atoms in the center. Furthermore, it appeared to be severely disordered over three or six non-equal positions with the P_5 and C_5 rings occupying very close positions. A prominent feature is the face-to-face orientation of the ligands of **1b** towards the *cyclo*-P_5 ligands of the host, respectively, revealing π-stacking interactions (*Figure 10.9*c). However, the $P_5 \cdots P_5$ distances range from 3.80 Å to 3.95 Å (preliminary values) and are therefore slightly longer than twice the van-der-Waals radius of phosphorus (1.8 Å).[32] The same stacking interaction with similar distances has been observed for **1a** molecules encapsulated in a 90-vertex sphere.[11e]

The supramolecules **5a-c** are all obtained by diffusion reactions and their synthesis can always be accompanied by the formation of the polymeric networks $[Cp^*Fe(\eta^5\text{-}P_5)(CuX)]_n$[10a] (X = Cl, Br, I). In addition, for X = Cl, Br, also the 90-vertex spheres $[Cp^*Fe(\eta^5\text{-}P_5)]@[\{Cp^*Fe(\eta^5\text{-}P_5)\}_{12}(CuX)_{25}(CH_3CN)_{10}]$[11e] can be formed within these self-assembly processes. However, a precise observation during the diffusion process revealed that for X = Cl, Br first of all big black rhombohedra of **5a**/**5b** crystallize at the phase boundary, respectively. After approximately one to two days, brownish plates of $[Cp^*Fe(\eta^5\text{-}P_5)(CuX)]_n$ are visible at the ground of the Schlenk tube. Finally, after complete diffusion, rods of the 90-vertex sphere start appearing. Therefore, to get pure **5a**, one has to take the crystals as soon as possible only from the Schlenk wall with a spatula (see experimental part). *Via* this method, pure **5a** is obtained in still very good crystalline yields of 64%. Unfortunately, this separation procedure is not possible for X = I, since crystals of **5c** and $[Cp^*Fe(\eta^5\text{-}P_5)(CuI)]_n$ start to grow at the same place as well as at the same time.

All obtained nanoballs are completely insoluble in common solvents like hexane, toluene, CH_3CN, Et_2O and thf. However, in pyridine they show fragmentation. Therefore in the corresponding ^1H and $^{31}P\{^1H\}$ NMR spectra only signals of the starting complexes **1a** and **1b** can be obtained. On the other hand, this also means that the encapsulated pentaphosphaferrocene **1b** can be released by degradation of its host.

Surprisingly and on the contrary to previously reported 80-vertex supramolecules,[11c,f] **5a** and **5b** are also very poorly soluble in CH_2Cl_2. Thus, even a characterization by NMR spectroscopy is enabled. In the $^{31}P\{^1H\}$ NMR spectrum of **5a** three very broad signals at δ = 70, 76 and 103 ppm, one sharp singlet at δ = 152.1 ppm and one slightly broadened singlet at δ = 170.5 ppm can be observed. According to a detailed NMR study of soluble nanoballs, where $Cp^R = Cp^{Bn}$, the broad signals can be assigned to the coordinated P atoms of spheres with varying porosity.[33] In addition, a small amount of **1a** might be released, causing the singlet at δ = 152.1 ppm. Due to the

broadening, the singlet at δ = 170.5 ppm is related to the encapsulated complex **1b**, thus it is slightly downfield-shifted, compared to free **1b** (in CD_2Cl_2: δ = 168.6 ppm). This observation is in contrast to previously reported guest molecules, which all show a slight shift to higher field. Therefore, **1b** displays the first template which might rather act as electron donor. The quality of the $^{31}P\{^1H\}$ NMR spectrum of the analogous compound **5b** is already quite poor, since its solubility is even worse. Nevertheless, also two singlets for **1a** and **1b** as well as one very broad signal for **5b** can be obtained. Other broad signals, as they were observed for **5a**, can only be adumbrated and disappear below the noise floor.

Conclusions

In summary, the synthesis of the parent compound [CpFe(η^5-P_5)] (**1b**) is presented. Replacement of decalin by an even higher-boiling solvent makes the general route feasible for the formation of the desired sandwich complex. X-ray structural analysis reveals an eclipsed sandwich complex with slightly shorter bond lengths than the computed ones. Cyclic voltammetry data show an irreversible oxidation and a reversible reduction and DFT computations reveal a slightly stronger acceptor and weaker donor ability, compared to the Cp* derivative **1a**. To investigate the coordination behavior of **1b**, it was allowed to react with CuX (X = Cl, Br, I). In all reactions the formation of unprecedented 2D polymers (**2a**, **2b** and **3**) and even the first 3D polymer (**4**) based on pentaphosphaferrocene can be obtained. The networks **2a** and **2b** show an 1,2,3,4-coordination mode of the *cyclo*-P_5 ligand, whereas in **3** and **4** a 1,3-coordination is present. Furthermore, the incorporation of **1b** into 80-vertex nanoballs (**5a-c**) is shown. The host molecules differ in the halide and for the first time an iodine-containing supramolecule with fullerene topology is obtained. The behavior in solution shows that in CH_2Cl_2 **1b** remains incorporated in the host, whereas fragmentation and therefore release of the template is observed in the donor solvent pyridine. All in all, the influence of the unsubstituted Cp ligand is demonstrated: beginning from different conditions during its synthesis, through its deviating coordination behavior up to changes in host-guest chemistry owing to its smaller size.

10.3 Experimental Part

General Remarks:

All reactions were performed under an inert atmosphere of dry nitrogen or argon with standard vacuum, Schlenk and glove-box techniques. Solvents were purified, dried and degassed prior to use by standard procedures. $[CpFe(CO)_2]_2$[34,35] and [Cp*Fe(η^5-P_5)][36] were synthesized following reported procedures. White phosphorus (P_4) was sublimed and stored under argon. Commercially

available chemicals (CuCl, CuBr, CuI) were used without further purification. Solution NMR spectra were recorded on a Bruker Avance 300 or 400 spectrometer. The corresponding ESI-MS spectra were acquired on a ThermoQuest Finnigan MAT TSQ 7000 mass spectrometer, whereas EI-MS spectra were measured on a Finnigan MAT 95 mass spectrometer. Elemental analyses were performed on a Vario EL III apparatus.

Synthesis of [CpFe(η^5-P$_5$)] (1b)

[CpFe(CO)$_2$]$_2$ (1.0 g, 2.83 mmol) and P$_4$ (1.4 g, 11.3 mmol) are dissolved in 1,3-diisopropylbenzene (DIB, bp = 203 °C) and refluxed for 15 hours. The solvent is removed and the dark residue is dissolved in CH_2Cl_2. Afterwards this solution is filtered over celite and the solvent is again removed. The solid is adsorbed on silica and loaded onto a column filled with silica (20 cm x 3 cm). Using hexane, a yellow band of residual P$_4$ can be eluted. With a hexane/toluene (10/1) solvent mixture a bright green band of **1b** can be eluted. The solvent is removed and pure [CpFe(η^5-P$_5$)] can be isolated as green powder (0.22 mmol, 8%). Crystals suitable for X-ray diffraction analysis can be obtained by layering a solution of **1b** in CH_2Cl_2 with CH_3CN or by cooling a saturated solution of **1b** in hexane to -28 °C. Solvent-free **1b** can also be sublimed (10^{-3} mbar, 80 °C). Also 1,3,5-triisopropylbenzene (TIP, bp = 235 °C) can be used as a solvent, hereby the refluxing time is reduced to 2 hours.

Analytical data of **1b**:

Yield: 60 mg (0.22 mmol, 8%)

^{1}H NMR (C_6D_6): δ [ppm] = 3.39 (s, [(C$_5$<u>H</u>$_5$)Fe(η^5-P$_5$)]).

^{13}C{^{1}H} NMR (C_6D_6): δ [ppm] = 75.96 (s, [(<u>C</u>$_5$H$_5$)Fe(η^5-P$_5$)]).

^{31}P{^{1}H} NMR (C_6D_6): δ [ppm] = 169.49 (s, [(C$_5$H$_5$)Fe(η^5-<u>P</u>$_5$)]).

EI-MS (70 eV): 275.9 [CpFe(η^5-P$_5$)], 214.0 [{CpFe(η^5-P$_5$)}-P$_2$].

Elemental analysis: Calculated (%) for [CpFeP$_5$] (275.8 g/mol): C 21.77, H 1.83; found: C 21.93, H 1.94.

Synthesis of [{CpFe(η$^{5:1:1:1:1}$-P$_5$)}Cu$_2$(μ-Cl)$_2$]$_n$ (2a)

In a thin Schlenk tube a green solution of [CpFe(η^5-P$_5$)] (22 mg, 0.08 mmol) in CH_2Cl_2 (5 mL) is carefully layered with a colorless solution of CuCl (16 mg, 0.16 mmol) in CH_3CN (8 mL). Thereby, the phase boundary turns orange and gets turbid. Already after one day the formation of small orange plates of **2a** at the phase boundary can be observed. After complete diffusion the mother liquor is decanted, the crystals are washed with hexane (3 x 5 mL) and dried *in vacuo*.

Analytical data of **2a**:

Yield: 25 mg (0.053 mmol, 66%)

^{1}H NMR (pyridine-d_5): δ [ppm] = 1.83 (s, CH_3CN), 4.52 (s, [($C_5\underline{H}_5$)Fe(η^5-P_5)]).

^{31}P{^{1}H} NMR (pyridine-d_5): δ [ppm] = 136.96 (s, [(C_5H_5)Fe(η^5-$\underline{P}_5$)]).

Positive ion ESI-MS (pyridine): *m/z* (%) = 320.7 $[Cu_2Cl\{C_5H_5N\}_2]^+$, 220.8 (100) $[Cu\{C_5H_5N\}_2]^+$.

Negative ion ESI-MS (pyridine): *m/z* (%) = 332.5 $[Cu_3Cl_4]^-$, 232.4 $[Cu_2Cl_3]^-$, 134.5 (100) $[CuCl_2]^-$.

Elemental analysis: Calculated (%) for $[\{CpFe(\eta^5\text{-}P_5)\}(CuCl)_2(CH_3CN)_{0.1}]$ (478 g/mol): C 13.07, H 1.12, N 0.29; found: C 14.23, H 1.37, N 0.15.

Synthesis of $[\{CpFe(\eta^{5:1:1:1:1}\text{-}P_5)\}Cu_2(\mu\text{-}Br)_2]_n$ (2b)

In a thin Schlenk tube a green solution of [$CpFe(\eta^5$-$P_5)$] (10 mg, 0.036 mmol) in CH_2Cl_2 (6 mL) is carefully layered with a colorless solution of CuBr (16 mg, 0.11 mmol) in CH_3CN (10 mL). Thereby, the phase boundary turns orange and gets turbid. Already after one day the formation of small orange plates of **2b** at the phase boundary can be observed. After complete diffusion the mother liquor is decanted, the crystals are washed with hexane (3 x 5 mL) and dried *in vacuo*.

Analytical data of **2b**:

Yield: 18 mg (0.032 mmol, 89%)

^{1}H NMR (pyridine-d_5): δ [ppm] = 0.88 (m, *hexane*-CH_3), 1.32 (m, *hexane*-CH_2), 1.84 (s, CH_3CN), 4.34 (s, [($C_5\underline{H}_5$)Fe(η^5-P_5)]).

^{31}P{^{1}H} NMR (pyridine-d_5): δ [ppm] = 155.57 (s, [(C_5H_5)Fe(η^5-$\underline{P}_5$)]).

Positive ion ESI-MS (pyridine): *m/z* (%) = 381.9 $[Cu\{C_5H_5N\}_4]^+$, 220.9 $[Cu\{C_5H_5N\}_2]^+$.

Negative ion ESI-MS (pyridine): *m/z* (%) = 222.6 (100) $[CuBr_2]^-$, 80.9 $[Br]^-$.

Elemental analysis: Calculated (%) for $[\{CpFe(\eta^5\text{-}P_5)\}(CuBr)_2(C_6H_{14})_{0.25}]$ (584 g/mol): C 13.36, H 1.47; found: C 13.32, H 1.33.

Synthesis of $[\{CpFe(\eta^{5:1:1}\text{-}P_5)\}Cu(\mu\text{-}I)]_n$ (3) and $[\{CpFe(\eta^{5:1:1}\text{-}P_5)\}Cu(\mu\text{-}I)]_n$ (4)

In a thin Schlenk tube a green solution of [$CpFe(\eta^5$-$P_5)$] (22 mg, 0.08 mmol) in CH_2Cl_2 (5 mL) is carefully layered with a colorless solution of CuI (31 mg, 0.16 mmol) in CH_3CN (9 mL). Thereby, the phase boundary turns orange and gets turbid. Already after one day the formation of small orange plates of **3** and red prisms of **4** at the phase boundary can be observed. After complete diffusion the mother liquor is decanted, the crystals are washed with hexane (3 x 5 mL) and dried *in vacuo*.

Analytical data of **3** and **4**:

Yield: 24 mg (0.052 mmol, 64%)

^{1}H NMR (pyridine-d_5): δ [ppm] = 1.83 (s, CH_3CN), 4.34 (s, [($C_5\underline{H}_5$)Fe(η^5-P_5)]).

^{31}P{^{1}H} NMR (pyridine-d_5): δ [ppm] = 154.80 (s, [(C_5H_5)Fe(η^5-$\underline{P}_5$)]).

Positive ion ESI-MS (pyridine): *m/z* (%) = 220.9 (100) $[Cu\{C_5H_5N\}_2]^+$.

Negative ion ESI-MS (pyridine): *m/z* (%) = 506.5 $[Cu_2I_3]^-$, 380.6 $[I_3]^-$, 316.6 (100) $[CuI_2]^-$, 126.9 $[I]^-$.

Synthesis of $[CpFe(\eta^5\text{-}P_5)]@[\{Cp^*Fe(\eta^5\text{-}P_5)\}_{12}(CuCl)_{17.6}]$ (5a)

In a Schlenk tube a green solution of $[Cp^*Fe(\eta^5\text{-}P_5)]$ (50 mg, 0.145 mmol) and $[CpFe(\eta^5\text{-}P_5)]$ (4.5 mg, 0.016 mmol) in CH_2Cl_2 (12 mL) is carefully layered with a colorless solution of CuCl (36 mg, 0.36 mmol) in CH_3CN (12 mL). Thereby the phase boundary turns yellow-brownish. Already after one day the formation of black rhombohedra of **5a** at the phase boundary can be observed. After a longer period of time, a small amount of the polymer $[Cp^*Fe(\eta^5\text{-}P_5)(CuCl)]_n$[10a] at the bottom as well as, later on, of the 90-vertex supramolecule $[Cp^*Fe(\eta^5\text{-}P_5)]@[\{Cp^*Fe(\eta^5\text{-}P_5)\}_{12}(CuCl)_{25}(CH_3CN)_{10}]$[11e] appear. After complete diffusion the mother liquor is decanted, the crystals are washed with hexane (3 x 10 mL) and dried *in vacuo*.

The only way to get pure **5a** is to take the crystals as soon as possible from the Schlenk wall (when the solutions are not yet diffused completely) with a spatula and quickly dip it into a Schlenk tube with hexane.

Analytical data of **5a**:

Yield: 48 mg (7.8 µmol, 64%)

^{1}H NMR (CD_2Cl_2): δ [ppm] = 1.43 (s, $[(C_5\underline{Me}_5)Fe(\eta^5\text{-}P_5)]$), 2.10 (s, br), 2.18 (s, br), 2.26 (s, br), 3.65 (s, $[(C_5\underline{H}_5)Fe(\eta^5\text{-}P_5)]$).

^{31}P{^{1}H} NMR (CD_2Cl_2): δ [ppm] = 70.4 (s, br), 76.3 (s, br), 110.3 (s, br), 152.08 (s, $[Cp^*Fe(\eta^5\text{-}\underline{P}_5)]$), 170.50 (s, $[CpFe(\eta^5\text{-}\underline{P}_5)]$).

Positive ion ESI-MS (CH_2Cl_2): *m/z* (%) = 1894.3 $[\{Cp^*Fe(\eta^5\text{-}P_5)\}_3Cu_9Cl_8]^+$, 1794.4 $[\{Cp^*Fe(\eta^5\text{-}P_5)\}_3Cu_8Cl_7]^+$, 1744.7 $[\{Cp^*Fe(\eta^5\text{-}P_5)\}_4Cu_4Cl_3]^+$, 1696.5 $[\{Cp^*Fe(\eta^5\text{-}P_5)\}_3Cu_7Cl_6]^+$, 1596.6 $[\{Cp^*Fe(\eta^5\text{-}P_5)\}_3Cu_6Cl_5]^+$, 1496.5 $[\{Cp^*Fe(\eta^5\text{-}P_5)\}_3Cu_5Cl_4]^+$, 1398.7 $[\{Cp^*Fe(\eta^5\text{-}P_5)\}_3Cu_4Cl_3]^+$, 1298.7 $[\{Cp^*Fe(\eta^5\text{-}P_5)\}_3Cu_3Cl_2]^+$, 1150.6 $[\{Cp^*Fe(\eta^5\text{-}P_5)\}_2Cu_5Cl_4]^+$, 1052.6 $[\{Cp^*Fe(\eta^5\text{-}P_5)\}_2Cu_4Cl_3]^+$, 952.7 $[\{Cp^*Fe(\eta^5\text{-}P_5)\}_2Cu_3Cl_2]^+$, 854.8 $[\{Cp^*Fe(\eta^5\text{-}P_5)\}_2Cu_2Cl]^+$, 754.9 (100) $[\{Cp^*Fe(\eta^5\text{-}P_5)\}_2Cu]^+$, 449.9 $[\{Cp^*Fe(\eta^5\text{-}P_5)\}Cu(CH_3CN)]^+$, 408.8 $[\{Cp^*Fe(\eta^5\text{-}P_5)\}Cu]^+$.

Negative ion ESI-MS (CH_2Cl_2): *m/z* (%) = 530.4 $[Cu_5Cl_6]^-$, 332.5 $[Cu_3Cl_4]^-$, 232.6 $[Cu_2Cl_3]^-$, 134.7 $[CuCl_2]^-$.

EI-MS (70 eV): 345.9 $[Cp^*Fe(\eta^5\text{-}P_5)]$, 283.9 $[\{Cp^*Fe(\eta^5\text{-}P_5)\}\text{-}P_2]$.

Elemental analysis: Calculated (%) for $[\{CpFe(\eta^5\text{-}P_5)\}\{Cp^*Fe(\eta^5\text{-}P_5)\}_{12}(CuCl)_{17}]$ (6110 g/mol): C 24.57, H 3.05; found: C 25.77, H 3.42.

Synthesis of [CpFe(η5-P5)]@[{Cp*Fe(η5-P5)}12(CuBr)17.6] (5b)

In a Schlenk tube a green solution of [Cp*Fe(η5-P5)] (50 mg, 0.145 mmol) and [CpFe(η5-P5)] (4.5 mg, 0.016 mmol) in CH_2Cl_2 (12 mL) is carefully layered with a colorless solution of CuBr (52 mg, 0.36 mmol) in CH_3CN (12 mL). Thereby, the phase boundary turns yellow-brownish. Already after one day the formation of black rhombohedra of **5b** at the phase boundary can be observed. After a longer period of time, a considerable amount of the polymer $[Cp^*Fe(\eta^5\text{-}P_5)(CuBr)]_n$[10a] as well as, later on, of the 90-vertex supramolecule $[Cp^*Fe(\eta^5\text{-}P_5)]@[\{Cp^*Fe(\eta^5\text{-}P_5)\}_{12}(CuBr)_{25}(CH_3CN)_{10}]$[11e] appear. After complete diffusion the mother liquor is decanted, the crystals are washed with hexane (3 x 10 mL) and dried *in vacuo*.

Analytical data of **5b** and $[Cp^*Fe(\eta^5\text{-}P_5)(CuBr)]_n$:

Yield: 79 mg

^{1}H NMR (CD_2Cl_2): δ [ppm] = 1.43 (s, [($C_5\underline{Me}_5$)Fe(η5-P5)]), 2.23 (s, br), 2.32 (s, br), 2.34 (s, br), 3.69 (s, br, [($C_5\underline{H}_5$)Fe(η5-P5)]).

^{31}P{^{1}H} NMR (CD_2Cl_2): δ [ppm] = 67.0 (s, br), 152.05 (s, [Cp*Fe(η5-$\underline{P}_5$)]), 170.73 (s, [CpFe(η5-$\underline{P}_5$)]).

Positive ion ESI-MS (CH_2Cl_2): *m/z* (%) = 1042.6 $[\{Cp^*Fe(\eta^5\text{-}P_5)\}_2Cu_3Br_2]^+$, 898.7 $[\{Cp^*Fe(\eta^5\text{-}P_5)\}_2Cu_2Br]^+$, 754.8 $[\{Cp^*Fe(\eta^5\text{-}P_5)\}_2Cu]^+$, 696.9 $[\{Cp^*Fe(\eta^5\text{-}P_5)\}_2Cu_3Br_2]^+$, 552.7 $[\{Cp^*Fe(\eta^5\text{-}P_5)\}Cu_2Br]^+$, 408.8 $[\{Cp^*Fe(\eta^5\text{-}P_5)\}Cu]^+$

Negative ion ESI-MS (CH_2Cl_2): *m/z* (%) = 366.6 $[Cu_2Br_3]^-$, 222.7 (100) $[CuBr_2]^-$

EI-MS (70 eV): 346.1 [Cp*Fe(η5-P5)], 284.1 [{Cp*Fe(η5-P5)}-P_2].

Elemental analysis: Calculated (%) for $[\{CpFe(\eta^5\text{-}P_5)\}\{Cp^*Fe(\eta^5\text{-}P_5)\}_{12}(CuBr)_{17}]$ (6292 g/mol): C 21.87, H 2.72; calculated (%) for $[Cp^*Fe(\eta^5\text{-}P_5)(CuBr)]$ (489.4 g/mol): C 24.54, H 3.09; found: C 24.52, H 3.05.

Synthesis of [CpFe(η5-P5)]@[{Cp*Fe(η5-P5)}12(CuI)19.05] (5c)

In a Schlenk tube a green solution of [Cp*Fe(η5-P5)] (50 mg, 0.145 mmol) and [CpFe(η5-P5)] (4.5 mg, 0.016 mmol) in CH_2Cl_2 (12 mL) is carefully layered with a colorless solution of CuI (69 mg, 0.36 mmol) in CH_3CN (12 mL). Thereby, the phase boundary turns yellow-brownish and turbid. Already after one day the formation of black rhombohedra of **5c** at the phase boundary and brown plates of the 2D polymer $[\{Cp^*Fe(\eta^5\text{-}P_5)\}(CuI)]_n$[10a] can be observed. After complete diffusion the mother liquor is decanted, the crystals are washed with hexane (3 x 10 mL) and dried *in vacuo*. Unfortunately, a 'one after the other'-crystallization or a spatial separation of the crystals of the sphere and the polymer (see **5a** and **5b**) is not observed for **5c**, hence **5c** and $[\{Cp^*Fe(\eta^5\text{-}P_5)\}(CuI)]_n$ cannot be separated from each other.

Analytical data of **5c** and $[\{Cp^*Fe(\eta^5\text{-}P_5)\}(CuI)]_n$:

Yield: 78 mg

^{1}H NMR (pyridine-d_5): δ [ppm] = 1.32 (s, [(C$_5$*Me*$_5$)Fe(η^5-P$_5$)]), 4.44 (s, [(C$_5$*H*$_5$)Fe(η^5-P$_5$)]).

^{31}P{^{1}H} NMR (pyridine-d_5): δ [ppm] = 146.25 (s, [Cp*Fe(η^5-*P*$_5$)]), 148.64 (s, [CpFe(η^5-*P*$_5$)]).

Positive ion ESI-MS (pyridine): *m/z* (%) = 948.7 [{Cp*Fe(η^5-P$_5$)}Cu$_3$I$_2${C$_5$H$_5$N}$_2$]$^+$, 869.7 [{Cp*Fe(η^5-P$_5$)}Cu$_3$I$_2${C$_5$H$_5$N}]$^+$, 790.5 [{Cp*Fe(η^5-P$_5$)}Cu$_3$I$_2$]$^+$, 756.9 [{Cp*Fe(η^5-P$_5$)}Cu$_2$I{C$_5$H$_5$N}$_2$]$^+$, 677.8 [{Cp*Fe(η^5-P$_5$)}Cu$_2$I{C$_5$H$_5$N}]$^+$, 600.7 [{Cp*Fe(η^5-P$_5$)}Cu$_2$I]$^+$, 487.9 [{Cp*Fe(η^5-P$_5$)}Cu{C$_5$H$_5$N}]$^+$.

Negative ion ESI-MS (pyridine): *m/z* (%) = 888.4 [Cu$_4$I$_5$]$^-$, 698.4 [Cu$_3$I$_4$]$^-$, 316.7 (100) [CuI$_2$]$^-$.

EI-MS (70 eV, pyridine): 346.0 [Cp*Fe(η^5-P$_5$)], 284.0 [{Cp*Fe(η^5-P$_5$)}-P$_2$], 79.1 [C$_5$H$_5$N].

Elemental analysis: Calculated (%) for [{CpFe(η^5-P$_5$)}{Cp*Fe(η^5-P$_5$)}$_{12}$(CuI)$_{19.05}$] (8055 g/mol): C 18.64, H 2.32; calculated (%) for [Cp*Fe(η^5-P$_5$)(CuI)] (536.4 g/mol): C 22.39, H 2.82; found: C 21.80, H 2.73.

10.4 Crystallographic Details

Crystals of **1b-5c** were taken from a Schlenk flask under a stream of argon and immediately covered with mineral oil or perfluorinated Fomblin® mineral oil to prevent both decomposition and a loss of solvent. The quickly chosen single crystals covered by a drop of the oil were taken to the pre-centered goniometer head with CryoMount® and directly attached to the diffractometer into a stream of cold nitrogen. X-ray diffraction studies of **2a**, **2b**, **3** and **4** faced many challenges, since the crystals are very small and systematically twinned owing to their layered structure. Therefore, the single crystals chosen for measurement had low diffraction power and the collection of data at high theta angles required high exposure times.

The data for **1b** and **5b** were collected on an Agilent Technologies Gemini R-Ultra diffractometer equipped with Atlas^{S2} CCD detector and an Enhanced Ultra CuK_α sealed tube (λ = 1.54178 Å) using 1° ω scans. The data for **2a**, **2b, 3, 4, 5a** and **5c** were collected on an Agilent Technologies diffractometer equipped with Titan^{S2} CCD detector and a SuperNova CuK_α microfocus source using 0.5 or 1° ω scans depending on the unit cell parameters. All measurements (except for **1b** r.t.) were performed at 123 K. The data for **1b** at r.t. were collected on an Agilent Technologies diffractometer equipped with Atlas CCD detector and a SuperNova CuK_α microfocus source using 1° ω scans.

All structures were solved by direct methods with *SHELX97*.[37] The structures were refined by full-matrix least-squares method against $|F|^2$ in anisotropic approximation using *SHELXL97* or the multiprocessor and variable memory version *SHELXL2013*. All non-hydrogen atoms were refined anisotropically, while the hydrogen atoms were refined riding on pivot atoms. Compounds **2a** and **2b** proved to be isostructural; and **2b** was refined using the model found for **2a**. The model of **5b** was used to refine the two other crystal structures of the isostructural series **5**. Nevertheless, the distribution of vacancies in the core of the supramolecules proved to be different. The enlarged

displacement parameters for Cu and X indicated partial occupancies for several CuX fragments. The occupancies were refined with equated to average displacement parameters for the heavy atoms in every structure. The occupancies were fixed at the resulting values and the refinement of the displacement parameters was performed.

5b crystallizes as solvate **5b**·2.19CH_2Cl_2·6.15CH_3CN. The solvent molecules are severely disordered in the packing voids of the supramolecules. Therefore the solvent portion can be seriously underestimated from X-ray diffraction data. For **5a** and **5c** a final solvent content cannot be given at this stage of refinement.

The occupancy factors of the Fe atoms of **1b** indicate that the cavities are fully occupied by the guest molecule in all supramolecules **5a-c**. They appeared to be disordered over three or six positions in the inner cavity of the host supramolecules, unexpectedly with different probability for every position. Since there are two independent positions ($\bar{1}$ and $\bar{3}$ point symmetry), the way of disorder is not identical, because some of the disordered positions are related by symmetry operations, which are different. In addition, the P_5 and C_5 rings occupy very close positions. For these reasons the disorder of the **1b** molecule as a guest is very sophisticated. An algorithm for non-contradictory positions of the guest in accordance with the electron density needs to be developed. Therefore only preliminary data can be given for **5a-c**.

Crystallographic data and details of the diffraction experiments are given in *Table 10.2 – Table 10.6*.

Table 10.2 Experimental details for compound **1b** (at 123 K and at r.t.).

Crystal Data	1b	1b r.t.
Chemical formula	$C_5H_5FeP_5$	$C_5H_5FeP_5$
M_r	275.79	275.79
Crystal system, space group	monoclinic, $P2_1/m$	monoclinic, $P2_1/m$
Temperature (K)	123(1)	298(1)
a, *b*, *c* (Å)	6.7227(4), 10.7738(5), 6.9507(4)	6.7805(2), 10.9485(3), 7.0045(2)
α, β, γ (°)	90, 110.893(6), 90	90, 111.057(4) , 90
V (Å^3)	470.33(4)	485.26(2)
Z	2	2
F(000)	272	272
Radiation type	Cu K_α	Cu K_α
μ (mm^{-1})	20.31	19.74
Crystal color and shape	green prism	green prism
Crystal size (mm)	0.22 × 0.21 × 0.12	0.17 × 0.10 × 0.08
Data collection		
Diffractometer	Xcalibur, Atlas, Gemini ultra diffractometer	SuperNova, Single source at offset, Atlas diffractometer

Absorption correction	analytical	gaussian
T_{min}, T_{max}	0.058, 0.238	0.105, 0.365
No. of measured, independent and observed [$I > 2\sigma(I)$] reflections	1606, 867, 792	4279, 1020, 963
R_{int}	0.025	0.026
$(\sin\theta/\lambda)_{max}$ (Å^{-1})	0.597	0.621
Range of h, k, l	h = -7→7, k = -12→8, l = -8→8	h = -8→8, k = -13→13, l = -7→8
Refinement		
$R[F^2 > 2\sigma(F^2)]$, $wR(F^2)$, S	0.029, 0.074, 1.00	0.034, 0.090, 1.10
No. of reflections	867	1020
No. of parameters	56	56
No. of restraints	0	0
H-atom treatment	H-atom parameters constrained	H-atom parameters constrained
$\Delta\rangle_{max}$, $\Delta\rangle_{min}$ (e Å^{-3})	0.56, -0.38	0.63, -0.61

Table 10.3 Experimental details for compounds **2a** and **2b**.

Crystal Data	**2a**	**2b**
Chemical formula	$C_5H_5Cl_2Cu_2FeP_5$	$C_5H_5Br_2Cu_2FeP_5$
M_r	473.77	562.69
Crystal system, space group	triclinic, $P\bar{1}$	triclinic, $P\bar{1}$
Temperature (K)	123(1)	123(1)
a, b, c (Å)	7.1920(12), 7.3682(9), 12.724(1)	7.1319(8), 7.4112(7), 13.043(1)
α, β, γ (°)	91.817(8), 91.11(1), 117.41(2)	91.262(7), 91.052(8), 115.83(1)
V (Å^3)	597.83(13)	620.07(12)
Z	2	2
F(000)	456	528
Radiation type	Cu K_α	Cu K_α
μ (mm^{-1})	23.82	26.58
Crystal color and shape	orange plate	orange plate
Crystal size (mm)	0.13 × 0.10 × 0.03	0.07 × 0.04 × 0.01
Data collection		
Diffractometer	SuperNova, Titan^{S2} diffractometer	SuperNova, Titan^{S2} diffractometer
Absorption correction	gaussian	gaussian
T_{min}, T_{max}	0.161, 0.569	0.363, 0.795
No. of measured, independent and observed [$I > 2\sigma(I)$] reflections	3377, 2250, 1489	3581, 2367, 1609
R_{int}	0.088	0.075
$(\sin\theta/\lambda)_{max}$ (Å^{-1})	0.623	0.623
Range of h, k, l	h = -8→8, k = -7→9, l = -12→15	h = -8→8, k = -9→8, l = -15→16
Refinement		

$R[F^2 > 2\sigma(F^2)]$, $wR(F^2)$, S	0.086, 0.240, 1.01	0.059, 0.176, 1.09
No. of reflections	2250	2367
No. of parameters	136	136
No. of restraints	0	12
H-atom treatment	H-atom parameters constrained	H-atom parameters constrained
$\Delta\rangle_{max}$, $\Delta\rangle_{min}$ (e Å^{-3})	2.15, -1.79	1.88, -1.44

Table 10.4 Experimental details for compounds **3** and **4**.

Crystal Data	**3**	**4**
Chemical formula	$C_5H_5CuFeIP_5$	$C_5H_5CuFeIP_5$
M_r	466.23	466.23
Crystal system, space group	monoclinic, $P2_1/c$	orthorhombic, $Pna2_1$
Temperature (K)	123	123(1)
a, b, c (Å)	19.7543(5), 13.9715(4), 12.6806(5)	13.4299(2), 11.5468(2), 7.4118(1)
α, β, γ (°)	90, 95.104(3), 90	90, 90, 90
V (Å^3)	3485.93(19)	1149.37(3)
Z	12	4
F(000)	2616	872
Radiation type	Cu K_α	Cu K_α
μ (mm^{-1})	39.35	39.67
Crystal color and shape	orange plate	red prism
Crystal size (mm)	0.11 × 0.06 × 0.01	0.10 × 0.06 × 0.05
Data collection		
Diffractometer	SuperNova, Titan^{S2} diffractometer	SuperNova, Titan^{S2} diffractometer
Absorption correction	gaussian	gaussian
T_{min}, T_{max}	0.139, 0.732	0.097, 0.322
No. of measured, independent and observed [$I > 2\sigma(I)$] reflections	11998, 6679, 2798	12912, 2281, 2131
R_{int}	0.158	0.055
$(\sin\theta/\lambda)_{max}$ (Å^{-1})	0.624	0.624
Range of h, k, l	h = -24→24, k = -17→15, l = -15→15	h = -16→16, k = -12→13, l = -9→9
Refinement		
$R[F^2 > 2\sigma(F^2)]$, $wR(F^2)$, S	0.085, 0.238, 0.89	0.023, 0.055, 0.98
No. of reflections	6679	2281
No. of parameters	352	118
No. of restraints	90	1
H-atom treatment	H-atom parameters constrained	H-atom parameters constrained

$\Delta\rangle_{max}$, $\Delta\rangle_{min}$ (e Å^{-3})	3.08, -2.67	0.49, -0.80
Absolute structure parameter[38]	-	0.004(4)

Table 10.5 Experimental details for compounds **5a** and **5b** (* = preliminary data).[39]

Crystal Data	5a	5b
Chemical formula	$C_{125}H_{185}Cl_{17.6}Cu_{17.6}Fe_{13}P_{65}$*	$C_{125}H_{185}Br_{17.6}Cu_{17.6}Fe_{13}P_{65}\cdot 2.19CH_2Cl_2\cdot 6.15CH_3CN$*
M_r	6169.46*	7204.33*
Crystal system, space group	trigonal, $R\bar{3}$	trigonal, $R\bar{3}$
Temperature (K)	123(1)	123(1)
a, *b*, *c* (Å)	41.9137(2), 41.9137(2), 51.6343(4)	42.3428(2), 42.3428(2), 52.2621(4)
α, β, γ (°)	90, 90, 120	90, 90, 120
V (Å^3)	78556.2(8)	81147.7(8)
Z	12	12
Radiation type	Cu K_α	Cu K_α
μ (mm^{-1})	> 12.95	> 15.38
Crystal color and shape	black rhombohedron	black rhombohedron
Crystal size (mm)	0.29 x 0.19 x 0.16	0.63 x 0.29 x 0.20
Data collection		
Diffractometer	SuperNova, Single source at offset, Atlas diffractometer	Xcalibur, Atlas, Gemini ultra diffractometer
Absorption correction	gaussian	analytical
T_{min}, T_{max}	3.591, 73.580	3.285, 66.815
No. of measured reflections	213840	495971
R_{int}	0.057	0.066
Range of h, k, l	*h* = -37→42, *k* = -51→52, *l* = -58→63	*h* = -50→50, *k* = -50→50, *l* = -62→62
Refinement	*	*
$R[F^2 > 2\sigma(F^2)]$, $wR(F^2)$, *S*	0.0868, 0.2524, 1.050	0.0439, 0.1425, 1.055
No. of reflections	28960	26604
No. of parameters	1567	1827
No. of restraints	0	27
H-atom treatment	H-atom parameters constrained	H-atom parameters constrained
$\Delta\rangle_{max}$, $\Delta\rangle_{min}$ (e Å^{-3})	3.798, -3.887	2.090, -2.034

Table 10.6 Experimental details for compound **5c** (* = preliminary data).[39]

Crystal Data	5c
Chemical formula	$C_{150}H_{185}I_{19.05}Cu_{19.05}Fe_{13}P_{65}$*

M_r	8055.22*
Crystal system, space group	trigonal, $R\bar{3}$
Temperature (K)	123(1)
a, *b*, *c* (Å)	42.49380(10), 42.49380(10), 52.3369(2)
α, β, γ (°)	90, 90, 120
V (Å^3)	81844.5(5)
Z	12
Radiation type	Cu K_α
μ (mm^{-1})	> 27.733
Crystal color and shape	black rhombohedron
Crystal size (mm)	0.21 x 0.18 x 0.12
Data collection	
Diffractometer	SuperNova, Titan^{S2} diffractometer
Absorption correction	gaussian
T_{min}, T_{max}	0.117, 0.396
No. of measured reflections	36703
R_{int}	0.0850
Range of h, k, l	*h* = -47→51, *k* = -53→42, *l* = -61→65
Refinement	*
$R[F^2 > 2\sigma(F^2)]$, $wR(F^2)$, *S*	0.0739, 0.2495, 1.074
No. of reflections	30434
No. of parameters	1563
No. of restraints	0
H-atom treatment	H-atom parameters constrained
$\Delta\rangle_{max}$, $\Delta\rangle_{min}$ (e Å^{-3})	4.358, 5.097

Topological classification of the coordination networks in 2a, 2b, 3 and 4

The topological classification of the coordination networks was done by the method described in references [30] and [40] using the ToposPro[29] program set. With this method, the initial network is represented as an underlying net, whose nodes correspond to centroids of structural groups and whose edges correspond to μ_2-ligands. Any other 2-coordinated fragments display spacers. The simplification of the crystal structure to the underlying net was done using the ADS subroutine of the ToposPro program set.

The 2D underlying net in the isostructural compounds **2a** and **2b** consists of three types of nodes, namely, two topologically different 3-coordinated Cu^+ cations and one 4-coordinated {$CpFeP_5$} fragment (*Figure 10.10*). The μ-X (X = Cl, Br) ligands display spacers. The resulting 3-nodal 3,3,4-

connected net with the stoichiometry (3-c)(3-c)(4-c) consists of 4-, 5- and 6-membered rings (*Figure 10.10*). With the point (Schlafli) symbol of $\{4.5^2.6.7^2\}\{4.5^2\}\{5.6^2\}$ it belongs to a new topological type that is not yet recorded in the current TTD collection of the TOPOSPro system.

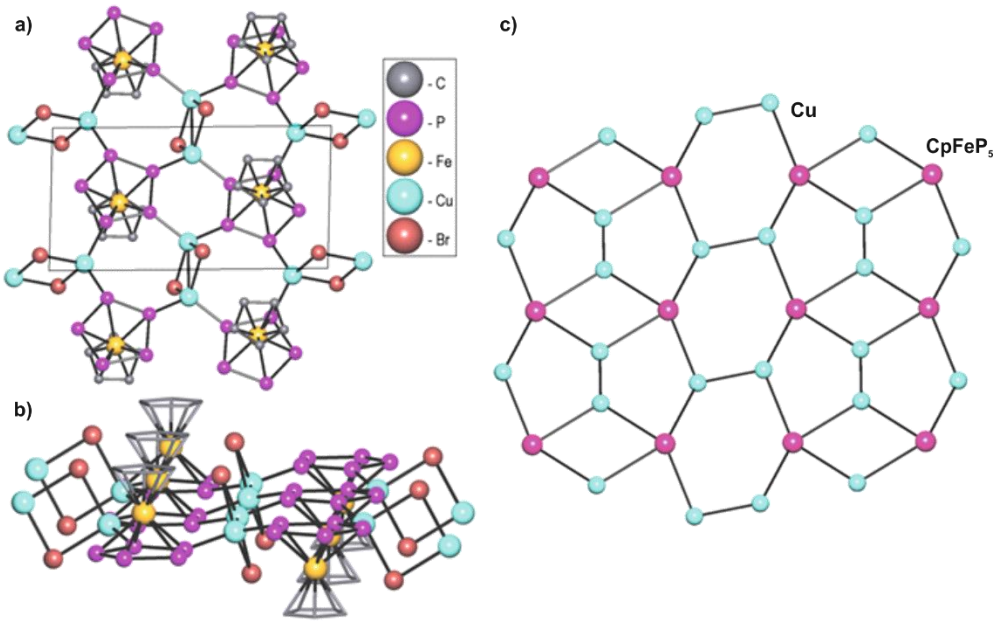

Figure 10.10 Section of a layer in the crystal of **2b**: a) view along *a* axis; b) side view; hydrogen atoms are omitted for clarity; c) the corresponding underlying net.

The $\{CpFeP_5\}$ fragments in compounds **3** and **4**, being 2-coordinated, play the role of non-linear bulky spacers. Together with the μ-I spacers they join Cu^+ nodes into the distorted planar honeycomb layer in **3** (*Figure 10.11*) and the diamond-like network in **4** (*Figure 10.11*). According to the RCSR notation, the corresponding topological types are **hcb** and **dia** respectively.[31]

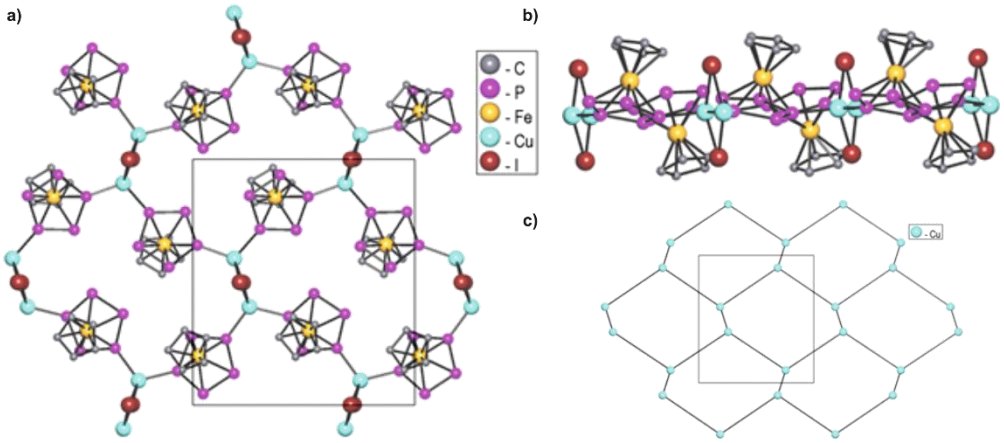

Figure 10.11 Section of a layer in the crystal of **3**: a) view along *a*; b) side view; hydrogen atoms are omitted for clarity; c) the 2D underlying net with **hcb** topology in **3**, view along *a* axis.

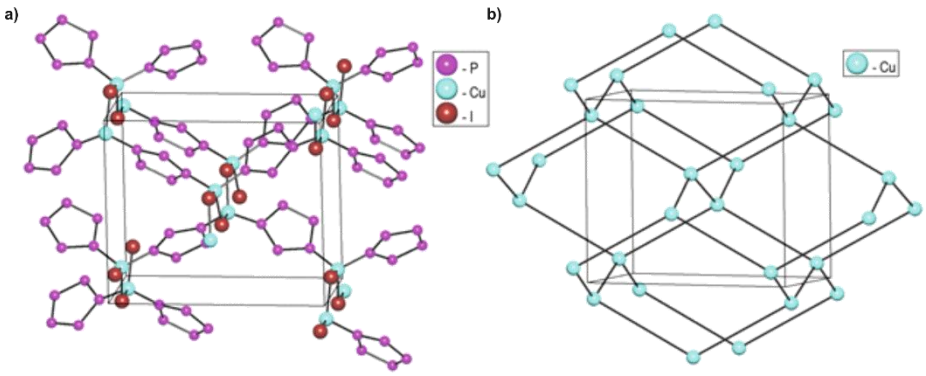

Figure 10.12 a) Fragment of the 3D framework in **4**; Fe atoms and Cp ligands are omitted for clarity; b) the 3D underlying net with **dia** topology.

10.5 Author Contributions

- The syntheses and characterization of all compounds **1b** – **5c** were performed by Claudia Heindl
- X-ray structural analyses of **1b** – **5c** were performed by Dr. Eugenia V. Peresypkina, Dr. Alexander V. Virovets and Claudia Heindl
- The manuscript (introduction, results and discussion, experimental part; including figures and graphical abstract) was written by Claudia Heindl; with the following exceptions:
- The section 'crystallographic details' was written by Dr. Eugenia V. Peresypkina
- The TOPOS analysis and description in the crystallographic part was done by Dr. Alexander V. Virovets
- The cyclovoltammetric measurement of **1b** was performed and interpreted by Eric Mädl
- DFT computations and their description regarding **1b** were performed by Dr. Gábor Balázs

10.6 References

[1] a) T. J. Kealy, P. L. Pauson, *Nature* **1951**, *168*, 1039; b) G. Wilkinson, M. Rosenblum, M. C. Whiting, R. B. Woodward, *J. Am. Chem. Soc.* **1952**, *74*, 2125.

[2] G. Wilkinson, *Angew. Chem.* **1974**, *86*, 664.

[3] a) G. Gritzner, J. Kuta, *Pure Appl. Chem.* **1984**, *56*, 461; b) N. G. Connelly, W. E. Geiger, *Chem. Rev.* **1996**, *96*, 877.

[4] a) A. Togni, in *Metallocenes: Synthesis - Reactivity - Applications*, Volume 11 (Eds.: A. Togni, R. Halterman), WILEY-VCH, **1998**, pp. 685–718; b) C. J. Richards, A. J. Locke, *Tetrahedron: Asymmetry* **1998**, *9*, 2377.

[5] a) T. Fukino, H. Joo, Y. Hisada, M. Obana, H. Yamagishi, T. Hikima, M. Takata, N. Fujita, T. Aida, *Science* 2014, *344*, 499; b) Z. M. Hudson, I. Manners, *Science* 2014, *344*, 482; c) P. Nguyen, P. Gomez-Elipe, I. Manners, *Chem. Rev.* 1999, *99*, 1515.

[6] a) I. P. Chang, K. C. Hwang, C.-S. Chiang, *J. Am. Chem. Soc.* 2008, *130*, 15476; b) H. Kumari, C. L. Dennis, A. V. Mossine, C. A. Deakyne, J. L. Atwood, *J. Am. Chem. Soc.* 2013, *135*, 7110.

[7] a) F. Mathey, A. Mitschler, R. Weiss, *J. Am. Chem. Soc.* 1977, *99*, 3537; b) L. Weber, *Angew. Chem. Int. Ed.* 2002, *41*, 563.

[8] O. J. Scherer, T. Brück, *Angew. Chem.* 1987, *99*, 59.

[9] a) O. J. Scherer, T. Brück, G. Wolmershäuser, *Chem. Ber.* 1989, *122*, 2049; b) M. Detzel, T. Mohr, O. J. Scherer, G. Wolmershäuser, *Angew. Chem.* 1994, *106*, 1142; c) B. Rink, O. J. Scherer, G. Wolmershäuser, *Chem. Ber.* 1995, *128*, 71.

[10] a) J. Bai, A. V. Virovets, M. Scheer, *Angew. Chem. Int. Ed.* 2002, *41*, 1737; b) M. Scheer, L. J. Gregoriades, A. V. Virovets, W. Kunz, R. Neueder, I. Krossing, *Angew. Chem. Int. Ed.* 2006, *45*, 5689; c) F. Dielmann, A. Schindler, S. Scheuermayer, J. Bai, R. Merkle, M. Zabel, A. V. Virovets, E. V. Peresypkina, G. Brunklaus, H. Eckert, M. Scheer, *Chem. Eur. J.* 2012, *18*, 1168; d) C. Heindl, S. Heinl, D. Luedeker, G. Brunklaus, W. Kremer, M. Scheer, *Inorg. Chim. Acta* 2014, *422*, 218; e) M. Fleischmann, L. Duetsch, M. E. Moussa, A. Schindler, G. Balázs, C. Lescop, M. Scheer, *Chem. Commun.* 2015, *51*, 2893; f) M. Fleischmann, S. Welsch, H. Krauss, M. Schmidt, M. Bodensteiner, E. V. Peresypkina, M. Sierka, C. Groeger, M. Scheer, *Chem. Eur. J.* 2014, *20*, 3759.

[11] a) E. V. Peresypkina, C. Heindl, A. Schindler, M. Bodensteiner, A. V. Virovets, M. Scheer, *Z. Kristallogr.* 2014, *229*, 735; b) C. Schwarzmaier, A. Schindler, C. Heindl, S. Scheuermayer, E. V. Peresypkina, A. V. Virovets, M. Neumeier, R. Gschwind, M. Scheer, *Angew. Chem. Int. Ed.* 2013, *52*, 10896; c) A. Schindler, C. Heindl, G. Balázs, C. Groeger, A. V. Virovets, E. V. Peresypkina, M. Scheer, *Chem. Eur. J.* 2012, *18*, 829; d) S. Welsch, C. Groeger, M. Sierka, M. Scheer, *Angew. Chem. Int. Ed.* 2011, *50*, 1435; e) M. Scheer, A. Schindler, J. Bai, B. P. Johnson, R. Merkle, R. Winter, A. V. Virovets, E. V. Peresypkina, V. A. Blatov, M. Sierka H. Eckert, *Chem. Eur. J.* 2010, *16*, 2092; f) M. Scheer, A. Schindler, C. Groeger, A. V. Virovets, E. V. Peresypkina, *Angew. Chem. Int. Ed.* 2009, *48*, 5046; g) M. Scheer, A. Schindler, R. Merkle, B. P. Johnson, M. Linseis, R. Winter, C. E. Anson, A. V. Virovets, *J. Am. Chem. Soc.* 2007, *129*, 13386; h) M. Scheer, J. Bai, B. P. Johnson, R. Merkle, A. V. Virovets, C. E. Anson, *Eur. J. Inorg. Chem.* 2005, 4023; i) J. Bai, A. V. Virovets, M. Scheer, *Science* 2003, *300*, 781.

[12] O. J. Scherer, T. Brück, G. Wolmershäuser, *Chem. Ber.* 1988, *121,* 935.

[13] M. Fleischmann, J. S. Jones, F. P. Gabbai, M. Scheer, *Chem. Sci.* 2015, *6*, 132.

[14] O. J. Scherer, T. Hilt, G. Wolmershäuser, *Organometallics* 1998, *17*, 4110.

[15] F. Dielmann, R. Merkle, S. Heinl, M. Scheer, *Z. Naturforsch.* 2009, *64*, 3.

[16] S. Heinl, G. Balázs, M. Scheer, *Phosphorus, Sulfur Silicon Relat. Elem.* 2014, *189*, 924.

[17] a) T. P. Gryaznova, S. A. Katsyuba, V. A. Milyukov, O. G. Sinyashin, *J. Organomet. Chem.* 2010, *695*, 2586; b) E. J. Padma Malar, *Eur. J. Inorg. Chem.* 2004, 2723; c) J. Frunzke, M. Lein, G. Frenking, *Organometallics* 2002, *21*, 3351; d) G. Frison, F. Mathey, A. Sevin, *J. Phys. Chem. A* 2002, *106*, 5653.

[18] O. J. Scherer, G. Kemény, G. Wolmershäuser, *Chem. Ber.* 1995, *128*, 1145.

[19] M. Fleischmann, C. Heindl, M. Seidl, G. Balázs, A. V. Virovets, E. V. Peresypkina, M. Tsunoda, F. P. Gabbaï, M. Scheer, *Angew. Chem. Int. Ed.* 2012, *51*, 9918.

[20] Y.-P. Wang, P. Wu, H.-Y. Cheng, T.-S. Lin, S.-L. Wang, *J. Organomet. Chem.* 2009, *694*, 285.

[21] G. L. Hardgrove, D. H. Templeton, *Acta Cryst.* 1959, *12*, 28.

[22] J. C. A. Boeyens, D. C. Levendis, M. I. Bruce, M. L. Williams, *J. Crystallogr. Spectrosc. Res.* 1986, *16*, 519.

[23] P. Seiler, J. D. Dunitz, *Acta Cryst. sect. B* 1982, *B38*, 1741.

[24] R. G. Winter, W.E. Geiger, *Organometallics* 1999, *18*, 1827.

[25] M. V. Butovskiy, G. Balázs, M. Bodensteiner, E. V. Peresypkina, A. V. Virovets, J. Sutter, M. Scheer, *Angew. Chem. Int. Ed.* 2013, *52*, 2972.

[26] All calculations have been performed with the Gaussian 09 at the B3LYP/6-31++G(3df,3pd) level of theory. The geometry of **1b** has been optimised without symmetry restrains, although the optimized geometry is C_{5v} symmetric. The orbital labelling is according to C_{5v} point group. Program: gaussian 09, Revision D.01, M. J. Frisch, G. W. Trucks, H. B. Schlegel, G. E. Scuseria, M. A. Robb, J. R. Cheeseman, G. Scalmani, V. Barone, B. Mennucci, G. A. Petersson, H. Nakatsuji, M. Caricato, X. Li, H. P. Hratchian, A. F. Izmaylov, J. Bloino, G. Zheng, J. L. Sonnenberg, M. Hada, M. Ehara, K. Toyota, R. Fukuda, J. Hasegawa, M. Ishida, T. Nakajima, Y. Honda, O. Kitao, H. Nakai, T. Vreven, J. A. Montgomery, Jr., J. E. Peralta, F. Ogliaro, M. Bearpark, J. J. Heyd, E. Brothers, K. N. Kudin, V. N. Staroverov, T. Keith, R. Kobayashi, J. Normand, K. Raghavachari, A. Rendell, J. C. Burant, S. S. Iyengar, J. Tomasi, M. Cossi, N. Rega, J. M. Millam, M. Klene, J. E. Knox, J. B. Cross, V. Bakken, C. Adamo, J. Jaramillo, R. Gomperts, R. E. Stratmann, O. Yazyev, A. J. Austin, R. Cammi, C. Pomelli, J. W. Ochterski, R. L. Martin, K. Morokuma, V. G. Zakrzewski, G. A. Voth, P. Salvador, J. J. Dannenberg, S. Dapprich, A. D. Daniels, O. Farkas, J. B. Foresman, J. V. Ortiz, J. Cioslowski, and D. J. Fox, gaussian, Inc., Wallingford CT, 2013.

[27] H. Krauss, G. Balázs, M. Bodensteiner, M. Scheer, *Chem. Sci.* 2010, 1, 337.

[28] F. Dielmann, C. Heindl, F. Hastreiter, E. V. Peresypkina, A. V. Virovets, R. M. Gschwind, M. Scheer, *Angew. Chem. Int. Ed.* 2014, *53*, 13605.

[29] V. A. Blatov, A. P. Shevchenko, D. M. Proserpio. *Cryst. Growth Des*. 2014, *14*, 3576; http://rcsr.anu.edu.au

[30] T. G. Mitina, V. A. Blatov, *Cryst. Growth Des.* 2013, *13*, 1655.

[31] M. O'Keeffe, M. A. Peskov, S. J. Ramsden, O. M. Yaghi, *Accts. Chem. Res.* 2008, *41*, 1782.

[32] A. Bondi, *J. Phys. Chem.* 1964, *68*, 441.

[33] F. Dielmann, M. Fleischmann, C. Heindl, E. V. Peresypkina, A. V. Virovets, R. M. Gschwind, M. Scheer, *Chem. Eur. J.* 2015, *21*, 6208.

[34] R. B. King, F. G. A. Stone, *Inorg. Syn.* 1963, *7*, 99.

[35] This compound was in-house available.

[36] M. Detzel, G. Friedrich, O. J. Scherer, G. Wolmershäuser, *Angew. Chem. Int. Ed.* 1995, *34*, 1321.

[37] G. M. Sheldrick, *Acta Cryst. sect. C* 2015, *C71*, 3.

[38] H. D. Flack, *Acta Cryst. sect. A* 1983, *A39*, 876.

[39] Please note: Due to the uncompleted refinement, not all parameters (e.g. F(000)) can be stated and some given parameters, such as μ, R_{int}, as well as the sum formula have to be treated as temporarily values and may change at a later stage.

[40] V. A. Blatov, D. M. Proserpio, A. R. Oganov in: *Modern Methods of Crystal Structure Prediction,* Wiley-VCH: Weinheim, 2011, Chapter 1.

11. Template Controlled Formation of 80-vertex Fullerene-like Spheres – A Study on Template Requirements

C. Heindl, E. V. Peresypkina, S. Reisinger, A. Biegerl, D. Lüdeker, U. Zenneck, G. Brunklaus, A. V. Virovets, M. Scheer

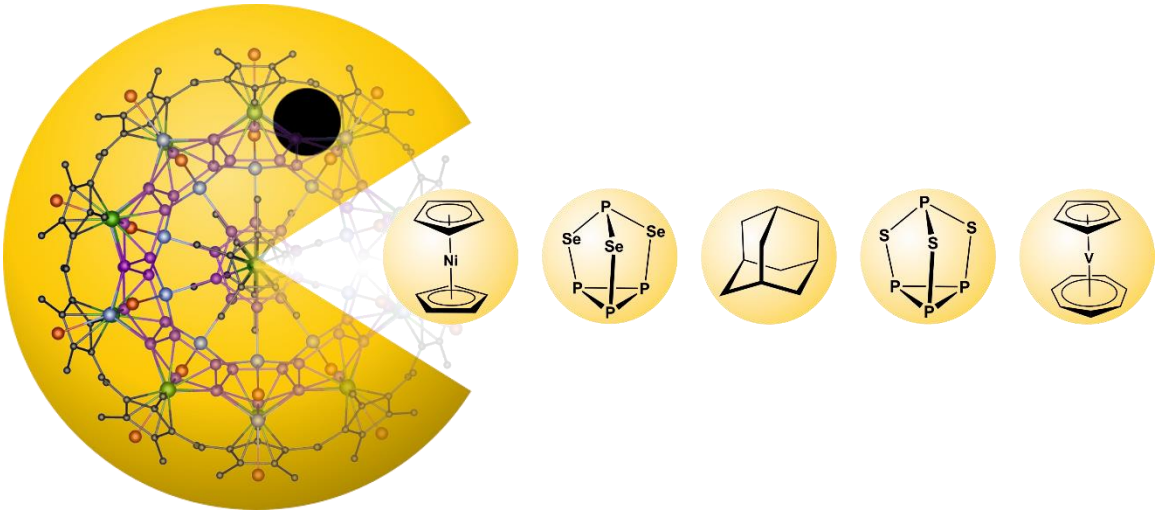

Abstract:

The template-directed self-assembly of [Cp*Fe(η^5-P_5)] with Cu(I) halides leads to the formation of a nano-sized supramolecule exhibiting I_h-C_{80} topology. Herein, a comprehensive study on the required template properties for a successful incorporation is presented. Thereby, a variety of small molecules has been tested for their template capability and nickelocene [$NiCp_2$], trovacene [CpV(η^7-C_7H_7)], the cage molecules P_4Q_3 (Q = S, Se) as well as adamantane $C_{10}H_{16}$ were successfully trapped in this fullerene-like sphere in good to excellent yields. The supramolecules were comprehensively characterized in the solid state by X-ray structural analysis as well as IR and MAS NMR spectroscopy and also in solution by mass spectrometry, NMR and EPR spectroscopy, respectively. In addition, an unprecedented hybrid polymer containing pentaphosphaferrocene, P_4S_3 and CuI could be obtained as a by-product.

11.2 Introduction

Despite earlier hints,[1] finally in 1985, the structure of a cluster consisting of 60 carbons was published by Kroto *et al.*[2] and beside suggestions like 'ballene', 'spherene' or 'soccerene' the name 'Buckminster-fullerene' became established for this third allotrope of carbon. This discovery marked the beginning of a still ongoing success story of the class of fullerenes.[3] For aesthetic reasons alone these compounds exert a special fascination for scientists. However, in addition, they also show interesting properties making them potentially important in many disciplines like biomedicine,[4] catalysis,[5] electrochemistry[6] and cosmetics.[7] In fundamental research much expense is also applied to the synthesis of less stable fullerenes, which either do not fulfill the isolated pentagon rule (IPR)[8] or dispense without spherical aromaticity.[9] C_{80} is one example for the latter and among seven possible isomers the icosahedral topology is even the most unstable one.[10] Nevertheless, its structure could be obtained in endohedral fullerenes like $Sc_3N@I_h\text{-}C_{80}$,[11] $La_2@I_h\text{-}C_{80}$,[12] and $Sc_4O@I_h\text{-}C_{80}$.[13]

Recently, we have introduced an approach to carbon-free supramolecules constructed by pentaphosphaferrocenes and bearing fullerene topology.[14] Applying special conditions, the self-assembly of [Cp*Fe(η^5-P_5)] (Cp* = C_5Me_5) (**1**, *Figure 11.1*a) and CuX (X = Cl, Br) not only leads to the formation of the polymeric products [{Cp*Fe(η^5-P_5)}(CuX)]$_n$ (**2**; **2-Cl**: X = Cl, **2-Br**: X = Br)[15] but also to spherical nano-sized balls of the general formula [Cp*Fe(η^5-P_5)]@[{Cp*Fe(η^5-P_5)}$_{12}$(CuX)$_{25}$(CH_3CN)$_{10}$] (**3**; **3-Cl**: X = Cl, **3-Br**: X = Br). Concerning CuI, only the polymer [{Cp*Fe(η^5-P_5)}(CuI)]$_n$ (**2-I**).[15] The encapsulation of one molecule of **1** in the spheres **3** encourages the assumption of a template effect. Gratifyingly, the addition of *o*-carborane (*Figure 11.1*b) as a template results in its enclosure in the 80-vertex supramolecule to give *o*-$C_2B_{10}H_{12}$@[{Cp*Fe(η^5-P_5)}$_{12}$(CuX)$_{20\text{-}n}$] (**4**; **4-Cl**: X = Cl, n = 0; **4-Br**: X = Br, n = 1.2), whose $Cu_{20}P_{60}$ scaffold represents an inorganic analogue of the I_h-C_{80} fullerene.[16] Shortly afterwards, the metallocenes [$FeCp_2$], [CpCr(η^5-As_5)] and [CpFe(η^5-P_5)] (*Figure 11.1*c,d) could also be encapsulated into this 80-vertex ball to give [$FeCp_2$]@[{Cp*Fe(η^5-P_5)}$_{12}$(CuX)$_{20\text{-}n}$][17] (**5**; **5-Cl**: X = Cl, n = 0; **5-Br**: X = Br, n = 2.7), [CpCr(η^5-As_5)]@[{Cp*Fe(η^5-P_5)}$_{12}$(CuCl)$_{20}$][17b] (**6-Cl**) and [CpFe(η^5-P_5)]@[{Cp*Fe(η^5-P_5)}$_{12}$(CuX)$_{20\text{-}n}$][18] (**7**; **7-Cl**: X = Cl, n = 1.4; **7-Br**: X = Br, n = 1.4; **7-I**: X = I, n = 0.95).

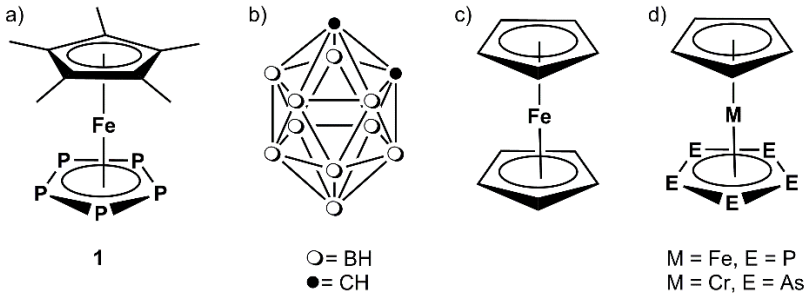

Figure 11.1 a) Pentaphosphaferrocene **1** as building block for carbon-free fullerenes; b)-d) templates incorporated into a carbon-free I_h-C_{80} sphere: b) *o*-carborane; c) [$FeCp_2$]; d) [$CpFe(\eta^5\text{-}P_5)$], [$CpCr(\eta^5\text{-}As_5)$].

Furthermore, the analogous 80-vertex nanoball is obtained exclusively, when the sterically more demanding pentaphosphaferrocene [$Cp^{Bn}Fe(\eta^5\text{-}P_5)$] ($Cp^{Bn}$ = $C_5(CH_2C_6H_5)_5$) (**1-Bn**) is reacted with CuX (X = Cl, Br). Yet its formation is not template-directed and the cavity is filled with CH_2Cl_2 solvent molecules.[19] Nonetheless, these spheres can also be applied in host-guest chemistry and ferrocene has successfully been trapped within the cavity.

On the contrary, the formation of supramolecules built up by the Cp* derivative could exclusively be observed in the presence of the mentioned small molecules, hence their template-dependency is obvious. Therefore, we were interested whether the assembly to the I_h-C_{80} analogue is restricted to templates of icosahedral shape like *o*-carborane or to five-fold symmetric metallocenes.

Herein, we describe the independence of templates possessing five-fold symmetry and present a wide variety of templates, which can be enclosed into the 80-vertex supramolecules [$\{Cp^*Fe(\eta^5\text{-}P_5)\}_{12}(CuX)_{20}$] (X = Cl, Br, I) (*Figure 11.2*). The used molecules all differ in shape, symmetry, number of valence electrons and donor capability. Therefore, a comprehensive study was carried out and will be described in the following.

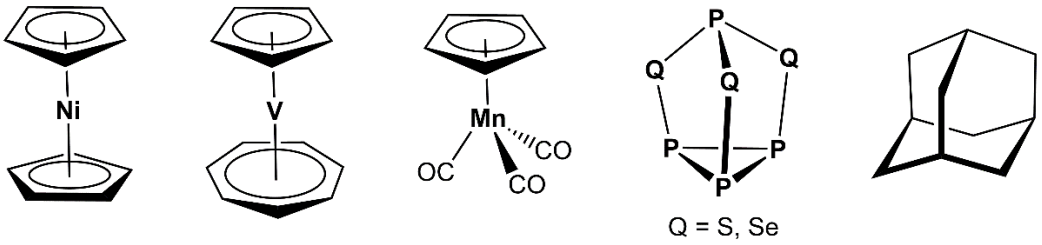

Figure 11.2 Incorporated templates in this chapter: nickelocene [$NiCp_2$], trovacene [$CpV(\eta^7\text{-}C_7H_7)$], cymantrene [$CpMn(CO)_3$], P_4S_3, P_4Se_3 and adamantane $C_{10}H_{16}$.

11.3 Results and Discussion

Synthesis of the Supramolecules

For the synthesis of the supramolecules one unitary procedure is applied: A solution of **1** and the template in CH_2Cl_2 or toluene is carefully layered with a solution of CuX (X = Cl, Br, I) in CH_3CN. Already after several hours crystal growth occurs and the following products were isolated after complete diffusion:

$[NiCp_2]$@$[\{Cp^*Fe(\eta^5\text{-}P_5)\}_{12}(CuBr)_{18.95}]$ (**8-Br**),

$[NiCp_2]$@$[\{Cp^*Fe(\eta^5\text{-}P_5)\}_{12}(CuI)_{18.125}]$ (**8-I**),

$[CpV(\eta^7\text{-}C_7H_7)]$@$[\{Cp^*Fe(\eta^5\text{-}P_5)\}_{12}(CuCl)_{18.20}]$ (**9-Cl**),

$[CpV(\eta^7\text{-}C_7H_7)]$@$[\{Cp^*Fe(\eta^5\text{-}P_5)\}_{12}(CuBr)_{18.83}]$ (**9-Br**),

$[CpV(\eta^7\text{-}C_7H_7)]$@$[\{Cp^*Fe(\eta^5\text{-}P_5)\}_{12}(CuI)_{17.65}]$ (**9-I**),

$[CpMn(CO)_3]_{0.33}$@$[\{Cp^*Fe(\eta^5\text{-}P_5)\}_{12}(CuBr)_{18.05}]$ (**10-Br**),

$[CpMn(CO)_3]_{0.2}$@$[\{Cp^*Fe(\eta^5\text{-}P_5)\}_{12}(CuI)_{18.15}]$ (**10-I**),

$[P_4S_3]_{0.5}$@$[\{Cp^*Fe(\eta^5\text{-}P_5)\}_{12}(CuCl)_{19.5}]$ (**11-Cl**),

$[P_4S_3]_{0.38}$@$[\{Cp^*Fe(\eta^5\text{-}P_5)\}_{12}(CuBr)_{19.025}]$ (**11-Br**),

$[P_4S_3]_{0.44}$@$[\{Cp^*Fe(\eta^5\text{-}P_5)\}_{12}(CuI)_{18.95}]$ (**11-I**),

$[P_4Se_3]_{0.54}$@$[\{Cp^*Fe(\eta^5\text{-}P_5)\}_{12}(CuCl)_{17.375}]$ (**12-Cl**),

$[P_4Se_3]_{0.75}$@$[\{Cp^*Fe(\eta^5\text{-}P_5)\}_{12}(CuBr)_{18.35}]$ (**12-Br**) and

$[C_{10}H_{16}]_{0.425}$@$[\{Cp^*Fe(\eta^5\text{-}P_5)\}_{12}(CuCl)_{17.52}]$ (**13-Cl**).

The respective crystalline yields cover a range from < 5% for **10-Br** and **10-I** up to 97% for **12-Br**, since the synthesis can always be accompanied by the polymers **2-Cl**, **2-Br** and **2-I** as well as the slightly larger nanoball **3-Cl** and **3-Br**, respectively (*Table 11.1*). However, **3** is only formed in diluted solutions (c(**1**) ≤ 3.75 mmol·L^{-1})[14a] and after longer reaction times, and the polymeric products **2** contain a lower molar ratio of copper (CuX:**1** = 1:1 for **2**; roughly 1.7:1 for **4**-**13**). Thus, the formation of the by-products can be suppressed to a certain extent by the use of higher concentrations and two equivalents of CuX (for full details see experimental part).

Table 11.1 Overview of the respective yields (for the isolation of the pure compounds see experimental part).

Template	CuCl	CuBr	CuI
$NiCp_2$	-	**8-Br**: 39%	**8-I**: 23%
$CpV(\eta^7\text{-}C_7H_7)$	**9-Cl**: 87%	**9-Br**: 91%	**9-I**: 72%
$CpMn(CO)_3$	-	**10-Br**: < 5%	**10-I**: < 1%
P_4S_3	**11-Cl**: 84%	**11-Br**: 71%	**11-I**: 66%
P_4Se_3	**12-Cl**: 94%	**12-Br**: 97%	-
$C_{10}H_{16}$	**13-Cl**: 72%	-	-

The still wide discrepancy of the obtained yields might also be traced back to the suitability and resulting template capability of the used molecules and complexes. Especially [CpV(η^7-C_7H_7)], [P_4S_3] and [P_4Se_3] show such a strong template effect that the nanoballs can be isolated in unprecedented excellent yields. Emphasized by these results, the synthesis of **9-Cl** was repeated on a larger scale and 650 mg of **9-Cl** can be isolated without a decreasing effect on the yield. Hence, in contrast to fullerene chemistry[3b] and previous examples of this system,[16a,b] one is not restricted to a mg- or even sub-mg scale.

In addition, trovacene [CpV(η^7-C_7H_7)] has also been added to a solution of the pentaphosphaferrocene derivative **1-Bn** and CuBr in CH_2Cl_2. In this system, the sandwich complex has to compete with the solvent for an encapsulation into the 80-vertex nanoball. But also in this case, [CpV(η^7-C_7H_7)] shows a strong template effect and [CpV(η^7-C_7H_7)]@[{Cp^{Bn}Fe(η^5-P_5)}$_{12}$(CuBr)$_{18.8}$] (**14-Br**) is obtained exclusively.

A Hybrid Polymer as an interesting By-Product

Noteworthy, the templates P_4Q_3 (Q = S, Se) are also capable of a coordination to copper to form polymeric products, as it has been shown by Wachter *et al.*[20] Therefore, their formation cannot be avoided completely and the formation of the balls **11-Cl**, **11-Br**, **11-I** as well as **12-Cl** and **12-Br** as respective main products is even more astonishing. Furthermore, since the cage compounds as well as pentaphosphaferrocene **1** form polymers, one can also think of a hybrid product containing all three components **1**, P_4Q_3 and the Cu(I) salt. In fact, this has been observed once for Q = S and X = I with the polymer [(**1**)$_4$(P_4S_3)(CuI)$_{12}$]$_n$ (**15-I**). However, **15-I** appeared only in a low amount and reproduction, let alone its selective synthesis, failed. Therefore, **15-I** has to be treated as a chance product. It crystallizes as brown plates in the tetragonal space group $P42_12$ with four molecules CH_3CN per formula unit. Thus, the crystals optically differ from the supramolecules (big, dark brown rhombohedra), yet not from the polymer **2-I** (brownish plates). The X-ray structural analysis reveals a two-dimensional polymeric structure with the *cyclo*-P_5 ligands in a 1,2,3,4-coordination mode and the basal phosphorus atoms of the P_4S_3 cage in a 1,2-coordination (*Figure 11.3*a). Both coordination modes are well-known for these ligands.[20,21] The extended CuI framework for the most part consists of four-membered {Cu_2I_2} and five-membered {P_2Cu_2I} rings, in which the copper atoms show a tetrahedral environment and the iodine atoms act as μ_2, μ_3 or even μ_4 bridging ligands. Thereby, distorted double layers are formed, with the Cp* ligands pointing outside. Surprisingly, short contacts (3.584(2) Å – 3.815(2) Å) between the opposite *cyclo*-P_5 ligands of such a double layer are obtained (*Figure 11.3*b). Since these distances are partly below the sum of the v.d.W radii of phosphorus (3.6 Å), π-π-stacking interactions can be proposed for the first time for

pentaphosphaferrocene-containing polymers. Such a π-stacking fashion has so far only been observed once in a double-layered polymer constructed by a 1,2,3-triphosphaferrocene.[22] The only $P_5 \cdots P_5$ interactions could be found in the supramolecules **3** and **7** with encapsulated pentaphosphaferrocenes.[14a,18]

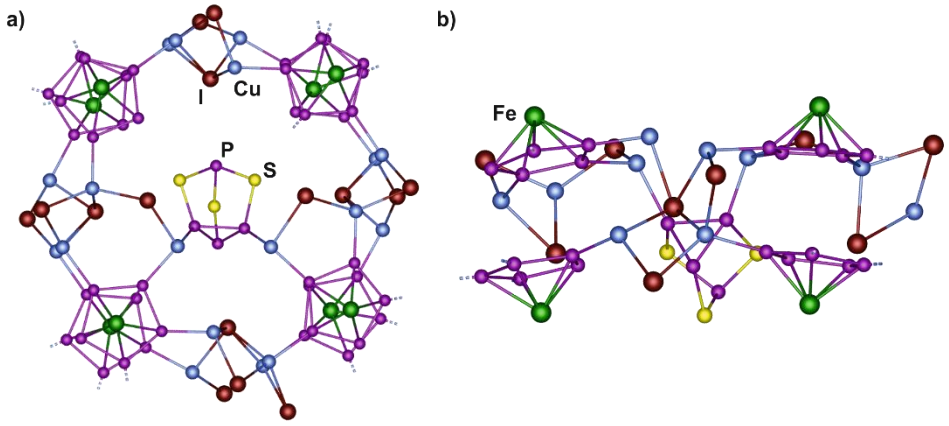

Figure 11.3 Section of the 2D polymeric structure of **15-I** in the crystal: a) top view; b) side view. The 1,2,3,4-coordination mode of the P_5 ligands is indicated by broken-off bonds. Cp* ligands, minor parts of disorder and solvents are omitted for clarity.

Efforts for the synthesis of hybrid polymers containing the P_4S_3 molecule have already been made by the group of Wachter. They succeeded in the synthesis of frameworks incorporating P_4S_3, CuI and the triple decker complex $[(Cp°Mo)_2(P_4S)]$ (Cp° = 1-^{t}Bu-3,4-$Me_2C_5H_2$).[23] However, previous attempts with pentaphosphaferrocene did not lead to the formation of hybrid polymers,[24] hence **15-I** displays the first representative.

Crystal Structures of the Supramolecules

Except of **11-Cl** and **9-Br**, all compounds **8-13** are isostructural and crystallize as dark brown to black rhombohedra in the trigonal space group $R\bar{3}$ with unit cell parameters of a = b = ~42 Å, c= ~52 Å regardless of the used halide (*Table 11.2*). The asymmetric unit contains one half (on the $\bar{1}$ position) and one sixth (on the $\bar{3}$ position) of the supramolecule. On the contrary, **11-Cl** crystallizes as brown laths in the monoclinic space group *C*2/*c* (a = 41.322(2) Å, b = 41.291(1) Å, c = 41.430(1) Å, β = 112.427(4)) with 2·0.5 spheres in the asymmetric unit. Furthermore, **9-Br** crystallizes as black laths in the triclinic space group $P\bar{1}$ (a = 29.4982(4) Å, b = 29.5875(5) Å, c = 29.7525(4) Å, α = 90.862(1), β = 90.291(1), γ = 90.324(1)). The reason for these outliers can most likely be attributed to the use of toluene instead of CH_2Cl_2 for the synthesis of **11-Cl** and **9-Br**. However, with toluene as solvent, the obtained crystals (not only of **11-Cl** and **9-Br**, also for the other supramolecules) decompose within seconds, when removed from the mother liquor due to the loss of solvent. Therefore, the diffraction quality is insufficient for an X-ray structural analysis in most cases. In

contrast, the use of CH_2Cl_2 leads to the formation of more stable crystals, which allow a satisfactory diffraction experiment. In comparison with the previously reported compounds **4-7**, it can be stated that the use of CH_2Cl_2 leads to a crystallization in the trigonal crystal system, whereas with toluene three different structural types (cubic, monoclinic and triclinic) are obtained (*Table 11.2*).

Table 11.2 Comparison of the four different structural types observed for 80-vertex balls. For exact parameters see section 'crystallographic details'.

Crystal system	cubic	trigonal	monoclinic	triclinic
Space group	$Fm\bar{3}c$	$R\bar{3}$	$C2/c$	$P\bar{1}$
Z	8	12	8	3
a, b, c [Å]	~41, ~41, ~41	~42, ~42, ~52	41.322(2), 41.292(1), 41.430(1)	~29, ~29, ~29
α, β, γ [°]	90, 90, 90	90, 90, 120	90, 112.43(1), 90	~90.5, ~90.5, ~90.5
V [Å^3]	~70000	~80000	65344(4)	~26000
Spheres per asymmetric unit	$\frac{1}{12}$	$\frac{1}{2}+\frac{1}{6}$	$2\cdot\frac{1}{2}$	$3\cdot\frac{1}{2}$
Point symmetry	$m\bar{3}$	$\bar{1}$, $\bar{3}$	$\bar{1}$	$\bar{1}$
Packing	primitive cubic (pcu)	face-centered cubic (fcu)	primitive hexagonal (hex)	ReO_3 (reo)
Compounds	**4-Cl**, **5-Cl**, **6-Cl**	**5-Br**, **7**, **8**, **9-Cl**, **9-I**, **10**, **11-Br**, **11-I**, **12**, **13-Cl**	**11-Cl**	**4-Br**, **9-Br**
Used solvents	toluene, CH_3CN	CH_2Cl_2, CH_3CN	toluene, CH_3CN	toluene, CH_3CN

Inorganic Scaffold of the Supramolecules

The host molecules **8-13** each consist of 12 moieties of **1** and 20-n CuX units with X acting as a terminal ligand. Thereby, the ideal 80-vertex scaffold with n = 0 is constructed by 30 six-membered $\{Cu_2P_4\}$ rings and 12 *cyclo*-P_5 ligands with the phosphorus atoms in a 1,2,3,4,5-coordination mode to copper (*Figure 11.4*a). Since they also obey the isolated pentagon rule (IPR), the scaffolds represent carbon-free I_h-C_{80} analogues. As it is already mentioned in the introduction, these hosts could also be obtained in the structures **4**, **5**, **6** and **7**, when *o*-carborane, ferrocene, $[CpCr(\eta^5\text{-}As_5)]$ and $[CpFe(\eta^5\text{-}P_5)]$ are incorporated, respectively.

Table 11.3 Number of CuX (X = Cl, Br, I) units in the reduced scaffolds (20-n) due to vacancies n.

	8-Br	**8-I**	**9-Cl**	**9-Br**	**9-I**	**10-Br**	**10-I**	**11-Cl**	**11-Br**	**11-I**	**12-Cl**	**12-Br**	**13-Cl**	**14-Br**
n	1.05	1.87	1.80	1.17	2.35	1.95	1.85	0.5	0.97	1.05	2.63	1.65	2.48	1.2
20-n	18.95	18.13	18.20	18.83	17.65	18.05	18.15	19.5	19.03	18.95	17.37	18.35	17.52	18.8

However, in all host molecules reported herein, some CuX positions show site occupancy factors < 1, resulting in incomplete, porous spheres. Therefore, the number of CuX moieties is reduced from 20 to 20-n with n being different for every compound and in the range of $0.5 \leq n \leq 2.63$ (see *Table 11.3*). Apparently, neither a correlation with the used halide nor the template becomes evident. Noteworthy, also the use of an excess of CuX (X = Cl, Br, I) does not lead to a significantly less porous sphere. Since the values for n are not integer, the molecular structures all have to be treated as solid solutions of incomplete spheres and/or complete spheres. For example, **11-Cl** (19.5 CuCl units per ball) can be considered as a 1:1 mixture of the complete $Cu_{20}P_{60}$ and the porous $Cu_{19}P_{60}$ sphere (0.5·20 + 0.5·19 = 19.5). However, also the combination of 75% $Cu_{20}P_{60}$ and 25% $Cu_{18}P_{60}$ is conceivable (0.75·20 + 0.25·18 = 19.5). Of course, one can think of numerous other combinations. This phenomenon also occurred in the previously reported derivatives **4-Br**, **5-Br** and **7** as well as in analogous balls containing **1-Bn** as building block, such as **14-Br**.[19]

Remarkably, host molecules without any vacancies (**4-Cl**, **5-Cl** and **6-Cl**) all crystallize in the cubic space group *Fm*$\bar{3}$*c*, whereas the ones with partial vacancies all belong to a structural type of lower symmetry (trigonal, monoclinic, triclinic) (*Table 11.2*). This reduction of symmetry might be traced back to the presence of solvent molecules at the positions of missing halide ligands. For example, in **11-Cl** a CH group of toluene is pointing exactly into the 'hole' in the ball (*Figure 11.4*b), whereas it is either a Cl atom from CH_2Cl_2 or the nitrogen atom of CH_3CN in **12-Br** (*Figure 11.4*c, d). These solvent molecules might act as kind of anchor, fix the orientation of the supramolecule and be responsible for a different packing of the spheres. Furthermore, the presence of these solvent molecules is in contradiction with fully occupied CuX units, therefore they also serve as further evidence for the porosity of the hosts.

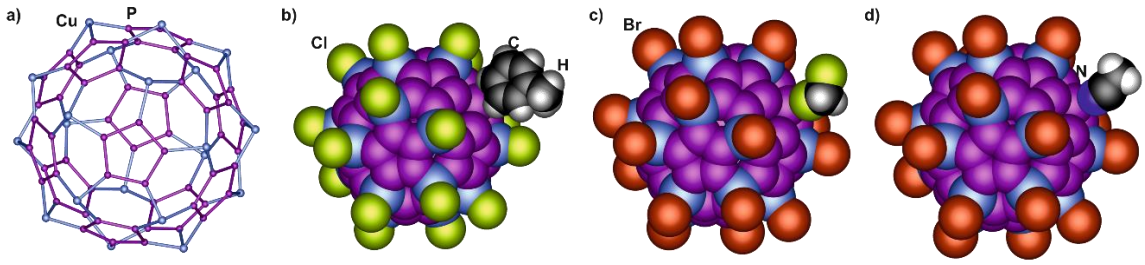

Figure 11.4 a) Ideal inorganic $Cu_{20}P_{60}$ scaffold; b) toluene c) dichloromethane and d) acetonitrile solvent molecules pointing into a CuX vacancy.

The outer shell of these 80-vertex balls is comprised by the Cp* ligands of **1**, thus the halide used does not have a significant impact on the outer diameter, which is roughly 2.3 nm in size (e.g. in **11-Cl**: 2.31 nm, **8-Br**: 2.30 nm, **8-I**: 2.31 nm).[25] All nano-sized spheres provide a defined bowl-shaped cavity with an approximate uniform inner diameter of 0.78 nm (e.g. in **11-Cl**: 0.783 nm, **8-Br**: 0.773 nm, **8-I**: 0.776 nm) capable to accommodate small molecules.[26]

On the other hand, compound **14-Br** with **1-Bn** as building block crystallizes in the cubic space group *Pm*$\bar{3}$*n* and the structure of the 80-vertex host molecule is isostructural to the solvent-filled nano-ball[19] and analogous to the Cp* derivatives **4**-**13**. Solely the outer diameter of 3.1 nm differs dramatically, since the phenyl rings of the sterically demanding Cp^{Bn} ligands protrude outwards.

Properties of the Guests

As mentioned above, the icosahedral 80-vertex supramolecule provides a cavity, which is spherical in shape. Furthermore, the scaffold contains twelve *cyclo*-P_5 rings available for π-π-interactions with the five-fold symmetric rings of metallocenes. These mechanistic ideas have been proved by the incorporation of the predestinated templates *o*-carborane, [$FeCp_2$], [$CpCr(\eta^5\text{-}As_5)$] and [$CpFe(\eta^5\text{-}P_5)$]. To study, if these properties are strictly required, play only supporting role or give negligible impacts, a variety of different templates was tested. Successfully incorporated molecules are shown in *Figure 11.2*.

The most evident characteristic of the templates are their sizes, which are listed in *Table 11.4*. Since the inner cavity with a diameter of 7.8 Å limits the maximum size, $Cr(CO)_6$ (9.1 Å) and [$Ce(COT)_2$] (COT = $\eta^8\text{-}C_8H_8$, 9.3 Å) cannot be incorporated. Also no any larger supramolecule can be obtained in these reactions. Since the van-der-Waals radii are taken into consideration for the size calculations,[26,27] also templates slightly larger than 7.8 Å (e.g. nickelocene, trovacene) can be enclosed within the nanoballs.

Cymantrene [$CpMn(CO)_3$] with a length of 8.34 Å can be treated as a borderline case. Its template effect is highly disputed, since the formation of **10-Br** and **10-I** was only observed twice and once, respectively. All further attempts to reproduce its incorporation failed in favor of the formation of **2-Br** and **2-I**, respectively. Since with **1-Bn** as building block no polymeric products are obtained, cymantrene was tested for its template ability also in this system, yet solely the incorporation of CH_2Cl_2 is observed. Even a change to 1,3-diisopropylbenzene as solvent, which is larger than the provided cavity, did not result in the encapsulation of [$CpMn(CO)_3$].

Table 11.4 Sizes of the templates.[27]

Template	Size	Incorporation in 80-vertex ball	Reference
o-$C_2B_{10}H_{12}$	7.95 Å	yes	Ref. [16]
[$FeCp_2$]	6.9 Å	yes	Ref. [17]
[$CpCr(\eta^5\text{-}As_5)$]	7.5 Å	yes	Ref. [17b]
[$CpFe(\eta^5\text{-}P_5)$]	7.0 Å	yes	Chapter 10
[$NiCp_2$]	7.95 Å[28]	yes	this chapter
[$CpV(\eta^7\text{-}C_7H_7)$]	8.12 Å[29]	yes	this chapter

$[CpMn(CO)_3]$	8.34 Å[30]	sporadically	this chapter
P_4S_3	6.99 Å[31]	yes	this chapter
P_4Se_3	7.26 Å[32]	yes	this chapter
$C_{10}H_{16}$	7.30 Å[33]	yes	this chapter
$Cr(CO)_6$	9.10 Å[34]	no	
$[Ce(COT)_2]$	9.29 Å[35]	no	
P_4	5.80 Å[36]	no (different host)	Ref. [37]

In contrast to the maximum size, a minimum size cannot be taken for granted. However, P_4 does not show a template effect for the formation of the C_{80} analogue despite numerous trials. However, recently we were able to show that this small molecule as well as As_4 are rather incorporated in a different sphere providing a smaller cavity.[37] This points to the fact that for the formation of the 80-vertex ball a minimum size of the template is strictly required.

The second already mentioned key factor might be the icosahedral or five-fold symmetry (D_{5h}, D_{5d}). Yet, the successful incorporation of trovacene $[CpV(\eta^7\text{-}C_7H_7)]$, whose symmetry is reduced to mirror plane (C_s), refutes this idea.

Another plain similarity (except for *o*-carborane) is the sandwich structure. In these complexes the cyclic ligands provide optimum prerequisites for π-π-interactions with the respective host molecule. However, also the cage molecules P_4S_3 and P_4Se_3 can be enclosed even in the highest yields. One might assume that the lone pairs on the P and Q (Q = S, Se) atoms are responsible for their template force. As a counterexample for this hypothesis the trapping of adamantane $C_{10}H_{16}$ is presented. Furthermore, this template displays the first organic compound, which is trapped within this inorganic host.

Our selection of templates also represents a variation in the electronic properties. Nickelocene, containing 20 valence electrons, is an electron-rich metallocene, whereas the electron-poor complex $[CpV(\eta^7\text{-}C_7H_7)]$ possesses only 17 valence electrons.

Summarizing these observations, it can be stated that only the size of the molecule is an imperative factor for the formation of these 80-vertex fullerene analogues.

(Half-) Sandwich Complexes as Guests (Nickelocene, Trovacene, Cymantrene)

In all supramolecules the enclosed guest molecules are severely disordered. When there is a central heavy atom in the template, which is the case for $[NiCp_2]$, $[CpV(\eta^7\text{-}C_7H_7)]$ and $[CpMn(CO)_3]$, a strong electron density peak is found exactly in the center of the cavity (point symmetry $\bar{1}$ and $\bar{3}$ for two crystallographically independent positions). In the case of $[NiCp_2]$ (in **8-Br** and **8-I**, *Figure 11.5*a), each sandwich complex is disordered over six orientations, whereby only two of them are

symmetrically independent in the $\bar{3}$ position (*Figure 11.5*b). This number of positions results from the preferred stacking orientations of the Cp ligands of [$NiCp_2$] to the twelve *cyclo*-P_5 rings of **1** revealing Cp···P_5 π-π-interactions (*Figure 11.5*c). Thereby, the distance between the centroids is with 3.8 Å just above the sum of the van-der-Waals radii (3.5 Å) and thus similar to the observations of previously encapsulated sandwich complexes in **5**-**7**.[17,18] Unexpectedly, each position of disorder has slightly different occupation factors and therefore unequal probabilities (for details see crystallographic section). In total, the nickelocene guest molecules show occupancy factors of 1.0 each and are therefore present in every ball of **8-Br** and **8-I**.

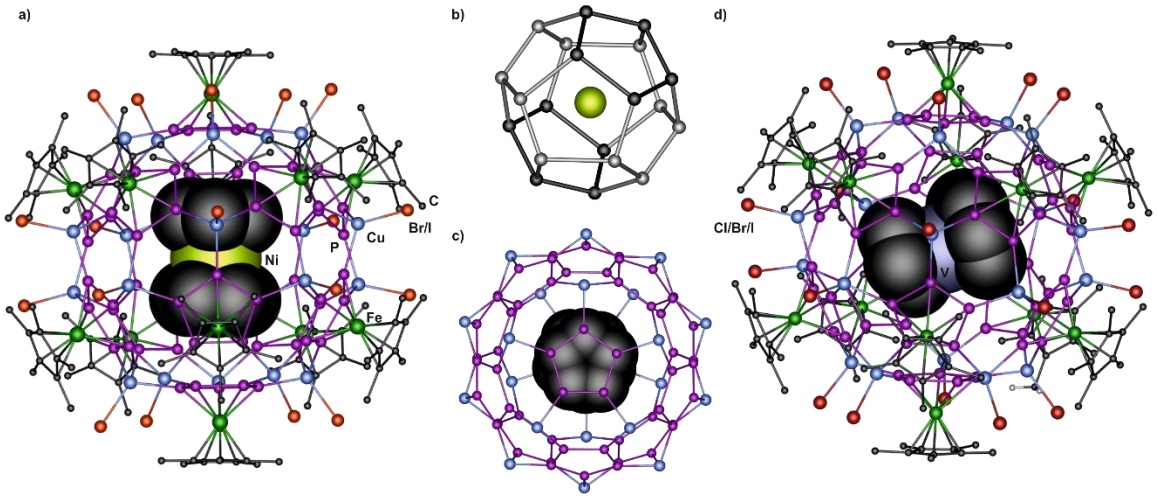

Figure 11.5 a) Molecular structure of **8-Br** and **8-I**. H atoms, minor parts of disorder, vacant CuX positions and solvents are omitted for clarity, the guest is shown in the space-filling model; b) illustration of the disorder of nickelocene in **8-Br** and **8-I**, respectively. The different positions form a dodecahedron with each vertex belonging to three different positions of the guest. One position is highlighted by darkened carbon atoms; c) illustration of the Cp···P_5 stacking interactions in **8-Br** and **8-I**; d) molecular structure of **9-Cl**, **9-Br** and **9-I**. H atoms, minor parts of disorder, vacant CuX positions and solvents are omitted for clarity, the guest is shown in the space-filling model.

The situation is similar for [$CpV(\eta^7\text{-}C_7H_7)$] in **9-Cl**, **9-Br**, **9-I** as well as in **14-Br**. The molecular structure with one possible orientation of the trovacene complex in **9** is depicted in *Figure 11.5*d. However, the refinement of the disorder of the template, especially of the seven-membered tropylium ligand, is even more complicated due to the lack of symmetry. In good agreement with the proposed excellent template effect of trovacene, the sandwich complex is fully occupied in all derivatives **9-Cl**, **9-Br**, **9-I** and **14-Br** and thus present in every supramolecule.

On the contrary, the site occupancy factors for [$CpMn(CO)_3$] in **10-Br** and **10-I** are 0.33 and 0.2, respectively, indicated by the electron density exactly in the center of the host molecule. Hence, cymantrene is only present in 33% and 20% of the bromide- and iodide-ball, respectively. The remaining 'template-free' cavities are most likely filled with solvent molecules. Such a partial occupancy of the guest has also been found in previous examples, such as **3-Cl**[14a] and **4-Br**.[16a] Due

to the low occupancy factors and the disorder of the template as well as of the additional solvent molecules the entire guest molecule cannot be refined. The low presence of cymantrene within the host molecule is in good agreement with the treatment of **10-Br** and **10-I** as a chance product (see above).

Cage Molecules as Guests (P_4S_3, P_4Se_3, Adamantane)

Different positions within the cavity can also be found for the cage molecules P_4Q_3 (Q = S, Se). In the monoclinic structural type of **11-Cl** (*Figure 11.6*a), the sulfur atoms of P_4S_3 are disordered over two positions (*Figure 11.6*b). In addition, the whole molecule shows a disorder over the center of symmetry (*Figure 11.6*c), hence in total, P_4S_3 shows four different, but equally distributed orientations. In contrast to the incorporated nickelocene (**8-Br** and **8-I**), the overall occupation factor of the guest in **11-Cl** is 0.5, therefore P_4S_3 is present only in every second supramolecule.[38]

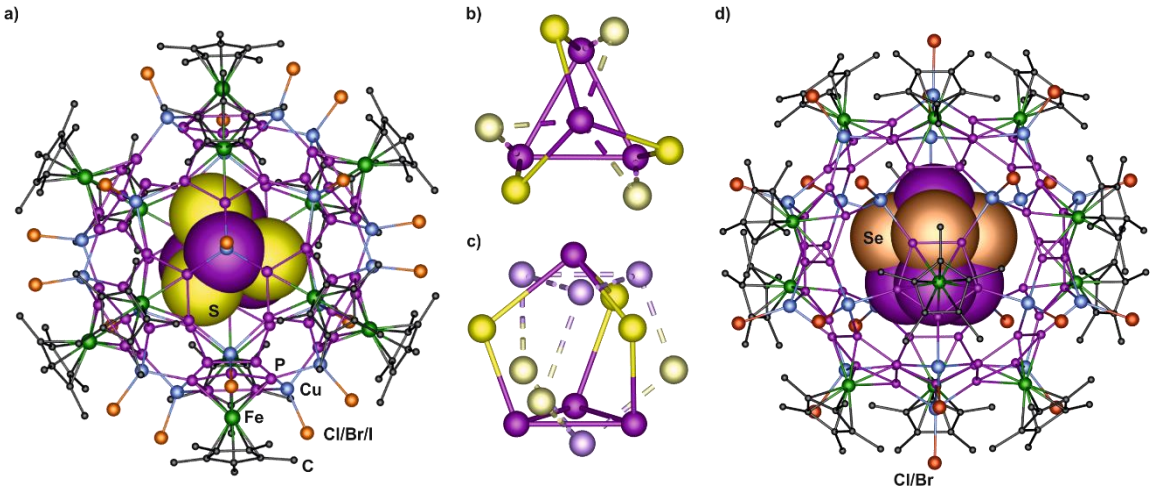

Figure 11.6 a) Molecular structure of **11-Cl**, **11-Br**, and **11-I**. H atoms, minor parts of disorder, vacant CuX positions and solvents are omitted for clarity, the guest is shown in the space-filling model; b) illustration of the disorder of the sulfur atoms and c) of P_4S_3 over the center of symmetry (only one position of S is shown). The second positions are highlighted by brighter color and dashed bonds; d) molecular structure of **12-Cl** and **12-Br**. H atoms, minor parts of disorder, vacant CuX positions and solvents are omitted for clarity, the guest is shown in the space-filling model.

For the trigonal structures **11-Br**, **11-I**, as well as **12-Cl** and **12-Br** (with the supramolecules in the $\bar{1}$ and $\bar{3}$ positions), the disorder and occupancy of P_4Se_3 in **12-Br** will be described exemplarily (*Figure 11.6*d). Similar to **11-Cl**, the cage molecule in $\bar{1}$ shows a disorder over the center of symmetry and an additional disorder of the selenium atoms, this time even over three close positions (two in **11-Cl**). In total, in **12-Br**, the template is present in two out of three host molecules (average occupation factor 0.667). On the contrary, the P_4Se_3 molecule in the $\bar{3}$ position is found on six equal positions due to the three-fold screw axis with an overall occupation of 100%. It is interesting to note that the supramolecule in this position is more porous. This fact is also found in

other rhombohedral phases, such as **12-Cl** ($\bar{1}$ position: $(P_4Se_3)_{0.52}@[(\mathbf{1})_{12}(CuBr)_{17.7}]$ and $\bar{3}$ position: $(P_4Se_3)_{0.6}@[(\mathbf{1})_{12}(CuBr)_{16.4}]$) and **11-I** ($\bar{1}$ position: $(P_4S_3)_{0.40}@[(\mathbf{1})_{12}(CuI)_{19.1}]$ and $\bar{3}$ position: $(P_4S_3)_{0.57}@[(\mathbf{1})_{12}(CuI)_{18.5}]$). Thus, the trend is emerging that a higher porosity of the nanoball is associated with a higher occupation factor of the guest molecule (at least for the cage molecules P_4Q_3 (Q = S, Se)).

Unfortunately, adamantane appeared to be even more disordered within the cavity of **13-Cl**. Since there is no possibility for π-stacking interactions, the cycloalkane most likely can reorientate without any predominant orientation. On the contrary to P_4Q_3, no heavy atoms facilitate the localization of a position. Nevertheless, some positions could be refined (*Figure 11.7*) revealing the spherical shape of $C_{10}H_{16}$ in **13-Cl**.

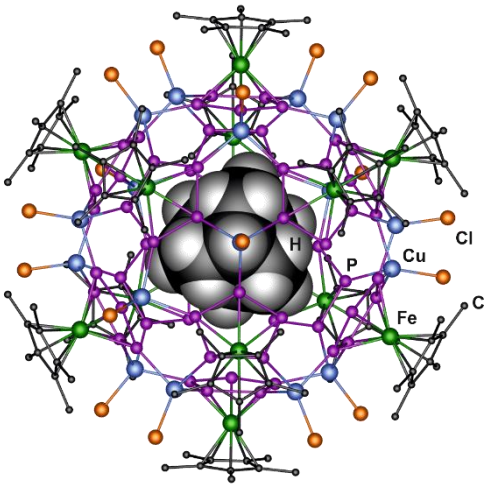

Figure 11.7 Molecular structure of **13-Cl**. H atoms, minor parts of disorder, vacant CuCl positions and solvents are omitted for clarity, the guest is shown in the space-filling model.

Characterization in Solution: Solubilities

The supramolecules are insoluble in common solvents like hexane, toluene, Et_2O, thf and CH_3CN. Astonishingly and on the contrary to the complete spheres **4-Cl**, **5-Cl** and **6-Cl**, they are soluble in CH_2Cl_2, even though very poor. Nevertheless, NMR spectroscopic and mass spectrometric investigations could be performed. Due to the failed reproduction of the cymantrene encapsulation, no comprehensive analytical data can be provided for **10-Br** and **10-I**. In addition, the solubility decreases from the chloride to the iodide derivatives and thus for the latter a characterization in dichloromethane was only feasible for **8-I**.

Furthermore, all obtained supramolecules are soluble in the donor solvent pyridine, though accompanied by complete fragmentation of the host molecules. Therefore, in the corresponding ^1H and $^{31}P\{^1H\}$ NMR spectra only one sharp singlet at δ = 1.3 ppm and δ = 152 ppm are obtained, which are assigned to the methyl groups and the P_5 ring of the starting complex **1**, respectively.

On the other hand, this degradation compulsorily implies that the encapsulated molecules are released from their host molecules. In addition, a characterization of the compounds in pyridine is useful for a further detection of the template (see experimental part).

In the following, the results of the characterization of the supramolecules in CH_2Cl_2 and CD_2Cl_2 are described, respectively.

Characterization in Solution: Mass spectrometry

In most cases, the anionic ESI mass spectra of dissolved crystals only display peaks corresponding to copper halide units, whereas in the cationic ESI mass spectra pentaphosphaferrocene containing peaks can be detected. Among them, the largest fragments for the respective halide can be assigned to $[\{Cp^*Fe(\eta^5\text{-}P_5)\}_3Cu_8Cl_7]^+$ (in the spectrum of **12-Cl** at *m/z* = 1794.4), $[\{Cp^*Fe(\eta^5\text{-}P_5)\}_4Cu_7Br_6]^+$ (in the spectrum of **9-Br** at *m/z* = 2308.5) and $[\{Cp^*Fe(\eta^5\text{-}P_5)\}_3Cu_{10}I_9]^+$ (in the spectrum of **8-I** at *m/z* = 2815.9). Furthermore, in the spectra of **8-Br** and **8-I**, also peaks corresponding to $[NiCp_2]^+$ are observed. Though the used crystals were carefully washed several times with solvents, which dissolve the respective templates, one has to keep in mind the high sensitivity of mass spectrometry. Hence, the evidence of the molecule does not definitely proof its presence inside the cavity, but rather displays a supporting method. For the detection of the other templates, EI mass spectrometry has been proved beneficial and peaks for $[NiCp_2]$, $[CpV(\eta^7\text{-}C_7H_7)]$, P_4S_3, and P_4Se_3 are found in the respective spectra of **8-I**, **9-Cl**, **9-Br**, **11-Cl**, **11-Br**, **12-Cl** and **12-Br**. Unfortunately, the evidence of adamantane is not possible, because the molecular formulae of Cp* and adamantane only differ by one hydrogen atom that could easily be lost or absorbed ($[Cp^*]^-$ = $C_{10}H_{15}$ = 135.23 g/mol, adamantane = $C_{10}H_{16}$ = 136.23 g/mol). Also the unambiguous detection of trovacene is hampered, since at *m/z* = 207.03 also a fragment of silicon grease ($C_5H_{15}O_3Si_3$) often appears. Gratifyingly, high resolution MS has successfully been applied in this case to verify the presence of $[CpV(\eta^7\text{-}C_7H_7)]$ in the spectra of **9-Cl** and **9-Br**, respectively.

Characterization in Solution: NMR spectroscopy

The $^{31}P\{^1H\}$ NMR spectrum of **8-Br** in CD_2Cl_2 shows a small singlet at δ = 151.4 ppm and three very broad signals at δ = 66, 80 and 104 ppm in an integral ratio of 1:11:3:3. This resembles the obtained spectra of 80-vertex balls containing **1-Bn**. A comprehensive NMR and solid state study concerning these more soluble derivatives revealed that the broad signals can be attributed to supramolecules of different porosities.[19] Therefore, they might be attributed to a $Cu_{20}P_{60}$, $Cu_{19}P_{60}$ and a $Cu_{18}P_{60}$ scaffold, respectively. However, the singlet at δ = 151.4 ppm can be assigned to the free complex **1**. Thus, a minimal dissociation of moieties of **1** from the ball might take place, resulting in spheres also with a deficit of phosphorus. This is also in accordance with the behavior of $[\{Cp^{Bn}Fe(\eta^5\text{-}P_5)\}_{12}(CuX)_{20\text{-}n}]$ (X = Cl, Br, n ≤ 4.6) in solution.[19] The $^{31}P\{^1H\}$ NMR spectra of **9-Cl**, **9-Br**, **10-Br** and **11-Cl** in CD_2Cl_2, respectively, look similar, though sometimes the two broad signals with lower intensities do not appear. This can probably traced back to the poor solubility and the disappearance of the signals below the noise floor.

The ^1H NMR spectra in CD_2Cl_2 are in accordance with these observations and show, exemplified by compound **9-Cl**, a sharp singlet at δ = 1.43 ppm and three further broad signals at δ = 2.12, 2.18

and 2.25 ppm. Hence, the first one can be assigned to the free complex **1**, whereas the broad singlets correspond to the Cp* ligands in the supramolecule.

Also evidences for some templates can be gained from NMR spectroscopic investigations, such as the cage molecule P_4S_3 in **11-Cl**. In the corresponding $^{31}P\{^1H\}$ NMR spectrum a doublet at δ = -128.5 ppm ($^2J_{PP}$ = 70.5 Hz) is obtained for the three basal P atoms of P_4S_3. In comparison to free P_4S_3 (δ = -127.3 ppm, $^2J_{PP}$ = 70.0 Hz)[39] it displays a minimal shift to higher field. Thus, the guest molecule rather acts as electron acceptor, which is in agreement with the observations made in other encapsulation processes.[14,16,17,40] Unfortunately, the signal for the apical P atom of P_4S_3 (free: δ = 65.1 ppm) is superimposed by the broad signal of the supramolecule. The integral ratio of the basal phosphorus atoms of P_4S_3 to the broad signals (assigned to the 60 P atoms of the supramolecule plus the apical P atom of P_4S_3) is 3:146, hence P_4S_3 is present in 42% of the spheres. This value nicely fits to the one observed in the solid state (50%).

Interestingly, in the ^1H NMR spectrum of **8-Br** in CD_2Cl_2 a broad signal for the paramagnetic nickelocene complex is observed at an impressive chemical shift of δ = -249 ppm (literature data for free nickelocene in toluene-d_8: δ = -257 ppm).[41]

Characterization in Solution: EPR spectroscopy

Due to the paramagnetic nature of trovacene, displaying a $V^0(d^5)$ complex with one unpaired electron, EPR spectroscopy seems a promising tool for its detection.[42] Hence, measurements of dissolved crystals of **9-Cl**, **9-Br** and **9-I** were carried out. In fact, all compounds show an EPR signal with hyperfine splitting into eight absorption lines due to the interaction with the ^{51}V nucleus (I = 7/2). Due to the diamagnetic nature of the host molecule and the similarity to the g- and hyperfine anisotropy of free [CpV(η^7-C_7H_7)][43] the signal clearly can be assigned to the trovacene complex. Because of the similarity of the received spectra, the counterion in the host does play a negligible role. The obtained spectra of **9-Cl** in CH_2Cl_2 at r.t. and in rigid solution at 90 K, respectively, are displayed in *Figure 11.8*. The isotropy of the signal at r.t. as well as the anisotropy at lower temperature is in accordance with the free complex.[43] The EPR parameter of the obtained spectrum of **9-Br** in CH_2Cl_2 compared to free [V(Cp)(C_7H_7)] are given in *Table 11.5*. The small changes of the parameters, especially $A_{\|}(^{51}V)$, can therefore be traced back to the incorporation in the supramolecular host. However, the differences between free and incorporated trovacene are rather low, hence a strong interaction between the scaffold and the unpaired electron in the $d(z^2)$-orbital of vanadium can be excluded.

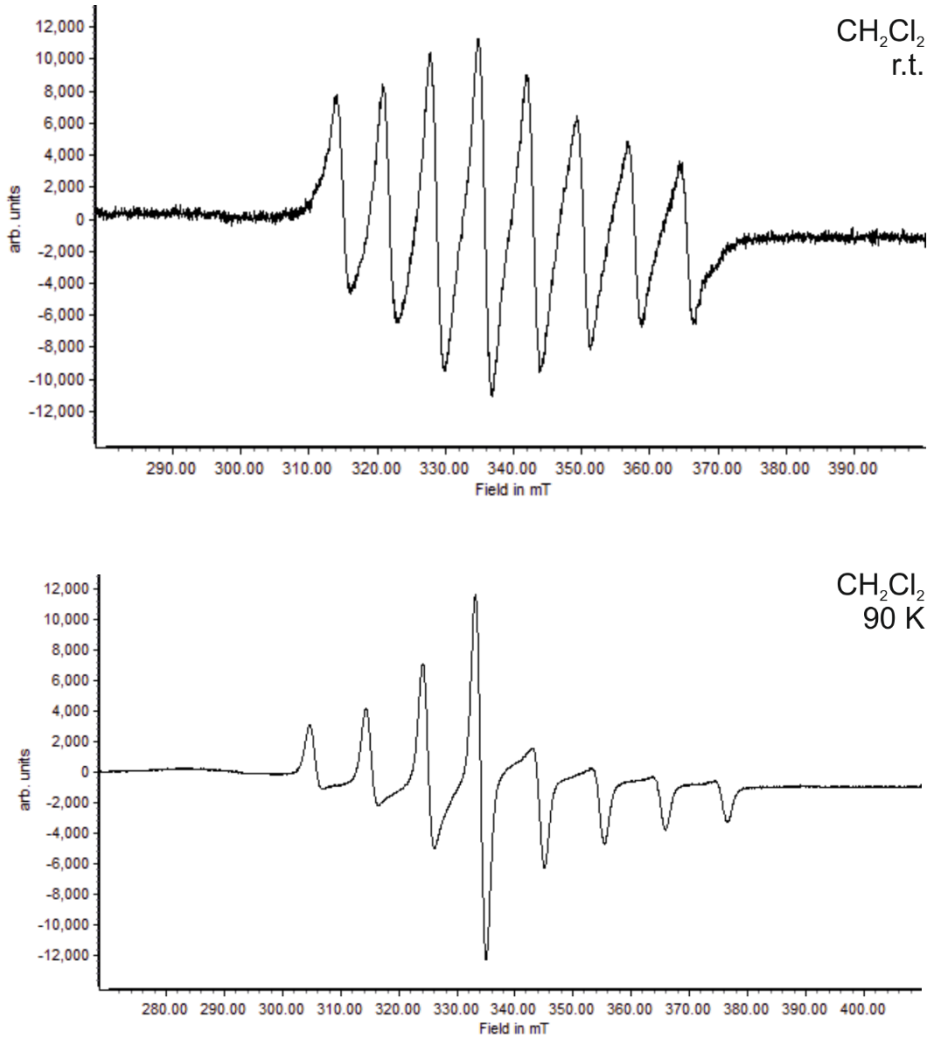

Figure 11.8 EPR spectra of **9-Cl** (9.44 GHz, CH_2Cl_2) at r.t. (top) and at 90 K (bottom).

Table 11.5 EPR parameters of **9-Br** (8.96 GHz, CH_2Cl_2, 90 K) in comparison to the data reported for free trovacene.

	$g_\perp$	$g_\parallel$	<g>	$A_\perp(^{51}V)$/mT	$A_\parallel(^{51}V)$/mT	$<A(^{51}V)>$/mT
9-Br	1.9742	2.0059	1.9848	9.99	1.57	7.18
$[CpV(\eta^7\text{-}C_7H_7)]$[43]	1.9725	1.9994	1.9815	10.37	0.97	7.20

Solid State Studies

Compound **12-Cl** was investigated by $^{31}P\{^1H\}$ magic angle spinning (MAS) NMR spectroscopy, in particular to demonstrate a successful inclusion of P_4Se_3 into the supramolecular host. Based on previous experimental data,[44] the presence of a host typically results in significant shifts to lower ppm values for the ^{31}P resonances compared to free P_4Se_3 (δ = 63.4 and -76.0 ppm).[45] Indeed, the corresponding $^{31}P\{^1H\}$ MAS NMR spectrum of **12-Cl** exhibits two rather sharp peaks at δ = -108.8 and 40.7 ppm, while the major signals at δ = 72.9, 118.7 and 131.0 ppm reflect the *cyclo*-P_5 rings of the host.

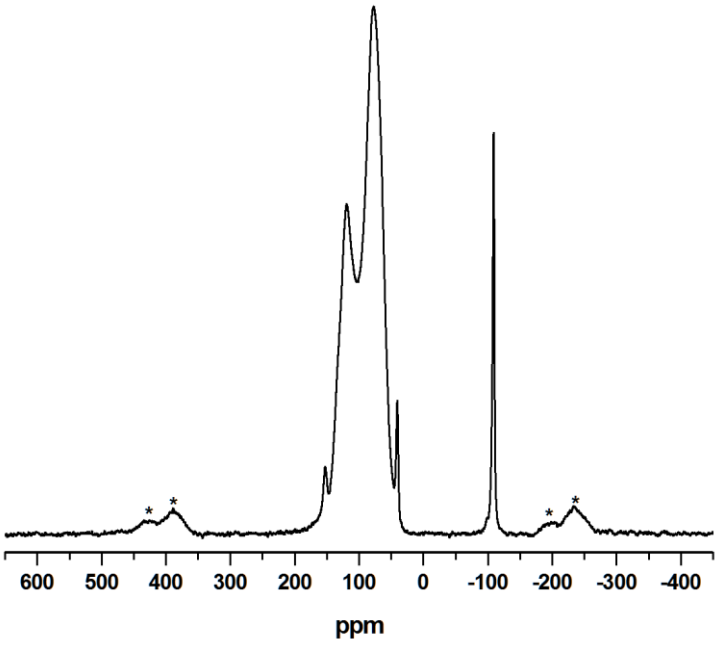

Figure 11.9 $^{31}P\{^{1}H\}$ MAS NMR spectrum of **12-Cl** acquired at 81.1 MHz and 25 kHz MAS using a Bruker Avance III 200 spectrometer. 4096 scans were accumulated at a relaxation delay of 30s; the dwell time was set to 0.5 µs recording 32k points. After zero-filling to 128k points, the resulting spectrum was obtained by FFT. The sharp signals at δ = -108.8 and 40.7 ppm are attributed to the P_4Se_3 cage molecule embedded within the sphere; spinning sidebands are marked with asterisks.

These $^{31}P\{^{1}H\}$ chemical shifts are reminiscent of **2-Br**,[21b] indicating similar coordination environments. The minor peak at 153.2 ppm (0.5% of the overall signal intensity) can most likely be assigned to the free complex **1**. Further deconvolution of the ^{31}P MAS NMR line-shape revealed an overall signal fraction of about 5.8% for P_4Se_3 reflecting an occupancy of ca. 87% of the supramolecular spheres. The discrepancy, when compared to the crystal structure of **12-Cl** (54%), can probably be attributed to a slight underestimation of the occupation factor derived from the X-ray structural analysis due to not refined additional disorder.[38] Another reason might be the variation of the guest occupancy from crystal to crystal.

Furthermore, two-dimensional radio-frequency driven (homo-nuclear) dipolar recoupling (RFDR) ^{31}P MAS NMR spectra were recorded at different mixing times.[46] This experiment uses an adjustable, longitudinal mixing period of π-pulses applied as a compensated echo sequence to generate magnetization transfer among coupled spins, as evidenced by resulting cross-peaks in a resulting 2D NMR spectrum.[47] In the case of short mixing times (less than 3 ms), merely strongly coupled spins (e.g., P atoms comprising the P_5 ring or the P_4Se_3 cage) showed cross-peaks among themselves in the obtained 2D spectra (data not shown) simply reflecting spatial proximity imposed by chemically bonded P sites (^{31}P-^{31}P dipolar coupling constant: 5.8 kHz (1.5 Å), 2.5 kHz (2.0 Å), 0.3 kHz (4.0 Å)). In contrast, weak dipolar couplings originating from either large intermolecular distances and/or pronounced rotational tumbling (the P_4Se_3 cage is considered to be rather mobile

within the host) require rather long mixing times to achieve an effective magnetization transfer (*Figure 11.10*).

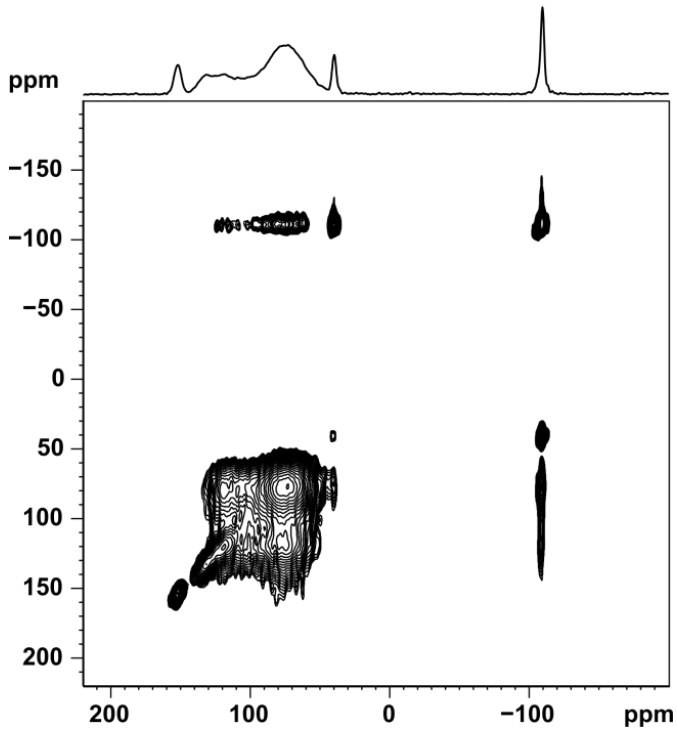

Figure 11.10 ^{31}P-25 kHz MAS RFDR spectrum of **12-Cl** at 4.7 T (81.1 MHz), acquired with a BRUKER Avance III spectrometer and commercially available BRUKER 2.5 mm double-resonance probe under the following experimental conditions: $\tau_{(mix)}$ = 12.8 ms, 256 t_1-increments at steps of 10 µs, accumulating 64 scans at a relaxation delay of 15 s. Quadrature detection in the F_1 dimension was achieved by STATES-TPPI.[48] Thirty-two positive contour levels between 5% and 100% of the maximum peak intensity were plotted; the F_2 projection corresponding to the 1D ^{31}P MAS NMR spectrum of **12-Cl** is shown on the top.

Most notably, reasonably strong cross-peaks among the peak at δ = -108.8 ppm (basal P sites of P_4Se_3) and the peaks at δ = 72.9 and 118.7 ppm, respectively, (both attributed to the P_5 ring) clearly corroborate an inclusion of P_4Se_3 within the host sphere. This is in good agreement with the significantly shifted ^{31}P resonances of the P_4Se_3 cage.

As another characterization method in the solid state, IR spectroscopy has been applied. Due to its sensitivity, it displays a promising tool especially for the detection of cymantrene. And in fact, the IR spectrum of a mixture of **10-Br** and **2-Br** shows two very weak bands corresponding to the CO stretch vibrations of [CpMn(CO)$_3$] at $\tilde{\nu}_{CO}$ = 2016 and 1931 cm^{-1}, which are shifted to lower wavenumbers when compared to the free halfsandwich complex ($\tilde{\nu}_{CO}$ = 2019 and 1947 cm^{-1}).

Conclusion

In summary, a comprehensive study of incorporation experiments of small molecules into a I_h-C_{80} fullerene-like nanoball based on **1** and CuX (X = Cl, Br, I) is presented. Thereby, a variety of templates with distinctive features was used in order to determine the required template

properties. The successful encapsulation of [$NiCp_2$], [$CpV(\eta^7\text{-}C_7H_7)$], P_4Q_3 (Q = S, Se) and adamantane into this 80-vertex sphere demonstrates that characteristics such as sandwich structure, symmetry, number of valence electrons and magnetism only play a negligible role. On the contrary, the size of the template and the ability to interact with the *cyclo*-P_5 rings of the host turned out to be the imperative factors, since not only larger templates such as $Cr(CO)_6$ and [$Ce(\eta^8\text{-}C_8H_8)_2$] cannot be enclosed, but also smaller templates like P_4 show no template effect for the formation of the carbon-free I_h-C_{80} analogue. All obtained supramolecules exhibit CuX vacancies with solvent molecules pointing into these holes and therefore fixing the orientation. Furthermore, besides the X-ray structural analyses the guest molecules are additionally detected by (MAS) NMR spectroscopy, mass spectrometry, IR and EPR spectroscopy, respectively.

11.4 Experimental Part

General Remarks:

All reactions were performed under an inert atmosphere of dry nitrogen or argon with standard vacuum, Schlenk and glove-box techniques. Solvents were purified, dried and degassed prior to use by standard procedures. [$Cp^*Fe(\eta^5\text{-}P_5)$],[49] [$Cp^{Bn}Fe(\eta^5\text{-}P_5)$][50] and [$NiCp_2$][51] were synthesized following reported procedures and [$CpV(\eta^7\text{-}C_7H_7)$],[52] [$CpMn(CO)_3$],[53] P_4S_3, P_4Se_3 and adamantane were in-house available. Commercially available chemicals (CuCl, CuBr, CuI) were used without further purification. Solution NMR spectra were recorded on either Bruker Avance 300 or 400 spectrometer. The corresponding ESI-MS spectra were acquired on a ThermoQuest Finnigan MAT TSQ 7000 mass spectrometer, whereas EI-MS spectra were measured on a Finnigan MAT 95 mass spectrometer. Elemental analyses were performed on a Vario EL III apparatus. The X-Band EPR measurements of **9-Cl** and **14-Br** were carried out with a MiniScope MS400 device with a frequency of 9.5 GHz and rectangular resonator TE102 of Magnettech GmbH. The EPR spectra of **9-Br** were recorded on a JEOL JES-FA200 CW X-Band EPR spectrometer.

Synthesis of [$NiCp_2$]@[{$Cp^*Fe(\eta^5\text{-}P_5)$}$_{12}$($CuBr)_{18.95}$] (8-Br)

In a Schlenk tube a dark green solution of [$Cp^*Fe(\eta^5\text{-}P_5)$] (50 mg, 0.15 mmol) and [$NiCp_2$] (10 mg, 0.053 mmol) in CH_2Cl_2 (28 mL) is carefully layered first with a solvent mixture of CH_2Cl_2/CH_3CN (2 mL, 2/1), afterwards with a colorless solution of CuBr (42 mg, 0.29 mmol) in CH_3CN (25 mL). After a short time, the phase boundary turns yellow-brownish. The formation of black rhombohedra of **8-Br** at the phase boundary and brownish plates of **2-Br** at the bottom can be observed. After complete diffusion the mother liquor is decanted, the crystals are carefully washed with hexane (3 x 5 mL) and toluene (3 x 5 mL) and dried *in vacuo*. The only way to get pure **8-Br** is to take the

crystals of the Schlenk wall (and not from the bottom) with a spatula and quickly dip it into a Schlenk tube with hexane. However, the yield of pure **8-Br** is always underestimated, since bigger crystals of **8-Br** fall to the bottom due to their higher weight and are not isolated using this method.

Analytical data of **8-Br**:

Yield: 35 mg (4.85 µmol, 39%)

^{1}H NMR (CD_2Cl_2): δ [ppm] = -248.8 (s, br, $NiCp_2$], 1.44 (s, [Cp*Fe(η^5-P_5)]), 1.51 (s, [Cp*Fe(η^5-P_5)]), 2.45 (m, br).

^{31}P{^{1}H} NMR (CD_2Cl_2): δ [ppm] = 66 (s, br), 80 (s, br), 104 (s, br), 151.4 (s, [Cp*Fe(η^5-P_5)]).

^{1}H NMR (pyridine-d_5): δ [ppm] = 1.31 (s, [Cp*Fe(η^5-P_5)]).

^{31}P{^{1}H} NMR (pyridine-d_5): δ [ppm] = 148.23 (s, [Cp*Fe(η^5-P_5)]).

Positive ion ESI-MS (CH_2Cl_2): *m/z* = 898.7 [{Cp*Fe(η^5-P_5)}$_2$$Cu_2Br$]$^+$, 754.9 [{Cp*Fe($\eta^5$-$P_5$)}$_2$Cu]$^+$, 188.3 [$NiCp_2$]$^+$.

Elemental analysis: Calculated (%) for [($NiCp_2$){Cp*Fe(η^5-P_5)}$_{12}$($CuBr)_{18.95}$($CH_3CN)_3$] (7222 g/mol): C 22.95, H 2.82, N 0.78; found: C 23.81, H 3.05, N 0.40.

Synthesis of [$NiCp_2$]@[{Cp*Fe(η^5-P_5)}$_{12}$($CuI)_{18.125}$] (8-I)

In a thin Schlenk tube a dark green solution of [Cp*Fe(η^5-P_5)] (60 mg, 0.17 mmol) and [$NiCp_2$] (13 mg, 0.069 mmol) in CH_2Cl_2 (12 mL) is carefully layered first with a solvent mixture of CH_2Cl_2/CH_3CN (2 mL, 2/1), afterwards with a colorless solution of CuI (99 mg, 0.52 mmol) in CH_3CN (10 mL). After a short time, the phase boundary turns yellow-brownish and turbid. The formation of a small amount of black rhombohedra of **8-I** at the phase boundary and brownish plates of **2-I** at the bottom can be observed. After complete diffusion the mother liquor is decanted, the crystals are washed with hexane (3 x 5 mL) and CH_2Cl_2 (5 x 5 mL) and dried *in vacuo*. The only way to get pure **8-I** is to take the crystals of the Schlenk wall (and not from the bottom) with a spatula and quickly dip it into a Schlenk tube with hexane. However, the yield of pure **8-I** is always underestimated, since bigger crystals of **8-I** fall to the bottom due to their higher weight and are not isolated using this method.

Analytical data of **8-I**:

Yield: 25 mg (3.2 µmol, 23%)

^{1}H NMR (pyridine-d_5): δ [ppm] = 1.30 (s, [Cp*Fe(η^5-P_5)]).

^{31}P{^{1}H} NMR (pyridine-d_5): δ [ppm] = 151.1 (s, [Cp*Fe(η^5-P_5)]).

Positive ion ESI-MS (CH_2Cl_2/CH_3CN): *m/z* (%) = 2815.9 [{Cp*Fe(η^5-P_5)}$_3$$Cu_{10}I_9$]$^+$, 2777.9 [{Cp*Fe($\eta^5$-$P_5$)}$_4$$Cu_8I_7$]$^+$, 2624.8 [{Cp*Fe($\eta^5$-$P_5$)}$_3$$Cu_9I_8$]$^+$, 2435.2 [{Cp*Fe($\eta^5$-$P_5$)}$_3$$Cu_8I_7$]$^+$, 2244.9 [{Cp*Fe($\eta^5$-$P_5$)}$_3$$Cu_7I_6$]$^+$, 2052.8 [{Cp*Fe($\eta^5$-$P_5$)}$_3$$Cu_6I_5$]$^+$, 1862.5 [{Cp*Fe($\eta^5$-$P_5$)}$_3$$Cu_5I_4$]$^+$, 1671.8 [{Cp*Fe($\eta^5$-

$P_5)\}_3Cu_4I_3]^+$, 1326.3 $[\{Cp^*Fe(\eta^5\text{-}P_5)\}_2Cu_4I_3]^+$, 1136.5 $[\{Cp^*Fe(\eta^5\text{-}P_5)\}_2Cu_3I_2]^+$, 944.6 $[\{Cp^*Fe(\eta^5\text{-}P_5)\}_2Cu_2I]^+$, 754.8 $[\{Cp^*Fe(\eta^5\text{-}P_5)\}_2Cu]^+$, 449.9 (100) $[\{Cp^*Fe(\eta^5\text{-}P_5)\}Cu(CH_3CN)]^+$, 408.9 $[\{Cp^*Fe(\eta^5\text{-}P_5)\}Cu]^+$, 188.0 $[NiCp_2]^+$.

Negative ion ESI-MS (CH_2Cl_2): *m/z* (%) = 506.6 $[Cu_2I_3]^-$, 316.7 (100) $[CuI_2]^-$

EI-MS (70 eV): 345.9 $[Cp^*Fe(\eta^5\text{-}P_5)]$, 284.0 $[\{Cp^*Fe(\eta^5\text{-}P_5)\}\text{-}P_2]$, 190.10 $[^{60}NiCp_2]$, 188.10 $[^{58}NiCp_2]$.

Elemental analysis: Calculated (%) for $[(NiCp_2)\{Cp^*Fe(\eta^5\text{-}P_5)\}_{12}(CuI)_{18.125}]$ (7833 g/mol): C 20.24, H 2.48; found: C 20.66, H 2.65.

Synthesis of $[CpV(\eta^7\text{-}C_7H_7)]@[\{Cp^*Fe(\eta^5\text{-}P_5)\}_{12}(CuCl)_{18.20}]$ (9-Cl)

In a thick Schlenk tube a green solution of $[Cp^*Fe(\eta^5\text{-}P_5)]$ (500 mg, 1.45 mmol) and $[CpV(\eta^7\text{-}C_7H_7)]$ (50 mg, 0.24 mmol) in CH_2Cl_2 (150 mL) is carefully layered with a colorless solution of CuCl (300 mg, 3.03 mmol) in CH_3CN (130 mL). Thereby, the phase boundary turns yellow-brownish. Already after a few days the formation of black rhombohedra of **9-Cl** at the phase boundary can be observed. After complete diffusion the mother liquor is decanted, the crystals are washed with pentane (3 x 10 mL) and dried *in vacuo*. Of course, **9-Cl** can also be synthesized in smaller quantities. Analytical data of **9-Cl**:

Yield: 650 mg (0.101 mmol, 87%)

^{1}H NMR (CD_2Cl_2): δ [ppm] = 1.43 (s, $[Cp^*Fe(\eta^5\text{-}P_5)]$), 2.12 (s, br), 2.18 (s, br), 2.25 (s, br).

^{31}P{^{1}H} NMR (CD_2Cl_2): δ [ppm] = 76 (s, br), 152.2 (s, $[Cp^*Fe(\eta^5\text{-}P_5)]$).

^{1}H MAS NMR: δ [ppm] = 1.9 (s, br).

^{31}P{^{1}H} MAS NMR: δ [ppm] = 105 (m, br).

EI-MS (70 eV): 346.0 $[Cp^*Fe(\eta^5\text{-}P_5)]$, 284.1 $[\{Cp^*Fe(\eta^5\text{-}P_5)\}\text{-}P_2]$, 207.1 $[CpV(\eta^7\text{-}C_7H_7)]$, 84.0 $[CH_2Cl_2]$, 49.0 $[CH_2Cl]$.

HR-MS: 207.03775 $[CpV(\eta^7\text{-}C_7H_7)]$.

Positive ion ESI-MS (CH_2Cl_2): *m/z* (%) = 1644.9 $[\{Cp^*Fe(\eta^5\text{-}P_5)\}_4Cu_3Cl_2]^+$, 1398.7 $[\{Cp^*Fe(\eta^5\text{-}P_5)\}_3Cu_4Cl_3]^+$, 1298.8 $[\{Cp^*Fe(\eta^5\text{-}P_5)\}_3Cu_3Cl_2]^+$, 952.7 (2) $[\{Cp^*Fe(\eta^5\text{-}P_5)\}_2Cu_3Cl_2]^+$, 854.8 (12) $[\{Cp^*Fe(\eta^5\text{-}P_5)\}_2Cu_2Cl]^+$, 754.9 (43) $[\{Cp^*Fe(\eta^5\text{-}P_5)\}_2Cu]^+$, 587.8 (100) $[\{Cp^*Fe(\eta^5\text{-}P_5)\}Cu_2Cl(C_5H_5N)]^+$, 487.8 (45) $[\{Cp^*Fe(\eta^5\text{-}P_5)\}Cu(C_5H_5N)]^+$.

Negative ion ESI-MS (CH_2Cl_2): *m/z* (%) = 134.7 (100) $[CuCl_2]^-$.

Elemental analysis: Calculated (%) for $[\{CpV(\eta^7\text{-}C_7H_7)\}\{Cp^*Fe(\eta^5\text{-}P_5)\}_{12}(CuCl)_{18.20}(CH_2Cl_2)_6]$ (6669 g/mol): C 24.85, H 3.08; found: C 24.60, H 3.58.

Synthesis of [CpV(η^7-C_7H_7)]@[{Cp*Fe(η^5-P_5)}$_{12}$($CuBr)_{18.83}$] (9-Br)

In a Schlenk tube a green solution of [Cp*Fe(η^5-P_5)] (50 mg, 0.145 mmol) and [CpV(η^7-C_7H_7)] (20 mg, 0.097 mmol) in CH_2Cl_2 (15 mL) is carefully layered first with a solvent mixture of CH_2Cl_2/CH_3CN (2 mL, 2/1), afterwards with a colorless solution of CuBr (42 mg, 0.289 mmol) in CH_3CN (15 mL). After a short time, the phase boundary turns yellow-brownish. Already after a few days the formation of black rhombohedra of **9-Br** at the phase boundary can be observed. After complete diffusion the mother liquor is decanted, the crystals are washed with hexane (3 x 10 mL) and dried *in vacuo*.

Analytical data of **9-Br**:

Yield: 75 mg (0.011 mmol, 91%)

^{1}H NMR (CD_2Cl_2): δ [ppm] = 1.52 (s, [Cp*Fe(η^5-P_5)]), 2.22 (s, br), 2.30 (s, br).

^{31}P{^{1}H} NMR (CD_2Cl_2): δ [ppm] = 68 (s, br), 152.1 (s, [Cp*Fe(η^5-P_5)]); signals almost below noise floor.

^{31}P{^{1}H} NMR (pyridine-d_5): δ [ppm] = 146.4 (s, [Cp*Fe(η^5-P_5)]).

EI-MS (70 eV): 346.0 [Cp*Fe(η^5-P_5)], 284.1 [{Cp*Fe(η^5-P_5)}-P_2], 207.1 [CpV(η^7-C_7H_7)], 84.0 [CH_2Cl_2], 49.0 [CH_2Cl].

HR-MS : 207.03842 [CpV(η^7-C_7H_7)].

Positive ion ESI-MS (CH_2Cl_2): *m/z* (%) = 2308.5 [{Cp*Fe(η^5-P_5)}$_4$$Cu_7Br_6$]$^+$, 1674.2 [{Cp*Fe($\eta^5$-$P_5$)}$_3$$Cu_5Br_4$]$^+$, 1532.3 [{Cp*Fe($\eta^5$-$P_5$)}$_3$$Cu_4Br_3$]$^+$, 1471.9 [{Cp*Fe($\eta^5$-$P_5$)}$_2$$Cu_6Br_5$]$^+$, 1388.2 [{Cp*Fe($\eta^5$-$P_5$)}$_3$$Cu_3Br_2$]$^+$, 1328.1 [{Cp*Fe($\eta^5$-$P_5$)}$_2$$Cu_5Br_4$]$^+$, 1184.4 [{Cp*Fe($\eta^5$-$P_5$)}$_2$$Cu_4Br_3$]$^+$, 1042.5 [{Cp*Fe($\eta^5$-$P_5$)}$_2$$Cu_3Br_2$]$^+$, 898.6 [{Cp*Fe($\eta^5$-$P_5$)}$_2$$Cu_2Br$]$^+$, 754.8 [{Cp*Fe($\eta^5$-$P_5$)}$_2$Cu]$^+$, 593.7 [{Cp*Fe($\eta^5$-$P_5$)}$Cu_2Br(CH_3CN)$]$^+$, 449.8 (100) [{Cp*Fe($\eta^5$-$P_5$)}$Cu(CH_3CN)$]$^+$.

Negative ion ESI-MS (CH_2Cl_2): *m/z* (%) = 222.8 (100) [$CuBr_2$]$^-$.

Elemental analysis: Calculated (%) for [{CpV(η^7-C_7H_7)}{Cp*Fe(η^5-P_5)}$_{12}$($CuBr)_{18.83}$] (7060 g/mol): C 22.46, H 2.74; found: C 22.38, H 3.16.

Synthesis of [CpV(η^7-C_7H_7)]@[{Cp*Fe(η^5-P_5)}$_{12}$($CuI)_{17.65}$] (9-I)

In a Schlenk tube a green solution of [Cp*Fe(η^5-P_5)] (30 mg, 0.087 mmol) and [CpV(η^7-C_7H_7)] (35 mg, 0.17 mmol) in CH_2Cl_2 (20 mL) is carefully layered first with a solvent mixture of CH_2Cl_2/CH_3CN (2 mL, 2/1), afterwards with a colorless solution of CuI (33 mg, 0.17 mmol) in CH_3CN (10 mL). After a short time, the phase boundary turns yellow-brownish and turbid. Already after a few hours the formation of black crystals of **9-I** and brown plates of **2-I** can be observed. After complete diffusion the mother liquor is decanted, the crystals are washed with hexane (3 x 10 mL) and shaken up with CH_2Cl_2 to remove the smaller and thinner plates of [{Cp*Fe(η^5-P_5)}CuI]$_n$ and dried *in vacuo*.

Analytical data of **9-I**:

Yield: 41 mg (5.2 µmol, 72%)

^{1}H NMR (pyridine-d_5): 1.25 (s, [Cp*Fe(η^5-P_5)]).

^{31}P{^{1}H} NMR (pyridine-d_5): δ [ppm] = 152.90 (s, [Cp*Fe(η^5-P_5)]).

Positive ion ESI-MS (pyridine): *m/z* (.%) = 756.9 (5) [{Cp*Fe(η^5-P_5)}$Cu_2I(C_5H_5N)_2]^+$, 677.9 (10) [{Cp*Fe(η^5-P_5)}$Cu_2I(C_5H_5N)]^+$, 487.8 (18) [{Cp*Fe(η^5-P_5)}$Cu(C_5H_5N)]^+$, 220.9 (100) $[Cu(C_5H_5N)_2]^+$.

Negative ion ESI-MS (pyridine): *m/z* (%) = 316.6 (100) $[CuI_2]^-$, 126.7 (17) $[I]^-$.

EI-MS (70 eV, pyridine): 346.1 [Cp*Fe(η^5-P_5)], 284.0 [{Cp*Fe(η^5-P_5)}-P_2], 79.1 [C_5H_5N].

Elemental analysis: Calculated (%) for [{CpV(η^7-C_7H_7)}{Cp*Fe(η^5-P_5)}$_{12}$$(CuI)_{17.65}(CH_3CN)_5$] (7925 g/mol): C 21.52, H 2.63, N 0.88; found: C 22.39, H 2.85, N 0.28.

Synthesis of $[CpMn(CO)_3]_{0.33}$@[{Cp*Fe(η^5-P_5)}$_{12}$$(CuBr)_{18.05}$] (10-Br)

In a Schlenk tube a green solution of [Cp*Fe(η^5-P_5)] (100 mg, 0.29 mmol) and $[CpMn(CO)_3]$ (120 mg, 0.58 mmol) in CH_2Cl_2 (30 mL) is carefully layered first with a solvent mixture of CH_2Cl_2/CH_3CN (2 mL, 2/1), afterwards with a colorless solution of CuBr (126 mg, 0.88 mmol) in CH_3CN (30 mL). After a short time, the phase boundary turns yellow-brownish. The formation of black rhombohedra of **10-Br** (sporadically) and brownish plates of **2-Br** (main product) can be observed. After complete diffusion the mother liquor is decanted, the crystals are washed with hexane (3 x 10 mL) and shaken up with CH_2Cl_2 several times to remove traces of $[CpMn(CO)_3]$. Unfortunately, a separation of **10-Br** and **2-Br** is not possible. Furthermore, the synthesis of **10-Br** was successful only twice, numerous attempts to reproduce **10-Br** failed and only crystals of **2-Br** are obtained, even when an excess of the template is used. For an interpretation of this fact, see discussion.

Analytical data of **10-Br** and **2-Br**:

Yield: 25 mg

^{1}H NMR (CD_2Cl_2): δ [ppm] = 1.52 (s, [Cp*Fe(η^5-P_5)]), 2.15 (s, br), 2.22 (s, br), 2.31 (s,br), 4.79 (s, $[CpMn(CO)_3]$).

^{31}P{^{1}H} NMR (CD_2Cl_2): δ [ppm] = 66 (s, br), 151.8 (s, [Cp*Fe(η^5-P_5)]); signals almost below noise floor.

EI-MS (70 eV): 346.0 [Cp*Fe(η^5-P_5)], 284.0 [{Cp*Fe(η^5-P_5)}-P_2].

Positive ion ESI-MS (CH_2Cl_2): *m/z* (%) = 537.0 (100) $[(Cp^*Fe)_2P_5]^+$.

Negative ion ESI-MS (CH_2Cl_2): *m/z* (%) = 222.5 (100) $[CuBr_2]^-$.

IR (KBr pellet): $\tilde{\nu}_{CO}$ [cm^{-1}] = 2017 (s), 1931 (br).

Elemental analysis: Calculated (%) for [{$CpMn(CO)_3$}$_{0.2}${Cp*Fe(η^5-P_5)}$_{12}$$(CuBr)_{18.05}(CH_3CN)$] (6363 g/mol): C 21.76, H 2.72, N 0.21; calculated (%) for [Cp*Fe(η^5-P_5)CuBr]$_n$ (489 g/mol): C 24.54, H 3.09; found: C 24.50, H 3.03, N 0.2.

Synthesis of $[CpMn(CO)_3]_{0.2}@[\{Cp^*Fe(\eta^5\text{-}P_5)\}_{12}(CuI)_{18.15}]$ (10-I)

In a Schlenk tube a green solution of $[Cp^*Fe(\eta^5\text{-}P_5)]$ (50 mg, 0.15 mmol) and $[CpMn(CO)_3]$ (60 mg, 0.29 mmol) in CH_2Cl_2 (10 mL) is carefully layered first with a solvent mixture of CH_2Cl_2/CH_3CN (2 mL, 2/1), afterwards with a colorless solution of CuI (55 mg, 0.29 mmol) in CH_3CN (8 mL). After a short time, the phase boundary turns yellow-brownish and gets turbid. The formation of a small amount of black rhombohedra of **10-I** (sporadically, <1%) and brownish plates of **2-I** (main product) can be observed once. After complete diffusion the mother liquor is decanted, the crystals are washed with hexane (4 x 5 mL) and and toluene (3 x 5 mL) to remove traces of $[CpMn(CO)_3]$ and dried *in vacuo*. Unfortunately, a separation of **10-I** and **2-I** was not possible. Furthermore, numerous attempts to reproduce **10-I** failed and only crystals of **2-I** are obtained, even when an excess of the template is used. Also variations in concentration and solvent were not successful. Therefore no analytical data can be provided for **10-I**. For an interpretation of this fact, see discussion.

Synthesis of $(P_4S_3)_{0.5}@[\{Cp^*Fe(\eta^5\text{-}P_5)\}_{12}(CuCl)_{19.5}]$ (11-Cl)

In a Schlenk tube a green solution of $[Cp^*Fe(\eta^5\text{-}P_5)]$ (100 mg, 0.29 mmol) and P_4S_3 (11 mg, 0.048 mmol) in CH_2Cl_2 (30 mL) is carefully layered first with a solvent mixture of CH_2Cl_2/CH_3CN (3 mL, 2/1), afterwards with a colorless solution of CuCl (58 mg, 0.58 mmol) in CH_3CN (30 mL). After a short time the phase boundary turns yellow-brownish. Already after one day the formation of black rhombohedra of **11-Cl** and sometimes accompanied by a small amount of **2-Cl** as well as of the polymer $[(P_4S_3)_3(CuCl)_7]_n$[20c] can be observed. After complete diffusion the mother liquor is decanted, the crystals are washed and shaken up with hexane (3 x 5 mL) and toluene (3 x 5 mL) to remove the thin plates of the polymeric by-products and dried *in vacuo*.

Analytical data of **11-Cl**:

Yield: 130 mg (0.02 mmol, 84%)

^{1}H NMR (CD_2Cl_2): δ [ppm] = 1.52 (s, $[Cp^*Fe(\eta^5\text{-}P_5)]$), 2.18 (s, br), 2.26 (s, br).

$^{31}P\{^1H\}$ NMR (CD_2Cl_2): δ [ppm] = -128.1 (d, $^2J_{PP}$ = 70.4 Hz, $P_4S_{3,\ basal}$), 72 (s, br), 110 (s, br).

$^{31}P\{^1H\}$ MAS NMR: δ [ppm] = -126.6 (m, $P_4S_{3,\ basal}$), -62.6 (m, $P_4S_{3,\ Polymer}$),[20c] 67.8 (m, $P_4S_{3,\ apical}$), 72 (m, br), 110 (m, br).

EI-MS (70 eV): 346.0 $[Cp^*Fe(\eta^5\text{-}P_5)]$, 284.1 $[\{Cp^*Fe(\eta^5\text{-}P_5)\}\text{-}P_2]$, 219.9 $[P_4S_3]$.

Elemental analysis: Calculated (%) for $[(P_4S_3)_{0.5}\{Cp^*Fe(\eta^5\text{-}P_5)\}_{12}(CuCl)_{19.5}(C_7H_8)_2]$ (6376 g/mol): C 25.24, H 3.10, S 0.75; found: C 25.68, H 3.24, S 1.45.

Synthesis of $(P_4S_3)_{0.38}$@[{Cp*Fe(η^5-P_5)}$_{12}$($CuBr)_{19.025}$] (11-Br)

In a Schlenk tube a green solution of [Cp*Fe(η^5-P_5)] (100 mg, 0.29 mmol) and P_4S_3 (11 mg, 0.048 mmol) in CH_2Cl_2 (30 mL) is carefully layered first with a solvent mixture of CH_2Cl_2/CH_3CN (3 mL, 2/1), afterwards with a colorless solution of CuBr (83 mg, 0.58 mmol) in CH_3CN (30 mL). After a short time, the phase boundary turns yellow-brownish. After one day the formation of black rhombohedra of **11-Br** at the phase boundary can be observed in addition to a small amount of **2-Br**. After complete diffusion the mother liquor is decanted, the crystals are carefully washed and shaken up with hexane (3 x 5 mL) and toluene (2 x 5 mL) to remove the thin plates of **2-Br** and dried *in vacuo*.

Analytical data of **11-Br**:

Yield: 125 mg (0.02 mmol, 71%)

^{1}H NMR (CD_2Cl_2): δ [ppm] = 1.51 (s, [Cp*Fe(η^5-P_5)]), 2.22 (s, br), 2.32 (s, br).

^{1}H NMR (pyridine-d_5): δ [ppm] = 1.39 (s, [Cp*Fe(η^5-P_5)]).

^{31}P{^{1}H} NMR (pyridine-d_5): δ [ppm] = -111.4 (d, $P_4S_{3,\,basal}$, $^2J_{PP}$ = 57.4 Hz), 90.1 (q, $P_4S_{3,\,apical}$, $^2J_{PP}$ = 56.8 Hz), 142.6 (s, [Cp*Fe(η^5-P_5)]).

Positive ion ESI-MS (CH_2Cl_2): *m/z* (%) = 898.7 [{Cp*Fe(η^5-P_5)}$_2$$Cu_2Br]^+$, 839.6 [{Cp*Fe($\eta^5$-$P_5$)}$Cu_4Br_3]^+$, 754.9 [{Cp*Fe($\eta^5$-$P_5$)}$_2$$Cu]^+$, 696.6 [{Cp*Fe($\eta^5$-$P_5$)}$Cu_3Br_2]^+$, 408.7 [{Cp*Fe($\eta^5$-$P_5$)}$Cu]^+$.

Negative ion ESI-MS (CH_2Cl_2): *m/z* (%) = 366.4 $[Cu_2Br_3]^-$, 222.5 $[CuBr_2]^-$, 78.8 $[Br]^-$.

EI-MS (70 eV): 346.1 [Cp*Fe(η^5-P_5)], 284.0 [{Cp*Fe(η^5-P_5)}-P_2], 219.8 [P_4S_3].

Elemental analysis: Calculated (%) for [$(P_4S_3)_{0.5}${Cp*Fe(η^5-P_5)}$_{12}$$(CuBr)_{19}$$(C_7H_8)_3$] (7263 g/mol): C 23.32, H 2.83, S 0.66; found: C 23.84, H 2.95, S 0.57.

Synthesis of $(P_4S_3)_{0.44}$@[{Cp*Fe(η^5-P_5)}$_{12}$($CuI)_{18.95}$] (11-I)

In a Schlenk tube a green solution of [Cp*Fe(η^5-P_5)] (20 mg, 0.058 mmol) and P_4S_3 (6 mg, 0.027 mmol) in CH_2Cl_2 (10 mL) is carefully layered first with a solvent mixture of CH_2Cl_2/CH_3CN (2 mL, 2/1), afterwards with a colorless solution of CuI (22 mg, 0.12 mmol) in CH_3CN (6 mL). After a short time, the phase boundary turns yellow-brownish and turbid. Already after one day the formation of small black crystals of **11-I** and plates of **2-I** at the phase boundary can be observed. After complete diffusion the mother liquor is decanted, the crystals are washed with hexane (2 x 5 mL), toluene (2 x 5 mL) and Et_2O (2 x 5 mL) and dried *in vacuo*. Sometimes, also crystals of $[(P_4S_3)(CuI)]_n$ are observed.[20c] Furthermore, the formation of the hybrid polymer [{Cp*Fe(η^5-P_5)}$_4$$(P_4S_3)(CuI)_{12}]_n$ (**15-I**) was detected once as a small by-product, yet could not be reproduced. A molar ratio of 1:0.5 for **1**:P_4S_3 turned out to be the optimum for the synthesis of **11-I**.

Analytical data of **11-I**:

Yield: 25 mg (3.2 µmol, 66%)

^{1}H NMR (pyridine-d_5): 1.31 (s, [Cp*Fe(η^5-P_5)]).

^{31}P{^{1}H} NMR (pyridine-d_5): δ [ppm] = -110.63 (d, $^2J_{P\text{-}P}$ = 58.0 Hz, $P_4S_{3,basal}$), 148.37 (s, [Cp*Fe(η^5-P_5)]).

Positive ion ESI-MS (pyridine): *m/z* (%) = 756.9 (15) [{Cp*Fe(η^5-P_5)}$Cu_2I(C_5H_5N)_2]^+$, 677.8 (20) [{Cp*Fe(η^5-P_5)}$Cu_2I(C_5H_5N)]^+$, 220.9 (100) $[Cu(C_5H_5N)_2]^+$.

Negative ion ESI-MS (pyridine): *m/z* (%) = 316.6 (100) $[CuI_2]^-$, 126.8 (7) $[I]^-$.

EI-MS (70 eV): 346.1 [Cp*Fe(η^5-P_5)], 284.0 [{Cp*Fe(η^5-P_5)}-P_2], 79.1 [C_5H_5N].

Elemental analysis: Calculated (%) for $[(P_4S_3)_{0.44}${Cp*Fe(η^5-P_5)}$_{12}(CuI)_{18.95}]$ (7857 g/mol): C 18.34, H 2.31, S 0.54; found: C 17.71, H 2.18, S 1.37.

Synthesis of $(P_4Se_3)_{0.54}$@[{Cp*Fe(η^5-P_5)}$_{12}(CuCl)_{17.375}$] (12-Cl)

In a Schlenk tube a green solution of [Cp*Fe(η^5-P_5)] (50 mg, 0.145 mmol) and P_4Se_3 (26 mg, 0.072 mmol) in CH_2Cl_2 (10 mL, a minimal amount of P_4Se_3 remains undissolved at the bottom even after ultrasonic treatment) is carefully layered first with a solvent mixture of CH_2Cl_2/CH_3CN (2 mL, 2/1), afterwards with a colorless solution of CuCl (29 mg, 0.289 mmol) in CH_3CN (10 mL). After a short time, the phase boundary turns yellow-brownish. After one day the formation of black rhombohedra of **12-Cl** at the phase boundary can be observed (sometimes accompanied by the formation of plates of **2-Cl** at the bottom). After complete diffusion the mother liquor is decanted, the crystals are washed with hexane (3 x 5 mL) and toluene (3 x 5 mL) to remove residues of P_4Se_3 and dried *in vacuo*. For the case, a considerable amount of **2-Cl** is present: the only way to get pure **12-Cl** is to take the crystals of the Schlenk wall (and not from the bottom) with a spatula and quickly dip it into a Schlenk tube with hexane.

Analytical data of **12-Cl**:

Yield: 69 mg (0.011 mmol, 94%)

^{1}H NMR (CD_2Cl_2): δ [ppm] = 1.51 (s, [Cp*Fe(η^5-P_5)]), 2.18 (s, br), 2.26 (s, br).

^{1}H NMR (pyridine-d_5): 1.41 (s, [Cp*Fe(η^5-P_5)]).

^{31}P{^{1}H} NMR (pyridine-d_5): δ [ppm] = 3.04 (m, $P_4Se_{3,apical}$), 133.95 (s, [Cp*Fe(η^5-P_5)]).

EI-MS (70 eV): 361.8 [P_4Se_3], 346.1 [Cp*Fe(η^5-P_5)], 284.1 [{Cp*Fe(η^5-P_5)}-P_2].

Positive ion ESI-MS (CH_2Cl_2): *m/z* (%) = 1794.4 [{Cp*Fe(η^5-P_5)}$_3Cu_8Cl_7]^+$, 1694.1 [{Cp*Fe(η^5-P_5)}$_3Cu_7Cl_6]^+$, 1596.6 [{Cp*Fe(η^5-P_5)}$_3Cu_6Cl_5]^+$, 1498.5 [{Cp*Fe(η^5-P_5)}$_3Cu_5Cl_4]^+$, 1396.6 [{Cp*Fe(η^5-P_5)}$_3Cu_4Cl_3]^+$, 1052.2 [{Cp*Fe(η^5-P_5)}$_2Cu_4Cl_3]^+$, 952.6 [{Cp*Fe(η^5-P_5)}$_2Cu_3Cl_2]^+$, 854.7 [{Cp*Fe(η^5-P_5)}$_2Cu_2Cl]^+$, 754.9 [{Cp*Fe(η^5-P_5)}$_2Cu]^+$, 449.4 (100) [{Cp*Fe(η^5-P_5)}$Cu(CH_3CN)]^+$.

Negative ion ESI-MS (CH_2Cl_2): *m/z* (%) = 232.6 $[Cu_2Cl_3]^-$, 134.7 (100) $[CuCl_2]^-$.

Elemental analysis: Calculated (%) for $[(P_4Se_3)_{0.54}\{Cp^*Fe(\eta^5\text{-}P_5)\}_{12}(CuCl)_{17.375}]$ (6066 g/mol): C 23.76, H 2.99; found: C 24.06, H 3.10.

Synthesis of $(P_4Se_3)_{0.75}@[\{Cp^*Fe(\eta^5\text{-}P_5)\}_{12}(CuBr)_{18.35}]$ (12-Br)

In a Schlenk tube a green solution of $[Cp^*Fe(\eta^5\text{-}P_5)]$ (50 mg, 0.145 mmol) and P_4Se_3 (26 mg, 0.072 mmol) in CH_2Cl_2 (10 mL, a minimal amount of P_4Se_3 remains undissolved at the bottom even after ultrasonic treatment) is carefully layered first with a solvent mixture of CH_2Cl_2/CH_3CN (2 mL, 2/1), afterwards with a colorless solution of CuBr (42 mg, 0.289 mmol) in CH_3CN (10 mL). After a short time, the phase boundary turns yellow-brownish. Already after one day the formation of black rhombohedra of **12-Br** at the phase boundary can be observed (sometimes accompanied by the formation of plates of **2-Br** at the bottom). After complete diffusion the mother liquor is decanted, the crystals are washed with hexane (3 x 5 mL) and toluene (3 x 5 mL) to remove residues of P_4Se_3 and dried *in vacuo*. For the case, a considerable amount of **2-Br** is present: the only way to get pure **12-Br** is to take the crystals of the Schlenk wall (and not from the bottom) with a spatula and quickly dip it into a Schlenk tube with hexane. Analytical data of **12-Br**:

Yield: 83 mg (0.012 mmol, 97%)

^{1}H NMR (CD_2Cl_2): δ [ppm] = 1.51 (s, $[Cp^*Fe(\eta^5\text{-}P_5)]$), 2.14 (s, br), 2.22 (s, br), 2.31 (s, br).

^{1}H NMR (pyridine-d_5): 1.36 (s, $[Cp^*Fe(\eta^5\text{-}P_5)]$).

^{31}P{^{1}H} NMR (pyridine-d_5): δ [ppm] = -107.12 (d, $^2J_{PP}$ = 67.2 Hz, $P_4Se_{3,basal}$), 2.87 (m, $P_4Se_{3,apical}$), 141.42 (s, $[Cp^*Fe(\eta^5\text{-}P_5)]$).

EI-MS (70 eV): 361.7 $[P_4Se_3]$, 346.0 $[Cp^*Fe(\eta^5\text{-}P_5)]$, 284.0 $[\{Cp^*Fe(\eta^5\text{-}P_5)\}\text{-}P_2]$.

Negative ion ESI-MS (CH_2Cl_2): *m/z* (%) = 368.5 $[Cu_2Br_3]^-$, 322.5 $[Cu_2Br_2Cl]^-$, 266.6 $[CuBr_2(CH_3CN)]^-$, 222.6 (100) $[CuBr_2]^-$, 178.6 $[CuClBr]^-$.

Elemental analysis: Calculated (%) for $[(P_4Se_3)_{0.75}\{Cp^*Fe(\eta^5\text{-}P_5)\}_{12}(CuBr)_{18.35}]$ (7054 g/mol): C 20.43, H 2.57, found: C 21.23, H 2.77.

Synthesis of $(C_{10}H_{16})_{0.452}@[\{Cp^*Fe(\eta^5\text{-}P_5)\}_{12}(CuCl)_{17.52}]$ (13-Cl)

In a thin Schlenk tube a green solution of $[Cp^*Fe(\eta^5\text{-}P_5)]$ (30 mg, 0.087 mmol) and adamantane $C_{10}H_{16}$ (10 mg, 0.07 mmol) in CH_2Cl_2 (2 mL) is carefully layered with a colorless solution of CuCl (17 mg, 0.17 mmol) in CH_3CN (2 mL). Thereby, the phase boundary turns yellow-brownish. Already after one day the formation of black rhombohedra of **13-Cl** at the phase boundary can be observed. After complete diffusion the mother liquor is decanted, the crystals are washed with toluene (2 x 1 mL) and quickly with CH_2Cl_2 (1 mL) and dried *in vacuo*.

Analytical data of **13-Cl**:

Yield: 31 mg (5.2 µmol, 72%)

^{1}H NMR (pyridine-d_5): δ [ppm] = 1.36 (s, [Cp*Fe(η^5-P_5)]), 1.65 (s, adamantane-CH_2), 1.81 (s, adamantane-CH).

^{31}P{^{1}H} NMR (pyridine-d_5): δ [ppm] = 140.0 (s, [Cp*Fe(η^5-P_5)]).

^{1}H MAS NMR: δ [ppm] = -3.2 (s, $C_{10}H_{16}$), 1.7 (s, br, $\omega_{1/2}$ = 727 Hz, [Cp*Fe(η^5-P_5)]).

Positive ion ESI-MS (CH_2Cl_2): *m/z* (%) = 1596.3 [{Cp*Fe(η^5-P_5)}$_3$$Cu_6Cl_5$]$^+$, 1496.3 [{Cp*Fe($\eta^5$-$P_5$)}$_3$$Cu_5Cl_4$]$^+$, 1396.5 [{Cp*Fe($\eta^5$-$P_5$)}$_3$$Cu_4Cl_3$]$^+$, 1298.5 [{Cp*Fe($\eta^5$-$P_5$)}$_3$$Cu_3Cl_2$]$^+$, 1052.6 [{Cp*Fe($\eta^5$-$P_5$)}$_2$$Cu_4Cl_3$]$^+$, 952.6 [{Cp*Fe($\eta^5$-$P_5$)}$_2$$Cu_3Cl_2$]$^+$, 854.7 [{Cp*Fe($\eta^5$-$P_5$)}$_2$$Cu_2Cl$]$^+$, 754.8 (100) [{Cp*Fe($\eta^5$-$P_5$)}$_2$Cu]$^+$, 449.4 [{Cp*Fe($\eta^5$-$P_5$)}Cu($CH_3CN$)]$^+$, 408.8 [{Cp*Fe($\eta^5$-$P_5$)}Cu]$^+$

Elemental analysis: Calculated (%) for [($C_{10}H_{16}$){Cp*Fe(η^5-P_5)}$_{12}$($CuCl$)$_{17}$] (5971 g/mol): C 25.11, H 3.17; found: C 26.13, H 3.34.

Synthesis of [CpV(η^7-C_7H_7)]@[{Cp^{Bn}Fe(η^5-P_5)}$_{12}$($CuBr$)$_{18.8}$] (14-Br)

In a Schlenk tube [Cp^{Bn}Fe(η^5-P_5)] (10 mg, 0.014 mmol), [CpV(η^7-C_7H_7)] (10 mg, 0.049 mmol) and CuBr (12 mg, 0.084 mmol) are stirred in *m*-diisopropylbenzene (DIB, 10 mL) or CH_2Cl_2 (10 mL). In DIB, a color change from green to brownish red is observed overnight, whereas in CH_2Cl_2 due to a better solubility of all compounds the red color is already observed after one hour. After this, the slightly turbid solution is filtered and layered with hexane or toluene resulting in the crystallization of black blocks of **14-Br**. After complete diffusion the mother liquor is decanted, the crystals are washed with hexane (3 x 10 mL) and dried *in vacuo*. The reason for the use of DIB is the size of the solvent, since it does not fit into the cavity of the sphere of **14-Br**.

Analytical data of **14-Br**:

Yield: 10 mg (0.86 µmol, 74%)

^{1}H NMR (CD_2Cl_2): δ [ppm] = 1.23 (d, DIB-CH_3), 2.88 (sept, DIB-CH), 4.6 – 5.3 (br, C$\underline{H}_2C_6H_5$), 6.4 – 6.8 (br, $CH_2C_6\underline{H}_5$), 7.03 (dd, DIB-CH), 7.08 (t, DIB-CH), 7.20 (t, DIB-CH).

^{31}P{^{1}H} NMR (CD_2Cl_2): δ [ppm] = 71 (s, br), 78 (s, br), 115.1 (s, br), 161.8 (s, [Cp^{Bn}Fe(η^5-P_5)]).

EI-MS (70 eV): 726.1 [Cp^{Bn}Fe(η^5-P_5)], 207.0 [CpV(η^7-C_7H_7)].

Positive ion ESI-MS (CH_2Cl_2): *m/z* (%) = 1803.2 [{Cp^{Bn}Fe(η^5-P_5)}$_2$$Cu_3Br_2$]$^+$, 1659.4 [{Cp^{Bn}Fe($\eta^5$-$P_5$)}$_2$$Cu_2Br$]$^+$, 1515.4 [{Cp^{Bn}Fe($\eta^5$-$P_5$)}$_2$Cu]$^+$, 830.2 [{Cp^{Bn}Fe($\eta^5$-$P_5$)}Cu($CH_3CN$)]$^+$, 789.1 [{Cp^{Bn}Fe($\eta^5$-$P_5$)}Cu]$^+$.

Negative ion ESI-MS (CH_2Cl_2): *m/z* (%) = 222.6 (100) [$CuBr_2$]$^-$.

Elemental analysis: Calculated (%) for [{CpV(η^7-C_7H_7)}{Cp^{Bn}Fe(η^5-P_5)}$_{12}$($CuBr$)$_{18.8}$($C_{12}H_{18}$)$_6$] (12595 g/mol): C 53.79, H 4.32; found: C 53.90, H 4.31.

11.5 Crystallographic Details

Crystals of **8-15** were taken from a Schlenk flask under a stream of argon and immediately covered with mineral oil or perfluorinated Fomblin® mineral oil to prevent both decomposition and a loss of solvent. The quickly chosen single crystals covered by a drop of the oil were taken to the pre-centered goniometer head with CryoMount® and directly attached to the diffractometer into a stream of cold nitrogen. X-ray diffraction studies faced many challenges, since the crystals decompose rapidly losing solvent molecules. The diffraction power of the crystals at high theta angles was very low, and the collection of data required high exposure times.

The data for **14-Br** and **10-Br** were collected on an Agilent Technologies Gemini R-Ultra diffractometer equipped with a Ruby CCD detector and an Enhanced Ultra CuK_α sealed tube (λ = 1.54178 Å) using 0.5 (**14-Br**) or 1° (**10-Br**) ω scans. The data for **12-Cl** were collected on an Agilent Technologies diffractometer equipped with a Titan^{S2} CCD detector and a SuperNova CuK_α microfocus source using 0.5° ω scans. The data for **8-Br**, **8-I**, **9-Cl**, **9-Br, 9-I, 10-I** and **11-Cl** were collected on an Agilent Technologies diffractometer equipped with an Atlas CCD detector and a SuperNova CuK_α microfocus source using 0.5° (**8-Br**, **9-Br**) or 1° (**8-I**, **9-Cl**, **9-I**, **10-I**, **11-Cl**) ω scans. The data for **11-I**, **12-Br** and **13-Cl** were collected on an Agilent Technologies diffractometer equipped with an Eos CCD detector and a SuperNova MoK_α microfocus source using 0.5° (**12-Br**, **13-Cl**) or 0.25° (**11-I**) ω scans. All measurements were performed at 123 K.

The structures were solved by direct methods with *SIR97*,[54] *SHELX97* or *SHELX2013*.[55] The structures were refined by full-matrix least-squares method against $|F|^2$ in an anisotropic approximation using the *SHELXL97* or the multiprocessor and variable memory version *SHELXL2013*. All non-hydrogen atoms were refined anisotropically, while the hydrogen atoms were refined riding on pivot atoms. Due to isostructurality, the model of **8-Br** was used to refine all structures crystallizing in the same trigonal structural type. The refinement task was reduced to the determination of vacant positions in the inorganic scaffolds, disorder modes of the different guest molecules and solvent molecules.

The compound **11-Cl** is the only representative of the monoclinic structural type. The crystal was twinned due to similar magnitudes of *a* and *c* parameters according to the twinning law {0 0 1, 0 1 0, 1 0 0}. The twin batches were refined to 0.2540(8)/0.746(8) that allowed to improve the quality factors from R_1 = 0.12 to 0.0566.

In every supramolecule some positions of CuX are partly vacant indicated by enlarged displacement parameters. The occupancies for these positions were refined with fixed isotropic U_{iso} similar to average U_{iso} (usually 0.03 – 0.04 Å^{-2}) for fully occupied heavy atoms in the corresponding

structure. The constraints on the Cu and X displacement parameters were then removed and anisotropic approximation was used for the further refinement.

The refinement of the [$NiCp_2$] guest molecules in **8-Br** and **8-I** required additional modeling. The [$NiCp_2$] molecules occupy two positions with point symmetry $\bar{1}$ and $\bar{3}$ providing the Ni atom in the respective special position and 10 and 4 unique positions of carbon atoms, respectively. Each molecule is disordered over 6 *unequally* probable orientations, whereby only 6 and 2 of them are symmetrically independent for $\bar{1}$ and $\bar{3}$ positions. Every C atom site belongs simultaneously to three possible orientations of the guest molecule. Therefore correlation between the refined occupancy factors for the C atoms and the probability of the molecule in the defined orientation were tested for each case to bring physical sense into the model. The probabilities of $NiCp_2$ were described as 7.4%+15.8%+38.3%+13.7%+9.4%+15.4%=100% (in $\bar{1}$) and 15.7%+84.3%=100% (in $\bar{3}$) for **8-Br** and 7.8%+9.3+41.8+14.7+14.6+11.8%=100% (in $\bar{1}$) and 9.34%+90.66%=100% (in $\bar{3}$) for **8-I**.

Some solvent molecules in **8-Br**, **8-I**, **11-Cl**, **12-Br** and **14-Br** could be located from the difference Fourier map. The solvent molecules in most cases are disordered, and their molecular occupancy factors were refined using the FVAR instruction of SHELX with isotropic displacement parameters fixed at U_{iso} = 0.05 Å^{-2}. The resulting occupancies were fixed and the C and N atoms with occupancy more than 0.5 were refined anisotropically. Most dichloromethane molecules in **8-Br**, **8-I** and **12-Br** were refined with restraint geometry. The restraints were removed at the final stage of the refinement if possible. Due to the disorder, the solvent content is generally underestimated. In **11-Cl**, most of the disordered solvent toluene molecules had to be refined with geometrical restraints (AFIX 66).

Table 11.6 Experimental details for compounds **8-Br** (final data) and **8-I** (final data).

Crystal Data	8-Br	8-I
Chemical formula	$NiC_{10}H_{10}{\cdot}C_{120}H_{180}Br_{18.95}Cu_{18.95}Fe_{12}P_{60}{\cdot}(CH_3CN)_{6.3}{\cdot}(CH_2Cl_2)_{1.065}$	$NiC_{10}H_{10}{\cdot}C_{120}H_{180}I_{18.125}Cu_{18.125}Fe_{12}P_{60}{\cdot}(CH_3CN)_{6.225}{\cdot}(CH_2Cl_2)_{1.4}$
M_r	7407.38	8160.03
Crystal system, space group	trigonal, $R\bar{3}$	trigonal, $R\bar{3}$
Temperature (K)	123	123
a, *b*, *c* (Å)	42.1828(1), 42.1828(1), 52.1008(2)	42.6637(5), 42.6637(5), 52.7745(11)
α, β, γ (°)	90, 90, 120	90, 90, 120
V (Å^3)	80287.1(5)	83190(3)
Z	12	12
F(000)	43274	46632
Radiation type	Cu K_α	Cu K_α
μ (mm^{-1})	13.87	26.03
Crystal color and shape	brown lath	dark brown prism

Crystal size (mm)	0.43 × 0.12 × 0.08	0.16 × 0.15 × 0.11
Data collection		
Diffractometer	SuperNova, Single source at offset, Atlas diffractometer	SuperNova, Single source at offset, Atlas diffractometer
Absorption correction	gaussian	analytical
T_{min}, T_{max}	0.165, 0.584	0.077, 0.225
No. of measured, independent and observed [$I > 2\sigma(I)$] reflections	216861, 35806, 27319	186066, 37719, 21124
R_{int}	0.045	0.086
$(\sin\theta/\lambda)_{max}$ (Å^{-1})	0.622	0.630
Range of h, k, l	h = -48→52, k = -49→51, l = -61→64	h = -51→53, k = -53→49, l = -46→66
Refinement		
$R[F^2 > 2\sigma(F^2)]$, $wR(F^2)$, S	0.048, 0.163, 1.03	0.052, 0.157, 0.96
No. of reflections	35806	37719
No. of parameters	1738	1725
No. of restraints	12	21
H-atom treatment	H-atom parameters constrained	H-atom parameters constrained
$\Delta\rangle_{max}$, $\Delta\rangle_{min}$ (e Å^{-3})	2.77, -1.97	2.47, -2.48

Table 11.7 Experimental details for compounds **9-Cl** and **9-Br** (* = preliminary data).[56]

Crystal Data	9-Cl	9-Br
Chemical formula	$VC_{12}H_{12}{\cdot}C_{120}H_{180}Br_{18.2}Cu_{18.2}Fe_{12}P_{60}$*	$VC_{12}H_{12}{\cdot}C_{120}H_{180}Br_{18.83}Cu_{18.83}Fe_{12}P_{60}$*
M_r	6939.72*	7059.66*
Crystal system, space group	trigonal, $R\bar{3}$	triclinic, $P\bar{1}$
Temperature (K)	123	123
a, b, c (Å)	41.9658(2), 41.9658(2), 51.8408(3)	29.4982(4), 29.5875(5), 29.7525(4)
α, β, γ (°)	90, 90, 120	90.862(1), 90.291(1), 90.324(1)
V (Å^3)	79066.6(8)	25963.7(6)
Z	12	3
Radiation type	Cu K_α	Cu K_α
μ (mm^{-1})	> 12.69	> 10.75
Crystal color and shape	dark brown rhombohedron	black lath
Crystal size (mm)	0.33 x 0.25 x 0.06	0.20 × 0.08 × 0.03
Data collection		
Diffractometer	SuperNova, Single source at offset, Atlas diffractometer	SuperNova, Single source at offset, Atlas diffractometer
Absorption correction	analytical	gaussian
T_{min}, T_{max}	0.117, 0.522	0.047, 0.574

No. of measured, independent and observed [$I > 2\sigma(I)$] reflections	106450, 34592, 28058	188697, 103142, 71322
R_{int}	0.0484	0.0359
Range of h, k, l	h = -52→36, k = -51→49, l = -47→62	h = -36→25, k = -36→37, l = -37→33

Table 11.8 Experimental details for compounds **9-I** and **10-Br** (* = preliminary data).[56]

Crystal Data	9-I	10-Br
Chemical formula	$VC_{12}H_{12}{\cdot}C_{120}H_{180}I_{17.65}Cu_{17.65}Fe_{12}P_{60}$*	$(MnC_8H_5O_3)_{0.33}{\cdot}C_{120}H_{180}Br_{18.05}Cu_{18.05}Fe_{12}P_{60}$*
M_r	7719.95*	6781.41*
Crystal system, space group	trigonal, $R\bar{3}$	trigonal, $R\bar{3}$
Temperature (K)	123	123
a, b, c (Å)	42.4302(4), 42.4302(4), 52.2040(8)	42.3557(5), 42.3557(5), 52.2801(8)
α, β, γ (°)	90, 90, 120	90, 90, 120
V (Å^3)	81392(2)	81225(2)
Z	12	12
Radiation type	Cu K_α	Cu K_α
μ (mm^{-1})	> 28.60	> 14.98
Crystal color and shape	black plate	black rhombohedron
Crystal size (mm)	0.21 × 0.14 × 0.04	0.50 × 0.27 × 0.16
Data collection		
Diffractometer	SuperNova, Single source at offset, Atlas diffractometer	Xcalibur, Atlas, Gemini ultra diffractometer
Absorption correction	gaussian	analytical
T_{min}, T_{max}	0.047, 0.421	0.057, 0.253
No. of measured, independent and observed [$I > 2\sigma(I)$] reflections	587116	263092, 31781, 23960
R_{int}	0.092	0.075
Range of h, k, l	h = -52→39, k = -36→53, l = -64→65	h = -48→50, k = -50→46, l = -62→54

Table 11.9 Experimental details for compounds **10-I** (* = preliminary data)[56] and **11-Cl** (final data)

Crystal Data	10-I	11-Cl
Chemical formula	$(MnC_8H_5O_3)_{0.2}{\cdot}C_{120}H_{180}I_{18.15}Cu_{18.15}Fe_{12}P_{60}$*	$C_{214.30}H_{289.20}Cl_{19.50}Cu_{19.50}Fe_{12}N_2P_{62}S_{1.50}$
M_r	7675.34*	7461.99
Crystal system, space group	trigonal, $R\bar{3}$	monoclinic, $C2/c$
Temperature (K)	123	123
a, b, c (Å)	42.5787(7), 42.5787(7), 52.6957(6)	41.3224(15), 41.2915(7), 41.4301(10)

α, β, γ (°)	90, 90, 120	90, 112.427(4), 90
V (Å^3)	82735(2)	65344(4)
Z	12	8
F(000)	> 46178.3	30016
Radiation type	Cu K_α	Cu K_α
μ (mm^{-1})	> 28.10	10.41
Crystal color and shape	black rhombohedron	brown lath
Crystal size (mm)	0.15 × 0.13 × 0.08	0.26 × 0.09 × 0.04
Data collection		
Diffractometer	SuperNova, Single source at offset, Atlas diffractometer	SuperNova, Single source at offset, Atlas diffractometer
Absorption correction	gaussian	analytical
T_{min}, T_{max}	0.070, 0.286	0.185, 0.668
No. of measured, independent and observed [$I > 2\sigma(I)$] reflections	227563, 37156, 28226	111226, 63497, 40310
R_{int}	0.054	0.046
$(\sin\theta/\lambda)_{max}$ (Å^{-1})		0.624
Range of h, k, l	*h* = -53→52, *k* = -53→52, *l* = -52→63	*h* = -49→51, *k* = -31→50, *l* = -51→48
Refinement		
$R[F^2 > 2\sigma(F^2)]$, $wR(F^2)$, *S*	0.064, 0.207, 1.06	0.057, 0.171, 1.01
No. of reflections	37156	63497
No. of parameters	1703	3015
No. of restraints	4	44
H-atom treatment	H-atom parameters constrained	H-atom parameters constrained
$\Delta\rangle_{max}$, $\Delta\rangle_{min}$ (e Å^{-3})	3.743, -4.558	2.03, -1.53

Table 11.10 Experimental details for compounds **11-Cl** (final data) and **11-Br** (* = preliminary data).[56]

Crystal Data	11-Cl	11-Br
Chemical formula	$C_{214.30}H_{289.20}Cl_{19.50}Cu_{19.50}Fe_{12}N_2P_{62}S_{1.50}$	$C_{131.16}H_{180}Cl_{0.78}Cu_{19.025}Fe_{12}Br_{19.025}N_{5.10}P_{61.52}S_{1.14}$*
M_r	7461.99	8091.40*
Crystal system, space group	monoclinic, *C*2/*c*	trigonal, $R\bar{3}$
Temperature (K)	123	123(2)
a, *b*, *c* (Å)	41.3224(15), 41.2915(7), 41.4301(10)	42.0935(3), 42.0935(3), 51.8785(4)
α, β, γ (°)	90, 112.427(4), 90	90, 90, 120
V (Å^3)	65344(4)	79607(1)
Z	8	12
F(000)	30016	45744
Radiation type	Cu K_α	Cu K_α

μ (mm^{-1})	10.41	> 15.71
Crystal color and shape	brown lath	black rhombohedron
Crystal size (mm)	0.26 × 0.09 × 0.04	0.24 × 0.16 × 0.08
Data collection		
Diffractometer	SuperNova, Single source at offset, Atlas diffractometer	SuperNova, Single source at offset, Titan^{S2} diffractometer
Absorption correction	analytical	gaussian
T_{min}, T_{max}	0.185, 0.668	0.096, 0.420
No. of measured, independent and observed [$I > 2\sigma(I)$] reflections	111226, 63497, 40310	187828, 35688, 29980
R_{int}	0.046	0.0660
$(\sin\theta/\lambda)_{max}$ ($Å^{-1}$)	0.624	
Range of h, k, l	h = -49→51, k = -31→50, l = -51→48	h = -52→38, k = -40→49, l = -63→63
Refinement		*
$R[F^2 > 2\sigma(F^2)]$, $wR(F^2)$, S	0.057, 0.171, 1.01	0.0630, 0.2168, 1.100
No. of reflections	63497	35688
No. of parameters	3015	1663
No. of restraints	44	
H-atom treatment	H-atom parameters constrained	H-atom parameters constrained
$\Delta\rangle_{max}$, $\Delta\rangle_{min}$ (e $Å^{-3}$)	2.03, -1.53	3.181, -4.544

Table 11.11 Experimental details for compounds **11-I** and **12-Cl** (* = preliminary data).[56]

Crystal Data	**11-I**	**12-Cl**
Chemical formula	$C_{126.67}H_{183.33}Cl_{4.33}Cu_{18.95}Fe_{12}I_{18.95}N_{1.05}P_{61.77}S_{1.33}$*	$(P_4Se_3)_{0.54}\cdot C_{120}H_{180}Cl_{17.375}Cu_{17.375}Fe_{12}P_{60}$*
M_r	8109.01*	6066.20*
Crystal system, space group	trigonal, $R\bar{3}$	trigonal, $R\bar{3}$
Temperature (K)	123(2)	123
a, b, c (Å)	42.5307(3), 42.5307(3), 52.3268(6)	41.9360(2), 41.9360(2), 51.6445(2)
α, β, γ (°)	90, 90, 120	90, 90, 120
V ($Å^3$)	81970(1)	78655.7(6)
Z	12	12
F(000)	46056	> 38036.1
Radiation type	Mo K_α	Cu K_α
μ (mm^{-1})	> 4.64	> 13.19
Crystal color and shape	black rhombohedron	black rhombohedron
Crystal size (mm)	0.14 × 0.12 × 0.08	0.52 × 0.27 × 0.13
Data collection		
Diffractometer	SuperNova, Single source at	SuperNova, Single source at

	offset, Eos diffractometer	offset, Titan[S2] diffractometer
Absorption correction	gaussian	gaussian
T_{min}, T_{max}	0.643, 0.750	0.040, 0.354
No. of measured, independent and observed [$I > 2\sigma(I)$] reflections	576068, 62185, 34125	171749
R_{int}	0.0803	0.089
Range of h, k, l	h = -60→63, k = -62→63, l = -77→77	h = -49→52, k = -50→41, l = -64→64
Refinement	*	
$R[F^2 > 2\sigma(F^2)]$, $wR(F^2)$, S	0.0686, 0.2333, 1.074	0.0841, 0.2618, 1.058
No. of reflections	62185	34390
No. of parameters	1652	1651
No. of restraints	8	
H-atom treatment	H-atom parameters constrained	H-atom parameters constrained
$\Delta\rangle_{max}$, $\Delta\rangle_{min}$ (e Å^{-3})	4.033, -5.772	3.849, -2.650

Table 11.12 Experimental details for compounds **12-Br** (final data) and **13-Cl** (* = preliminary data).[56]

Crystal Data	12-Br	13-Cl
Chemical formula	$C_{131.18}H_{197.10}Br_{18.35}Cl_{1.35}Cu_{18.35}Fe_{12}N_{5.25}P_{63}Se_{2.25}$	$(C_{10}H_{16})_{0.425}\cdot C_{120}H_{180}Cl_{17.52}Cu_{17.52}Fe_{12}P_{60}$*
M_r	7326.76	6144.01*
Crystal system, space group	trigonal, $R\bar{3}$	trigonal, $R\bar{3}$
Temperature (K)	123(1)	123
a, b, c (Å)	42.1062(1), 42.1062(1), 51.7973(3)	41.6741(5), 41.6741(5), 50.0101(7)
α, β, γ (°)	90, 90, 120	90, 90, 120
V (Å^3)	79529.8(6)	75218(2)
Z	12	12
F(000)	42621	36570.7
Radiation type	Mo K_α	Mo K_α
μ (mm^{-1})	5.58	> 2.74
Crystal color and shape	brown rhombohedron	brown rhombohedron
Crystal size (mm)	0.25 × 0.12 × 0.07	0.120 × 0.070 × 0.056
Data collection		
Diffractometer	SuperNova, Single source at offset, Eos diffractometer	SuperNova, Single source at offset, Eos diffractometer
Absorption correction	gaussian	gaussian
T_{min}, T_{max}	0.450, 0.720	0.802, 0.897
No. of measured, independent and observed [$I > 2\sigma(I)$] reflections	516760, 30095, 20873	178758, 40272, 16640
R_{int}	0.069	0.0832

$(\sin\theta/\lambda)_{max}$ (Å^{-1})	0.588	
Range of h, k, l	*h* = -49→49, *k* = -49→49, *l* = -60→60	*h* = -44→56, *k* = -54→56, *l* = -59→66
Refinement		*
$R[F^2 > 2\sigma(F^2)]$, $wR(F^2)$, *S*	0.054, 0.181, 1.13	0.0462, 0.1260, 0.847
No. of reflections	30095	40272
No. of parameters	1669	1594
No. of restraints	106	0
H-atom treatment	H-atom parameters constrained	H atom parameters constrained
$\Delta\rangle_{max}$, $\Delta\rangle_{min}$ (e Å^{-3})	3.90, -2.24	0.983, -1.065

Table 11.13 Experimental details for the supramolecule **14-Br** (final data) and the polymer **15-I** (final data).

Crystal Data	**14-Br**	**15-I**
Chemical formula	$VC_{12}H_{12}{\cdot}C_{480}H_{420}Br_{18.8}Cu_{18.8}Fe_{12}P_{60}{\cdot}4.8(C_7H_8)$	$C_{48}H_{72}Cu_{12}Fe_4I_{12}N_4P_{24}S_3$
M_r	11948.06	4053.24
Crystal system, space group	cubic, *Pm*$\bar{3}$*n*	tetragonal, $P42_12$
Temperature (K)	123	123(2)
a, *b*, *c* (Å)	31.6670(3), 31.6670(3), 31.6670(3)	18.8634(1), 18.8634(1), 17.8339(2)
α, β, γ (°)	90, 90, 90	90, 90 , 90
V (Å^3)	31755.6(5)	6345.80(9)
Z	2	2
F(000)	12022	3768.0
Radiation type	Cu K_α	Cu K_α
μ (mm^{-1})	5.96	32.120
Crystal color and shape	black block	brown plate
Crystal size (mm)	0.19 × 0.15 × 0.11	0.15 × 0.14 × 0.01
Data collection		
Diffractometer	SuperNova, Single source at offset, Titan^{S2} diffractometer	SuperNova, Single source at offset, Atlas diffractometer
Absorption correction	gaussian	gaussian
T_{min}, T_{max}	0.205, 0.364	0.024, 0.660
No. of measured, independent and observed [$I > 2\sigma(I)$] reflections	22682, 5536, 3243	30416, 6379, 5851
R_{int}	0.047	0.0604
$(\sin\theta/\lambda)_{max}$ (Å^{-1})	0.624	
Range of h, k, l	*h* = -13→25, *k* = -18→38, *l* = -38→27	*h* = -16→21, *k* = -19→23, *l* = -21→21
Refinement		

$R[F^2 > 2\sigma(F^2)]$, $wR(F^2)$, S	0.081, 0.273, 0.98	0.047, 0.136, 1.028
No. of reflections	5536	6379
No. of parameters	196	298
No. of restraints	33	3
H-atom treatment	H-atom parameters constrained	H-atom parameters constrained
$\Delta\rangle_{max}$, $\Delta\rangle_{min}$ (e Å^{-3})	1.69, -0.80	3.57, -1.70
Flack parameter	-	-0.006(6)

11.6 Author Contributions

- The syntheses and characterization of compounds **8-Br**, **8-I**, **9-Cl**, **9-Br**, **9-I**, **10-Br**, **10-I**, **11-Cl**, **11-Br**, **11-I**, **12-Cl**, **12-Br**, **14-Br** and **15-I** were performed by Claudia Heindl
- The synthesis and characterization of compound **13-Cl** were performed by Dr. Sabine Reisinger and are also part of her dissertation thesis (University of Regensburg, **2014**)
- The initial synthesis and X-ray structural analysis of **11-I** were done by Dr. Andreas Biegerl and are also part of his dissertation thesis (University of Regensburg, **2010**)
- X-ray structural analyses of **8-12** and **14-15** were performed by Dr. Eugenia V. Peresypkina, Dr. Alexander V. Virovets and Claudia Heindl
- X-ray structural analysis of **13-Cl** was performed together by Dr. Eugenia V. Peresypkina, Dr. Alexander V. Virovets and Dr. Sabine Reisinger
- The manuscript (introduction, results and discussion, experimental part; including figures and graphical abstract) was written by Claudia Heindl; with the following exceptions:
- The section 'crystallographic details' was written by Dr. Eugenia V. Peresypkina
- The MAS NMR investigations on **12-Cl** and **12-Br** as well as their description and figures were performed by David Lüdeker and PD Dr. Gunther Brunklaus.
- The EPR spectra of **9-Br** were recorded and interpreted by Prof. Dr. Ulrich Zenneck

11.7 References

[1] a) P. A. Thrower, *Carbon* **1999**, *37*, 1677; b) D. A. Bochvar, E. G. Gal'pern, *Dokl. Akad. Nauk SSSR* **1973**, *209*, 610.

[2] H. W. Kroto, J. R. Heath, S. C. O'Brien, R. F. Curl, R. E. Smalley, *Nature* **1985**, *318*, 162.

[3] a) A. A. Popov, S. Yang, L. Dunsch, *Chem. Rev.* **2013**, *113*, 5989; b) A. Rodriguez-Fortea, A. L. Balch, J. M. Poblet, *Chem. Soc. Rev.* **2011**, *40*; c) A. Hirsch, M. Brettreich in *Fullerenes* –

Chemistry and Reactions, Wiley-VCH, Weinheim, 2005; d) M. S. Dresselhaus, G. Dresselhaus, P. C. Eklund in *Science of Fullerenes and Carbon Nanotubes,* Academic Press, 1996.

[4] a) M. D. Tzirakis, M. Orfanopoulos, *Chem. Rev.* 2013, *113*, 5262; b) Z. Chen, L. Ma, Y. Liu, C. Chen, *Theranostics* 2012, *2*, 238; c) P. Anilkumar, F. Lu, L. Cao, P. G. Luo, J. H. Liu, S. Sahu, K. N. Tackett, II, Y. Wang, Y. P. Sun, *Curr. Med. Chem.* 2011, *18*, 2045.

[5] a) K. Yang, B. Xing, *Chem. Rev.* 2010, *110*, 5989; b) R. Tenne, M. Redlich, *Chem. Soc. Rev.* 2010, *39*, 1423.

[6] a) C.-Z. Li, H.-L. Yip, A. K. Y. Jen, *J. Mater. Chem.* 2012, *22*, 4161; b) Y. He, Y. Li, *Phys. Chem. Chem. Phys.* 2011, *13*, 1970.

[7] a) S. Raj, S. Jose, U. S. Sumod, M. Sabitha, *J. Pharm. BioAllied Sci.* 2012, *4*, 186; b) M. Lens, *Recent Pat. Biotechnol.* 2011, *5*, 67.

[8] None of the pentagons are in contact with each other.

[9] P. W. Fowler, D. E. Manolopoulos in *An Atlas of fullerenes*, Clarendon Press, 1995.

[10] F. Furche, R. Ahlrichs, *J. Chem. Phys.* 2001, *114*, 10362.

[11] S. Stevenson, G. Rice, T. Glass, K. Harich, F. Cromer, M. R. Jordan, J. Craft, E. Hadju, R. Bible, M. M. Olmstead, K. Maitra, A. J. Fisher, A. L. Balch, H. C. Dorn, *Nature* 1999, *402*, 898.

[12] M. Yamada, C. Someya, T. Wakahara, T. Tsuchiya, Y. Maeda, T. Akasaka, K. Yoza, E. Horn, M. T. H. Liu, O. N. Mizorogi, S. Nagase, *J. Am. Chem. Soc.* 2008, *130*, 1171.

[13] S. Stevenson, M. A. Mackey, M. A. Stuart, J. P. Phillips, M. L. Easterling, C. J. Chancellor, M. M. Olmstead, A. L. Balch, *J. Am. Chem. Soc.* 2008, *130*, 11844.

[14] a) M. Scheer, A. Schindler, J. Bai, B. P. Johnson, R. Merkle, R. Winter, A. V. Virovets, E. V. Peresypkina, V. A. Blatov, M. Sierka, H. Eckert, *Chem. Eur. J.* 2010, *16*, 2092; b) J. Bai, A. V. Virovets, M. Scheer, *Science* 2003, *300*, 781.

[15] J. Bai, A. V. Virovets, M. Scheer, *Angew. Chem. Int. Ed.* 2002, *41*, 1737.

[16] a) E. V. Peresypkina, C. Heindl, A. Schindler, M. Bodensteiner, A. V. Virovets, M. Scheer, *Z. Kristallogr.* 2014, *229*, 735; b) M. Scheer, A. Schindler, C. Groeger, A. V. Virovets, E. V. Peresypkina, *Angew. Chem. Int. Ed.* 2009, *48*, 5046.

[17] a) see chapter 9 in this work; b) A. Schindler, C. Heindl, G. Balázs, C. Groeger, A. V. Virovets, E. V. Peresypkina, M. Scheer, *Chem. Eur. J.* 2012, *18*, 829.

[18] see chapter 10 in this work.

[19] F. Dielmann, M. Fleischmann, C. Heindl, E. V. Peresypkina, A. V. Virovets, R. M. Gschwind, M. Scheer, *Chem. Eur. J.* 2015, *21*, 6208.

[20] a) A. Biegerl, C. Groeger, H. R. Kalbitzer, A. Pfitzner, J. Wachter, R. Weihrich, M. Zabel, *J. Solid State Chem.* 2011, *184*, 1719; b) J. Wachter, *Coord. Chem. Rev.* 2010, *254*, 2078; c) A. Biegerl, E. Brunner, C. Groeger, M. Scheer, J. Wachter, M. Zabel, *Chemistry* 2007, *13*, 9270.

[21] a) C. Heindl, S. Heinl, D. Luedeker, G. Brunklaus, W. Kremer, M. Scheer, *Inorg. Chim. Acta* 2014, *422*, 218; b) F. Dielmann, A. Schindler, S. Scheuermayer, J. Bai, R. Merkle, M. Zabel, A. V. Virovets, E. V. Peresypkina, G. Brunklaus, H. Eckert, M. Scheer, *Chem. Eur. J.* 2012, *18*, 1168.

[22] S. Deng, C. Schwarzmaier, C. Eichhorn, O. Scherer, G. Wolmershauser, M. Zabel, M. Scheer, *Chem. Commun.* 2008, 4064.

[23] C. Groeger, H. R. Kalbitzer, M. Pronold, D. Piryazev, M. Scheer, J. Wachter, A. Virovets, M. Zabel, *Eur. J. Inorg. Chem.* 2011, 785.

[24] A. Biegerl, Dissertation thesis (Universität Regensburg) 2010.

[25] The outer diameters were calculated as the maximum distance between two hydrogen atoms situated at two opposite methyl groups plus two times the van-der-Waals radius of the hydrogen atom (0.11 nm).

[26] The inner diameter were calculated as the distance between the centroids of two opposite *cyclo*-P_5 ligands minus two times the van-der-Waals radius of phosphorous (0.18 nm).

[27] The size of the templates was calculated as the maximum distance between two opposite atoms plus the van der Waals radii of these atoms. Hence, for templates of elongated and non-spherical shape, such as sandwich complexes, only the length is given.

[28] P. Seiler, J. D. Dunitz, *Acta Cryst. sect. B* 1980, *B36*, 2255.

[29] K. A. Lyssenko, M. Y. Antipin, S. Y. Ketkov, *Russ. Chem. Bull.* 2001, *50*, 130.

[30] P. J. Fitzpatrick, Y. Le Page, J. Sedman, I. S. Butler, *Inorg. Chem.* 1981, *20*, 2852.

[31] L. Y. Goh, W. Chen, R. C. S. Wong, K. Karaghiosoff, *Organometallics* 1995, *14*, 3886.

[32] J. R. Rollo, G. R. Burns, W. T. Robinson, R. J. H. Clark, H. M. Dawes, M. B. Hursthouse, *Inorg. Chem.* 1990, *29*, 2889.

[33] J. Donohue, S. H. Goodman, *Acta Cryst.* 1967, *22*, 352.

[34] A. Whitaker, J. W. Jeffery, *Acta Cryst.* 1967, *23*, 977.

[35] a) B. L. Kalsotra, R. K. Multani, B. D. Jain, *Chem. Ind.* 1972, 339; b) M. D. Walter, C. H. Booth, W. W. Lukens, R. A. Andersen, *Organometallics* 2009, *28*, 698.

[36] A. Simon, H. Borrmann, H. Craubner, *Phosphorus Sulfur* 1987, *30*, 507.

[37] C. Schwarzmaier, A. Schindler, C. Heindl, S. Scheuermayer, E. V. Peresypkina, A. V. Virovets, M. Neumeier, R. Gschwind, M. Scheer, *Angew. Chem. Int. Ed.* 2013, *52*, 10896.

[38] The overall occupancy of the guest can be underestimated because of the severe disorder and the fact that therefore not all positions of the guest molecule can be localized. It is especially true for the centrosymmetric position $\bar{1}$, where more than one (three are expected) crystallographically independent position of the guest must be found. For comparison, in the $\bar{3}$ position, only one orientation of the guest completely describes the disorder.

[39] l. I. Rios, F. Mani, M. Peruzzini, P. Stoppioni, *J. Organomet. Chem.* 2004, *689*, 164.

[40] M. Scheer, A. Schindler, R. Merkle, B. P. Johnson, M. Linseis, R. Winter, C. E. Anson, A. V. Virovets, *J. Am. Chem. Soc.* 2007, *129*, 13386.

[41] N. Hebendanz, F. H. Koehler, F. Scherbaum, B. Schlesinger, *Magn. Reson. Chem.* 1989, *27*, 798.

[42] Also [$NiCp_2$] is paramagnetic, though due to the presence of two unpaired electrons EPR inactive.

[43] C. Elschenbroich, F. Paganelli, M. Nowotny, B. Neumüller, O. Burghaus, *Z. Anorg. Allg. Chem.* 2004, *630*, 1599-1606.

[44] G. Brunklaus, *Dissertation,* University of Münster, Germany, 2003.

[45] D. Lathrop, H. Eckert, *Phys. Chem.* 1989, *93*, 7895.

[46] Y. Ishii, *J. Chem. Phys.* 2001, *114*, 8473.

[47] R. Zhang, Y. Nishiyama, P. Sun, A. Ramamoorthy, *J. Magn. Reson.* 2015, *252*, 55.

[48] A. D. Bain, I. W. Burton, *Concepts Magn. Reson.* 1996, *8*, 191.

[49] M. Detzel, G. Friedrich, O. J. Scherer, G. Wolmershäuser, *Angew. Chem. Int. Ed.* 1995, *34*, 1321.

[50] F. Dielmann, R. Merkle, S. Heinl, M. Scheer, *Z. Naturforsch.* 2009, *64*, 3.

[51] a) G. Wilkinson, P. L. Pauson, J. M. Birmingham, F. A. Cotton, *J. Am. Chem. Soc.* 1953, *75*, 1011; b) E. O. Fischer, R. Jira, *Z. Naturforsch.* 1953, *8b*, 217.

[52] R. B. King, F. G. A. Stone, *J. Am. Chem. Soc.* 1959, *81*, 5263.

[53] E. O. Fischer, R. Jira, *Z. Naturforsch.* 1954, *9b*, 618.

[54] G. M. Sheldrick. *Acta Cryst. sect. C* 2015, *C71*, 3.

[55] A. Altomare, M. C. Burla, M. Camalli, G. L. Cascarano, C. Giacovazzo, A. Guagliardi, A. G. G. Moliterni, G. Polidori, R. Spagna, *J. Appl. Cryst.* 1999, *32*, 115.

[56] Please note: Due to the uncompleted refinement, not all parameters (e.g. F(000)) can be stated and some given parameters, such as μ, R_{int}, as well as the sum formula have to be treated as temporarily values and may change at a later stage.

12. From Nano-Balls to Nano-Bowls

C. Heindl, E. V. Peresypkina, A. V. Virovets, M. Scheer

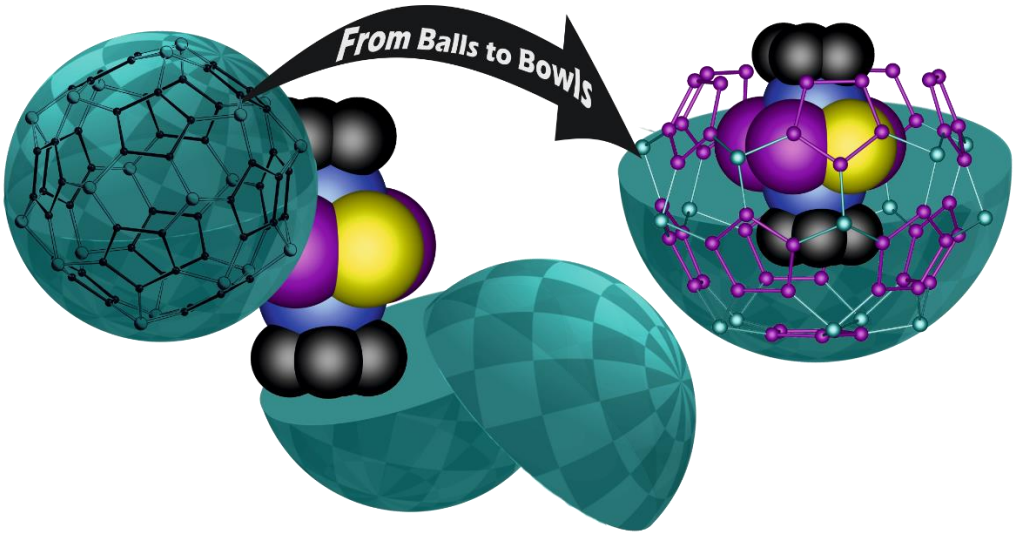

Abstract:

Pentaphosphaferrocene [Cp*Fe(η^5-P_5)] in combination with Cu(I) halides is capable of the template-directed synthesis of fullerene-like spheres. Herein, we present the use of two triple decker complexes as template: [$(CpMo)_2(\mu,\eta^{3:3}\text{-}P_3)(\mu,\eta^{2:2}\text{-}PS)$] (**2**) and [$(CpMo)_2(\mu,\eta^{6:6}\text{-}P_6)$] (**3**). Thereby, the hitherto unknown former complex **2** is synthesized by using a very high-boiling solvent. Surprisingly, the self-assembly processes of pentaphosphaferrocene and CuBr in presence of **2** and **3**, respectively, leads to the formation of the unprecedented 'nano-bowls' [**2**]@[$\{Cp^*Fe(\eta^5\text{-}P_5)\}_{11}\{CuBr\}_{15\text{-}n}$] (**4a**) and [**3**]@[$\{Cp^*Fe(\eta^5\text{-}P_5)\}_{11}\{CuBr\}_{15\text{-}n}$] (**5a**). Both compounds exhibit a scaffold of a spherical dome resembling a truncated 80-vertex ball. This enables the incorporation of the rather large guest molecules, since they are allowed to tower above the host molecule. Furthermore, within this study, the novel polymer [$\{Cp^*Fe(\eta^{5:1:1:1}\text{-}P_5)\}_3Cu_4(\mu\text{-}I)_4]_n$ (**6**) consisting of pentaphosphaferrocene and CuI can be obtained. Despite the large variety of known polymers, compound **6** displays the first three-dimensional assembly derived from [Cp*Fe(η^5-P_5)] and CuX (X = Cl, Br, I).

12.1 Introduction

Supramolecular chemistry, although as old as the mankind itself, is one of the most fascinating topics in current research. For instance, almost all biological actions refer to highly complex systems that are based on small subunits and held together by weak interactions. During the last decades supramolecular chemistry was successfully implemented in non-biological systems for the synthesis of large assemblies built up by small building blocks. Within this field, the coordinative bond turned out to be a great tool, since it combines the advantages of both covalent bonds as well as weak interactions: it is relatively strong, but often weak enough to allow dynamic behavior in solution. Hence, the self-assembly of metal salts and organic linkers has produced a wide variety of metal-organic frameworks (MOFs) and porous coordination polymers on the one hand[1] and discrete nano-sized supramolecules on the other.[2] The latter often provide defined inner cavities and can be used as molecular containers.

Recently, we have introduced the pentaphosphaferrocene $[Cp^RFe(\eta^5\text{-}P_5)]$ (Cp^R = Cp* = $\eta^5\text{-}C_5Me_5$; Cp^{Bn} = $\eta^5\text{-}C_5(CH_2Ph)_5$; Cp^{BIG} = $\eta^5\text{-}C_5(4\text{-}^nBuC_6H_4)_5$) as an outstanding five-fold symmetric organometallic building block as an auspicious alternative to the often used di- or tridentate organic linkers (*Figure 12.1*a). Astonishingly, under certain conditions the *cyclo*-P_5 ligand in combination with Cu(I) halides leads to the formation of spheres with, *inter alia*, fullerene topology.[3]

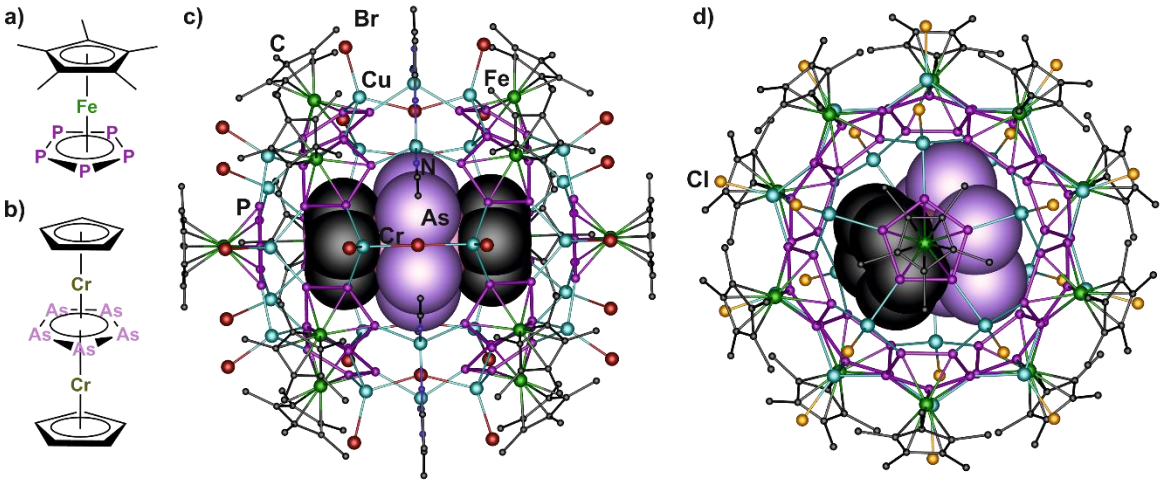

Figure 12.1 a) The building block $[Cp^*Fe(\eta^5\text{-}P_5)]$; b) the template $[(CpCr)_2(\mu,\eta^{5:5}\text{-}As_5)]$ (**1**); c) inclusion of **1** into the 90-vertex sphere **A**; d) inclusion of the fragment $[CpCr(\eta^5\text{-}As_5)]$ generated from **1** into the 80-vertex sphere **B**.

Their synthesis is often template-directed, thus, various molecules like C_{60}[3f] and ferrocene[3d] are encapsulated within these nano-balls. Among all templates the triple decker complex $[(CpCr)_2(\mu,\eta^{5:5}\text{-}As_5)]$ (**1**) displays an exceptional case (*Figure 12.1*b). With CuBr, it is incorporated into the 90-vertex host $[\{Cp^*Fe(\eta^5\text{-}P_5)\}_{12}(CuBr)_{25}(CH_3CN)_{10}]$ (host **A**), whereas with CuCl cleavage of the template appears and the fragment $[CpCr(\eta^5\text{-}As_5)]$ is encapsulated into the slightly smaller 80-

vertex ball [{Cp*Fe(η^5-P_5)}$_{12}$(CuCl)$_{20}$] (host **B**) (*Figure 12.1*c,d).[3d] Encouraged by this result, we were interested in the use of other triple decker complexes in this host-guest system to verify the generality of the observations.

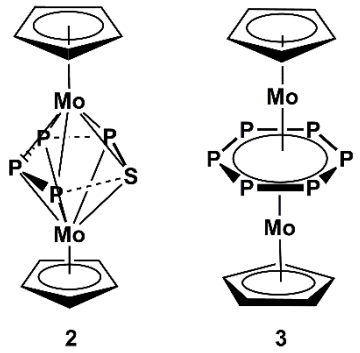

Figure 12.2 Triple decker complexes **2** and **3**.

For this purpose, the choice fell on two complexes bearing interesting middle decks and unsubstituted Cp ligands: [(CpMo)$_2$(μ,$\eta^{3:3}$-P_3)(μ,$\eta^{2:2}$-PS)] (**2**) and [(CpMo)$_2$(μ,$\eta^{6:6}$-P_6)] (**3**) (*Figure 12.2*). Whereas the latter complex **3** was obtained for the first time very recently,[4] the hitherto unknown parent compound **2** could be synthesized and characterized within the scope of this work. Herein, the template function of the triple decker complexes **2** and **3** in the system [Cp*Fe(η^5-P_5)]/CuBr will be described. Remarkably, in the presence of **2** and **3** the self-assembly of the building blocks leads to the generation of unprecedented nano-bowls with fullerene topology. These truncated spheres are able to incorporate the intact triple decker complexes.

12.2 Results and Discussion

The triple decker complex of the type [(Cp^{R}Mo)$_2$(μ,$\eta^{3:3}$-P_3)(μ,$\eta^{2:2}$-PS)] is known for Cp^R = Cp* = η^5-C_5Me_5[5] and Cp° = η^5-1-^{t}Bu-3,4-$Me_2C_5H_2$.[6] However, due to sterical reasons and favored Cp···P_5 π-π-interactions between guest and host, complexes with unsubstituted Cp ligands are unambiguously preferred for the incorporation in fullerene-like spheres. Both known derivatives are synthesized by the reaction of [Cp^{R}Mo(CO)$_2$]$_2$ with P_4S_3 in refluxing toluene. Unfortunately, the target compound **2** (Cp^R = Cp) could not be obtained applying the analogue reaction route. As we demonstrated earlier, the use of a higher-boiling solvent sometimes is expedient in thermolysis reactions.[4,7] Hence, [CpMo(CO)$_2$]$_2$ was allowed to react with P_4S_3 in refluxing 1,3-diisopropylbenzene (DIB, b.p. = 205 °C) (*Scheme 12.1*). In fact, after chromatographic work-up the desired parent compound **2** could be isolated in 18% crystalline yield (for a comparison: 13% for the Cp° derivative).[6]

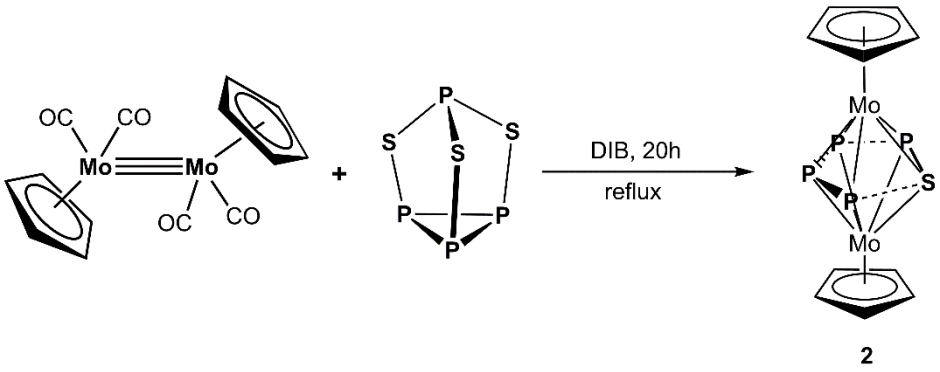

Scheme 12.1 Synthesis of **2**.

Compound **2** is soluble in rather nonpolar solvents like toluene and CH_2Cl_2, yet only sparingly soluble in hexane and insoluble in CH_3CN. The ^{1}H and $^{13}C\{^{1}H\}$ NMR spectra of **2** in C_6D_6 each show one singlet at δ = 4.73 ppm and δ = 91.2 ppm for the Cp ligand, respectively. In the $^{31}P\{^{1}H\}$ spectrum four multiplets, spread over a wide range of almost 750 ppm, represent an ABMX spin system: δ = 336.6 (ddd, P_A), 318.9 (ddd, P_B), -168.6 (ddd, P_M), -403.8 (ddd, P_X) ppm with respective coupling constants of J_{PP}(AB) = 19 Hz, J_{PP}(AM) = 59 Hz, J_{PP}(AX) = 376 Hz, J_{PP}(BM) = 6 Hz, J_{PP}(BX) = 376 Hz and J_{PP}(MX) = 20 Hz. These observations are in accordance with a weakly interacting η^3-P_3 and a η^2-PS ligand. Compared to the Cp* and Cp° derivative all signals are shifted to higher field up to 18 ppm.[5,6]

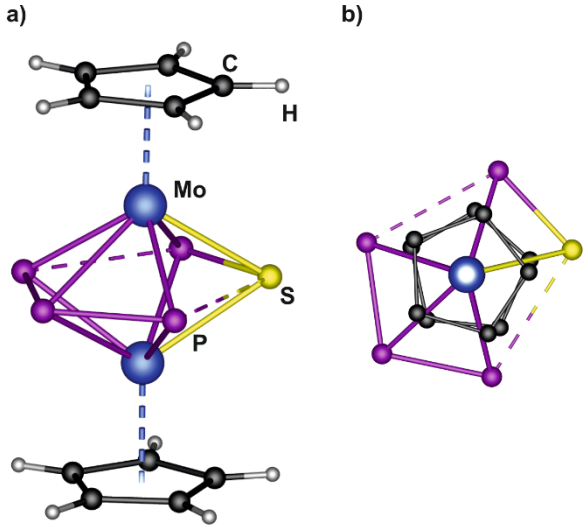

Figure 12.3 Molecular structure of **2** a) side view; b) top view, hydrogen atoms are omitted for clarity.

By layering a solution of **2** in CH_2Cl_2 with CH_3CN, red plate-like crystals suitable for X-ray structural analysis can be obtained for the first time for $[(Cp^RMo)_2(\mu,\eta^3\text{-}P_3)(\mu,\eta^2\text{-}PS)]$. For Cp^R = Cp* or Cp°, only coordination compounds containing the complex and not the starting compound itself were characterized by X-ray crystallography.[5,6,8] Compound **2** crystallizes in the monoclinic space group *C*2/*c*. Its molecular structure reveals a triple decker complex bearing a *pseudo* five-membered middle deck (*Figure 12.3*). In accordance with the $^{31}P\{^{1}H\}$ NMR spectrum, it can best be described as a η^3-P_3 and a η^2-PS ligand. The latter is disordered in the crystal structure by rotation about the 2-fold axis, passing through the center of the PS bond and the middle P atom of the η^3-P_3 ligand. The P-S distance of 2.079(1) Å as well as the P-P bond lengths of 2.159(1) Å are in the region between a single and a double bond.[9] The P_3 and the PS ligand are separated by 2.890(1) Å in the middle deck and the

Mo-P distances range from 2.417(1) Å to 2.600(1) Å. The Cp ligands deviate from an eclipsed conformation by 9.9(1)°. In the crystal structure, the molecules form lengthwise chains with short Cp···Cp distances of 3.22 Å – 3.23 Å evident for quite strong π-π-interactions.

With both triple decker complexes **2** and **3** in hand, they were applied as templates in the [Cp*Fe(η^5-P_5)]/CuBr system. For this purpose, a solution of [Cp*Fe(η^5-P_5)] and **2** or **3** in CH_2Cl_2 is layered with a solution of CuBr in CH_3CN, respectively. In all reactions the crystallization of brown plates of the 2D polymer [Cp*Fe(η^5-P_5)CuBr]$_n$[10] and sometimes also of brown rods of [Cp*Fe(η^5-P_5)]@**A** are observed. The latter displays the known 90-vertex supramolecule, which incorporates the building block [Cp*Fe(η^5-P_5)] itself.[11] Astonishingly, also black rhombohedra of the supramolecules **4** (in the presence of **2**) and **5** (in the presence of **3**) appear.[12] Unfortunately, the formation of **5** is observed only sporadically and solely the polymer and/or the 90-vertex sphere **A** is obtained in many attempts. On the other hand, the synthesis of **4** is reproducible without exception. A principle behind this discrepancy could not be figured out. Compound **4** crystallizes in the trigonal space group $R\bar{3}$ in the giant unit cell a = b = 41.7763(5) Å, c = 104.785(1) Å, V = 158377(4) Å^3, whereas the unit cell of **5** is half the volume ($R\bar{3}$, a = b = 42.0956(6) Å, c = 52.239(1) Å, V = 80167(2) Å^3). Hence, both crystalline phases are related as structure (**5**) and superstructure (**4**).

The X-ray structural analyses reveal that these crystals represent solid solutions of different spherical compounds consisting of [Cp*Fe(η^5-P_5)] and copper bromide. The respective idealized scaffolds are all derived from the icosahedral 80-vertex nano-ball [{Cp*Fe(η^5-P_5)}$_{12}${CuBr}$_{20}$] mentioned above (*Figure 12.1*d, type **B**). In these, twelve *cyclo*-P_5 ligands are coordinated to copper *via* all their phosphorus atoms in a 1,2,3,4,5-fashion, whereas the bromine atoms are all terminal. The hereby constructed scaffold contains 12 five-membered P_5 ligands and 30 six-membered {Cu_2P_4} rings and resembles the I_h-C_{80} fullerene. As in most cases,[3b,7,13,14] in **4** and **5** some positions of the CuBr fragments are partly vacant indicated by enlarged displacement parameters leading to the reduced scaffolds [{Cp*Fe(η^5-P_5)}$_{12}${CuBr}$_{20-n}$].[15]

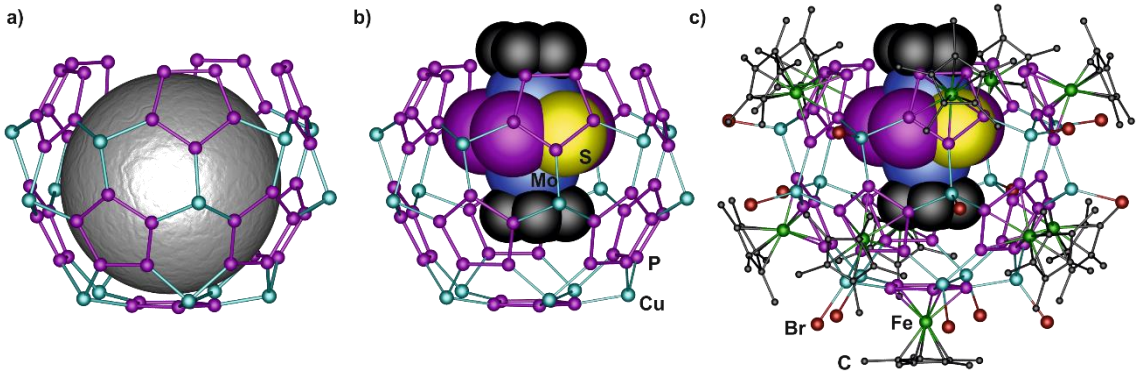

Figure 12.4 a) Inorganic scaffold of **4a** and **5a**; b) inorganic scaffold of **4a** with encapsulated template **2**; c) molecular structure of **4a**. Hydrogen atoms, solvents and minor parts of disorder are omitted for clarity; the template is shown in the space-filling-model.

Surprisingly, in **4** and **5** also a pentaphosphaferrocene vacancy is observed for the first time, which in addition correlates with adjacent vacant CuBr positions. As a consequence of this, a {Cp*Fe(η^5-P_5)$(CuBr)_5$} moiety is cutted off leaving the bowl-like truncated spheres [**2**]@[{Cp*Fe(η^5-P_5)}$_{11}${CuBr}$_{15-n}$] (**4a**) and [**3**]@[{Cp*Fe(η^5-P_5)}$_{11}${CuBr}$_{15-n}$] (**5a**) (*Figure 12.4*). These nano-bowls represent the predominant part of the solid solutions of **4** and **5**, respectively. However, in **5**, also the closed sphere [{Cp*Fe(η^5-P_5)}$_{12}${CuBr}$_{20-n}$] (**5b**) is present, whose cavity is most likely filled with solvent molecules. Hence, the crystal of **5** not only displays a solid solution of supramolecules of varying porosities, but also a mixture of 'balls' and 'bowls' in a rough ratio of 25% and 75%, respectively (for details see crystallographic part).

In the unprecedented spherical globes **4a** and **5a**, the coordination of the P_5 rings on the 'bottleneck' is reduced to a 1,2,3-fashion and the idealized scaffold of the globe consists of 70 atoms (55 P + 15 Cu) (*Figure 12.4*a). The diameter of the roughly spherical cavity of the ball is therefore reduced to a maximum width of 0.78 nm at the base of the bowl and 0.58 nm at the bottleneck.[16] In turn, the cavity is open at the top so that the templates **2** and **3** with a size of 1.01 x 0.71 nm and 1.00 x 0.80 nm, respectively,[17] are allowed to protrude and can be incorporated despite their bigger size (*Figure 12.4*b,c).

This result of a nano-bowl is observed for the first time and demonstrates that the formation of pentaphosphaferrocene-based host molecules is really template-directed. Thus, the previously reported cleavage of the triple decker complex **1** is not observed in the presence of **2** and **3**, respectively. The different reactivity of **1** bearing a *cyclo*-As_5 middle deck ('intact' sphere, fragmentation of the template) on the one hand and **2** and **3** (intact template, 'fragmentation' of the sphere) on the other hand might be traced back to a lower stability of **1**.

The guest molecules are disordered over at least two positions *via* an inversion center. In addition, they show an eclipsed orientation towards the *cyclo*-P_5 ligands of the host molecule, indicating π-π-host-guest interactions with Cp···P_5 distances of 3.7 Å – 3.8 Å in **4a** and 3.6 Å – 3.7 Å in **5a**.

The previously encapsulated triple-decker complex **1** in **1@A** forms similar eclipsed stacking with the P_5 ring of the 90-vertex host **A**.[3d] However, the middle *cyclo*-As_5 deck of **1** is disordered over three positions through the lack of interactions with the host **A**, since the *cyclo*-As_5 ligand is surrounded by alternating {$Cu(CH_3CN)_2$} and Br bridges of the middle belt of **A** (*Figure 12.1*c). The As···Br distances exceed the sum of the van-der-Waals radii by ~0.2 Å. In contrast, in the structure of **4a**, the middle deck of the P_3 and PS ligand is ordered and each P-P or P-S edge is arranged parallel (line-to-plane angles deviate by 0.1° – 0.8°) to the *cyclo*-P_5 ligand of the host. The corresponding six intermolecular contacts, namely five P···P and one P···S (two per middle deck

atom), are 3.58 Å – 3.65 Å, which is in a range for normal van-der-Waals contacts. Interestingly, the other intermolecular distances corresponding to the terminal atoms of the middle deck ligands are somewhat longer, 3.67 Å – 3.77 Å, and the line-to-plane angles between P···P or P···S and the P_5 ring of the host deviate by 1.1 – 1.5°. Therefore, the guest molecule has a preferable orientation in the host molecule supported by a system of van-der-Waals interactions.

The supramolecules **4** and **5** are insoluble in common solvents such as hexane, toluene, thf, Et_2O, and CH_3CN. Surprisingly, **4** is sparingly soluble in dichloromethane allowing ESI mass spectrometric analyses of dissolved crystals. Whereas in the anionic ESI mass spectrum only copper halide fragments are detected, the respective cationic spectrum shows numerous pentaphosphaferrocene-containing fragments. The largest fragment found is $[\{Cp^*Fe(\eta^5\text{-}P_5)\}_3Cu_{11}Br_{10}]^+$ (*m/z* = 2573.8). Notably, in the EI mass spectrum of **4** also a peak at *m/z* = 477.9 is found corresponding to the intact guest molecule **2**.

Furthermore, **4** and **5** are well soluble in pyridine, though accompanied by a complete fragmentation of the supramolecular scaffold. Hence, in the respective NMR spectra only signals corresponding to the free complex $[Cp^*Fe(\eta^5\text{-}P_5)]$ are detected (see experimental part). Nonetheless, dissolving of crystals of **4** and **5** in pyridine-d_5 displays an appropriate method for the detection of the triple decker complex. In fact, a singlet for the *cyclo*-P_6 ligand in **3** is observed in the $^{31}P\{^1H\}$ NMR spectrum of **5**, whereas four mulitplets resembling the ABMX spin system of the $(\mu,\eta^{3:3}\text{-}P_3)(\mu,\eta^{2:2}\text{-}PS)$ middle deck are perceived in the $^{31}P\{^1H\}$ NMR spectrum of **4**. The largest fragment in the cationic mass spectrum of **5** in pyridine appears at *m/z* = 1075.7 and corresponds to $[\{Cp^*Fe(\eta^5\text{-}P_5)\}Cu_4Br_3(C_5H_5N)_3]^+$.

Within the unsuccessful attempts to synthesize a CuI derivative of this bowl-like host molecule, the novel polymer $[\{Cp^*Fe(\eta^{5:1:1:1}\text{-}P_5)\}_2\{Cp^*Fe(\eta^{5:1:1}\text{-}P_5)\}Cu_4(\mu\text{-}I)_4]_n$ (**6**) is obtained. It crystallizes as brownish-red needles in the orthorhombic space group *Pmna* and its X-ray structural analysis reveals a three-dimensional assembly of $[Cp^*Fe(\eta^5\text{-}P_5)]$ and CuI (*Figure 12.5*).[18] This is in particular astonishing, since a huge variety of polymers containing pentaphosphaferrocene and copper halides is known, though only one- and two-dimensional networks.[10,19] Hence, compound **6** represents the first 3D aggregate containing $[Cp^*Fe(\eta^5\text{-}P_5)]$.

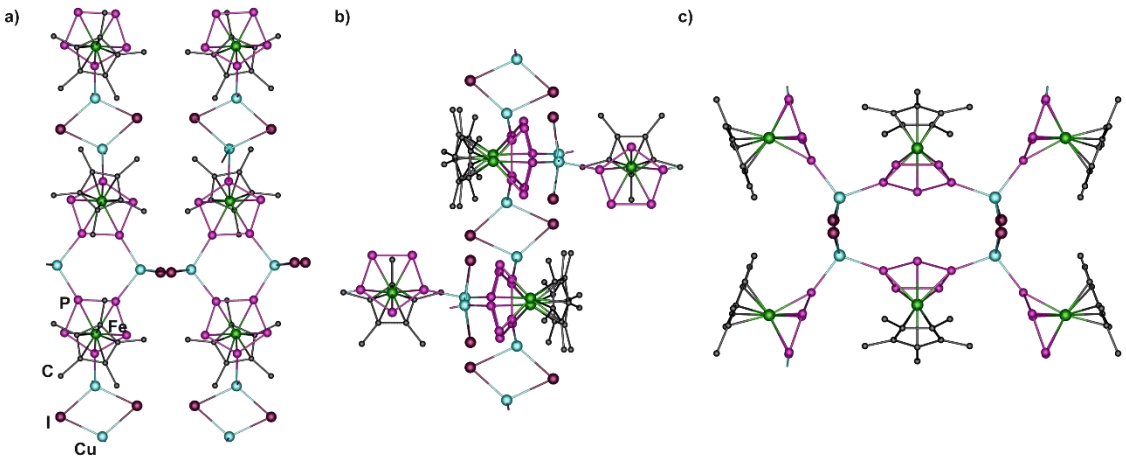

Figure 12.5 Sections of the polymeric structure of **6** along the crystallographic axes *a*, *b* and *c*, respectively.

The *cyclo*-P_5 ligands in **6** show two different coordination modes: Two thirds of the P_5 rings are connected to copper *via* three atoms in a 1,2,4-fashion, whereas the remaining ones show a 1,3-bridging coordination mode of two P atoms. In turn, each Cu atom links two P_5 rings and is additionally coordinated by two iodine atoms to reach a tetrahedral environment. By this, 12-membered $\{Cu_4P_6I_2\}$ rings, six-membered $\{Cu_2P_4\}$ rings and four-membered $\{Cu_2I_2\}$ rings are formed. The individual structural motifs and linkage pattern are well-known in this chemistry.[10,19] Despite this, the combination of two different coordination modes leads to a hitherto unknown topological type of 3-connected 3-periodic nets. Thereby, the Cu atoms and the 1,2,4-coordinating [Cp*Fe(η^5-P_5)] moieties form the nodes of the polymeric framework with iodine and the 1,3-coordinating [Cp*Fe(η^5-P_5)] molecules acting as spacers (see crystallographic part, *Figure 12.6*)

Compound **6** is insoluble in all common solvents (hexane, toluene, CH_2Cl_2, CH_3CN, thf, Et_2O). Only in the strong donor solvent pyridine the network is disassembled into the building blocks [Cp*Fe(η^5-P_5)] and CuI as evidenced by $^{31}P\{^1H\}$ NMR spectroscopy. Unfortunately, its formation was accompanied by the crystallization of the 2D network $[Cp^*Fe(\eta^5\text{-}P_5)CuI]_n$,[10] which could not be separated from **6**. Furthermore, almost all attempts of reproduction, much less of a selective synthesis, failed. Noteworthy, the first appearance of **6** is obtained when the triple decker complex **3** is present and the only successful reproduction also occurs in the presence of **3** despite its absence in the polymer.

In summary, the synthesis of the parent compound [$(CpMo)_2(\mu,\eta^{3:3}\text{-}P_3)(\mu,\eta^{2:2}\text{-}PS)$] (**2**) is enabled *via* the common thermolytic route by the use of the higher-boiling solvent 1,3-diisopropylbenzene. The triple decker complex **2** bears unsubstituted Cp ligands and an interesting mixed group 15/16 middle deck. This compound as well as the *cyclo*-P_6 containing complex [$(CpMo)_2(\mu,\eta^{6:6}\text{-}P_6)$] (**3**) were used as templates for the formation of supramolecules based on [Cp*Fe(η^5-P_5)] and CuBr. Thereby, two unprecedented host molecules incorporating the respective triple decker complex

can be obtained: [**2**]@[{Cp*Fe(η^5-P_5)}$_{11}${CuBr}$_{15-n}$] (**4a**) and [**3**]@[{Cp*Fe(η^5-P_5)}$_{11}${CuBr}$_{15-n}$] (**5a**). They both exhibit the same fullerene-like spherical cap, which is open at the top. It resembles the known 80-vertex nano-ball, though truncated and therefore can be entitled as 'nano-bowl'. Since the guest molecules are allowed to protrude, they can be trapped despite their bigger size. In addition, a novel polymer consisting of [Cp*Fe(η^5-P_5)] and CuI is obtained, which builds up a three-dimensional assembly for the first time.

12.3 Experimental Part

General Remarks:

All reactions were performed under an inert atmosphere of dry nitrogen or argon with standard vacuum, Schlenk and glove-box techniques. Solvents were purified, dried and degassed prior to use by standard procedures. [CpMo(CO)$_2$]$_2$,[20] [(CpMo)$_2$(μ,$\eta^{6:6}$-P_6)][4] and [Cp*Fe(η^5-P_5)][21] were synthesized following reported procedures and P_4S_3 was in-house available. CuCl and CuBr are commercially available and were used without further purification. Solution NMR spectra were recorded on a Bruker Avance 300 or 400 spectrometer. The corresponding ESI-MS spectra were acquired on a ThermoQuest Finnigan MAT TSQ 7000 mass spectrometer, whereas EI-MS and FD-MS spectra were measured on a Finnigan MAT 95 mass spectrometer. Elemental analyses were performed on a Vario EL III apparatus.

Synthesis of [(CpMo)$_2$(μ,$\eta^{3:3}$-P_3)(μ,$\eta^{2:2}$-PS)] (2)

[CpMo(CO)$_2$]$_2$ (1.0 g, 2.30 mmol) and P_4S_3 (506 g, 2.30 mmol) are dissolved in 1,3-diisopropylbenzene (DIB, bp = 203 °C, 150 mL) and refluxed for 20 hours. The solvent was removed and the dark residue was dissolved in toluene. Subsequently, this solution is filtered over celite and the solvent is again removed. The solid is adsorbed on silica and loaded onto a column filled with silica and hexane (20 cm x 3 cm). Compound **2** can be eluted as a red band using a hexane/toluene (1/1) solvent mixture. The solvent is removed and pure **2** can be isolated as dark red powder. Crystals suitable for X-ray diffraction analysis are obtained by layering a solution of **2** in CH_2Cl_2 with CH_3CN.

Analytical data of **2**:

Yield: 200 mg (crystalline yield, 0.42 mmol, 18%)

^{1}H NMR (C_6D_6): δ [ppm] = 4.73 (s, $C_5\underline{H}_5$)

^{13}C{^{1}H} NMR (C_6D_6): δ [ppm] = 91.2 (s, $\underline{C}_5H_5$)

^{31}P{^{1}H} NMR (C_6D_6): δ [ppm] = 336.6 (ddd, P_A), 318.9 (ddd, P_B), -168.6 (ddd, P_M), -403.8 (ddd, P_X); J_{PP}(AB) = 19 Hz, J_{PP}(AM) = 59 Hz, J_{PP}(AX) = 376 Hz, J_{PP}(BM) = 6 Hz, J_{PP}(BX) = 376 Hz, J_{PP}(MX) = 20 Hz.

FD-MS (toluene): 479.9 (M^+).

Elemental analysis: Calculated (%) for [$C_{10}H_{10}Mo_2P_4S$] (478.0 g/mol): C 25.13, H 2.11, S 6.71; found: C 24.81, H 2.10, S 7.19.

Synthesis of 4

In a Schlenk tube a dark green solution of [Cp*Fe(η^5-P_5)] (50 mg, 0.145 mmol) and **2** (15 mg, 0.03 mmol) in CH_2Cl_2 (10 mL) is carefully layered with a colorless solution of CuBr (42 mg, 0.29 mmol) in CH_3CN (10 mL). Thereby the phase boundary turns yellow-brownish. Already after one day the formation of black rhombohedra of **4** (at the phase boundary) in addition to brown plates of the polymer [{Cp*Fe(η^5-P_5)}CuBr]$_n$[10] (at the bottom) is observed. After some time also brown rods of the 90-vertex nanoball [Cp*Fe(η^5-P_5)]@[{Cp*Fe(η^5-P_5)}$_{12}$(CuBr)$_{25}$(CH_3CN)$_5$][11] appear. After complete diffusion the mother liquor is decanted, the crystals are washed with hexane (4 x 10 mL) and dried *in vacuo*. The only way to get pure **4** is to take the crystals of the Schlenk wall (and not from the bottom) with a spatula and quickly dip it into a Schlenk tube with hexane. However, the yield of pure **4** is always underestimated, since bigger crystals of **4** fall to the bottom due to their higher weight and are not isolated using this method

Analytical data of **4**:

Yield: 25 mg (3.9 µmol, 29%)

^{1}H NMR (pyridine-d_5): δ [ppm] = 1.41 (s, [Cp*Fe(η^5-P_5)]), 5.66 (s, [(CpMo)$_2$(µ,η^3-P_3)(µ,η^2-PS)].

^{31}P{^{1}H} NMR (pyridine-d_5): δ [ppm] = 311.3 (dd, P_A), 289.9 (d, P_B), 133.2 (s, [Cp*Fe(η^5-P_5)]), -167.5 (dd, P_M), -414.3 (ddd, P_X); J_{PP}(AM) = 32 Hz, J_{PP}(AX) = 386 Hz, J_{PP}(BX) = 401 Hz, J_{PP}(MX) = 21 Hz.

Positive ion ESI-MS (CH_2Cl_2): *m/z* (%) = 2573.8 [{Cp*Fe(η^5-P_5)}$_3$Cu$_{11}$Br$_{10}$]$^+$, 2394.0 [{Cp*Fe(η^5-P_5)}$_3$Cu$_{10}$Br$_9$]$^+$, 2248.0 [{Cp*Fe(η^5-P_5)}$_3$Cu$_9$Br$_8$]$^+$, 2106.0 [{Cp*Fe(η^5-P_5)}$_3$Cu$_8$Br$_7$]$^+$, 1960.2 [{Cp*Fe(η^5-P_5)}$_3$Cu$_7$Br$_6$]$^+$, 1818.4 [{Cp*Fe(η^5-P_5)}$_3$Cu$_6$Br$_5$]$^+$, 1676.6 [{Cp*Fe(η^5-P_5)}$_3$Cu$_5$Br$_4$]$^+$, 1530.7 [{Cp*Fe(η^5-P_5)}$_3$Cu$_4$Br$_3$]$^+$, 1328.3 [{Cp*Fe(η^5-P_5)}$_2$Cu$_5$Br$_4$]$^+$, 1040.6 [{Cp*Fe(η^5-P_5)}$_2$Cu$_3$Br$_2$]$^+$, 898.7 [{Cp*Fe(η^5-P_5)}$_2$Cu$_2$Br]$^+$, 754.8 (100) [{Cp*Fe(η^5-P_5)}$_2$Cu]$^+$, 449.8 [{Cp*Fe(η^5-P_5)}Cu(CH_3CN)]$^+$, 408.8 [{Cp*Fe(η^5-P_5)}Cu]$^+$

Negative ion ESI-MS (CH_2Cl_2): *m/z* = 510.3 [Cu_3Br_4]$^-$, 366.5 [Cu_2Br_3]$^-$, 222.6 [$CuBr_2$]$^-$

EI-MS (70 eV): 477.9 [(CpMo)$_2$(µ,η^3-P_3)(µ,η^2-PS)], 415.9 [{(CpMo)$_2$(µ,η^3-P_3)(µ,η^2-PS)}-P_2], 346.0 [Cp*Fe(η^5-P_5)], 284.1 [{Cp*Fe(η^5-P_5)}-P_2]

Elemental analysis: Calculated (%) for [{(CpMo)$_2$(µ,η^3-P_3)(µ,η^2-PS)}{Cp*Fe(η^5-P_5)}$_{11}$(CuBr)$_{15}$] (6435 g/mol): C 22.40, H 2.74, S 0.50; found: C 22.47, H 2.83, S 1.16.

Synthesis of 5

In a Schlenk tube a dark green solution of [Cp*Fe(η^5-P_5)] (30 mg, 0.087 mmol) and [(CpMo)$_2$(μ,$\eta^{6:6}$-P_6)] (10 mg, 0.019 mmol) in CH_2Cl_2 (10 mL) is carefully layered with a colorless solution of CuBr (25 mg, 0.17 mmol) in CH_3CN (10 mL). Thereby, the phase boundary turns yellow-brownish. After complete diffusion black rhombohedra of **5** in addition to brown plates of [{Cp*Fe(η^5-P_5)}(CuBr)]$_n$[10] can be observed. The mother liquor is decanted, the crystals are washed with hexane (4 x 10 mL) and dried *in vacuo*. Unfortunately, attempts to reproduce **5** have not always been successful. Frequently, only the polymeric product [{Cp*Fe(η^5-P_5)}(CuBr)]$_n$[10] crystallizes, sometimes also the crystallization of the 90-vertex ball [Cp*Fe(η^5-P_5)]@[{Cp*Fe(η^5-P_5)}$_{12}$(CuBr)$_{25}$(CH_3CN)$_5$][11] can be observed. Variations of the solvent as well as concentration were not successful. One reason might be the poor solubility of **3**, though only a small amount is needed. However, even performing the layering reactions with hot solutions did not lead to the formation of **5**.

Instead of CuBr, also the corresponding Cu(II) salt $CuBr_2$ once lead to the formation of **5**, though only as a minor phase.

Analytical data of **5** and [{Cp*Fe(η^5-P_5)}(CuBr)]$_n$:

Yield: 50 mg

^{1}H NMR (pyridine-d_5): δ [ppm] = 1.34 (s, [Cp*Fe(η^5-P_5)]), 2.47 (s, [(CpMo)$_2$(μ,$\eta^{6:6}$-P_6)]).

^{31}P{^{1}H} NMR (pyridine-d_5): δ [ppm] = -345.3 (s, [(CpMo)$_2$(μ,$\eta^{6:6}$-P_6)]), 152.0 (s, [Cp*Fe(η^5-P_5)]).

^{13}C{^{1}H} NMR (pyridine-d_5): δ [ppm] = 10.7 (s, $C_5\underline{Me}_5$), 91.7 (s, $\underline{C}_5Me_5$).

Positive ion ESI-MS (pyridine): *m/z* (%) = 1075.7 [{Cp*Fe(η^5-P_5)}$Cu_4Br_3(C_5H_5N)_3]^+$, 998.7 [{Cp*Fe(η^5-P_5)}$Cu_4Br_3(C_5H_5N)_2]^+$, 933.8 [{Cp*Fe(η^5-P_5)}$Cu_3Br_2(C_5H_5N)_3]^+$, 854.8 [{Cp*Fe(η^5-P_5)}$Cu_3Br_2(C_5H_5N)_2]^+$, 710.9 (100) [{Cp*Fe(η^5-P_5)}$Cu_2Br(C_5H_5N)_2]^+$, 631.9 (22) [{Cp*Fe(η^5-P_5)}$Cu_2Br(C_5H_5N)]^+$, 487.9 (70) [{Cp*Fe(η^5-P_5)}$Cu(C_5H_5N)]^+$, 351.3 (90), not assigned.

Negative ion ESI-MS (pyridine): *m/z* (%) = 366.6 (3) $[Cu_2Br_3]^-$, 222.8 (100) $[CuBr_2]^-$.

EI-MS (70 eV): 345.9 [Cp*Fe(η^5-P_5)], 284.0 [{Cp*Fe(η^5-P_5)}-P_2].

Elemental analysis: Calculated (%) for [{(CpMo)$_2$(μ,$\eta^{6:6}$-P_6)}{Cp*Fe(η^5-P_5)}$_{11}$(CuBr)$_{15}$] (6465 g/mol): C 22.29, H 2.73; calculated (%) for [Cp*Fe(η^5-P_5)CuBr] (489 g/mol): C 24.54, H 3.09; found: C 24.11, H 3.05.

Analytical Data of the mother liquor of **5**:

^{31}P{^{1}H} NMR (C_6D_6 capillary): δ [ppm] = -354.0 (s, [(CpMo)$_2$(μ,$\eta^{6:6}$-P_6)]).

Synthesis of $[\{Cp^*Fe(\eta^{5:1:1:1}\text{-}P_5)\}_2\{Cp^*Fe(\eta^{5:1:1}\text{-}P_5)\}Cu_4(\mu\text{-}I)_4]_n$ (6)

In a Schlenk tube a dark green solution of $[Cp^*Fe(\eta^5\text{-}P_5)]$ (30 mg, 0.087 mmol) and $[(CpMo)_2(\mu,\eta^{6:6}\text{-}P_6)]$ (15 mg, 0.030 mmol) in CH_2Cl_2 (10 mL) is carefully layered with a colorless solution of CuI (33 mg, 0.17 mmol) in CH_3CN (10 mL). Thereby, the phase boundary turns yellow-brownish and gets turbid. After complete diffusion black brownish-red needles of **6** as well as brown plates of $[\{Cp^*Fe(\eta^5\text{-}P_5)\}(CuI)]_n$[10] can be observed. The mother liquor is decanted, the crystals are washed with hexane (3 x 10 mL) and dried *in vacuo*. Unfortunately, attempts to reproduce **6**, with and without the addition of $[(CpMo)_2(\mu,\eta^{6:6}\text{-}P_6)]$, mostly failed. In total, **6** was observed only twice (both times when the triple decker complex **3** was present).

Analytical data of **6** and $[\{Cp^*Fe(\eta^5\text{-}P_5)\}(CuI)]_n$:

Yield: 30 mg

$^{31}P\{^1H\}$ NMR (pyridine, C_6D_6 capillary): δ [ppm] = 152.0 (s, $[Cp^*Fe(\eta^5\text{-}P_5)]$).

Elemental analysis: Calculated (%) for $[\{Cp^*Fe(\eta^5\text{-}P_5)\}_3(CuI)_4]$ (**6**; 1800 g/mol): C 20.02, H 2.52; calculated (%) for $[Cp^*Fe(\eta^5\text{-}P_5)CuI]$ (536 g/mol): C 22.39, H 2.82; found: C 21.94, H 2.84.

12.4 Crystallographic Details

Crystals of **2** and **4-6** were taken from a Schlenk flask under a stream of argon and immediately covered with mineral oil (**2**, **6**) or perfluorinated Fomblin® mineral oil (**4**, **5**) to prevent both decomposition and a loss of solvent. The quickly chosen single crystals covered by a drop of the oil were taken to the pre-centered goniometer head with CryoMount® and directly attached to the diffractometer into a stream of cold nitrogen. The X-ray diffraction study of **4** and **5** faced many challenges, since the crystals quickly decompose due to the loss of solvent. Due to the low diffraction power of **4** and **5** at high theta angles the collection of data required high exposure times.

The data for **2, 4,** and **6** were collected using 0.5° (**4**) or 1° (**2**, **6**) ω scans on an Agilent Technologies diffractometer equipped with an Atlas CCD detector and a SuperNova CuK_α microfocus source. The data for **5** were collected on an Agilent Technologies diffractometer equipped with Titan^{S2} CCD detector and a SuperNova CuK_α microfocus source using 0.5 ω scans. All measurements were performed at 123K.

The structures were solved by direct methods with *SHELX97*[22] and refined by full-matrix least-squares method on $|F|^2$ using multiprocessor and variable memory version *SHELXL2013*. All ordered non-hydrogen atoms were refined in an anisotropic approximation, while the disordered atoms with occupancy factors less that 0.5 were refined isotropically. The hydrogen atoms were

refined riding on pivot atoms. Crystallographic data and details of the diffraction experiments are given in in *Table 12.1* and *Table 12.2*.

The triple-decker complex **2** lies on the 2-fold axis and the $\mu,\eta^{2:2}$-PS ligand is represented by one crystallographically independent atom. To refine the disordered ligand both the coordinates and displacement parameters of the P and S atom were equated.

The crystal structure of **4** relates to **5** as a superstructural phase of doubled unit cell volume. The nature of this superstructural ordering is not yet clear. In **5**, the supramolecules occupy two independent positions of $\bar{1}$ and $\bar{3}$ symmetry, in **4** these are general and 3 positions. All three structures possess various types of disorder. First, some positions of the CuBr fragments are partly vacant indicated by enlarged displacement parameters. The occupancies for these positions were refined with fixed isotropic U_{iso} similar to average U_{iso} = 0.04 for the fully occupied heavy atoms in the corresponding structure. The constraints on the Cu and Br displacement parameters were then removed and an anisotropic approximation was used for the further refinement. Second, the positions of two pentaphosphaferrocene molecules per supramolecule are partly vacant. In the general position (in **4**) these occupancies were refined using the same procedure to 0,833 (⅚) and 0,167 (⅙), returning an incomplete bowl-like supramolecule. In $\bar{1}$ positions (in **5**) there is one independent vacant position. Since equal occupancies are imposed by symmetry the overall ratio per supramolecule was refined to ~0.75 for **5**. The vacancy of the pentaphosphaferrocene is strictly complementary (in **4**) or correlates well (in **5**) with the occupancies of adjacent CuBr units. The molecular occupancy refined for the entire guest molecule (**4**) or derived from occupancies of the Mo atoms (**5**) is less than (or equal to for the minor ⅙ part in $\bar{1}$ position) the corresponding vacancy of $\{Cp^*FeP_5(CuBr)_5\}$ unit. The direct refinement of the molecular occupancy of the guest in **5** is hindered by still unresolved disorder of the *cyclo*-P_6 ligand. The guest molecule in the general position (in **4**) is disordered over two independent positions. In **5**, one Mo atom of the triple-decker complex occupies an inversion center and the other Mo atom together with the *cyclo*-P_6 and the Cp ligands are disordered. The preliminary data show that the guest molecule is present in 0.667 and 0.167 (⅔ and ⅙) of cases in the general position of the structure **4** and ~0.5 in the 1 position for **5**. Interestingly, the compound **5** demonstrates more deficient CuBr scaffolds than **4**, where all vacant CuBr positions strictly correspond to the vacancy of pentaphosphaferrocene. For supramolecules in $\bar{3}$ (**5**) and 3 (**4**) positions, possible vacancies of pentaphosphaferrocene molecules are subject of further refinement.

These data prove that a complicated mixture of supramolecules, both nano-bowls and confined balls, co-exist at least in $\bar{1}$ position in **5**, where confined spheres $[(Cp^*FeP_5)_{12}(CuBr)_{20-n}]$ are present in 25% of cases. Additionally, a number of CuBr vacancies apart from the vacant

pentaphosphaferrocene position in **5** do not allow to state which type of supramolecules, nano-bowl or ball, is vacant. The higher symmetry for the other one complicates the refinement and assignment of the entities, although the general conclusions about **4**-**5** as solid solution cannot be withdrawn. Further refinement of the guest molecules and modeling of their disorder is only possible with concurrent refinement of all other structural parameters (mostly corresponding to the occupancies and disorder of solvent molecules).

The refinement of the 3D polymer **6** is not yet complete, since not all solvent molecules could be localized yet. The framework represents a new topological type of 3-connected 3-periodic nets. In this structure, the Cu atoms and the 1,2,4-coordinated [Cp*Fe(η^5-P_5)] molecules form nodes of the polymeric framework, connected by 1,3-coordinated [Cp*Fe(η^5-P_5)] spacers (*Figure 12.6*).

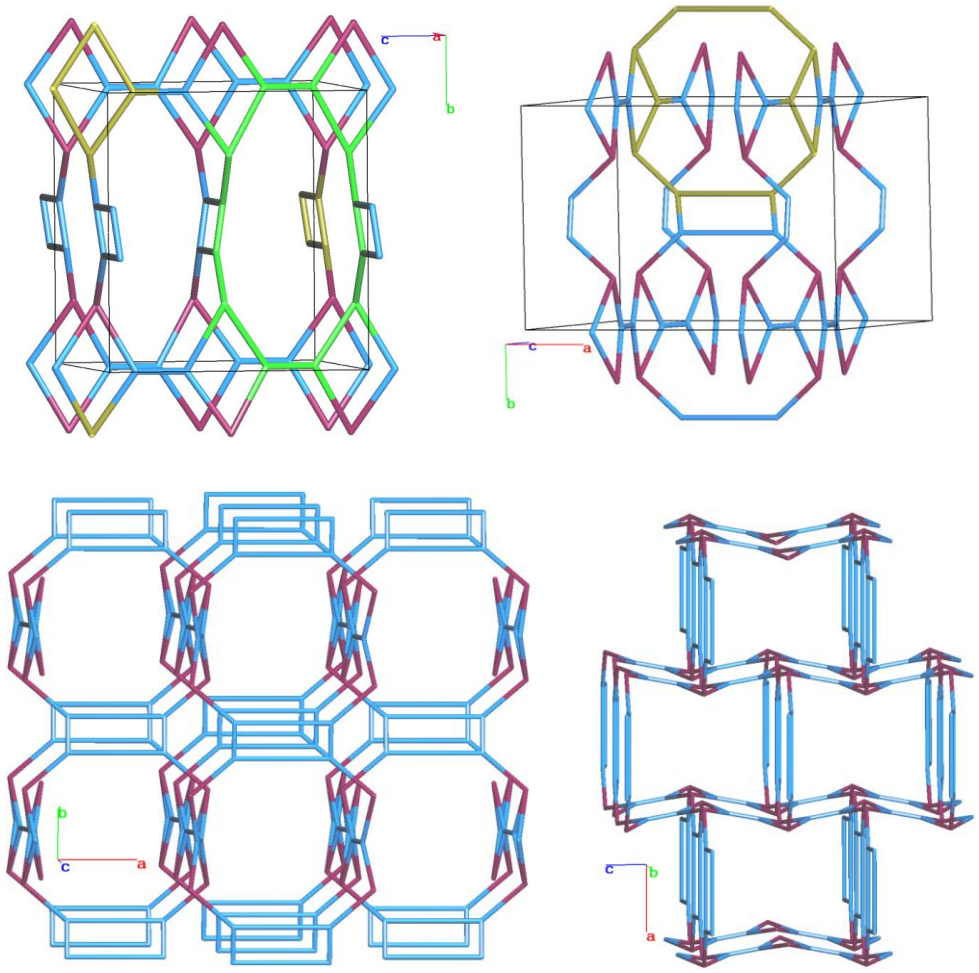

Figure 12.6 The 3-connected net of the new topology in **6**, containing 4, 10 (yellow highlighted) and 12-membered rings (green highlighted). Blue nodes correspond to Cu, purple ones to pentaphosphaferrocene.

Table 12.1 Experimental details for compounds **2** (final data) and **4** (* = preliminary data).[23]

Crystal Data	2	4
Chemical formula	$C_{10}H_{10}Mo_2P_4S$	$C_{237.5}H_{250}Br_{26.9}Cl_{5.75}Cu_{26.9}Fe_{21.5}Mo_{2.58}N_{2.33}P_{114.17}S$*
M_r	478.00	6276.76*

Crystal system, space group	monoclinic, *C*2/*c*	trigonal, $R\bar{3}$
Temperature (K)	123.0(2)	123
a, *b*, *c* (Å)	11.4167(5), 10.9669(3), 12.1695(6)	41.7763(8), 41.7763(8), 104.785(1)
α, β, γ (°)	90, 117.231(6), 90	90, 90, 120
V (Å^3)	1354.82(10)	158377(4)
Z	4	12
F(000)	920	> 70880
Radiation type	Cu K_α	Cu K_α
μ (mm^{-1})	20.84	> 12.39
Crystal color and shape	dark red rhombohedron	black block
Crystal size (mm)	0.13 × 0.07 × 0.06	0.61 × 0.18 × 0.03
Data collection		
Diffractometer	SuperNova, Single source at offset, Atlas diffractometer	SuperNova, Single source at offset, Atlas diffractometer
Absorption correction	multi-scan	gaussian
T_{min}, T_{max}	0.356, 1.000	0.024, 0.239
No. of measured, independent and observed [$I > 2\sigma(I)$] reflections	3339, 1345, 1243	104864, 67895, 38205
R_{int}	0.013	0.1066
$(\sin\theta/\lambda)_{max}$ (Å^{-1})	0.624	0.804
Range of h, k, l	*h* = -14→11, *k* = -12→13, *l* = -14→13	*h* = -33→31, *k* = -23→24, *l* = -44→53
Refinement		*
$R[F^2 > 2\sigma(F^2)]$, $wR(F^2)$, *S*	0.021, 0.058, 1.07	0.1528, 0.4104, 1.340
No. of reflections	1345	43976
No. of parameters	78	2614
No. of restraints	0	3
H-atom treatment	H-atom parameters constrained	H-atom parameters constrained
$\Delta\rangle_{max}$, $\Delta\rangle_{min}$ (e Å^{-3})	1.09, -1.20	1.87, -4.47

Table 12.2 Experimental details for compounds **5** and **6** (* = preliminary data).[23]

Crystal Data	5	6
Chemical formula	$C_{128.89}H_{153.46}Br_{14.85}Cl_{1.69}Cu_{14.85}Fe_{11.63}Mo_{0.92}N_{3.22}P_{59.89}$*	$C_{35}H_{52.5}Cu_4Fe_3I_4N_{2.5}P_{15}$*
M_r	6847.33*	1902.16*
Crystal system, space group	trigonal, $R\bar{3}$	orthorhombic, *Pnma*
Temperature (K)	123(2)	123(2)
a, *b*, *c* (Å)	42.0956(6), 42.0956(6), 52.239(1)	25.1960(5), 16.1506(3), 15.0851(3)

α, β, γ (°)	90, 90, 120	90, 90, 90
V (Å^3)	80167(2)	6138.6(5)
Z	12	4
F(000)	> 40230	> 3732
Radiation type	Cu K_α	Cu K_α
μ (mm^{-1})	> 13.21	> 26.95
Crystal color and shape	brown rhombohedron	brown needle
Crystal size (mm)	0.20 × 0.15 × 0.11	0.24 × 0.02 × 0.01
Data collection		
Diffractometer	SuperNova, Single source at offset, Titan^{S2} diffractometer	SuperNova, Single source at offset, Atlas diffractometer
Absorption correction	gaussian	gaussian
T_{min}, T_{max}	0.240, 0.387	0.141, 0.770
No. of measured, independent and observed [$I > 2\sigma(I)$] reflections	56621, 34462, 17327	25789, 6541, 5457
R_{int}	0.0770	0.0443
(sin θ/λ)$_{max}$ (Å^{-1})	0.801	0.792
Range of h, k, l	h = -39→50, k = -50→52, l = -45→63	h = -31→30, k = -19→20, l = -18→18
Refinement	*	*
$R[F^2 > 2\sigma(F^2)]$, $wR(F^2)$, S	0.0891, 0.2641, 0.940	0.0378, 0.1137, 1.045
No. of reflections	34462	6541
No. of parameters	1731	320
No. of restraints	7	0
H-atom treatment	H atom parameters constrained	H atom parameters constrained
Δ⟩$_{max}$, Δ⟩$_{min}$ (e Å^{-3})	2.856, -1.160	2.139, -0.955

12.5 Author Contributions

- The syntheses and characterization of the triple decker complex **2** as well as of the coordination products **4 – 6** were performed by Claudia Heindl
- X-ray structural analyses of **2** and **4 – 6** were performed by Dr. Eugenia V. Peresypkina, Dr. Alexander V. Virovets and Claudia Heindl
- The manuscript (introduction, results and discussion, experimental part; including figures and graphical abstract) was written by Claudia Heindl with the following exception:
- The section 'crystallographic details' was written by Dr. Eugenia V. Peresypkina

12.6 References

[1] a) L. E. Kreno, K. Leong, O. K. Farha, M. Allendorf, R. P. Van Duyne, J. T. Hupp, *Chem. Rev.* 2012, *112*, 1105; b) O. K. Farha, J. T. Hupp, *Acc. Chem. Res.* 2010, *43*, 1166; c) C. Janiak, J. K. Vieth, *New J. Chem.* 2010, *34*, 2366; d) J. L. C. Rowsell, O. M. Yaghi, *Microporous Mesoporous Mater.* 2004, *73*, 3; e) S. L. James, *Chem. Soc. Rev.* 2003, *32*, 276.

[2] a) S. Zarra, D. M. Wood, D. A. Roberts, J. R. Nitschke, *Chem. Soc. Rev.* 2015, *44*, 419; b) N. J. Young, B. P. Hay, *Chem. Commun.* 2013, *49*, 1354; c) Y. Fang, T. Murase, S. Sato, M. Fujita, *J. Am. Chem. Soc.* 2013, *135*, 613; d) T. Mitra, K. E. Jelfs, M. Schmidtmann, A. Ahmed, S. Y. Chong, D. J. Adams, A. I. Cooper, *Nat. Chem.* 2013, *5*, 276; e) R. W. Saalfrank, A. Scheurer, *Top. Curr. Chem.* 2012, *319*, 125; f) M. Schmidtendorf, T. Pape, F. E. Hahn, *Angew. Chem. Int. Ed.* 2012, *51*, 2195; g) J. S. Mugridge, R. G. Bergman, K. N. Raymond, *J. Am. Chem. Soc.* 2012, *134*, 2057; h) K. Tiefenbacher, D. Ajami, J. Rebek, *Angew. Chem. Int. Ed.* 2011, *50*, 11805; i) Z. Laughrey, B. C. Gibb, *Chem. Soc. Rev.* 2011, *40*, 363; j) J. Rabone, Y. F. Yue, S. Y. Chong, K. C. Stylianou, J. Bacsa, D. Bradshaw, G. R. Darling, N. G. Berry, Y. Z. Khimyak, A. Y. Ganin, P. Wiper, J. B. Claridge, M. J. Rosseinsky, *Science* 2010, *329*, 1053; k) S. Horike, S. Shimomura, S. Kitagawa, *Nat. Chem.* 2009, *1*, 695; l) M. Yoshizawa, J. K. Klosterman, M. Fujita, *Angew. Chem. Int. Ed.* 2009, *48*, 3418; m) S. J. Dalgarno, N. P. Power, J. L. Atwood, *Coord. Chem. Rev.* 2008, *252*, 825; n) T. S. Koblenz, J. Wassenaar, J. N. H. Reek, *Chem. Soc. Rev.* 2008, *37*, 247; o) C. Schmuck, *Angew. Chem. Int. Ed.* 2007, *46*, 5830.

[3] a) S. Heinl, E. V. Peresypkina, A. V. Virovets, M. Scheer, *Angew. Chem. Int. Ed.* 2015, submitted; b) F. Dielmann, M. Fleischmann, C. Heindl, E. V. Peresypkina, A. V. Virovets, R. M. Gschwind, M. Scheer, *Chem. Eur. J.* 2015, *21*, 6208; c) F. Dielmann, C. Heindl, F. Hastreiter, E. V. Peresypkina, A. V. Virovets, R. M. Gschwind, M. Scheer, *Angew. Chem. Int. Ed.* 2014, *53*, 13605; d) A. Schindler, C. Heindl, G. Balázs, C. Groeger, A. V. Virovets, E. V. Peresypkina, M. Scheer, *Chem. Eur. J.* 2012, *18*, 829; e) M. Scheer, A. Schindler, C. Groeger, A. V. Virovets, E. V. Peresypkina, *Angew. Chem. Int. Ed.* 2009, *48*, 5046; f) M. Scheer, A. Schindler, R. Merkle, B. P. Johnson, M. Linseis, R. Winter, C. E. Anson, A. V. Virovets, *J. Am. Chem. Soc.* 2007, *129*, 13386; g) J. Bai, A. V. Virovets, M. Scheer, *Science* 2003, *300*, 781.

[4] M. Fleischmann, C. Heindl, M. Seidl, G. Balázs, A. V. Virovets, E. V. Peresypkina, M. Tsunoda, F. P. Gabbaï, M. Scheer, *Angew. Chem. Int. Ed.* 2012, *51*, 9918.

[5] H. Brunner, U. Klement, W. Meier, J. Wachter, O. Serhadle, M. L. Ziegler, *J. Organomet. Chem.* 1987, *335*, 339.

[6] C. Groeger, H. R. Kalbitzer, M. Pronold, D. Piryazev, M. Scheer, J. Wachter, A. Virovets, M. Zabel, *Eur. J. Inorg. Chem.* 2011, 785.

[7] See chapter 10.

[8] L. J. Gregoriades, G. Balázs, E. Brunner, C. Groeger, J. Wachter, M. Zabel, M. Scheer, *Angew. Chem. Int. Ed.* 2007, *46*, 5966.

[9] a) P. Pyykkö, M. Atsumi, *Chem. Eur. J.* 2009, *15*, 186; b) P. Pyykkö, M. Atsumi, *Chem. Eur. J.* 2009, *15*, 12770.

[10] J. Bai, A. V. Virovets, M. Scheer, *Angew. Chem. Int. Ed.* 2002, *41*, 1737.

[11] a) M. Scheer, A. Schindler, J. Bai, B. P. Johnson, R. Merkle, R. Winter, A. V. Virovets, E. V. Peresypkina, V. A. Blatov, M. Sierka, H. Eckert, *Chem. Eur. J.* 2010, *16*, 2092; b) M. Scheer, J. Bai, B. P. Johnson, R. Merkle, A. V. Virovets, C. E. Anson, *Eur. J. Inorg. Chem.* 2005, 4023.

[12] Due to the incomplete refinement of these complicated solid solutions no final sum formula can be given at this state.

[13] E. V. Peresypkina, C. Heindl, A. Schindler, M. Bodensteiner, A. V. Virovets, M. Scheer, *Z. Kristallogr.* 2014, *229*, 735.

[14] See chapter 11.

[15] For a more detailed discussion of these vacancies see: a) chapter 10; b) chapter 11.

[16] The width is measured as the distance between the centroids of two opposite *cyclo*-P_5 ligands minus twice the van-der-Waals radius of phosphorus (1.80 Å); the bottleneck is measured as the distance between two opposite P atoms of the open top minus twice the van-der-Waals radius of phosphorus.

[17] The sizes of the templates are measured as the distances between two opposite P atoms of the middle deck and the distance between the centroids of the Cp rings, respectively, plus twice the van-der-Waals radius of P (1.80 Å) and C (1.70 Å), respectively.

[18] For the only 3D polymer containing a pentaphosphaferrocene see: chapter 10.

[19] F. Dielmann, A. Schindler, S. Scheuermayer, J. Bai, R. Merkle, M. Zabel, A. V. Virovets, E. V. Peresypkina, G. Brunklaus, H. Eckert, M. Scheer, *Chem. Eur. J.* 2012, *18*, 1168.

[20] M. D. Curtis, M. S. Hay, *Inorg. Synth.* 1990, *28*, 150.

[21] M. Detzel, G. Friedrich, O. J. Scherer, G. Wolmershäuser, *Angew. Chem. Int. Ed.* 1995, *34*, 1321.

[22] G. M. Sheldrick, *Acta Cryst. sect. C.*, 2015, *C71*, 3.

[23] Please note: Due to the incomplete refinement, not all parameters (e.g. F(000)) can be stated and some given parameters, such as μ, R_{int}, as well as the sum formula have to be treated as preliminary values and may change at a later stage.

13. From Halides to Triflates: Synthesis of the first Ag-containing supramolecules based on pentaphosphaferrocenes

C. Heindl, B. Krämer, E. V. Peresypkina, A. V. Virovets, M. Scheer

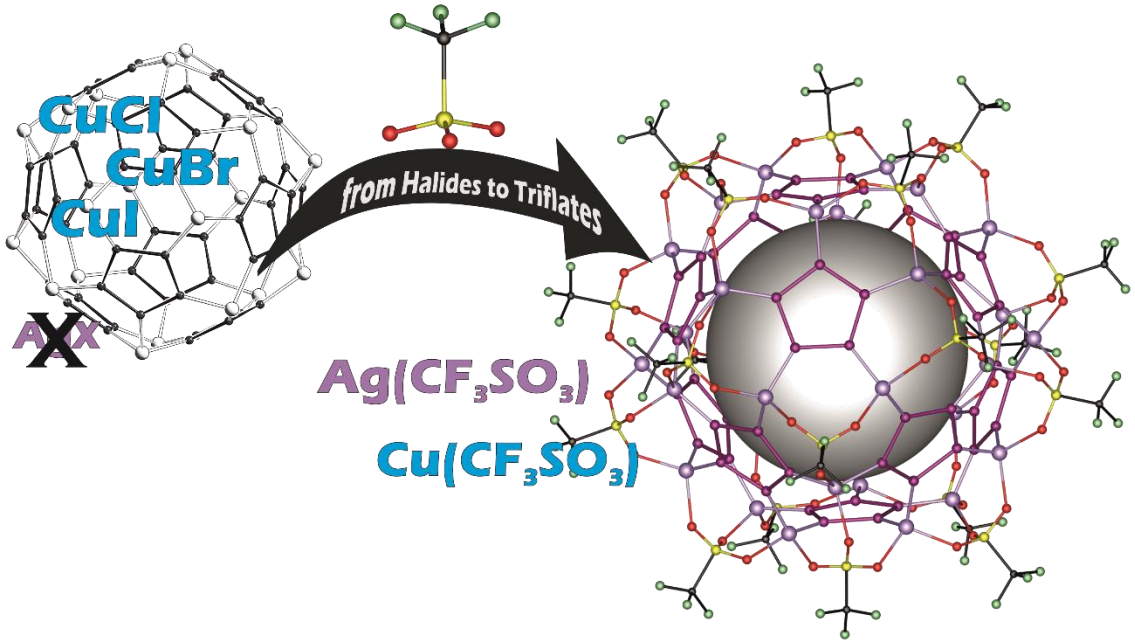

Abstract:

Pentaphosphaferrocenes [$Cp^RFe(\eta^5\text{-}P_5)$] and Cu(I) halides display excellent building blocks for the formation of discrete supramolecules. Herein, we demonstrate the potential of $M(CF_3SO_3)$ (M = Cu, Ag) for the construction of novel 2D polymers as well as of nano-sized spheres: $[\{Cp^*Fe(\mu_4,\eta^{5:1:1:1}\text{-}P_5)\}\{Cu(CF_3SO_3)\}]_n$ (**2**), $(CH_2Cl_2)_{1.4}@[\{Cp^{Bn}Fe(\eta^5\text{-}P_5)\}_{12}\{Cu(CF_3SO_3)\}_{19.6}]$ (**3**), $[\{Cp^*Fe(\mu_3,\eta^{5:1:1:1}\text{-}P_5)\}\{Ag(CF_3SO_3)\}_2]_n$ (**4**), $[Cp^*Fe(\eta^5\text{-}P_5)]@[\{Cp^*Fe(\eta^5\text{-}P_5)\}_{12}\{Ag(CF_3SO_3)\}_{20\text{-}n}]$ (**5**) and $[\{Cp^{Bn}Fe(\eta^5\text{-}P_5)\}_{12}\{Ag(CF_3SO_3)\}_{20\text{-}n}]$ (**6**). Thereby, the supramolecules **3**, **5** and **6** exhibit an identical and unprecedented scaffold beyond the fullerene topology with the copper atoms forming an icosidodecahedron and the tridentate triflate ligands in a μ_3 coordination mode. Remarkably, **5** and **6** display the first representatives of an Ag-containing 'ball' derived from pentaphosphaferrocenes. Furthermore, one molecule of $[Cp^*Fe(\eta^5\text{-}P_5)]$ is encapsulated within the cavity of **5**. The outer diameters are defined by the Cp^R ligands and amount to 2.3 nm for **5** (Cp^R = Cp*) and even 3.3 nm for **3** and **6** (Cp^R = Cp^{Bn}). The benzyl ligands in **3** and **6** also significantly enhance the solubility allowing NMR spectroscopic and mass spectrometric investigations.

13.2 Introduction

Though supramolecular chemistry is rooted in nature, it has also become a fascinating and indispensable field of current research in chemistry over the last few decades. Among the obtained assemblies discrete spherical supramolecules are particularly astonishing, since they reach several nanometers in size and often provide defined inner cavities suitable for guest enclosure.[1] For their synthesis based on the self-assembly approach, especially the metal-ligand dative bond provides many advantages, such as the combination of strength and reversibility. Since this type of bonding is directional, a rational design is enabled by the variation of symmetry and geometry of the respective building blocks.[2] Our group therefore uses substituent-free complexes of phosphorus, such as [{CpMo(CO)$_2$}$_2$(η^2-P$_2$)],[3] [CpMo(CO)$_2$(η^3-P$_3$)],[4] [Cp''Ta(CO)$_2$(η^4-P$_4$)][5] (Cp'' = η^5-C$_5$H$_3$^{t}Bu$_2$) and especially [Cp^{R}Fe(η^5-P$_5$)] (**1**, Cp^R = Cp* = η^5-C$_5$Me$_5$ (**1a**); Cp^{Bn} = η^5-C$_5$(CH$_2$Ph)$_5$ (**1b**); Cp^{BIG} = η^5-C$_5$(4-^{n}BuC$_6$H$_4$)$_5$ (**1c**)), the latter type containing a planar five-fold symmetric P$_5$ ligand (*Figure 13.1*a). Such pentatopic nodes are predestinated for the construction of ball-shaped spheres, as it has also been recognized recently by two other groups: Williams *et al.* use the pentakis(4-pyridyl)cyclopentadienide (*Figure 13.1*b)[6] as well as the pentakis(1-methylpyrazole)cyclopentadienide ligand (*Figure 13.1*c),[7] whereas the group of Wright focuses on [C$_5$(CN)$_5$]$^-$ (*Figure 13.1*d).[8] In contrast to **1**, these ligands all contain nitrogen as the donating element.

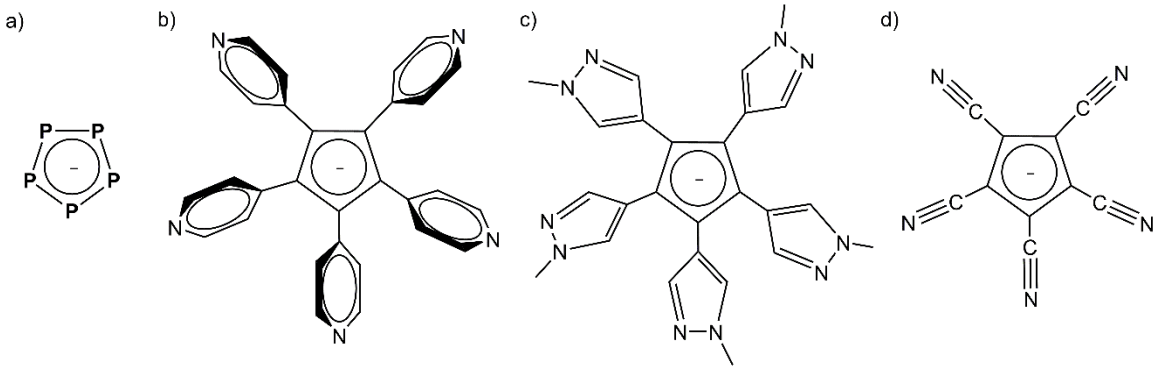

Figure 13.1 Five-fold symmetric linking units.

Pentaphosphaferrocenes [Cp^{R}Fe(η^5-P$_5$)] provide a large variety of coordination compounds in combination with various Lewis-acidic metal atoms. Thereby, the *cyclo*-P$_5$ ligand shows different coordination modes and one- and two-dimensional polymers (coordination *via* two, three or four P atoms)[9] as well as discrete spherical compounds (coordination *via* five P atoms)[10] could be synthesized and investigated over the past decade. Selected examples are depicted in *Figure 13.2*. Exemplarily, the self-assemblies with CuCl and Ag[Al{OC(CF$_3$)$_3$}$_4$], lead to the formation of neutral and cationic chains, respectively (*Figure 13.2*a,b).[9c,e] Astonishingly, the addition of small molecules to the mixtures of **1** and CuX (X = Cl, Br, I) allows the formation of supramolecules accompanied by

the trapping of these templates within their cavities. A common feature among these is the fullerene topology: they are constructed by five- and six-membered rings according to the isolated pentagon rule (*Figure 13.2*c).[10a,b,e,f] However, also a few supramolecules with deviating topologies and shapes have been synthesized (*Figure 13.2*d).[10c,d] Furthermore, the structural motifs as well as the properties of the obtained products can be tuned by altering the electronic and sterical influence of the substitution pattern of the cyclopentadienyl ligand. In this manner it was possible to increase substantially the solubility of the spheres by using sterically demanding organic residues as in **1b** and **1c**.[10a-c]

Whereas for the synthesis of polymeric compounds various transition metal atoms, such as copper,[9c,e] silver,[9b,d] and thallium[9a] could be implemented, the field of spherical compounds was restricted to Cu(I) halides up to the present.[10] Attempts to include other types of metal cations as well as anions as scaffold-constructing building blocks failed so far. A promising approach might be the use of multifunctional anions like triflouromethanesulfonate $(CF_3SO_3)^-$ (or triflate) which shows varying coordination properties. Since it can act as non-coordinating, terminal, multidentate or bridging ligand,[11] we are interested in its application as building block in combination with pentaphosphaferrocenes.

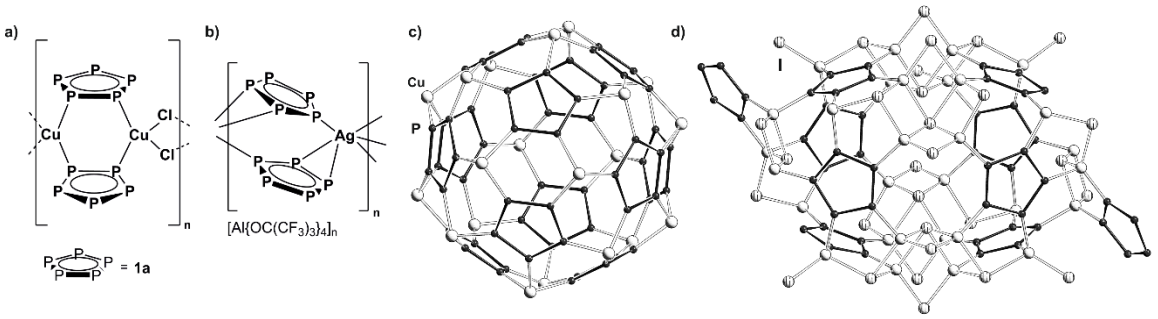

Figure 13.2 Selected coordination products based on **1a** as building block: a) 1D polymer containing Cu; b) 1D polymer containing Ag; c) a Cu-based supramolecule with fullerene topology; d) a Cu-based supramolecule with non-fullerene topology.

Herein we report on the results of the self-assembly of the pentaphosphaferrocenes **1a** and **1b** with $M(CF_3SO_3)$ (M = Cu, Ag), respectively. Thereby, the copper salt is capable of the formation of the novel 2D polymer $[\{Cp^*Fe(\mu_4,\eta^{5:1:1:1}\text{-}P_5)\}\{Cu(CF_3SO_3)\}]_n$ (**2**) and an unprecedented supramolecule $(CH_2Cl_2)_{1.4}@[\{Cp^{Bn}Fe(\eta^5\text{-}P_5)\}_{12}\{Cu(CF_3SO_3)\}_{19.6}]$ (**3**). Furthermore, going to Ag, the formation of the 2D network $[\{Cp^*Fe(\mu_3,\eta^{5:1:1:1}\text{-}P_5)\}\{Ag(CF_3SO_3)\}_2]_n$ (**4**) and gratifyingly of the first silver containing spheres $[Cp^*Fe(\eta^5\text{-}P_5)]@[\{Cp^*Fe(\eta^5\text{-}P_5)\}_{12}\{Ag(CF_3SO_3)\}_{20\text{-}n}]$ (**5**) and $[\{Cp^{Bn}Fe(\eta^5\text{-}P_5)\}_{12}\{Ag(CF_3SO_3)\}_{20\text{-}n}]$ (**6**) based on pentaphosphaferrocenes is observed.

13.3 Results and Discussion

When a solution of $Cu(CF_3SO_3)\cdot 0.5C_7H_8$ in CH_2Cl_2 is layered with a solution of **1a** in a toluene/hexane mixture, a color change to yellow at the phase boundary is observed. Within one day yellow plates of the polymer $[\{Cp^*Fe(\mu_4,\eta^{5:1:1:1}\text{-}P_5)\}\{Cu(CF_3SO_3)\}]_n$ (**2**) start to crystallize (*Scheme 13.1*). On the contrary, **1b** is reacted with $Cu(CF_3SO_3)\cdot 0.5C_7H_8$ by stirring a CH_2Cl_2 solution of both compounds. Within ten minutes the solution turns yellowish brown. After filtration and layering with toluene brown prisms of the supramolecule $[\{Cp^{Bn}Fe(\eta^5\text{-}P_5)\}_{12}\{Cu(CF_3SO_3)\}_{19.6}]$ (**3**) crystallize (*Scheme 13.1*). Both compounds **2** and **3** are obtained in reasonable yields of 56% and 65%, respectively.

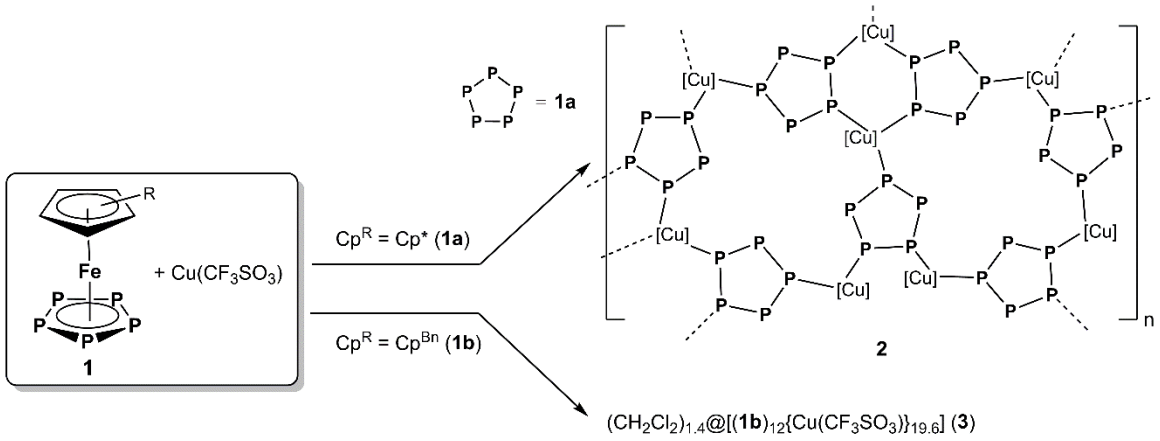

Scheme 13.1 Reaction of **1a** and **1b** with $Cu(CF_3SO_3)$, respectively.

The X-ray structural analysis of **2** reveals a two-dimensional network with the P_5 ligands of **1a** in a 1,2,4-coordination mode to copper, which displays a known structural motif in pentaphosphaferrocene containing polymers.[9c,e] Thereby, six-membered $\{Cu_2P_4\}$ rings and also distorted 16-membered $\{Cu_4P_{12}\}$ rings resembling a porphyrin-like structure are formed (*Figure 13.3*a). The triflate anion acts as a terminal ligand with one oxygen coordinated to copper and therefore completing the preferred tetrahedral environment of the metal center (3 x P, 1 x O). This geometry is also responsible for the distortion of the Cu-containing rings, hence the 2D network consists of corrugated layers with the triflate and pentaphosphaferrocene units orientated upwards and downwards alternatively (*Figure 13.3*b).

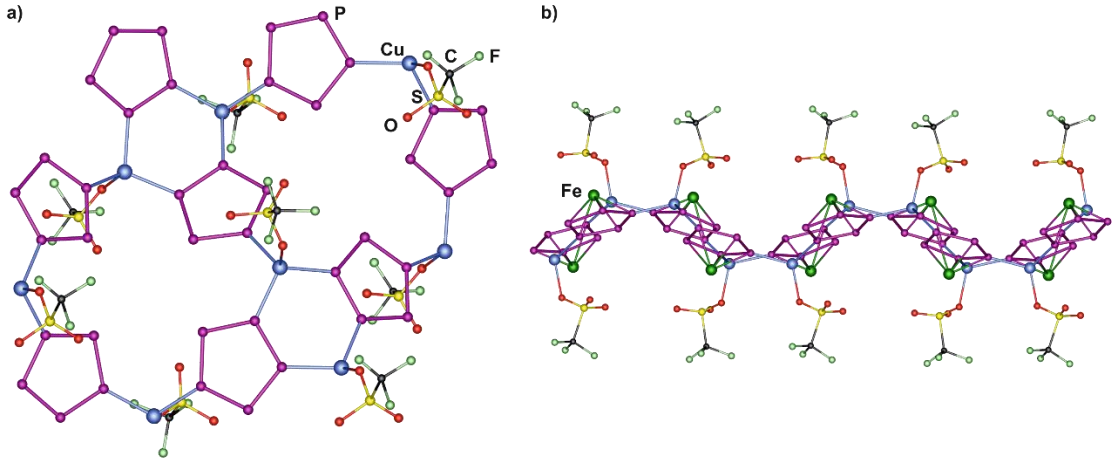

Figure 13.3 Section of the polymeric structure of **2**: a) top view and b) side view of a layer.

Compound **3** crystallizes in the monoclinic space group *C*2/*c* with giant unit cell parameters of 45.771(1) Å, 31.615(1) Å, 91.429(1) Å and β = 98.008(1)°. Its X-ray structural analysis reveals an unprecedented spherical supramolecule. The idealized 90-vertex scaffold of **3** is constructed by 12 moieties of **1b**, which are coordinated to 30 copper positions *via* all their phosphorus atoms in a 1,2,3,4,5-coordination mode. In turn, the Cu atoms in **3** link two P_5 rings forming nine-membered Cu_3P_6 rings (*Figure 13.4*a-c).

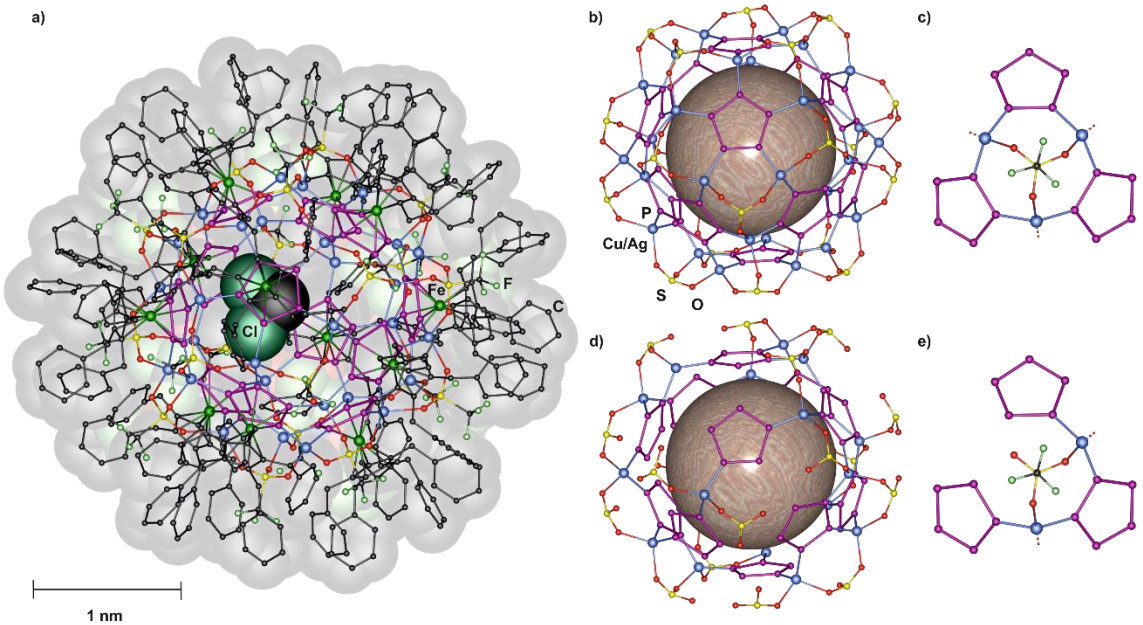

Figure 13.4 Molecular idealized structure of **3** in the crystal. H atoms, solvents and minor parts of disorder are omitted for clarity. Only one position of a CH_2Cl_2 molecule is shown in the space-filling model; b) idealized $Cu_{30}P_{60}$ scaffold of **3**; c) connective pattern in the idealized scaffold of **3**; d) one possible isomer of **3** with Cu vacancies; e) one possible connectivity in the reduced scaffold of **3**.

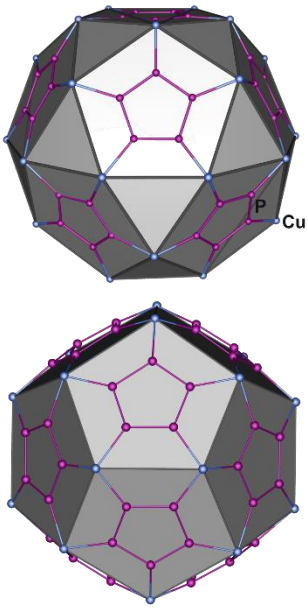

Figure 13.5 Icosidodecahedron of **3** (top) and dodecahedron of 80-vertex balls (bottom)

This structural motif differentiates **3** from other pentaphosphaferrocene-based supramolecules, in which a copper atom connects three P_5 ligands and $\{Cu_2P_4\}$ hexagons are formed. Since in **3** no six-membered rings are found, it does not show fullerene topology in the narrow sense despite the presence of 12 P_5 rings. As a further consequence, in the idealized framework of **3** no dodecahedron as in the halide containing 80-vertex spheres is formed. The copper atoms rather build up an icosidodecahedron consisting of twelve pentagonal and twenty triangular faces (*Figure 13.5*).

The 20 triflate anions cap these $\{Cu_3P_6\}$ rings in a μ_3 fashion *via* coordination of all oxygen atoms to Cu. To reach a tetrahedral environment, every Cu atom is bound to two CF_3SO_3 ligands (*Figure 13.4*c).

However, according to the diffraction data all 30 Cu and two triflate positions in **3** show site occupancy factors < 1 and therefore the scaffold is partly vacant. The idealized $\{Cu_{30}(CF_3SO_3)_{20}\}$ scaffold is thus reduced to its ordered part comprising of 19.6 copper and 19.6 triflate moieties. This is also in agreement with the required charge balance. The porosity of **3** also entails the reduction of the number of coordinated phosphorus atoms from five in the idealized scaffold to four, three or even only two in the observed supramolecule (*Figure 13.4*d,e). Also one or two oxygen atoms of the triflate ligands remain uncoordinated when situated next to a copper vacancy. Therefore, the crystal of **3** represents a solid solution of different supramolecules with an average sum formula of $[(\mathbf{1b})_{12}\{Cu(CF_3SO_3)\}_{19.6}]$. The number of possible isomers cannot be derived accurately, since different compositions are conceivable. For example, it can be treated as a mixture of $[(\mathbf{1b})_{12}\{Cu(CF_3SO_3)\}_{20}]$ (**3a**, 80 vertices) and $[(\mathbf{1b})_{12}\{Cu(CF_3SO_3)\}_{19}]$ (**3b**, 79 vertices) with contributions of 60% and 40%, respectively. However, also the more porous sphere $[(\mathbf{1b})_{12}\{Cu(CF_3SO_3)\}_{18}]$ (**3c**, 78 vertices) might be present, and **3** represents a solid solution of 80% of **3a** and 20% of **3c** or a mixture of 70% of **3a**, 20% of **3b** and 10% of **3a**. This series can be continued for spheres of even higher porosities. One can think of far more examples and isomers taking into account also the statistical distribution of the 30 copper positions. The phenomenon of porosity and the crystallization of solid solutions of different supramolecules has recently also been found in other pentaphosphaferrocene-based spheres.[10b,c]

Since the Cp^{Bn} ligands in **3** are all pointing outwards, the whole assembly reaches an outer diameter of 3.3 nm. Compound **3** is therefore 0.2 nm larger than the 80-vertex fullerene-analogue

[(**1b**)$_{12}$(CuX)$_{20-n}$] (X = Cl, Br; n < 7) and exceeds the Cp* derivatives [(**1a**)$_{12}$(CuX)$_{20-n}$] (X = Cl, Br, I) by approximately 1.2 nm in size.[10] For a more vivid comparison, the volume of the ball roughly amounts to 18.8 nm^3, which is 36 times larger than the Buckminster fullerene C_{60} (V = 0.52 nm^3).

Furthermore, **3** provides a spherical cavity with an inner diameter of 1.0 nm, which is 0.2 nm larger than the CuX-derived (X = Cl, Br) 80-vertex balls. This void is filled with one or two severely disordered dichloromethane molecules.

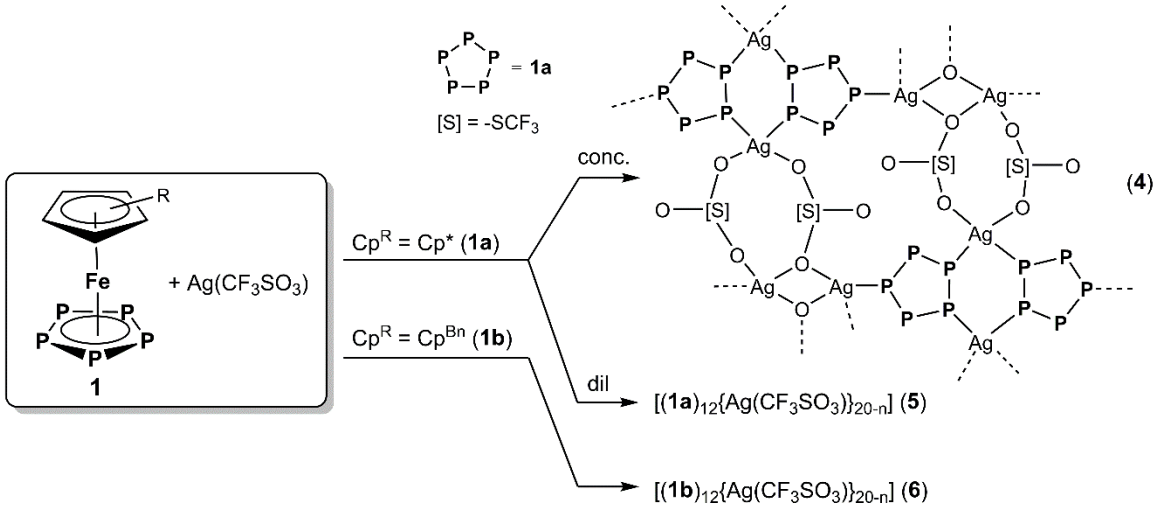

Scheme 13.2 Reaction of **1a** and **1b** with Ag(CF_3SO_3), respectively.

The synthesis of **3** demonstrates that the formation of pentaphosphaferrocene-based supramolecules is not any more restricted to halide ligands and can rather be extended also to the triflate anion in the combination with **1b**.[12] Since attempts for the synthesis of an silver-containing sphere by using Ag(I) halides failed so far, the self-assembly of **1a** and **1b** with Ag(CF_3SO_3) was investigated.

For this purpose, a solution of Ag(CF_3SO_3) in CH_2Cl_2 is carefully layered with a solution of **1a** and **1b** in toluene, respectively. Thereby, with **1a** the phase boundary turns yellow and small yellow plates of the 2D polymer [{Cp*Fe(μ_3,$\eta^{5:1:1:1}$-P_5)}{Ag(CF_3SO_3)}$_2$]$_n$ (**4**) start to grow during the diffusion process. However, when the same reaction is carried out in more diluted solutions, the crystallization of brown prisms of the supramolecule [Cp*Fe(η^5-P_5)]@[{Cp*Fe(η^5-P_5)}$_{12}$ {Ag(CF_3SO_3)}$_{20-n}$] (**5**) is observed, occassionally accompanied by the crystallization of **4**. On the other hand, the layering experiment of **1b** with Ag(CF_3SO_3) gratifyingly always leads to the formation of red blocks of the discrete sphere [{Cp^{Bn}Fe(η^5-P_5)}$_{12}$ {Ag(CF_3SO_3)}$_{20-n}$] (**6**). All three compounds can be obtained in reasonable to excellent yields of 94% for **4**, 45% for **5** and 49% for **6**.

Compound **4** crystallizes in the monoclinic space group $P2_1/c$ and the X-ray structural analysis reveals a two-dimensional network (*Figure 13.6*a). Similarly to **2**, the P_5 ligands show a 1,2,4-

coordination mode to silver atoms, which in turn possess a tetrahedral environment (2 x O, 2 x P or 3 x O, 1 x P). Despite these common features the structural motif of **4** differs from that of **2**, primarily because of the coordination mode of the triflate anions. These act as μ_2 or even μ_3 bridging ligands *via* coordination of two oxygen atoms to silver, whereas they are terminal in **2**. Thereby, four-membered $\{Ag_2O_2\}$, six-membered $\{Ag_2P_4\}$ and eight membered $\{Ag_2O_4S_2\}$ rings are formed within the network. Noteworthy, between the 2D layers toluene molecules are intercalated explaining the rapid decomposition of crystals of **4** when removed from the mother liquor. The parallel arrangement of toluene and the *cyclo*-P_5 ligands as well as short phosphorus carbon distances (3.58 Å to 3.62 Å) indicate π-stacking interactions (*Figure 13.6*b).[13]

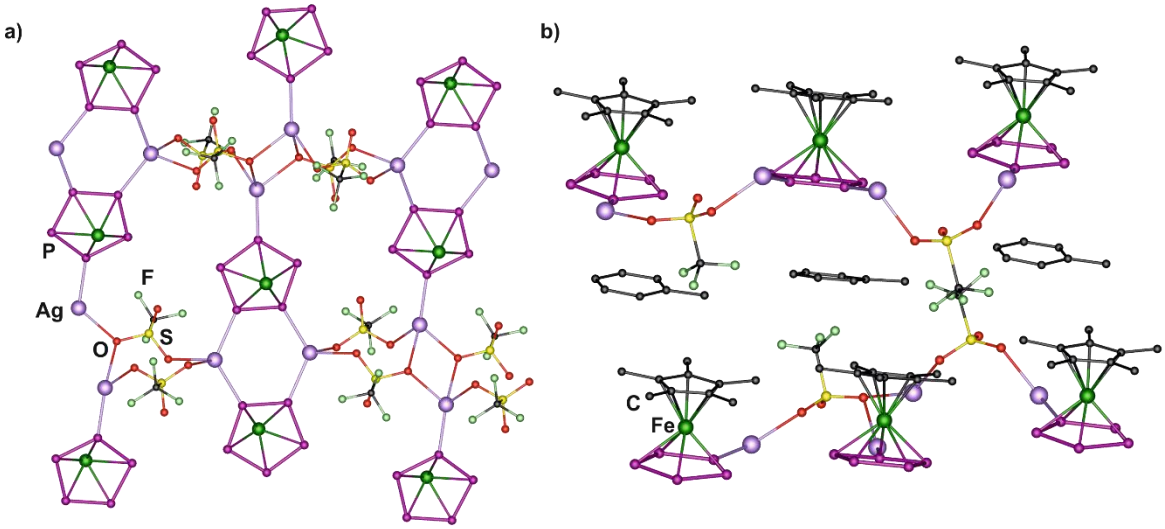

Figure 13.6 a) Section of the polymeric network of **4**. Cp* ligands and solvent molecules are omitted for clarity; b) illustration of the π-π-interaction between intercalated toluene molecules and the *cyclo*-P_5 ligands. H atoms are omitted for clarity.

Compound **5** crystallizes in the triclinic space group $P\bar{1}$, whereas **6** is isostructural to **3**. The X-ray structural analyses of **5** and **6** both reveal giant supramolecules of the same framework like in **3**. Hence, **5** and **6** display the silver derivatives of compound **3** and thus are the first representatives of a pentaphosphaferrocene-based supramolecule containing silver(I). In all previously reported spheres the *cyclo*-P_5 ligands are linked by copper(I). Furthermore, **5** displays the first triflate containing supramolecule with **1a** as building block (*Figure 13.7*). Both **5** and **6** show the same idealized scaffold with 30 positions of silver constructing an icosidodecahedron and the Ag_3P_6 rings capped by the CF_3SO_3 ligands. As in **3**, in terms of the diffraction data and the required charge balance the Ag positions are not fully occupied leading to the reduced sum formula of $[(\mathbf{1})_{12}\{Ag(CF_3SO_3)\}_{20-n}]$. Since only preliminary data for **5** and **6** can be given within this work and the exact value of n can only be determined at the very end of the refinement process of the crystal structure, the amount of n cannot be stated at this point. Yet it will very likely be in a similar range

than other supramolecules (0 < n < 4.7). Due to the ensured presence of silver vacancies, also the crystals of **5** and **6** represent solid solutions of different isomers of the supramolecule.

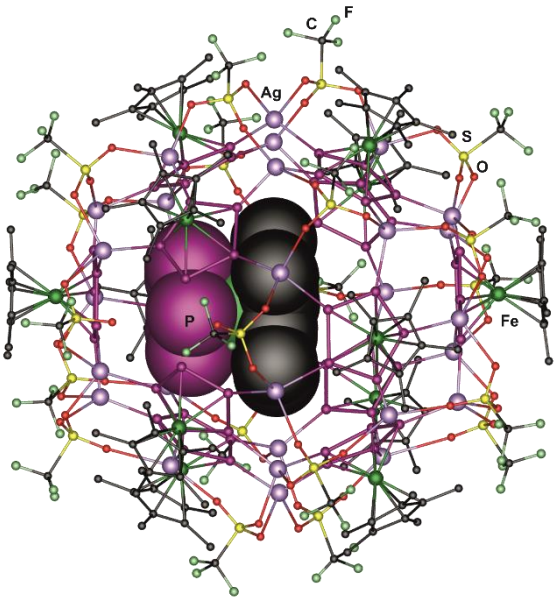

Figure 13.7 Molecular idealized structure of **5** in the crystal. H atoms, solvents, vacancies and minor parts of disorder are omitted for clarity, the guest molecule is shown in the space-filling model.

The provided cavity with an inner diameter of 1.0 nm is most likely filled with CH_2Cl_2 solvent molecules in **6**, as it has been observed for **3**. On the contrary in **5**, one molecule of **1a** is encapsulated. This is enabled by the smaller size of **1a** (length: 0.7 nm), whereas the benzyl ligands of **1b** (length: 1.2 nm) impede its inclusion in **3** and **6**, respectively. Noteworthy, the enclosed **1b** moiety is shifted from the center of the cavity allowing π-stacking interactions of the *cyclo*-P_5 ligands of the guest and host molecule, respectively (*Figure 13.7*). This resembles the encapsulation of **1a** in a 90-vertex supramolecule based on copper halides.[14]

Since **1a** is 0.5 nm smaller in length than **1b**, accordingly the supramolecule **6** reaches an outer diameter of 2.3 nm, whereas it is 3.3 nm in **6**.

All compounds containing **1a** (**2**, **4**, **5**) are insoluble in common solvents such as hexane, toluene, CH_2Cl_2, thf and Et_2O. Only in CH_3CN they are poorly soluble, though accompanied by partial fragmentation of the coordination network. Therefore in the $^{31}P\{^1H\}$ NMR spectra and ^1H NMR spectra of **2** and **5** in CD_3CN, respectively, the only signals present can be assigned to the free complex **1a**. However, mass spectrometric investigations reveal the presence of at least oligomeric moieties. For example, in the respective cationic ESI MS spectra of **2** and **5** in CH_3CN numerous peaks of fragments containing pentaphosphaferrocene units are observed. Thereby, the largest peak in the spectrum of **5** at *m/z* = 2946.0 can be assigned to $[\{Cp^*Fe(\eta^5\text{-}P_5)\}_3Ag_8(CF_3SO_3)_7]^+$, whereas in the case of copper the largest peak is found for $[\{Cp^*Fe(\eta^5\text{-}P_5)\}_4Cu_9(CF_3SO_3)_8]^+$ at *m/z* = 3148.2.

The benzyl ligands of **1b** increase the solubility of supramolecular compounds remarkably. Therefore, **3** shows a low solubility in toluene and a moderate solubility in CH_2Cl_2, whereas the Ag-derivative **6** is even well soluble in CH_2Cl_2, thf and toluene. Nonetheless, fragmentation is observed again when dissolved in CH_3CN.

As expected, in the ^{1}H NMR spectra of the isostructural compounds **3** and **6** in CD_2Cl_2, respectively, a set of four broad signals corresponding to the methylene as well as the aromatic protons (*o*-CH, *m*-CH and *p*-CH) for the Cp^{Bn} ligand is observed (**3**: δ = 4.48, 6.23, 6.67, 6.93 ppm; **5**: δ = 4.21, 6.34, 6.75, 6.93 ppm). In addition, the triflate ligand can be detected in the $^{19}F\{^{1}H\}$ NMR spectrum exhibiting one broad singlet at δ = -76.7 ppm for **3** and at δ = -77.6 for **6**, respectively. Unfortunately, in the $^{31}P\{^{1}H\}$ NMR spectrum of **3** no signal appears, which can most likely be attributed to the only moderate solubility of **3** in CD_2Cl_2. Gratifyingly, the enhanced solubility of **6** allows the detection of broad signals at δ = -62, 65, 134 ppm as well as a sharp singlet at δ = 159.8 ppm in the corresponding $^{31}P\{^{1}H\}$ NMR spectrum. This is reminiscent of the obtained spectra of the copper halide derivatives $[(\mathbf{1b})_{12}(CuX)_{20-n}]$ (X = Cl, Br; n ≤ 4.6),[10b] though the signals of **6** are distributed over a wider range. A comprehensive NMR study concerning these fullerene derivatives revealed that the broad signals can be attributed to supramolecules of different porosities. Therefore, the broad signals in the $^{31}P\{^{1}H\}$ NMR spectrum of **6** might be assigned in an analogous manner to spheres with a different Ag content. However, the singlet at δ = 159.8 ppm corresponds to the free complex **1b**. Therefore also a dissociation of moieties of **1** might take place in solution.

In the cationic ESI MS spectra of **3** and **6** numerous peaks attributed to fragments containing pentaphosphaferrocene, the coinage metal and triflate are detected. The largest peak in the spectrum of **3** at *m/z* = 2879.4 can be assigned to $[\{Cp^{Bn}Fe(\eta^5\text{-}P_5)\}_3Cu_4(CF_3SO_3)_3]^+$, whereas the spectrum of **6** reveals the largest peak at *m/z* = 2331.6 attributed to the species $[\{Cp^{Bn}Fe(\eta^5\text{-}P_5)\}_2Ag_4(CF_3SO_3)_3]^+$.

In summary, we have shown that the formation of pentaphosphaferrocene-derived supramolecules is not restricted to copper halides any more, but also feasible using the triflate salts $M(CF_3SO_3)^-$ (M = Cu, Ag). Thereby, three nano-sized spheres can be isolated: $(CH_2Cl_2)_{1.4}@[\{Cp^{Bn}Fe(\eta^5\text{-}P_5)\}_{12}\{Cu(CF_3SO_3)\}_{19.6}]$ (**3**); $[Cp^*Fe(\eta^5\text{-}P_5)]@[\{Cp^*Fe(\eta^5\text{-}P_5)\}_{12}\{Ag(CF_3SO_3)\}_{20-n}]$ (**5**) and $[\{Cp^{Bn}Fe(\eta^5\text{-}P_5)\}_{12}\{Ag(CF_3SO_3)\}_{20-n}]$ (**6**), of which **5** and **6** display the first silver-containing spheres of phosphaferrocenes. All three supramolecules exhibit an identical unprecedented scaffold of 12 moieties of pentaphosphaferrocene and 20-n $M(CF_3SO_3)^-$ units forming an icosidodecahedron. Furthermore, in the host molecule of **5** one molecule of **1a** is encapsulated. Hence, this system might also be capable of further template-directed syntheses, which will be investigated in future. In addition, the combination of **1a** and $Cu(CF_3SO_3)$ as well as concentrated solutions of **1a** and $Ag(CF_3SO_3)$, respectively, reveal two novel 2D coordination polymers: $[\{Cp^*Fe(\mu_4,\eta^{5:1:1:1}\text{-}P_5)\}\{Cu(CF_3SO_3)\}]_n$ (**2**) and $[\{Cp^*Fe(\mu_3,\eta^{5:1:1:1}\text{-}P_5)\}\{Ag(CF_3SO_3)\}_2]_n$ (**4**) with different topologies and π-stacking interactions in **4**.

13.4 Experimental Part

General Remarks:

All reactions were performed under an inert atmosphere of dry nitrogen or argon with standard vacuum, Schlenk and glove-box techniques. Solvents were purified, dried and degassed prior to use by standard procedures. $[Cp^{Bn}Fe(\eta^5\text{-}P_5)]$[15] and $[Cp^*Fe(\eta^5\text{-}P_5)]$[16] were synthesized following reported procedures. Commercially available chemicals ($Cu(CF_3SO_3)\cdot 0.5C_7H_8$, $Ag(CF_3SO_3)$) were used without further purification. Solution NMR spectra were recorded on a Bruker Avance 300 or 400 spectrometer. The corresponding ESI-MS spectra were acquired on a ThermoQuest Finnigan MAT TSQ 7000 mass spectrometer, whereas EI-MS spectra were measured on a Finnigan MAT 95 mass spectrometer. Elemental analyses were performed on a Vario EL III apparatus.

Synthesis of $[\{Cp^*Fe(\mu_4,\eta^{5:1:1:1}\text{-}P_5)\}\{Cu(CF_3SO_3)\}]_n$ (2)

In a Schlenk tube a solution of $Cu(CF_3SO_3)\cdot 0.5C_7H_8$ (30 mg, 0.116 mmol) in CH_2Cl_2 (15 mL) is carefully layered with a green solution of $[Cp^*Fe(\eta^5\text{-}P_5)]$ (20 mg, 0.058 mmol) in a solvent mixture of hexane (10 mL) and toluene (5 mL). Thereby, the phase boundary turns yellow. After a few days the formation of small yellow crystals of **2** below the phase boundary can be observed. After complete diffusion the mother liquor is decanted, the crystals are washed with hexane (3 x 10 mL) and dried *in vacuo*.

Analytical data of **2**:

Yield: 18 mg (0.032 mmol, 56% referred to $[Cp^*Fe(\eta^5\text{-}P_5)]$)

^{1}H NMR (CD_3CN): δ [ppm] = 1.44 (s, $[Cp^*Fe(\eta^5\text{-}P_5)]$), 1.95 (s, CH_3CN)

$^{31}P\{^1H\}$ NMR (CD_3CN): δ [ppm] = 146.25 (s, $[Cp^*Fe(\eta^5\text{-}P_5)]$).

Positive ion ESI-MS (CH_2Cl_2/CH_3CN): *m/z* (%) = 3148.2 $[\{Cp^*Fe(\eta^5\text{-}P_5)\}_4Cu_9(CF_3SO_3)_8]^+$, 2937.4 $[\{Cp^*Fe(\eta^5\text{-}P_5)\}_4Cu_8(CF_3SO_3)_7]^+$, 2723.0 $[\{Cp^*Fe(\eta^5\text{-}P_5)\}_4Cu_7(CF_3SO_3)_6]^+$, 2376.9 $[\{Cp^*Fe(\eta^5\text{-}P_5)\}_3Cu_7(CF_3SO_3)_6]^+$, 2164.8 $[\{Cp^*Fe(\eta^5\text{-}P_5)\}_3Cu_6(CF_3SO_3)_5]^+$, 1950.9 $[\{Cp^*Fe(\eta^5\text{-}P_5)\}_3Cu_5(CF_3SO_3)_4]^+$, 1604.5 $[\{Cp^*Fe(\eta^5\text{-}P_5)\}_2Cu_5(CF_3SO_3)_4]^+$, 1392.7 $[\{Cp^*Fe(\eta^5\text{-}P_5)\}_2Cu_4(CF_3SO_3)_3]^+$, 1180.7 $[\{Cp^*Fe(\eta^5\text{-}P_5)\}_2Cu_3(CF_3SO_3)_2]^+$, 966.8 $[\{Cp^*Fe(\eta^5\text{-}P_5)\}_2Cu_2(CF_3SO_3)]^+$, 754.9 (12) $[\{Cp^*Fe(\eta^5\text{-}P_5)\}_2Cu]^+$, 449.8 (100) $[\{Cp^*Fe(\eta^5\text{-}P_5)\}Cu(CH_3CN)]^+$, 408.8 $[\{Cp^*Fe(\eta^5\text{-}P_5)\}Cu]^+$

Negative ion ESI-MS (CH_2Cl_2/CH_3CN): *m/z* (%) = 360.6 (100) $[Cu(CF_3SO_3)_2]^-$, 148.8 (39) $[CF_3SO_3]^-$

Elemental analysis: Calculated (%) for $[\{Cp^*Fe(\eta^5\text{-}P_5)\}Cu(CF_3SO_3)(CH_2Cl_2)]$ (643 g/mol): C 22.40, H 2.66, S 4.98; found: C 21.89, H 2.34, S 4.94.

Synthesis of $[\{Cp^{Bn}Fe(\eta^5\text{-}P_5)\}_{12}\{Cu(CF_3SO_3)\}_{19.6}]$ (3)

[$Cp^{Bn}Fe(\eta^5\text{-}P_5)$] (40 mg, 0.055 mmol) and $Cu(CF_3SO_3)\cdot 0.5C_7H_8$ (43 mg, 0.166 mmol) are dissolved in CH_2Cl_2 (22 mL) to give a yellowish brown solution that gets turbid after 10 minutes. This solution is stirred for 2 hours, then filtered into a Schlenk tube and carefully layered with toluene (15 mL). After several days the formation of small crystals of **3** can be observed at the phase boundary. After complete diffusion, the mother liquor is decanted, the crystals are washed with hexane (3 x 10 mL) and dried *in vacuo*. By concentrating the mother liquor, a second crop of crystals can be obtained.

Analytical data of **3**:

Yield: 38 mg (0.003 mmol, 65% referred to [$Cp^{Bn}Fe(\eta^5\text{-}P_5)$])

^{1}H NMR (CD_2Cl_2): δ [ppm] = 4.48 (m, br, 120H, CH_2), 6.23 (m, br, 120H, *ortho*-CH), 6.67 (m, br, 120H, *meta*-CH), 6.93 (m, br, 60H, *para*-CH).

^{19}F{^{1}H} NMR (CD_2Cl_2): δ [ppm] = -76.7 (s, br, $(CF_3SO_3)^-$).

Positive ion ESI-MS (CH_2Cl_2/CH_3CN): *m/z* (%) = 2879.4 $[\{Cp^{Bn}Fe(\eta^5\text{-}P_5)\}_3Cu_4(CF_3SO_3)_3]^+$, 2792.6 $[\{Cp^{Bn}Fe(\eta^5\text{-}P_5)\}_2Cu_7(CF_3SO_3)_6]^+$, 2669.5 $[\{Cp^{Bn}Fe(\eta^5\text{-}P_5)\}_3Cu_3(CF_3SO_3)_2]^+$, 2579.1 $[\{Cp^{Bn}Fe(\eta^5\text{-}P_5)\}_2Cu_6(CF_3SO_3)_5]^+$, 2454.6 $[\{Cp^{Bn}Fe(\eta^5\text{-}P_5)\}_3Cu_2(CF_3SO_3)]^+$, 2366.9 $[\{Cp^{Bn}Fe(\eta^5\text{-}P_5)\}_2Cu_5(CF_3SO_3)_4]^+$, 2153.1 $[\{Cp^{Bn}Fe(\eta^5\text{-}P_5)\}_2Cu_4(CF_3SO_3)_3]^+$, 1941.1 $[\{Cp^{Bn}Fe(\eta^5\text{-}P_5)\}_2Cu_3(CF_3SO_3)_2]^+$, 1728.7 $[\{Cp^{Bn}Fe(\eta^5\text{-}P_5)\}_2Cu_2(CF_3SO_3)]^+$, 1515.4 $[\{Cp^{Bn}Fe(\eta^5\text{-}P_5)\}_2Cu]^+$, 1002.9 (20) $[\{Cp^{Bn}Fe(\eta^5\text{-}P_5)\}Cu_2(CF_3SO_3)]^+$, 830.1 (73) $[\{Cp^{Bn}Fe(\eta^5\text{-}P_5)\}Cu(CH_3CN)]^+$, 789.0 (100) $[\{Cp^{Bn}Fe(\eta^5\text{-}P_5)\}Cu]^+$.

Negative ion ESI-MS (CH_2Cl_2/CH_3CN): *m/z* (%) = 572.6 (3) $[Cu_2(CF_3SO_3)_3]^-$, 360.7 (100) $[Cu(CF_3SO_3)_2]^-$, 148.8 (12) $[CF_3SO_3]^-$.

Elemental analysis: Calculated (%) for $[\{Cp^{Bn}Fe(\eta^5\text{-}P_5)\}_{12}\{Cu(CF_3SO_3)\}_{20}(CH_2Cl_2)_7]$ (13564 g/mol): C 44.89, H 3.23, S 4.73; found: C 44.82, H 3.45, S 4.71.

Synthesis of $[\{Cp^*Fe(\mu_3,\eta^{5:1:1:1}\text{-}P_5)\}\{Ag(CF_3SO_3)\}_2]_n$ (4)

In a Schlenk tube a solution of $Ag(CF_3SO_3)$ (114 mg, 0.44 mmol) in CH_2Cl_2 (10 mL) is carefully layered with a green solution of [$Cp^*Fe(\eta^5\text{-}P_5)$] (55 mg, 0.16 mmol) in toluene (11 mL). Thereby, the phase boundary turns yellow. During the diffusion process the formation of small yellow plates of **4** below the phase boundary can be observed. After complete diffusion the mother liquor is decanted, the crystals are washed with hexane (3 x 10 mL) and dried *in vacuo*.

Analytical data of **4**:

Yield: 125 mg (0.15 mmol, 94% referred to [$Cp^*Fe(\eta^5\text{-}P_5)$])

Positive ion ESI-MS (CH_3CN): *m/z* (%) = 798.9 (38) $[\{Cp^*Fe(\eta^5\text{-}P_5)\}_2Ag]^+$, 493.9 (100) $[\{Cp^*Fe(\eta^5\text{-}P_5)\}Ag(CH_3CN)]^+$

Negative ion ESI-MS (CH_3CN): *m/z* (%) = 404.7 (6) $[Ag(CF_3SO_3)_2]^-$, 148.7 (100) $[CF_3SO_3]^-$

Elemental analysis: Calculated (%) for [{Cp*Fe(η^5-P_5)}{Ag(CF_3SO_3)}$_2$] (860 g/mol): C 16.76, H 1.76, S 7.46; found: C 15.81, H 2.29, S 6.76.

Synthesis of [Cp*Fe(η^5-P_5)]@[{Cp*Fe(η^5-P_5)}$_{12}${Ag(CF_3SO_3)}$_{20-n}$] (5)

In a thin Schlenk tube a solution of Ag(CF_3SO_3) (32 mg, 0.125 mmol) in CH_2Cl_2 (12 mL) is carefully layered with a green solution of [Cp*Fe(η^5-P_5)] (15 mg, 0.043 mmol) in toluene (12 mL). Thereby the phase boundary turns yellow. During the diffusion process the formation of greenish brown rods of **5** can be observed, though sometimes accompanied by the crystallization of a minor amount of **4**. After complete diffusion the mother liquor is decanted, the crystals are washed with hexane (3 x 5 mL) and dried *in vacuo*.

Analytical data of **5**:

Yield: 15 mg (1.6 µmol, 45% referred to [Cp*Fe(η^5-P_5)])

^{1}H NMR (CD_3CN): δ [ppm] = 1.46 (s, [Cp*Fe(η^5-P_5)]).

^{31}P{^{1}H} NMR (CD_3CN): δ [ppm] = 135.00 (s, [Cp*Fe(η^5-P_5)]).

^{19}F{^{1}H} NMR (CD_3CN): δ [ppm] = -77.8 (s, br, $(CF_3SO_3)^-$).

Positive ion ESI-MS (CH_3CN): *m/z* (%) = 2946.0 [{Cp*Fe(η^5-P_5)}$_3$Ag$_8$(CF_3SO_3)$_7$]$^+$, 2686.1 [{Cp*Fe(η^5-P_5)}$_3$Ag$_7$(CF_3SO_3)$_6$]$^+$, 2430.2 [{Cp*Fe(η^5-P_5)}$_3$Ag$_6$(CF_3SO_3)$_5$]$^+$, 2172.2 [{Cp*Fe(η^5-P_5)}$_3$Ag$_5$(CF_3SO_3)$_4$]$^+$, 2172.6 [{Cp*Fe(η^5-P_5)}$_3$Ag$_5$(CF_3SO_3)$_4$]$^+$, 2084.3 [{Cp*Fe(η^5-P_5)}$_2$Ag$_6$(CF_3SO_3)$_5$]$^+$, 1916.6 [{Cp*Fe(η^5-P_5)}$_3$Ag$_4$(CF_3SO_3)$_3$]$^+$, 1826.6 [{Cp*Fe(η^5-P_5)}$_2$Ag$_5$(CF_3SO_3)$_4$]$^+$, 1660.7 [{Cp*Fe(η^5-P_5)}$_3$Ag$_3$(CF_3SO_3)$_2$]$^+$, 1570.5 [{Cp*Fe(η^5-P_5)}$_2$Ag$_4$(CF_3SO_3)$_3$]$^+$, 1312.7 [{Cp*Fe(η^5-P_5)}$_2$Ag$_3$(CF_3SO_3)$_2$]$^+$, 1056.6 (1) [{Cp*Fe(η^5-P_5)}$_2$Ag$_2$(CF_3SO_3)]$^+$, 798.8 (22) [{Cp*Fe(η^5-P_5)}$_2$Ag]$^+$, 493.8 (100) [{Cp*Fe(η^5-P_5)}Ag(CH_3CN)]$^+$, 452.8 (12) [{Cp*Fe(η^5-P_5)}Ag]$^+$.

Negative ion ESI-MS (CH_3CN): *m/z* (%) = 406.7 (16) [Ag(CF_3SO_3)$_2$]$^-$, 360.7 (46) [Cu(CF_3SO_3)$_2$]$^-$, 148.8 (70) [CF_3SO_3]$^-$.

Elemental analysis: Calculated (%) for [{Cp*Fe(η^5-P_5)}$_{12}${Ag(CF_3SO_3)}$_{20}$] (9290 g/mol): C 18.10, H 1.95, S 6.90; found: C 17.69, H 2.76, S 6.35.

Synthesis of [{Cp^{Bn}Fe(η^5-P_5)}$_{12}${Ag(CF_3SO_3)}$_{20-n}$] (6)

A solution of $AgCF_3SO_3$ (14 mg, 0,055 mmol) in CH_2Cl_2 (8 mL) is carefully layered with a green solution of [Cp^{Bn}Fe(η^5-P_5)] (20 mg, 0.028 mmol) in toluene (8 mL). After complete diffusion the brownish solution is layered with hexane. A few hours later, the growth of deep red crystals of **6** can be observed at the phase boundary. After complete diffusion the mother liquor is decanted, the crystals are washed with hexane (3 x 5 mL) and dried *in vacuo*.

Analytical data of **6**:

Yield: 17 mg (1.1 µmol, 49% referred to [$Cp^{Bn}Fe(\eta^5\text{-}P_5)$])

^{1}H NMR (CD_2Cl_2): δ [ppm] = 4.21 (m, br, 120H, CH_2), 6.34 (m, br, 120H, *ortho*-CH), 6.75 (s, br, 120H, *meta*-CH), 6.93 (s, br, 60H, *para*-CH).

^{31}P{^{1}H} NMR (CD_2Cl_2): δ [ppm] = 160 (s, [$Cp^{Bn}Fe(\eta^5\text{-}P_5)$]), 134 (s, br), 65 (s, br), -62 (s, br)

^{19}F{^{1}H} NMR (CD_2Cl_2): δ [ppm] = -77.55 (s, br, $(CF_3SO_3)^-$).

Positive ion ESI-MS (CH_2Cl_2/CH_3CN): *m/z* (%) = 2331 (1) $[\{Cp^{Bn}Fe(\eta^5\text{-}P_5)\}_2Ag_4(CF_3SO_3)_3]^+$, 2075 (1) $[\{Cp^{Bn}Fe(\eta^5\text{-}P_5)\}_2Ag_3(CF_3SO_3)_2]^+$, 1817 (1) $[\{Cp^{Bn}Fe(\eta^5\text{-}P_5)\}_2Ag_2CF_3SO_3]^+$, 1561 (6) $[\{Cp^{Bn}Fe(\eta^5\text{-}P_5)\}_2Ag]^+$, 1347 (1) $[\{Cp^{Bn}Fe(\eta^5\text{-}P_5)\}Ag_2(CF_3SO_3)_2]^+$, 1091 (50) $[\{Cp^{Bn}Fe(\eta^5\text{-}P_5)\}Ag_2CF_3SO_3]^+$, 874 (32) $[\{Cp^{Bn}Fe(\eta^5\text{-}P_5)\}Ag(CH_3CN)]^+$, 833 (17) $[\{Cp^{Bn}Fe(\eta^5\text{-}P_5)\}Ag]^+$, 531 (100) $[Cp^{Bn}O]^+$.

Negative ion ESI-MS (CH_2Cl_2/CH_3CN): *m/z* (%) = 502 (21) $[Fe(CF_3SO_3)_3]^-$, 406 (13) $[Ag(CF_3SO_3)_2]^-$, 148 (100) $[CF_3SO_3]^-$.

Elemental analysis: Calculated (%) for $[\{Cp^{Bn}Fe(\eta^5\text{-}P_5)\}_{12}\{Ag(CF_3SO_3)\}_{20}(CH_2Cl_2)_{15}]$ (15130 g/mol): C 40.88, H 3.00, S 4.24; found: C 40.29, H 3.19., S 4.48.

13.5 Crystallographic Data

Crystals of **2-6** were taken from a Schlenk flask under a stream of argon and immediately covered with mineral oil or perfluorinated Fomblin® mineral oil to prevent both decomposition and a loss of solvent. The quickly chosen single crystals covered by a drop of the oil were taken to the pre-centered goniometer head with CryoMount® and directly attached to the diffractometer into a stream of cold nitrogen. The X-ray diffraction study of **2-6** faced many challenges, since the crystals have very small size and low diffraction power. The crystals of the polymers **2** and **6** proved to be multi-layered in agreement with their 2D structures. The collection of data at high theta angles required extremely high exposure times, and even that sometimes did not allow collection of the sufficient quality data (compounds **4** and **5**). Therefore, for crystal structures of **4** and **5** only a preliminary model can be reported.

The data for **2** were collected using 1° ω scans on an Agilent Technologies diffractometer equipped with Atlas CCD detector and a SuperNova CuK_α microfocus source. The data for **3, 4, 5** and **6** were collected on an Agilent Technologies diffractometer equipped with Titan^{S2} CCD detector and a SuperNova CuK_α microfocus source using 0.5°, 0.33°, 0.5° and 1° ω scans, respectively. All measurements were performed at 123 K. The structures were solved by direct methods with *SHELX97*.[17] The structures were refined by full-matrix least-squares method against $|F|^2$ in anisotropic approximation using multiprocessor and variable memory version *SHELXL2013*. All non-hydrogen atoms were refined anisotropically, while the hydrogen atoms were refined riding on pivot atoms.

In the crystal structure of **2** the nature and the disorder pattern of the solvent molecule is not yet clear. Therefore, preliminary data are reported.

In the crystal structure of **3** the partly vacant positions of heavy atoms were indicated by high displacement parameters. The occupancy factors were therefore refined at displacement parameters equated to the average displacement parameters for fully occupied heavy atoms in the structure. After the refinement, the occupancy factors were fixed at the resulted values and displacement parameters were refined in a usual way. The structure is featured by a disorder of the benzyl groups of the Cp^{Bn} ligands and solvent toluene molecules as well. The phenyl rings of the disordered species were sometimes refined in a rigid body approximation, and the molecular occupancy factors were a subject of the refinement. If the occupancy factors for these groups were less than 0.5, the groups were refined isotropically.

Table 13.1 Experimental details for compounds **2** (* = preliminary data)[18] and **3** (final data).

Crystal Data	2	3
Chemical formula	$C_{12.50}H_{22.50}Cl_{0.25}CuF_3FeO_3P_5S$*	$C_{533.29}H_{485.27}Cl_{3.88}Cu_{19.60}F_{58.80}Fe_{12}O_{59.30}P_{60}S_{19.60}$
M_r	592.97*	13499.44
Crystal system, space group	orthorhombic, *I*222	monoclinic, *C*2/*c*
Temperature (K)	123	123
a, *b*, *c* (Å)	12.3655(3), 12.9713(3), 26.4575(7)	45.7712(7), 31.6154(6), 91.4285(12)
α, β, γ (°)	90, 90, 90	90, 98.008(1), 90
V (Å^3)	4243.69(18)	131014(4)
Z	8	8
F(000)	> 2390	54788
Radiation type	Cu K_α	Cu K_α
μ (mm^{-1})	> 11.66	5.37
Crystal color and shape	yellow plate	brown prism
Crystal size (mm)	0.09 × 0.08 × 0.01	0.15 × 0.10 × 0.05
Data collection		
Diffractometer	SuperNova, Atlas diffractometer	SuperNova, Titan^{S2} diffractometer
Absorption correction	gaussian	gaussian
T_{min}, T_{max}	0.525, 0.864	0.577, 0.775
No. of measured, independent and observed [$I > 2\sigma(I)$] reflections	8162, 4085, 3785	142481, 92366, 39030
R_{int}	0.0309	0.060
$(\sin\theta/\lambda)_{max}$ (Å^{-1})		0.556
Range of h, k, l	*h* = -15→12, *k* = -16→12, *l* = -32→32	*h* = -49→50, *k* = -35→19, *l* = -101→98

Refinement	*	
$R[F^2 > 2\sigma(F^2)]$, $wR(F^2)$, S	0.0294, 0.0769, 0.976	0.103, 0.307, 1.02
No. of reflections	4085	92366
No. of parameters	244	6937
No. of restraints	0	39
H-atom treatment	H-atom parameters constrained	H-atom parameters constrained
Flack parameter	-0.009(4)	-
$\Delta\rangle_{max}$, $\Delta\rangle_{min}$ (e Å^{-3})	0.949, -0.455	1.03, -0.57

Table 13.2 Experimental details for compounds **4** (final data) and **5** (* = preliminary data).[18]

Crystal Data	**4**	**5**
Chemical formula	$C_{12}H_{15}Ag_2F_6FeO_6P_5S_2 \cdot C_7H_8$	$C_{187.66}H_{180}Ag_{18.68}Cl_{2.17}F_{57.47}Fe_{13.04}N_{1.50}O_{57.7}P_{65.17}S_{19.47}$*
M_r	951.97	> 9900*
Crystal system, space group	monoclinic, $P2_1/c$	triclinic, $P\bar{1}$
Temperature (K)	123	123
a, b, c (Å)	11.0744(2), 18.3563(4), 15.3723(3)	26.7610(3), 37.4100(4), 46.1376(3)
α, β, γ (°)	90, 97.712(2), 90	84.2426(7), 82.8411(7), 87.1584(9)
V (Å^3)	3096.68(12)	45566.4(8)
Z	4	4
F(000)	1864	> 19623.0
Radiation type	Cu K_α	Cu K_α
μ (mm^{-1})	18.12	> 12.84
Crystal color and shape	yellow plate	greenish-brown block
Crystal size (mm)	0.24 × 0.16 × 0.01	0.58 × 0.27 × 0.21
Data collection		
Diffractometer	SuperNova, Titan^{S2} diffractometer	SuperNova, Titan^{S2} diffractometer
Absorption correction	gaussian	gaussian
T_{min}, T_{max}	0.045, 0.447	0.052, 0.212
No. of measured, independent and observed [$I > 2\sigma(I)$] reflections	10748, 6012, 4541	300045, 176494, 107377
R_{int}	0.0637	0.117
Range of h, k, l	h = -11→13, k = -21→14, l = -18→18	h = -32→33, k = -46→46, l = -56→57
Refinement		*
$R[F^2 > 2\sigma(F^2)]$, $wR(F^2)$, S	0.0632, 0.166, 0.977	0.1387, 0.3482, 1.889
No. of reflections	6012	176494
No. of parameters	376	6898

No. of restraints	0	-
H-atom treatment	H-atom parameters constrained	H-atom parameters constrained
$\Delta\rangle_{max}$, $\Delta\rangle_{min}$ (e Å^{-3})	2.820, -2.296	6.346, -2.702

Table 13.3 Experimental details for compound **6** (* = preliminary data).[18]

Crystal Data	6
Chemical formula	$C_{500}H_{420}Ag_{20}F_{60}Fe_{12}O_{60}P_{60}S_{20}$*
M_r	13856.01*
Crystal system, space group	monoclinic, *C*2/*c*
Temperature (K)	123
a, *b*, *c* (Å)	46.408(1), 31.916(1), 91.334(2)
α, β, γ (°)	90, 97.436(2), 90
V (Å^3)	134142(6)
Z	8
F(000)	> 57610
Radiation type	Cu K_α
μ (mm^{-1})	> 9.12
Crystal color and shape	red prism
Crystal size (mm)	0.26 x 0.16 x 0.08
Data collection	
Diffractometer	SuperNova, Titan^{S2} diffractometer
Absorption correction	gaussian
T_{min}, T_{max}	0.280, 0.533
No. of measured, independent and observed [$I > 2\sigma(I)$] reflections	127434, 73110, 28590
R_{int}	0.062
Range of h, k, l	h = -16→46, k = -26→32, l = -93→89
Refinement	*
$R[F^2 > 2\sigma(F^2)]$, $wR(F^2)$, S	0.14
No. of reflections	73110
No. of parameters	6313
No. of restraints	8
H-atom treatment	H-atom parameters constrained

13.6 Author Contributions

- The syntheses and characterization of the polymers **2** and **4** as well as of the supramolecules **3** and **5** were performed by Claudia Heindl

- The synthesis and characterization of the supramolecule **6** as well as the initial use of the triflate salt were done by Barbara Krämer and are also part of her master thesis (University of Regensburg, 2014)
- The manuscript (introduction, results and discussion, experimental part; including figures and graphical abstract) was written by Claudia Heindl and Barbara Krämer
- The section 'crystallographic details' was written by Dr. Eugenia V. Peresypkina
- X-ray structural analyses of **2, 3, 4, 5** were performed by Dr. Eugenia V. Peresypkina, Dr. Alexander V. Virovets and Claudia Heindl
- X-ray structural analysis of **6** was performed by Dr. Eugenia V. Peresypkina, Dr. Alexander V. Virovets and Barbara Krämer

13.7 References

[1] a) S. Zarra, D. M. Wood, D. A. Roberts, J. R. Nitschke, *Chem. Soc. Rev.* 2015, *44*, 419; b) M. D. Wise, J. J. Holstein, P. Pattison, C. Besnard, E. Solari, R. Scopelliti, G. Bricogne, K. Severin, *Chem. Sci.* 2015, *6*, 1004; c) T. Mitra, K. E. Jelfs, M. Schmidtmann, A. Ahmed, S. Y. Chong, D. J. Adams, A. I. Cooper, *Nat. Chem.* 2013, *5*, 276; d) D. Ajami, J. Rebek, *Acc. Chem. Res.* 2013, *46*, 990; e) L. F. Lindoy, K.-M. Park, S. S. Lee, *Chem. Soc. Rev.* 2013, *42*, 1713; f) R. W. Saalfrank, A. Scheurer, *Top. Curr. Chem.* 2012, *319*, 125; g) Z. Laughrey, B. C. Gibb, *Chem. Soc. Rev.* 2011, *40*, 363; h) M. Yoshizawa, J. K. Klosterman, M. Fujita, *Angew. Chem. Int. Ed.* 2009, *48*, 3418; i) P. Jin, S. J. Dalgarno, J. L. Atwood, *Coord. Chem. Rev.* 2010, *254*, 1760.

[2] a) L. Chen, Q. Chen, M. Wu, F. Jiang, M. Hong, *Acc. Chem. Res.* 2015, *48*, 201; b) R. W. Saalfrank, H. Maid, A. Scheurer, *Angew. Chem. Int. Ed.* 2008, *47*, 8794; c) G. F. Swiegers, T. J. Malefetse, *Coord. Chem. Rev.* 2002, *225*, 91.

[3] a) B. Attenberger, S. Welsch, M. Zabel, E. Peresypkina, M. Scheer, *Angew. Chem. Int. Ed.* 2011, *50*, 11516; b) M. Scheer, L. J. Gregoriades, M. Zabel, J. Bai, I. Krossing, G. Brunklaus, H. Eckert, *Chem. Eur. J.* 2008, *14*, 282; c) M. Scheer, L. Gregoriades, J. Bai, M. Sierka, G. Brunklaus, H. Eckert, *Chem. Eur. J.* 2005, *11*, 2163; d) J. Bai, E. Leiner, M. Scheer, *Angew. Chem. Int. Ed.* 2002, *41*, 783.

[4] L. J. Gregoriades, B. K. Wegley, M. Sierka, E. Brunner, C. Groeger, E. V. Peresypkina, A. V. Virovets, M. Zabel, M. Scheer, *Chem. Asian J.* 2009, *4*, 1578.

[5] B. P. Johnson, F. Dielmann, G. Balázs, M. Sierka, M. Scheer, *Angew. Chem. Int. Ed.* 2006, *45*, 2473.

[6] O. Oms, T. Jarrosson, L. H. Tong, A. Vaccaro, G. Bernardinelli, A. F. Williams, *Chem. Eur. J.* 2009, *15*, 5012.

[7] L. H. Tong, L. Guenee, A. F. Williams, *Inorg. Chem.* 2011, *50*, 2450.

[8] a) R. J. Less, T. C. Wilson, B. Guan, M. McPartlin, A. Steiner, P. T. Wood, D. S. Wright, *Eur. J. Inorg. Chem.* 2013, 1161; b) J. Bacsa, R. J. Less, H. E. Skelton, Z. Soracevic, A. Steiner, T. C. Wilson, P. T. Wood, D. S. Wright, *Angew. Chem. Int. Ed.* 2011, *50*, 8279.

[9] a) M. Fleischmann, S. Welsch, H. Krauss, M. Schmidt, M. Bodensteiner, E. V. Peresypkina, M. Sierka, C. Groeger, M. Scheer, *Chem. Eur. J.* 2014, *20*, 3759; b) C. Heindl, S. Heinl, D. Luedeker, G. Brunklaus, W. Kremer, M. Scheer, *Inorg. Chim. Acta* 2014, *422*, 218; c) F. Dielmann, A. Schindler, S. Scheuermayer, J. Bai, R. Merkle, M. Zabel, A. V. Virovets, E. V. Peresypkina, G. Brunklaus, H. Eckert, M. Scheer, *Chem. Eur. J.* 2012, *18*, 1168; d) M. Scheer, L. J. Gregoriades, A. V. Virovets, W. Kunz, R. Neueder, I. Krossing, *Angew. Chem. Int. Ed.* 2006, *45*, 5689; e) J. Bai, A. V. Virovets, M. Scheer, *Angew. Chem. Int. Ed.* 2002, *41*, 1737.

[10] a) S. Heinl, E. V. Peresypkina, A. V. Virovets, M. Scheer, *Angew. Chem. Int. Ed.* 2015, submitted; b) F. Dielmann, M. Fleischmann, C. Heindl, E. V. Peresypkina, A. V. Virovets, R. M. Gschwind, M. Scheer, *Chem. Eur. J.* 2015, *21*, 6208; c) F. Dielmann, C. Heindl, F. Hastreiter, E. V. Peresypkina, A. V. Virovets, R. M. Gschwind, M. Scheer, *Angew. Chem. Int. Ed.* 2014, *53*, 13605; d) C. Schwarzmaier, A. Schindler, C. Heindl, S. Scheuermayer, E. V. Peresypkina, A. V. Virovets, M. Neumeier, R. Gschwind, M. Scheer, *Angew. Chem. Int. Ed.* 2013, *52*, 10896; e) M. Scheer, A. Schindler, C. Groeger, A. V. Virovets, E. V. Peresypkina, *Angew. Chem. Int. Ed.* 2009, *48*, 5046; f) J. Bai, A. V. Virovets, M. Scheer, *Science* 2003, *300*, 781.

[11] a) S. H. Strauss, *Chem. Rev.* 1993, *93*, 927; b) W. Beck, K. Suenkel, *Chem. Rev.* 1988, *88*, 1405; c) G. A. Lawrance, *Chem. Rev.* 1986, *86*, 17.

[12] For a further example of the self-assembly of **1b** with $Cu(BF_4)$ forming a supramolecule, though accompanied by oxidation of **1b** and most likely a fragmentation of the BF_4 anion, see: F. Dielmann, Dissertation thesis (Universität Regensburg) 2011.

[13] P. Pyykkö, M. Atsumi, *Chem. Eur. J.* 2009, *15*, 186.

[14] M. Scheer, A. Schindler, J. Bai, B. P. Johnson, R. Merkle, R. Winter, A. V. Virovets, E. V. Peresypkina, V. A. Blatov, M. Sierka, H. Eckert, *Chem. Eur. J.* 2010, *16*, 2092.

[15] F. Dielmann, R. Merkle, S. Heinl, M. Scheer, *Z. Naturforsch.* 2009, *64*, 3.

[16] M. Detzel, G. Friedrich, O. J. Scherer and G. Wolmershäuser, *Angew. Chem. Int. Ed.* 1995, *34*, 1321.

[17] G. M. Sheldrick. *Acta Cryst. sect. C* 2015, *C71*, 3.

[18] Please note: Due to the uncompleted refinement, not all parameters (e.g. F(000)) can be stated and some given parameters, such as μ, R_{int}, as well as the sum formula have to be treated as preliminary values and may change at a later stage.

14. A Giant Self-Assembled Rugby Ball from Pentaphosphaferrocene and $CuBr_2$

Reprinted (adapted) with permission from C. Heindl, E. V. Peresypkina, A. V. Virovets, W. Kremer, M. Scheer, *J. Am. Chem. Soc.* 2015, *137*, 10938-10941.

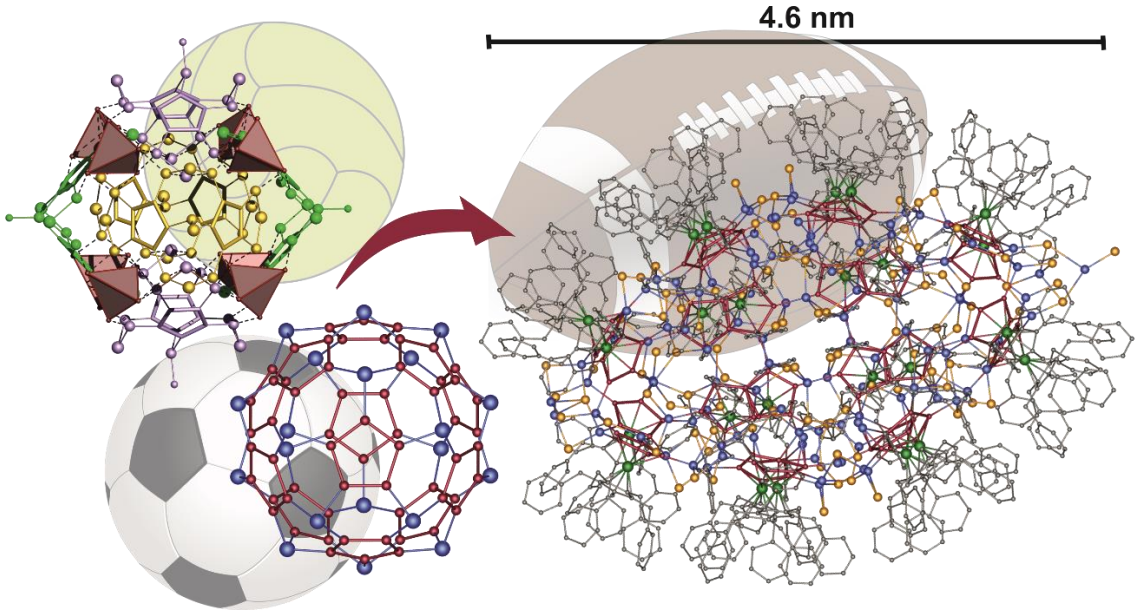

Abstract:

The self-assembly of $[Cp^{Bn}Fe(\eta^5\text{-}P_5)]$ (Cp^{Bn} = $\eta^5\text{-}C_5(CH_2Ph)_5$) with $CuBr_2$ leads to the formation of an unprecedented rugby ball-shaped supramolecule consisting of 24 units of the pentaphosphaferrocene and an extended CuBr framework. The resulting scaffold of 312 inorganic atoms reveals three different coordination modes of the *cyclo*-P_5 ligand including the unfavored π-coordination. The outer dimensions of 3.7 x 4.6 nm exceed the values of hitherto known pentaphosphaferrocene-based spheres. In fact, this range of size is almost on the scope of proteins, such as hemoglobin with a diameter of 5 nm. Furthermore, this giant rugby ball features a slight solubility in CH_2Cl_2. NMR spectroscopic investigations indicate that in solution phosphorus is still coordinated to copper.

14.1 Introduction

The construction of discrete nano-sized clusters and supramolecules is a fascinating frontier in modern molecular chemistry. A challenge within this field is the constant increase of the size to enter the field of nano and material science. For the design of ever larger spheres, already in the size category of proteins, two different connectivity approaches are applied. In inorganic chemistry, the clusters are held together mostly by covalent bonds, as it is the case for fullerenes,[1] highly symmetric polyoxometallates,[2] Cu and Ag chalcogenide clusters[3] or (inter-)metalloid clusters.[4] Among them are the largest structurally characterized aggregates: Concerning the size, the 'hedgehog' cluster $[H_xMo_{368}O_{1032}(H_2O)_{240}(SO_4)_{48}]^{48-}$ (x ~ 16) reaches an outer diameter of *ca.* 6 nm and therefore ranks first.[5] Regarding the number of metal atoms, Fenske and coworkers succeeded in the synthesis of $[Ag_{490}S_{188}(S\mathit{t}C_5H_{11})_{114}]$ containing 490 metal atoms.[6] The other, supramolecular, approach utilizes weaker interactions such as coordinative bonds and is based on the self-assembly of metal salts or complexes and multitopic organic linkers. Thereby, the rational design of a huge variety of spheres, though of smaller size, is enabled, which often can act as host for small molecules.[7]

We are interested in the expansion of this self-assembly approach to organometallic connecting units and use $[Cp^RFe(\eta^5\text{-}P_5)]$ ($Cp^R = Cp^{Bn} = \eta^5\text{-}C_5(CH_2Ph)_5$ (**1**); Cp* = η^5-C_5Me_5; $Cp^{Et} = \eta^5\text{-}C_5Me_4Et$; $Cp^{BIG} = \eta^5\text{-}C_5(4\text{-}^nBuC_6H_4)_5$) as building blocks for this purpose (*Figure 14.1*). Furthermore, these pentaphosphaferrocene complexes provide the advantage of phosphorus as donating element and an outstanding five-fold symmetry provided by the *cyclo*-P_5 ring.

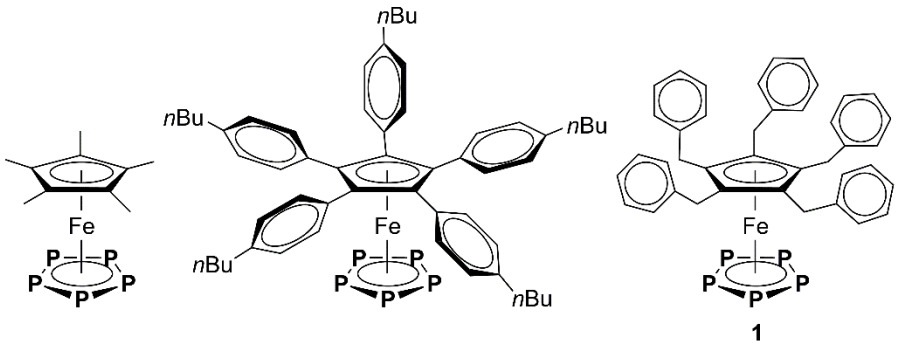

Figure 14.1 Phosphaferrocenes $[Cp^RFe(\eta^5\text{-}P_5)]$ (Cp^R = Cp*, Cp^{BIG}, Cp^{Bn}) for the construction of discrete supramolecules.

In combination with Cu(I) halides these benefits gratifyingly lead to the formation of nano-sized supramolecules with and beyond fullerene-like topology. Depending on the substitution pattern of the Cp^R ligand, various spheres with different scaffolds, shapes and outer diameters can be obtained.[8] A selection of the obtained scaffolds is shown in *Figure 14.2*. For example, *Figure 14.2*a shows a sphere constructed according to the isolated pentagon-rule (IPR).[8b,e] Hence, it shows fullerene topology and displays a carbon-free I_h-C_{80} analogue. The integration of a middle belt leads

to a slightly larger ball (*Figure 14.2*b) with 90 vertices.[8e,h] Even more giant supramolecules with deviating topologies and extended CuX (X = Br, I) frameworks can also be obtained (*Figure 14.2*c-e).[8c,d,g] Among them, there is one common feature concerning the number of pentaphosphaferrocene units per supramolecule: it is always equal 12 for fullerene-like balls[8a,b,e,h] (*Figure 14.2*a,b) and less than[8d, f] or equal to[8c] 12 for spheres with deviating topology (*Figure 14.2*c-e). A slightly higher number of *cyclo*-P_5 moieties, namely 13, occurred solely once, when C_{60} is encapsulated into a 99-vertex sphere.[8g] The hitherto largest spheres are constructed by sterically demanding phosphaferrocenes, such as the Cp^{Bn} and Cp^{BIG} derivative. The maximum size-record of 3.7 nm is held by $[\{Cp^{Bn}Fe(\eta^5\text{-}P_5)\}_{12}(CuI)_{54}]$, owed to an extensive CuI aggregate (*Figure 14.2*d).[8c]

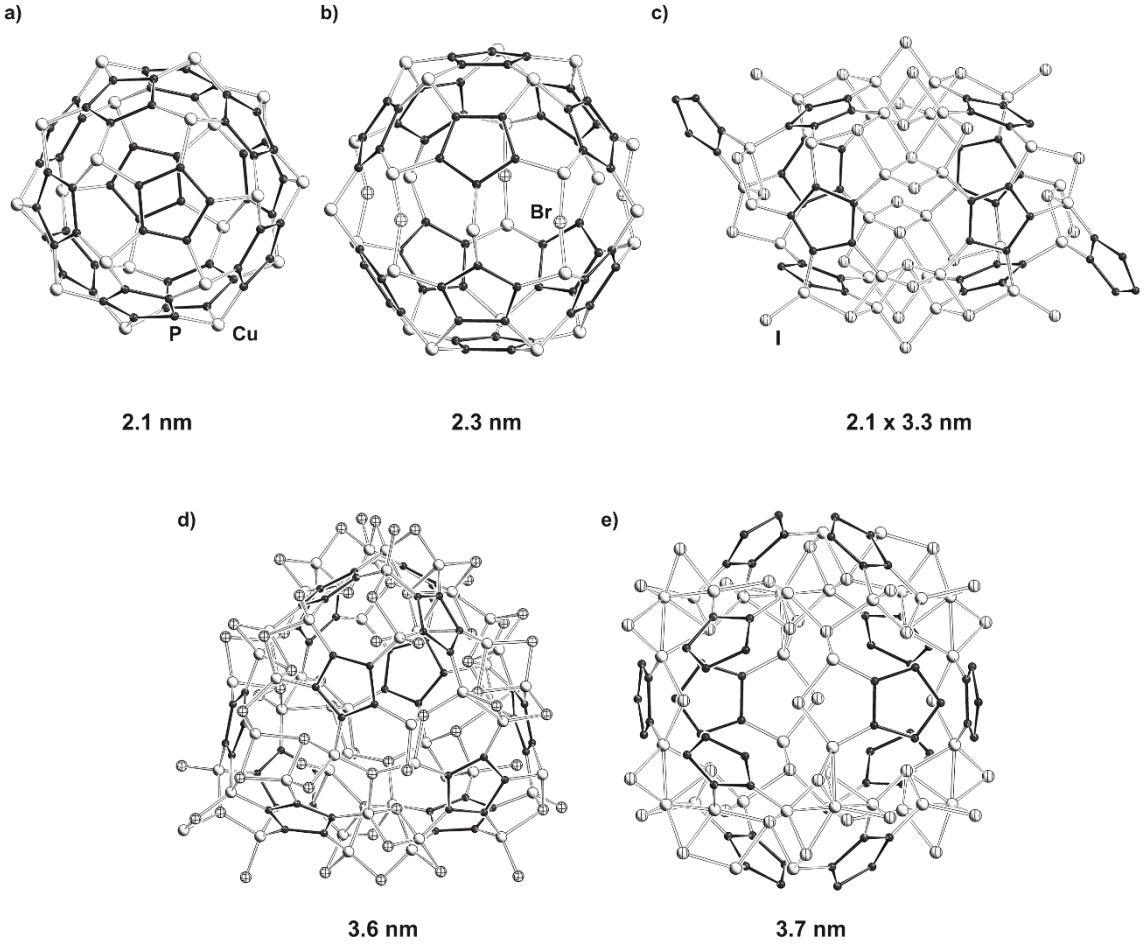

Figure 14.2 Inorganic scaffolds of selected pentaphosphaferrocene-based supramolecules: a) 80-vertex ball containing 12 P_5 moieties; b) 90-vertex ball containing 12 P_5 ligands; c) cuboid-shaped sphere with 10 P_5 moieties; d) tetrahedral-shaped supramolecule containing 12 P_5 units; e) 168-vertex ball with 12 P_5 units. The size indications refer to the maximal outer diameter including the Cp* and Cp^{Bn} ligands.

Herein we report on the synthesis and characterization of the unprecedented giant rugby-ball $[\{Cp^{Bn}Fe(\eta^5\text{-}P_5)\}_{24}Cu_{96}Br_{96}]$]·$6.2CH_2Cl_2$·$4.6C_7H_8$·$2.4CH_3CN$ (**2**) obtained by the reaction of **1** with $CuBr_2$. Neither such a high number of P_5 units, nor such an extended CuBr framework has been found in a supramolecule before. With an outer size of 4.6 x 3.7 nm it also overcomes all the other examples based on five-fold symmetric building blocks.

14.2 Results and Discussion

When a dark green solution of $CuBr_2$ in CH_3CN is added to a green solution of **1**, an immediate color change to an intensive red is observed. After one day of stirring and removal of the solvent, the residue is dissolved in CH_2Cl_2 and carefully layered with toluene. Within a few weeks, red rods of **2** crystallize, mostly accompanied by the crystallization of black blocks of the 80-vertex supramolecule $[(\mathbf{1})_{12}(CuBr)_{20-x}]$ (x < 7) (**3**; *Figure 14.2*a). A comprehensive solid-state and NMR spectroscopic study regarding the formation conditions and structure of **3** has been reported by our group recently.[8b] Studies on a selective synthesis reveal that the amount of acetonitrile seems to play a crucial role for the formation of **2** (see experimental part). Therefore the yields of pure **2** vary, though with an astonishing maximum of 84%, when a solvent mixture of 8 mL CH_2Cl_2 and 6 mL CH_3CN is applied.

Compound **2** crystallizes in the orthorhombic space group *I*222 with unit cell dimensions of a = 33.2127(2) Å, b = 42.4597(2) Å and c = 50.9189(3) Å. Its X-ray structural analysis reveals a giant rugby ball-shaped sphere built up by 24 moieties of **1** connected by 96 units of CuBr (*Figure 14.3*). In the crystal the supramolecules form a distorted face-centered cubic packing.

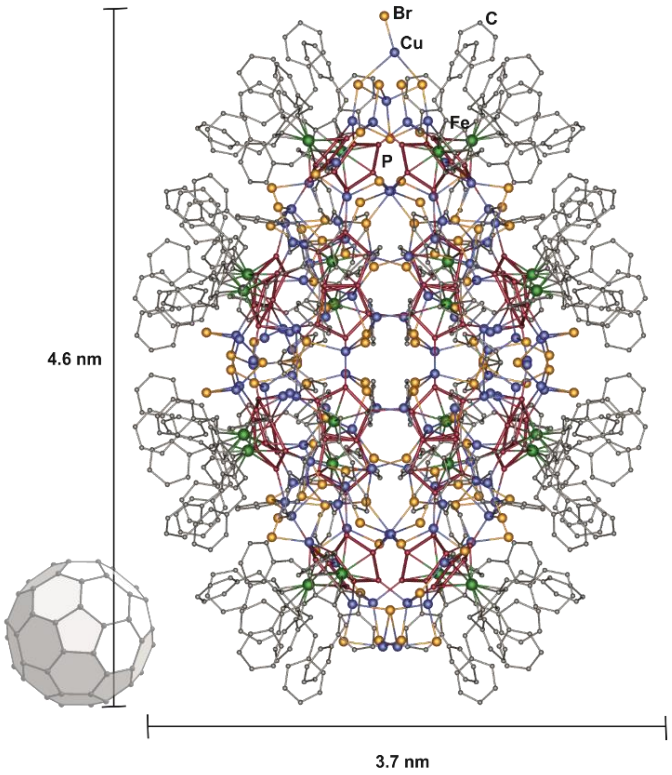

Figure 14.3 Molecular structure of **2**. Hydrogens, solvents and minor parts of disorder are omitted for clarity. For a size comparison, C_{60} is depicted in semitransparent color.

In compound **2**, the *cyclo*-P_5 ligands show three different coordination modes to copper (*Figure 14.4*): (i) each phosphorus atom shows a η^1-coordination to Cu (10 x {$Cp^{Bn}Fe(\eta^{5:1:1:1:1}$-$P_5)$}); (ii) four P atoms feature a η^1-coordination (6 x {$Cp^{Bn}Fe(\eta^{5:1:1:1:1}$-$P_5)$}) and (iii) in addition to a η^1-coordination of three P atoms, two P-P edges surprisingly each show a η^2-bond to copper (8 x {$Cp^{Bn}Fe(\eta^{5:2:2:1:1:1:1}$-$P_5)$}). Both σ-coordination modes are well known for this ligand, since (i) is present in all spherical supramolecules[8] and (ii) is obtained in two polymeric products.[8c,9] On the contrary, type (iii) is unprecedented for this ligand. Comparative studies of [Cp*Fe(η^5-E_5)] (E = P, As) rather revealed that the σ-interaction is clearly preferred by the phosphorus derivative, whereas it is the π-coordination mode for the arsenic analogue.[10] There are few exceptions with only one η^2-bond per P_5 ligand,[8a,b,9] though **2** displays the first compound with two η^2-bonds per P_5 ring.

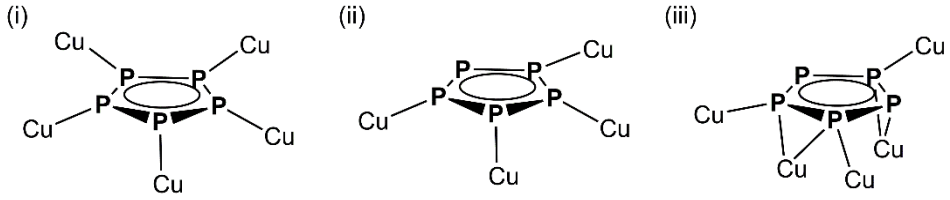

Figure 14.4 Illustration of the different coordination modes of the P_5 ligand in **2**.

In compound **2**, the different coordination modes show a noticeable effect on the corresponding bond lengths. The σ-Cu-P distances range between 2.210 Å and 2.293 Å and are therefore significantly shorter than the π-Cu-P bonds (2.345 Å – 2.420 Å). Furthermore, also the P-P bond lengths in the still planar *cyclo*-P_5 rings are affected: Those, which are involved in the π bonding, range from 2.116 Å to 2.133 Å and are therefore slightly elongated in comparison to the free complex **1** (2.110(1) Å).[11] On the contrary, the P-P bond lengths in type (i) and (ii) are quite uniform (2.066 Å – 2.113 Å) and slightly shorter than in **1**.

The Cu atoms show a characteristic tetrahedral environment, whereas the bromine atoms act as terminal as well as bridging (μ_2, μ_3, μ_4) ligand. The constructed framework includes a variety of different ring sizes, such as {Cu_2Br_2}, {P_2Cu_2Br}, {P_2Cu_3Br}, {P_4Cu_2}, {Cu_3Br_3} and {$P_2Cu_4Br_3$} rings, hence a comparison to the fullerene topology would be too far-fetched.

The whole sphere can formally be divided into two caps, which frame two identical middle belt parts (*Figure 14.5*). The caps each comprise four pentaphosphaferrocene molecules bound to Cu atoms in a 1,2,3,4,5-mode (type (i)). In addition, the very ends show a severe disorder of Cu and Br positions, respectively, which can be attributed to the possibility of the Cu atoms to form dimers and can also be present in a triangular environment. Therefore, two different non-contradictory possibilities are shown as the upper and lower part, respectively (*Figure 14.5*b,d). On the other

hand, each middle belt contains eight moieties of **1** with all three observed coordination modes (1 x (i), 4 x (ii), 3 x (iii); *cf. Figure 14.4*, *Figure 14.5*c).

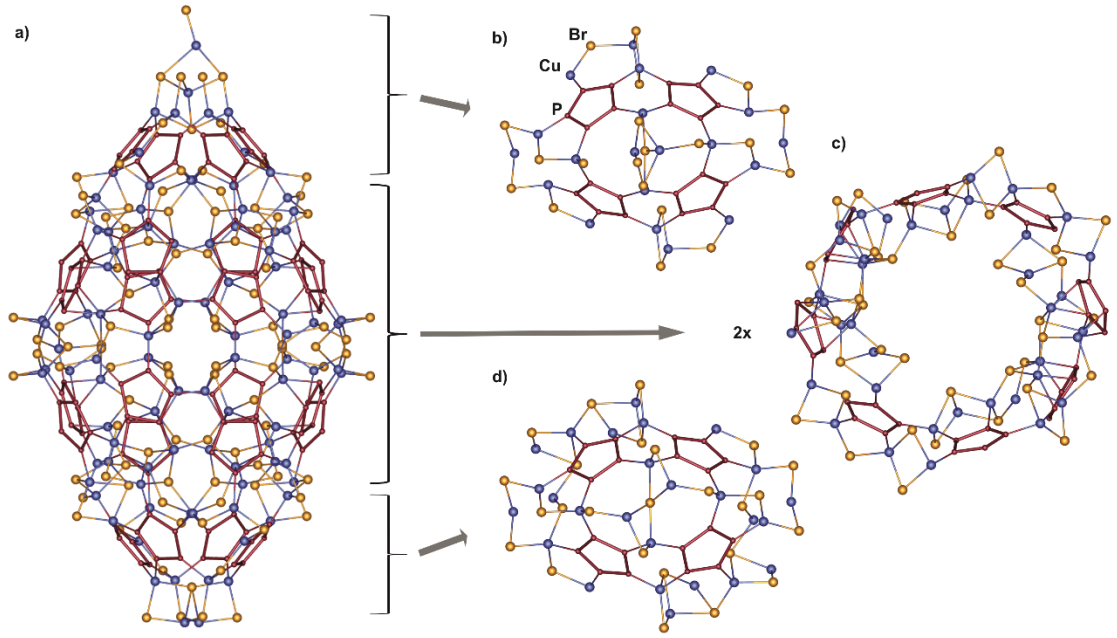

Figure 14.5 a) Inorganic scaffold of **2** containing 312 atoms; top view of the b) upper part, c) middle part and d) lower part.

In total, the scaffold of **2** consists of 312 atoms (120 P, 96 Cu, 96 Br; *Figure 14.5*a). This number far exceeds all hitherto reported pentaphosphaferrocene-based spheres, which mostly contain 80 up to 100 framework atoms. Recently we have shown, that the use of **1** instead of the well explored Cp* derivative [Cp*Fe(η^5-P_5)] allows the agglomeration of more CuX units (X = Br, I). However, the maximal numbers of scaffold atoms amount to 162 for X = Br (*Figure 14.2*d)[8b] and 168 for X = I (*Figure 14.2*e).[8b] The use of the sterically even more demanding Cp^{BIG} derivative allows the isolation of a 170-vertex skeleton.[8a] Therefore in **2**, almost twice the number is present.

Concerning the size, the giant rugby-ball **2** reaches 4.6 nm in length and 3.7 nm in width (*Figure 14.3*). These values again top all other [Cp^RFe(η^5-P_5)] containing supramolecules (*cf*. *Figure 14.2*). Though **2** has less metal atoms than $[Ag_{490}S_{188}(StC_5H_{11})_{114}]$ (see introduction), it is larger than this hourglass shaped cluster (2.8 x 3.1 nm).[6] Remarkably, the size of **2** is already on the verge of protein dimensions, e.g. hemoglobin shows a diameter of 5 nm.[12]

For another spectacular comparison: the diameter of the Buckminster fullerene C_{60} is close to 1 nm, therefore compound **2** is almost five times as long and four times as wide.[13]

Since the shape of **2** matches well the one of a protrude ellipsoid, the volume of the supramolecule can be calculated and amounts to 32.1 nm^3 with the values of the half-axes being 2.3 nm, 1.85 nm and 1.8 nm, respectively.[14] Hence staggeringly, the volume of **2** is 62 times larger than the ball-shaped C_{60} fullerene (V = 0.52 nm^3).

Despite the extended copper halide framework, which is partly protruding inside, the size of the inner cavity still amounts to 2.5 x 1.2 nm. It is filled with disordered CH_2Cl_2 and CH_3CN molecules.

Note, that in the rugby-ball **2** as well as in the 80-vertex ball **3** only Cu(I) units are present, though starting from $CuBr_2$ and thus indicating a reduction. This is also supported by the absence of a signal in the EPR spectrum of crystals of **2** in CH_2Cl_2 at r.t. as well as at T = 77 K. However, no corresponding oxidation product could be identified. This phenomenon already occurred several times, when [Cp*Fe(η^5-P_5)] or [{CpMo(CO)$_2$}$_2$(η^2-P_2)] is combined with Cu(II) halides.[9,15] Recently, our group succeeded in the isolation of the oxidation product of [Cp*Fe(η^5-P_5)], which is a dimer of the formula [Cp*Fe(η^4-P_5)]$_2^{2+}$ and readily decomposes.[16] Therefore, an analogous reaction might also take place during the formation of **2** and **3**.

Due to the organic shell of benzyl substituents, **2** is slightly soluble in CH_2Cl_2, which is absolutely remarkable for this giant aggregate. In the ^{1}H NMR spectrum of crystals of **2** in CD_2Cl_2 broad multiplets for the methylene groups (δ = 3.6 – 4.9 ppm) as well as for the aromatic protons (δ = 5.8 – 7.0 ppm) with the correct integral ratio of 2:5 are detected. However, in the ^{31}P{^{1}H} NMR spectrum no signal is observed, even when applying more than 10.000 scans. Solely an extremely vast hill straddling over several hundreds of ppm appears, yet cannot be counted as a signal. Unfortunately, even recording a low temperature (T = 193 K) ^{31}P{^{1}H} NMR spectrum does not lead to a sharpening or appearance of a signal worthy of interpretation. Nonetheless, signals for both nuclei corresponding to free molecules of **1** are not visible, yet should appear already at low concentrations due to their sharpness. This indicates the persisting coordination of Cu (nuclear spin I = 3/2) to the P_5 ligand in solution. In the ^{31}P{^{1}H} solid state NMR spectrum of **2** a broad multiplet at δ = 155 ppm ($\omega_{1/2}$ = 2460 Hz) is detected, which is comparable to ^{31}P{^{1}H} MAS studies of other pentaphosphaferrocene containing assemblies with more than three coordinated phosphorus atoms.[8e,9,17] Due to similar chemical shifts a distinction of the different coordination modes is impossible. In addition, the cationic ESI mass spectrum shows small peaks corresponding to the fragments [{Cp^{Bn}Fe(η^5-P_5)}$_2$$Cu_3Br_2$]$^+$, [{Cp^{Bn}Fe($\eta^5$-$P_5$)}$_2$$Cu_2Br$]$^+$ and [{Cp^{Bn}Fe(η^5-P_5)}$_2$Cu]$^+$ at m/z = 1803.2, 1659.5 and 1515.4, respectively. On the other hand, in the anionic ESI-MS spectrum only peaks, which are assigned copper bromide units up to $[Cu_3Br_4]^-$, are obtained.

In summary, the giant rugby ball-shaped supramolecule **2** is obtained by the self-assembly of the pentaphosphaferrocene **1** with $CuBr_2$. Whereas for nano-sized spherical molecules the number of P_5 rings was hitherto restricted to a maximum of 13, with 24 moieties of **1** in compound **2**, this trend is not any more true. Including the unprecedented extended $Cu_{96}Br_{96}$ framework the inorganic scaffold consists of 312 atoms. The outer size of the entire sphere amounts to 3.7 nm in width and 4.6 nm in length with a corresponding volume of 32.1 nm^3, hence it is one of the largest

discrete supramolecules, which was yet structurally characterized. More vividly, it is only slightly smaller than the human protein hemoglobin (d = 5 nm) and even 62 times larger in volume than the C_{60} fullerene (V = 0.5 nm^3). The *cyclo*-P_5 ligands in **2** show three different coordination modes, whereas one of them includes the rather uncommon η^2-π-coordination to copper. In addition, the giant molecule is slightly soluble in CH_2Cl_2 allowing NMR spectroscopic investigations. Since **2** provides a large cavity, future investigations will be concerned with the replacement of the enclosed solvent molecules and potential incorporation reactions.

14.3 Experimental Part

General Remarks:

All reactions were performed under an inert atmosphere of dry nitrogen or argon with standard vacuum, Schlenk and glove-box techniques. Solvents were purified, dried and degassed prior to use by standard procedures. [$Cp^{Bn}Fe(\eta^5\text{-}P_5)$] was synthesized following the reported procedure.[11] $CuBr_2$ was commercially available and was used without further purification. Solution NMR spectra were recorded on a Bruker Avance 400 spectrometer. The $^{31}P\{^1H\}$ MAS NMR spectrum was measured on a Bruker Avance 300. The corresponding ESI-MS spectra were acquired on a ThermoQuest Finnigan MAT TSQ 7000 mass spectrometer, while the elemental analysis was performed on a Vario EL III apparatus.

Synthesis of $[\{Cp^{Bn}Fe(\eta^5\text{-}P_5)\}_{24}Cu_{96}Br_{96}] \cdot 6.2(CH_2Cl_2) \cdot 4.6(C_7H_8) \cdot 2.4(CH_3CN)$ (2):

In a Schlenk tube [$Cp^{Bn}Fe(\eta^5\text{-}P_5)$] (50 mg, 0.07 mmol) and $CuBr_2$ (31 mg, 0.14 mmol) are dissolved in CH_2Cl_2 (8 mL) and CH_3CN (6 mL). The immediately dark red solution is stirred for one day, before the solvent is removed. The red residue is dissolved in pure CH_2Cl_2 (15 mL), filtered and layered with toluene (10 mL). After diffusion a small amount of crystals of **2** can be obtained at the bottom of the Schlenk tube. The yield is increased by layering the solvent mixture with Et_2O resulting in the crystallization of red rods below the phase boundary. Mostly, also black blocks of the 80-vertex supramolecule **3** crystallize, sometimes even as a single phase.[8b] It turned out that the amount of CH_3CN is determining: It is crucial for the formation of **2**, however only small amounts (at least less than the amount of CH_2Cl_2) are needed. Otherwise (without or too much CH_3CN) the formation of **3** is obtained exclusively. Although compound **2** and **3** significantly differ in their copper content (molar ratio Cu:**1** = 4.0 in **2**; 1.7 in **3**) a stoichiometric control of the starting materials was without any influence. Gratifyingly, due to different color and shape of the crystals, **2** and **3** can be separated mechanically under the microscope. After diffusion the crystals are washed with hexane (5 x 5 mL) and dried *in vacuo*.

Yield: varying on the amount of cocrystallized blocks of **3**; maximum: 38 mg (1.2 µmol, 84% referred to $CuBr_2$)

^{1}H NMR (CD_2Cl_2): δ [ppm] = 3.6 – 4.9 (m, br, 240 H, CH_2), 5.8 – 7.0 (m, br, 600 H, C_6H_5).

$^{31}P\{^1H\}$ NMR (CD_2Cl_2; NS = 10240): no signal detectable, see text.

$^{31}P\{^1H\}$ NMR (CD_2Cl_2; 193 K): no signal detectable, see text.

$^{31}P\{^1H\}$ MAS NMR: δ [ppm] = 155 (br, $\omega_{1/2}$ = 2460 Hz)

Positive ion ESI-MS (CH_2Cl_2): *m/z* = 1803.2 $[\{Cp^{Bn}Fe(\eta^5\text{-}P_5)\}_2Cu_3Br_2]^+$, 1659.5 $[\{Cp^{Bn}Fe(\eta^5\text{-}P_5)\}_2Cu_2Br]^+$, 1515.4 $[\{Cp^{Bn}Fe(\eta^5\text{-}P_5)\}_2Cu]^+$.

Negative ion ESI-MS (CH_2Cl_2): *m/z* (%) = 510.4 (10) $[Cu_3Br_4]^-$, 366.4 (36) $[Cu_2Br_3]^-$, 222.5 (100) $[CuBr_2]^-$.

Elemental analysis: Calculated (%) for $[C_{966}H_{852}Br_{96}Cl_{12}Cu_{96}Fe_{24}P_{120}]$ (31715 g/mol): C 36.58, H 2.71; found: C 35.62, H 2.97.

14.4 Crystallographic Details

Crystals of **2** were taken from a Schlenk flask under a stream of argon and immediately covered with perfluorinated Fomblin® mineral oil to prevent both decomposition and a loss of solvent. The quickly chosen single crystals covered by a drop of the oil were taken to the pre-centered goniometer head with CryoMount® and directly attached to the diffractometer into a stream of cold nitrogen. X-ray diffraction studies faced many challenges, since the crystals decompose rapidly losing solvent molecules and the collection of data at high theta angles required high exposure times.

The data for **2** were collected on an Agilent Technologies SuperNova diffractometer equipped with Atlas^{S2} CCD detector and an SuperNova CuK_α source (λ = 1.54178 Å) using 0.5° ω scans at 123 K. Crystallographic data and details of the diffraction experiment are given in *Table 14.1*. The structure of **2** was solved by direct methods with *SHELX97*[18] and refined by full-matrix least-squares method against $|F|^2$ in anisotropic approximation using the multiprocessor and variable memory version *SHELXL2013* with an increased to 5000 maximum number of full-matrix parameters. The structure was refined as an inversion twin with twin batches 0.515(5)/0.485(5). The non-hydrogen atoms were refined anisotropically if their occupancies exceeded 0.1 for heavy atoms (Cu, Br) or 0.8 for light atoms (C, N), while the hydrogen atoms were refined riding on pivot atoms. The enlarged displacement parameters for Cu and Br atoms indicated partial occupancies for several Cu_xBr_y fragments. The disorder of the heavy part was refined as follows: The occupancies were refined with equated to average displacement parameters for the heavy atoms in the structure, U_{iso} = 0.035. The occupancies were fixed at the resulting values and the refinement of

the displacement parameters was performed. Many phenyl rings of the Cp^{Bn} ligands are disordered *via* rotation around the CH_2-Ph bond over at least two positions and therefore were refined with restraint geometry. One entire Cp^{Bn} ligand is disordered over two positions. Sometimes it was necessary to restrain also displacement parameters of the rotating Ph fragments as a result of unresolved disorder.

Some solvent molecules in **2** could be located from the difference Fourier map. The solvent molecules in most cases are disordered, and their molecular occupancy factors were refined using the FVAR instruction of SHELX with isotropic displacement parameters fixed at U_{iso} = 0.05. The resulting occupancies were fixed and were refined isotropically due to low molecular occupancy factors. Most of the toluene and dichloromethane molecules were refined with restraint geometry. The restraints were removed at the final stage of the refinement if possible. Due to the disorder the solvent content is generally underestimated. In the cavity only one MeCN and 0.8 CH_2Cl_2 molecules were localized. There are cavities in the structure accessible for solvent molecules, however no residual electron density that can be attributed to some solvent molecule with reasonable geometry was found.

Table 14.1 Experimental details for compound **2**.

Crystal Data	2
Chemical formula	$C_{960}H_{840}P_{120}Fe_{24}Cu_{96}Br_{96}\cdot 6.2(CH_2Cl_2)\cdot 4.6(C_7H_8)\cdot 2.4(CH_3CN)$
M_r	32345.16
Crystal system, space group	orthorhombic, *I222*
Temperature (K)	123(2)
a, *b*, *c* (Å)	33.2127(2), 42.4597(2), 50.9189(3)
α, β, γ (°)	90, 90, 90
V (Å^3)	71805.9(7)
Z	2
F(000)	31517
Radiation type	CuK_α
μ (mm^{-1})	8.28
Crystal color and shape	red-brown rod
Crystal size (mm)	0.98 x 0.14 x 0.10
Data collection	
Diffractometer	SuperNova, Single source at offset, Atlas[S2]
Absorption correction	gaussian
T_{min}, T_{max}	0.093, 0.535
No. of measured, independent and observed [$I > 2\sigma(I)$] reflections	229206, 69900, 62895

R_{int}	0.046
$(\sin\theta/\lambda)_{max}$ ($Å^{-1}$)	0.618
Range of h, k, l	h = -37→40, k = -52→52, l = -62→62
Refinement	
$R[F^2 > 2\sigma(F^2)]$, $wR(F^2)$, S	0.061, 0.175, 1.04
No. of reflections	69900
No. of parameters	3079
No. of restraints	46
H-atom treatment	H-atom parameters constrained
$\Delta\rangle_{max}$, $\Delta\rangle_{min}$ (e $Å^{-3}$)	3.31, -2.38

14.5 Author Contributions

- The synthesis and characterization of the rugby ball **2** was performed by Claudia Heindl
- X-ray structural analysis of **2** was performed by Dr. Eugenia V. Peresypkina, Dr. Alexander V. Virovets and Claudia Heindl
- The manuscript (introduction, results and discussion, experimental part; including figures and graphical abstract) was written by Claudia Heindl
- The section 'crystallographic details' was written by Dr. Eugenia V. Peresypkina
- The $^{31}P\{^1H\}$ MAS NMR spectrum of **2** was recorded by Werner Kremer

14.6 References

[1] a) A. Hirsch, M. Brettreich in *Fullerenes – Chemistry and Reactions,* Wiley-VCH, Weinheim, 2005; b) P. W. Fowler, D. E. Manolopoulos in *An Atlas of Fullerenes*, Clarendon Press, 1995; c) M. S. Dresselhaus, G. Dresselhaus, P. C. Eklund in *Science of Fullerenes and Carbon Nanotubes*, Academic Press, 1996.

[2] a) D.-L. Long, R. Tsunashima, L. Cronin, *Angew. Chem. Int. Ed.* 2010, *49*, 1736; b) M. T. Pope, A. Mueller, *Angew. Chem.* 1991, *103*, 56; *Angew. Chem. Int. Ed.* 2006, *1930*, 1934; c) S. Kopilevich, A. Gil, M. Garcia-Rates, J. Bonet-Avalos, C. Bo, A. Muller, I. A. Weinstock, *J. Am. Chem. Soc.* 2012, *134*, 13082.

[3] a) O. Fuhr, S. Dehnen, D. Fenske, *Chem. Soc. Rev.* 2013, *42*, 1871; b) J. F. Corrigan, O. Fuhr, D. Fenske, *Adv. Mater.* 2009, *21*, 1867.

[4] a) H. Schnöckel, A. Schnepf, Robert L. Whetten, C. Schenk, P. Henke, *Z. Anorg. Allg. Chem.* 2011, *637*, 15; b) J. Vollet, J. R. Hartig, H. Schnöckel, *Angew. Chem. Int. Ed.* 2004, *43*, 3186; c)

S. Scharfe, F. Kraus, S. Stegmaier, A. Schier, T. F. Faessler, *Angew. Chem. Int. Ed.* 2011, *50*, 3630; d) N. T. Tran, D. R. Powell, L. F. Dahl, *Angew. Chem. Int. Ed.* 2000, *39*, 4121.

[5] a) A. Mueller, B. Botar, S. K. Das, H. Boegge, M. Schmidtmann, A. Merca, *Polyhedron* 2004, *23*, 2381; b) A. Müller, E. Beckmann, H. Bögge, M. Schmidtmann, A. Dress, *Angew. Chem. Int. Ed.* 2002, *41*, 1162.

[6] a) O. Fuhr, S. Dehnen, D. Fenske, *Chem. Soc. Rev.* 2013, *42*, 1871; b) C. Anson, A. Eichhoefer, I. Issac, D. Fenske, O. Fuhr, P. Sevillano, C. Persau, D. Stalke, J. Zhang, *Angew. Chem. Int. Ed.* 2008, *47*, 1326.

[7] a) Y. Inokuma, M. Kawano, M. Fujita, *Nat. Chem.* 2011, *3*, 349; b) S. Li, J. Huang, F. Zhou, T. R. Cook, X. Yan, Y. Ye, B. Zhu, B. Zheng, P. J. Stang, *J. Am. Chem. Soc.* 2014, *136*, 5908; c) J. S. Mugridge, R. G. Bergman, K. N. Raymond, *J. Am. Chem. Soc.* 2012, *134*, 2057; d) O. Oms, T. Jarrosson, L. H. Tong, A. Vaccaro, G. Bernardinelli, A. F. Williams, *Chem. Eur. J.* 2009, *15*, 5012; e) S. R. Seidel, P. J. Stang, *Acc. Chem. Res.* 2002, *35*, 972.

[8] a) S. Heinl, E. V. Peresypkina, A. V. Virovets, M. Scheer, *Angew. Chem. Int. Ed.* 2015, submitted; b) F. Dielmann, M. Fleischmann, C. Heindl, E. V. Peresypkina, A. V. Virovets, R. M. Gschwind, M. Scheer, *Chem. Eur. J.* 2015, *21*, 6208; c) F. Dielmann, C. Heindl, F. Hastreiter, E. V. Peresypkina, A. V. Virovets, R. M. Gschwind, M. Scheer, *Angew. Chem. Int. Ed.* 2014, *53*, 13605; d) C. Schwarzmaier, A. Schindler, C. Heindl, S. Scheuermayer, E. V. Peresypkina, A. V. Virovets, M. Neumeier, R. Gschwind, M. Scheer, *Angew. Chem. Int. Ed.* 2013, *52*, 10896; e) A. Schindler, C. Heindl, G. Balázs, C. Groeger, A. V. Virovets, E. V. Peresypkina, M. Scheer, *Chem. Eur. J.* 2012, *18*, 829; f) S. Welsch, C. Groeger, M. Sierka, M. Scheer, *Angew. Chem. Int. Ed.* 2011, *50*, 1435; g) M. Scheer, A. Schindler, R. Merkle, B. P. Johnson, M. Linseis, R. Winter, C. E. Anson, A. V. Virovets, *J. Am. Chem. Soc.* 2007, *129*, 13386; h) J. Bai, A. V. Virovets, M. Scheer, *Science* 2003, *300*, 781.

[9] F. Dielmann, A. Schindler, S. Scheuermayer, J. Bai, R. Merkle, M. Zabel, A. V. Virovets, E. V. Peresypkina, G. Brunklaus, H. Eckert, M. Scheer, *Chem. Eur. J.* 2012, *18*, 1168.

[10] a) M. Fleischmann, J. S. Jones, F. P. Gabbai, M. Scheer, *Chem. Sci.* 2015, *6*, 132; b) H. Krauss, G. Balázs, M. Bodensteiner, M. Scheer, *Chem. Sci.* 2010, *1*, 337.

[11] F. Dielmann, R. Merkle, S. Heinl, M. Scheer, *Z. Naturforsch.* 2009, *64*, 3.

[12] H. P. Erickson, *Biological Procedures Online* 2009, *11*, 32.

[13] S. Liu, Y.-J. Lu, M. M. Kappes, J. A. Ibers, *Science* 1991, *254*, 408.

[14] The formula for the determination of the volume of a protrude ellipsoid is: V = 4/3πabc with a, b, c being the semi-axes. Their values are half of the major and minor axes, respectively: a = 4.6/2 nm; b = 3.7/2 nm; c = 3.6/2 nm.

[15] M. Scheer, L. Gregoriades, J. Bai, M. Sierka, G. Brunklaus, H. Eckert, *Chem. Eur. J.* 2005, *11*, 2163.

[16] a) M. V. Butovskiy, G. Balázs, M. Bodensteiner, E. V. Peresypkina, A. V. Virovets, J. Sutter, M. Scheer, *Angew. Chem. Int. Ed.* 2013, *52*, 2972; b) R. G. Winter, W.E. Geiger, *Organometallics* 1999, *18*, 1827.

[17] a) M. Scheer, A. Schindler, J. Bai, B. P. Johnson, R. Merkle, R. Winter, A. V. Virovets, E. V. Peresypkina, V. A. Blatov, M. Sierka, H. Eckert, *Chem. Eur. J.* 2010, *16*, 2092; b) M. Scheer, A. Schindler, C. Groeger, A. V. Virovets, E. V. Peresypkina, *Angew. Chem. Int. Ed.* 2009, *48*, 5046.

[18] G. M. Sheldrick, *Acta Cryst. sect. C* 2015, *71*, 3.

15. Conclusion

This work deals with the formation of polymeric and spherical assemblies derived from polyphospholyl ligands as building blocks *via* self-assembly processes. The introductory part (chapter 1) elucidates general aspects of supramolecular chemistry as well as the current state of literature especially involving phosphaferrocenes. After the research objectives (chapter 2), the results obtained within this thesis are presented in the self-contained chapters 3 – 14.

The main objective was the investigation of the coordination behavior of selected polyphospholyl ligands towards Lewis-acidic metal salts, especially Cu(I) halides. These are as following (*Figure 15.1*): the triple decker complex $[(CpMo)_2(\mu,\eta^{6:6}\text{-}P_6)]$ (chapter 3), the triphosphaferrocene $[Cp^*Fe(\eta^5\text{-}P_3C_2Mes_2)]$ (chapter 4), the triphospholyl salts $K[1,2,4\text{-}P_3C_2R_2]$ (R = Mes, ^{t}Bu; chapter 5) and the pentaphosphaferrocenes $[Cp^RFe(\eta^5\text{-}P_5)]$ (Cp^R = Cp*, chapters 8-13; Cp^R = Cp^{Bn}, chapters 11, 13, 14).

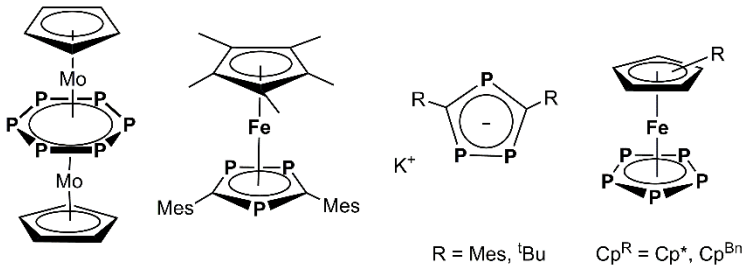

Figure 15.1 Building blocks used for the self-assembly with Lewis-acidic metal salts.

In addition, several hitherto unknown building blocks could be synthesized within the scope of this work (*Figure 15.2*): the tri- and tetra-pentelyl salts $Cs[E_3C_2(trip)_2]$ and $Cs[E_4C(trip)]$ (E = P, As; chapter 6), a series of ^{i}Pr-substituted phosphaferrocenes (chapter 7) as well as the parent compounds $[CpFe(\eta^5\text{-}P_5)]$ (chapter 10) and $[(CpMo)_2(\mu,\eta^{3:3}\text{-}P_3)(\mu,\eta^{2:2}\text{-}PS)]$ (chapter 13).

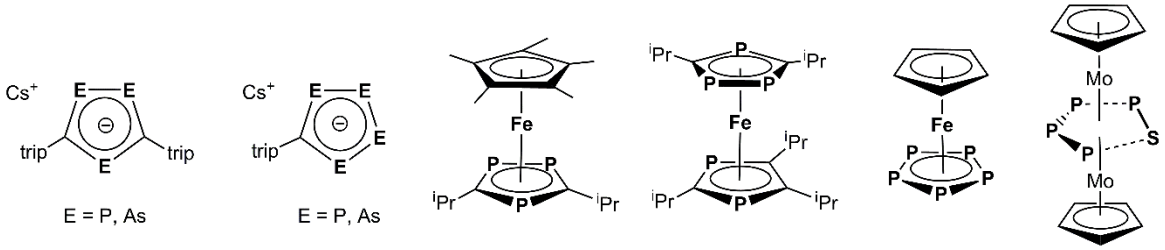

Figure 15.2 Hitherto unknown starting compounds synthesized within this work.

In the following, all topics are summarized according to the type of the building block: (a) is concerned with the hexaphosphabenzene ligand, (b) describes the reactivity of 1,2,4-triphospholyl ligands and in (c) an overview of the coordination behavior of pentaphospholyl ligands is given.

Whereas in (a) and (b) mainly polymeric assemblies are obtained, section (c) emphasizes the template-directed formation of spherical supramolecules.

(a) The Hexaphosphabenzene Ligand – A versatile Building Block for the Formation of 2D Networks

The triple decker complex $[(CpMo)_2(\mu,\eta^{6:6}\text{-}P_6)]$ (**1**) displays an excellent building block in supramolecular chemistry, since its planar *cyclo*-P_6 middle deck offers variable coordination sites and the formation of planar graphene-like sheet structures might be conceivable. Therefore, it was reacted with CuX (X = Br, I), resulting in the formation of the unprecedented two-dimensional networks $[\{(CpMo)_2(\mu,\eta^{3:3:1:1:1:1}\text{-}P_3)(\mu,\eta^{3:2:1:1:1:1}\text{-}P_3)\}Cu_4(\mu\text{-}Br)_4]_n$ (**2**) and $[\{(CpMo)_2(\mu,\eta^{3:3:1:1}\text{-}P_3)(\mu,\eta^{3:2:1:1}\text{-}P_3)\}_{0.84}\{(CpMo)_2(\mu,\eta^{6:6:1:1:1:1}\text{-}P_6)\}_{0.16}Cu_2(\mu\text{-}I)_2]_n$ (**3**) (*Scheme 15.1*). Surprisingly, in both compounds the P_6 ligands show deformation, namely a bisallylic distortion as well as a bending of one phosphorus atom in an 'envelope' conformation. In addition, 1D and 2D $^{31}P\{^1H\}$ MAS NMR investigations give evidence for this spatial arrangement. Despite this, planar layers are formed for the first time *via* a 1,2,4,5-coordination mode of **1** to copper.

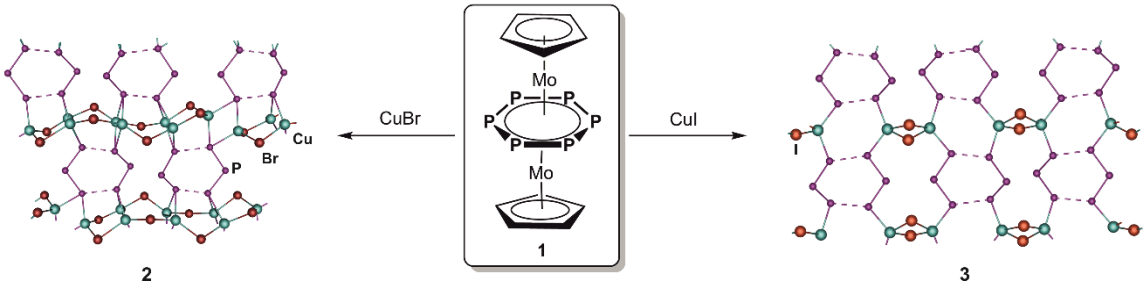

Scheme 15.1 Coordination compounds based on **1**.

(b) The 1,2,4-Triphospholyl Ligand – A versatile Building Block for the Formation of Oligomeric and Polymeric compounds

A variety of coordination compounds based on the 1,2,4-triphosphaferrocenes $[Cp^RFe(\eta^5\text{-}P_3C_2{}^tBu_2)]$ (Cp^R = Cp, Cp*, Cp''') as building blocks is known. Depending on the steric bulk of the Cp^R ligand, different products are formed. Hence, also the substitution pattern of the phospholyl ligand should profoundly affect the self-assembly with Cu(I) halides. These investigations were an elementary part of this thesis. Therefore, in the first instance the sterically more demanding triphosphaferrocene $[Cp^*Fe(\eta^5\text{-}P_3C_2Mes_2)]$, bearing mesityl ligands adjacent to the phosphorus atoms, was reacted with CuX (X = Cl, Br, I). Surprisingly, the sandwich complex undergoes an unique fragmentation into decamethylferrocene, FeX_2 (X = Cl, Br, I) and $[P_3C_2Mes_2]^-$ units in all reactions. Subsequently, the triphospholyl ligand $[1,2,4\text{-}P_3C_2Mes_2]^-$ (**4a**) acts as versatile building block for the

formation of monomeric, dimeric, one- and even two-dimensional polymeric coordination products (*cf. Scheme 15.2*) with Cu(I) halides:

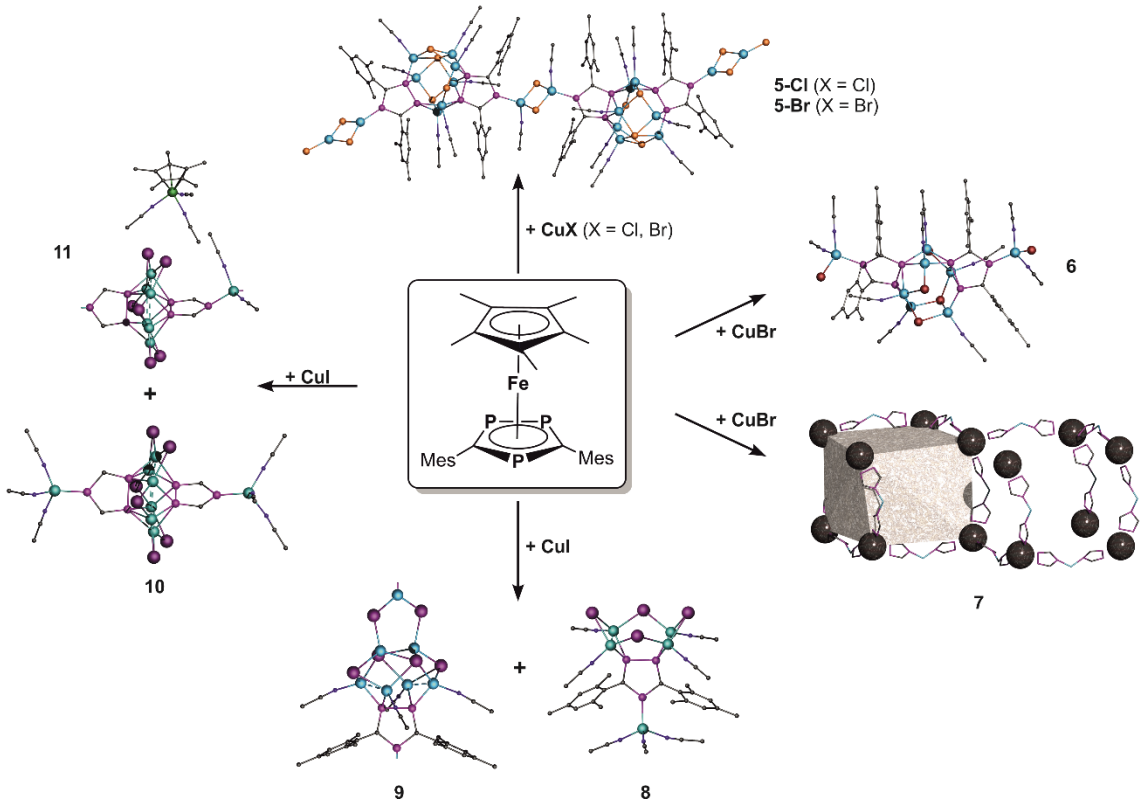

Scheme 15.2 Coordination compounds based on the triphospholyl ligand **4a** after fragmentation of [Cp*Fe(η^5-$P_3C_2Mes_2$)].

By the reaction of [Cp*Fe(η^5-$P_3C_2Mes_2$)] with CuX (X = Cl, Br) in both cases the dimeric complex [($\mu,\eta^{1:2:2}$-$P_3C_2Mes_2$)($\mu,\eta^{1:3:3}$-$P_3C_2Mes_2$){$Cu_7(CH_3CN)_7(\mu_4$-X)(μ_3-X)$_2$(μ-X)}{$Cu_2(\mu_2$-X)$_2$X}{Cu(CH_3CN)(μ_2-X)}]$_2$ (X = Cl: **5-Cl**; X = Br: **5-Br**) is obtained. Here, the **4a** moieties are connected *via* a novel P-, Cu-, X-containing cage (*Scheme 15.2*, *Figure 15.3*a). Whereas this reaction is selective for X = Cl, the self-assembly of **4a** with CuBr is much more sensitive to the stoichiometry and concentration used and two additional products can be isolated (*Scheme 15.2*): [($\mu,\eta^{1:2:3}$-$P_3C_2Mes_2$)$_2${Cu(CH_3CN)}$_6$(μ-Br)$_2$(μ_3-Br)$_2${Cu(CH_3CN)$_2$Br}$_2$] (**6**) and [($\mu,\eta^{1:1:2}$-$P_3C_2Mes_2$)$_3$($\mu,\eta^{1:2:3}$-$P_3C_2Mes_2$){$Cu_5(CH_3CN)_5(\mu_2$-Br)}{Cu(CH_3CN)$_2$$CuBr_2$}$_2${Cu($CH_3CN$)$_2$}]$_n$[$CuBr_2$]$_n$ (**7**). Compound **6** can be regarded as the monomer of the dimeric assembly **5-Br** with a slight deviation in the central CuBr-cage motif. On the other hand, a deficit of CuBr leads to the formation of a two-dimensional network despite the steric bulk of the mesityl ligands. The **4a** moieties are again linked *via* a cage composed by P, Cu and Br atoms, though with a completely different, hitherto unknown topology (*Figure 15.3*b).

By combining **1** and CuI, products with two different very rare structural motifs of CuI units can be realized: the {Cu_4I_4} 'crown' (*Figure 15.3*c) and the {Cu_6I_6} 'hexagram' motif (*Figure 15.3*d). Both are found either in a monomeric coordination compound or in a 1D polymer (*Scheme 15.2*):

$[(\mu,\eta^{1:2:2}\text{-}P_3C_2Mes_2)\{Cu(CH_3CN)(\mu\text{-}I)\}_4\{Cu(CH_3CN)_3\}]$ (**8**) and $[(\mu,\eta^{1:2:2}\text{-}P_3C_2Mes_2)Cu_7(CH_3CN)_4(\mu_4\text{-}I)_2(\mu_3\text{-}I)_2(\mu\text{-}I)_2]_n$ (**9**) containing the 'crown' and $[(\mu,\eta^{1:3:3}\text{-}P_3C_2Mes_2)\{Cu(CH_3CN)_3\}_2\{Cu(\mu\text{-}I)\}_6]$ (**10**) and $[Cp^*Fe(CH_3CN)_3]_n[(\mu,\eta^{1:3:3}\text{-}P_3C_2Mes_2)_2\{Cu(CH_3CN)_2\}\{Cu(\mu\text{-}I)\}_6]_n$ (**11**) containing the 'hexagram'. The negative charge of the latter polymer is surprisingly balanced by the extremely labile cation $[Cp^*Fe(CH_3CN)_3]^+$. This represents another possible decomposition pathway of the initial triphosphaferrocene.

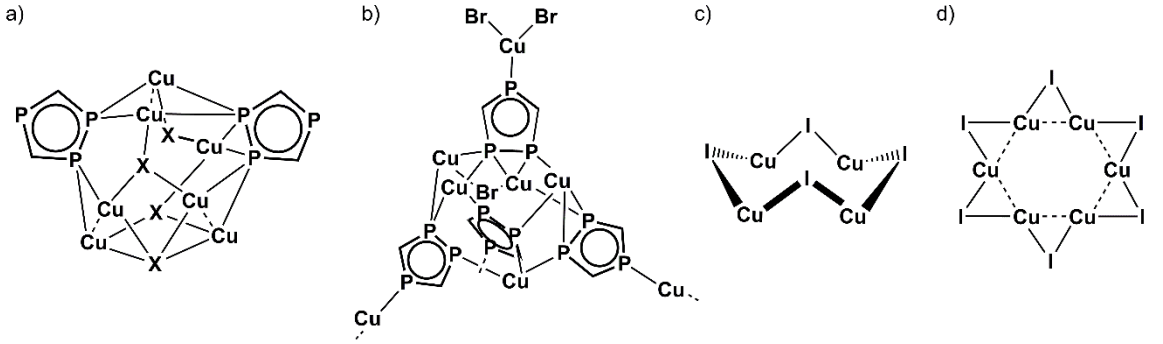

Figure 15.3 Structural motifs of the copper halide assemblies in a) **5-Cl**, **5-Br** and **6** (slightly different); b) **7**; c) **8** and **9**; d) **10** and **11**.

To conclude, an enhancement of the steric bulk from ^{t}Bu to mesityl substituents induces instability of the 1,2,4-triphosphaferrocene in terms of fragmentation *via* a split-off of the phospholyl ligand.

Since **5-Cl** – **11** all contain **4a** as building block, the question arose whether the detour of the synthesis and subsequent fragmentation of $[Cp^*Fe(\eta^5\text{-}P_3C_2Mes_2)]$ can be avoided. To investigate this issue, the potassium salt K[**4a**] was used as building block in combination with Cu(I) halides (*Scheme 15.3*).

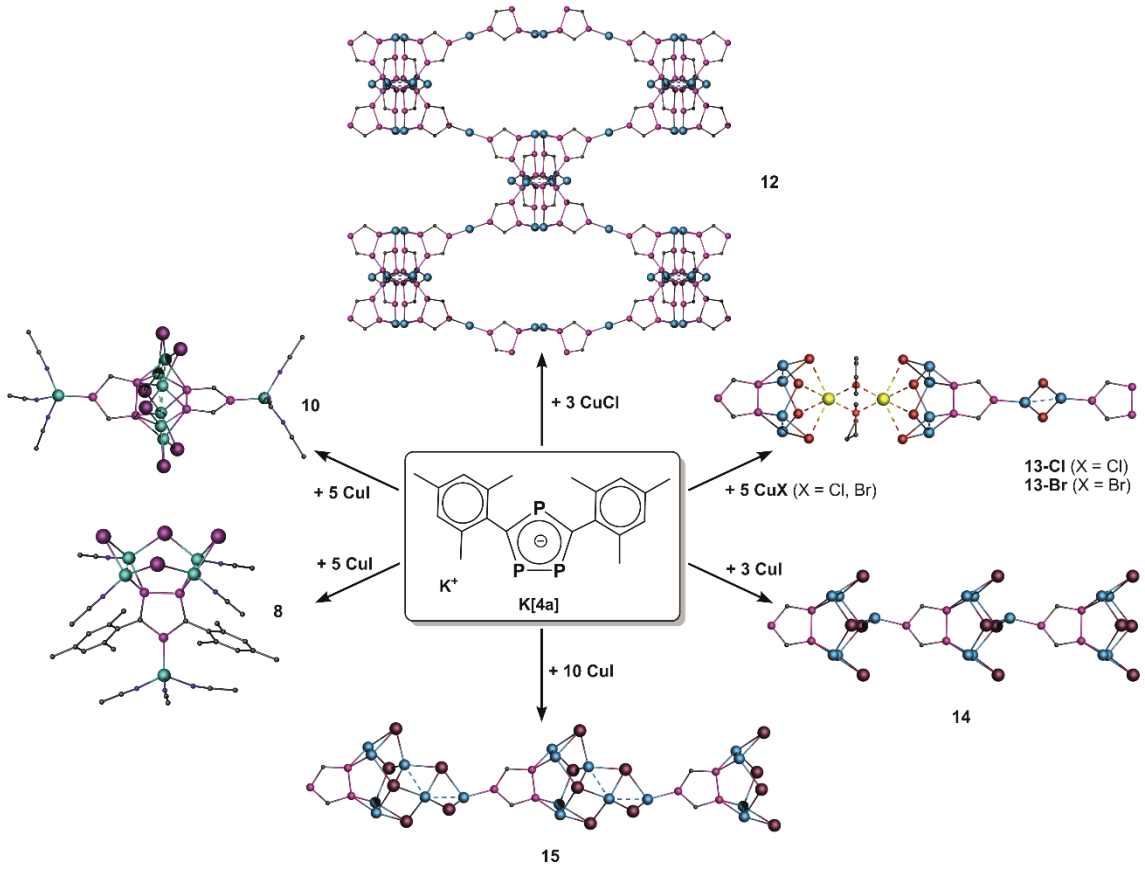

Scheme 15.3 Coordination compounds based on **4a** starting from its potassium salt.

Thereby, two known monomeric coordination products are obtained, namely the 'crown' **8** and the 'hexagram' **10**. However, in addition to this, unprecedented one-dimensional chains and for the first time even a three-dimensional assembly can be isolated (*Scheme 15.3*): $[(\mu,\eta^{1:1:2}\text{-}P_3C_2Mes_2)_2\{Cu(CH_3CN)\}_2\{Cu(CH_3CN)_2\}]^+_n[Cl]^-_n$ (**12**), $[(\mu,\eta^{1:2:2}\text{-}P_3C_2Mes_2)\{Cu(CH_3CN)(\mu_2\text{-}X)\}_4\{K(\mu_2\text{-}solv)\}\{Cu(\mu_2\text{-}X)\}]_n$ (**13-Cl**: X = Cl, solv = dme; **13-Br**: X = Br, solv = thf), $[(\mu,\eta^{1:2:2}\text{-}P_3C_2Mes_2)\{Cu(CH_3CN)(\mu_2\text{-}I)\}_2\{Cu(CH_3CN)(\mu_3\text{-}I)\}_2Cu]_n$ (**14**) and $[(\mu,\eta^{1:2:2}\text{-}P_3C_2Mes_2)\{Cu(CH_3CN)(\mu_3\text{-}I)\}_2\{Cu(CH_3CN)(\mu_4\text{-}I)\}_2Cu_2\{Cu(CH_3CN)\}(\mu_3\text{-}I)(\mu_2\text{-}I)]_n$ (**15**). The 1D polymers **13-Cl**, **13-Br**, **14** and **15** all have the rather uncommon $\{Cu_4X_4\}$ 'crown' motif in common (*cf.* **8**, **9**), though the linkage of **4a** moieties and this 'crown' is different, for example *via* K^+ (in **13-Cl** and **13-Br**) or a more extended CuI-aggregate (in **15**). In contrast to these 1D chains, due to tetrahedral $\{Cu_4(\mathbf{4a})_4\}$ nodes the net of **12** is extended in three dimensions and exhibits topologic relationships with diamond. These results nicely demonstrate the potential of the salt K[**4a**] as a building block in metallosupramolecular chemistry. In comparison to the corresponding triphosphaferrocene (*vide supra*), rather novel polymers are formed in addition to a few analogous products.

Furthermore, in order to study the influence of the steric bulk of the R group in $K[1,2,4\text{-}P_3C_2R_2]$, analogous reactions were carried out using the ^{t}Bu derivative $K[1,2,4\text{-}P_3C_2{}^tBu_2]$ (K[**4b**]). Here, the

self-assembly processes with Cu(I) halides once more reveal unprecedented coordination compounds with hitherto unknown structural motifs (*Scheme 15.4*):

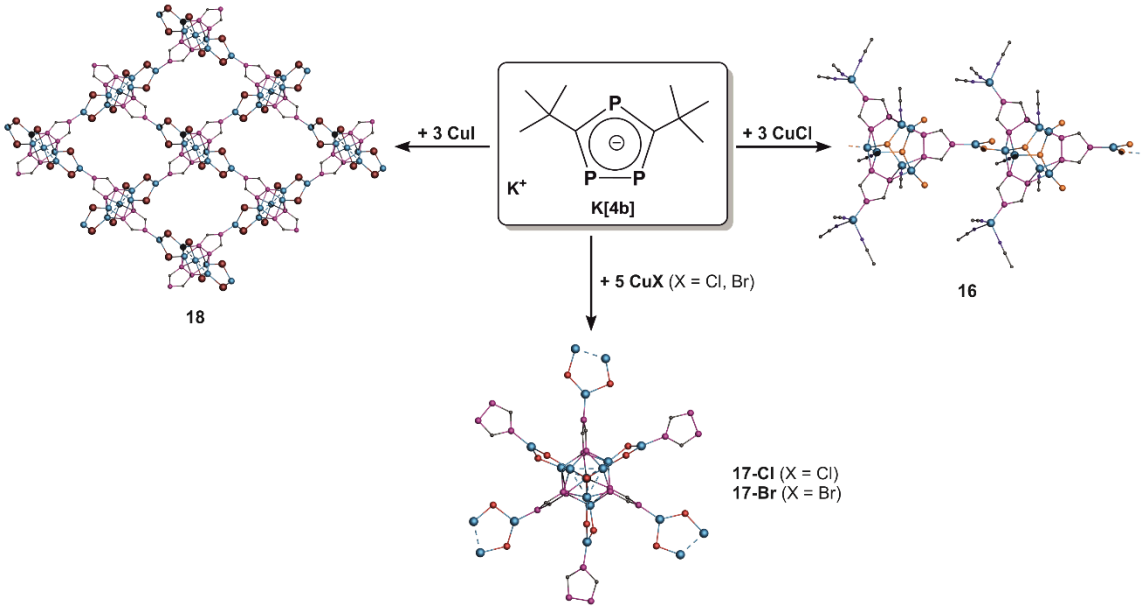

Scheme 15.4 Coordination Compounds based on **4b** starting from its potassium salt.

In the 1D polymer $[(\mu,\eta^{1:2:2}\text{-}P_3C_2{}^tBu_2)(CuCl)_3(\mu_3\text{-}Cl)_2\{Cu(CH_3CN)\}_3\{Cu(\mu_2\text{-}Cl)\}\{Cu(CH_3CN)_3\}_2]_n$ (**16**) the central core consists of a Cu_6 triangular prism capped by chloride and **4b** ligands, whereas $[K(thf)_6]_n[(\mu,\eta^{1:3:3}\text{-}P_3C_2{}^tBu_2)_2\{Cu_3(\mu_2\text{-}I)_2\}_2\{Cu(\mu_2\text{-}I)_2\}]_n$ (**18**) shows a mesh-like 2D structure with embedded $K(thf)_6^+$ cations. Astonishingly, **4b** is also capable of the formation of the isotypical three-dimensional aggregates $[(P_3C_2{}^tBu_2)_3Cu_{9.85}Cl_{6.85}(CH_3CN)_{1.9}]_n$ (**17-Cl**) and $[(P_3C_2{}^tBu_2)_3Cu_{10.1}Br_{7.1}(CH_3CN)_{1.2}]_n$ (**17-Br**). In these polymers, the central structural motif is continued stellar-like to give a 6-fold-connected 3D network, which shows topological analogy to 'polybenzene'. This allotrope of carbon is proposed to be rather stable, however it could not be synthesized so far.

In summary, the 1,2,4-triphospholyl ligands **4a** and **4b** were introduced as building blocks in supramolecular chemistry, whereby the negative charge of this cyclic ligand favors the generation of cationic Cu_aX_b (a > b, X = Cl, Br, I) assemblies, a challenging area within the well-studied coordination chemistry of CuX units. In addition, the results give evidence of the considerable impact of the substitution pattern (R = Mes, ^{t}Bu) as well as of the phospholyl source ([Cp*Fe(η^5-$P_3C_2Mes_2$)], K[**4a**]).

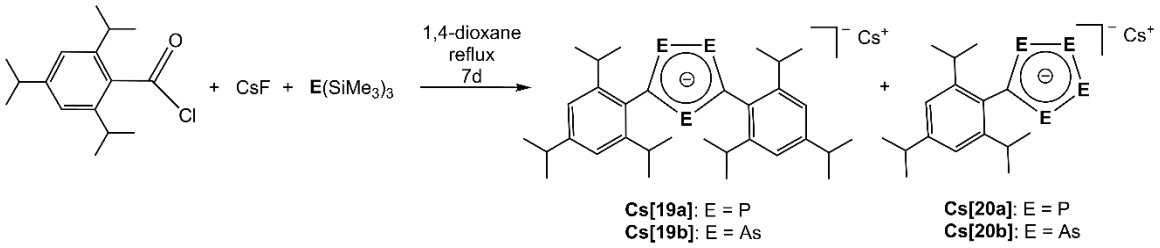

Scheme 15.5 Synthesis of **19a** and **19b** and **20a** and **20b**, respectively.

Not only was the preparation of supramolecular assemblies containing phospholyl ligands part of this work, but also the synthesis of hitherto unknown derivatives bearing even bigger substituents. Within the scope of this, a one-pot-synthesis applied by the group of Ionkin for the synthesis of Cs[1,2,4-($P_3C_2Mes^*_2$)] and Cs[P_4CMes^*] was successfully transferred to the slightly smaller 2,4,6-tri-*iso*-propylphenyl (trip) ligand. *Via* this method (*Scheme 15.5*) Cs[1,2,4-$P_3C_2(trip)_2$] (Cs[**19a**]) and Cs[$P_4C(trip)$] (Cs[**20a**]) can be isolated. More astonishingly, this synthetic approach is also applicable for the synthesis of the respective arsenic derivatives Cs[1,2,4-$As_3C_2(trip)_2$] (Cs[**19b**]) and Cs[$As_4C(trip)$] (Cs[**20b**]) (*Scheme 15.5*), of which the latter compound Cs[**20b**] could also be structurally characterized. Cs[**19b**] and Cs[**20b**] display the first representatives of a 1,2,4-triarsolyl and a tetraarsolyl ligand, respectively.

In contrast to the continuous enhancement of the steric bulk at the 1,2,4-triphospholyl ligands (from ^{t}Bu to Mes), also the synthesis and reactivity of phosphaferrocenes bearing rather small substituents was part of this thesis. Therefore a mixture of K[1,2,4-$P_3C_2{}^i Pr_2$] and K[1,3-$P_2C_3{}^i Pr_3$] was reacted with Fe(II) halide and LiCp* to give a series of partially novel phosphaferrocenes (*Scheme 15.6*): The 1,3-diphosphaferrocene [Cp*Fe(η^5-$P_2C_3iPr_3$)] (**21**), the 1,2,4-triphosphaferrocene [Cp*Fe(η^5-$P_3C_2{}^i Pr_2$)] (**22**), the 1,1',3,3'-tetraphosphaferrocene [(η^5-$P_2C_3{}^i Pr_3$)$_2$Fe] (**23**), the 1,1',2,3',4-pentaphosphaferrocene [(η^5-$P_3C_2{}^i Pr_2$)Fe(η^5-$P_2C_3{}^i Pr_3$)] (**24**), as well as the 1,1',2,2',4,4'-hexaphosphaferrocene [(η^5-$P_3C_2{}^i Pr_2$)$_2$Fe] (**25**).

Previous results on the coordination behavior have shown the tendency of ^{t}Bu-substituted triphosphaferrocenes [Cp^{R}Fe(η^5-$P_3C_2{}^t Bu_2$)] (Cp^R = Cp, Cp*, Cp''') to form di- and oligomeric products with intact sandwich complexes or, on the other hand, polymeric products, though with fragmented and/or rearranged moieties of the building block. In addition, as explained above, the mesityl ligands in [Cp*Fe(η^5-$P_3C_2Mes_2$)] lead to a split-off of the phospholyl ligand (*Scheme 15.2*). By contrast, using the ^{i}Pr-substituted derivative **22**, isolation of the 2D mesh-like networks [{Cp*Fe(μ_4,$\eta^{5:1:1:1}$-$P_3C_2{}^i Pr_2$)}Cu_2(μ-X)$_2$]$_n$ (**26-Cl**: X = Cl, **26-Br**: X = Br) (*Scheme 15.6*) is possible. Both compounds contain intact units of **22** and therefore display the second and third representative of a triphosphaferrocene-based polymer, respectively.

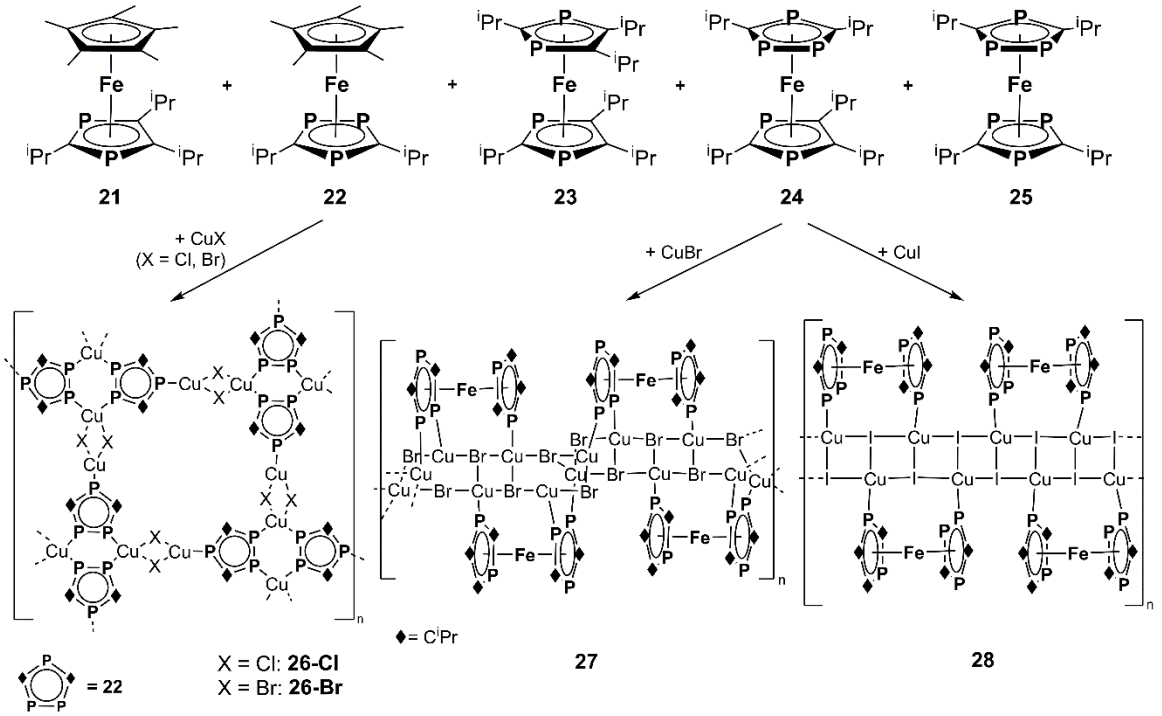

Scheme 15.6 Synthesized phosphaferrocenes bearing ^{i}Pr substituents and subsequently obtained coordination polymers based on **22** and **24**, respectively.

Since no supramolecular assemblies are known for a 1,1',2,3',4-pentaphosphaferrocene, the coordination behavior of **24** towards Cu(I) halides has also been studied. By the reaction with CuBr and CuI, the ladder-like infinite chains $[\{(\mu_3,\eta^{5:1:1}\text{-}P_3C_2{}^iPr_2)Fe(\mu,\eta^{5:1}\text{-}P_2C_3{}^iPr_3)\}Cu_3(\mu\text{-}Br)(\mu_3\text{-}Br)(\mu_4\text{-}Br)]_n{\cdot}0.5C_7H_8$ (**27**) and $[\{(\mu,\eta^{5:1}\text{-}P_3C_2{}^iPr_2)Fe(\mu,\eta^{5:1}\text{-}P_2C_3{}^iPr_3)\}Cu_2(\mu_3\text{-}I)_2]_n$ (**28**) are obtained (*Scheme 15.6*). These first representatives both contain the moieties of **24** in a chelating coordination mode.

In summary, rather small substituents (^{i}Pr) in the phospholyl ligand entail an enhanced stability of the corresponding phosphaferrocenes and polymeric products are formed in combination with Cu(I) halides. Triphosphaferrocenes bearing rather large R groups (^{t}Bu) tend to form oligomeric compounds and already a few fragmentations and rearrangement processes occur. On the other hand, the sterically even more demanding mesityl ligand leads to the cleavage of the triphospholyl ligands from iron without exception.

(c) The Pentaphospholyl Ligand – A versatile Building Block for the Template-Directed Synthesis of Spherical Supramolecules

The pentaphosphaferrocenes $[Cp^RFe(\eta^5\text{-}P_5)]$ (**29a**: $Cp^R = Cp^*$; **29b**: $Cp^R = Cp^{Bn}$) bearing a *cyclo*-P_5 ligand in combination with Cu(I) halides display excellent building blocks for the formation of neutral nano-sized supramolecules. Among them, a fullerene-like 80-vertex ball exhibiting I_h-C_{80} topology is capable of the encapsulation of small molecules, e.g. $[FeCp_2]$ and *o*-carborane, respectively (*Figure 15.4*). Therefore it was of special interest to expand this host-guest system to

other small molecules while focusing on the required properties of the template molecules to be incorporated into this 80-vertex sphere.

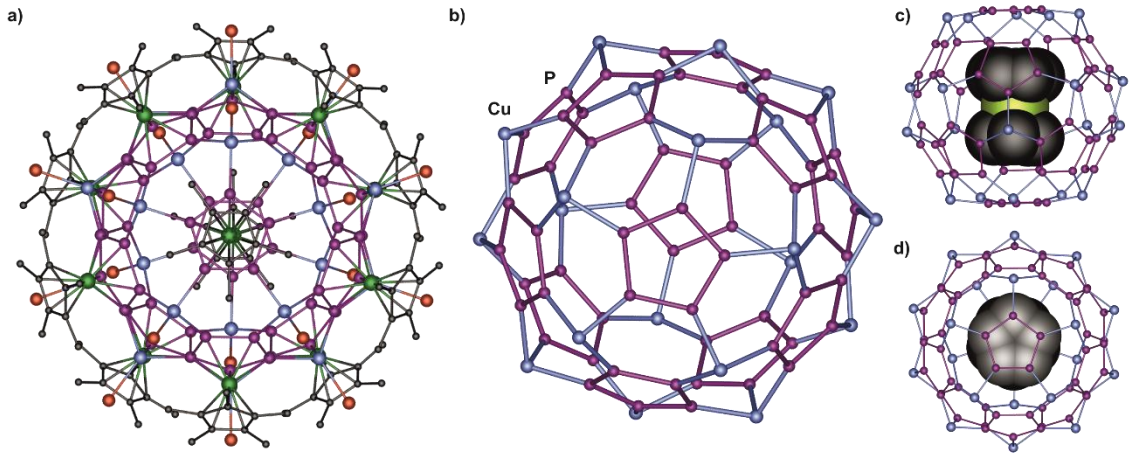

Figure 15.4 a) 80-vertex sphere without guest; b) scaffold of the 80-vertex sphere: c) illustration of an enclosed sandwich complex; d) illustration of π-π-interactions between host and guest.

To investigate this, a variety of small molecules exhibiting different properties, such as size, symmetry, the presence of Cp ligands, redox potential, number of valence electrons, stability and magnetism have been tested. Those which show a template effect for the formation of a nano-sized supramolecule, are displayed in *Figure 15.5* and an overview of the obtained host-guest complexes is given in *Table 15.1*.

.

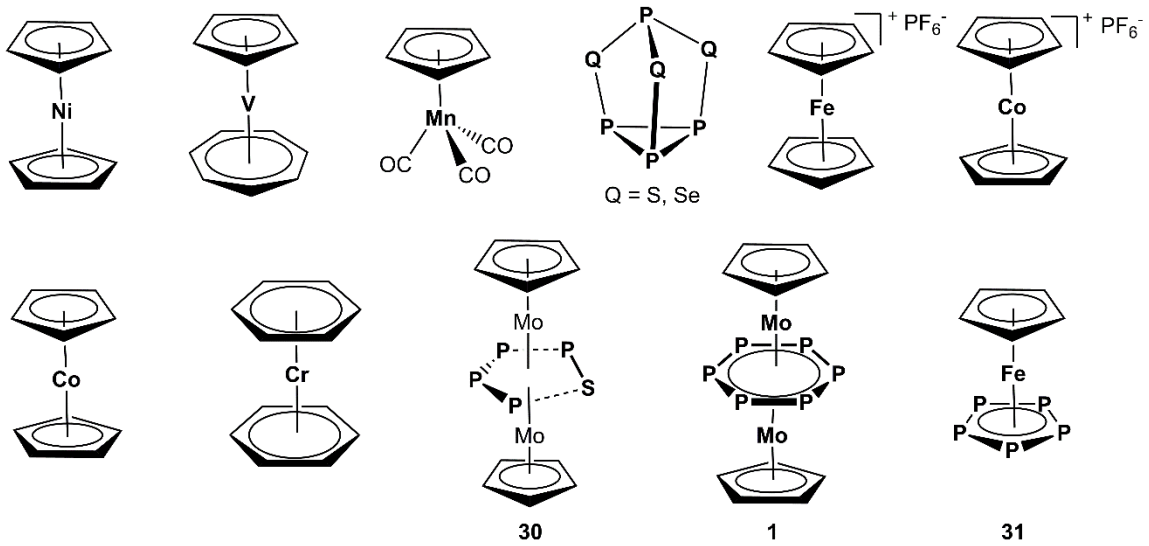

Figure 15.5 Overview of the molecules used with template effect for the formation of supramolecular hosts.

Table 15.1 Obtained products of the template-dependant formation of supramolecules based on **29a** and CuX (X = Cl, Br, I). The 80-vertex sphere exhibiting I_h-C_{80} topology (see above) is stated as 'C_{80}'.

Template	Guest (if not the template)	Host	X	Sum Formula	Label
$[NiCp_2]$		'C_{80}'	Br	$[NiCp_2]@[\{Cp^*Fe(\eta^5\text{-}P_5)\}_{12}(CuBr)_{18.95}]$	**32-Br**
$[NiCp_2]$		'C_{80}'	I	$[NiCp_2]@[\{Cp^*Fe(\eta^5\text{-}P_5)\}_{12}(CuI)_{18.125}]$	**32-I**
$[CpV(\eta^7\text{-}C_7H_7)]$		'C_{80}'	Cl	$[CpV(\eta^7\text{-}C_7H_7)]@[\{Cp^*Fe(\eta^5\text{-}P_5)\}_{12}(CuCl)_{18.20}]$	**33-Cl**
$[CpV(\eta^7\text{-}C_7H_7)]$		'C_{80}'	Br	$[CpV(\eta^7\text{-}C_7H_7)]@[\{Cp^*Fe(\eta^5\text{-}P_5)\}_{12}(CuBr)_{18.83}]$	**33-Br**
$[CpV(\eta^7\text{-}C_7H_7)]$		'C_{80}'	I	$[CpV(\eta^7\text{-}C_7H_7)]@[\{Cp^*Fe(\eta^5\text{-}P_5)\}_{12}(CuI)_{17.65}]$	**33-I**
$[CpMn(CO)_3]$		'C_{80}'	Br	$[CpMn(CO)_3]_{0.2}@[\{Cp^*Fe(\eta^5\text{-}P_5)\}_{12}(CuBr)_{18.05}]$	**34-Br**
$[CpMn(CO)_3]$		'C_{80}'	I	$[CpMn(CO)_3]_{0.33}@[\{Cp^*Fe(\eta^5\text{-}P_5)\}_{12}(CuI)_{18.15}]$	**34-I**
$[P_4S_3]$		'C_{80}'	Cl	$[P_4S_3]_{0.5}@[\{Cp^*Fe(\eta^5\text{-}P_5)\}_{12}(CuCl)_{19.5}]$	**35-Cl**
$[P_4S_3]$		'C_{80}'	Br	$[P_4S_3]_{0.38}@[\{Cp^*Fe(\eta^5\text{-}P_5)\}_{12}(CuBr)_{19.025}]$	**35-Br**
$[P_4S_3]$		'C_{80}'	I	$[P_4S_3]_{0.44}@[\{Cp^*Fe(\eta^5\text{-}P_5)\}_{12}(CuI)_{18.95}]$	**35-I**
$[P_4Se_3]$		'C_{80}'	Cl	$[P_4Se_3]_{0.54}@[\{Cp^*Fe(\eta^5\text{-}P_5)\}_{12}(CuCl)_{17.375}]$	**36-Cl**
$[P_4Se_3]$		'C_{80}'	Br	$[P_4Se_3]_{0.75}@[\{Cp^*Fe(\eta^5\text{-}P_5)\}_{12}(CuBr)_{18.35}]$	**36-Br**
$[FeCp_2][PF_6]$	$[FeCp_2]$	'C_{80}'	Br	$[FeCp_2]@[\{Cp^*Fe(\eta^5\text{-}P_5)\}_{12}(CuBr)_{17.3}]$	**37**
$[CoCp_2][PF_6]$	$[CoCp_2]^+$	'prism'	Br	$[CoCp_2]^+@[\{Cp^*Fe(\eta^5\text{-}P_5)\}_8Cu_{24.25}Br_{28.25}(CH_3CN)_6]^{4-}\cdot 3[CoCp_2]^+$	**38**
$[CoCp_2]$	$[CoCp_2]^+$	'prism'	Br	$[CoCp_2]^+@[\{Cp^*Fe(\eta^5\text{-}P_5)\}_8Cu_{24.25}Br_{28.25}(CH_3CN)_6]^{4-}\cdot 3[CoCp_2]^+$	**38**
$[CoCp_2]$	none	'C_{80}'	Br	$[\{Cp^*Fe(\eta^5\text{-}P_5)\}_9\{Cp^*Fe(\eta^4\text{-}P_5OH)\}_3(CuBr)_{20}]^{3-}\cdot 3[CoCp_2]^+$	**39**
$[CoCp_2]$	$[CoCp_2]^+$	'cube'	I	$\{[Cp_2Co]^+@[\{Cp^*Fe(\eta^5\text{-}P_5)\}Cu_{24.4}I_{26.4}(CH_3CN)_8]^{2-}\}\{[Cp_2Co]^+@[\{Cp^*Fe(\eta^5\text{-}P_5)\}_8Cu_{28}I_{28}(CH_3CN)_{9.8}]\}$	**40**
$[CoCp_2]$	none	'hemisphere'	I	$[\{Cp^*Fe(\eta^5\text{-}P_5)\}_3\{(Cp^*Fe(\eta^4\text{-}P_5))_2O\}_3Cu_{16}I_{10}(CH_3CN)_7]$	**41**
$[Cr(\eta^6\text{-}C_6H_6)_2]$	$[Cr(\eta^6\text{-}C_6H_6)_2]^+$	'C_{80}'	Br	$[Cr(C_6H_6)_2]^+{}_{0.6}@[\{Cp^*Fe(\eta^5\text{-}P_5)\}_{12}Cu_{17.925}Br_{18.525}]$	**42**
$[(CpMo)_2(\mu,\eta^{3:3}\text{-}P_3)(\mu,\eta^{2:2}\text{-}PS)]$		'nano-bowl'	Br	$[(CpMo)_2(\mu,\eta^{3:3}\text{-}P_3)(\mu,\eta^{2:2}\text{-}PS)]@[\{Cp^*Fe(\eta^5\text{-}P_5)\}_{11}(CuBr)_{15\text{-}n}]$	**43**
$[(CpMo)_2(\mu,\eta^{6:6}\text{-}P_6)]$		'nano-bowl'	Br	$[(CpMo)_2(\mu,\eta^{6:6}\text{-}P_6)]@[\{Cp^*Fe(\eta^5\text{-}P_5)\}_{11}(CuBr)_{15\text{-}n}]$	**44**
$[CpFe(\eta^5\text{-}P_5)]$		'C_{80}'	Cl	$[CpFe(\eta^5\text{-}P_5)]@[\{Cp^*Fe(\eta^5\text{-}P_5)\}_{12}(CuCl)_{17.6}]$	**45-Cl**
$[CpFe(\eta^5\text{-}P_5)]$		'C_{80}'	Br	$[CpFe(\eta^5\text{-}P_5)]@[\{Cp^*Fe(\eta^5\text{-}P_5)\}_{12}(CuBr)_{17.6}]$	**45-Br**
$[CpFe(\eta^5\text{-}P_5)]$		'C_{80}'	I	$[CpFe(\eta^5\text{-}P_5)]@[\{Cp^*Fe(\eta^5\text{-}P_5)\}_{12}(CuI)_{19.05}]$	**45-I**

The results demonstrate that only the correct size and the ability to interact with the inner surface of a host are determining factors for the formation of the carbon-free I_h-C_{80} analogue and $[NiCp_2]$ (in **32-Br**, **32-I**), $[CpV(\eta^7\text{-}C_7H_7)]$ (in **33-Cl**, **33-Br**, **33-I**), $[CpMn(CO)_3]$ (in **34-Br**, **34-I**), P_4S_3 (in **35-**

Cl, **35-Br**, **35-I**) and P_4Se_3 (in **36-Cl**, **36-Br**) can be enclosed within its cavity. Moreover, [CpV(η^7-C_7H_7)] was also trapped in the analogous sphere constructed by the Cp^{Bn} derivative **29b** to give [CpV(η^7-C_7H_7)]@[{Cp^{Bn}Fe(η^5-P_5)}$_{12}$(CuBr)$_{18.8}$] (**46**). It is noteworthy that some of the templates even allow the isolation of the iodide derivative of this fullerene-like sphere (**32-I**, **33-I**, **34-I**, **35-I**, **45-I**), whereas previous attempts failed.

Furthermore, more instable templates such as the ferricinium cation $[FeCp_2]^+$ and cobaltocene $[CoCp_2]$ are readily reduced or oxidized to their more stable corresponding forms $[FeCp_2]$ and $[CoCp_2]^+$, respectively. Particularily astonishing is the subsequent incorporation of the cobaltocinium cation resulting in the formation of the unprecedented 'prism'- and 'cube'-shaped supramolecules **38** and **40** (*Scheme 15.7*). They represent the first inorganic/organometallic host molecules encapsulating a $[MCp_2]^+$ species and in contrast to the neutral 80-vertex ball they bear a negative charge.

Since the use of [$(CpCr)_2(\mu,\eta^{5:5}$-$As_5)$] entails its fragmentation followed by an encapsulation of the remnant [CpCr(η^5-As_5)], the use of further triple decker complexes bearing Cp ligands as end decks is of special interest. For this purpose, the hitherto unknown parent compound [$(CpMo)_2(\mu,\eta^{3:3}$-$P_3)(\mu,\eta^{2:2}$-PS)] (**30**) was successfully synthesized by means of the commonly applied thermolysis reaction though using a higher-boiling solvent. Surprisingly, the self-assembly of **29a** and CuBr in presence of **30** leads to the formation of the unprecedented nano-sized 'bowl' **43**, which is open at the top (*Scheme 15.7*). The host molecule of **43** can be derived from the 80-vertex ball by cutting of a {Cp*Fe(η^5-P_5)$(CuBr)_5$} moiety in a way so that the triple decker complex is allowed to protrude upwardly and is incorporated despite its larger size. To investigate whether the formation of this truncated sphere only displays a random event, also the triple decker complex **1** has been applied in this system. Astonishingly, also this template induces the self-assembly of the spherical dome (**44**).

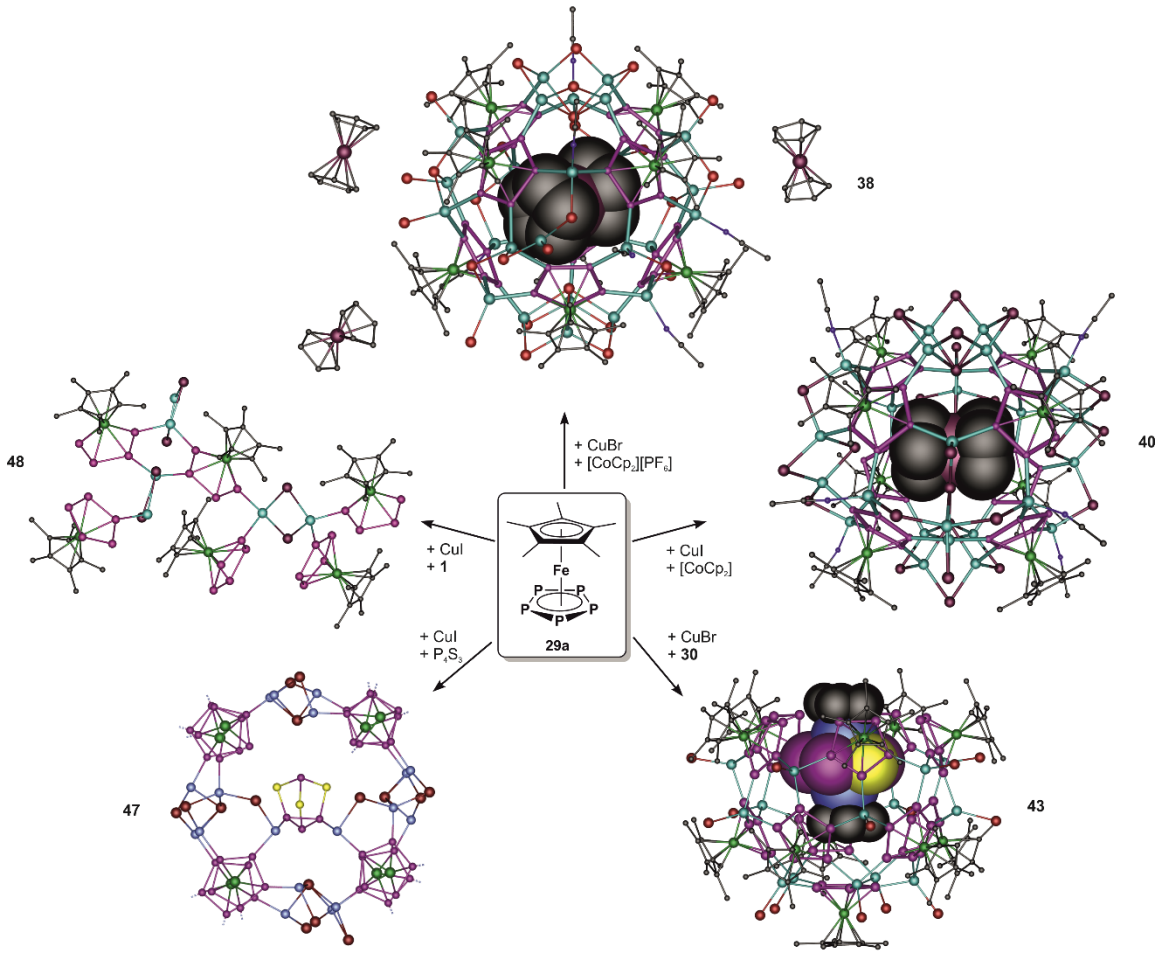

Scheme 15.7 Spherical and polymeric coordination products from **29a** and Cu(I) halides apart from the 80-vertex ball.

In the course of these host-guest reactions, also two novel polymers could be obtained (*Scheme 15.7*): the hybrid polymer $[\{Cp^*Fe(\eta^{5:1:1:1:1}\text{-}P_5)\}_4(P_4S_3)(CuI)_{12}]_n$ (**47**) constructed by the three components **29a**, P_4S_3 and CuI as well as the three-dimensional network $[\{Cp^*Fe(\eta^{5:1:1:1}\text{-}P_5)\}_2\{Cp^*Fe(\eta^{5:1:1}\text{-}P_5)\}Cu_4(\mu\text{-}I)_4]_n$ (**48**). Amazingly, among the huge variety of pentaphosphaferrocene-based polymers, **48** displays the first representative of a 3D assembly despite its simple linkage pattern. Unfortunately, **48** was only observed twice.

Another interesting template of the appropriate size is the previously unknown parent compound $[CpFe(\eta^5\text{-}P_5)]$ (**31**). By applying slightly different reaction conditions its synthesis and comprehensive characterization was possible for the first time within the scope of this thesis. Despite its variable coordination sites, it also acts as a template for the construction of the 80-vertex balls **45-Cl**, **45-Br** and **45-I** when added to the **29a**/CuX system.

Moreover, **31** displays a promising building block itself and the coordination behavior towards Cu(I) halides was investigated revealing the three novel 2D mesh-like assemblies $[\{CpFe(\eta^{5:1:1:1:1}\text{-}P_5)\}Cu_2(\mu\text{-}X)_2]_n$ (**49-Cl**: X = Cl, **49-Br**: X = Br) and $[\{CpFe(\eta^{5:1:1}\text{-}P_5)\}Cu(\mu\text{-}I)]_n$ (**50**) as well as the 3D

network [{CpFe($\eta^{5:1:1}$-P_5)}Cu(μ-I)]$_n$ (**51**) (*Scheme 15.8*). Noteworthy, **51** displays the first reproducible three-dimensional polymer containing *cyclo*-P_5 ligands.

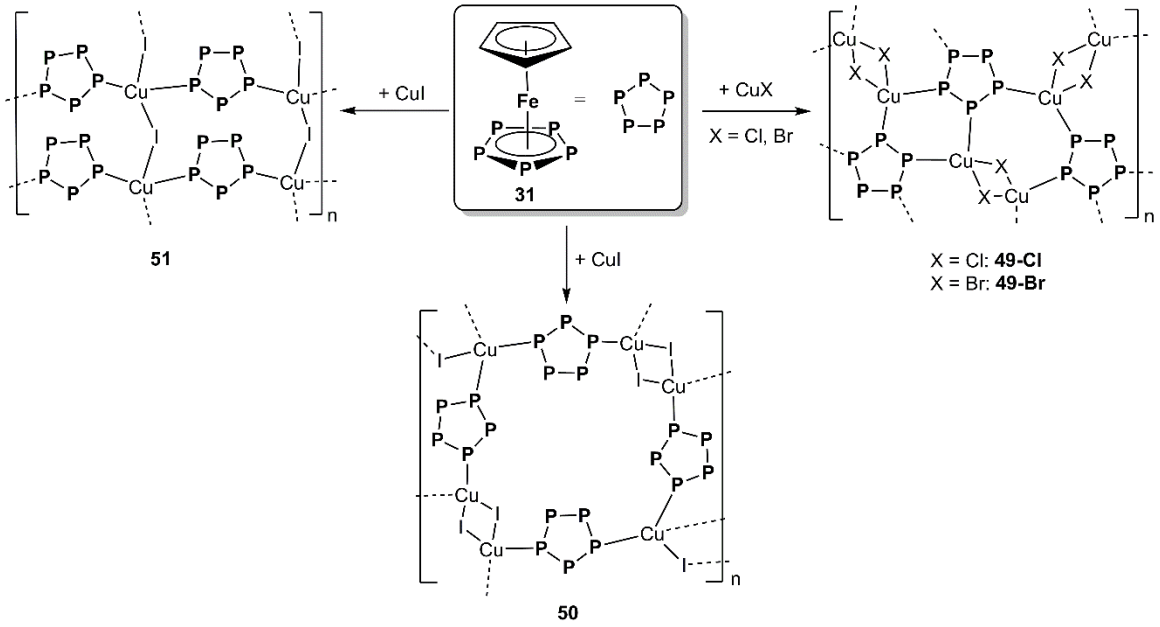

Scheme 15.8 Coordination compounds based on **31**.

This thesis also deals with the variation of the copper source with the goal being the synthesis of novel supramolecules regarding different topologies and shapes. For this purpose, Cu($GaCl_4$) and Cu(CF_3SO_3) were reacted with **29a**, respectively, to yield the novel 2D undulated sheet-like polymers [{Cp*Fe(η^5-P_5)}{Cu($GaCl_4$)$_2$}]$_n$ (**52**) and [{Cp*Fe(μ_4,$\eta^{5:1:1:1}$-P_5)}{Cu(CF_3SO_3)}]$_n$ (**53**) (*Scheme 15.9*). On the other hand, the self-assembly process of the pentabenzyl derivative **29b** with the triflate salt reveals the unprecedented ball-shaped sphere [{Cp^{Bn}Fe(η^5-P_5)}$_{12}${Cu(CF_3SO_3)}$_{19.6}$] (**54**) (*Scheme 15.9*). Therein, the skeleton is beyond the fullerene topology with the copper atoms forming an icosidodecahedron and the tridentate triflate ligands bridging them in a μ_3 coordination mode. Within the scope of a cooperation with Barbara Krämer, isostructural spheres are also obtained by using the respective silver salt Ag(CF_3SO_3) in combination with **29b** as well as **29a** (*Scheme 15.9*): [{Cp^{Bn}Fe(η^5-P_5)}$_{12}${Ag(CF_3SO_3)}$_{20-n}$] (**55**) and [Cp*Fe(η^5-P_5)]@[{Cp*Fe(η^5-P_5)}$_{12}${Ag(CF_3SO_3)}$_{20-n}$] (**56**), the latter additionally encapsulating one molecule of **29a**. These two compounds represent the first Ag-containing supramolecules based on pentaphosphaferrocenes. Depending on the concentration, sometimes also the novel two-dimensional assembly [{Cp*Fe(μ_3,$\eta^{5:1:1:1}$-P_5)}{Ag(CF_3SO_3)}$_2$]$_n$ (**57**) is obtained, which exhibits a different linkage pattern compared to the copper-containing polymer **53** (*Scheme 15.9*).

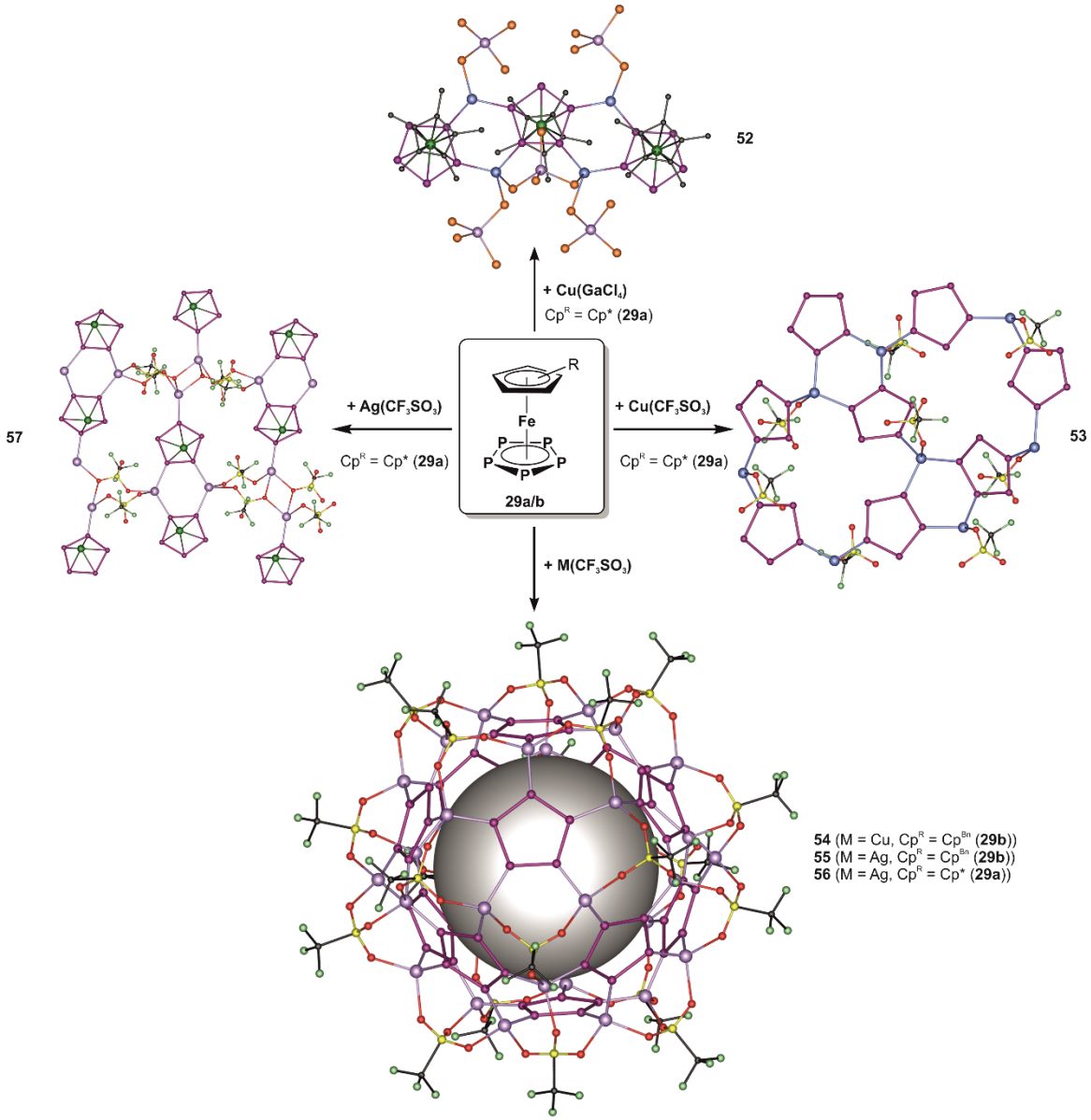

Scheme 15.9 Variation of the metal salt: coordination compounds based on **29a/b** and $Cu(GaCl_4)$ or $M(CF_3SO_3)$ (M = Cu, Ag), respectively.

Finally, a particular highlight is the self-assembly of **29b** with $CuBr_2$ leading to the formation of the staggering rugby ball-shaped supramolecule $[\{Cp^{Bn}Fe(\eta^5\text{-}P_5)\}_{24}Cu_{96}Br_{96}]$ (**58**) (*Figure 15.6*). It consists of 24 units of **29b** and an extended $Cu_{96}Br_{96}$ framework, therefore the inorganic scaffold alone contains 312 atoms already. The outer size of the entire sphere amounts to 3.7 nm in width and 4.6 nm in length with a corresponding volume of 32.1 nm^3, hence it is one of the largest discrete supramolecules which was structurally characterized up to date. More vividly, it is only slightly smaller than the human protein hemoglobin (d = 5 nm) and even 62 times larger in volume than the C_{60} fullerene (V = 0.5 nm^3).

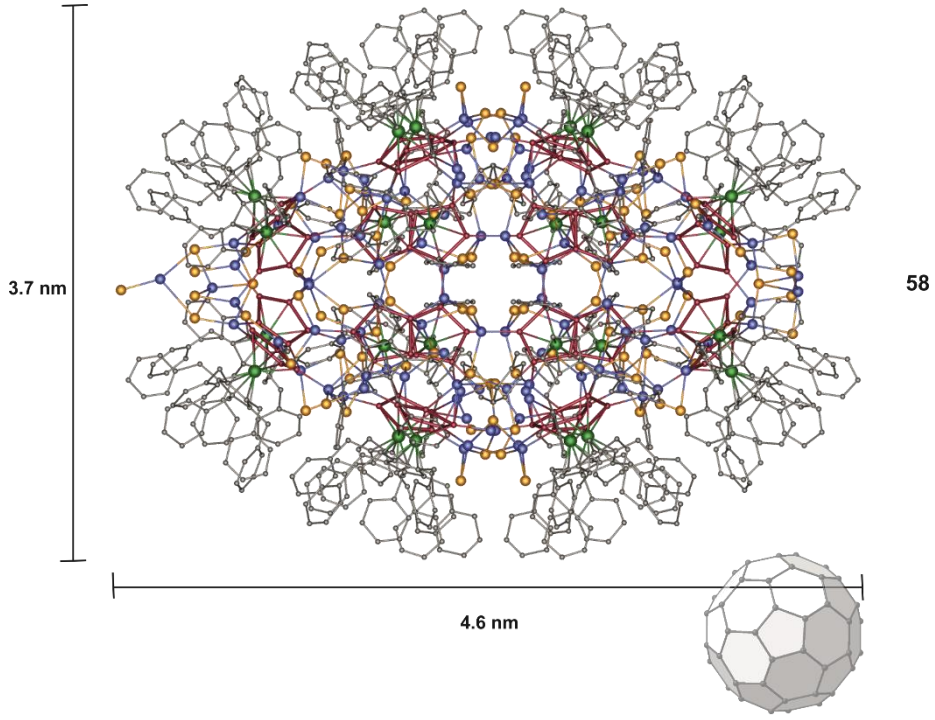

Figure 15.6 Rugby ball-shaped sphere **58**. For a size comparison, C_{60} is depicted in semitransparent color.

16. Appendices

16.1 Alphabetic List of Abbreviations

Å	Angstroem, 1 Å = $1 \cdot 10^{-10}$ m
°C	degree Celsius
0D	*pseudo*-zero-dimensional
1D	one-dimensional
2D	two-dimensional
3D	three-dimensional
av.	Average
Bn	benzyl
bp	boiling point
br (NMR)	broad
^{n}Bu	*n*-butyl
^{t}Bu	*tert*-butyl
COSY	correlation spectroscopy
Cp	cyclopentadienyl, C_5H_5
Cp''	1,3-di-*tert*-butylcyclopentadienyl, $C_5H_3{}^{t}Bu_2$
Cp'''	1,2,4-tris-*tert*-butylcyclopentadienyl, $C_5H_2{}^{t}Bu_3$
Cp°	1-*tert*-butyl-3,4-dimethylyclopentadienyl, $C_5H_2Me_2{}^{t}Bu_2$
Cp*	pentametyhlcyclopentadienyl, C_5Me_5
Cp^{BIG}	pentakis-4-*n*butylphenylcyclopentadienyl, $C_5(4\text{-}{}^{n}BuC_6H_4)_5$
Cp^{Bn}	pentabenzylcyclopentadienyl, $C_5(CH_2Ph)_5$
Cp^{Et}	tetramethyl-ethylcyclopentadienyl, C_5Me_4Et
Cp^{R}	substituted cyclopentadienyl ligand
CV	Cyclic voltammetry
d	distance or day(s)
d (NMR)	doublet
δ	chemical shift
DFT	density functional theory
DIB	1,3-diisopropylbenzene
dme	1,2-dimethoxyethane

E	heavier element of the 15th group, E = P, As, Sb
e^-	electron
EI MS	electron impact mass spectrometry
EPR	electron paramagnetic resonance
ESI MS	electron spray ionization mass spectrometry
Et	ethyl
FD MS	field desorption ionization mass spectrometry
h	hour(s)
HOMO	highest occupied molecular orbital
Hz	Hertz
IR	infrared
J (NMR)	coupling constant
L	ligand (specified in text)
LUMO	lowest unoccupied molecular orbital
m (NMR)	multiplet
M	metal
m/z	mass to charge ratio
MAS	magic angle spinning
Me	methyl
Mes	mesityl, 2,4,6-trimethylphenyl
Mes*	supermesityl, 2,4,6-tri-*tert*-butylphenyl
MO	molecular orbital
MOF	metal-organic framework
NMR	nuclear magnetic resonance
v	frequency
$\tilde{\nu}$	wavenumber
$\omega_{1/2}$	half width
OTf	triflate, CF_3SO_3
ppm	parts per million
^{i}Pr	*iso*-propyl
q (NMR)	quartett
R	organic substituent
r.t.	room temperature
s (IR)	strong

s (NMR)	singlet
sept (NMR)	septet
t (NMR)	triplet
thf	tetrahydrofurane, C_4H_8O
TIP	1,3,5-triisopropylbenzene
trip	2,4,6-tri-*iso*-propylphenyl
UV-Vis	Ultraviolet-visible
vdW	van-der-Waals
VE	valence electrons
VT	various temperature
w (IR)	weak
X	any halide, X = Cl, Br, I

16.2 Acknowledgments

Finally, I would like to express my gratitude to:

- Prof. Dr. Manfred Scheer for giving me the opportunity to work on such an interesting project and always ensuring excellent working conditions
- Dr. Gábor Balázs for his very helpful advices on every need instead of answering 'Ich nix verstehen'
- Dr. Eugenia Peresypkina and Dr. Alexander V. Virovets for the untiring efforts concerning the X-ray structure analyses, without whom this work would not have been possible
- The Fonds der chemischen Industrie for a Ph.D. fellowship
- Prof. Dr. Werner Kremer, PD Dr. Gunther Brunklaus and David Lüdeker for a very successful MAS NMR cooperation
- Dr. Gábor Balázs and PD Dr. Gunther Brunklaus for DFT calculations
- Dr. Thomas Hirsch for the UV-Vis spectra
- All staff and co-workers of the Central Analytical Services: X-Ray (Dr. Michael Bodensteiner, Sabine Stempfhuber, Katharina Beier), NMR (Dr. Ilya Shenderovich, Anette Schramm, Georgine Stühler, Fritz Kastner), MS (Josef Kiermaier, Wolfgang Söllner), Elemental analysis (Helmut Schüller, Barbara Baumann, Wilhelmina Krutina)
- The staff of the glass blowing, electronics and mechanics facilities of the University of Regensburg
- Dr. Sebastian Heinl, Dr. Eugenia Peresypkina, Dr. Gábor Balázs and Eva-Maria Rummel for accurate proof reading
- Dr. Andrea Kuntz, Dr. Christine Thoms, Dr. Sabine Reisinger, Barbara Krämer and Helena Brake for the fantastic atmosphere in the girls' lab
- Sebi, Fabi, Moni, Eva, Andi and sμ for the funny 'statement'-meetings
- All present and former members of the research group for an unforgettable time, also beyond research: Andi (nein, nicht euer Ernst), Andrea, Andrea K., Babsi-Barbara, Barbara, Bianca, Biegi, Boudi, Conny, Dani, David, (Chol-)Eric, Eva (print the legend), Fabi D., Felix, Gábor, Helena (Hells-Bells), Hias, Jens, Julian, Karin, Küken (alias Gockl), Liese, Luigi, Luis, Matthias, Mehdi, Mia, Michi, Miriam, ML, Moartl, Mobbsi-Fabi, Moni (hat wer Moni gesagt?), Moritz, Musch, Muschine, Oime, (Pr-)Olli, Patrick, Petra, Rasta, Reini, Robert, Rudi, Sabine-Bienchen, Schotti, Sebi Hein(d)l, sμ (alias das μ), Stubi, Susanne, Thomsi, Tobi, Valentin, Walter, Wast, Welschi, Wurzl
- My family for their enduring support and…

…Sebi for loving me, supporting me, making me laugh